Université de Toulouse

THÈSE

En vue de l'obtention du

DOCTORAT DE L'UNIVERSITÉ DE TOULOUSE

Délivré par :
Université Toulouse III Paul Sabatier (UT3 Paul Sabatier)

Discipline ou spécialité :

Sciences de la Terre

Présentée et soutenue par :
Mélanie LOUTERBACH

le : vendredi 24 octobre 2014

Titre :

Propagation du front orogénique Subandin et réponse sédimentaire associée dans le bassin d'avant-pays Amazonien (Madre de Dios, Pérou)

Ecole doctorale :
Sciences de l'Univers, de l'Environnement et de l'Espace (SDU2E)

Unité de recherche :
UMR 5563-GET / Institut Polytechnique Lasalle Beauvais

Directeur(s) de Thèse :

Patrice BABY, Julien BAILLEUL et Martin RODDAZ

Rapporteurs :

Michel LOPEZ, Jaume VERGÉS

Membre(s) du jury :

Patrice BABY (IRD), Julien BAILLEUL (Lasalle-Beauvais), Elton DANTAS (Brasilia), Jean GÉRARD (Repsol S.A.), Michel LOPEZ (Montpellier), Martin RODDAZ (Toulouse-UPS), Olivier VANDERHAEGHE (Toulouse-UPS), Jaume VERGÉS (Barcelone),

Remerciements

Voici la fin de « quelques » mois de rédaction. Une telle quantité de mots en tous genres est sortie de ma tête pour finir sur Word Microsoft, que j'aimerai ne plus avoir à écrire quoi que ce soit pendant quelques années. Je me fourvoie évidemment. Rien qu'hier, je pensais en avoir fini avec les ultimes corrections, et j'allais, émue, figer pour l'éternité mon manuscrit dans un pdf irréversible quand l'évidence m'a soudain sauté aux yeux : « *Meeeeeeeeeeerde j'ai oublié les remerciements……* ». Eh oui car dans les remerciements on a le droit d'écrire un peu n'importe comment et même d'être grossière, dans une certaine mesure. Mais le but principal reste tout de même, si j'ai bien compris, de remercier toute la *smala*. Eh bien soit, me suis-je dit, remercions tout le monde. Ceux qui ne m'ont pas aidée à écrire, ceux qui m'ont corrigée tellement de fois que je ne suis plus sûre par moment d'être l'auteure de certains paragraphes, et même ceux qui n'ont jamais réellement compris ce que je faisais avec tous ces cailloux… ! Eh Oui ! J'ai bien eu un moment de *blues* post-rédaction, un moment honteux j'en conviens, au cours duquel je me suis dit « *Vraiment ? Faut-il même remercier….mes directeurs de thèse ?!!* ». Puis une vague d'émotion s'est emparée de moi, les souvenirs ont commencé à affluer et je me suis remémorée toutes ces missions de terrain passées ensemble, nos discussions houleuses, tout. Et j'ai repensé à toutes les personnes sans qui effectivement je n'aurais pas pu faire cette thèse. En effet, les remerciements sont de rigueur.

Puis un problème premier s'est imposé à moi : oui, remercier tout le monde, d'accord, mais dans quel ordre ? Vais-je grouper les personnes par importance ? Ce serait totalement indélicat, et un casse-tête évident pour établir une telle hiérarchie. Les regrouper selon leur appartenance à un groupe socio-culturel ? Martin me poserait problème…Devrait-il entrer dans le groupe des Toulousains-rugbymen à l'accent du sud ? Ou bien dans le groupe des intellectuels trentenaires-grincheux à polo rose? Trop difficile. Pas assez de polos roses. La méthode graphique aurait été parfaite : une photo par personne ! Mais certains ne sont vraiment pas photogéniques…Alors j'ai finalement décidé que pour une fois je ne suivrai aucune méthode. Honnêtement, je ne sais pas ce que ça va donner…Mais ce qu'il y a de bien avec les remerciements c'est qu'il s'agit d'une zone de non-droit : on peut à peu près faire ce que l'on veut, il n'y a pas de règles, on ne peut pas nous évaluer sur ces quelques pages, et si le lecteur n'est pas content il ne peut s'en prendre qu'à lui-même d'avoir eu la curiosité de les lire.

Je commencerai par remercier mes parents, qui se sont pourtant inquiétés de mes orientations académiques et demandés à plusieurs reprises « *Mais quand va-t-elle vraiment commencer à travailler ?* » (« *C'est un travail, Maman !! J'ai signé un CDD !!!* »). Ils m'ont tout simplement appris à m'intéresser à ce qui m'entoure, et mon père m'a appris à réfléchir par moi-même (merci Mimi !). Ça peut paraître dérisoire, dit comme ça, mais que c'est utile dans une vie !! Et maintenant que l'occasion se présente, Maman, vraiment, merci pour ta cuisine et tes gâteaux. C'est un régal pour l'âme. Ceux qui connaissent la maison Louterbach en conviendront j'en suis certaine.

Je remercie aussi ceux qui ont eu confiance en moi très tôt, et qui m'ont permis de réaliser cette thèse en amont. Merci donc à Jean Gérard et à Julien Bailleul, qui ont porté et défendu ce projet de thèse dans les

hautes sphères administratives et décisionnelles (sisi !), que ce soit à Repsol ou à l'Institut Polytechnique Lasalle Beauvais. Moment anecdote : saviez-vous que l'accord mutuel entre Repsol et Lasalle au sujet de la thèse se fit en haut d'une montagne des Pyrénées, lors de la rencontre fortuite et non planifiée Jean et Julien lors d'une randonnée? Merci à eux.

Merci aussi à toute l'équipe de Lasalle Beauvais. Que de bons souvenirs !! Mes premières heures de cours en tant qu'enseignante, les moments de détente avec Julien D. et Loïc, les apéros chez Julien B. et Poupou…C'était le bon temps ! Merci aussi à Yannick, Thuan, Sébastien, Stéphane, Pascal, Olivier, Bastien et Michel-Bières. J'ai pourtant beaucoup critiqué Beauvais mais je me sens désormais comme chez moi en Picardie! Et rien n'aurait été pareil sans PH, évidemment.

Au Pérou, merci à Willy Gil et Mayssa, qui nous ont toujours accueillis et hébergés, à Lima ou à Cuzco.

Du coté Toulousain, je remercie toute l'équipe du laboratoire GET, et en particulier Ludo, à qui les doctorants manquent toujours un peu quand ils partent… Merci à Stéphanie Brichau, qui fut la première à me loger à Toulouse et qui m'a initiée au monde étrange de la thermochronologie et des traces de fissions (merci.. ?). Que de fous rires aussi pendant les missions de terrain ! Merci Steph ! Et puis je dois évidemment remercier Stéphane Brusset, d'abord pour son aide en structurale (c'est peu dire) mais aussi pour son tempérament ours-bourru que j'aime bien. Et puis surtout, merci aux co-bureaux et autres acolytes !! Jean-Louis, Guillaume et Angela tout particulièrement. J'ai aimé partager ces trois années à vos côtés, c'était parfait. Jean-Louis et sa musique des années 80, Guillaume et ses blagues souvent drôles, Angela et ses questionnements intérieurs (souvent drôles eux aussi). Et puis Merci à Manuel Henry (de son nom entier), hétérosexuel de son état, par nature et par choix (c'est dit Manu !!). Quel art ! Quelle manière de manier la pipette et les solvants! Ma vie à Toulouse n'aurait pas été la même sans toi. Merci aussi à Sophie, Caro, Alysson, Masbou, Maria, Vincent, Léandre, Alex, et tous les autres ! Spéciale dédicace à Adrien, avec qui nous avons partagé bien des douleurs et quelques épopées Péruviennes. Et à Alexandra Robert, qui ne peut apporter que du bien au labo. Elle est tellement drôle vous comprenez…

Que serait une vie sans amis ? Pour leur humour (qui va au-delà du trente-sixième degré), leur bonne humeur et leur amitié sincère, je remercie en particulier Alizée, Chonchon, Clémentine, Leslie, copain Canard-Dimitri et évidemment Eugénie Pérouse. Et Angela bien sûr, mais elle a déjà été citée plus haut alors je ne peux pas la mettre dans deux catégories, je suis mal à l'aise avec les doublons !

Ma nouvelle vie commençant tout juste à Madrid, je tiens à remercier tout particulièrement Brice et Narimane pour leur bonne humeur et leur soutient (les pauses thés sont nécessaires à l'équilibre de l'employé), sans oublier Roger, Cédric et Amandine, Alexandre, Thomas et tous les autres.

Enfin, parce qu'il le faut bien n'est-ce pas ? Je remercie mes directeurs de thèse. Eh oui, malgré les quelques mésententes par-ci par-là, il faut bien avouer que c'est grâce à eux que j'ai pu réaliser cette thèse. C'est avec eux que j'ai découvert le Pérou, l'Amazonie, le terrain en bateau. A chacun d'eux je dois quelque chose de différent, mais merci à eux trois. Merci à Patrice pour son soutient, son hospitalité, ses histoires mystiques qui font parfois peur (« *Vraiment, tu as été capturé par des indiens à moitié nus avec des arcs et des*

flèches ??! ») et ses corrections tardives (il fallait que je le dise, c'est sorti tout seul !). Merci à Julien pour sa patience, sa gentillesse, sa rigueur scientifique et tout ce qu'il m'a appris pendant ces trois (quatre) années. Je n'oublierai pas la découverte du Machu Pichu avec toi !

Et puis ne la cachons pas, je suis parfois exaspérante et obstinée, ça n'a pas dû être facile tous les jours de me gérer…La palme revient donc à Martin, que j'ai souvent rendu chèvre, il est vrai. Que j'ai appelé presque tous les deux jours, même une fois installée à Madrid, afin d'avoir des précisions sur telle ou telle chose. J'ai même été jusqu'à l'appeler pour lui demander « *Mais Martiiiiiin Pourquoi tu as encore fait des corrections sur cette partie ??! Tu ne vas donc jamais t'arrêter ?!* ». Bon, c'est difficile les corrections…Je demande pardon (ça sert aussi à ça les remerciements). Mais tu as toujours été là pour moi, et tu m'as soutenue au jour le jour, alors merci. Je n'aurais pas dû gratter tes piqures de moustique sur le terrain, c'est l'unique chose dont je me sente coupable.

Pour finir cette longue liste, je tiens à remercier mes deux rapporteurs Michel Lopez et Jaume Vergés pour leurs remarques constructives et le temps passé (cet été !) à lire cette thèse. Merci aussi à Olivier Vanderaghe de faire partie de mon jury de thèse ainsi qu'à Elton Dantas pour sa bonne humeur sur le terrain et pour s'être déplacé de si loin pour être examinateur lors de la soutenance.

Et puis parce que je fais ce que je veux dans les remerciements, et que je n'écrirai jamais de roman, j'en profite pour dédier ma thèse à mon frère Thomas et sa femme Lucita (malgré le fait que je trouve ça un peu mégalo, tout de même).

MERCI

SOMMAIRE

C. Evidences for a late Paleocene marine incursion in Southern Amazonia (Madre de Dios Sub-Andean Zone, Peru) (p. 152)

D. Facies analysis and sedimentary evolution of the Neogene southern Amazonian foreland basin (p. 188)

Introduction

1. Généralités

La Cordillère des Andes est la plus longue chaîne de montagne actuelle, s'étendant sur plus de 8000 km le long de la bordure occidentale du continent sud-américain, depuis le Vénézuela au nord, jusqu'à la Terre de Feu au Sud. Elle constitue un exemple classique de chaîne de montagne non-collisionnelle, formée le long d'une marge active par la subduction de plusieurs plaques océaniques (Nazca, Antarctique) sous la plaque Amérique du Sud (Dewey and Bird, 1970; James, 1971; Kay et al., 2005).

Les Andes Centrales (~3º-33º latitudes S) (Figure 1-A) se caractérisent par la présence dans leur domaine interne du plateau Andin. Le plateau Andin, qui comprend l'Altiplano et le plateau de Puna, se définit par des altitudes dépassant 3000 m (Isacks, 1988), une longueur de plus de 1800 km (12°-27° latitudes S) et une largeur variant entre 350 et 500 km. Ces caractéristiques font du plateau Andin le second plus grand plateau sur Terre derrière le plateau Tibétain et un exemple type de haut plateau formé en contexte de subduction. La surrection de ces plateaux, en influençant le flux de sédiments exporté vers les océans et la chimie des océans, est supposée avoir contrôlé le refroidissement climatique planétaire au cours du Cénozoïque (Richter et al., 1992; Ruddiman et al., 1997).

De par leur extension Nord-Sud, les Andes constituent la seule barrière aux flux atmosphériques dans l'hémisphère Sud. Il en résulte des climats contrastés de part et d'autres de la chaîne. Les Andes sont donc considérées comme un lieu privilégié pour étudier les couplages entre les processus tectoniques et climatiques. Au Nord du 17° parallèle Sud, le contraste climatique est particulièrement marqué avec un versant amazonien (Cordillère Orientale et zone Subandine) soumis à de fortes précipitations et un versant pacifique (Cordillère Occidentale et Cordillère Côtière) où domine l'hyperaridité. L'absence de corrélation temporelle entre augmentation des taux d'érosions et timing de la déformation du prisme orogénique oriental andin (Cordillère Orientale et zone Subandine) est utilisé par certains auteurs comme argument majeur afin de montrer un contrôle climatique sur l'érosion et la surrection de la chaîne andine (p.e. Uba et al., 2007 ; Lease et Elhers, 2013). Cependant, avant de discuter les éventuels couplages entre tectonique et climat, il apparaît primordial de déterminer le style et la chronologie de la déformation dans le prisme orogénique oriental andin.

Les bassins du versant oriental des Andes Centrales sont considérés comme des exemples type de bassins d'avant-pays rétroarc (Horton and DeCelles, 1997; Jordan, 1995) et comme des équivalents modernes des bassins d'avant-pays retro-arc nord-américains. Le début de la formation de ces bassins d'avant-pays retro-arc, leur évolution au cours du Cénozoïque ainsi que les contrôles qui s'exercent sur leur remplissage restent débattus. Bien qu'une subduction océanique soit active depuis le début du Jurassique (Mamani et al., 2010), le début du raccourcissement crustal dans la plaque supérieur et donc la formation des bassins d'avant-pays retro-arc reste controversée pour les Andes centrales.

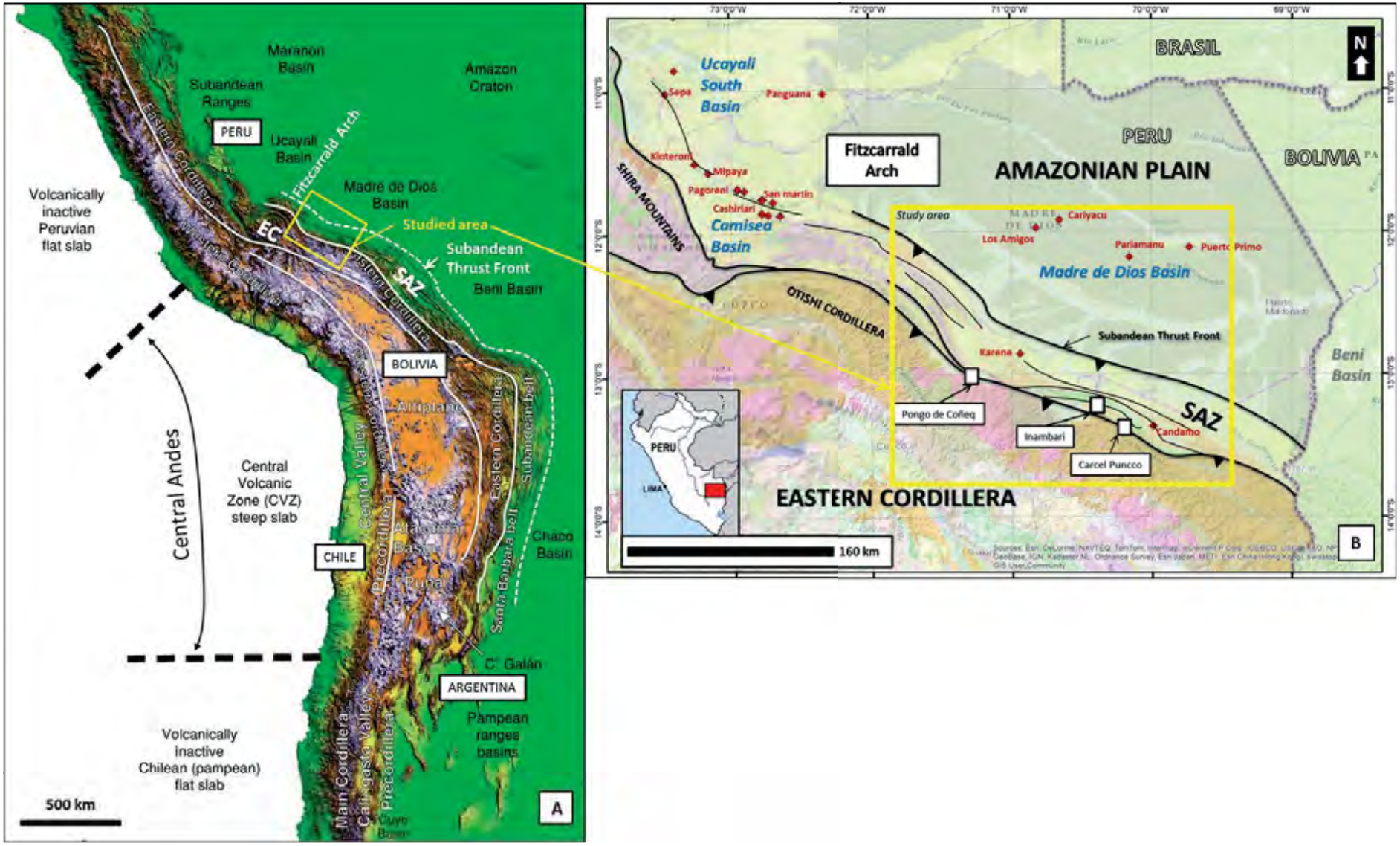

Figure 1 : A) Carte (DEM) de la partie centrale du continent sud-Américain montrant les principales caractéristiques géomorphologiques des Andes Centrales de Bolivie, du Pérou, du nord du Chili et de l'Argentine. La zone d'étude de la thèse est située par un rectangle jaune. B) Carte structural simplifiée du sud du Pérou montrant un agrandissement de la zone d'étude. EC= Eastern Cordillera (Cordillère Orientale); SAZ= Subandean Zone).

Certains auteurs suggèrent que les bassins d'avant-pays retro-arc commencent à se former au Crétacé Supérieur ou au Paléocène alors que d'autres proposent un début de formation au Néogène (Voir Roddaz et al., 2010 pour une synthèse). Des études récentes de modélisation ont suggéré que contrairement aux pro-bassins d'avant-pays (bassin se développant sur la lithosphère subductante), les retro-bassins d'avant-pays présentent un enregistrement sédimentaire plus complet de la phase de croissance de l'orogène (Sinclair et Naylor, 2012).

Enfin, outre l'intérêt académique, la zone Subandine des Andes Centrales possède un fort potentiel de réserves en hydrocarbures puisque les deux plus grands gisements de gaz d'Amérique latine s'y trouvent (San Alberto en Bolivie et Camisea au Pérou.) De plus, La zone Subandine a fait l'objet de découvertes récentes, notamment les champs de Kinteroni-1X dans le bassin d'Ucayali au Pérou (4ème découverte mondiale en 2008) et celui de Huacaya dans la zone Subandine du Chaco en Bolivie (5ème découverte mondiale en 2008).

2. Problématique et choix de la zone d'étude

L'histoire de la déformation des Andes Centrales, en particulier celle de la Cordillère Orientale et de la zone Subandine, ainsi que l'histoire paléogéographique et paléo-environnementale des bassins d'avant-pays amazoniens associés à la chaîne Andine au cours du Méso-Cénozoïque sont toujours au cœur d'intenses débats scientifiques. En termes d'exploration pétrolière, l'épaisseur des structures faillées et plissées ainsi que l'épaisseur du remplissage sédimentaire du bassin d'avant-pays ont un rôle très important sur la profondeur d'enfouissement du système pétrolier local, et donc sur la maturité organique et la génération d'hydrocarbures. Les failles au sens large étant étroitement liées aux chemins de migration des hydrocarbures et aux pièges structuraux, il apparaît tout aussi crucial de préciser la géométrie et la chronologie de déformation ainsi que l'histoire thermique de la zone Subandine, intensément déformée (Barnes et al., 2006b; Echavarria et al., 2003). Enfin, la chronologie précise de la déformation de la zone Subandine est de première importance pour déterminer la croissance du Plateau Andin au cours du Néogène supérieur (Espurt et al., 2011). Dans ces optiques, le prisme oriental orogénique du sud Pérou reste relativement peu étudié par rapport à ses équivalents boliviens (Barnes et al., 2006a) ; (McQuarrie et al., 2008b) et ceux du centre du Pérou (Espurt et al., 2008, 2011 ; Gautheron et al. 2013)

➔ *Le premier objectif de la thèse est donc de déterminer la géométrie précise et l'histoire de la déformation de la Cordillère Orientale et de la zone Subandine dans la zone d'étude (Sud du Pérou).*

Une des thématiques les plus controversées en géologie andine concerne le début de la formation du d'avant-pays Amazonien: quand le bassin retroarc se forme-t'il ? L'évolution paléo-environnementale du bassin Amazonien d'avant pays Sud-Péruvien au cours du Cénozoïque reste tout aussi peu contrainte. La forêt tropicale Amazonienne, caractérisée par le plus riche écosystème du monde, influe quant à elle sur le climat, le cycle du carbone ainsi que sur la biodiversité. Cependant, l'origine, la chronologie et les causes de cette biodiversité sont mal connues. Une synthèse récente de Hoorn et al. (2010) souligne les liens complexes existant dans le bassin Amazonien entre la création des Andes, la variabilité climatique et le développement

de la biodiversité au cours du Cénozoïque. La présence de mers intérieures s'avère tout particulièrement importante, pas seulement car celles-ci encouragent l'isolation bio-géographique et la spéciation allo-patrique mais aussi car elles contrôlent les taux de précipitation dans le bassin Amazonien (Jeffery et al., 2012) et donc les taux d'érosion et les flux sédimentaires. Déterminer le nombre, l'âge et la durée des incursions marines enregistrées dans le bassin Amazonien apparaît donc primordial.

➔ *En conséquence, le second objectif de la thèse est de déterminer l'évolution stratigraphique et paléogéographique du bassin d'avant-pays de Madre de Dios au cours du Méso-Cénozoïque. Un nouveau cadre spatio-temporel sera établi, et les diverses contraintes influant sur le remplissage sédimentaire du bassin (contraintes tectonique, climatique et eustatique principalement) seront discutées.*

3. Méthodologie

3.1. Analyse structurale

Deux principales coupes sont étudiées: celle de Pongo de Coñeq située au Nord-Ouest de la zone d'étude et celle d'Inambari située au Sud-Est (Figure 1-B). Les deux coupes traversent la bordure Est de la Cordillère Orientale, la zone Subandine dans son ensemble et une partie de la plaine de Madre de Dios. Une coupe équilibrée (Inambari) a été réalisée avec le logiciel 2D Move, et est principalement basée sur la sismique 2D disponible (données industrielles) et les données de terrain obtenues et analysées pendant la thèse (pendages et résultats biostratigraphiques). L'interprétation et les corrélations sismiques depuis le Nord-Ouest jusqu'au Sud-Ouest de la zone d'étude ont aussi été réalisées sur le logiciel Move ainsi que sur le logiciel OpenDtect. L'histoire de l'exhumation de la Cordillère Orientale et de la zone Subandine est basée sur l'interprétation des résultats de thermochronologie basse température (Traces de fission (AFTA) et (U-Th)/He sur apatites), réalisée sur chacune des unités tectoniques d'intérêt. L'histoire de la déformation est de plus complétée par l'interprétation des lignes sismiques 2D et des strates de croissances visibles sur la sismique comme sur le terrain. En combinant les données, deux premières restaurations séquentielles simplifiées de la zone d'étude sont finalement proposées.

3.2. Analyse de bassin

Afin de lier l'histoire de la déformation du prisme orogénique Andin (Cordillère Orientale et zone Subandine) à la réponse sédimentaire enregistrée dans le bassin d'avant-pays adjacent de Madre de Dios, nous proposons l'étude des deux principales coupes stratigraphiques de la zone d'étude (coupe de Pongo de Coñeq et coupe d'Inambari). Ces deux coupes sont contraintes par de nouvelles datations biostratigraphiques (palynologie, micro-paléontologie et paléontologie) et par quelques datations radiométriques (Ar/Ar). Les corrélations stratigraphiques réalisées entre les deux coupes sont majoritairement basées sur l'interprétation sismique 2D et les contraintes temporelles obtenues. Afin de proposer une reconstruction des paléo-environnements de dépôt au cours du Cénozoïque, des analyses de faciès ont été réalisées. Chacun des facies sédimentaires a été défini à partir de sa lithologie, de ses

structures sédimentaires et biogéniques, de son contenu palynologique et paléontologique et enfin sur les géométries sédimentaires observées. Sur la base de ces interprétations et en accord avec l'organisation dans l'espace de ces facies, plusieurs associations de faciès ont ensuite été définies, pour les environnements côtiers comme pour les environnements continentaux. Afin de déterminer la nature de la matière organique (marine versus *continentale), des analyses géochimiques de type « TOC » (Total Organic Carbon) et des mesures d'isotopes stables du Carbone (δ13CTOC) ont été réalisées. Des analyses supplémentaires (DRX, concentrations en éléments majeurs et traces et compositions isotopiques en Nd-Sr) sont proposées et permettent d'établir et d'interpréter l'évolution des sources au cours du remplissage du bassin. Grâce à cette méthode, les sédiments dérivés des reliefs andins (depuis l'Ouest) peuvent être différenciés des sédiments dérivés du craton brésilien (depuis l'Est). Pour contraindre l'histoire de la subsidence et l'évolution du flux sédimentaire dans le bassin d'avant-pays de Madre de Dios, les histoires d'enfouissement et les taux de sédimentation ont été calculés à l'aide du logiciel de modélisation PetroMod-1D pour les deux coupes stratigraphiques principales.*

4. Organisation générale de la thèse

La premier chapitre de la thèse (ou "Part A") est centré sur le cadre structural du prisme orogénique Andin (Cordillère Orientale et zone Subandine) au sud du Pérou. Dans un premier temps, la géométrie de la déformation est présentée pour chacune des deux coupes : coupe structurale, niveaux de décollement et style de déformation. Dans un second temps, la chronologie de la déformation ainsi que la mise en place progressive des structures au cours du Cénozoïque sont étudiées. Nous établissons finalement les principales périodes de déformation de la Cordillère Orientale et de la zone Subandine.

Le chapitre B est un court chapitre exposant les débuts de la formation du bassin d'avant-pays de Madre de Dios. L'étude est localisée dans le Nord de la zone Subandine actuelle, les affleurements décrits étant situés sur la coupe principale de Pongo de Coñeq. L'intervalle stratigraphique étudié correspond au Crétacé supérieur-Paléogène. Le but de ce chapitre est de déterminer l'âge du début du partitionnement classique des dépôts sédimentaires selon les « depozones » telles que décrites par DeCelles and Giles (1996) en Bolivie.

Le chapitre C de la thèse correspond à un article soumis et accepté à la revue scientifique « Palaeogeography, Palaeoclimatology and Palaeoecology » en mai 2014. Cet article présente les preuves sédimentaires, géochimiques, isotopiques et biostratigraphiques d'une incursion marine ayant atteint le bassin de Madre de Dios au cours du Paléocène supérieur. Cette incursion n'a été documentée qu'au Nord de la zone d'étude (coupe principale Pongo de Coñeq) et n'avait jamais été décrite auparavant.

Le chapitre D est quant à lui dédié au remplissage stratigraphique Néogène du bassin d'avant-pays de Madre de Dios, et se base sur deux coupes stratigraphiques réalisées selon les deux coupes principales de la zone d'étude : la coupe de Pongo de Coñeq et celle d'Inambari. Les facies sédimentaires, les contraintes biostratigraphiques et radiométriques ainsi que les résultats de provenance sédimentaires sont présentés, interprétés puis intégrés dans le but de discuter de l'évolution du bassin de Madre de Dios au cours du

Cénozoïque. Trois incursions marines sont notamment documentées pour cet intervalle stratigraphique. La discussion de cette partie tente d'évaluer l'influence et l'importance de chacun des contrôles tectonique, climatique et eustatique sur le remplissage sédimentaire du bassin, et en particulier sur les incursions marines documentées.

Les Annexes contiennent :

- *Les cartes principales de la thèse : cartes structurales (Cartes 1 et 2), localisation des affleurements (Carte 3), des résultats biostratigraphiques (Cartes 4 à 7), des résultats de provenance sédimentaire (Carte 8) et radiométriques (Carte 7).*
- *Les tables Excel relatives aux données géographiques des affleurements (Annexe nº9) et aux résultats biostratigraphiques (Annexes nº2 et 3).*
- *Un rapport de 2004 sur les analyses de thermochronologie effectuées dans la zone d'étude par R. Donnelick (Annexe nº 4).*
- *Les commentaires des reviewers sur l'article soumis et accepté au sujet de l'incursion marine Paléocène (Part C) (Annexe nº5).*
- *Deux papiers publiés (en 2012 et 2013) par l'équipe de paléontologues qui nous a à plusieurs reprises accompagnés sur le terrain (Annexes nº 6 et nº7).*
- *Neuf figures importantes de la thèse (Figures A à I) pouvant être consultées séparément lors de la lecture de la thèse si nécessaire (en grand format pour certaines). Il s'agit principalement des coupes stratigraphiques du Néogène et de la coupe structurale d'Inambari.*

5. References

Barnes, J.B., Ehlers, T.A., McQuarrie, N., O'Sullivan, P.B. and Pelletier, J.D., 2006a. Eocene to recent variations in erosion across the central Andean fold-thrust belt, northern Bolivia: Implications for plateau evolution. Earth and Planetary Science Letters, 248(1-2): 118-133.

Barnes, J.B., Ehlers, T.A., McQuarrie, N., O'Sullivan, P.B. and Pelletier, J.D., 2006b. Eocene to Recent variations in erosion across the Central Andean fold-thrust belt, northern Bolivia; Implications for plateau evolution: Earth and. Planetary Science Letters, v: 101016/jepsl200605018-101016/jepsl200605018.

DeCelles, P.G. and Giles, K.a., 1996. Foreland basin systems. Basin Research, 8(2): 105-123.

Dewey, J.F. and Bird, J.M., 1970. Mountain belts and the new global tectonics. Journal of Geophysical Research, 75(14): 2625-2647.

Echavarria, L., Hernandez, R., Allmendinger, R. and Reynolds, J., 2003. Subandean thrust and fold belt of northwestern Argentina; geometry and timing of the Andean evolution. AAPG Bull., 87: 965-985.

Espurt, N., Barbarand, J., Roddaz, M., Brusset, S., Baby, P., Saillard, M. and Hermoza, W., 2011. A scenario for late Neogene Andean shortening transfer in the Camisea Subandean zone (Peru, 12 S): Implications for growth of the northern Andean Plateau. Geological Society of America Bulletin, 123(9-10): 2050-2068.

Hoorn, C., Wesselingh, F.P., ter Steege, H., Mauricio, Mora, A., Sevink, J., Sanmartin, I., Sanchez-Meseguer, a., Anderson, C.L., Figueiredo, J.P., Jaramillo, C., Riff, D., Negri, F.R., Hooghiemstra, H., Lundberg, J.G., Stadler, T., Sarkinen, T. and Antonelli, A., 2010. Amazonia Through Time: Andean Uplift, Climate Change, Landscape Evolution, and Biodiversity. Science, 330(6006): 927-931.

Horton, B.K. and DeCelles, P.G., 1997. The modern foreland basin system adjacent to the Central Andes. Geology, 25(10): 895-895.

Isacks, B.L., 1988. Uplift of the Central Andean Plateau and Bending of the Bolivian Orocline. J. Geophys. Res., 93: 3211–3231.

James, D.E., 1971. Plate tectonic model for the evolution of the Central Andes. Geological Society of America Bulletin, 82(12): 3325-3346.

Jeffery, M.L., Poulsen, C.J. and Ehlers, T.A., 2012. Impacts of Cenozoic global cooling, surface uplift, and an inland seaway on South American paleoclimate and precipitation δ18O. Geological Society of America Bulletin, 124(3-4): 335-351.

Jordan, T.E., 1995. Retroarc foreland and related basins. In: C.J. Busby and R.V. Ingersoll (Editors), Tectonics of Sedimentary Basins. Blackwell Science, Oxford, pp. 331-362.

Kay, S.M., Mpodozis, C. and Ramos, V.A., 2005. Andes, pp. 118-131.

Mamani, M., Worner, G. and Sempere, T., 2010. Geochemical variations in igneous rocks of the Central Andean orocline (13° S to 18° S): tracing crustal thickening and magma generation through time and space. Geological Society of America Bulletin, 122: 162-182.

McQuarrie, N., Barnes, J.B. and Ehlers, T.A., 2008b. Geometric, kinematic, and erosional history of the central Andean Plateau, Bolivia (15–17°S). Tectonics, 27(3): 1-24.

Richter, F.M., Rowley, D.B. and DePaolo, D.J., 1992. Sr isotope evolution of seawater: the role of tectonics. Earth and Planetary Science Letters, 109(1-2): 11-23.

Ruddiman, W.F., Raymo, M.E., Prell, W.L. and Kutzbach, J.E., 1997. The uplift-climate connection; a synthesis. In: W.F. Ruddiman (Editor), Tectonic Uplift and Climate Change. Plenum Press, New York, pp. 471–515.

A. Geometry, kinematic and erosional history of the Eastern Cordillera and the Sub-Andean foreland thrust system, Madre de Dios basin, Peru.

Introduction au chapitre:

Le bassin de Madre de Dios se situe au sud du Pérou (12º-14ºS), à l'est des Andes Centrales constituées majoritairement de la bordure Est de l'Altiplano, de la Cordillère Orientale et de la zone Subandine dans la zone étudiée. La zone Subandine, où la majorité des travaux de terrains a été réalisée, constitue la zone de transition entre les hauts reliefs de la Cordillère Orientale et le bassin Amazonien situé plus à l'Est. Cette unité tectonique a été structurée par un système de chevauchements d'avant-pays alors que s'y accumulaient simultanément d'importantes épaisseurs de sédiments. La bordure Est de la zone Subandine correspond au front de déformation andine, qui sépare donc la zone interne et déformée du bassin d'avant-pays du foredeep amazonien à l'Est.

Les principales problématiques scientifiques liées à l'orogénèse Andine concernent les processus de création de reliefs, la géométrie de la déformation et la chronologie générale de mise en place de ces structures andines. À ces problématiques s'ajoute une composante économique, aux vues des importants gisements et prospects pétroliers découverts dans les zones Subandines jouxtant la Cordillère Andine depuis le Venezuela jusqu'en Bolivie.

Ce chapitre présente dans un premier temps les différentes caractéristiques géo-morpho-structurales ainsi que la stratigraphie générale de la Cordillère Orientale, de la zone Subandine et du reste bassin de Madre de Dios. Deux principaux transects ont été choisis : l'un au Nord-Ouest de la zone d'étude (Pongo de Coñeq) et l'autre au Sud-Est (Inambari). Afin de répondre aux problématiques scientifiques exposées, le chapitre est organisé en deux parties qui présentent respectivement:

1) *la géométrie de la déformation dans la zone Subandine, présentant pour chacun des transects une coupe géologique et structurale précise ainsi que les principaux niveaux de décollement impliqués dans cette déformation ;*
2) *la chronologie de la déformation dans la Cordillère Orientale comme dans la zone Subandine, basée pour chaque transect sur l'étude des déformations syn-sédimentaires ainsi que sur les résultats thermochronologiques (traces de fission sur apatites et (U-Th)/He sur apatites).*

Finalement, un des principaux buts de la thèse étant de déterminer la chronologie de la déformation dans la Cordillère Orientale et la zone Subandine, deux périodes de déformations sont proposées et permettent l'esquisse d'une « restauration séquentielle » de base pour chacun des transects.

Ce chapitre fera l'objet d'une publication (journal encore à déterminer). Il a été étendu (particulièrement la partie « stratigraphie ») en vue d'une meilleure lisibilité et d'une introduction générale à la thèse dans son ensemble. La version proposée pour l'article sera synthétisée.

Résumé:

La chronologie de la déformation des Andes Centrales, particulièrement celle de la Cordillère Orientale et de la Zone Subandine, tout comme l'évolution Cénozoïque des paléo-environnements de dépôts dans le bassin d'avant-pays amazonien au cours du temps sont encore controversées et débattues de nos jours.

Dans les Andes Centrales, la Cordillère Orientale a été déformée depuis environ 40 Ma (Oncken et al. (2006). Des taux de déformations ont été mesurés sur les bordures Est et Ouest de la Cordillère Orientale entre 30 et 17 Ma, et il est généralement admis que la déformation cesse entre 12 et 8 Ma (Gubbels et al., 1993; Kennan et al., 1995). Si certains auteurs considèrent que le début de la déformation dans la zone Subandine des Andes Centrales est Pliocène (Echavarria et al., 2003b; Mora et al., 2010; Oncken et al., 2006), la plupart des études récentes réalisées en Bolivie et au Pérou suggèrent plutôt que la zone Subandine subit d'importants taux de subsidence et de sédimentation pendant l'Oligocène et le Miocène inférieur, avant le raccourcissement résultant du développement du système de chevauchements dans cette zone (DeCelles and Horton, 2003; Espurt et al., 2011; Hermoza, 2004; Roddaz et al., 2010).

Dans la zone d'étude, au sud du Pérou (12-14ºS), une publication récente (Lease and Ehlers, 2013) se base sur des résultats de thermochronologie (U-Th)/He pour suggérer que le changement climatique brutal du Pliocène a certainement induit et par la suite régulé l'incision de la bordure Est de l'Altiplano pendant le Pliocène supérieur. Cependant, cette interprétation est contradictoire à nos résultats. En effet, notre étude montre que les résultats de thermochronologie (Traces de Fission sur Apatites et (U-Th)/He)) réalisée sur des échantillons provenant de la Cordillère Orientale comme de la zone Subandine, ainsi que les strates de croissance documentées sur le terrain et en profondeur (sismique 2D) dans le synclinal de Salvación et de Punquiri attestent d'au moins deux périodes de déformation : i) depuis la fin de l'Oligocène jusqu'au Miocène Moyen (~25-14 Ma, Période 1), et ii) pendant le Miocène supérieur jusqu'au Pléistocène (10-2.8, Période 2) au moins. La deuxième période peut probablement être étendue à l'époque actuelle puisque la zone Subandine présente encore de nos jours des indices de déformation active. Des différences mineures existent entre les deux transects en termes de géométrie de la déformation, ce qui implique par exemple une préservation différente des strates de croissance de la première période au Sud de la zone d'étude (Inambari).

Nos résultats ont des implications directes pour deux des plus importants problèmes fondamentaux en géologie Andine, à savoir : i) l'importance du contrôle climatique Pliocène sur l'érosion et ii) les mécanismes responsables de la croissance et du soulèvement de l'Altiplano. Concernant le premier point, nos résultats thermochronologiques suggèrent que le refroidissement induit par l'érosion de la Cordillère Orientale au sud du Pérou n'est pas contrôlé par un changement climatique mais plutôt par le développement d'un empilement d'écailles ou de duplex au front de la cordillère. Cette interprétation est en accord avec la présence de nombreuses strates de croissances identifiées dans les synclinaux transportés des deux transects et attribuées à la deuxième période de déformation. Concernant les mécanismes responsables de la formation de l'Altiplano, nos résultats thermochronologiques relatifs à la partie la plus interne des structures préservées du bassin de Madre de Dios ainsi que les restaurations structurales et les premiers essais de restauration séquentielle indiquent que le transfert du raccourcissement Andin depuis l'Altiplano vers la zone Subandine date de ~25 Ma. Nos résultats indiquent finalement que le soulèvement de l'Altiplano est un processus lent, résultant de la combinaison possible des processus d'épaississement crustal et de fluage de croûte inférieure.

Summary:

1. Introduction

The timing of deformation in the Central Andes, particularly in the Eastern Cordillera (EC) and the Sub-Andean Zone (SAZ), as well as the Cenozoic paleoenvironemental and paleogeographical history of the associated foreland basins, are still matter of intense debate. Nevertheless, in terms of petroleum exploration, the thickness of thrusts stacked structures and foreland basin deposits, and consequently the burial depth, has an important role on organic matter maturity and petroleum generation. Moreover, because faults are also closely related to hydrocarbon migration pathway, it is crucial to precise the geometry, the timing of deformation and the maturation history of the SAZ (Echavarria et al., 2003b). In terms of purely academic issues, research on the kinematic history of the EC and the SAZ provides an opportunity to compare geologic rates of shortening to modern displacements recently recorded by GPS studies (Bevis et al., 2001; Hindle et al., 2005; Horton, 1999; Khazaradze and Klotz, 2003; Lamb, 2000; Liu et al., 2000; Norabuena, 1998). The precise timing of deformation in the SAZ zone is also of first importance to decipher the Late Neogene growth of the Andean Plateau, the second greatest plateau in height and area after the Tibetan plateau (Espurt et al., 2011).

In the southern Central Andes, the EC deformed over a long time span starting 40 Ma ago (see review in Oncken et al. (2006)). Maximum shortening rates were measured at the western and eastern sides of the EC between 30 and 17 Ma, and deformation practically ceased between 12 and 8 Ma (Gubbels et al., 1993; Kennan et al., 1995) (Figure 1). If some authors consider the onset of deformation in the SAZ of the Central Andes to be Late Miocene to Pliocene in age (Echavarria et al., 2003b; Mora et al., 2010; Oncken et al., 2006), most of the recent studies realized in Bolivia and Peru suggest that the SAZ experienced high subsidence and sedimentation rates during Oligocene-Early Miocene times, prior to the shortening resulting from the development of thrust systems (DeCelles and Horton, 2003; Espurt et al., 2011; Hermoza, 2004; Roddaz et al., 2010). Espurt et al. (2011) calculated that the Andean shortening transfer into the southern Peruvian SAZ (12°S) initially started at c. 14 Ma. In northern Bolivia (15-22°S), temperature-time modelling of Apatite Fission Track (AFT) cooling ages suggests that shortening occurred between c. 25 and c. 8 Ma (McQuarrie et al., 2008b).

In the southernmost part of Peru, very few data exist, but a recent publication (Lease and Ehlers, 2013) used (U-Th)/He thermochronology to document a transition from Miocene faulting to Pliocene canyon incision across the north-eastern plateau margin of southern Peru and Bolivia. Authors conclude that Sea Surface Temperature (SST) – driven precipitation changes (related to a shift in Pliocene global Climate) could have provoked and regulated late Pliocene incision into the eastern Andean Plateau. However, this interpretation is based on the presumed lack of correlation between regional incision and deformational events, and appears to be contradictory to our observations.

In this chapter we will focus on the EC and the SAZ of southern Peru (Central Andes), between 12º and 14º south latitudes (Figure 2). The studied area comprises the Madre de Dios foreland thrust-system. The study aims to describe the structural architecture, the kinematics and the mechanism of the deformation from

new surface, subsurface and thermochronological data. Two main structural cross-sections (one of them balanced) are presented to analyse, geometrically and quantitatively, the SAZ deformation. These two new sections will update and correct the existing sections realized by W. Gil (2001) and W. Hermoza (2004) in the same area. We will particularly resolve issues related to the décollement levels and to the stratigraphic content of the duplex and the imbricate thrust system structures present in the SAZ. Field observations and interpretations of 2D seismic sections (Figure 3, Annex-Map nº2) are used to precise the deformation stages the SAZ suffered since the Cretaceous times. Seismic sections interpretations are mostly based on seismic data in time. Thermochronological data (AFT and (U-Th)/He ages) are also used to constrain the exhumation and uplift history of both the EC and the SAZ (Figure 4). A tentative sequential restoration of a synthetic section is finally proposed based on these observations.

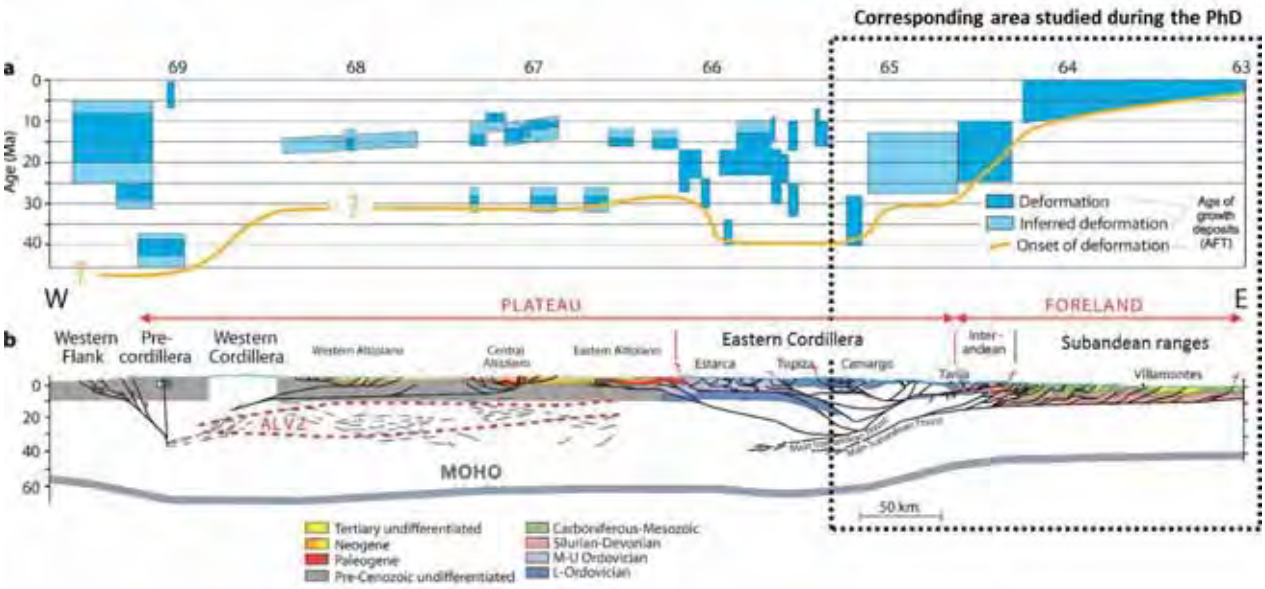

Figure 1: Distribution of deformation ages across the Southern Central Andes (21° S) based on published data from Oncken et al., (2006). A) Compilation of deformation ages: Western Flank (Victor et al., 2004), Precordillera (Haschke and Günther, 2003), Altiplano (Elger et al., 2005; Silva González, 2004), Eastern Cordillera (Gubbels et al., 1993; Müller et al., 2002), Interandean (Kley, 1996), and Sub-Andean (Kley, 1996). B) Balanced cross section at 21° S compiled from Victor et al. (2004) for the western flank of the Altiplano, Elger et al. (2005) for the Altiplano, and Müller et al. (2002) for the Eastern Cordillera and Sub-Andean zone. Moho and Andean Low Velocity Zone (ALVZ) from receiver function data (Yuan et al., 2000; Yuan et al., 2002). Line drawing in the middle crust indicates locations of strong reflectivity in the ANCORP seismic line (cf. ANCORP working group 2003).

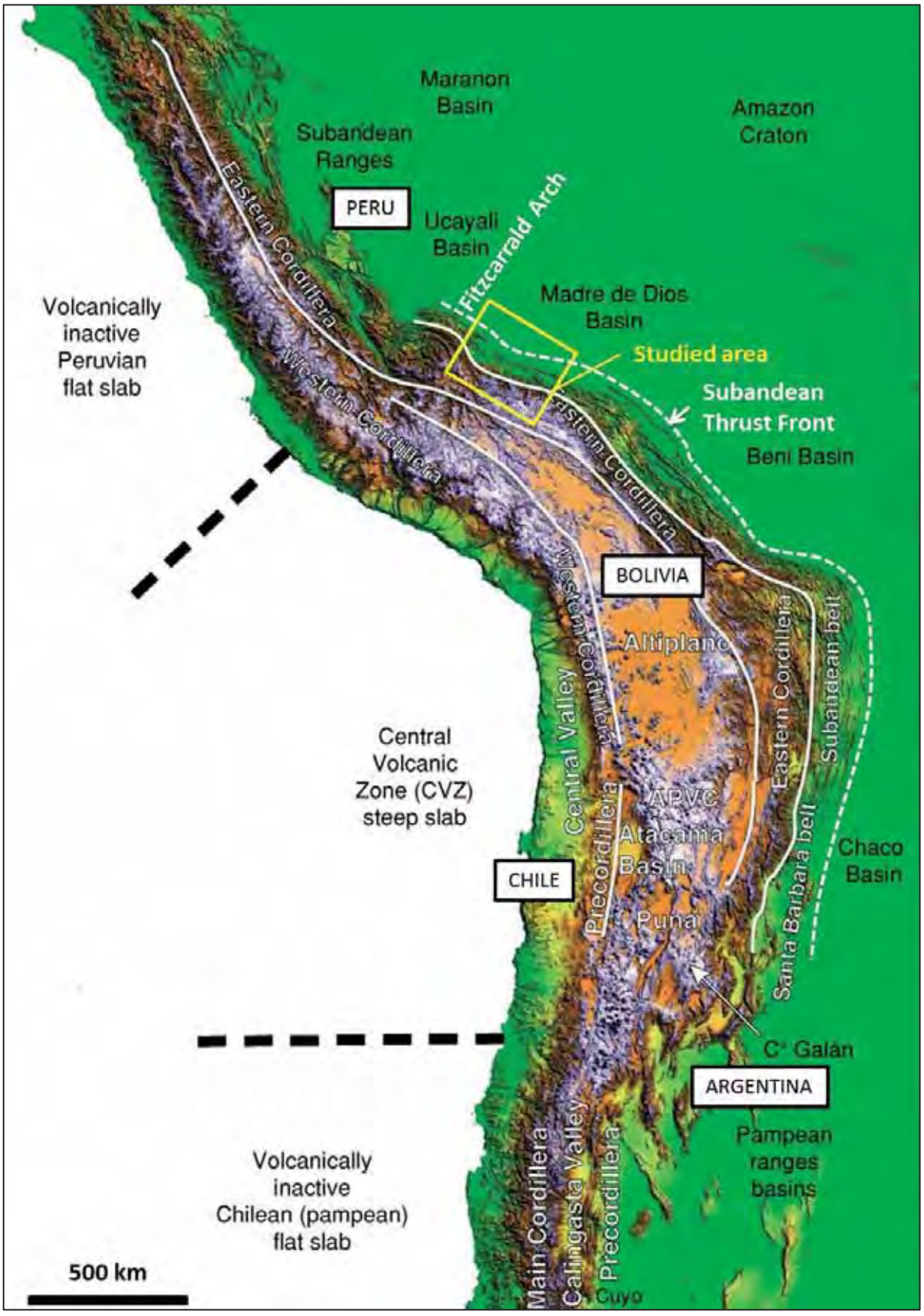

Figure 2: Digital Elevation Map (DEM) showing the principal features of the Central Andes of Peru, Bolivia, northern Chile and northern Argentina. Blue and white colours correspond to the highest elevations. Modified from Kay et al. (2005).

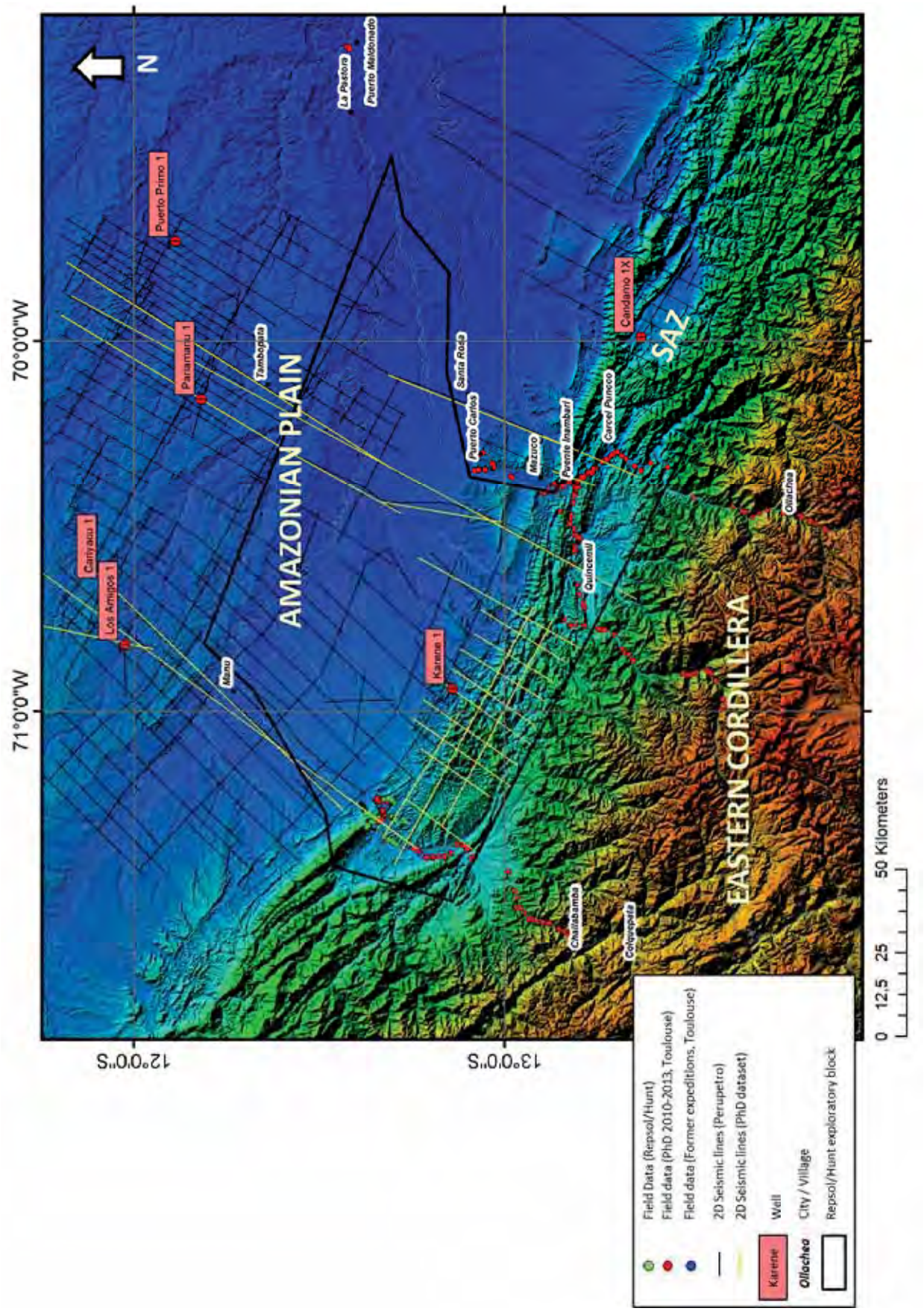

Figure 3: Map of the studied area focused on the Madre de Dios SAZ, with 2D seismic lines dataset, wells and field dataset from the University of Toulouse (red and blue dots) and from the Industry (green dots). Background image: colored Digital Elevation Map (DEM). See yellow rectangle of Figure 2 for geographic situation.

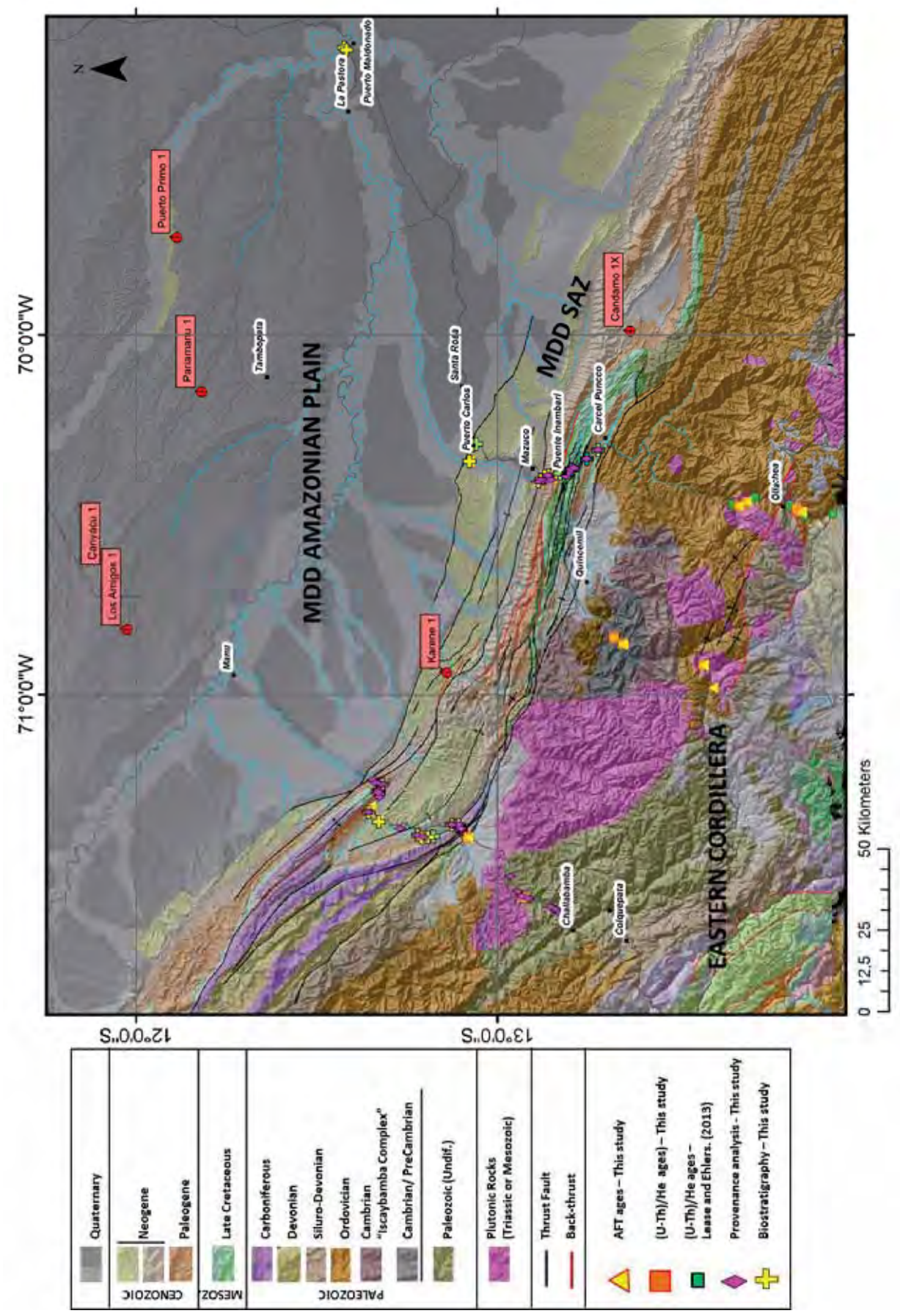

Figure 4: Geological map focused on the Madre de Dios (MDD) area. Main samples used in this study are displayed (sedimentary provenance, biostratigraphy, thermochronology). Geological map modified from INGEMMET Map. Background image: DEM.

2. Geological setting

2.1. Tectonic units

The Madre de Dios basin extends between 12º and 14º South latitudes on the Eastern side of the Peruvian Andes, adjacent to the EC. It belongs to the southern Amazonian foreland basin (Roddaz et al., 2005a), which is located south of the Fitzcarrald Arch (Espurt, 2007). It is limited on the southwest by the Azulmayo thrust, north and northeast by the Brazilian Shield and north and northwest by the Fitzcarrald Arch (Figure 6).

2.1.1. The Eastern Cordillera

Together with the Altiplano, the EC forms the "Central Andean Plateau" (Gubbels et al., 1993), the most distinctive morphological feature of the Central Andes which is underlain by continental crust at least 70 km thick (Beck et al., 1996; Wigger et al., 1994; Zandt et al., 1994).

The Eastern Cordillera of southern Peru is constituted by a deeply eroded pre-Cretaceous fold belt that mainly deformed Paleozoic anchimetarmophic sedimentary rocks locally intruded by Permian and Triassic granitoïds (Figure 4).

The oldest unit is a low-grade metasedimentary sequence for which a Precambrian age was first proposed (Mégard, 1996), before recent geochronological data show that orogenic events in the Peruvian Eastern Cordillera occurred during Lower Paleozoic times (Chew et al., 2007). This unit is unconformably overlain by Lower Paleozoic marine platform deposits which are covered by Late Paleozoic sediments of marine and continental facies. Cretaceous to Tertiary andean sediments rest upon an erosional surface over these former units (from Precambrian to Upper Paleozoic).

2.1.2. The Paleozoic Archs

The Madidi Arch plunges (Figure 5) west below the leading edge of the thrustbelt (House and al., 1999), and represents a basement uplift probably developed during the late Permian Tiahuanacu Orogeny (Jurua orogeny) as it appears eroded and overlain by Cretaceous deposits. South of the Madre de Dios basin, the Madidi Arch is interpreted to act as a buttress for foreland thrust propagation and accounts for complex duplex development in the SAZ (Aleman et al., 2003).

Similar to the Madidi Arch, the late Paleozoic units of the Manu Arch (Figure 5) are completely truncated to Precambrian crystalline rocks (House et al., 1999). However, regional seismic lines show onlap of Paleozoic rocks against a basement high in this area (Aleman et al., 2003). Manu arch is thought to have developed during Late Carboniferous times. According to Sheperd and al. (2002), the Cretaceous Vivian Formation top structural depth map shows this cross-basinal arch as a simple monocline that dips southeast into the Madre de Dios basin.

2.1.3. The Fitzcarralad Arch (synthesis from N. Espurt's PhD, 2007)

The Fitzcarrald Arch (Figure 5) corresponds to the topographic response to the Nazca Ridge subduction recorded in the eastern side of the Peruvian Andes. The Arch induces the North-South partitioning of the Amazonian foreland basin system (Roddaz et al., 2005b) and separates the Peruvian Ucayali-Marañon basins from the southern Peruvian and Bolivian Madre de Dios-Beni basins. In the Fitzcarrald Arch, the Subandean fold and thrust belt consists of two superimposed thrust-wedges. The lower one consists in the reactivation of a Carboniferous thrust-wedge whereas the upper one is deformed by thin-skinned thrust tectonics.

Apatite-fission track analysis (AFT) were used to determine an exhumation stage around 110 Ma linked to the opening of the South Atlantic Ocean. Since ~ 6 Ma, AFT recorded the thrust propagation in the Camisea South sub-basin (SAZ), where apatite thermochronometers have been reset. The underplating of the Nazca ridge had no influence on the short wavelength of the Subandes (Espurt, 2007). However, N. Espurt (2007) suggests that by compensating the flexure of the South American plate, the Fitzcarralad Arch prevents the classical partitioning of the Amazonian foreland basin sensu DeCelles and Gilles (1996) since ~4 Ma.

The Fitzcarrald Arch uplift is thus no older than Pliocene as constrained by the Neogene sediments and geomorphic markers and according to the kinemtatics of the Nazca Ridge subduction.

2.1.4. The Madre de Dios foreland Basin

The Madre de Dios foreland basin can be subdivided into the SAZ and the Madre de Dios plain (foredeep) tectonomorphic units (Figure 5 and Figure 6) (Gil, 2001; Hermoza, 2004). The SAZ is characterized by both sedimentary filling (wedge-top deposits) and active deformation. It is deformed by thin-skin tectonics involving detritic Palaeozoic marine platform, Cretaceous strata and Cenozoic deposits (Gil et al., 2001). The SAZ is limited to the southwest by the Azulmayo thrust that transports the Precambrian to Paleozoic units of the EC towards the NE. The propagation of the deformation towards the Madre de Dios plain is controlled by the development of a deep duplex structure, whose shortening is accommodated in surface by an hinterland imbricate thrust system (=Imbricates Zone, Figure 6) and by the Sub-Andean thrust front. The Sub-Andean thrust front corresponds to the north-eastern border of the SAZ and is responsible for the transportation of a piggy-back basin, which outcrops as large synclines such as the Salvación and the Punquiri synclines (Figure 6). The deformed and still active SAZ only corresponds to the internal (western) part of Madre de Dios foreland basin. The external (eastern) part of the basin is situated northeast to the Sub-Andean thrust front and corresponds to the non-deformed part of the system, the Madre de Dios foredeep (Figure 6).

In order to realize balanced cross-sections and to calculate shortening rates, we chose two sections perpendicular to the NE-SW trend direction of the Sub-Andes structures in the Madre de Dios area: one section through the Pongo de Coñeq Canyon and the Pantiacolla anticline (north-western area, section A displayed in Figure 6) and the other one through the Inambari River (southern area, section B displayed in Figure 6).

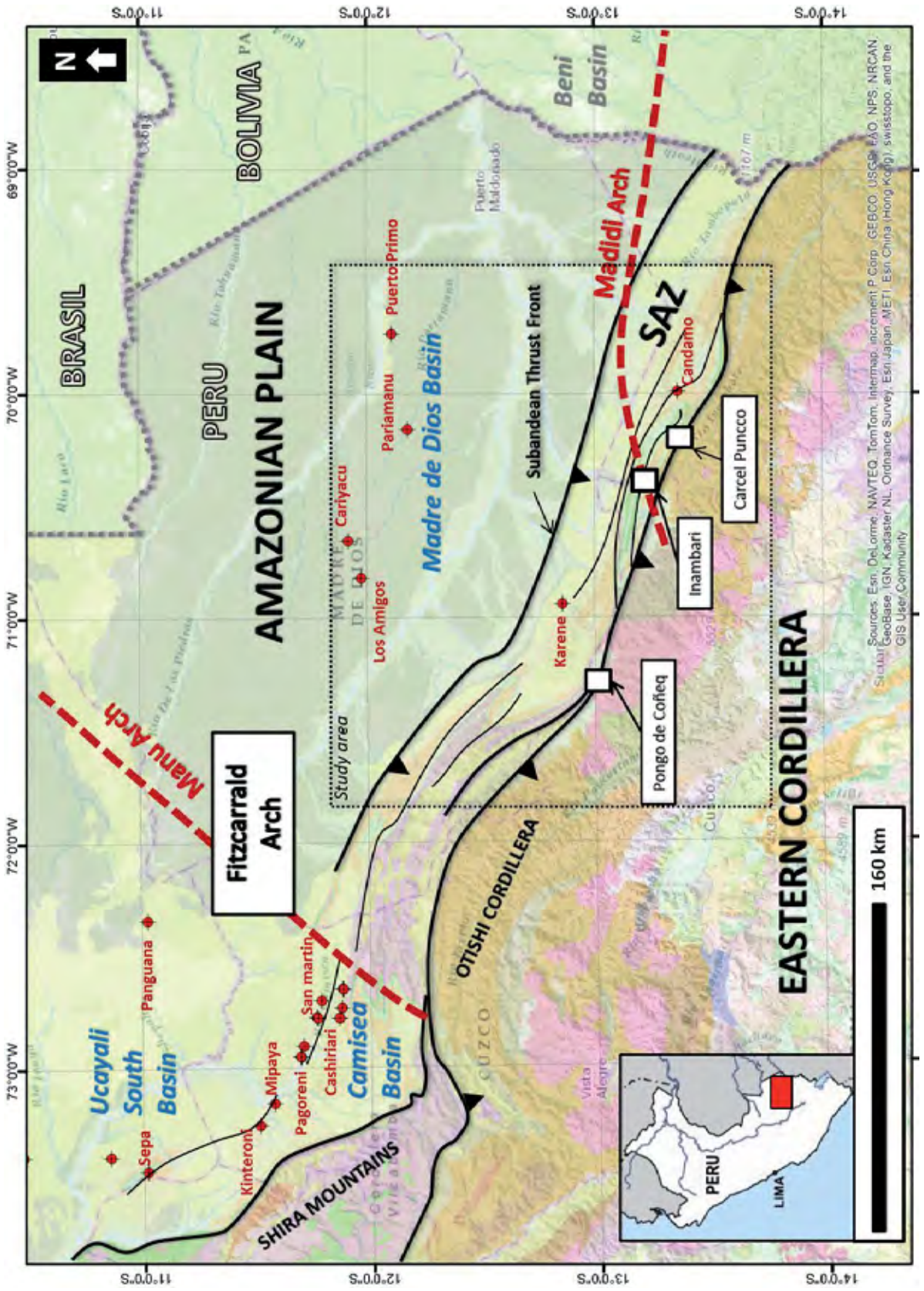

Figure 5: Synthetic structural map of southeast Peru including the Ucayali, the Camisea and the Madre de Dios basins. The main wells of the area are situated in red on the map. Important paleozoic features are displayed with red dashed lines. Recent Fitzcarrald Arch uplift is also situated according to Espurt (2007). The locations of the main three sedimentary sections available in the Madre de Dios SAZ are also indicated. The study area of the PhD (dashed black rectangle) only corresponds to the area located between the Manu Arch (which orientation is not very well constrained) and the Madidi Arch.

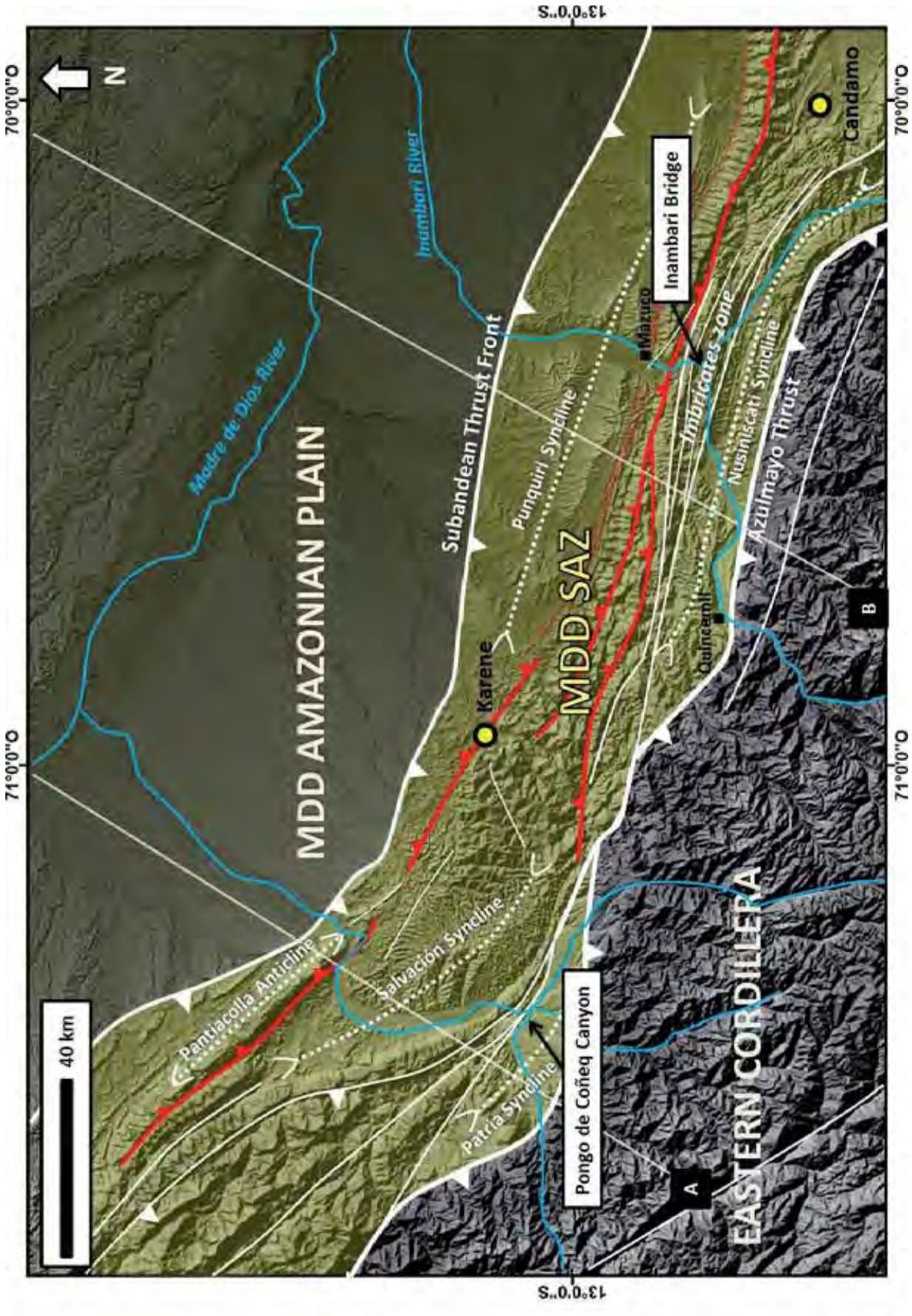

Figure 6: Structural map of the Madre de Dios (MDD) foreland basin, formed by the MDD Subandean Zone (SAZ) coloured in yellow in the map and the MDD plain. NE-verging thrusts are in white, SW-verging back-thrusts are in red. The two principal cross-sections described later in the study are situated in the north-western Pongo de Coñeq area (A) and in the south-eastern Inambari area (B). Karene and Candamo wells are the only two wells situated within the SAZ. The Karene well only shows undifferentiated cenozoic strata whereas the Candamo well shows cretaceous imbricates structures and discovered gas.

2.2. Stratigraphy

The basement is made up of Precambrian to Cambrian metamorphic rocks, Paleozoic metasediments and tardi-Hercynian igneous rocks (Audebaud et al., 1971; Laubacher, 1974; Willner et al., 2010). It outcrops in the Eastern Cordillera adjacent to the Madre de Dios basin where it is overlain by a heterogeneous sedimentary series ranging from Upper Paleozoic to Pleistocene (Dávila and Ponce de León, 1971; Gil et al., 1999; Gutierrez, 1982; Hermoza, 2004; Laubacher, 1974; Newell, 1945; Valdivia, 1974) (Figure 4). Paleozoic rocks outcrop in the EC and in the South-Eastern border of the SAZ. Cretaceous rocks outcrop in the most deformed internal part of the SAZ, whereas Cenozoic series are largely represented in the external part of the SAZ and in the Madre de Dios plain (Figure 4). The sedimentary series may be divided into eight stratigraphic units delimited by regional unconformities (Figure 7 and Figure 8).

2.2.1. Precambrian/ Cambrian

In Peru, the EC is partly formed by pre-Ordovician rocks affected by regional metamorphism, magmatism and pre-paleozoic deformations linked to a Late Precambrian orogenic cycle (600 to 500 Ma) (Audebaud et al., 1971). According to the absence of kyanite in the "andalousite-cordierite" paragenesis described in these Precambrian metamorphic rocks by audebaud et al. (1971), authors proposed a low pressure metamorphic type context. However, recent studies (Tassinari et al., 2011; Willner et al., 2010) proposed higher pressure metamorphic conditions in the Tapo massif, located in the EC of southern Peru. This Late Neoproterozoic metamorphic belt is now buried beneath the present-day Andean belt (Chew et al., 2008).

In the study area, the EC also presents a Cambrian metasedimentary unit: the "Iscaybamba complex" (Dalmayrac et al., 1980; Dalmayrac and Molnar, 1981; Laubacher et al., 1985; Marocco, 1978; Mégard, 1978). Rocks from the Iscaybamba complex have been recognized in the Inambari area during several field expeditions realized between 2010 and 2011. Outcrops are located along the Interoceanic road, between Camanti and Quicemil localities, along the Marcapata River (Figure 9). Metamorphic series of the Iscayabamba complex are made up of gneiss, andesites, anfibolites and quartzites (Figure 10). Metamorphic rocks from outcrops MD 112 and MD 216 have been used in this study for low-temperature thermochronology. The Iscayabamba complex has also been described in wells cores (Pando-1X) collected in the foredeep of the northern Bolivian foreland basin, adjacent to the Peruvian Madre de Dios basin (Isaacson and Diaz Martinez, 1995).

It is important to note that both Precambrian and Cambrian metamorphic rocks are not well-studied in the Eastern Cordillera of Peru, and that dating data are scarce. For this reason, some authors considered the Yscaybamba metamorphic unit outcropping near Quincemil to belong to the Precambrian unit instead of Cambrian (Audebaud et al., 1971; Gil, 2001). In this study we consider the Iscaybamba unit to be Neoproterozoic (Late Precambrian) to Early paleozoic in age, based on a recent study (Chew et al., 2007) that proposes an Early Paleozoic orogenic event in southern Peru.

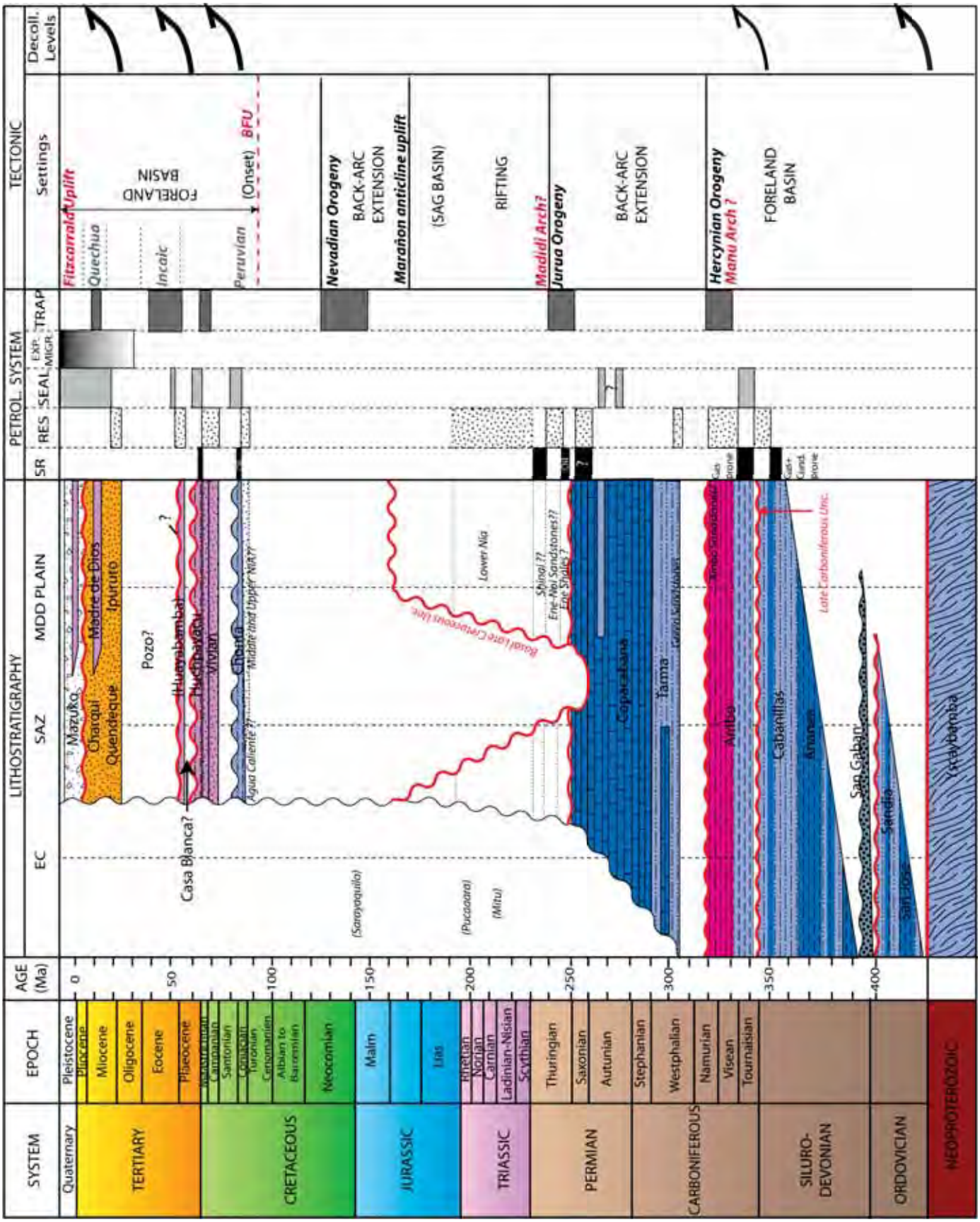

Figure 7: Stratigraphic chart including the eastern EC of southern Peru, the SAZ and the Amazonian plain of the Madre de Dios foreland basin (compilation of data from Gil (2001), Hermoza (2004), confidential industry reports and new data presented in this study).

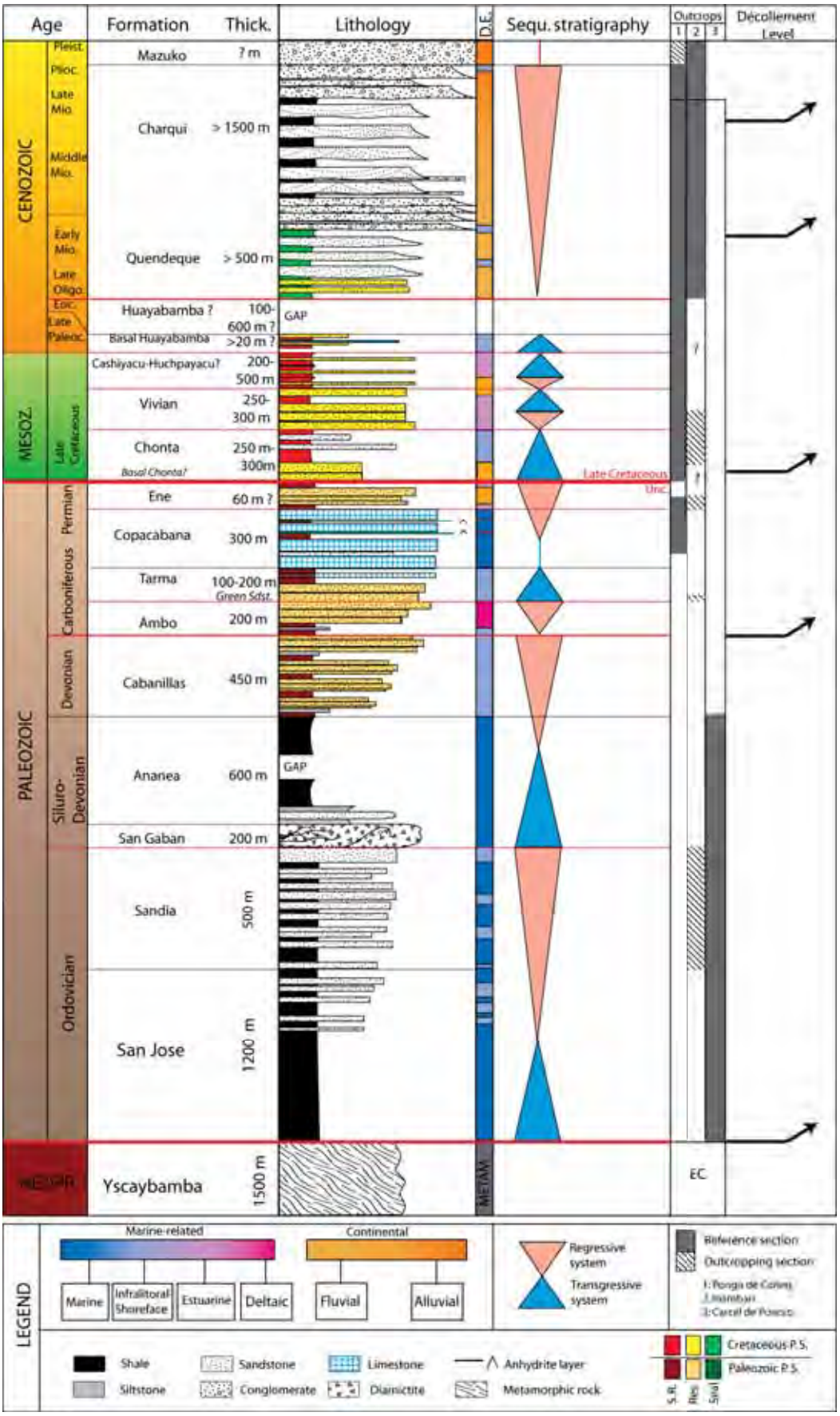

Figure 8: Synthetic sedimentary column for the SAZ of the Madre de Dios foreland basin. Thicknesses, lithologies and depositional environments interpretations are the results of a compilation of data from Hermoza (2004), Gil (1999; 2001), confidential reports and new data (this study). 1=Pongo de Coñeq section; 2= Inambari section; 3=Carcel de Puncco section. EC= Eastern Cordillera; PS= Petroleum System; S.R. = Source Rock; Res.= Reservoir.

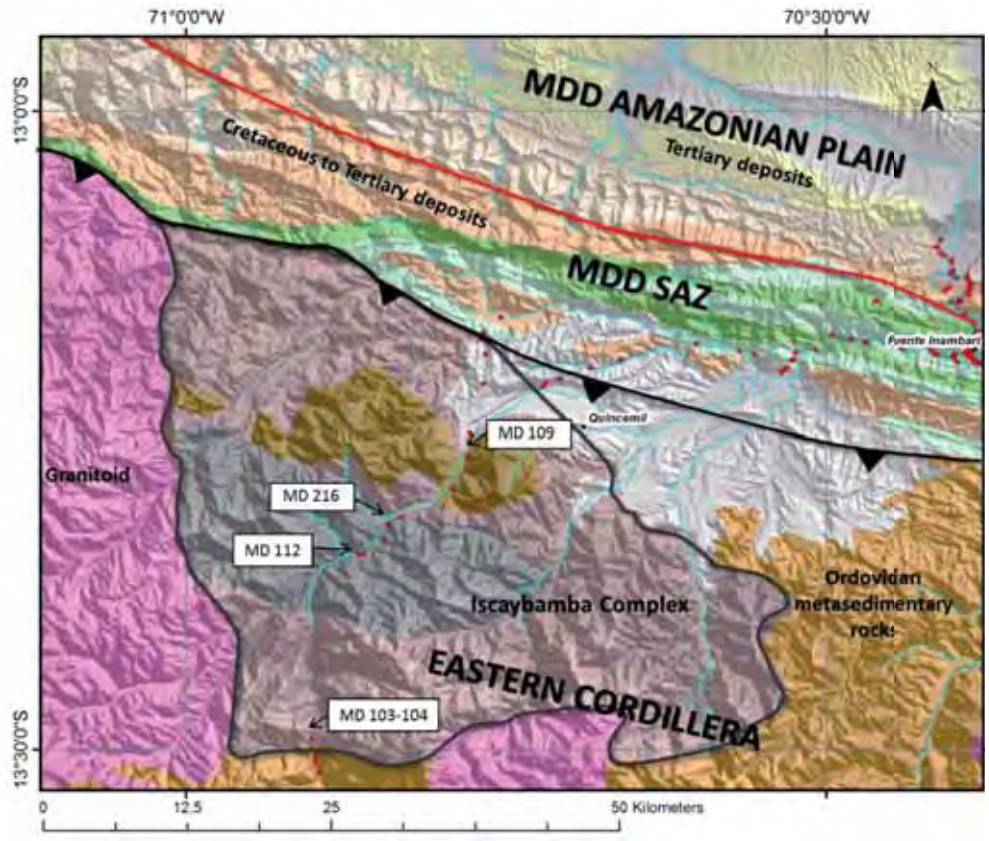

Figure 9: Geological map focused on Inambari area (south-eastern Madre de Dios basin). Structural interpretation is simplified. The metamorphic Yscaybamba complex is highlighted by brown bold contour. Field observations of Figure 10 are also situated in this figure and indicated by the number of the corresponding outcrop.

Figure 10: Field observations realized along the Transoceanic road, crossing over the EC. Photographs have been taken from 4 different outcrops, all situated within the Yscaybamba metamorphic unit (see map of Figure 9 for geographical locations of the outcrops).

2.2.2. Ordovician

This unit belongs to a Paleozoic southwest thickening wedge (House et al., 1999) formed by Ordovician to Devonian rocks.

The Ordovician unit unconformably overlies the metamorphic basement (Figure 7 and Figure 8). Ordovician strata correspond to black and grey shales and siltstones (**San Jose** Fm.) and white quartzites (**Sandia** Fm.) (Laubacher, 1977). San Jose Formation is 1200 m thick (Gil, 2001) and is Arenigian to Llanvirnian in age (Dávila and Ponce de León, 1971). Sandia Formation conformably overlies San Jose Formation, is 500 m thick and is interpreted to be Caradocian. Both formations are related to a marine or shallow marine paleo-depositional environment, and almost all the section presents slight low-grade metamorphism. Maximum thickness of this unit can be measured in the Altiplano, where it exceeds 7000 m (Aleman et al., 2003). In our study area, Ordovician metasediments outcrop in the EC, right by the Azulmayo thrust and the Yscaybamba metamorphic unit (see brownish orange area in Figure 9). The base of this unit constitutes an important regional décollement level or "sole thrust" for the SAZ thrust system, from Central Peru to northern Bolivia (Baby et al., 1989; Gil et al., 2001; Gil et al., 1999).

2.2.3. Siluro-Devonian

In Bolivia and Argentina, the entire Early Paleozoic basin suffers an emersion during the Asghillian and Llandovery period (Late Ordovician to basal Silurian), provoking a stratigraphic gap. In the EC of southern Peru, the absence of these strata is probable, and may be related to this emersion. However, in the Alto Inambari River section (SAZ), Siluro-Devonian strata are present and appear to be conformably deposited onto the Ordovician strata (Laubacher, 1974).

In southern Peru, the Siluro- Devonian unit corresponds to the **Ananea Formation** (Dávila and Ponce de León, 1971; Laubacher, 1978; Valdivia, 1974). It is composed of black shales interbedded with thin sandy layers and is 500 to 700 m-thick in the Carcel de Puncco section (Figure 5). In the Pongo de Coñeq section, Silurian strata are made up of green to yellow shales and breccia deposits associated to normal faults activity (Gil, 2001).

The sedimentation during Siluro-Devonian period was controlled by a glacio-marine depositional environment, and followed by widespread shelf deposition (Laubacher, 1978). Consequently, strata of the Ananea formation gradually evolve upwards into thick turbidites, shallow marine and episodic fluvial/deltaic sandstones of the Devonian **Cabanillas** Group (Aliaga Lopez, 1985; Müller, 1982; Newell, 1945). In the Pongo de Coñeq section (Figure 5), the Cabanillas Gp. is 450 m thick (Gil, 2001). It has also been documented in Pariamanu and Puerto Primo wells in the Madre de Dios foredeep (Gil, 2001) (Figure 5). Cabanillas Fm. must be regarded as a potential source rock in the Madre de Dios petroleum system, as it is known as a Type I/II world-class source rock. However, Devonian source rocks have a variable thickness, richness and regional distribution (Aleman et al., 2003). Sandstones of this unit can also constitute potential reservoirs for a lower Paleozoic petroleum system (Figure 8).

2.2.4. Carboniferous

Late Paleozoic strata (Carboniferous to Permian) correspond to mixed marine platform deposits, starting with Early Carboniferous (Mississipian) carbonaceous shales and coarse-grained sandstones of the **Ambo** Group (Aliaga Lopez, 1985; Müller, 1982; Newell, 1945; Valdivia, 1974). The base of this unit is erosive and can be highlighted by a conglomeratic level (Gil, 2001).

In the Madre de Dios basin, the Ambo group is Tournaisian to Visean in age (Aliaga Lopez, 1985). It outcrops in the Pongo de Coñeq section where it is approximately 200 m thick, in the Alto Manu area (Valdivia, 1974) and it has been documented in several wells (Gil, 2001). Strata consist of an intercalation of carbonaceous shales and sandstones deposited in an infralitoral to deltaic environment. The Ambo Group also contains interbedded tuff layers and sandstones with significant amount of volcanoclastics suggesting the presence of a contemporaneous volcanic arc (Alemán and León, 2002; Benavides, 1991; Diaz Martinez and Choque Mamani, 1995). In the southern Ucayali basin (Figure 5), the thickness of the Ambo group is variable, and the base of the unit constitutes an excellent décollement level for the main structures developed in Kinteroni and Camisea areas (Espurt et al., 2008).

Carbonaceous shales from the Ambo group contain abundant plant remains and discrete coal seams (Aleman et al., 2003) and constitute the main source rock of the giant Camisea gas/condensate field in the southern Ucayali basin. Oils seeps discovered in the Madre de Dios basin (Quebrada Petroleo and Quebrada Gallinazos) present similar geochemical signature than Cashiriari-1X well condensates (Camisea block, Figure 5), certifying a good potential source rock in this basin (Aleman et al., 2003).

2.2.5. Late Carboniferous to Late Permian

The basal part of this unit unconformably overlies former deposits (Hermoza, 2004). It is formed by Late Carboniferous and Permian strata corresponding to **Tarma** and **Copacabana** Groups (Dunbar and Newell, 1946).

Tarma Group consists of basal sandstones (green sandstones) grading upward into a sequence of thick-bedded lime mudstones and marls interbedded with thin dolomites and siltstones. The basal sandstones present good reservoir properties, and even better potential when stratigraphically stacked to the underlying Ambo sandstones (upper part of the formation). Tarma Group is interpreted to have been deposited in a shallow water inner shelf to supratidal, low energy environment (Aleman et al., 2003). It outcrops at the Pongo de Coñeq and the Pongo de Mainique (Ucayali Basin) sections and have been documented in both Puetro Primo and Pariamanu wells (Aleman et al., 2003; Gil, 2001) (Figure 5).

The **Copacabana Group** (Early Pennsylvanian to Early Permian) conformably overlies the Tarma Group, and mainly consists of limestones interbedded with shales. This unit is composed of normal to restricted marine, subtidal to supratidal deposits. In foreland wells, the carbonate sequence contains interbedded anhydrite layers probably associated to a lagoon depositional environment (Gil, 2001). These layers can constitute thin seal level for underlying petroleum system. In the Madre de Dios basin, the Copacabana Gp. outcrops in the

Alto Manu River and the Pongo de Coñeq area (~300 m thick). It has also been documented in Puerto Primo (810 m thick), Los Amigos (680 m thick), Pariamanu (1000 m thick) and Cariyacu wells (>750 m thick) (Figure 5). However, Copacabana strata can be partially eroded by the overlying Late Cretaceous unconformity, as observed in Panguana well (southern Ucayali basin, according to industry confidential report).

TOC values for marls layers of the Copacabana strata present values of ~2 to 9.7%, and maximum values of 444 to 692 for Hydrogen Index (Aleman et al., 2003; Baby et al., 1995). Copacabana source rocks are very similar to Type I Ene shales source rocks and should not been discarded.

Copacabana shelf series ends with a Late Permian unit, corresponding to Ene, Noi (?) and Shinai (??) formations. These series are not well-constrained, as no precise dating data exists. Note that the top of Copacabana unit can display a non-conformable contact with the overlying Upper Permian and/or Cretaceous strata (seismic data, confidential report). These Late Permian deposits are mainly correlated with the fluvio-aeolian **Ene formation** in the Pongo de Paquitzapango (Ene Basin, in the Ucayali area) and in the Pachitea area (Espurt, 2007; Hermoza, 2004; Leigh and Rejas, 1966). In Madre de Dios basin, Gil (2001) interpreted the quartzites and basal dark shales observed within the imbricate thrust system outcropping in The Inambari River as belonging to the Late Permian Ene formation. However, this interpretation is not attested by any biostratigraphical result, and we consider in this study that no Ene deposits outcrop in the SAZ of the Madre de Dios basin. When present, the basal black shale of Ene formation constitutes a good source rock, and the upper sandstones represent a potential reservoir (Camisea basin for example).

Noi formation is well-documented in the southern Ucayali and Camisea basin, where it is made up of fluvial and aeolian sandstones (Espurt et al., 2008). Some authors considered that Noi formation outcrops in the Pongo de Coñeq section and the Inamabri River cutbanks but no clear evidences nor precise dating exist to confirm this interpretation. However, the presence of eolian and fluvial facies of Ene and/or Noi formations where hydrocarbons are housed in Camisea and Kinteroni areas (Figure 6) has been recognized in the 2D seismic lines from the Madre de Dios foredeep (confidential report). Because we saw no aeolian deposits during the field expeditions realized in the SAZ of the Madre de dios basin, we consider in this study that Noi formation is absent.

Above the Noi unit lays the **Shinai** marly strata, deposited in a shallow marine to lagoonal environment. Shinai strata are sometimes eroded by the Basal Late Cretaceous unconformity or simply absent in the Madre de Dios basin (confidential report). Where Noi formation is conserved and Shinai unit is eroded, Noi deposits are in direct contact with the younger overlying Lower and Middle Nia sandstones, and the stacked sandy package created constitutes then an excellent reservoir level. It is most probably not the case in the Madre de Dios basin.

Lower Nia formation is situated above the Late Permian units and below the basal Late Cretaceous unconformity. They can consequently be Triasis (?) to Late Jurassic in age, as no dating material exists for these deposits. Strata of the Lower and Middle Nia formations are characterized by aeolian dunes and sebkas deposits, respectively. Thickness of these strata are difficult to asset, but may be comprised between

0 (when eroded) to up than 60 m thick. In the Madre de Dios SAZ, Lower Nia member has not been recognized at surface.

The presence and extend of the late Permian to pre-Late Cretaceous deposits are difficult to estimate in the Madre de Dios SAZ. Nevertheless, confidential report documents the presence of Permian aeolian deposits in the Madre de Dios foreland foredeep, based on the recognition of characteristic seismic facies (aeolian dunes). According to these subsurface seismic data, the late Permian to pre-Late Cretaceous formations may extend further to the northwestern part of the Madre de Dios foredeep (confidential report).

Based on field observations realized in the SAZ of the Madre de Dios foreland basin, we consider in this study that the Ene, Noi, Shinai and Nia (Lower and Middle members) formations are absent in surface. Nevertheless, it is possible that these units may be present in depth.

2.2.6. Late Cretaceous

In the Madre de Dios area, Permian-Triassic rift sequences, Jurassic and Early Cretaceous deposits are not preserved (Gil, 2001).

The Late Cretaceous sedimentary unit is underlined by a basal regional unconformity (breakup foreland unconformity) and consists of the Middle and Upper Nia (?), Chonta, Vivian, Cachiyacu, and possibly Huchpayacu formations (Gutierrez, 1982; Müller, 1982). This regional unconformity is largely erosional and is linked to a regional continental flexure as it corresponds to the basal unconformity of the incipient foreland basin (Crampton and Allen, 1995) (Louterbach et al., in preparation). In this study we bring new biostratigraphic dating related to the Late Cretaceous stratigraphic interval for samples collected in both the Pongo de Coñeq and the Inambari SAZ (see Annex nº2 and nº3 for detailed results).

In the Madre de Dios basin, Late Cretaceous series only outcrop in the SAZ. A complete section of vertical strata Late Cretaceous in age outcrops in the Pongo de Coñeq canyon. The fluvio-estuarine Late Campanian to Late Maastrichtian deposits of this section have recently been dated and analysed for sedimentary provenance study (Louterbach et al., in preparation). These deposits most probably correspond to the Chonta, the Vivian, the Cachiyacu and possibly the Huchpayacu Formations.

When conserved, the **Middle and Upper Nia** formations (>30 m?) lies above the Late Cretaceous unconformity. These units are constituted by fluvial to alluvial sandstones and correspond to the lower part of a transgressive sequence which also includes the Basal Chonta sands and part of the Chonta shale. The presence of the Middle and Upper Nia deposits is not obvious in the Madre de Dios basin. In the Pongo de Coñeq section, it is more convenient to merge the sandy packages of this unit with the basal Chonta formation. In Inambari area, it is even more difficult to separate the Middle and Upper Nia unit from the rest of Cretaceous strata. In this study we consider the Middle and Upper Nia formations to be absent of the southern SAZ of Madre de Dios basin.

The **Basal Chonta Fm** is made up of estuarine sandstones, mostly visible on well logs (Gamma Ray log curve). It evolves upwards into the **Chonta formation** (200 m thick), composed of gray carbonaceous shales and

mudstones interbedded by siltstone and sandstones. In the Madre de Dios basin, the Chonta Fm. is interpreted to be Cenomanian-Turonian in age (sample MD 282, see Annex 2) and corresponds to littoral to intertidal deposits. Shale deposits of this unit constitute a good seal level for the underlying petroleum system.

The next unit is formed by the **Vivian** sandstones, overlying the Chonta formation above a slightly angular erosional unconformity (10º in the Inambari area). This unconformity can be observed within the Cretaceous structures that form the Inambari SAZ (within the imbricate thrust system). In the Pongo de Coñeq area, due to poor outcropping conditions, this erosional unconformity has not been documented. The Vivian formation corresponds to a medium- to coarse-grained sandstone package about 60 m thick. These sandstones are vertically stacked and have been deposited in a fluvio-estuarine environment during Early Maastrichtian period (Müller, 1982). In the Pongo de Coñeq area these sandstones are probably partly removed and cut by an erosive surface which is dated Late Maastrichtian by biostratigraphic and paleontologic material (Louterbach et al., Submitted). Above this unconformity, estuarine deposits present subaerial exposure evidences such as paleosoil deposits (Cachiyacu-Huchpayacu formations?).

Section realized in the Pongo de Coñeq Canyon presents a gap of observation (50 m thick) above the Vivian formation, and restarts with more than 20 m of estuarine Late Paleocene deposits (Louterbach et al., Submitted). The gap may correspond to the Late Maastrichtian to Early Paleocene Cachiyacu and Huchpayacu formations (Gil, 2001). Another option is to consider an erosive surface between the Late Maastrichtian Vivian and the Late Paleocene deposits. These Late Paleocene estuarine strata correspond to the “Huayabamba” formation, formerly interpreted as made up of continental deposits.

In the Inambari area, the internal part of the SAZ is characterized by deformed and stacked Late Cretaceous strata which form a complex imbricate thrust system (see the Imbricates Zone indicated in Figure 6) (Gil, 2001; Hermoza, 2004). New biostratigraphical results obtained from samples collected in this zone indicate ages spanning from Cenomanian to Maastrichtian (Louterbach and al., in preparation, based on biostratigraphic analyses carried out by Francisco Parra), corresponding to the Chonta, the Vivian and probably the Huchpayacu formations. Facies are similar than those described in the Pongo de Coñeq section. Due to the complex structural settings, thicknesses are difficult to obtain. These Late Cretaceous strata show intense syn-sedimentary deformation features (mainly slumps and growth strata). Two new sauropods footsteps tracks have also been discovered at these top of Late Cretaceous strata during our field expeditions.

Sedimentary provenance data related to the Late Cretaceous deposits of the Inambari area indicate a different source than these of the Pongo de Coñeq section. Consequently, the presence of at least two different drainage watersheds in the Madre de Dios basin during Late Cretaceous times has been proposed (Sanchez, 2012).

2.2.7. Paleogene

In southern Peru, part of the Late Maastrichtian deposits and the basal part of the Paleocene deposits are absent (Jaillard, 1993a; Louterbach et al., Submitted). Consequently, Paleogene series of the Madre de Dios basin unconformably overlie Late Cretaceous series. This erosive surface is related to a chronological gap of several millions years. Paleogene strata rarely outcrop in the SAZ (Salvación syncline, Figure 6) and are poorly documented by previous studies (Gil, 2001; Hermoza, 2004; Kummel, 1948). Due to poor fauna content and difficult access, no reliable dating data existed before this study, and authors were used to consider the Paleogene "Red beds" from the "Huayabamba Group" to be Paleocene to Late Eocene in age (Gil, 2001; Hermoza, 2004; Jaillard et al., 1993b; Roddaz et al., 2010).

In the Pongo de Coñeq canyon and the northern flank of the Salvación syncline (Figure 6), the Late Cretaceous series previously described are directly covered by Late Paleocene (Thanetian) estuarine sandstones, marls and limestones, recently dated by new diverse biostratigraphical and paleontological material (Louterbach et al., Submitted)(see *Part C* of the manuscript for more details related to the Neogene stratorgaphy of the Madre de Dios basin). No direct evidence of Eocene or Early to Middle Oligocene strata has been documented in the Salvación syncline. In the Inambari area, no evidence of Paleogene deposits has been documented, as the Punquiri syncline (Figure 6) only yielded Neogene fauna until now. These Paleogene strata may lie between the Inambari Bridge and the first Neogene deposits described in the Punquiri Syncline. No dating result is available in this area but the deposits have been described and present similar facies than the Paleogene strata described in the Pongo de Coñeq area (estuarine deposits). However, because late Maastrichtian formations are also characterized by estuarine and shallow marine deposits, precaution must be taken before interpreting these unconstrained strata.

2.2.8. Neogene

Neogene deposits correspond to the thickest continental series and form the major part of the sedimentary filling of the SAZ and the Madre de Dios foredeep. Despite their importance, very few studies concern Neogene strata (Hermoza, 2004; Roddaz et al., 2010). This can be explained by the difficulty to find any biostratigraphical or paleontological material for dating. In this study, we bring new dating results and new sedimentological observations in order to propose a new chrono-stratigraphic framework for the Neogene sedimentary filling of the Madre de Dios SAZ (see *Part D* of the manuscript).

In the Madre de Dios basin, Neogene strata largely outcrop in the northern Salvación syncline as well as in the southern Punquiri syncline and around Santa Rosa locality (Figure 6). Neogene series from the SAZ of the Madre de Dios basin are traditionally divided into three coarsening- and thickening-up sequences mainly described in Bolivia (Hermoza, 2004; Kummel, 1948):

- the **Quendeque Formation** (Late Oligocene -Early Miocene),
- the **Charqui Formation** (Middle Miocene to Early Pliocene) and
- the **Mazuko Fm** (Middle Pliocene-Pleistocene).

In comparison with the thin marine-related Paleogene series, Neogene deposits are clearly more proximal, present coarser and thicker deposits with more and more frequent sandy to conglomeratic channelized fluvial bodies, and are characterized by increasing subsidence and sedimentation rates (Gil, 2001; Hermoza, 2004). Nevertheless, some shallow marine incursions have been documented and dated in the Neogene stratigraphic record of both the Salvación and the Punquiri synclines (see *Part D* of this manuscript). Many erosive surfaces and syn-sedimentary structures have also been documented within the Neogene deposits of the Madre de Dios foreland basin, and are well-documented by 2D seismic data.

3. Material and Method

3.1. Former studies

W. Gil (2001) and later W. Hermoza (Hermoza, 2004) proposed the first detailed structural studies realized in the Madre de Dios SAZ. They both constructed and restored two structural cross-sections: i) the Pongo de Coñeq section in the north-eastern part of the basin and ii) the Inambari section located in the south-western area. Locations of these sections are displayed in Figure 6 (sections A and B). They are oriented SW-NE, perpendicular to the general trends of the andean structures and parallel to the available seismic lines. These sections cross over part of the Eastern Cordillera, the whole SAZ and part of the Madre de Dios plain.

Mostly based on existing geological map and some additional field observations documented in the Eastern Cordillera, Gotberg et al (2010) also proposed an extended balanced cross-section realized across the EC and the Madre de Dios SAZ through Pongo de Coñeq area. Authors propose three different structural models with different shortening estimates according to the importance of the basement-involving controlling factor.

Based on refreshed subsurface data (Hunt survey, 2009-2010), new stratigraphic constraints and extended field observations, we propose in this study to review the geometry of deformation for both the Pongo de Coñeq and the Inambari sections.

3.2. New data

Surface data were obtained from 1:100,000 INGEMMET (Instituto Nacional Geológico, Minero y Metalúrgico del Peru) geologic maps, PERUPETRO S.A. geologic database, digital elevation models from SRTM data, LANDSAT images and from several field surveys carried out in 2010, 2011 and 2012 in this area by the University of Toulouse and the IRD (Annex-Map nº3). We collected samples for palynology, palaeontology, micro-fossil determination and sedimentary provenance studies (Figure 4). Biostratigraphical analyses have been realized thanks to the collaboration between the University of Montpellier (France), the University of Bonn (Germany), the University of Amsterdam (Netherlands) and the Smithsonian Institute (Panama). However, most of the biostratigraphic work presented in this study has been realized by Francisco Parra for his PhD project with the University of Toulouse and the IRD. Detailed biostratigraphic contents and results for the tertiary sedimentary filling of the Madre de Dios SAZ (both the Pongo de Coñeq and the Inambari areas) are shown further in this study (see *Part D*) and can be consulted in the supplementary dataset (Annex nº2 and 3 and Annex-Map nº 4 to 6). Sedimentary provenance analyses have been carried out at the University of Toulouse and the IRD (see Sanchez' master thesis (2012)) and at the University of Brasilia (Elton Dantas) (Annex-Map nº8).

Samples for low-temperature thermochronoly (AFTA and (U-Th)/He on apatites) have also been collected during the field expeditions, mainly through the eastern flank of the Eastern Cordillera. Samples have been prepared at the University of Toulouse and fission tracks on apatites have been counted under Stephanie

Brichau's supervision. (U-Th)/He analyses were carried out at Californian Institute of Technology (USA-Los Angeles) by Ken Farley.

Structural and sedimentological field observations were made for the Late Cretaceous to Pleistocene sedimentary interval in the Madre de Dios SAZ, in both the Pongo de Coñeq and the Inambari areas (north-western and south-eastern areas respectively).

Subsurface data consist of unpublished well and seismic reflection data provided by PERUPETRO S.A and Repsol Exploration S.A (see Figure 3 and Figure 12). These data have been used to interpret the structures at depth, the geometry of the thrust systems and the syn-tectonic sedimentation. Seismic lines interpretations shown further are all in time (TWT, ms). Figure 11 shows the resulting structural map in the Madre de Dios SAZ.

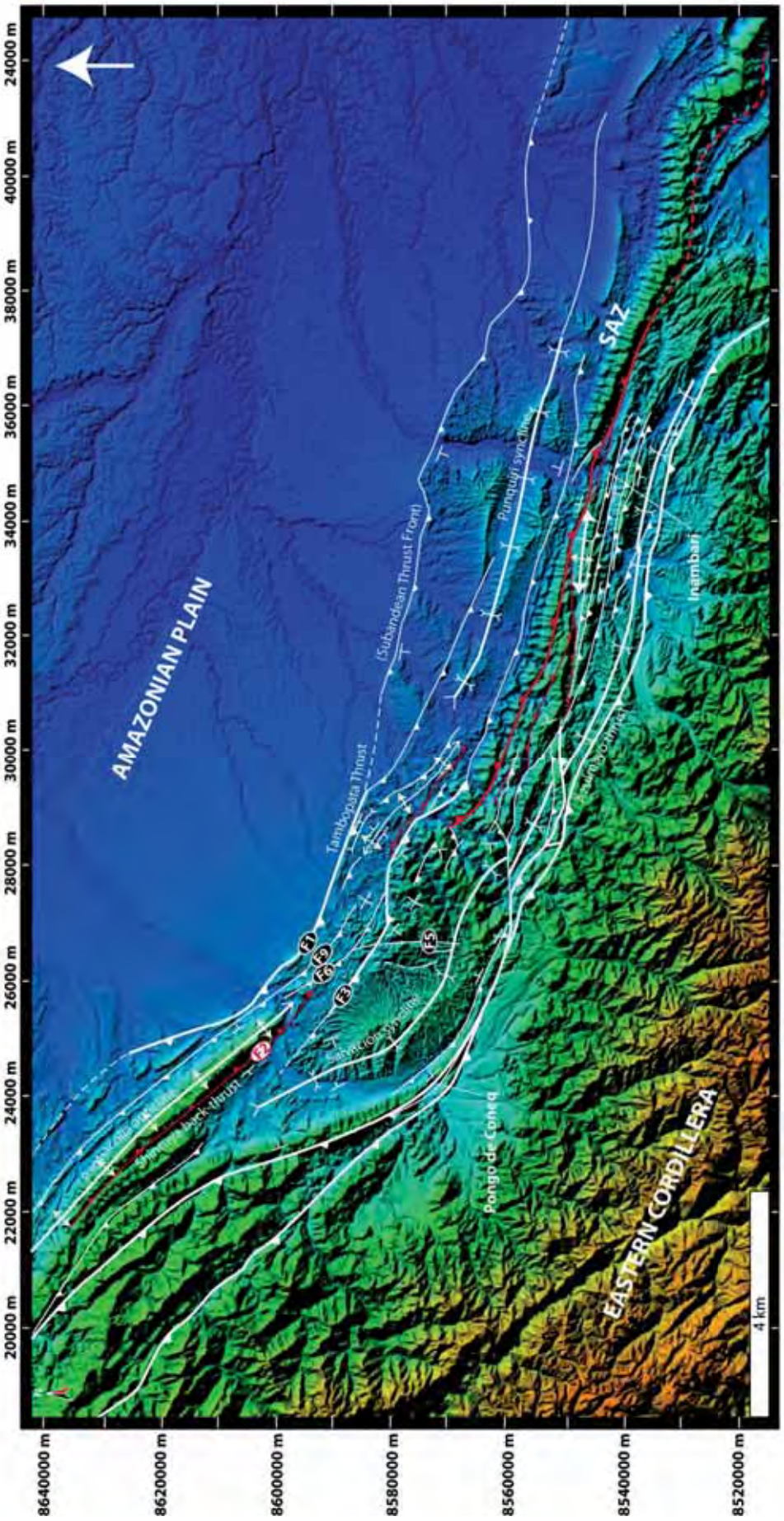

Figure 11: Structural map of the Madre de Dios SAZ. Thrust faults and fold axis are in white, back-thrust faults are in red. Background map: DEM colored map.

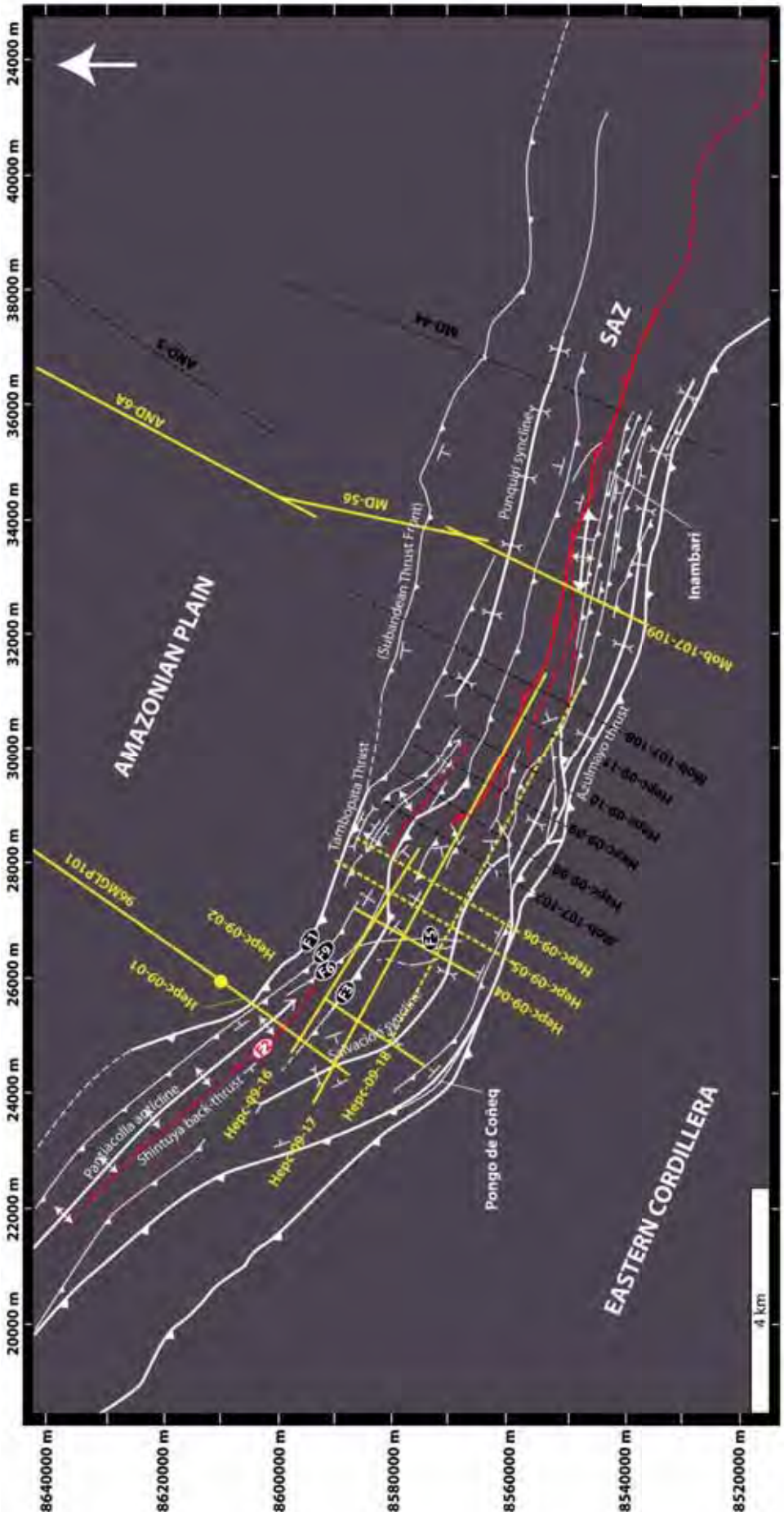

Figure 12: Structural map of the Madre de Dios SAZ with location of the 2D seismic lines interpreted and presented in this study (yellow bold lines), seismic lines that have been interpreted but which are not shown here (yellow dashed lines) and seismic lines not used for this study (black dashed lines). Thrust faults and fold axis are in white, back-thrust faults are in red.

3.2.1. Pongo de Coñeq dataset

In the north-western Pongo de Coñeq area, field observations have been realized along the road crossing-over the Andean belt from Cuzco city (Altiplano) to Atalaya village situated close the Pongo de Coñeq Canyon in the SAZ (Figure 6 and Figure 13). In this part of the SAZ, outcrops are only accessible by boat. They are situated along the cut banks of the Alto Madre de Dios River in the Salvación syncline and the Pantiacolla anticline (Figure 13).

For exploration geologists working on the Madre de Dios SAZ hydrocarbon potential appraisal, the Pongo de Coñeq area is of great interest. Indeed, the only seismic "line tie" to surface exposures of the Cretaceous Vivian sandstone (reservoir) in the whole seismic dataset of Block 76 is located along seismic line hepc-09-01 where it crosses over the Pantiacolla Anticline (Figure 13). It appears then critical to determine, with as much accuracy as possible, the Vivian contact around the Pantiacolla anticline, as well as the structural framework along the Pongo de Coñeq section. Realization of good correlation between the Vivian sandstones which have been recognized in Cariyacu well situated in the Madre de Dios foredeep (Figure 14) and the Vivian sandstones outcropping in the Pantiacolla anticline is primordial for the industry.

Biostratigraphical results and structural observations including dip data were adapted and loaded in Move software. Once loaded, structural data and other useful results have been projected onto a main section carefully chosen according to the trend direction of the strata. In the Pongo de Coñeq area, three seismic sections have been merged to construct the main composite section: one seismic section crossing over the Madre de Dios plain to Cariyacu well (96MGLP101), a second seismic section across the Salvación syncline and the Pantiacolla anticline (Hepc-09-01), and a third seismic sections crossing over the Pongo de Coñeq Canyon and the Salvación syncline (Hepc-09-02) (Figure 13). Seismic sections Hepc-09-01 and Hepc-09-02 have been recently acquired and processed by Hunt Oil Exploration and Production Company of Peru and their partner Repsol Exploration Company (2009-2010).

Figure 15 and Figure 16 show part of our Move database focused on the Pongo de Coñeq area and the correlations we made based on seismic sections, well data (Cariyacu-1X) and new biostratigraphic results. Thanks to these biostratigraphic constraints we projected onto Hepc-09-01 and Hepc-09-02 seismic sections, we propose a new stratigraphic framework for the Late Cretaceous to Pliocene sedimentary filling of the Salvación syncline (see *Parts B*, *C* and *D* of the manuscript for more details). Once we constructed the stratigraphic correlation between Cariyacu well, seismic section Hepc-09-01 and seismic line Hepc-09-02, we extended the interpretation towards the other seismic lines eastward (the interpretations of seismic sections Hepc-09-04, Hepc-09-16 and Hepc-09-17 are presented further in this study). However, due to complex structural settings of the SAZ, correlations are very difficult to manage between the Pongo de Coñeq and the Inambari areas. Indeed, the northern Salvación syncline appears to be partly or completely disconnected from the southern Punquiri syncline (Figure 11). Consequently, if the stratigraphic framework has been clearly re-established in the northern area, it is still uncertain towards the south (Inambari).

Thermochronological results, mainly situated in the Eastern Cordillera, as well as sedimentary provenance data documented in the Salvación syncline have also been loaded in Move software and then projected onto the main Pongo de Coñeq section.

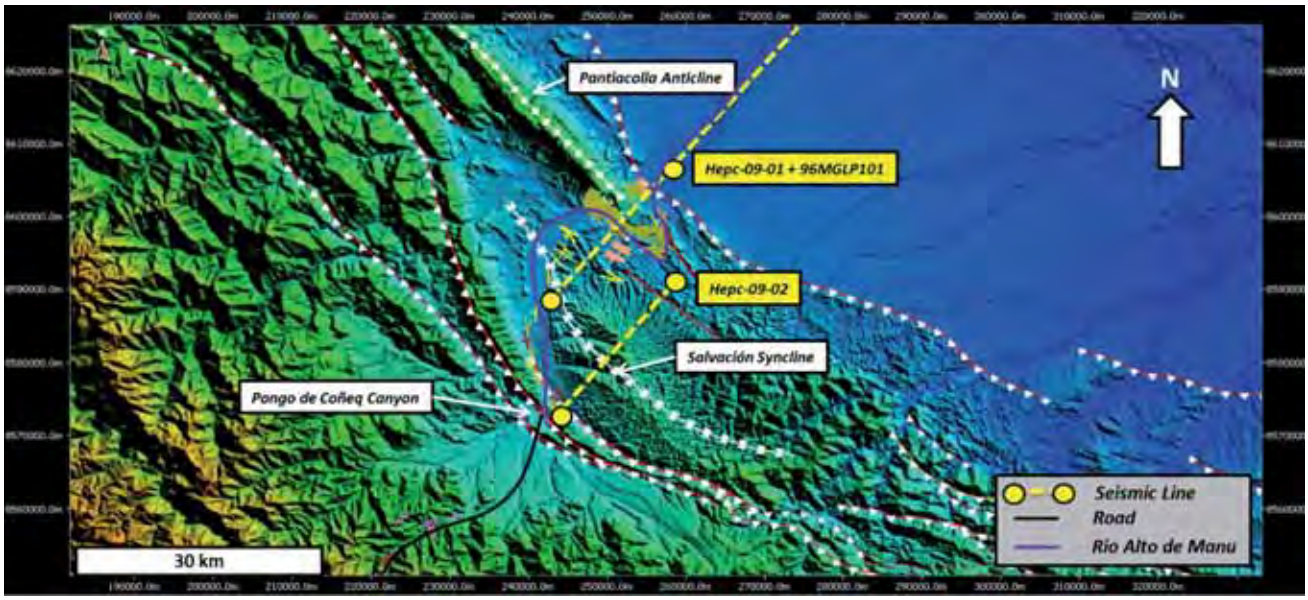

Figure 13: Structural map of the Pongo de Coñeq area focused on the Salvación syncline. Seismic lines used for the regional balanced cross-section construction are shown (yellow dashed lines). Dip data are also displayed (Map view from Move software).

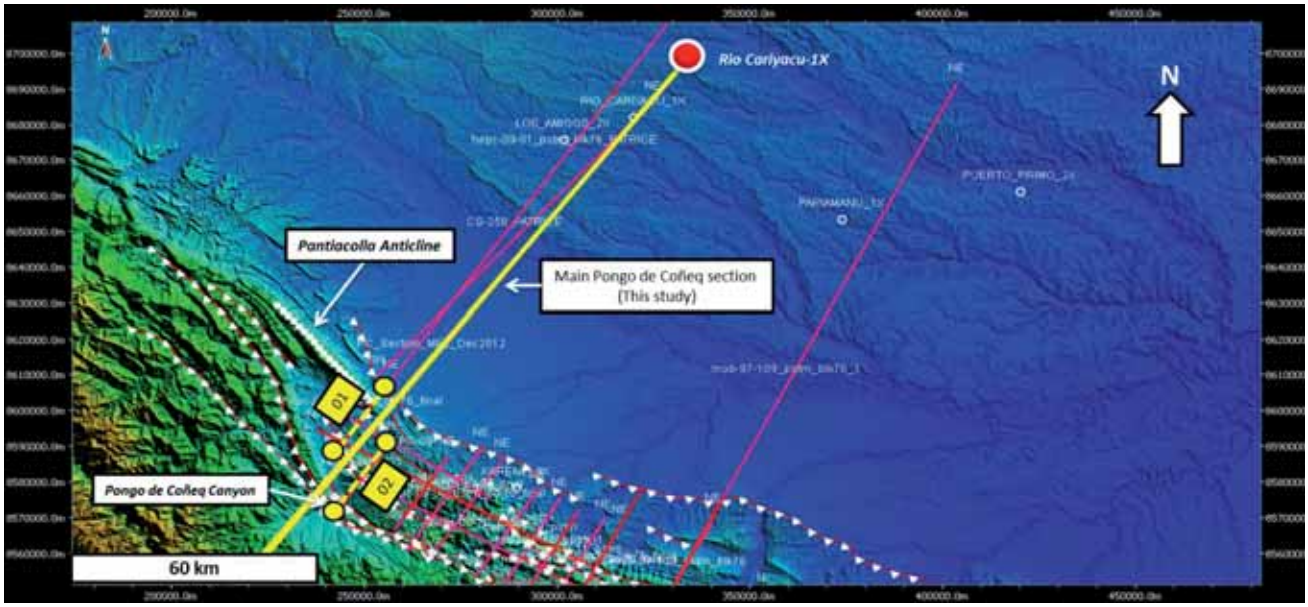

Figure 14: Location of the main Pongo de Coñeq section in the Madre de Dios basin (Map view from Move software). Section ends towards the north-east with the Rio Cariyacu-1X well.

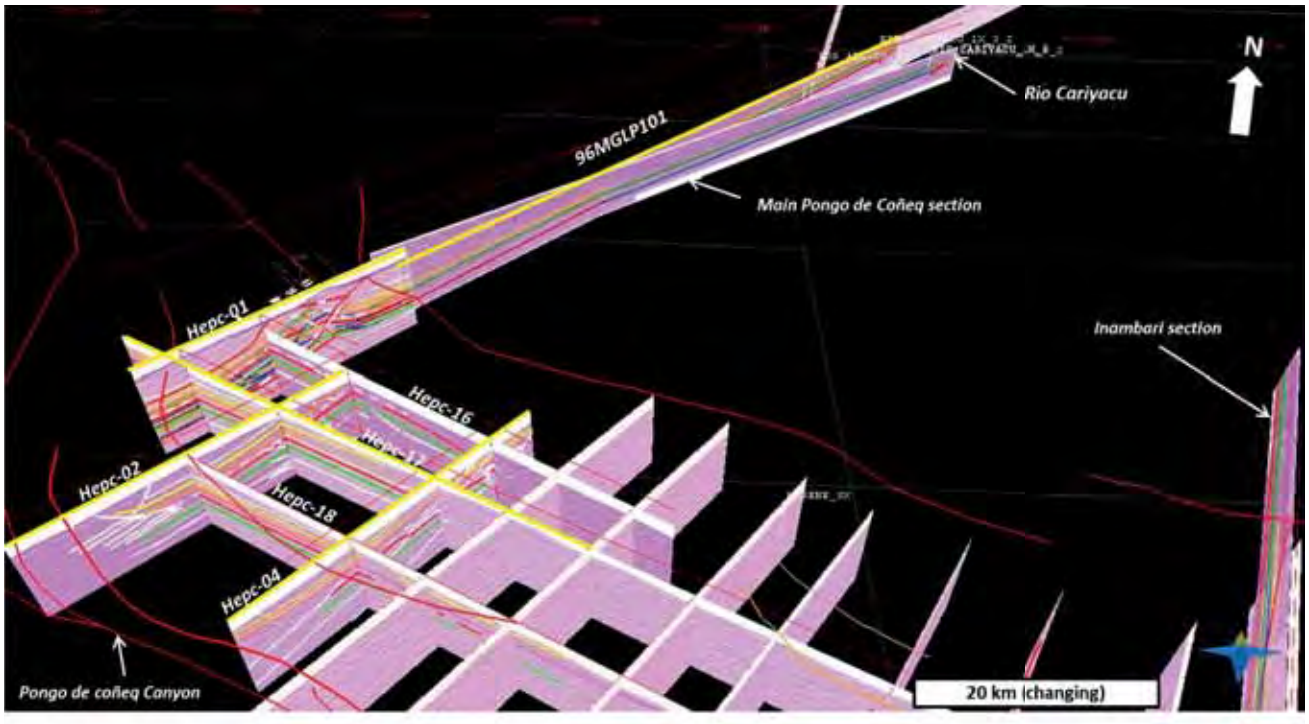

Figure 15: 3D view of the area shown in Figure 13 showing the available dataset for the Pongo de Coñeq area. Seismic lines are from Hunt's survey (see Figure 12 for geographic situation). The Main Pongo de Coñeq section is constructed based on Rio Cariyacu well and seismic sections Hepc-09-01, Hepc-09-02 and 96MGLP101. Biostratigraphic constraints are not displayed.

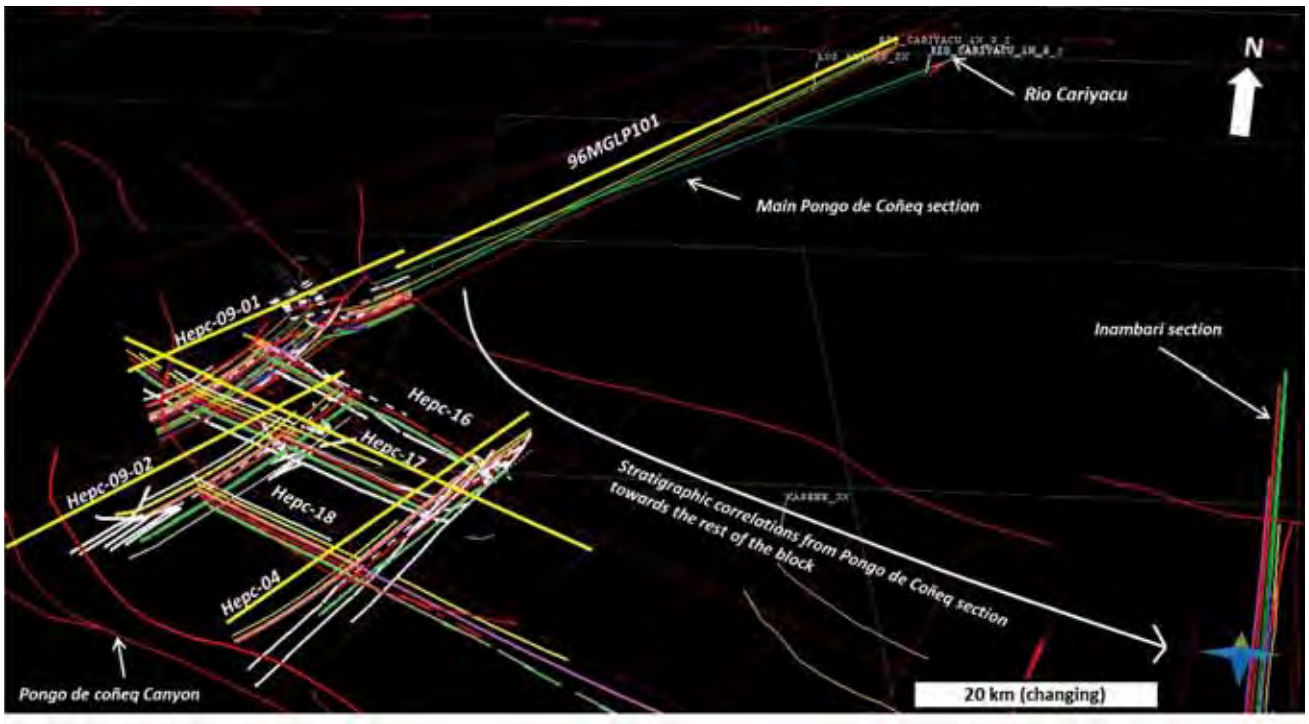

Figure 16: 3D view showing the stratigraphic correlations realized across the Pongo de Coñeq area, from the SAZ towards the northern Madre de Dios foredeep (Rio Cariyacu well). Based on the interpretation of seismic lines Hepc-09-01 and Hepc-09-02, seismic line Hepc-09-04 has also been interpreted. Strike sections (parallel to the Andean belt structures) correspond to seismic lines Hepc-09-16, Hepc-09-17 and Heoc-09-18 (from North to South).

3.2.2. *Inambari dataset*

Thanks to the recent Trans-oceanic road which crosses over the EC towards the Amazonian plain in our study area, we could realize precise structural field work in the south-eastern Madre de Dios SAZ and particularly in the complex "*Imbricates Area*" area situated between the Nusiniscati and the Punquiri Synclines (Figure 6, Figure 17 and Figure 18). As we did in the Pongo de Coñeq area, we collected samples for biostratigraphical analysis, sedimentary provenance study and thermochronology all along the section. A synthetic sedimentary column has been realized across one imbricate structure in the Imbricate area in order to constrain the stratigraphy and geological content of these important features.

Methodology is the same than this used for the Pongo de Coñeq area: all stratigraphic and useful results as well as structural data have been loaded in Move software before being projected onto a seismic line (Mob-97-109) (Figure 17).

Note that the seismic section used to construct the main Inambari balanced cross-section presented further is situated few kilometres eastwards from the field observations we realized along the road and the Inambari River cut banks (Figure 18). Data projection length is greater for the observations made around the Inambari Bridge in the Imbricates Area ("IA" in Figure 18) in comparison with the field observations realized along the road in the Eastern Cordillera which could be easily projected onto the Inambari section without any projection issue. To resolve this issue, we finally decided to mainly use the Mobil field data (PERUPETRO S.A. database) which are situated all along the seismic section Mob-97-109 to construct our structural section.

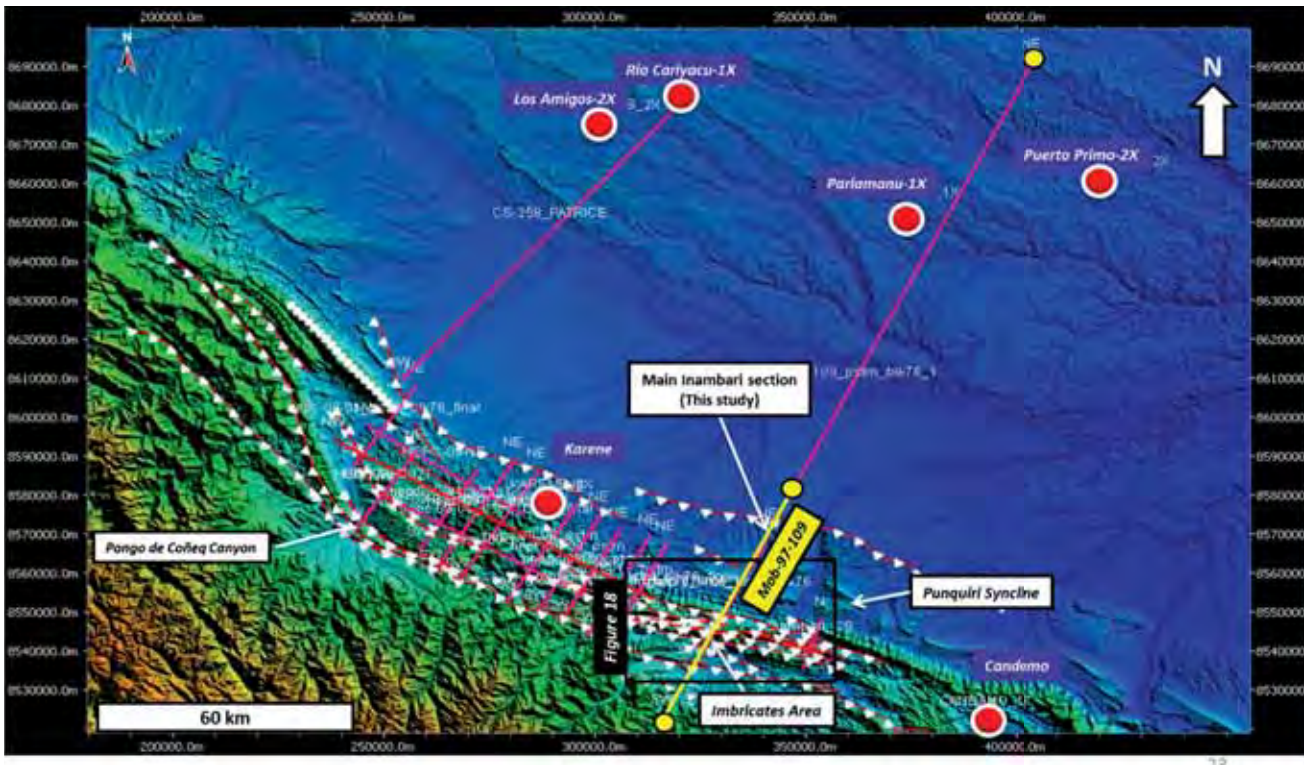

Figure 17: Location of the wells and the main Inambari section in the Madre de Dios basin (Map view from Move software).

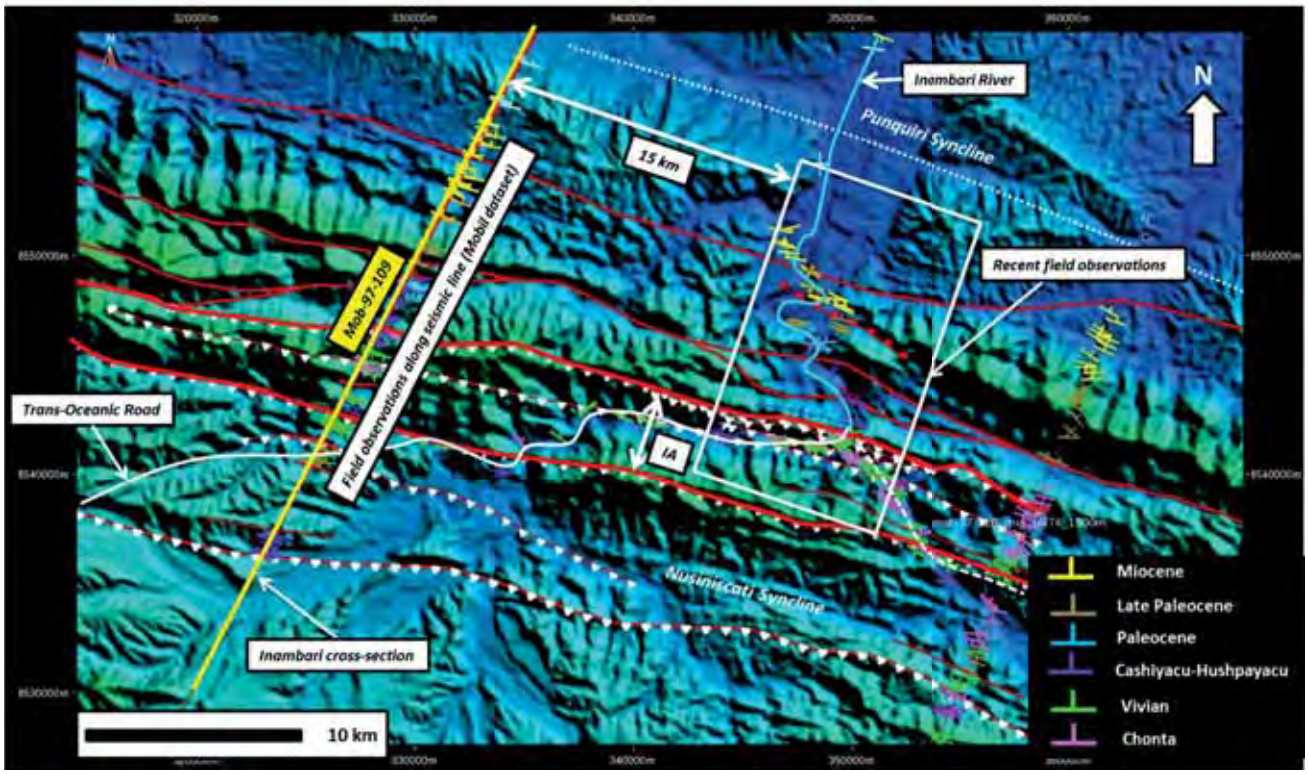

Figure 18: Enlarged view of the Inambari area focusing on the available dataset (see geographic situation in Figure 17). Recent field observations and dip data are situated along the road and along the Inambari River (Map view from Move software). Field and dip data used to construct the balanced cross-section are situated all along the seismic section (from Mobil survey).

4. Geometry of the deformation

In map view, differences in the surface geometry can be observed between the Pongo de Coñeq and the Inambari SAZ (Figure 11, or Annex-Map nº1). In the north-western Pongo de Coñeq sector, the EC directly thrusts over the Salvación syncline. No other fault-contact or structure is visible, a part from the northern Pantiacolla anticline which suggests a relation with a deeper thrust. The south-eastern Inambari SAZ presents a more complex organization in map view: the EC thrusts other a three-partite SAZ constituted by the Nusiniscati syncline, the Imbricates area and the Punquiri syncline (Figure 11). As documented in the Pongo de Coñeq area with the presence of the Pantiacolla anticline which is related with the Sub-Andean Thrust Front (STF), the Inambari SAZ ends towards the Santa Rosa anticline structure which is induced by the Tambopata thrust (local name of the STF).

4.1. Pongo de Coñeq area

The Pongo de Coñeq main section is based on three seismic sections: Hepc-09-01, Hepc-09-02 and 96MGLP101 (see Figure 13 and Figure 14 for location). Seismic sections Hepc-09-01 and Hepc-09-02 have been interpreted in details (Figure 20, Figure 21, Figure 24 and Figure 25). Various seismic markers were chosen based on their important amplitude, their easy identification across the all seismic dataset and on their relation with available stratigraphic constraints on surface (projected data). We thus tried to link a geological age or an age interval to each of these seismic markers. Correlation between Rio Cariyacu -1x well located in the Amazonian plain and the SAZ is based on seismic line 96 MGLP101 which crosses over all the un-deformed Madre de Dios foredeep to the location of the well (Figure 19). Based on new stratigraphic constraints, seismic interpretations and dip data projected with Move software onto the main section, we finally propose a simplified cross-section of the Pongo de Coñeq area (Figure 19).

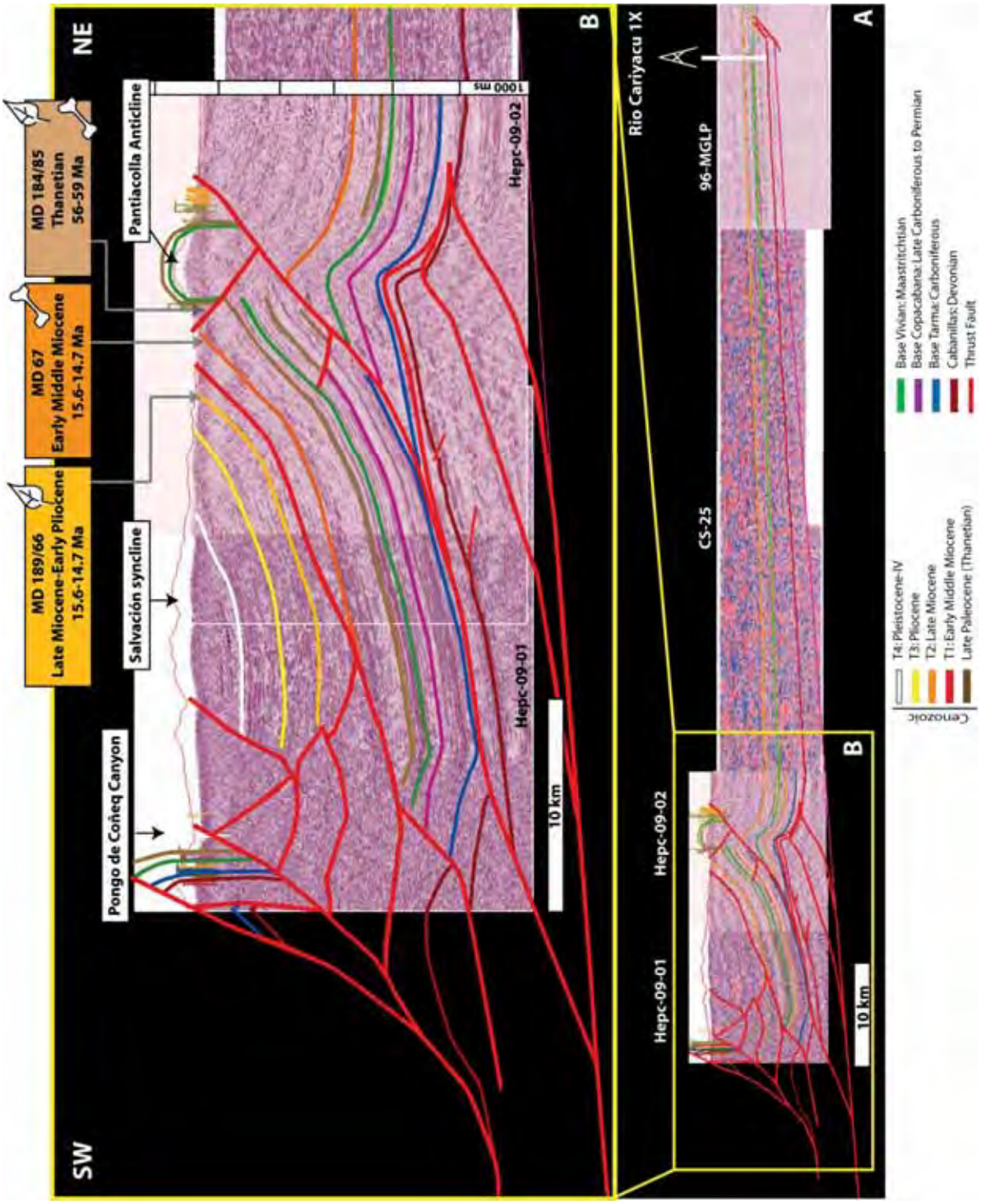

Figure 19: A) Main Pongo de Coñeq structural cross-section constructed with Move software based on dip data, seismic section and well calibration (Rio Cariyacu-1X well). B) Enlarged view of the synthetic Pongo de Coñeq structural section focused on the SAZ. Biostratigraphic constraints are projected above the topography (Move view).

4.1.1. Main geometry and seismic reflector calibration

Seismic section Hepc-09-01 (Figure 20 and Figure 21) crosses over part of the Salvación anticline and the Pantiacolla anticline which is deformed by a major north-vergent thrust (Figure 21). This thrust fault (F1 in this study, also named Tambopata thrust) corresponds to the Sub-Andean Thrust Front (STF) which delineates the deformed SAZ from the un-deformed foreland basin (see structural map, Figure 11). The

décollement level related to this thrust is situated at the base of the Ambo/Tarma Carboniferous formations. The northern flank of the Salvación syncline is thus partly transported and raised by the Tambopata thrust. The Tambopata thrust corresponds to the accommodation of a deep duplex developed in the Lower Paleozoic series. Part of the Paleozoic series, the Cretaceous strata and the whole Tertiary filling of the syncline is thus deformed by this thrust. The timing of deformation inferred from the syn-sedimentary depositional settings will be presented further. The southern flank of the Salvación syncline seems deformed by a duplex developed in Cenozoic syn-orogenic deposits. The geometry of this possible duplex is then poor constrained by seismic data.

Top Vivian Formation (Late Cretaceous) issue in seismic section

Seismic reflectors corresponding to Cretaceous strata are well calibrated in the northern part of the main Pongo de Coñeq section (just behind the Pantiacolla anticline and northwards), as they are directly related in depth to the Cretaceous rocks observed in Rio Cariyacu-1X well (Figure 19-A). Calibration between Rio Cariyacu-1X well and the northern flank of Pantiacolla anticline has been realized based on seismic line 96MGLP101 and Hepc09-01 in PERUPETRO office in Lima. However, correlation of the Vivian formation is much more problematic in the southern part of the main Pongo de Coñeq section due to thrust fault F1 activity and of the complex Pantiacolla structure (Figure 21).

In this study, the Cretaceous Vivian formation is interpreted much lower in the seismic stratigraphy (green seismic marker in Figure 21) in comparison with the recent interpretations realized by the Industry (confidential report by Hunt Oil, 2009). These former versions consider that the well-outcropping Cretaceous deposits of the Pantiacolla Anticline (Figure 21) can be directly connected to the folded strata of the Salvación syncline following the seismic horizons and respecting the surface dip data without being intersected by any back thrust in the southern flank of the Pantiacolla syncline. Depending on the structural interpretation of the Pantiacolla structure and particularly its southern limb, the exact location of the Late Cretaceous Vivian sandstones (reservoirs) in seismic is consequently significantly different. As we already discussed, the location of the Top Vivian formation must be exactly determined in seismic in order to extend the correlation towards the other seismic lines and to calibrate the seismic stratigraphic framework in the global Madre de Dios seismic dataset.

Methodology:

Considering that the main thrust F1 (Figure 21) cut and deformed a previously “one-piece” almost un-deformed Paleozoic to Tertiary stratigraphic sequence, correlation between the Salvación syncline and the foredeep situated eastward of F1 seems to be possible by comparing seismic facies and thicknesses in both areas. In addition to precise structural interpretations realized around the Pantiacolla anticline, we thus propose seismic facies classification and recognition as a complementary tool for Cretaceous correlation across the main Pongo de Coñeq section.

Seismic stratigraphic correlation has also been made based on new biostratigraphic constraints on surface (posted above the topography, Figure 20 and Figure 21).

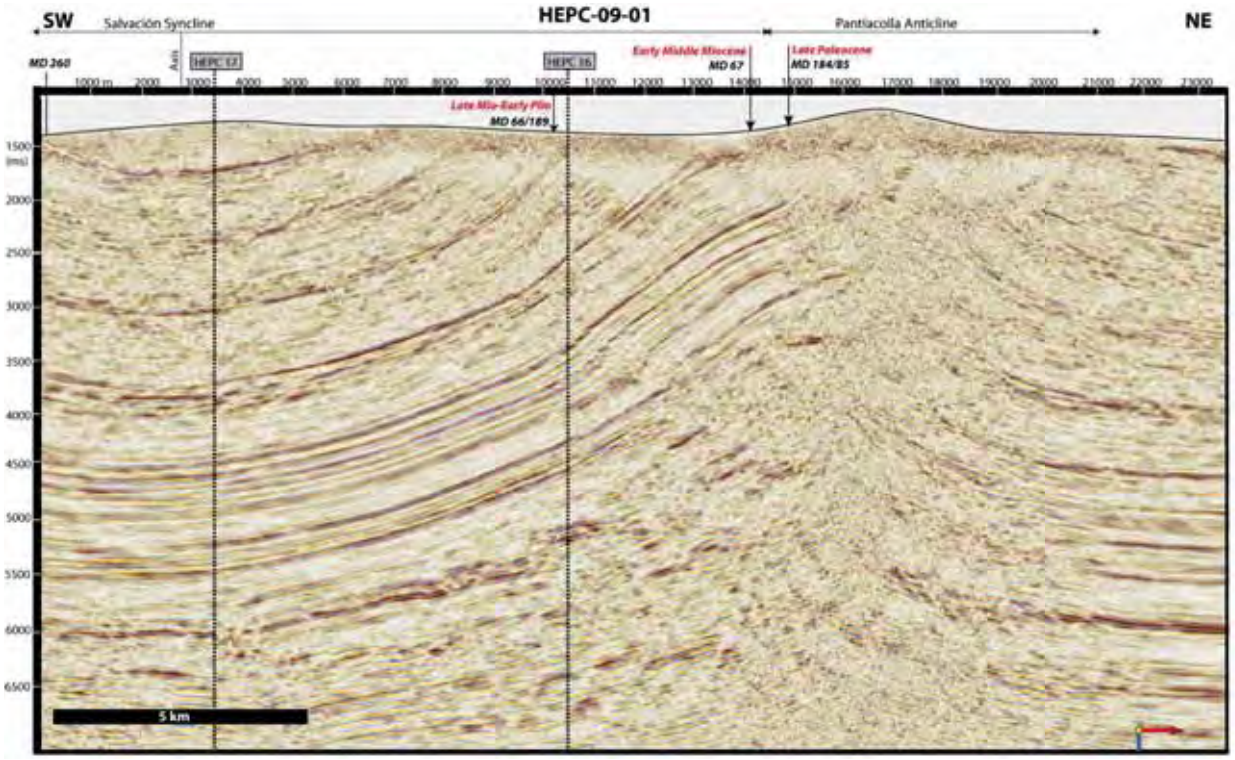

Figure 20: Seismic section Hepc-09-01 (see Figure 12 for location). Main stratigraphic constraints have been projected onto the section and placed above the topography.

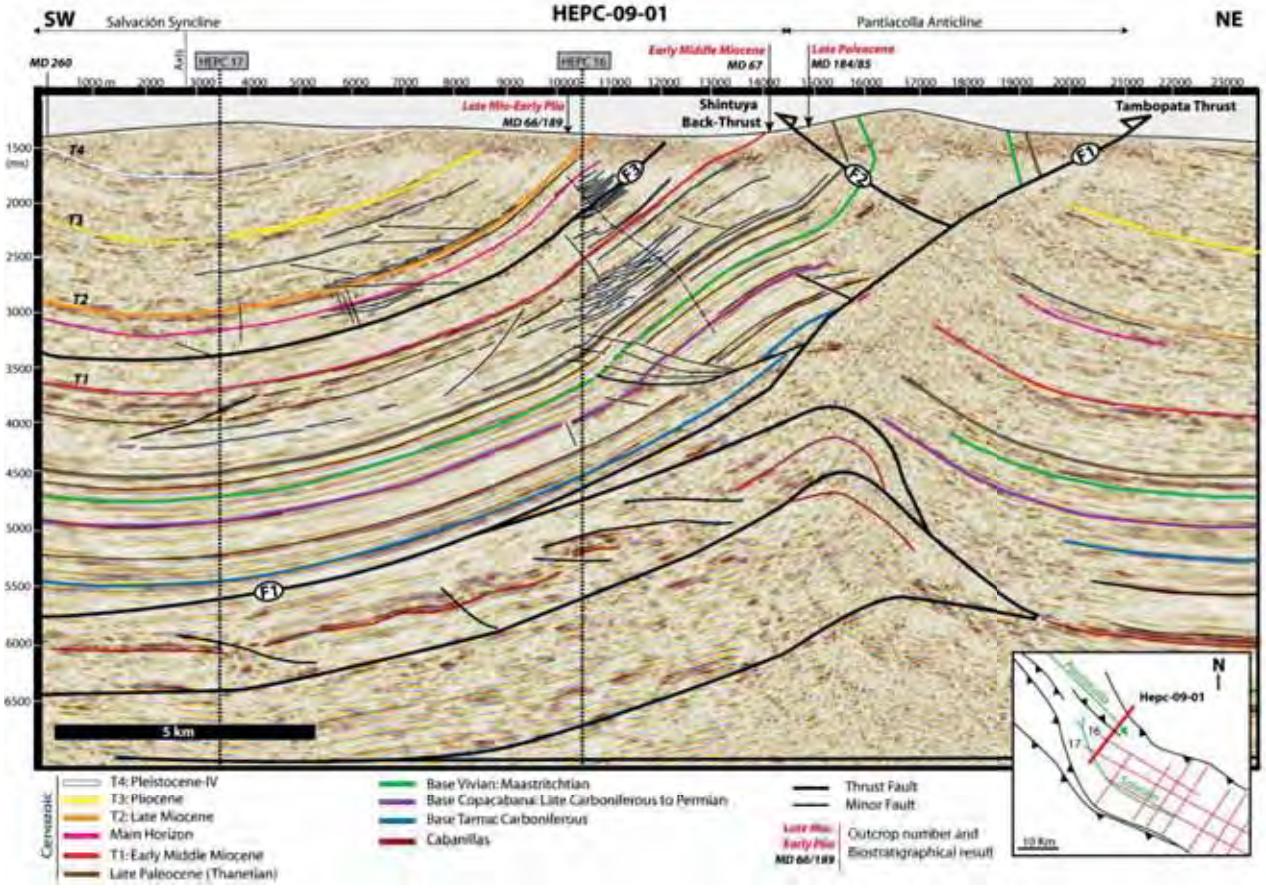

Figure 21: Interpreted seismic section Hepc-09-01. Main stratigraphic constraints have been projected onto the section and placed above the topography.

Seismic facies comparison:

In seismic section hepc-09-01 (Figure 20), the Late Paleozoic to Tertiary sedimentary filling of the Salvación syncline can be divided into different seismic facies forming distinct packages (Figure 22):

- The Late Paleozoic to Late Cretaceous sequence (situated between seismic markers blue and green) presents sheet to wedge geometry, thinning towards the north of the basin. The stratigraphic interval is characterized by regular, highly continuous and parallel seismic reflectors. Seismic horizons situated towards the base of this seismic package present moderate to high amplitude strength (SF-A) in comparison with seismic reflector of seismic facies B (SF-B) which is characterized by low-amplitude. These seismic facies is observed within a ~800 ms seismic interval.
- The Late Cretaceous to Late Paleocene strata (mainly situated between seismic markers green and brown) are characterized by highly regular and uninterrupted seismic facies, with very high amplitude (SF-C). These high amplitude seismic horizons are restricted to a thin interval (~100 ms) but they are easily recognisable across the overall seismic dataset.
- The first seismic interval related to Tertiary deposits is situated between seismic marker T1 (dated Early Middle Miocene thanks to MD 67 locality content, see also Antoine et al. (2013) and Annex nº7)) and the Late Paleocene horizon (brown color). The corresponding seismic facies (SF-D) is characterized by low amplitude strength and parallel to wavy, mainly continuous seismic reflectors in the lower part of the sequence. Seismic reflectors can present discontinuous pattern nearby faults. The amplitude of the reflector increases towards the top of the seismic sequence, and can present local high to very high amplitude strength.
- Seismic sequence situated between seismic markers T1 “Late Early Miocene” (red) and T2 “Late Miocene” (orange) is characterized by continuous to discontinuous and parallel to wavy seismic reflectors. These present high variability in the amplitude strength which can be low to high. The resulting seismic facies (SF-E) is not as homogeneous as this of the Late Cretaceous to Paleocene seismic sequence. Note that discontinuities due to faults activity or internal thrusting are frequent in this interval.
- Seismic facies F (SF-F) is related to the seismic sequence situated between seismic horizons T3 “Pliocene” (yellow) and T4 “Pleistocene-IV” (white). Very similar to seismic facies SF-E, seismic facies SF-F is also characterized by frequent discontinuities in the parallel to wavy seismic reflectors, but it presents slightly higher global amplitude than SF-E. The amplitude being the highest towards the top of the interval.

Thus, two vertical seismic sequences have been compared from one side to the other around the Pantiacolla anticline (one in the Salvación syncline and another one in the foredeep) in order to correlate the tow stratigraphic sequences separated by the main thrusts fault F1 (Hepc-09-01, Figure 22). Resulting interpretation corresponds to this of in Figure 21.

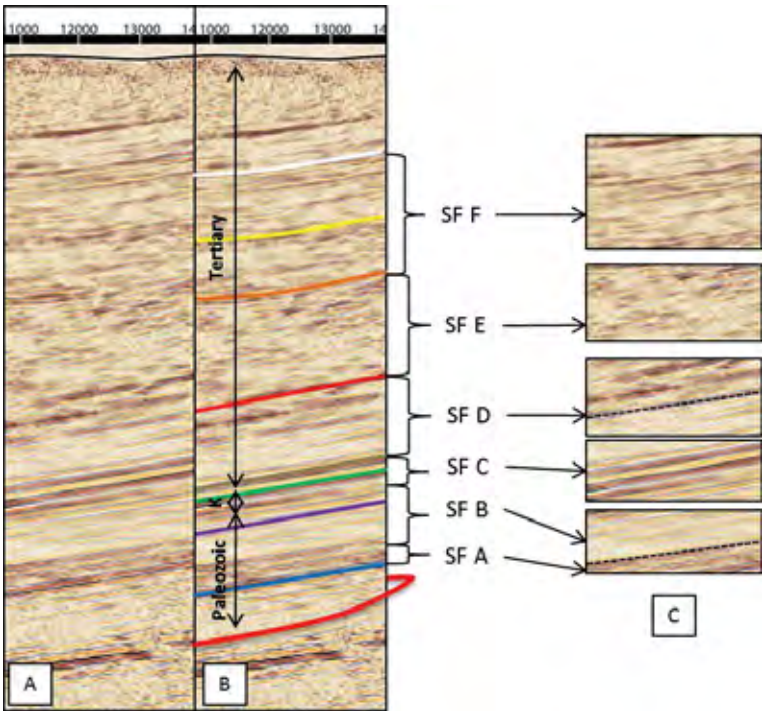

Figure 22: Seismic facies classification for the Paleozoic to Quaternary sedimentary filling of the Salvación syncline. A) Seismic section Hepc-09-01 between 10000 and 14000 m (X) and 1500 to 6000 ms (Y). B) Same seismic section with stratigraphic interpretation. C) Seismic facies (SF) classification from SF-A to SF-F.

Structural interpretation around the Pantiacolla anticline:

Further structural work has been realized around the Pantiacolla anticline in order to explain the resulting offset of the Cretaceous seismic markers on the northern flank of the structure (Figure 21).

For this, we used extended dip dataset collected from Repsol field expedition (2009) and from our own field work (2010-2012) and related to the Pantiacolla structure. These dip data have been projected with Move software onto several fictive cross-section lines oriented SW-NE and crossing over the anticline (Figure 23). Resulting 2D sections from 1 to 7 (Figure 23) show sudden and complete change in dip data direction in the exact locations where a geomorphological break is visible on surface, just at the foot of the Pantiacolla southern limb. Contrary to recent work (confidential report), we thus consider the geomorphological break on surface and the brutal change in dip data as clear evidences of the existence of a north-east dipping back-thrust developing in the Pantiacolla southern flank (thrust fault F2, also called Shintuya back thrust).

This interpretation allows a slight offset across the Pantiacolla back-thrust, which is consistent with our interpretation (Figure 21). Indeed, the stratigraphic position of the Top Cretaceous seismic horizon (green line) in the northern flank of the Salvación syncline and in the overriding Pantiacolla structure is consistent with a reverse-fault activity producing a little offset. The Cretaceous seismic marker location is also coherent with the Rio Cariyacu well top data in the Madre de Dios foreland.

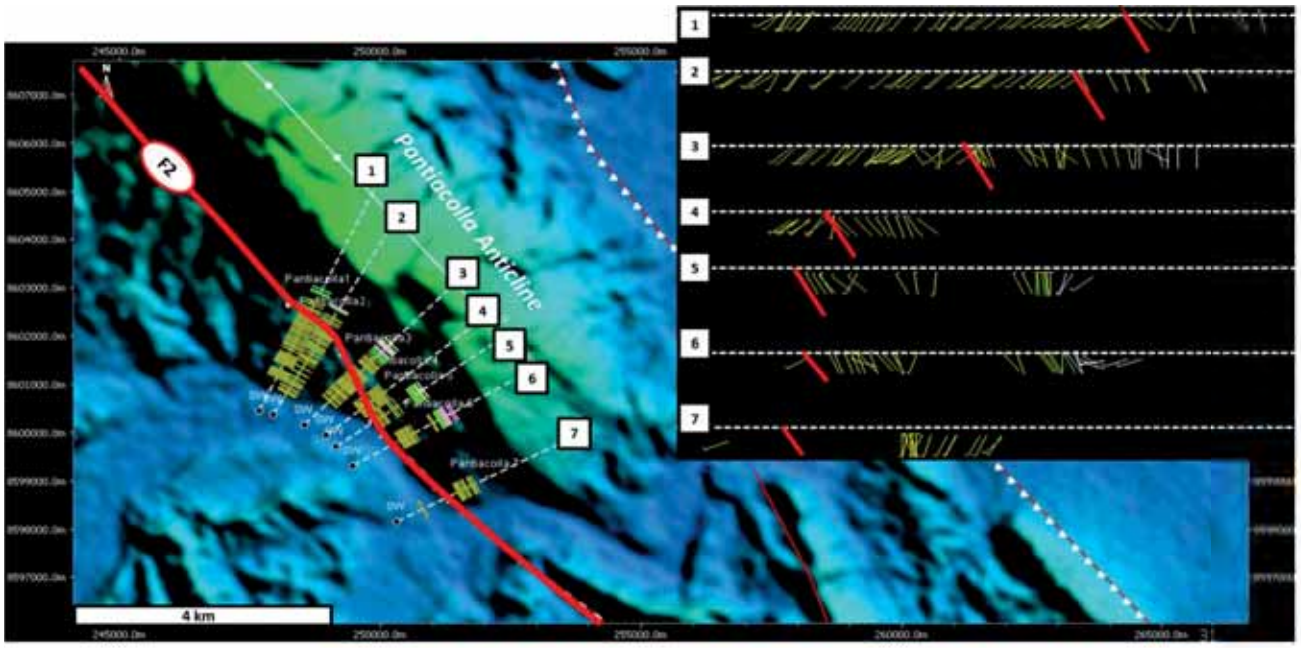

Figure 23: Structural map around the Pantiacolla anticline. Seven fictive sections realized across the Pantiacolla structure are presented. Note the brutal change in dip orientation in each of the sections indicating the presence of a back thrust in the southern flank of the Pantiacolla anticline (interpreted fault F2 is displayed in bold red line in each section). For location of the Pantiacolla anticline, refer to Figure 13. Back-thrust F2 is also displayed in the structural map Figure 11.

4.1.2. Pre-Carboniferous deformation

Note that in seismic section Hepc-09-01 (Figure 21), the Paleozoic deposits (Pre-Tarma formation?) which are situated below the Carboniferous to Cretaceous un-deformed strata and below the thrust F1 present ancient thrust deformation geometry. These deformed strata are also involved in Andean thrust sheet structures.

These Paleozoic structures are also visible on seismic line Hepc-09-02 (Figure 25). Strike line Hepc-09-17 also shows complex geometry related to these Paleozoic duplex which are probably oriented parallel to the section and thus, oriented E-W (Figure 27). Tectonic orogenesis responsible of these Paleozoic structures maybe the Hercynian deformation events. Hercynian thrusts have already been evidenced more to the north in the Ucayali basin by Espurt et al. (2008).

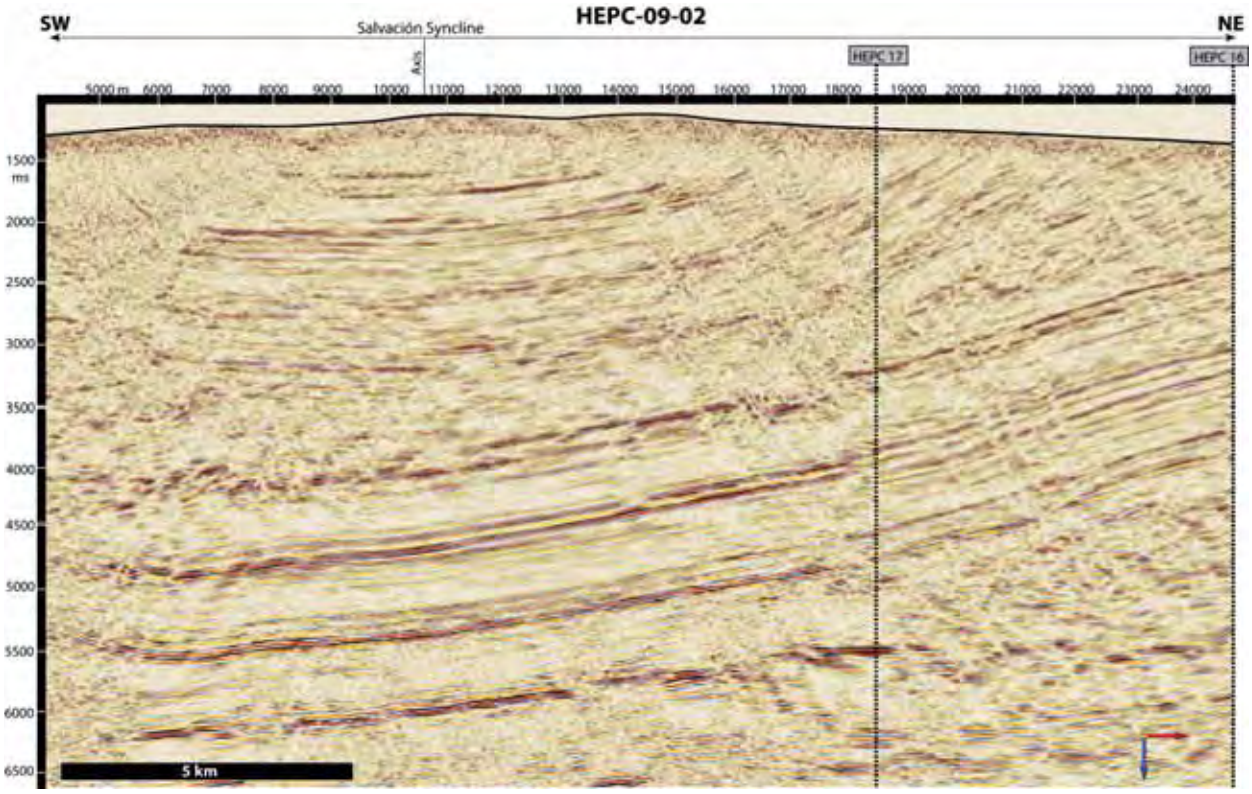

Figure 24: Seismic section Hepc-09-02. See Figure 12 for location.

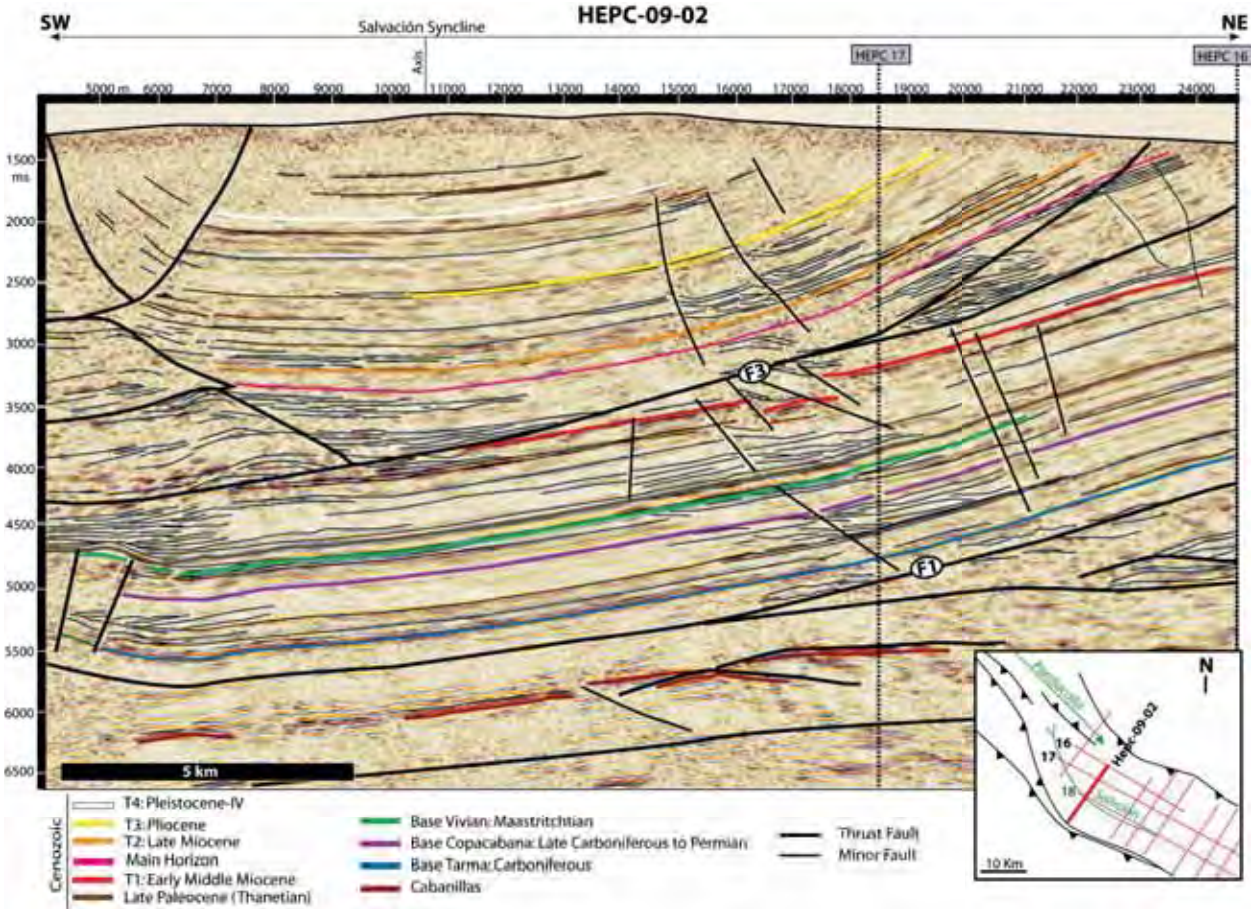

Figure 25: Interpreted seismic section Hepc-09-02. See Figure 12 for location.

4.1.3. Intra-Tertiary décollement

A part from the major Tambopata thrust fault (F1) and the possible Paleozoic horses situated below it, other brittle deformation structures have been interpreted. Based on seismic reflectors discontinuities and the main structural geometries visible on seismic, we propose a décollement level situated within the Middle Miocene sequence, situated between seismic markers T1 and T2. This décollement is referred as thrust fault F3 in this study (Figure 21). On seismic section Hepc-09-01, this décollement is almost invisible, even if some discontinuities are present between seismic markers T1 and T2 towards the surface (Figure 25).However, the décollement is clearly visible on seismic line Hepc-09-02 (Figure 24 and Figure 25) where F3 merged to the surface on a ramp. It seems connected to the duplex structure located at the south of the section.

Based on the only seismic sections Hepc-09-01 and Hepc-09-02, the unconformity observed between seismic markers T1 and T2 could be simply interpreted as a progressive unconformity linked to the syncline growth during Cenozoic times. However, strike seismic sections bring a pseudo 3D vision related to this surface. Indeed, seismic section Hepc-09-17 (Figure 26 and Figure 27) shows that the unconformity visible in Hepc-09-01 and Hepc-09-02 is most probably linked to a décollement level than a progressive erosive unconformity. According to seismic section Hepc-09-17, this level is situated at the base of the deformed syncline, and separates the “piggy-back” syncline structure from the underlying Paleozoic to Early Middle Miocene sequence (Figure 27). The eastern border of the Salvación syncline is thus deformed by thrust fault F3, situated below seismic marker T2. This thrust raises part of the Tertiary filling (mainly Late Miocene to Pliocene strata in this area) and is the principal cause of the piggy-back structure characterizing the Salvación syncline towards the east.

The Salvación synform structure is thus controlled by two important décollement levels: the main Tambopata thrust (F1) related to the Pantiacolla anticline towards the north and décollement level F4 which provokes the transport and deformation of the eastern part of the syncline (Figure 27). The “piggy-back” geometry deforming the syncline towards the north is visible on seismic lines Hepc-09-04, Hepc-09-05 and Hepc-09-06. In this study, we only propose to use the seismic section Hepc-09-04 (Figure 29 and Figure 30), in which the Late Miocene to Quaternary sequence forms a “piggy-back” syncline separated from the older sequences by the décollement level F3.

Towards the southeast of the Pongo de Coñeq area, décollement level F3 seems to branch on the roof thrust of a duplex. Composite seismic line presented in Figure 31 shows that the intra-Tertiary décollement level F3 is linked to this duplex structures which connects to the F1 sole thrust.. Décollement level F3 is one of the most important features of the area and it merges clearly visible on surface (see F3 on the colored DEM of Figure 11). It corresponds to the level of decoupling deformation between Cenozoic syn-orogenic series and pre-orogenic series (see interpretations of seismic line Hepc-09-04, Figure 30.

A 3D view of seismic sections Hepc-09-01, Hepc-09-02 and Hepc-09-16 is proposed in order to better visualize the main geometries and relationships existing between the main thrusts faults systems (F1 and F3) in the Pongo de Coñeq SAZ (Figure 32, Figure 33 and Figure 34).

4.1.4. Southern flank of the Salvación syncline

Southern part of seismic section Hepc-09-02 (Figure 25) is supposed to show the structures located below the Pongo de Coñeq Canyon area but seismic quality is poor and no unquestionable interpretation can be proposed. Poor seismic quality can be due to complicated or completely vertical structures. However, some stacked horses (two to three thrusts sheet?) can be deduced between 3000 and 4000 ms (Figure 24, Figure 25 and Figure 30). Is seems impossible to determine with absolute certainty the stratigraphic content of these thrust sheets as no indication or equivalent structure are available on surface. In this area, W. Gil's Pongo de Coñeq structural section shows several Ordovician thrust sheets involved in an important duplex system (Gil, 2001). This model indicates that the Salvación syncline is entirely transported by a thrust developing at the base of the Siluro-Devonian series. According to W. Gil's interpretation (2001), this décollement level corresponds to the roof-thrust of the Ordovician duplex system. However, according to new seismic line Hepc-09-02 (Figure 24 and Figure 25), the southern flank of the Salvación syncline which was formerly interpreted as entirely deformed and folded by a basal Paleozoic detachment level (Gil, 2001), seems finally to be characterized by more complex structural geometry. Two main interpretations remain:

1/ The vertical Paleozoic to Tertiary series outcropping in the Pongo de Coñeq Canyon can be simply and directly linked to the equivalent series outcropping in the Pantiacolla anticline following a simple transported syncline structure in depth as proposed in Gil's interpretation (2001).

2/ Another interpretation would be that the Pongo de Coñeq series corresponds to the short cut of a horse of the duplex system which occurred during an out of sequence propagation of hinterland thrusts.

In the synthetic structural cross-section proposed in this study (Figure 19), the vertical series outcropping in the Pongo de Coñeq canyon result from an out of sequence transported thrust sheet made up of Paleozoic to Early Tertiary deposits. Because this thrust sheet is the only outcropping structure available in this area, it can be considered as a possible transported cut of horse from the buried complex duplex situated below. Thus, we consider in this interpretation that the duplex is formed by several vertically stacked horses of Paleozoic to Early Tertiary (?) strata. The floor thrust is probably situated at the basement-Paleozoic interface, whereas the roof-thrust possibly develops within the Paleocene.

4.1.5. Pre- Late Miocene structures

Seismic section Hepc-09-04 (Figure 29 and Figure 30) displays different geometries than those displayed by seismic lines Hepc-09-01 (Figure 21) and Hepc-09-02 (Figure 25) situated northern ward. In section Hepc-09-04, the role of the intra-Tertiary décollement level is obvious as it induced the formation of an independent piggy-back syncline structure transported above the older strata. These older strata are also deformed and present a proper geometry including horses or fault bend fold structures (see interpretation of seismic lines Hepc-09-04, Figure 30). According to the new stratigraphic framework, these structures are most probably pre- Late Miocene in age as they are partially sealed by seismic marker T2. These newly described horses or ramp-anticline structures are of first importance in terms of oil and gas exploration in the Madre de Dios SAZ as they form perfect traps for hydrocarbon accumulation migrating from deeper Paleozoic source rocks.

Because deformation is probably less intense in the northern Madre de Dios SAZ, these structures are not documented in seismic sections Hepc-09-01 (Figure 21) and Hepc-09-02 (Figure 25). Because of this reduced pre- Late Miocene deformation in the north and because the intra-Tertiary décollement level (F3) is parallel to the stratigraphy, the two stratigraphic sequences which are disconnected towards the south (Hepc-09-04) appear to be conformably vertically stacked in seismic sections Hepc-09-01 and Hepc-09-02 toward the north. However, even in this northern area, the Paleozoic to Early-Middle Miocene (?) sequence is disconnected from the Late Miocene to Quaternary series by the Intra-Tertiary décollement level (F3).

4.1.6. Secondary faults and fractures

Finally, several secondary faults developed within the Paleozoic to Paleogene sedimentary sequence in the northern flank of the Salvación syncline, provoking slight offsets as interpreted in seismic section Hepc-09-01 (Figure 21). Several other secondary faults are also present within the whole sedimentary filling of the Salvación syncline. These small-scale structures can be important in terms of hydrocarbon potential appraisal in the Pongo de Coñeq area. As a matter of fact, several oil seeps have been discovered on surface around the Pantiacolla area (confidential reports) and can be easily interpreted as surface resurgences of hydrocarbon fluid migrating across the faulted net developed within the Pantiacolla southern flank from the Paleozoic (source rocks). Seismic line Hepc-09-02 also shows this fractures network (Figure 25).

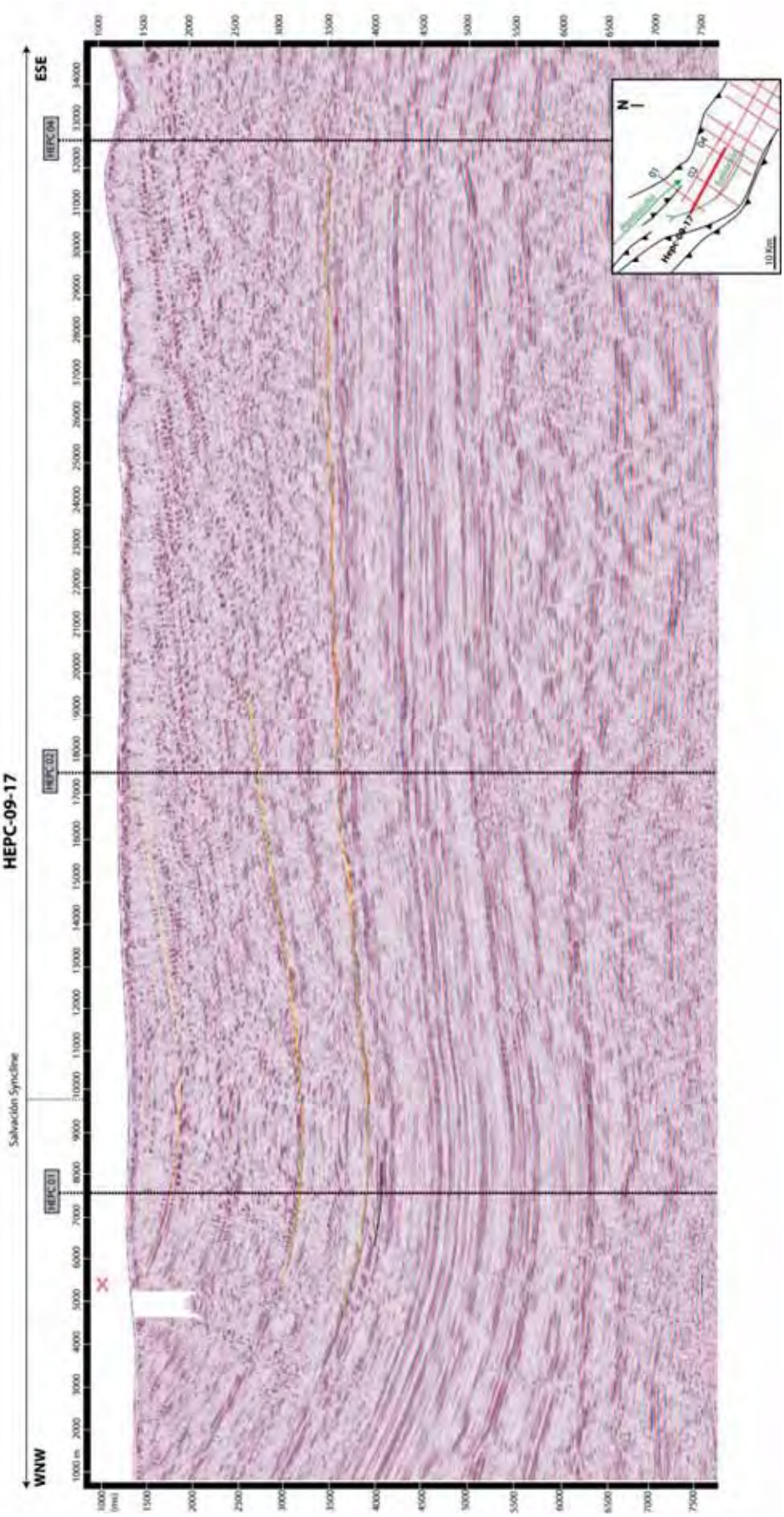

Figure 26: Seismic section Hepc-09-17. See Figure 12 for location.

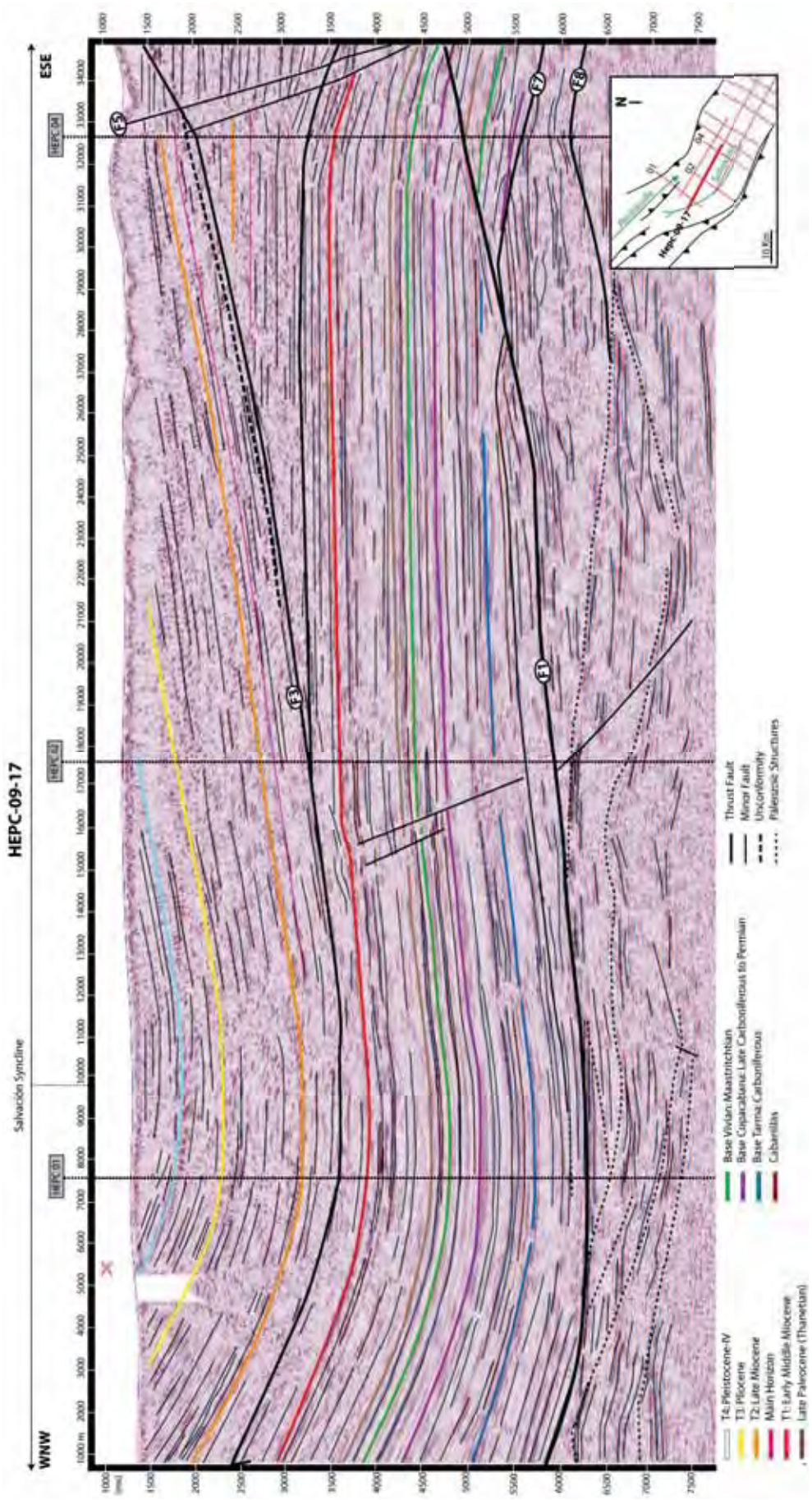

Figure 27: interpreted seismic section Hepc-09-17. See Figure 12 for location.

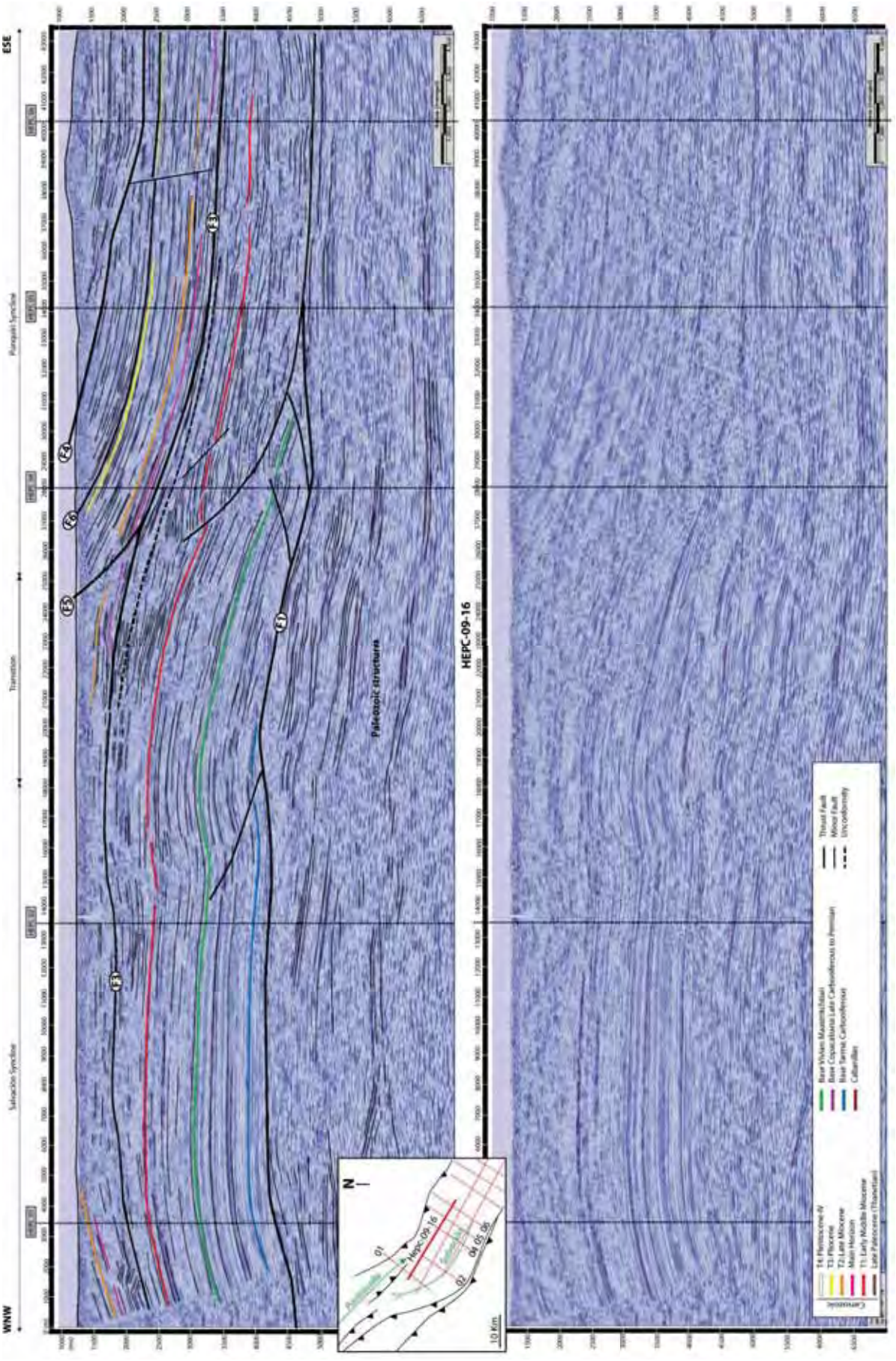

Figure 28: Non-interpreted (below) and interpreted (above) seismic section Hepc-09-16. See Figure 12 for location.

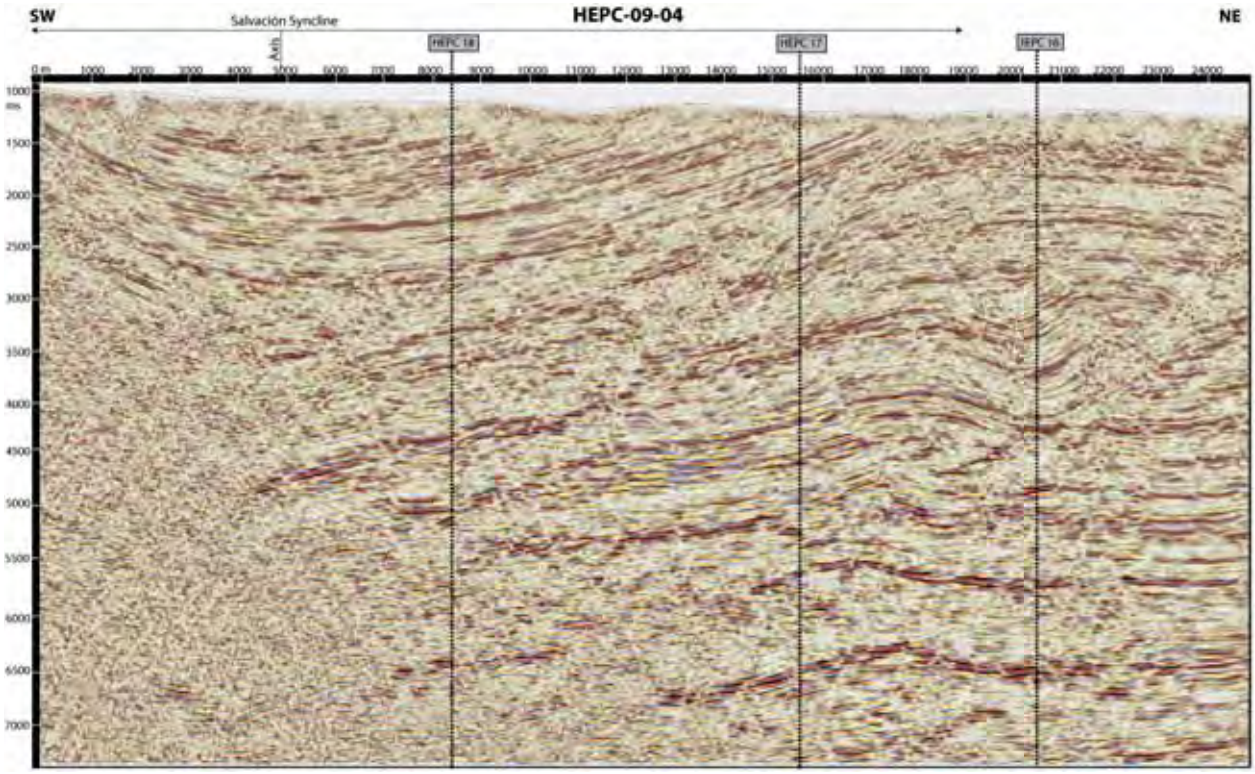

Figure 29: Seismic line Hepc-09-04. See Figure 12 for location.

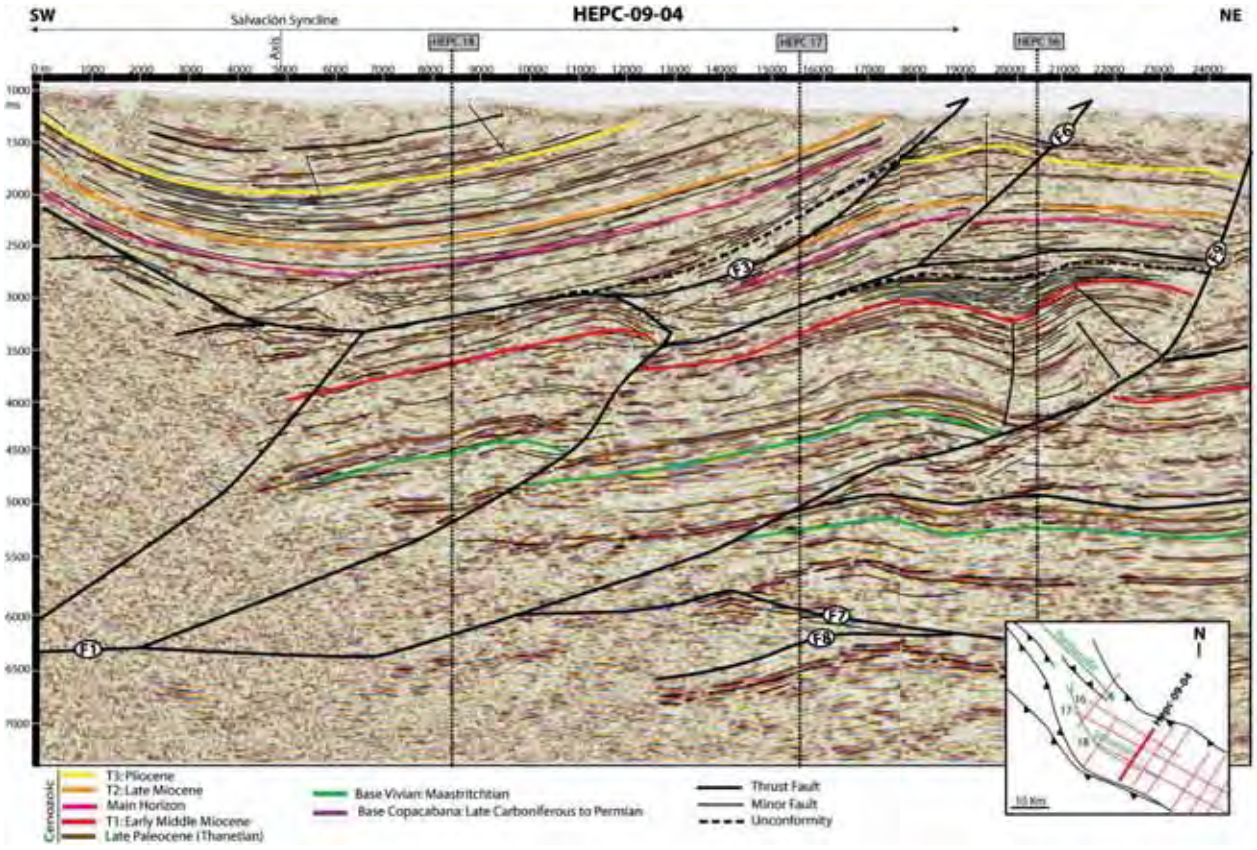

Figure 30: Interpreted seismic line Hepc-09-04. See Figure 12 for location.

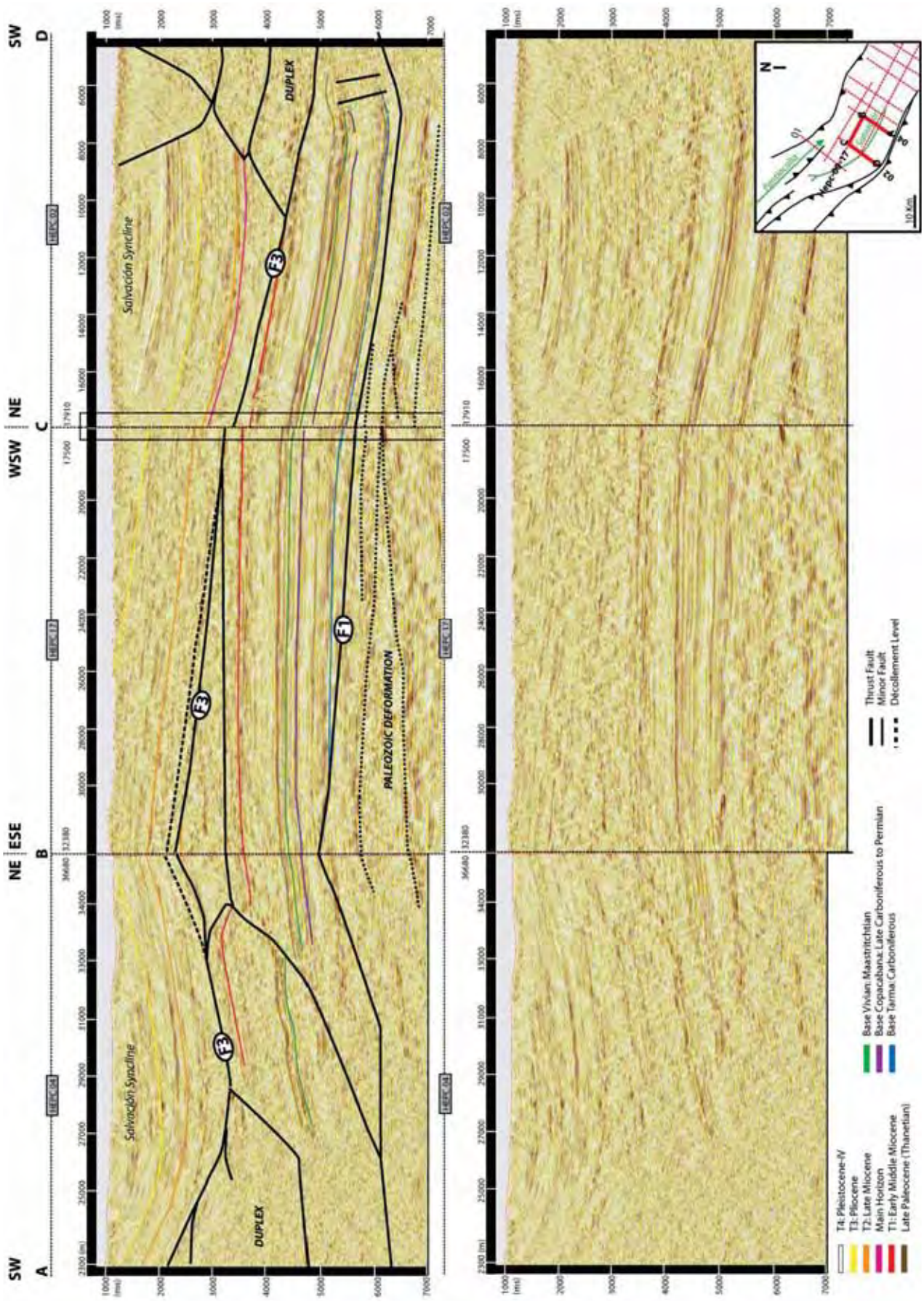

Figure 31: Non-interpreted (below) and interpreted (above) composite seismic sections (Hepc-09-04, Hepc-09-017-Hepc-09-02). See Figure 12 for location.

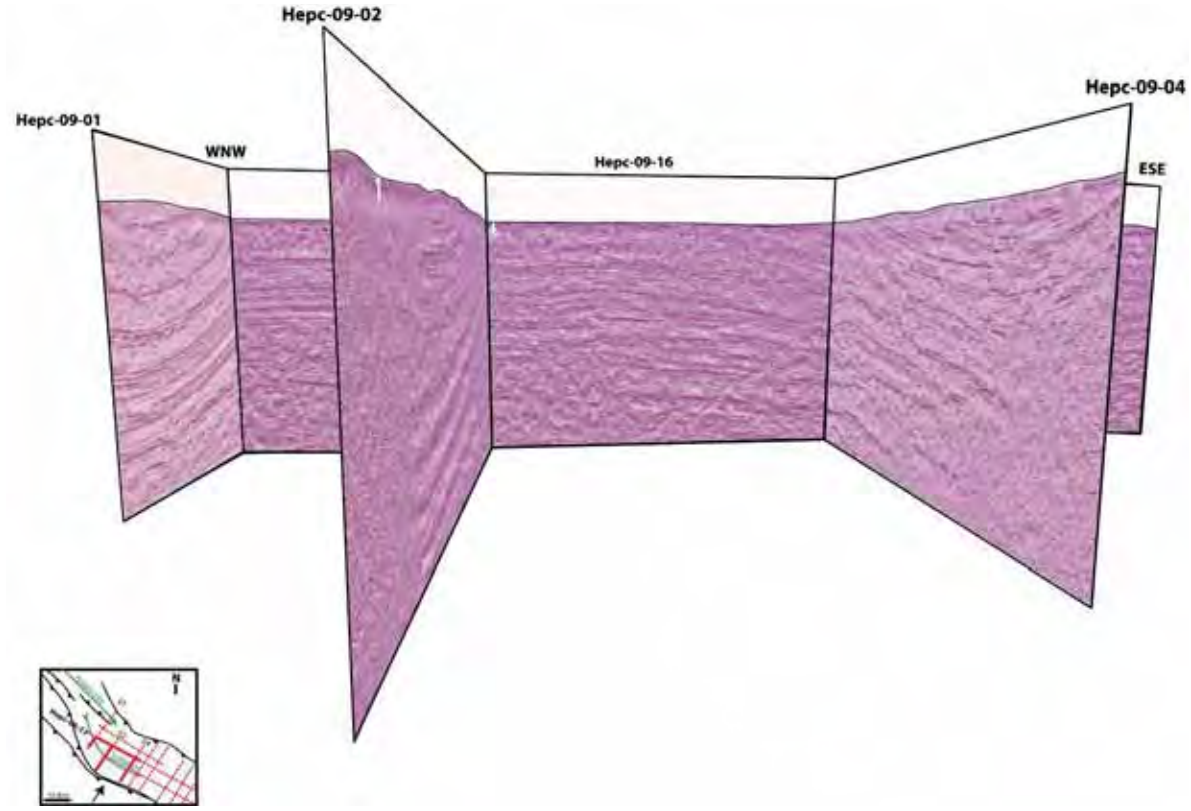

Figure 32: Non-interpreted 3D view of seismic sections Hepc-09-01, Hepc-09-02 and Hepc-09-16. See Figure 12 for location.

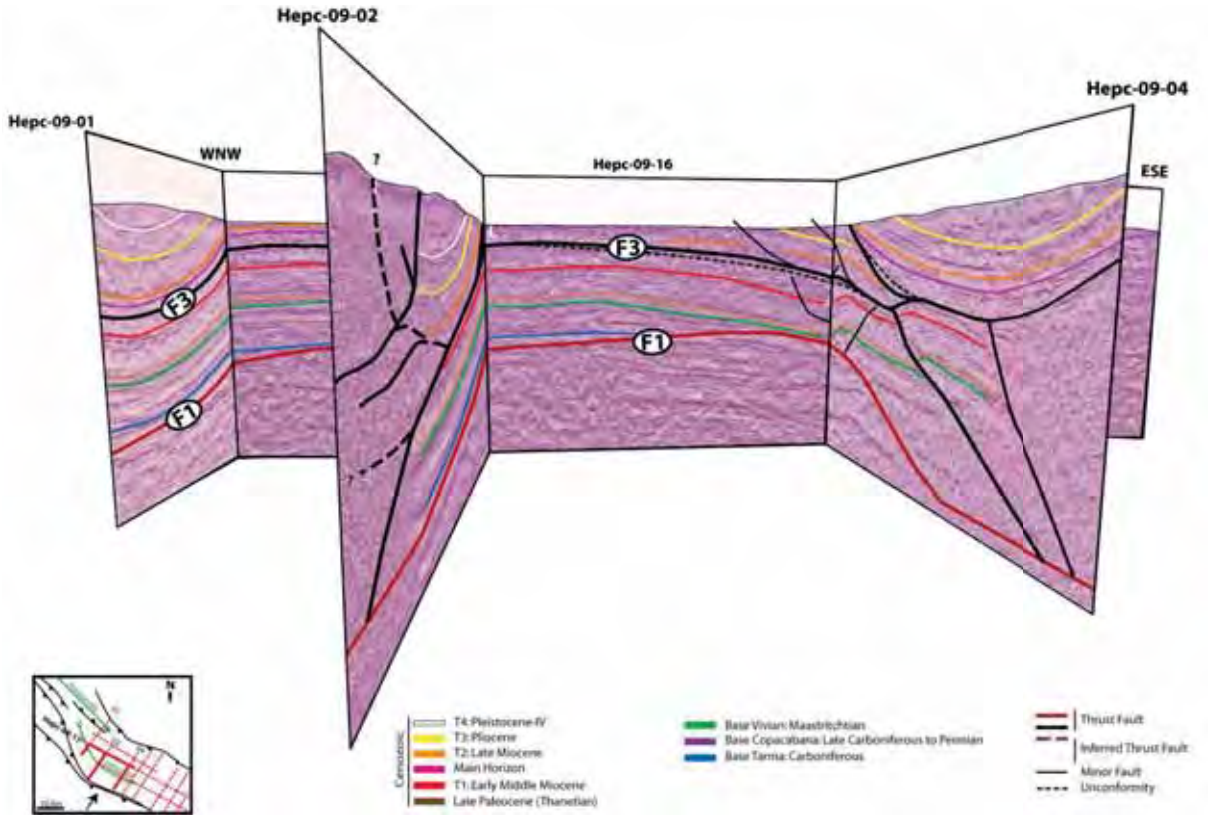

Figure 33: 3D view of interpreted seismic sections Hepc-09-01, Hepc-09-02 and Hepc-09-16. See Figure 12 for location.

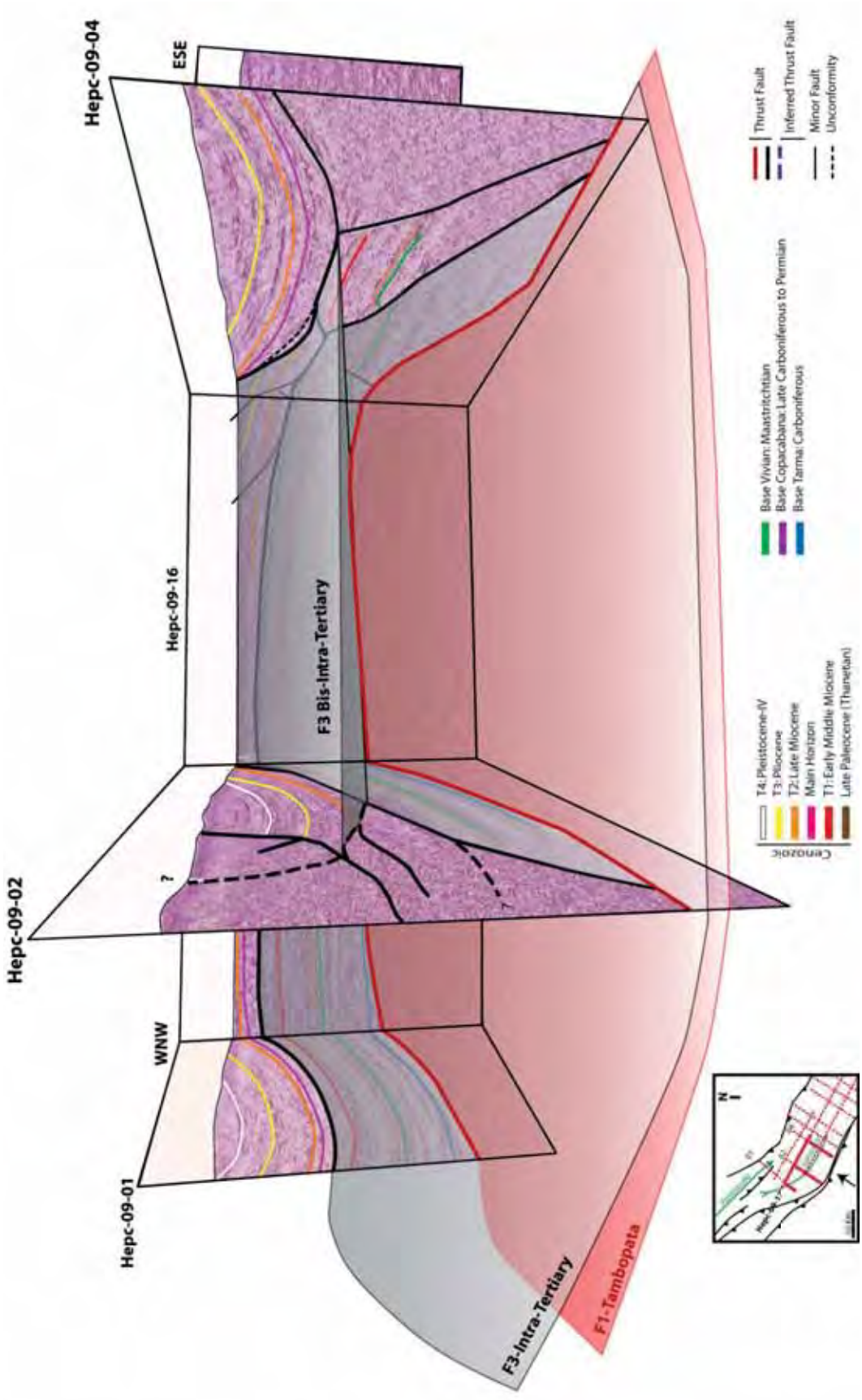

Figure 34: Interpreted 3D view of seismic sections Hepc-09-01, Hepc-09-02 and Hepc-09-16. Red surface corresponds to the décollement level of Tambopata Thrust (F1). Both grey surfaces correspond to the intra-Tertiary décollement level.

4.2. Inambari area

Before presenting the new version of the balanced and restored Inambari cross-section (Figure 42), we will first discuss the décollement levels issues and try to resolve it based on former studies interpretations (W. Hermoza's cross-section, Figure 35) and new field data observations for comparison (Figure 36 to Figure 39).

4.2.1. Décollement levels issues

4.2.1.1. Former studies

On a regional scale, several décollement levels are traditionally determined from the mechanical stratigraphy of the Ucayali-Madre de Dios SAZ.

In the Ucayali Basin, situated at the north-western border of the Madre de Dios basin (Figure 5), thick-skinedd tectonics with basement detachment provoked the uplift of different structural highs such as the Shira Mountain (Espurt et al., 2008). Similar detachment level does not exist in the basement of the Madre de Dios SAZ and is attested by seismic data. The basement-Paleozoic sediments interface situated at the base of the Ordovician unit is interpreted as the main décollement horizon within the SAZ of southern Peru by W. Gil (2001), W. Hermoza (2004) and Gotberg et al. (2010). This décollement level corresponds to the sole thrust of the Subandean thrusts wedge (Figure 42).

Note that Gotberg et al. (2010) interpret a major detachment horizon in a shale layer located in the middle of the Silurian-Devonian units. An intermediate décollement level is also proposed at the Cabanillas/Ambo interface or within the Ambo formation in the Ucayali-Camisea basin (Espurt et al., 2008). In the Madre de Dios basin, the floor-thrust of the internal duplex (Figure 35) seems to develop within the basal shale of the Carboniferous Ambo formation.

Next décollement levels have been problematic for a long time, and concerns: i) the deformation of the Imbricate thrust system outcropping in the Inambari area ("Imbricates" in Figure 35), and ii) the geometry of the buried complex duplex only visible on seismic lines (well displayed in the Inambari section, see the "Internal Duplex" in Figure 35).

- W. Gil (2001) considers that:
    - The buried internal duplex is constituted by Ordovician strata (San Jose, Sandia and San Gaban formations), with a floor-thrust situated at the base of the Ordovician series just above the basement and a roof-thrust situated at the base of Ene shale formation. The external part the duplex has a different roof thrust developed at the base of the Tertiary.
    - The imbricate thrust system outcropping in the Inambari SAZ is constituted by Late Permian to Cretaceous strata and the branch on the roof thrust of the internal duplex (Ene shale).
- Thanks to new field and subsurface data, W. Hermoza (2004) updated the structural model of the Madre de Dios SAZ and changed the interpretation of the internal duplex visible in the Inambari regional section (Figure 35). The only major difference with Gil's interpretation concerns the stratigraphic content of the internal duplex horses, which are replaced by Ordovician and Siluro-

Devonian strata in Hermoza's interpretation (Figure 35). The floor-thrust and the roof-thrust related to the internal duplex structure are still interpreted at the base of the Ordovician strata and at the base of the Ene shale formation, respectively.

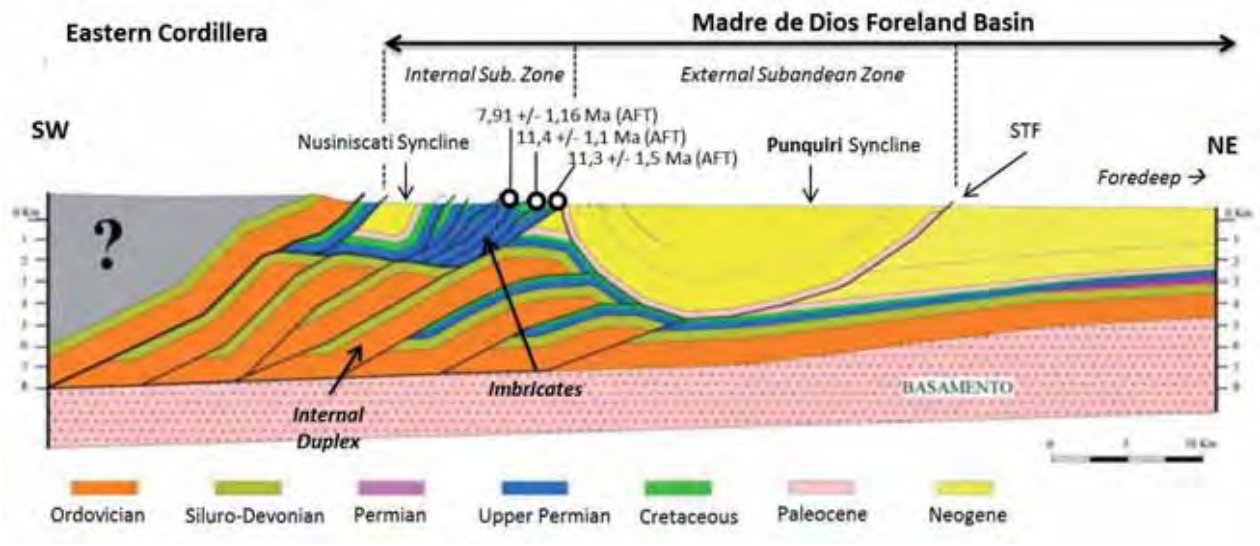

Figure 35: Inambari regional structural cross-section from Hermoza (2004). See location of the section in Figure 6, section B.

In our interpretation, the sole thrust of the Subandean wedge propagated first in the Ambo shale, then in the Cretaceous deposits before emerging with the Tambopata thrust (Figure 42). We agree with the uppermost décollement level situated at the Late Cretaceous-Lower Tertiary interface and traditionally interpreted by W. Gil (2001) and W. Hermoza (2004) as the roof thrust of the external duplex. This décollement level limit the southern border of the piggy-back structure of the Punquiri syncline transported on the Sub-Andean Thrust Front (STF) emerging in the northern Madre de Dios plain (Figure 35).

Based on recent structural field work, we propose in this study a new interpretation of the internal complex and the imbricate thrusts system visible on the main Inambari regional cross-section (Figure 42). We consequently propose to relocate the detachment level formerly situated within the Permian Ene shale formation within the Late Cretaceous series, as we consider Permian deposits to be absent of the Madre de Dios SAZ.

4.2.1.2. Imbricates geometry and stratigraphic content

According to the Digital Elevation Map model and the structural observations we made on surface in the Inambari SAZ, part of this area seems to be characterized by several closely related north-east vergent thrusts faults developing between the Nusiniscati and the Punquiri synclines (Figure 36). The overall structure has probably been uplifted and eroded through time, creating an eroded structure visible today. This imbricate system is best exposed south of the Inambari Bridge, but seems to extend towards the north-west (~20 km) and towards the south-east near Candamo well district (Figure 6). The Imbricate system is limited at the north by the south-west vergent back thrusts developing within the southern flank of the Punquiri syncline (Figure 36).

The main Inambari balanced cross-section proposed in this study (Figure 42) is located west to this complex area and crosses over 4 imbricates thrust sheets (see imbricates 3.1., 3.2., 3.3 and 3.4, Figure 36) according to the dip data measured along the seismic section by MOBIL's geologists and according to the 2D spatial distribution of thrust faults (DEM interpretation, Figure 11). Laterally towards the east, imbricates nº 3.1 corresponds to the complex area situated just before the Inambari Bridge and highlighted by a white rectangle. An enlarged view of this structurally complex area is displayed in Figure 35 and is characterized by several NW-SE oriented thrusts which are closely related as they are separated from each other from less than 500 m in some cases.

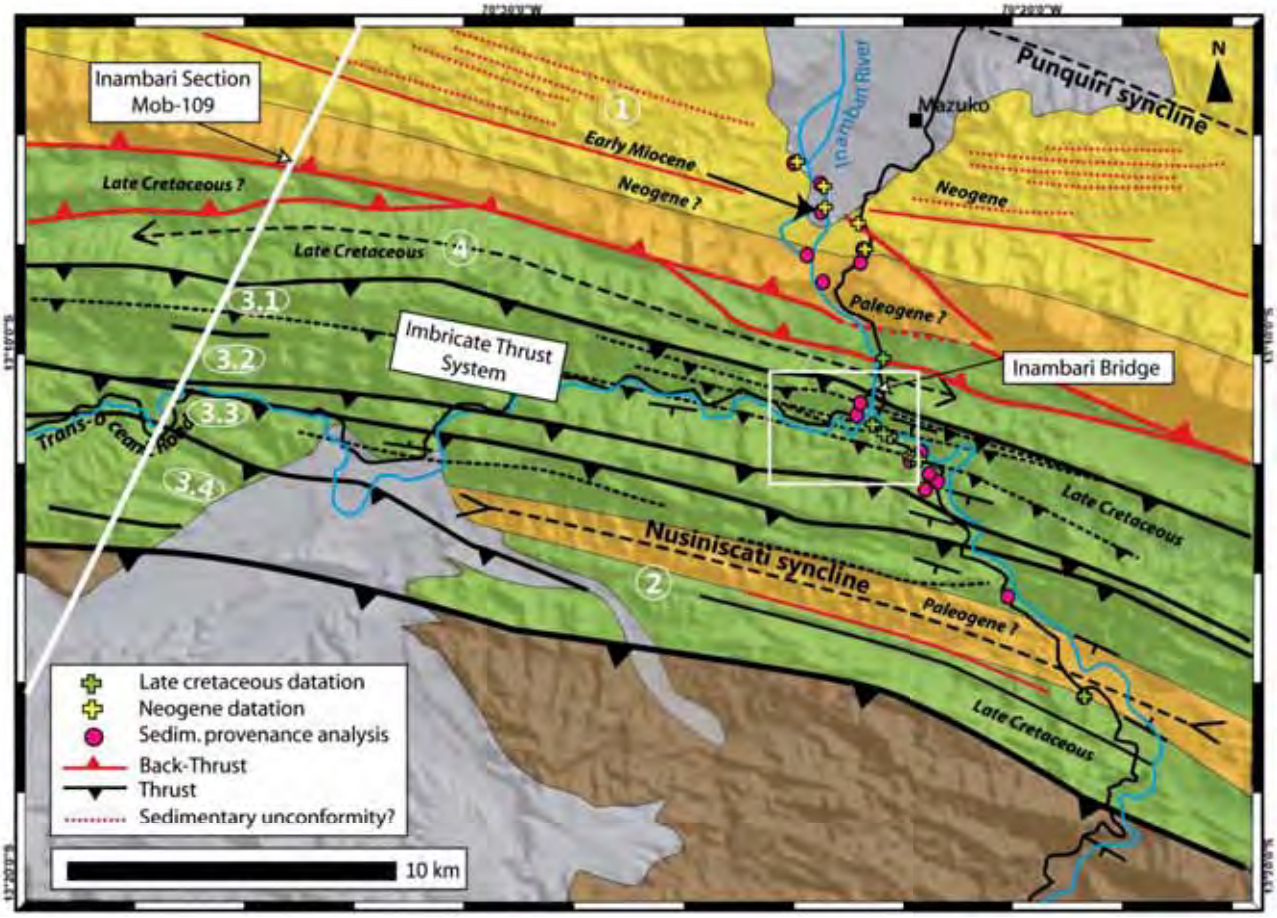

Figure 36: Geological map focused on the Inambari area, Madre de Dios SAZ. Numbers corresponds to those of Figure 43. White rectangle corresponds to the location of Figure 37.

Structural field observations realized in this complex area (Inambari bridge area) constitute a unique chance to understand and to detail the complex internal organization of each individual imbricates structures we interpreted much more eastwards for the balanced cross-section (main structures 3.1 to 3.4). The observations we made around the Inambari Bridge area have been mapped and are shown in Figure 37 and Figure 38. In Dip data, biostratigraphic results and lithological main characteristics are displayed. Thrusts sheets have been interpreted thanks to DEM interpretation and field mapping.

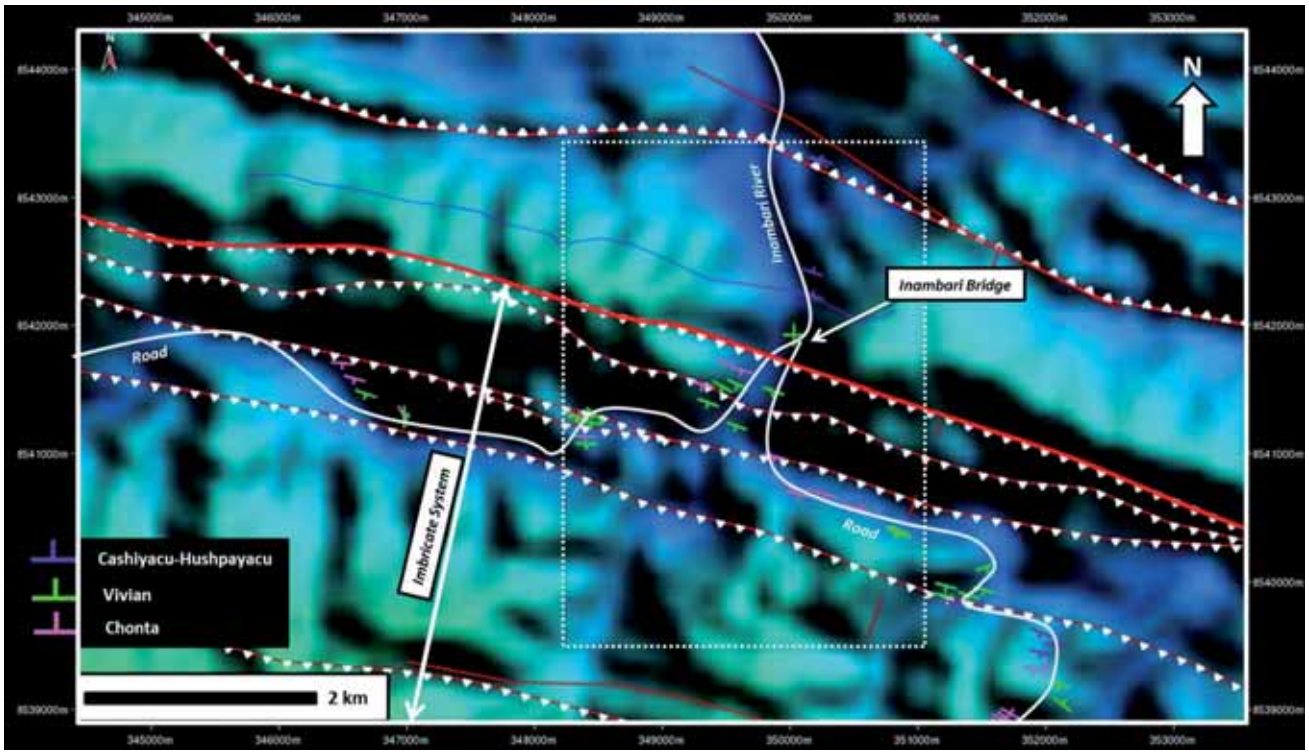

Figure 37: Map focused on the Inambari Bridge area and part of the Imbricate thrust system (Move dataset). The white rectangle (dashed line) corresponds to the location of Figure 38. Thrusts sheets situated south of the Inambari Bridge and within this dashed rectangle correspond laterally to one imbricate content (Imbricate nº3.1 in Figure 36).

Stratigraphic content of the thrust sheets:

Formerly interpreted to be made up of Late Permian and Cretaceous strata (Gil, 2001; Hermoza, 2004), new biostratigraphic constraints indicate that the imbricates are only composed by Cretaceous series (Figure 38). Indeed, the fluvio-estuarine deposits of the Late Cretaceous Chonta formation (Turonian to Santonian in age) and the Vivian formation (Campanian to Maastrichtian in age) have been documented all along the road from the Inambari Bridge toward the south (see Figure 38). No Permian facies (possible black shale or fluvio-aeolian deposits of the Ene formation) have been recognized. Deposits outcropping along the Inambari River just below the Inambari Bridge and north to this location show more distal facies in comparison with those of the Vivian and the Chonta formations. They are likely to correspond to shallow marine or tidal deposits, and may be related to Cashiyacu and/or Huchpayacu Late Cretaceous to Early Paleocene formations (mapped in violet in Figure 38). However, no stratigraphic constraints exist for these deposits as they yielded no useful material to date in this area.

South to the Inambari Bridge, we realized a sedimentary section across thrust sheet “A” which is part of the bigger Imbricate structure 3.1 (Figure 38, from point A to point B). The section starts with some shale deposits which are certainly related to the detachment level of the main thrust located near point A. Then, the section evolves into 80-m thick succession of fine-grained trough cross-bedded sandstones intercalated with shale deposits and some carbonate layers. Breccia deposits have also been observed within this unit. Possible Cretaceous palynomorphs have been yielded in the fine-grained strata at the base of this section (MD 261, Figure 38 and Table 1). Deposits are then cut off by an erosive angular unconformity (~10º), which

is overlain by 5 to 20 m -thick beds of medium- to coarse-grained quartzitic sandstones. Below the erosional surface, deposits probably correspond to the Late Cretaceous Chonta Formation. The overlying erosive tidal sandy packages are characteristic of the Vivian formation. The first thrust sheet documented here is then~200 m-thick and is made up of Late Cretaceous mostly sandy deposits from the Chonta and the Vivian formations. This sequence is repeated in each of the thrust sheets interpreted south to the Inambari Bridge (thrust sheets A to E, Figure 38). Finally, the presence of opposite dip data and very well outcropping Late Cretaceous folded structures both indicate additional complex internal structure in these thrust sheets.

Based on the detailed sedimentary and structural observations we realized on the field around the Inambari Bridge, we argue that:

i. Imbricates structures as interpreted in the Inambari regional balanced cross-section (Figure 42) correspond to main thrust faults and main geomorphological features on map (Figure 11 and Figure 36), but are clearly more complicated structures in details (Figure 38).
ii. There are some spatial differences in the structural geometry of the imbricate thrusts system. Each individual imbricate structure can be potentially made up of various stacked thrust sheets at smaller scale. For example, the main imbricate structure 3.1 corresponds laterally to four stacked smaller thrust sheets (thrust sheets A to D, Figure 37).
iii. Each of these thrust sheets is likely to contain majorly Late Cretaceous Chonta and Vivian strata, according to the sedimentary observations and the biostratigraphic constraints obtained in the Inambari Bridge area suggesting a Turonian to Maastrichtian age interval (Figure 38 and Table 1).
iv. Based on our sedimentary observations realized north to the Inambari Bridge, we also suggest the presence of the Late Cretaceous to Early Paleocene Cashiyacu and/or Huchpayacu formations in the anticline structure nº4 (Figure 36 and Figure 38).

According to these statements, it is thus very probable that the Imbricate thrust system is entirely made up of Late Cretaceous deposits, with a basal décollement level situated within the shaly facies of the Chonta formation.

Based on additional field observations made in the southern Inambari SAZ, we constructed a synthetic sedimentary column that is representative of an individual imbricate stratigraphic content (Figure 39). We finally propose that a classical imbricate thrust structure is more than 700 m –thick and that it is composed of mainly Late Cretaceous deposits (Chonta, Vivian, Huchpayacu and Cashiyacu formations). The imbricate-thrust system is characterized by a basal décollement level located at the base of the Chonta formation (Figure 38). Note that additional local décollement level can be interpreted within the Huchpayacu-Cashiyacu formations. The stratigraphic content of one Inambari imbricate can be duplicated and repeated due to such local décollement activity. This can explain the greater thicknesses of the imbricates structures interpreted in the Inambari balanced cross-section (Figure 42) in comparison with the 700m-thick synthetic section proposed here (Figure 38).

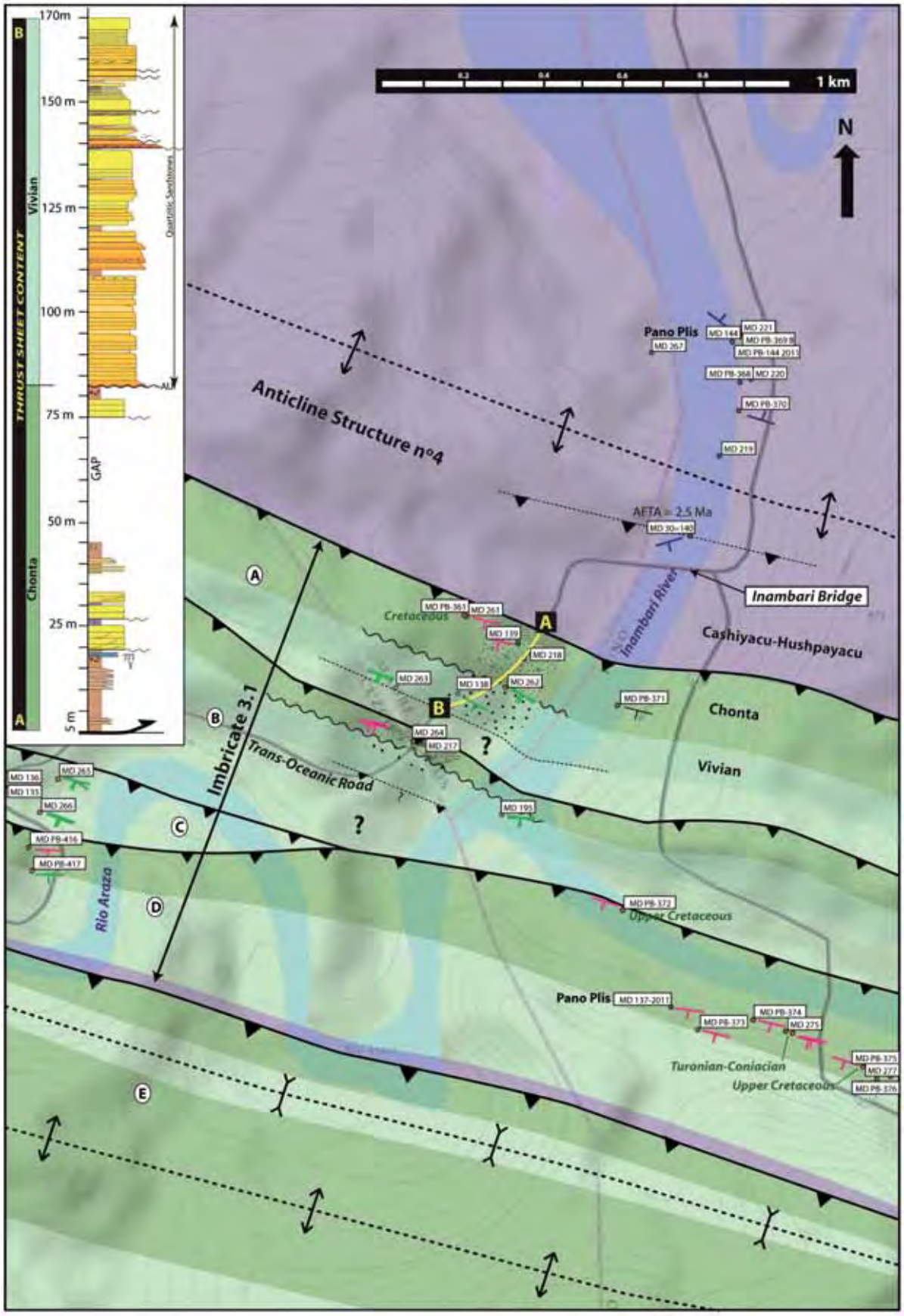

Figure 38: Geological map of the Inambari Bridge area realized from new structural, sedimentary and biostratigraphic constraints (see Figure 37 for geographic location). Sedimentary section has been realized from point A to point B south of the Inambari Bridge (yellow bold line).

Sample	Geological_Age	Depositional Environment	Specific Foram-Pollen associations for marine-influenced environements.	Location
MD 221	no age	Undetermined, continental?		SAZ- Imbricates
MD 125-2011 A	no age	Continental? No marine/ brackish element.	*Cyatheacidites annulatus? Striatriletes cf. saccolomoides*	SAZ- Nusiniscati syncline
MD 125-2011 B	no age	Continental? No marine/ brackish element.	*Psilatriletes spp. ; Pediastrum spp*	SAZ- Nusiniscati syncline
MD 302 Bio	Turonian to Coniacian	Bay or estuary. Strong freshwater influence	*Ostracodes (a lot) ; Ovocytheridea sp.*	SAZ- Imbricates
MD 309 Bio A	Late Cretaceous	Marine, high energy.	*Ostracodes: Cytheráceos; Cythereis sp. ; Bisulcocpris sp.*	SAZ- Imbricates
MD 275 Bio	Turoniao-Early Coniacian?	Marine	*Planctonic Foram.: Globotruncanidae and Helvetoglobotruncana*	SAZ- Imbricates
MD 280 Bio	Cenomanian?	Coastal, tidal?	*Benthic foram. (reworked)*	SAZ- Imbricates
MD 281 Bio (Dino)	Cenomanian	Shallow marine, anoxic floor (internal platform?)	*Planctonic Foram.: Guembelitria cretacea (Cushman, 1933), Rugoglobigerina rugosa (Plummer, 1926); Hedbergella holmdelensis Olsson, 1964; Archaeoglobigerina blowi Pessagno, 1967 Heterohelix globulosa (Ehrenberg, 1840); Benthic Foram.: Haplophragmoides walteri (Grzybowski, 1898); Haplophragmoides sp.; Rzehakina epigona (Rzehak, 1895); Silicosigmoilina sp.; Trochammina sp. Diatomea ? Others: Neocythere sp. (ostracode); Spicul*	SAZ- Imbricates
MD 282 Bio	Cenomanian-Turonian	FORAM: Estuarine. Mix of brackish and marine waters. PALY: Marine??	*Dordoniella sp., Cytherella sp., Isocythereis sp., Cythereis sp., Protocythere sp. y Timiriasevia sp. Dinoflagellates ?*	SAZ- Imbricates
MD 136-2011	no age	Undetermined, continental?		SAZ- Imbricates
MD 309 Bio A2	Late Cretaceous	Marine, high energy.		SAZ- Imbricates
MD 309 Bio B	Late Cretaceous	Quiet shallow marine water, shallower than 309 BIO A. Ostracodes badly preserved (tectonism?)	*Cytheracae Ostracodes: Cythereis sp., Bisulcocpris sp.*	SAZ- Imbricates
MD 309 Bio B2	Late Cretaceous	Quiet marine water, shallower than 309 BIO A	*Cyterelloidea, Bivalve*	SAZ- Imbricates
MD 270 Bio A	no age	Continental?	*Azolla type; Psilatriletes spp. Polen: Retitricolpites spp.;*	SAZ- Imbricates
MD 290 Bios	no age	Coastal, Tidal	*Benthic foram.: Silicosigmoilina Cushman & Church, 1929*	SAZ- Imbricates
MD 368	Maastrichtian?	Reductor context. Internal marine platform	*Reworked benthic foram.; Clavulina cf. clavata Cushman, 1926*	SAZ- Imbricates
MD 372	Upper Cretaceous?	Littoral. Bay or estuary.		SAZ- Imbricates
MD 375	Upper Cretaceous?	Littoral. Bay or estuary.	*Ostrácodos ; Ovocytheridea sp.*	SAZ- Imbricates
MD 6K	Cenomanian??	Coastal-Tidal?	*Foram.: Whiteinella sp. ?; Isocythereis? Algae: Carophyte. Paleonto.: Pelicipodes; Inoceramidus, Xilopale*	SAZ- Imbricates
MD 301 Bio	no age	Continental ??		SAZ- Imbricates
MD 318	no age	Marine, littoral	*Foram.: Saccammina sphaerica Brady, 1871*	SAZ- Imbricates
MD 318 Bio	no age	Coastal swamp, saline influence.	*Foram.: Sacamminidae*	SAZ- Imbricates
MD 261 Paly	Cretaceous?	Proximal Marine, Coastal	*Reworked benthic foram.: Glomospira Rzehak, 1888*	SAZ- Imbricates

Table 1: (Previous page) Biostratigraphic results in the Inambari area and the Nusiniscati syncline. Samples collected in the Punquiri syncline are not shown in this Table. For more details, see supplementary dataset (*Annex n°2*)

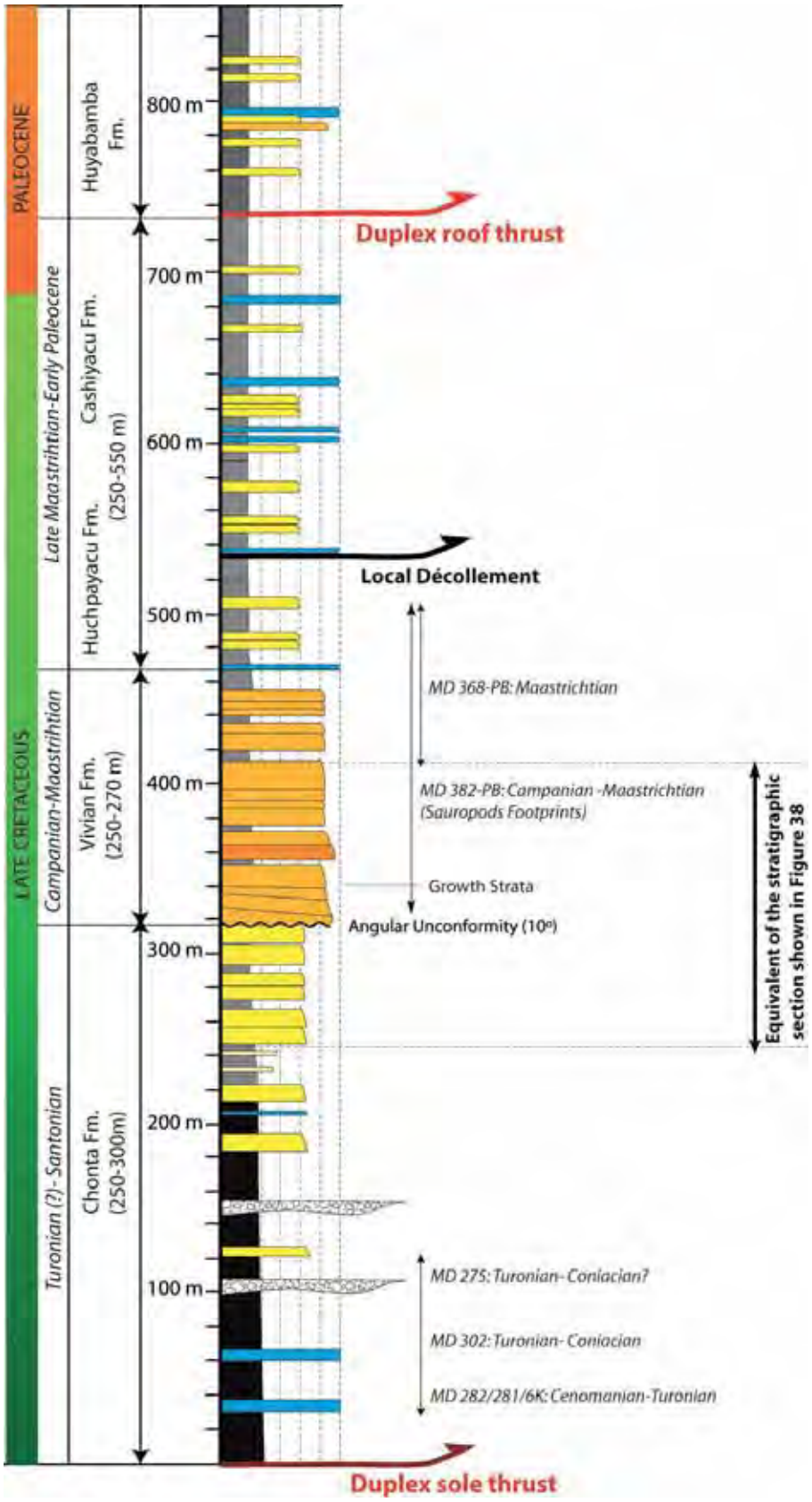

Figure 39: Synthetic sedimentary section presenting the stratigraphic content of one imbricate thrust sheet in the Inambari area. Biostratigraphic results are indicated as well as their corresponding locality number.

4.2.2. Balanced cross-section

The balanced and restored cross-section of the Inambari main regional section is presented in Figure 42. Figure 43 corresponds to an enlarged view of the structural cross-section focusing on the EC and the SAZ. This figure can also be consulted in the Annexes-Figure H for a more comfortable viewing

The NE flank of **the Punquiri syncline** (Figure 43, tectonic unit nº1) constitutes the front of the Andean deformation, materialized by the Sub-Andean Thrust Front (STF) or the Tambopata thrust (Gil, 2001; Hermoza, 2004). The Punquiri syncline is made up of Paleogene (?) to mainly Neogene sedimentary deposits. Its southern flank is uplifted and deformed on the passive roof thrust (base Tertiary) of the external duplex which emerged between Mazuko locality and the Inambari Bridge. The Punquiri syncline is interpreted as a piggy-back basin structure transported passively on the duplex and actively on the Tambopata thrust. A complete sedimentary study of the Tertiary sedimentary filling of the Madre de Dios basin is proposed further (see Parts B, C and D of this manuscript).

At the opposite southwest end of the section, the **Nusiniscati syncline** (Figure 43, tectonic unit nº2) is mainly made up of Late Cretaceous to Paleocene (?) strata (only Late Cretaceous biostratigraphic results, see above). The southwest flank of the syncline is directly cut by the main Azulmayo thrust which transports the EC towards the northeast. The faulted contact is clearly visible at the Antiocus Bridge locality (MD 319) along the Juliaca-Puno road, were Ordovician strata overthrust the Late Cretaceous-to Paleocene (?) deposits of the Nusiniscati syncline. The Nusiniscati syncline is a structure transported in the Inambari Imbricate system.

An imbricate thrust system is a structure formed by the stacking of two or more thrust sheets and are common in fold-and-thrust belts worldwide (Boyer and Elliott, 1982; Dahlstrom, 1969; McClay and Price, 1981; Price, 1986; Shaw et al., 1999). Such structures need closely related branching array of thrusts such that the thrust sheets overlap like roof tiles (McClay and Price, 1981). Each thrust sheet unit situated between two successive thrust faults is called an “Imbricate” sensu McClay (1981).

The Imbricate thrust system of the Inambari SAZ is outcropping in the Imbricate Area (IA) situated between the Nusiniscati and the Punquiri synclines (Figure 43, tectonic unit nº3). Our structural section shows four imbricates or thrust sheets all branched to the same floor thrust already interpreted for the Nusiniscati syncline and situated within the Late Cretaceous series. The imbricate system is eroded in surface and forms an Imbricate Fan sensu McKlay (1981) in depth. Each Imbricate is ~1000 to ~1300 m-thick according to our structural section. However, field observations made east of the seismic line along the Inambari River and along the road (this study) indicate that the imbricate system becomes more complex to the south.

North to the imbricate thrust system, dip data suggest an outcropping Late cretaceous **thrust-related fold** structure known as the “Inambari anticline” (Figure 43, tectonic unit nº4). In map view (DEM), west of the main section, this folded structure disappears below the Punquiri’s back-thrusts (Figure 36). This folded thrust sheet, dipping towards the foreland, is probably characterized by the same stratigraphic content than the western imbricates: mainly Late Cretaceous strata.

The Imbricate thrust system and the Punquiri piggy back basin both accommodate in surface deeper deformation characterized by the development of a complex area made up of two stacked or superimposed duplexes (the internal and external duplexes) as well as several basement-involved thrust structures.

The internal duplex (Figure 43, tectonic unit nº5) is situated below the Inambari anticline and the backthrust of the southern flank of the Punquiri syncline and is well displayed by seismic data in depth (Figure 40). It is formed by several overlapping ramp anticlines. The floor thrust of the duplex is situated within the Paleozoic series, probably at the base of the Ambo formation. The roof thrust is located within the Late Cretaceous unit, probably within the Chonta formation. More to the west, it connected to the imbricates system. The individual horses are stacked up on top of each other such that they form an antiform. The resulting structure is called an *antiformal stack* sensu McKley (1981), which corresponds to a passive roof duplex geometry (Jamison and Pope, 1996), generally linked to a complex Triangle Zone structure as described in the Bolivian Subandes (Baby et al., 1992), the Argentinean Sub-Andes (Echavarria et al., 2003a) and the Alberta foothills (Lawton et al., 1994). The duplex seems is displaced by an out of sequence thrust that emerges in the Punquiri syncline.

The external duplex is also a passive roof duplex. It is situated above the internal duplex and just below the Punquiri syncline (Figure 43, tectonic unit nº6). The floor-thrust of the external duplex corresponds to the roof-thrust of the internal duplex, situated within Late Cretaceous strata (probably at the base of the Chonta formation). The roof-thrust of the duplex corresponds to the basal part of the Tertiary (Paleogene?) series, which also forms the Punquiri's back-thrust. Presently, this external duplex appears to be deformed by the reactivation of the internal duplex.

Below the imbricates system, the basement of the EC is involved and constitutes the back-stop of the duplexes. It is transported on the décollement formed by the Ambo shale (Figure 43, tectonic unit nº7). This back-stop is made up of a basement rocks and Paleozoic to Late Cretaceous deposits (~8 km).

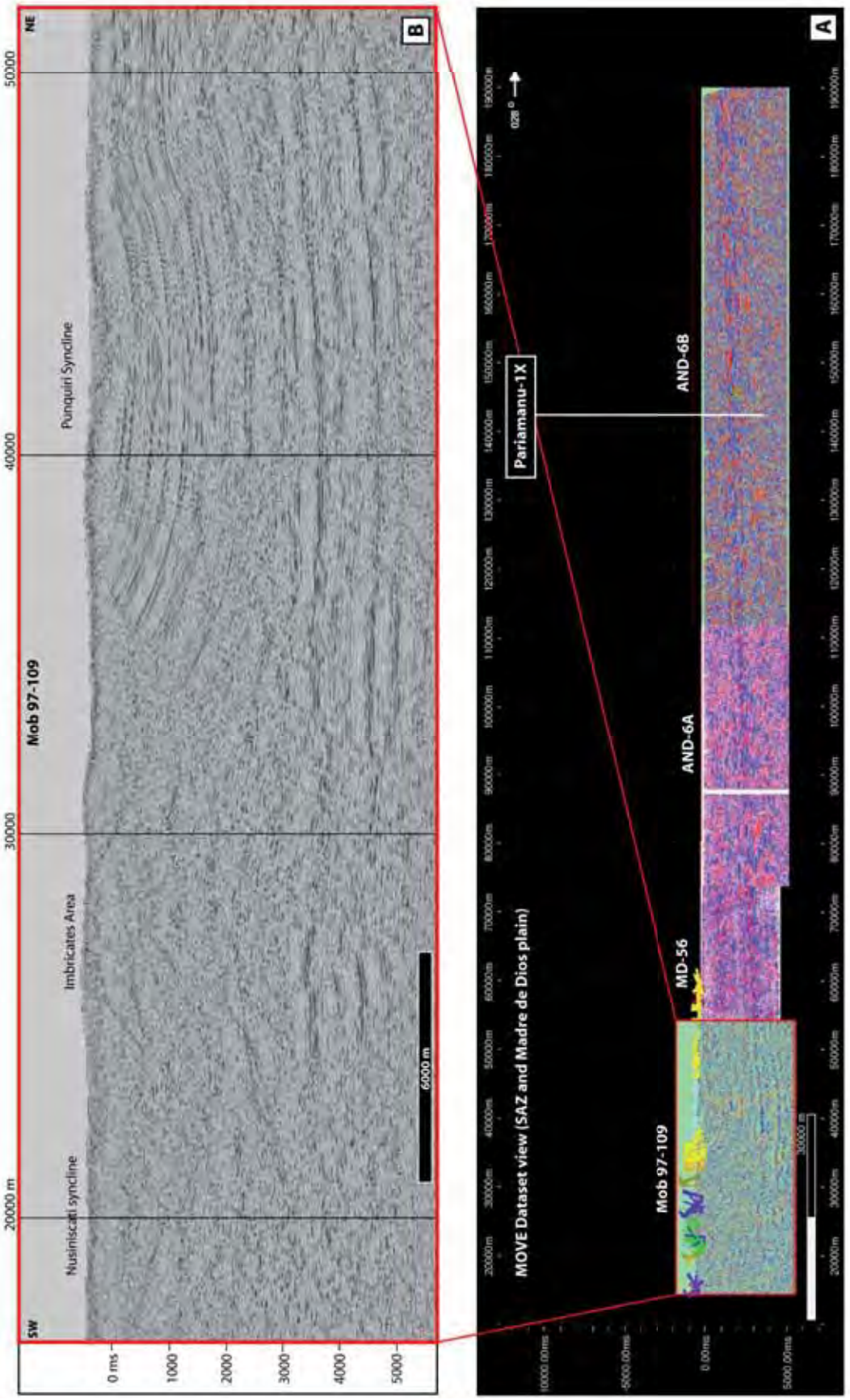

Figure 40: A) Seismic section and well data (Pariamanu-1X) representing the entire foreland system and used to construct the balanced cross-section in the Inambari area (Move view). Dip data are also represented. B) Seismic line Mob-109. See Figure 17 for location.

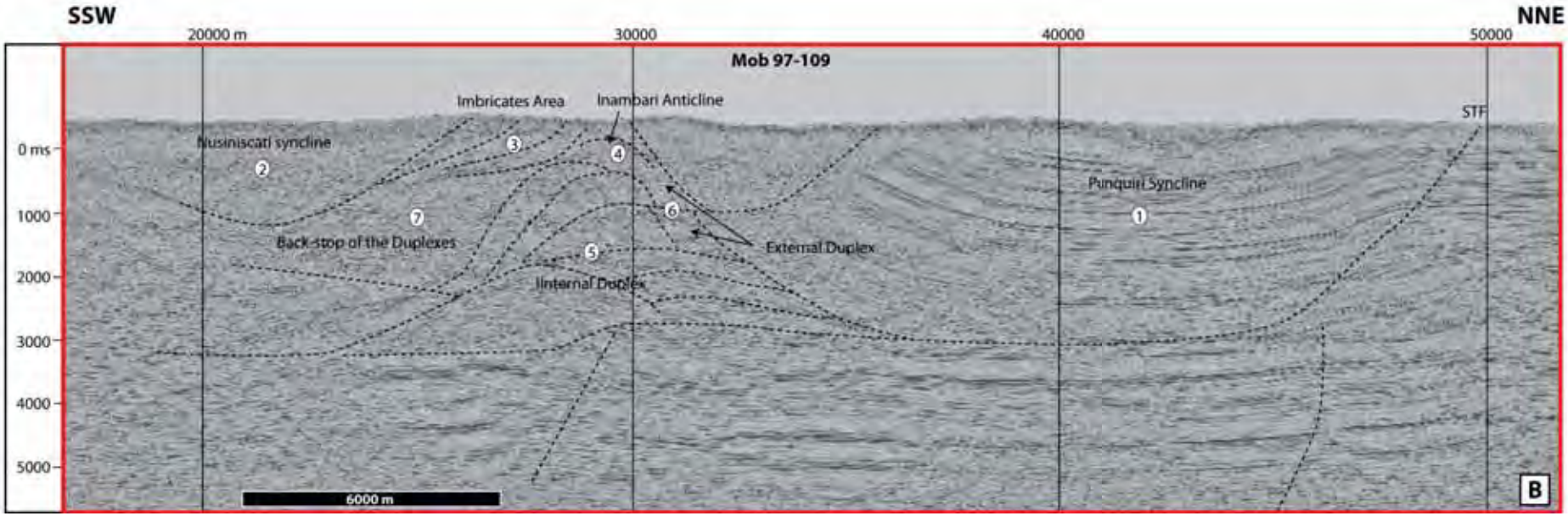

Figure 41: Interpreted seismic section Mob-109. See Figure 17 for location. Numbers corresponds to those shown in the main balanced cross-section in Figure 43.

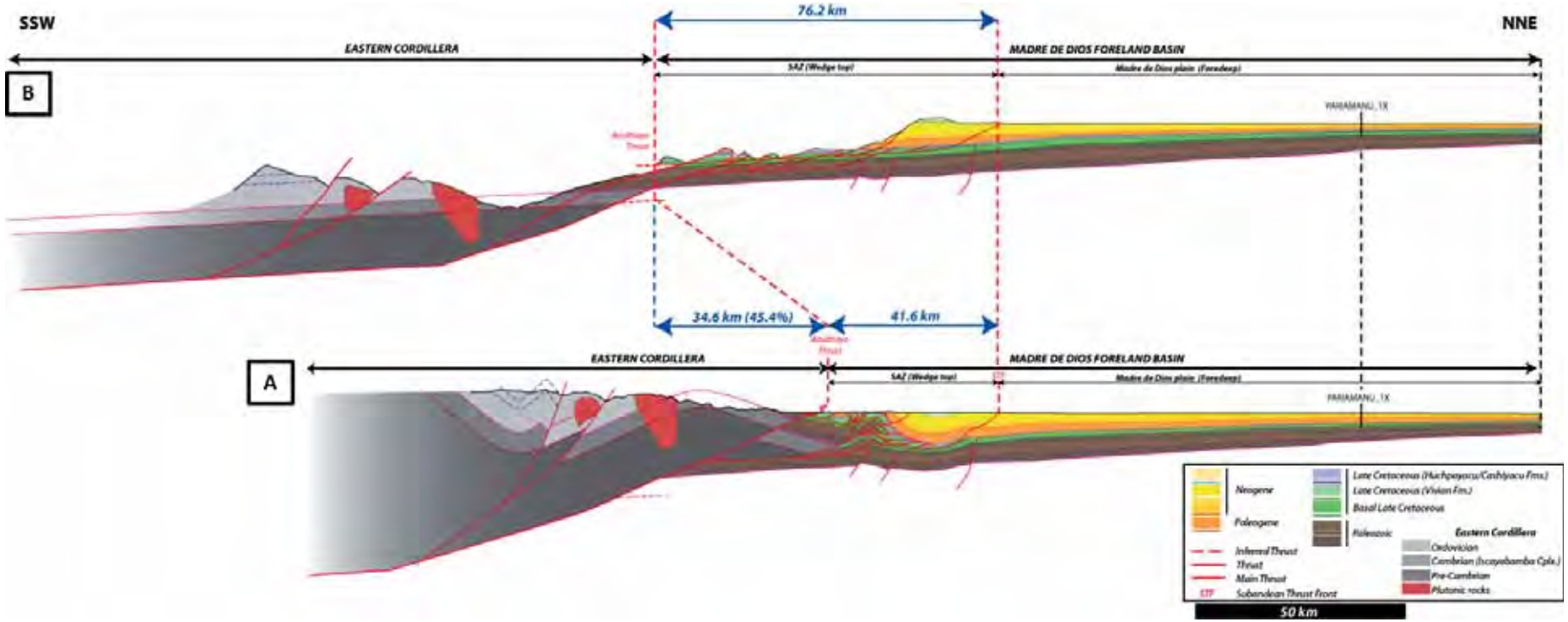

Figure 42: a) Inambari structural cross-section. B) Restored cross-section. See Figure 17 for location of the main cross-section.

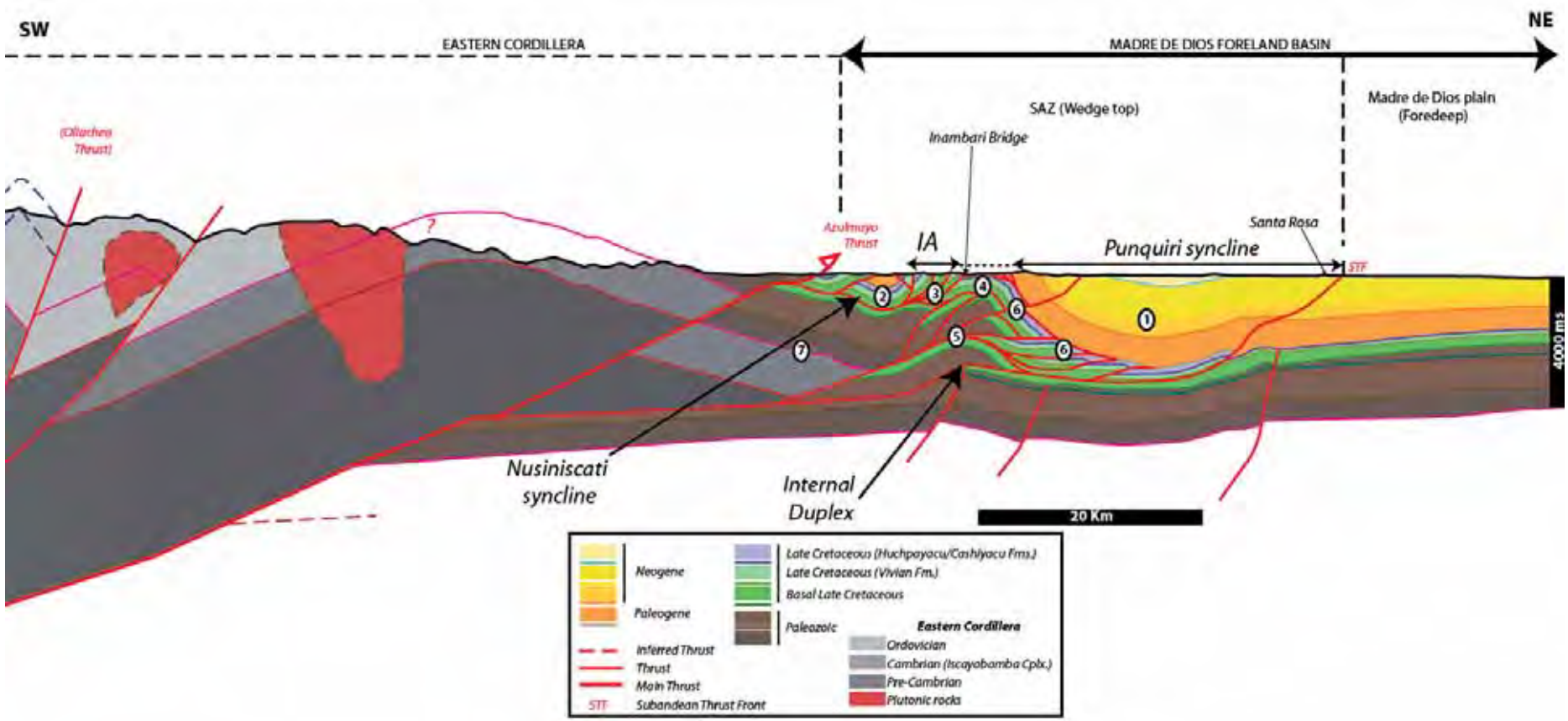

Figure 43: Enlarged view of the Inambari balanced cross-section (see Figure 42). 1= Punquiri syncline; 2= Nusiniscati syncline; 3= Imbricates Area (IA); 4= Inambari Anticline; 5= Internal duplex; 6= External duplex; 7= Basement wedge (back-stop).

4.2.3. Shortening estimates

Restoration of the Inambari balanced cross section provides a shortening estimate across the south-eastern SAZ of the Madre de Dios basin (Figure 44-section 6). The deformed cross section comprised between the Azulmayo thrust and the Tambopata thrust (SAZ) has a length of 41.6 km (Figure 42-A). The shortening model yields a 76.2-km-long un-deformed section (Figure 42-B) and a shortening estimate of 34.6 km, corresponding to a shortening rate ~45.4 % (Figure 42).

Cross-section balancing shows an along-strike homogenous horizontal shortening of ~56 km (~30%) across the Ene-southern Ucayali thrust system (Espurt et al., 2011) (Figure 44, section 1). According to the authors, this amount of shortening was vertically partitioned onto two stacked thrust wedges, and the N-S variations of the Paleozoic sedimentary prism controlled the eastward propagation of the upper thrust wedge. Major décollements and shortening rates are observed where Paleozoic series are thicker (Espurt et al., 2011).

In the SAZ of the Madre de Dios foreland basin, former works suggest shortening rates of 53% (corresponding to 55 km) in the Inambari area (Hermoza, 2004) and 56 % (or 121 km) in the Pongo de Coñeq district (Gil, 2001) (Figure 44-sections 5 and 2 respectively). However, these studies integrated part of the Eastern Cordillera. Recent structural work realized across the EC and the Pongo de Coñeq SAZ (Gotberg et al., 2010) suggests a ~46 % shortening rates (corresponding to 67.5 km) in the eastern side of the EC and the SAZ (calculated from the available section presented in their paper) (Figure 44-section 4).

In northern Bolivia, the SAZ of the Beni basin presents shortening rates that range between 40% (McQuarrie et al., 2008b) and ~50% (Baby et al., 1995) according to the authors (Figure 44-Sections 8 and 7 respectively).

Figure 44: Map showing the different balanced cross-sections available from the literature (green lines) and presented in this study (red lines). 1: Camisea basin (Espurt et al., 2011). 2: Madre de Dios basin, Pongo de Coñeq cross-section (this study). 3: Madre de Dios basin, Pongo de Coñeq cross-section (Gil, 2001). 4: Cross-section across the EC and the SAZ in Pongo de Coñeq area (Madre de Dios basin) (Gotberg et al., 2010). 5: Madre de Dios basin, Inambari section (Hermoza, 2004). 6: Madre de Dios basin, Inambari section (Gil, 2001). 7: Beni Basin (Baby et al., 1997). 8: Beni basin (McQuarrie et al., 2008b).

5. Timing of deformation

The geometry of the deformed EC and the Madre de Dios thrust system has been identified thanks to subsurfacae data and structural field observations in the SAZ in both the Pongo de Coñeq and the Inambari areas. In the following, we use the combination of growth strata sedimentary structures interpreted from dip data and seismic sections and low temperature thermochronology dating to decipher the timing of exhumation and deformation in the eastern Andean orogenic wedge (EC-SAZ).

5.1. Thermochronology and thermometry

5.1.1. Basics

Apatite fission-track ages are generally regarded as cooling ages that record the time since the apatite cooled through its closure temperature (Tc). The apatite Tc is commonly given as 100ºC (Wagner, 1968), but in reality the closure temperature can range from **120 to 160 ºC**, depending on the rate of cooling (Naeser et al., 1981). Unfortunately, fission track ages cannot be interpreted simply as cooling ages because of the annealing process occurring in the Partial Annealing Zone (or PAZ). Apatite from surface samples that resided in the PAZ prior to cooling will yield a "mixed age", that is an age that is younger than the primary age and older that the cooling event. Apatite fission-track ages from surface samples will always be either equal to (for samples that cooled quickly through their PAZ) or greater (mixed-age samples) than the age of the last cooling event. Track lengths and/or the relationship of apatite age with elevation can be used to determine whether the apatite ages are recording a geological event or are intermediate ages between two events (Laubacher and Naeser, 1994).

(U-Th)/He dating, like fission track analysis, provides information on a sample's low-temperature thermal history and not on its original, high-temperature igneous or metamorphic history. The low closure temperature of this technique has gained the interest of geologists because it is applicable to studies in structural geology across a range of different geodynamic settings. The nominal helium Tc is dependent on mineral properties, cooling rate, and grain size. For apatite crystals in the size range of ~140–180 µm, Tc will be 70ºC at a cooling rate of 10ºC/Ma. For smaller grain sizes and at lower cooling rates, it may be as low as 50ºC (Hendriks, 2005). As the method is sensitive to temperatures between ~**50-70°C,** (U-Th)/He ages document the latest stages of cooling in the uppermost crust, at even lower temperatures than the apatite fission track method (~100°C closure). The method can be used to record small changes in rock uplift not detectable by the FT method. Consequently, by combining FT analysis and (UTh)/ He dating in a single study it is possible to monitor cooling in the top 13km of the crust.

Vitrinite is one of the major elements of coal or organic matter in sedimentary rocks. Vitrinite reflectance (Ro for Reflectance in Oil) is the most widely used parameters for thermal history reconstruction of sedimentary basins and maturation evaluation of source rocks which is function of the kinetic transformation of the organic matter, commonly associated with burial. The Ro value depends on temperature and time and is irreversible (Peters and Cassa, 1994; Sweeney and Burnham, 1990). As vitrinite reflectance increases

irreversibly with temperature, it also retains indication of the maximum paleo-temperature (Barker and Pawlewicz, 1986; Teichmüller, 1987). Maximum of temperature or "Tmax" values (in ºC) are calculated by Rock-Eval pyrolysis technique following the methodology described by Esiptalié (1977).

The relation between Ro values and depth provides additional information about the thermal history of the main basin and the history of the sedimentary burial, and it can be used to decipher the existence of several heating episodes.

5.1.2. Methods

AFT analyses for samples located in the SAZ of the Inambari area (see MD 28, MD 29, MD 30, MD 13, MD 22, MD 26 and MD 20 in Figure 45) were carried out by Apatite to Zircon Inc. (former Donnelick Analytical Lab). See Annex nº4 for complete report. AFT analyses for samples located in the EC and in the Salvación syncline were carried out by the University of Toulouse at the Geosciences Environnement Toulouse (GET) laboratory under the supervision of Stéphanie Brichau. Apatite grains were isolated following classical densimetric and magnetic methods and then mounted in araldite, polished, and etched with 5 M HNO_3 for 20 s at 20 ± 0.5 ºC. AFT ages were obtained with the external detector method following the zeta procedure (Hurford and Green, 1982) with a CN5-zeta value of 303.32. Apatite mounts were covered by muscovite foils as external detector and irradiated in the FRM 11 thermal neutron facility at the University of Munich in Germany with a nominal fluence of 1.10^{16} neutron/cm^2. After irradiation, detectors were etched for 40 min in 40% HF at 20 ± 0.5ºC. The χ^2 test (Galbraith, 1981; Green, 1981) is currently used to discriminate between concordant ($P(\chi^2)$>5%) and discordant ($P(\chi^2)$<5%) grain-age distributions. When having a discordant grain-age distribution ($P(\chi^2)$<5%), the best-fit peaks were determined based on binomial model (Galbraith, 1988b; Galbraith and Green, 1990b) using the BINOMFIT program (Brandon, 1992a; Brandon, 1996b; Brandon, 2002). In the following, only the youngest peak ages or "minimum ages" (Brandon et al., 1998) are considered as other peaks may not have real geological signification (Moser et al., 2005).

Each sample aliquot for He, U and Th determinations typically comprises one to four apatite grains between 100-250 µm long and 60-150 µm wide. Evolved helium was spiked with 3He, cryogenically concentrated and purified, and the 4He/3He ratio determined by quadrupole mass spectrometry after quantitative He degassing of apatite at 1050°C for 5 min with a Photon Machines diode laser. Grains were retrieved from the vacuum system, dissolved in HNO3 for apatite, spiked with ^{230}Th, ^{235}U and ^{149}Sm, and analysed for U and Th by Inductively Coupled Plasma Mass Spectrometry. Reported He ages are corrected for alpha ejection effects based on measured grain dimensions (Farley et al., 1996) using the procedure of Gautheron et al., (2006). Each age typically comprises 2-5 replicates the mean of which is reported (Table 4). The estimated analytical uncertainty for He ages based on age standards is about 7% for Durango apatite (2σ). These are the default uncertainty values used on a sample unless the standard deviation from the sample replicate ages is higher in which case the latter is used.

Geochemical analyses (Rock-Eval, Vitrinite Reflectance) were performed by Repsol and the Paleo Sur Laboratory (Argentina).

5.1.3. Sampling strategy

We sampled vertical profiles in the EC and individual thrust structures in the SAZ (in both the Pongo de Coñeq and the Inambari areas) for AFTA/AHe double dating to constrain the timing of EC and SAZ exhumations (Figure 44). We present 18 new AFT ages (Table 3), 9 new (U-Th)/He ages (Table 4) and 35 new geochemical dataset (mainly Ro data, see Table 8).

Pongo de Coñeq

Sampling for AFT analyses has been made in the Permo-Triassic plutonic rocks of the eastern border of the EC (MD 191-FT), and along the SAZ in the Salvación syncline (MD 57-FT, MD 66-FT, MD 67-FT and MD 68-FT in Figure 45). Samples MD 56-FT and 57-FT have been collected in the Pongo de Coñeq Canyon within the Upper Carboniferous sandstones of the Tarma formation. MD 66-FT, MD 67-FT and MD 68-FT are all sandstones and have been collected within the Neogene deposits forming the northern flank of the Salvación syncline. MD 67-FT is Early Middle Miocene in age (Antoine et al., 2013). Because of its proximity to MD 67 locality, sample MD 68-FT is probably Early Middle Miocene too. MD 66-FT is the most recent sample collected in this section and is very likely to be Late Miocene to Early Pliocene in age (refer to PART D of this manuscript for more details related to the Neogene stratigraphy).

Sampling for (U-Th)/He analyses has only been carried out in the EC. Two Permo-Triassic plutonic rocks have been sampled: MD 173-He and MD 191-He (Figure 45). MD 191 is the only locality for which we provide both AFT and He ages.

Inambari

We collected 6 samples (5 crystallines and 1 meta-sedimentary) on two vertical profiles in the eastern flank of the EC adjacent to the inambari SAZ for AFTA dating (Figure 45).

Six samples have been collected in the EC: MD 192-FT, MD 194-FT, MD 112-FT, MD 170-FT, MD 164-FT and MD 211-FT. Almost all samples correspond to Permo-Triassic plutonic rocks as MD 216-FT is the only sample collected in the Pre-Cambrian or Cambrian meta-sedimentary unit (Figure 45).

Six sedimentary rocks have been collected in the SAZ of the Inambari area. MD 30-FT is located in the Imbricate Thrust System and corresponds to Late Cretaceous-Early Paleocene sandstone (Huchpayacu-Cashiyacu Formations). MD 29-FT corresponds to sandstone collected at the very beginning of the Punquiri syncline and is probably Late Cretaceous to Paleocene in age. MD 28-FT, MD 22-FT and MD 20-FT are also located in the southern flank of the Punquiri syncline and are Miocene in age (see PART D of this manuscript for more details related to the Neogene stratigraphy). MD 28-FT and MD 22-FT are sandstones whereas MD 20-FT corresponds to a tuffaceous level. MD 13-FT has been collected in the northern flank of the Punquiri syncline and corresponds to a Late Miocene to Pleistocene sand.

Seven samples were collected for (U-Th)/He analyses in the EC of the Inambari area (Figure 45). These correspond to samples MD 194-He, MD 216-He, MD 112-He, MD 169-He, MD 170-He, MD 164-He and MD

211-He. MD 216-He and MD112-FT were both collected in a Paleozoic (Cambrian?) meta-sedimentary unit (Figure 45). Other samples for (U-Th)/He analyses correspond to Permo-Triassic plutonic rocks.

In the Inambari area, we provide both FT and He thermochronological results for five localities: MD 170, MD 211, MD 164, MD 112 and MD 194 (Figure 45).

For this study, 35 samples for Rock-Eval and Vitrinite reflectance analyses were also sampled in both the EC and SAZ. See map of Figure 45 for samples localities and Table 8 for details.

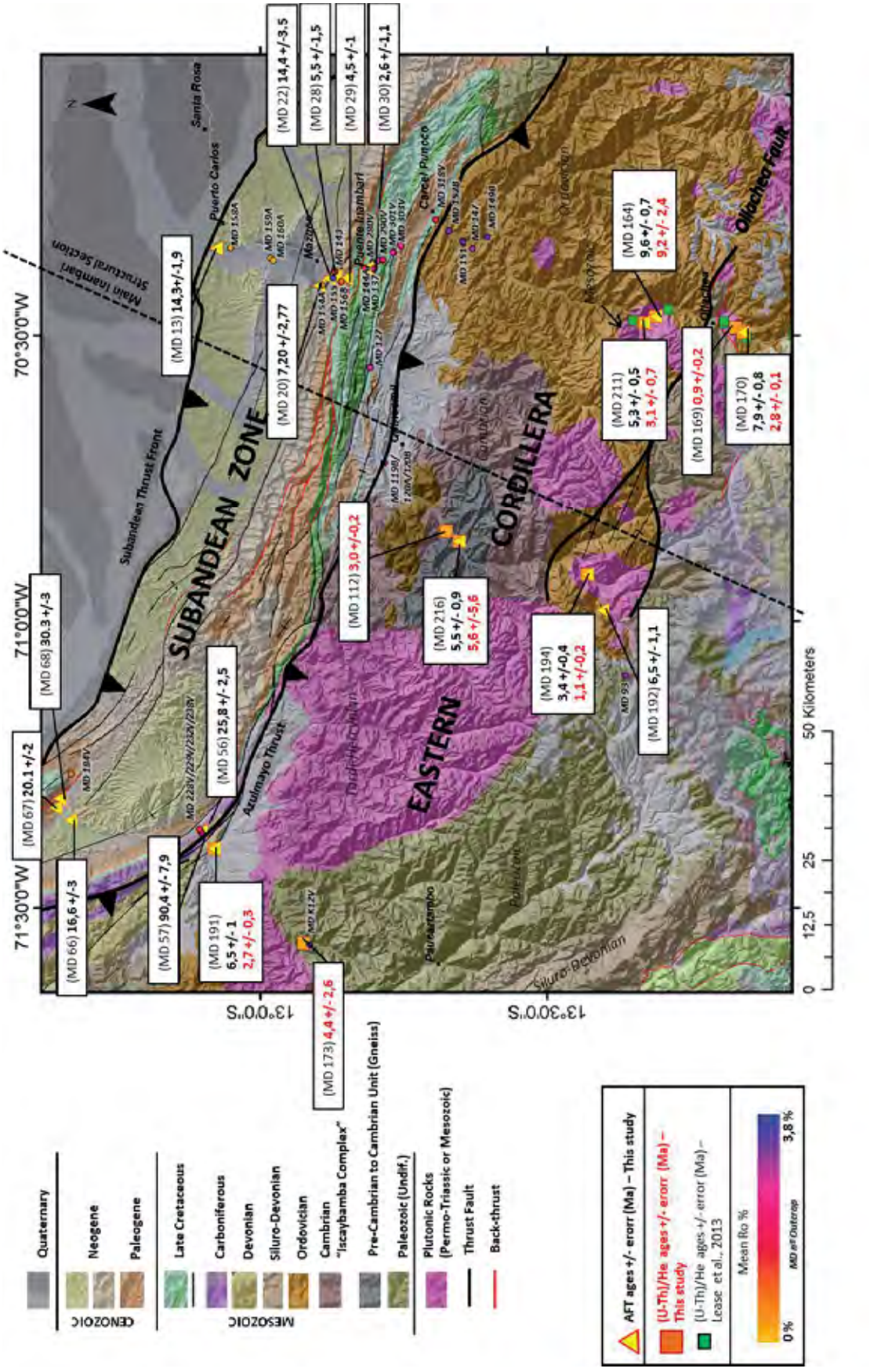

Figure 45: Low temperature thermochronological results (this study and others) in the Madre de Dios SAZ and the adjacent EC. Mean vitrinite reflectance (Ro%) results are also indicated and detailed in Table 8.

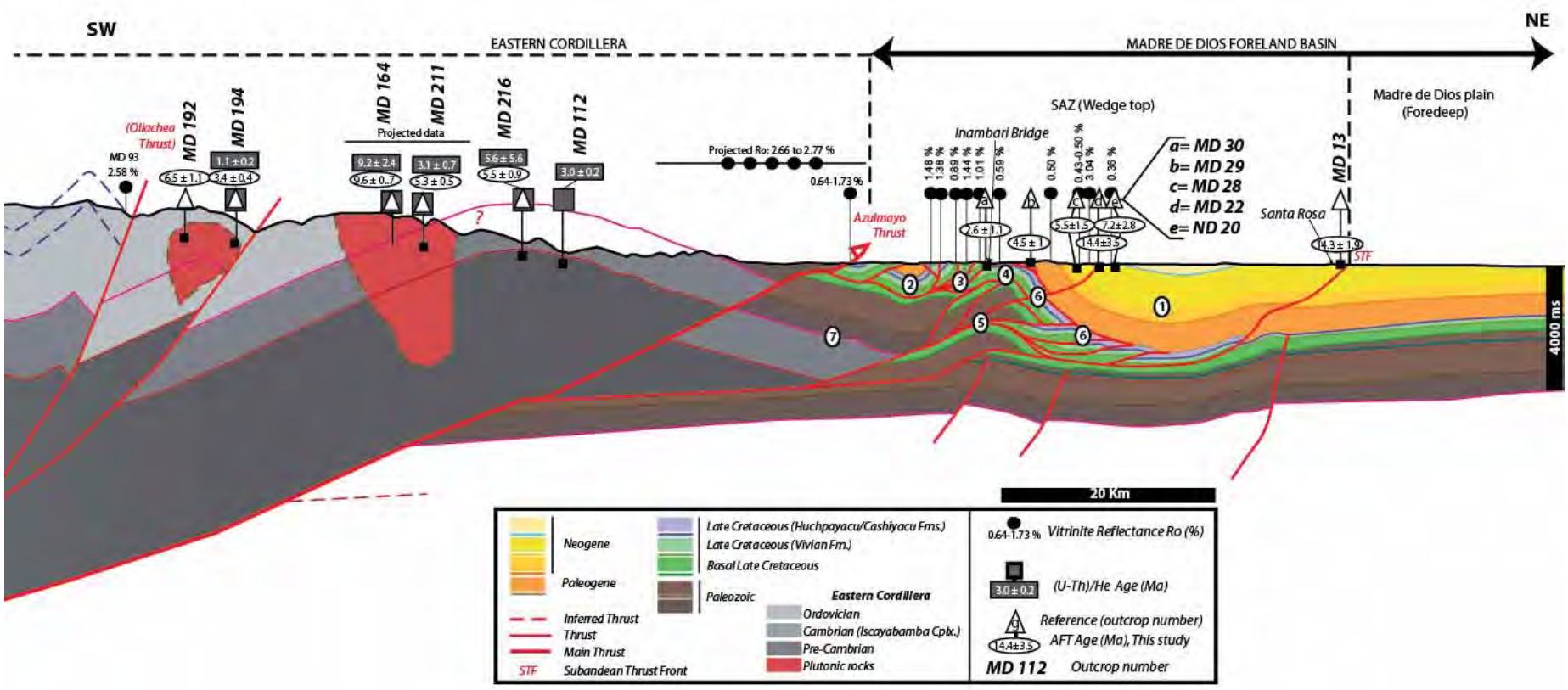

Figure 46: Low-temperature thermochronology (Ma) and Ro results (%) projected onto the main Inambari section (see Figure 45 for location of the section. Tectonic units of the main Inambari section: 1= Punquiri syncline; 2= Nusiniscati syncline; 3= Imbricates Area (IA); 4= Anticline; 5=Internal duplex; 6= External duplex; 7= detachment wedge (basement).

5.1.4. AFT and He Results

In the Inambari area, thermochronological results and Ro values were projected onto the main Inambari structural section (Figure 46). An enlarged view of these results projected onto the Inambari structural cross-section can be consulted in the Annexes-Figure I. In the Pongo de Coñeq area, results were also projected onto the main structural cross-section already presented (Figure 47).

5.1.4.1. Pongo de Coñeq area

Eastern Cordillera

The analyzed sample (MD 191-FT) of the Pongo de Coñeq EC passes χ2 test (P(χ2)>5%) indicating a concordant grain age distribution (Table 3). It has a central age of 6.5±1 (Figure 48) Ma with a Mean Track Length (MTL) of 12.1± 0.6 µm (Table 2; Figure 50). AFT age is younger than the primary age, indicating total resetting of the sample. The two AHe ages obtained for Pongo de Coñeq EC (MD 173-He and MD191-He) show Pliocene cooling with ages of 4.4 ±2.6 and 2.7±0.3 Ma respectively (Table 4 and Figure 49).

SAZ

Five samples from the Pongo de Coñeq SAZ were dated by AFT analysis (Table 3 and Figure 48). The five samples pass the χ2 test (P(χ2)>5%) indicating a concordant grain age distribution. The AFT central ages of Pongo de Coñeq SAZ range from 16.6±3 to 90.4±7.9 Ma with MTL ranging from 10.0±0.5 to 14.4±0.41 µm (Table 3 and Table 2).

5.1.4.2. Inambari area

Eastern Cordillera

All AFT ages pass the χ2 test (P(χ2)>5%) indicating a concordant grain age distribution (Table 3). The AFT central ages of Inambari EC range from 3.4±0.4 to 9.6±0.7 Ma with MTL ranging from 10.62±0.9 to 12.8 µm (Table 2 and Table 3). AHe ages range from 0.9±0.2 to 9.2± 2.4 Ma and except for one sample (i.e. MD 164-He), they show Plio-Pleistocene cooling (Table 4). Overall, where analyzed AHe ages are younger or similar to their associated AFT ages (see synthetic Table 5), there is no single relationship between AHe and AFT ages and elevation (Figure 49). However two trends can be observed. AFTA and AHe ages increase from elevation 986±10 to 1883±15 m in both profiles (from MD112 to MD216 and MD211 to MD164). Above ~1900 m, a strong shift toward younger AHe and AFT ages is observed (samples MD194 and MD169, Figure 49). MD192 and MD 170, the most elevated samples, have overall similar AFT central ages (6.5±1.1 Ma and 7.9±0.8 Ma respectively, Table 3) with an AHe age of 2.8±0.1 Ma older than AFT and AHe ages of lower in elevation MD 194 and MD 169 samples (Table 4 and synthetic Table 5).

Collected in the Eastern Cordillera, MD 191-FT is Permo-Triassic in age and corresponds to a plutonic rock (Figure 45). AFT analysis provided a Late Miocene age (6.5 ± 1.0 Ma; Table 3). This sample probably records a Late Miocene cooling event in the Eastern border of the Eastern Cordillera.

SAZ

Six samples from the Inambari SAZ were dated by AFTA (Table 3 and Figure 48). The tuffaceous levels (MD 20-FT) as well as the Neogene sandstones (MD 22-FT) and the Pliocene sand (MD 13B-FT) pass the χ2 test indicating that the apatite grains derived from homogenous sources. Their central ages range from 5.42±0.98 Ma to 14.4±3.5 Ma (Table 3 and Figure 48) with MTL varying between 13.71±0.29 to 14.7±0.18 µm and Dpar ranging from 1.52±0.27 to 2.28±0.70 µm (Table 2; Figure 50). Three sandstones (MD 28-FT, MD 29-FT and MD 3-FT0) failed the χ2 test with P(χ2) less than 1.4% (Table 3). Their single grain age distributions derived therefore from distinct sources. In each fission track grain age distribution, the best-fit peaks were determined based on binomial model described by (Galbraith, 1988a) using the BINOMFIT program (Brandon, 1992b; Brandon, 1996a; Brandon, 2002; Galbraith and Green, 1990a). In the following, only the youngest peak ages or "minimum ages" (Brandon et al., 1998; Galbraith and Green, 1990a) are considered since other peaks may not have real geological signification (Moser et al., 2005). The youngest peak ages for the samples that fail the χ2 test (i.e. MD 28-FT, MD 29-FT and MD 30-FT) are 5.5±1.5 Ma, 4.5±1 Ma and 2.6±1.1 Ma respectively (Table 3). The youngest peak age is the dominant component for MD 28-FT and MD 29-FT containing 60% and 64% of the distribution respectively. The youngest peak age of the MD 30-FT sample, although not dominant, represents a significant part of the grain ages (~30%).

5.1.5. Ro results

Ro values are presented in Table 8 and Figure 51 (see Figure 45 for samples location). Mean Ro values range between 0.29 and 3.8%. Values show a gradual increase toward the paleo-depth, with relative high values for the deepest horizons corresponding to Paleozoic formations and older ones forming the EC in comparison with Cretaceous to Tertiary deposits forming the SAZ (Table 8, Figure 46 and Figure 47). The EC is characterized by mean Ro values ranging from 2.52 to 3.8 % (Table 8). The SAZ is characterized by mean Ro values ranging from 0.29 to 1.72 % (Table 8) with anomalous value of 3.04 % at the very beginning of the Punquiri syncline (Figure 51).

Anomalous value of Ro=3.04 % registered in the Inambari SAZ might be due to back-thrust faults activity in the vicinity of the southern flank of the Punquiri syncline (Figure 46). The anomalous value would thus define an area of substantial uplift. However, this interpretation is not in agreement with the structural interpretation. The anomalous Ro value could also be the result of fluid circulation (hydrothermalism?). Because it is the unique anomalous result obtained in this area, we simply suggest that sample MD 155B should be disregarded.

Sample MD 93 is related to high vitrinite reflectance value (2.58 %). In map, MD 93 is the only sample situated so far toward the south-west (internal EC, Figure 45). MD 93 and the other samples collected in the north-eastern EC may belong to two different tectonic units (Figure 46). This is in agreement with the presence of the Ollachea fault in the EC (Figure 45 and Figure 46).

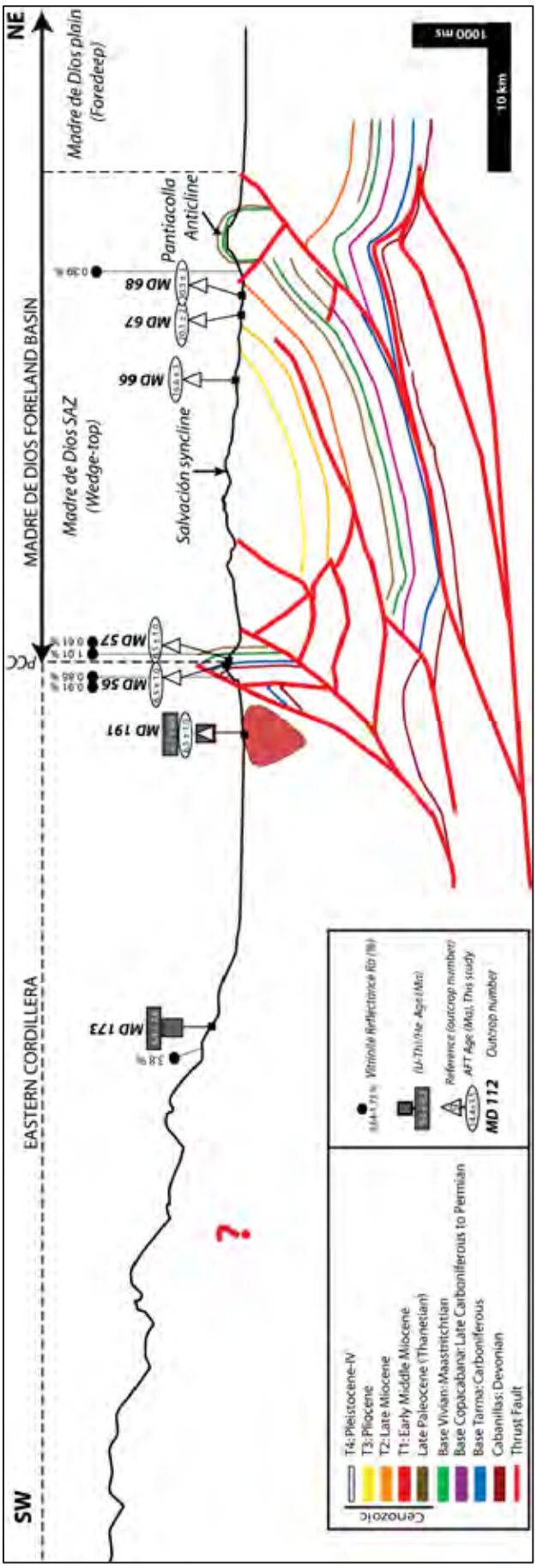

Figure 47: Low-temperature thermochronology (Ma) and Ro results (%) projected onto the main Pongo de Coñeq section. See Figure 45 for location of the section.

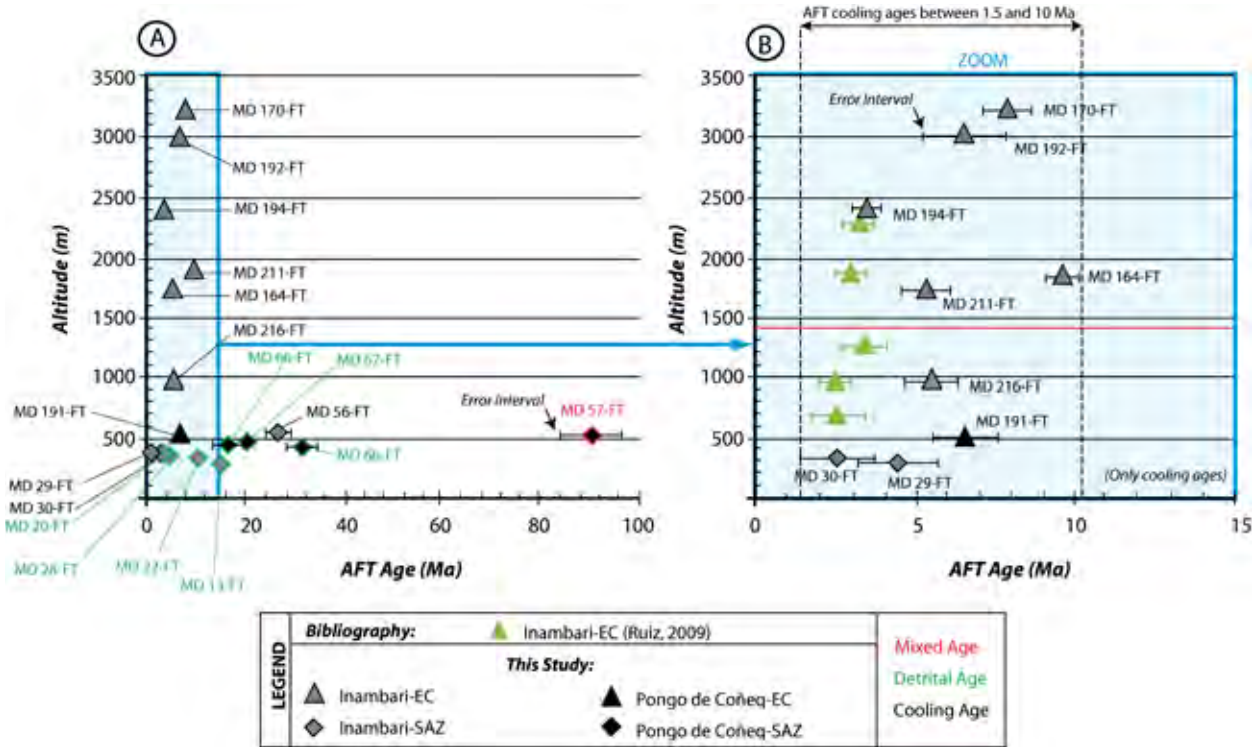

Figure 48: A) New AFT ages (this study). Ages are displayed in function of the altitude (m) and of their geographic location. Only MD 57-FT shows a consequent error interval. B) AFT ages of this study (only cooling ages are displayed) compared to AFT ages from Ruiz et al. (2009).

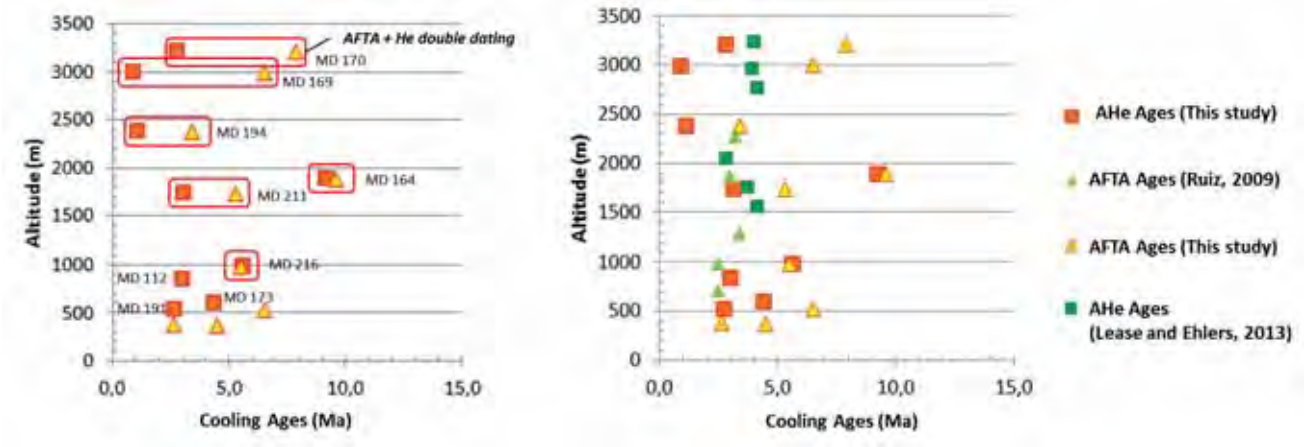

Figure 49: Left: Chart of the new AFT and He ages (Ma) presented in this study in function of the altitude (m). Only cooling ages are displayed. Note that six samples provided material for both AFT and (U-Th)/He analyses. AFT ages are shown by orange triangles whereas He ages are shown by red squares. Right: New AFT and He ages presented in this study compared with thermochronological results from the literature.

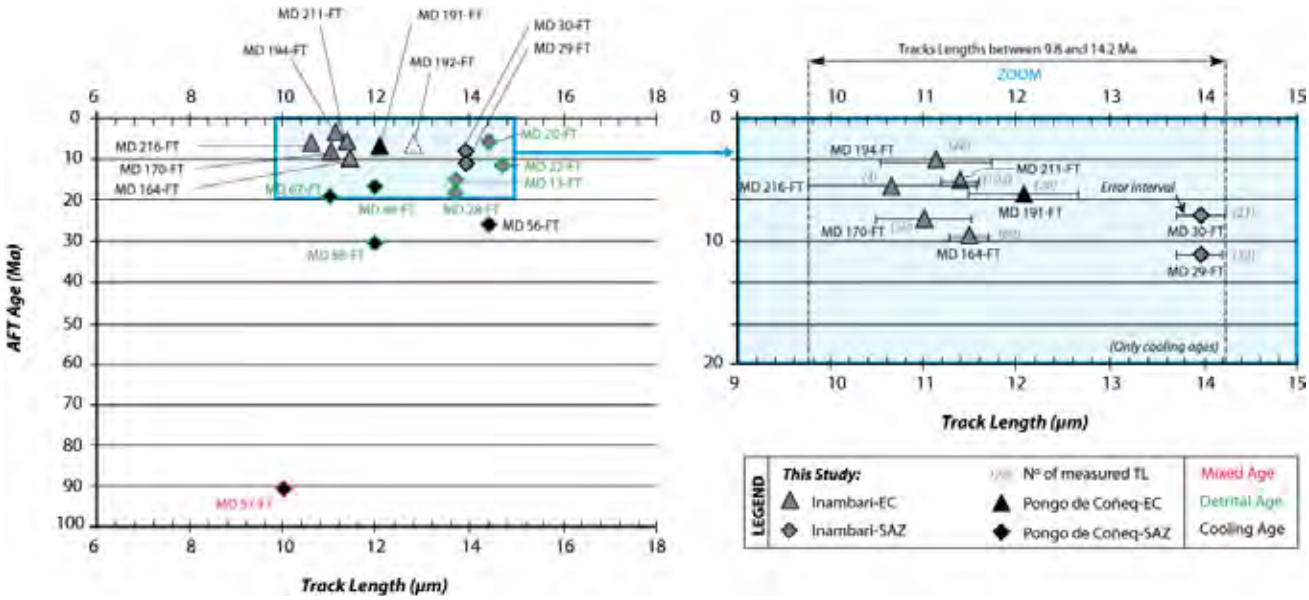

Figure 50: Tracks lengths distribution in function of AFT ages (this study).

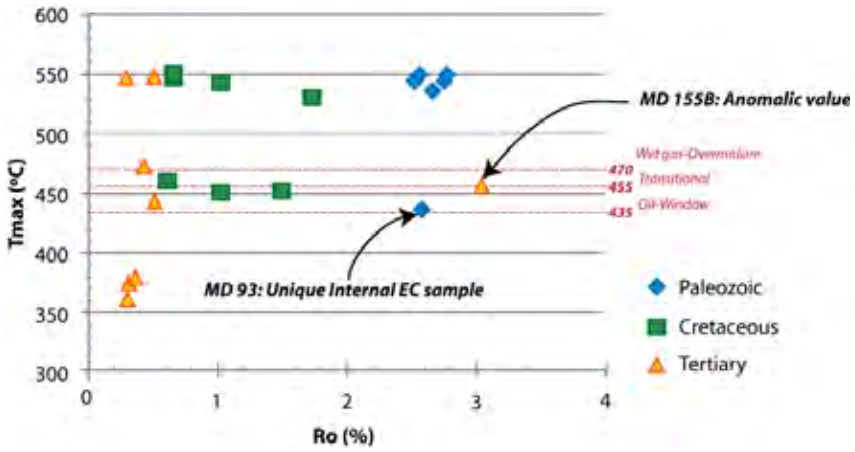

Figure 51: Ro (%) versus T max (ºC) diagramme (this study).

Zone	Unit	Sample Name	Central Age (Ma)	Pooled age (Ma)	Mean age (Ma)	Type	Tracks Lengths	Number of Tracks Lengths	Dpar (µm)	Std (µm)	Contact
Inambari	SAZ	MD 28 FT		18.0±1.8	13.4±3.0	Inherited	13,67±0,34	18	1,8	1,38	Donnelick
		MD 29 FT		11.4±1.1	11.4±1.1	Cooling	13,96±0,21	53	1,69	1,51	Donnelick
		MD 30 FT		7.91±1.16	13.9±3.8	Cooling	13,96±0,22	21	1,84	0,99	Donnelick
		MD 13 FT		15.2±1.5	14.3±1.9	Inherited	13,71±0,29	30	1.52±0.27	1,57	Donnelick
		MD 22 FT		11.0±1.6	14.4±3.5	Inherited	14,7±0,18	53	2.28±0.70	1,26	Donnelick
		MD 20 FT		5.58±1.17	5.42±0.98	Inherited	14,42±0,12	113	2.10±0.48	1,29	Donnelick
	EC	MD 164-2011 FT	9,6±0,7	9,6±0,7	9,0±0,6	Cooling	11,45±0,2	80			M. Louterbach
		MD 170 FT	7,9±0,8	7,9±0,8	8,1±1,3	Cooling	11,03±0,5	50			M. Louterbach
		MD 192 FT	6,5±1,1	6,5±1,1	6,1±0,9	Cooling	12,8	1			M. Louterbach
		MD 194 FT	3,4±0,4	3,4±0,4	3,4±0,4	Cooling	11,15±0,6	26			M. Louterbach
		MD 211 FT	5,3±0,5	5,3±0,5	5,4±0,3	Cooling	11,37±0,2	103			M. Louterbach
		MD 216 FT	5,5±0,9	5,5±0,9	5,5±1,0	Cooling	10,62±0,87	4			M. Louterbach
Pongo de Coñeq	EC	MD 191 FT	6,5±1	6,5±1,0	6,1±0,8	Cooling	12,1±0,6	20			M. Louterbach
	SAZ	MD 56 FT	25,8±2,5	25,8±2,5	27,4±2,8	Cooling (Mixed)	14,4±0,41	19			S. Brichau
		MD 57 FT	90,4±7,9	90,4±7,8	98,6±8,2	Cooling (Mixed)	10±0,5	11			S. Brichau
		MD 66 FT	16,6±3	17,1±2,6	15,4±2,6	Inherited	12,3±0,7	20			S. Brichau
		MD 67 FT	20,1±2	19,5±1,8	17,4±2,1	Inherited	11,5±1,2	4			S. Brichau
		MD 68 FT	30,3±3	30,3±3,0	28,9±2,1	Inherited	12,1±0,4	9			S. Brichau

Table 2: Tracks Length data (This study).

Zone 1	Unit	Sample Name	Age	Lithology	Longitude UTM 19	Latitute UTM 19	(Z)	ρS	Ns	ρi	Ni	ρd	Nd	P(χ^2) (%)	Dpar (µm)	Std (µm)	Mean U (ppm)	Central Age (Ma)	Pooled age (Ma)	Mean age (Ma)	P1 (Ma)	P2 (Ma)	REF
Inambari	SAZ	MD 28 FT	Miocene	Sandstone	348534,00	8548069,00	366	266000	126	2413000	1142	3126000	5154	0	1,65	0,39			18.0±1.8	13.4±3.0	5.5±1.5 (15)	29.6±3.5 (10)	1
		MD 29 FT	Late Cretaceous	Sandstone	348180,00	8545926,00	371	265000	131	3787000	1875	3124000	5154	0,0	1,70	0,39			11.4±1.1	11.4±1.1	4.5±1.0 (16)	19±2.1 (10)	1
		MD 30 FT	Late Cretaceous	Sandstone	350059,73	8541915,24	382	15000	51	3085000	1051	3122000	5154	1,4	1,80	0,42			7.91±1.16	13.9±3.8	2.6±1.1 (5)	11.6±2.0 (12)	1
		MD 13 FT	Late Mio.to Pleisto.	Sandstone	353644,01	8571093,54	290	221000	114	2382000	1230	3135000	5154	8,3	1,99	0,44			15.2±1.5	14.3±1.9			1
		MD 22 FT	Mio. to Early Pleisto.	Tuff	348162,00	8549280,00	338	82000	50	1227000	745	3131000	5154	27	2,36	0,71			11.0±1.6	14.4±3.5			1
		MD 20 FT	Pliocene (3.45 Ma)	Tuff	346741,00	8551191,00	355	36000	24	105000	704	3133000	5154	98,3	2,20	0,53			5.58±1.17	5.42±0.98			1
	EC	MD 164-2011 FT	Tardi-Hercynian	Granite	341372,20	8486309,41	1883	394400	186	9080000	4115	1406000	13542	81,8			80,8	**9,6±0,7**	9,6±0,7	9,0±0,6			2
		MD 170 FT	Tardi-Hercynian	Granite	338426,64	8469420,20	3213	231600	114	6134000	3124	1423000	41768	99,4			53,9	**7,9±0,8**	7,9±0,8	8,1±1,3			2
		MD 192 FT	Tardi-Hercynian	Granite	285652,50	8496115,17	3000	45540	39	1433000	1234	1367000	13741	92,4			13,1	**6,5±1,1**	6,5±1,1	6,1±0,9			2
		MD 194 FT	Tardi-Hercynian	Granite	292480,15	8499157,46	2385	82870	70	4796000	4283	1367000	13741	99,5			43,9	**3,4±0,4**	3,4±0,4	3,4±0,4			2
		MD 211 FT	Tardi-Hercynian	Granite	340201,32	8488514,87	1733	180712	107	7281816	4364	1438300	14485	99,9			63,3	**5,3±0,5**	5,3±0,5	5,4±0,3			2
		MD 216 FT	Siluro-Devonian	Metased.	298460,11	8523882,90	986	89265	37	3508563	1403	1377758	13741	75,4			31,8	**5,5±0,9**	5,5±0,9	5,5±1,0			2
Pongo de Coñeq	EC	MD 191 FT	Tardi-Hercynian	Granite	240020,79	8570716,57	528	71760	43	2261000	1389	1376000	27283	93,2			20,5	**6,5±1**	6,5±1,0	6,1±0,8			2
	SAZ	MD 56 FT	Lower Carboniferous	Sandstone	243182,00	8573184,00	532	127300	130	849800	587	998700	5537	38,7			10,6	**25,8±2,5**	25,8±2,5	27,4±2,8			3
		MD 57 FT	Carboniferous	Sandstone	243253,00	8573254,00	527	277200	209	495700	392	998700	5537	74,0			6,2	**90,4±7,9**	90,4±7,8	98,6±8,2			3
		MD 66 FT	Neogene	Sandstone	245115,00	8598378,00	435	520400	73	510900	729	998700	5537	22,5			6,4	**16,6±3**	17,1±2,6	15,4±2,6			3
		MD 67 FT	Neogene	Sandstone	247817,00	8600998,00	460	109200	137	1115000	1365	998700	5537	15,0			13	**20,1±2**	19,5±1,8	17,4±2,1			3
		MD 68 FT	Neogene	Sandstone	249180,00	8600546,00	423	175200	249	1008000	1391	998700	5537	23,7			12,6	**30,3±3**	30,3±3,0	28,9±2,1			3

Table 3: AFT age results (this study). Samples colored in dark grey are related to detrital AFT ages. Samples colored in bright grey are related to mixed AFT ages. Other samples (uncolored) are related to cooling events. REF. 1= Ray Donnelick (see Annex nº4). REF. 2=Mélanie Louterbach. REF. 3= Stéphanie Brichau.

Name	Corr Age Ma	1s Ma	U ppm	1s ppm	Th ppm	1s ppm	He nmol/g	mass (ug)	Ft	r um	l um	RE	Henmol/g	#gr	Sm ppm	Raw Age (Ma)	Dim Mass(ug)	He Age (Ma)
MD112(a)	3,321189	0,092232	54,348921	0,726718	9,720237	0,26444	0,754987	3,909837	0,735181	54,35	157,75	0	0,001327	2	162,391375	2,444924	7,522	
MD112(b)	2,695149	0,097241	48,397823	1,003673	7,981367	0,391842	0,48423	1,844055	0,654611	39,75	125,35	0	0,000416	2	127,998943	1,76729	3,202	3.0 ± 0.2
MD112(c)	34,223225	1,240113	43,193129	0,932046	7,250369	0,377664	5,485206	1,872732	0,652506	42,175	101,55	0	0,004603	2	86,545208	22,385824	2,908	
MD164(a)	11,241187	0,403441	69,221849	1,006536	5,657297	0,272342	2,633637	2,673194	0,607146	31,917	141,033	0	0,003156	3	200,949816	6,843278	3,515	
MD164(b)	9,655484	0,309223	72,121338	0,94364	3,470457	0,218848	2,521098	3,04831	0,654821	41,833	102,1	0	0,003445	3	212,23054	6,336466	4,369	9.2 ± 2.4
MD164(c)	6,567275	0,192874	100,44262	1,051197	3,828794	0,227204	2,477864	2,986497	0,682016	44,275	129,85	0	0,003317	2	240,850988	4,485931	4,095	
MD169(a)	0,950205	0,029936	34,946991	0,645128	1035,74548	4,949457	0,927239	3,336086	0,642065	41,538	152,075	1	0,001391	4	472,386742	0,610793	8,439	
MD169(b)	0,743388	0,039434	43,681625	1,204153	1996,69549	13,355051	0,905691	0,924314	0,434789	24,75	81,725	0	0,000392	4	666,896093	0,323876	1,611	0.9 ± 0.2
MD169(c)	1,092963	0,036141	7,429418	0,121989	257,344091	0,921959	0,248596	19,952602	0,61372	40,987	107,2	0	0,002225	4	92,493364	0,671472	5,833	
MD170(a)	2,371663	0,092443	57,207577	1,070702	356,858048	3,467332	1,039624	1,977578	0,568557	34,05	97,233	0	0,000928	3	328,093291	1,351355	2,731	
MD170(b)	2,991844	0,116657	46,108587	0,876643	264,824347	2,675448	1,009554	2,369638	0,569535	34,05	97,233	0	0,001078	3	283,418538	1,708125	2,731	2.8 ± 0.1
MD170(c)	2,929185	0,09521	42,123955	0,643182	217,250389	1,959268	0,961358	4,030802	0,643834	40,8	131,733	0	0,00174	3	299,765157	1,890045	5,355	
MD173(a)	3,256351	0,139442	8,779311	0,265285	24,235297	0,468614	0,162624	3,396849	0,592261	30,9	157,2	1	0,000273	3	509,950903	1,982803	3,8	
MD173(b)	2,556463	0,172231	6,603742	0,277779	19,442635	0,677554	0,096746	1,26112	0,572652	33,917	92,2	1	0,000127	3	468,106504	1,516522	2,572	4.4 ± 2.6
MD173(c)	7,33293	0,284073	9,390994	0,273685	24,859356	0,4665	0,407106	3,5887	0,634388	37,55	127,367	0	0,000665	3	453,665071	4,745558	4,529	
MD191(a)	2,937659	0,114768	19,291977	0,447548	45,143653	0,6999	0,290001	3,470583	0,595096	35,35	103,95	0	0,000465	4	304,445692	1,762747	4,17	
MD191(b)	2,384846	0,085621	15,808077	0,316252	37,685804	0,517735	0,202202	6,151462	0,622063	35,825	142,1	1	0,000569	4	211,915374	1,492851	5,906	2.7 ± 0.3
MD191(c)	2,911664	0,092653	16,00876	0,285509	37,318086	0,477951	0,268385	7,838566	0,672832	44,388	138,1	0	0,000949	4	236,712954	1,97003	8,762	
MD194(a)	1,196663	0,035759	46,379253	0,560199	27,009421	0,429965	0,235254	5,340166	0,683559	47,15	113,6	0	0,000574	4	115,962722	0,81902	8,185	
MD-194(b)	0,826563	0,022104	37,914946	0,343051	33,18616	0,417745	0,149491	9,416487	0,724572	48,217	209,867	0	0,000641	3	134,745318	0,599722	12,069	1.1 ± 0.2
MD-194(c)	1,29259	0,044875	28,01846	0,204371	39,213184	0,399798	0,156929	15,709398	0,595926	36,25	88,533	0	0,001111	3	126,310832	0,772447	2,829	
MD-211(a)	3,930251	0,152191	82,505404	1,227181	23,130253	0,550796	1,079132	2,170312	0,571827	29,633	121,767	1	0,001056	3	194,709917	2,252282	2,596	
MD-211(b)	2,741343	0,095371	79,447637	0,933209	30,410557	0,550539	0,787859	3,261381	0,607126	32,9	129,5	0	0,001157	4	260,810094	1,668412	4,546	3.1 ± 0.7
MD-211(c)	2,573648	0,097218	47,668955	0,811797	13,49173	0,36152	0,428062	2,915549	0,595999	34,737	94,5	0	0,000571	4	255,860326	1,54032	3,648	
MD-216(a)	1,141269	0,041052	17,50281	0,42839	531,403504	3,630936	0,53203	3,346598	0,59942	36,833	127,8	0	0,000806	3	249,31996	0,685071	4,205	
MD-216(b)	12,099964	0,502744	18,02801	0,505623	13,435006	0,423706	0,85971	2,167883	0,611925	36,5	99,825	0	0,000843	4	82,310376	7,429344	4,304	5.6 ± 5.6
MD-216(c)	3,607291	0,194566	10,137802	0,349728	26,367796	0,62628	0,162807	1,914519	0,501654	25,637	111,775	0	0,000179	4	89,45709	1,821621	2,355	

Table 4: (U-Th)/He age results (This study).

Sample name	He age Ma	FT Pooled age Ma	Tracks lenghts	number of TL	Contact
MD 56		25,8 ± 2,5	14,4±0,41	19	Stéphanie Brichau
MD 57	-	90,4 ± 7,9	10,0 ± 0,5	11	Stéphanie Brichau
MD 66	-	17,1 ± 2,6	12,3 ± 0,7	20	Stéphanie Brichau
MD 67	-	19,5 ± 1,8	11,5 ± 1,2	4	Stéphanie Brichau
MD 68	-	30,3 ± 3,0	12,1 ± 0,4	9	Stéphanie Brichau
MD 112	3,0 ± 0,2	-	-	-	Mélanie Louterbach
MD 164	9,2 ± 2,4	9,6 ± 0,7	11,45 ± 0,2	80	Mélanie Louterbach
MD 169	0,9 ± 0,2	-	-	-	Mélanie Louterbach
MD 170	2,8 ± 0,1	7,9 ± 0,8	11,03 ± 0,5	50	Mélanie Louterbach
MD 173	4,4 ± 2,6	-	-	-	Mélanie Louterbach
MD 191	2,7 ± 0,3	6,5 ± 1,0	12,1 ± 0,6	20	Mélanie Louterbach
MD 192	-	6,5 ± 1,1	12,8	1	Mélanie Louterbach
MD 194	1,1 ± 0,2	3,4 ± 0,4	11,15 ± 0,6	26	Mélanie Louterbach
MD 211	3,1 ± 0,7	5,3 ± 0,5	11,37 ± 0,2	103	Mélanie Louterbach
MD 216	5,6 ± 5,6	5,5± 0,9	10,62 ± 0,9	4	Mélanie Louterbach
MD 28 FT		5,5 ± 1,5			Donnelick
MD 29 FT		4,5 ± 1,5			Donnelick
MD 30 FT		2,6 ± 1,1			Donnelick
MD 13 FT		15,2 ± 1,5	13,71 ± 0,29		Donnelick
MD 22 FT		11 ± 1,6	14,7 ± 0,18		Donnelick
MD 20 FT		5,58 ± 1,17	14,42 ± 0,12		Donnelick

Table 5: Summary results: (U-Th)/He and AFT ages (this study).

Sample	Remarck	Latitude	Longitude	Elevation (m)	FT Age (Ma)	Error (± Ma)	Reference
03GR87	amfibolita	-13,258	-70,7799	713,00	2,5	0,9	Ruiz & Andriessen (2009)
03GR88	gneis	-13,3341	-70,8461	982,00	2,5	0,5	Ruiz & Andriessen (2009)
03GR91	gneis	-13,4772	-70,8981	1867,00	3	0,5	Ruiz & Andriessen (2009)
03GR92	gneis	-13,5179	-70,8963	2266	3,2	0,5	Ruiz & Andriessen (2009)
03GR89	gneis	-13,3938	-70,901	1285,00	3,4	0,7	Ruiz & Andriessen (2009)

Table 6: AFT ages in the studied area taken from Ruiz et al. (2009).

Sample	Latitude	Longitude	Y UTM	X UTM	Elevation (m)	He Age (mean, Ma)	Error1	Zhe age (Ma)	Error2	Bar age (Ma)	Error3	Incision depth (km)	Referencence
11PR01-COCA-343B	-13,65	-70,474	8490497	340568	1562	4,1	0,6	15	3	89,3	1,9	2,38	Lease et al. 2013
11PR04-COCA-344	-13,667	-70,478	8488614	340147	1759	3,7	0,4	15,7	0,7	103	2,1	2,25	Lease et al. 2013
11PR05-COCA-346	-13,711	-70,455	8483762	342664	2056	2,8	0,6	14,6	2,3	122,9	2,7	2,29	Lease et al. 2013
11PR09	-13,807	-70,479	8473126	340133	2775	4,1	0,9	75,5	17,7			2,08	Lease et al. 2013
11PR11	-13,808	-70,475	8473018	340567	2974	3,9	1,9					1,9	Lease et al. 2013
11PR16	-13,847	-70,504	8468684	337458	3240	4	0,2					1,91	Lease et al. 2013
11PR25	-13,929	-70,499	8459616	338056	4161	20,6	23,1	94,3	22,1			0,5	Lease et al. 2013

Table 7: He ages in the studied area taken from Lease et al. (2013).

Locality	Structural_Zone	Ref_Sample	Rockeval_TOC	Rockeval_TMax	Vitr_Mean	Vitr_Min	Vitr_Max	Confidence	Age	Reference
Inambari	EC	MD 147 A	6,107	549	2,56	2,15	2,89		Ordovician (Sandia Fm.)	2
		MD 147 B	6,794	544	2,52	2,34	2,75		Ordovician (Sandia Fm.)	2
		MD 149 B	4,25	549	2,77	2,32	3,05		Ordovician (Sandia Fm.)	2
		MD 151	5,395	544	2,75	2,46	3		Siluro-Devonian (Ananea Group)	2
		MD 152 B	0,293	536	2,66	2,11	3,11		Siluro-Devonian (Ananea Group)	2
		MD 93	1,495	437	2,58	1,93	2,82		Paleozoic	2
	SAZ	MD 119 B	0,268	549	0,64	0,64	0,64		Late Cretaceous to Paleogene ?	2
		MD 120 A	0,637	531	1,72	1,37	2,08		Late Cretaceous to Paleogene ?	2
		MD 120 B	0,571	547	0,64	0,54	0,78		Late Cretaceous to Paleogene ?	2
		MD 125 B	0,01	543	0	0	0		Late Cretaceous	2
		MD 127	0,358	453	1,48	1,2	1,81		Late Cretaceous	2
		MD 137 A	1,037	543	1	0,81	1,2		Late Cretaceous	2
		MD 137 B	1,126	450	1,01	0,81	1,25		Late Cretaceous	2
		MD 143 A	53,047	473	0,43	0,38	0,47		Neogene ?	2
		MD 143 B	0,116	548	0,51	0,46	0,56		Neogene ?	2
		MD 144 A	0,875	460	0,59	0,51	0,69		Late Cretaceous	2
		MD 154 A	51,654	379	0,36	0,3	0,43		Neogene ?	2
		MD 155 B	0,443	457	3,04	2,86	3,25		Miocene	2
		MD 156 B	46,963	443	0,5	0,38	0,62		Paleogene-Neogene?	2
		MD 158 A	57,412	361	0,3	0,27	0,33		Neogene	2
		MD 159 A	49,065	375	0,31	0,29	0,4		Neogene-Pleistocene	2
		MD 160 A	55,583	546	0,29	0,27	0,31		Neogene-Pleistocene	2
		MD 280 V			1,44	1,44	1,44	Very Low confidence	Late Cretaceous	1
		MD 290 V			0,89	0,78	1,03	Low confidence	Late Cretaceous	1
		MD 301 V			1,38	1,14	1,51	Middle confidence	Late Cretaceous	1
		MD 303 V			1,31	1,31	1,31	Very Low confidence	Late Cretaceous	1
		MD 318 V			0,58	0,47	0,68	Middle confidence	Late Cretaceous to Paleogene ?	1
Pongo de Coñeq	EC	MD K 5 V						Very Low confidence	Paleozoic	1
		MD K 10 Bis V						Very Low confidence	Paleozoic	1
		MD K 12 V			3,8	3,21	4,46	Very Low confidence	Paleozoic	1
	SAZ	MD 184 V			0,39	0,39	0,39	Low confidence	Paleogene	1
		MD 228 V			0,91	0,71	1,09	Low confidence	Carboniferous (Ambo Fm. ?)	1
		MD 229 V			0,85	0,7	1,01	Middle confidence	Carboniferous (Ambo - Tarma Fm.)	1
		MD 232 V			1,01	0,82	1,22	Low confidence	Late Carboniferous (Upper Copacabana Fm.)	1
		MD 238 V			0,61	0,57	0,67	Very Low confidence	Late Cretaceous	1

Table 8: Rock-Eval and vitrinite results (This study). Reference 1= analyses carried out by PaleoSur Laboratory (Argentina). Reference 2: analyses carried out by Repsol Exploration.

5.1.6. Interpretation

In the following, we first interpret the thermochronological ages regarding the age of crystallization or deposition of plutonic and sedimentary rocks. If the thermochronological ages are older than the depositional age, thus the grain ages are inherited from the source region and the thermochronological age is referred as detrital. If the thermochronological ages are similar to the age of crystallization or deposition, the thermochronological ages are referred as stratigraphic. If the thermochronological ages are younger than the age of deposition or crystallization, the ages are interpreted as reset or partially reset. AFT and AHe cooling reset or partially reset ages can result from either igneous activity, tectonic exhumation (normal faulting) or erosion (Ring, 1999). However, no tertiary intrusions or volcanism are found in the Madre de Dios SAZ and EC (Gotberg et al., 2010) and there is no evidence for significant normal faulting in the Peruvian SAZ and EC. Also, we assume that cooling has been caused by the rock erosion in response to thrust-related vertical motion.

5.1.6.1. Eastern Cordillera

Overall, AFTA and AHe ages of the Pongo de Coñeq EC and the Inambari EC show Late Miocene to Pliocene ages that are younger than the age of Permo-Triassic granite crystallization or Paleozoic sedimentary rocks (Figure 46 and Figure 47). Except for anomalous values, Ro results indicate that the maximum temperature reached by the EC Paleozoic rocks do not vary much with elevation and from one profile to another (536°C-549°C (Table 8). These temperatures are much higher than AFT and AHe closure temperatures indicating total resetting of EC AFT and AHe ages during Cenozoic burial. Hence, we interpret AFT and AHe ages as erosional cooling ages.

When compared with the AHe data published by Lease and Ehlers (2013) (Table 7) and AFT ages published in Ruiz and Andersen (2009) (Table 6), our analyzed AFT and AHe ages show co-variations with elevation for Inambari EC profiles (Figure 49). AHe ages from Lease et Ehlers (2013) were sampled across 1700-m range of elevation crossing over a fault (interpreted –without geometric evidences- by the authors as a back thrust and termed Eastern Cordillera fault or Ollachea fault, Figure 45) at ~2400 m in elevation. These authors argue that this fault has no significant effect on thermochronological ages as AHe ages have a narrow 4.1- to 2.8 Ma range, reflecting rapid, synchronous erosion both hanging-wall and footwall blocks caused by shift in global climate from early Pliocene warmth to late Pliocene cooling (Lease and Ehlers, 2013).

Contrary to what is found by these authors, our AHe and AFT data show younger ages above 2500 m suggesting that erosion is non uniform across the EC (Figure 49 and Figure 52). Rather, younger AFTA and AHe ages are best explained by the displacement on a east-verging thrust fault (Ollachea fault, re-interpreted as illustrated in Figure 45 and Figure 52 based on DEM analysis and geological mapping) that could drive surface uplift of the upper part of EC and Altiplano. Hence in the light of our thermochronological data, we do conclude that erosional cooling of the Southern Peruvian EC is not controlled by a Pliocene climatic shift but rather by Plio-pleistocene tectonic antiformal stacking of thrust faults (see structural section of Figure 46).

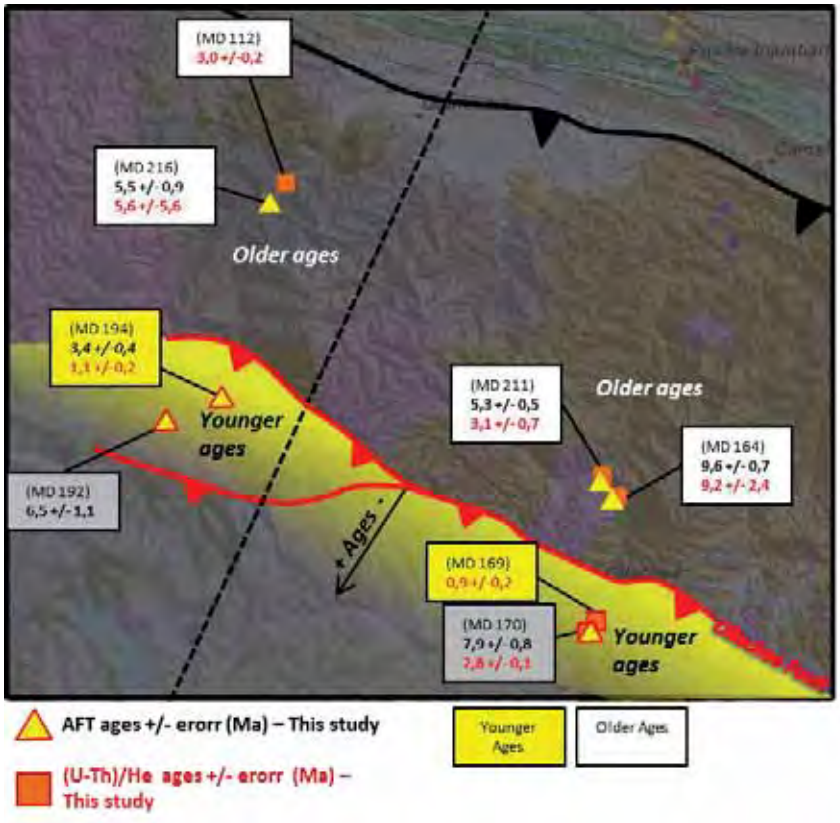

Figure 52: Enlarged view from Figure 45 focused on the EC and the Ollachea faults. See the shift in AFT and AHe ages in both sides of the fault. Yellow surface corresponds to the surface uplift created by the Ollachea thrust fault. Note that AFT and AHe ages also increase towards the Altiplano: they suffered less uplift than samples situated close to the fault.

5.1.6.2. SAZ

MD 56-FT and MD 57-FT are Carboniferous in age and have been collected in the vertical sedimentary section of the Pongo de Coñeq Canyon that includes strata from the Devonian to the Paleogene. In the Pongo de Coñeq sedimentary section, MD 57 FT is stratigraphically shallower than MD 56-FT. It has older AFT age (90.4±7.8 Ma vs 25.8±2.5 Ma) (Table 3, Figure 47 and Figure 48), shorter MTL (10±0.5 µm vs 14.4±0.41µm) and similar dpar (~2.5µm) (Table 2; Figure 50). Overall, AFT ages are younger than their stratigraphic ages, indicating resetting after deposition. The role of the structure or chemistry of apatite crystals in the explanation of the older AFT age of MD 57-FT with respect to MD 56-FT might be disregarded as Dpar values are quite similar (Barbarand et al., 2003a; Barbarand et al., 2003b; Burtner and Nigrini, 1994). We interpret the up-section shift in AFT ages from ~25 Ma to ~90 Ma as reflecting the transition from structural depths corresponding to full thermal resetting of the AFT system (Total Annealing Zone or TAZ) before Cenozoic exhumation to structural depths corresponding to the exhumed Partial Annealing Zone (PAZ). A prolonged stay within the Miocene PAZ for MD57-FT is also supported by short MTL (10±0.5 µm). High MTL (14.4±0.41µm) and younger AFT age for MD 56-FT also indicate rapid exhumation of this sample from the TAZ. Although we do not have as many samples as necessary to precisely locate the limit between the Miocene TAZ and PAZ as shown in Espurt et al. (2011), we do argue that this limit was between the Early and Late Carboniferous stratigraphic level in the Miocene times. Hence, the MD 56-FT AFT age indicates that the onset of exhumation has occurred as early as 25.8±2.5 Ma in this part of the Madre de Dios SAZ. Samples MD 67-FT and MD 68-FT are Early Middle Miocene in age and indicate Oligocene (MD 68-FT=30.3 ± 3 Ma) to Early Miocene (MD 67-FT=20.1 ± 2 Ma) AFT ages (Table 3, Figure 47 and Figure 48). AFT ages are older than

stratigraphic ages, within error bar. It is also the case for MD 66-FT which is Late Miocene to Pliocene in age and presents an older AFT age (16.6 ± 3 Ma). Thus, the three ages obtained from sedimentary samples in the Salvación syncline are detrital ages.

In the Inambari SAZ, MD 29-FT and MD 30-FT are Late Cretaceous in age (Figure 46). Their AFT ages are younger than their stratigraphic ages indicating total resetting after deposition (Table 3). It is likely that the younger AFT ages recorded the passage through the apatite PAZ to the surface and therefore these ages correspond to the minimum uplift ages of the Imbricates. Rapid uplift is support by the track length distribution and short MTL (~13.96 µm). Given the AFT ages of MD 29-FT and MD 30-FT, we consider that a major thrust-induced surface uplift occurred at ca. 4-5 Ma inducing the erosion of the imbricates. MD 28-FT has also been sampled in the Punquiri syncline. It is Neogene in age and is part of the growth strata deposits which are presented further in this study. MD 28-FT has a discordant grain age population that shows two peak ages P1 (5.5±1.5 Ma) and P2 (29.6±3.5 Ma) (Table 3; Figure 48). The youngest peak age (P1: 5.5±1.5 Ma) has the dominant population of grain (60% of the analyzed grains). Given the uncertainty of the depositional age of MD 28-FT, this age could ever be stratigraphic or a cooling age. A cooling age would indicate that MD 28 passed through the PAZ at approximately the same time as MD 29-FT and MD-30. This would imply that uplift of MD 28 is related to the forward propagation and erosion of the imbricate thrusts system (Figure 46). Structural data and balanced cross-section do not support this interpretation. In addition, MD 28-FT has been sampled within the growth-strata deposits that also include the tuffaceous sample MD 20-FT. Hence, we favor a detrital age for MD-28 FT. MD 22-FT has been sampled within the Punquiri syncline strata and is Pliocene in age (dated ~3.45 Ma by Ar/Ar method, see PART D for more details). It has a concordant grain-age distribution which indicates a pooled age of 11.0 ± 1.6 Ma (Table 3; Figure 48). Considering the AFT age is clearly older than the stratigraphic age, this implies that the AFT age corresponds to an inherited age. MD 20-FT is 3.45 Ma old and is tilted (Figure 59) indicating post depositional deformation. Hence, it is likely that the discordant grain-age distribution reflects heterogeneity in the source cooling rather than heterogeneous annealing of the apatites. Moreover, the youngest peak age (P1: 5.5 ± 1.5) has a similar age as those of MD 29-FT and MD-30 (Table 3). This youngest peak age P1 could be inherited from the uplift and erosion of the imbricates thrust system. MD 13-FT is interpreted to be Late Miocene to Pleistocene in age and is made of tidal deposits (Hovikoski et al., 2005) (also see Part C of he manuscript). MD 13-FT has been collected close to the Inambari thrust which corresponds to the active thrust front of the southern Peruvian Subandean zone (Figure 45 and Figure 46). This thrust front separates the present-day wedge-top depozone to the southwest from the present-day foredeep depozone to the northeast. Because MD 13 is Late Miocene to Pleistocene in age (see Part D), we interpret its AFT age as detrital.

5.2. Syn-sedimentary deformation

5.2.1. Syn-sedimentary deformation in fold-and-thrust belts

The study of the synorogenic sedimentary record, and the understanding of the geometric and relative age relationships between these synorogenic sediments and the structures is a powerful tool to deciphering the kinematic evolution of thrust and folds belt (Burbank et al., 1996; Carrera and Muñoz, 2008; Vergés et al., 2002), especially if the synorogenic strata are well dated by radiometric, magnetostratigraphic or biostratigraphical dating (Figure 53 Figure 54). In particular, growth strata (Medwedeff, 1989) that accumulated during and in the vicinity of growing structures facilitate remarkably precise dating of individual thrust movement histories in the Subandean zones (e.g. in Echavarria et al. (2003b)). Growth strata are commonly recognized on the basis of their cross-sectioned geometries (Anadón Monzón, 1986; Hardy et al., 1996; Medwedeff and Suppe, 1986; Suppe et al., 1992), but in the Subandean zones geometries at the scale of fold limbs are difficult to document. We identified growth strata and unconformities in the Cenozoic sedimentary filling of the Madre de Dios foreland basin from field observations, seismic data (2D lines) and Digital Elevation Map (DEM). Growth strata related to thrust fold motion have been observed in both the northern and the southern parts of the Madre de Dios SAZ.

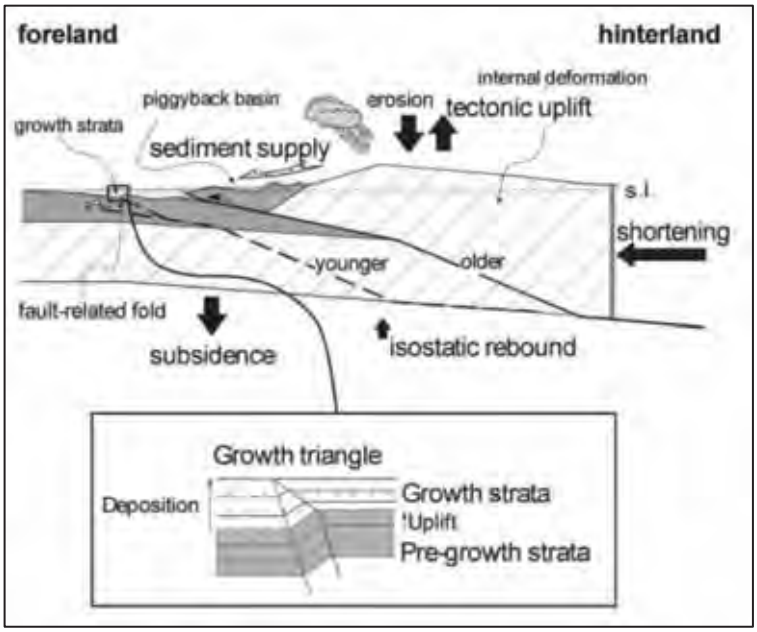

Figure 54: Cartoon showing superficial and deep processes acting during syn-tectonic foreland basin infill development and the position of growth strata linked to the foreland fold-and-thrust belt, from Verges et al. (2002).

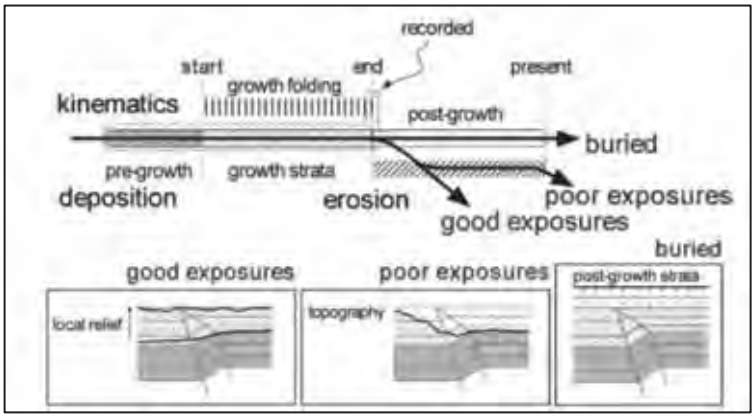

Figure 53: Folded sedimentary basins display different levels of growth strata preservation from buried at depth (typical of modern and still active fold-and-thrust belts) to uplifted and eroded examples (representative of old and inactive deformed belts).

5.2.2. Neogene syn-sedimentary deformation

5.2.2.1. Pongo de Coñeq: the Salvación syncline

In the Salvación syncline, Neogene strata are the thickest deposits of the Cenozoic sedimentary filling. They show high sedimentation rate, and their depositional environment is characterized by alternating of coastal and continental deposits (see *Part C* of the manuscript for details). Seismic section Hepc-09-04 (Figure 55; see Figure 12 for location) shows a main growth stratal geometry related to the piggy-back Salvación syncline between seismic marker T2 (Late Miocene) and the most recent deposits (Quaternary). The thickness corresponding to this stratigraphic interval is greater in the northern flank of the syncline than in its southern flank (Figure 56). Seismic sections Hepc-09-05 and Hepc-09-06 (see Figure 12 for location) also display global growth stratal geometry within the Neogene filling of the syncline, with strata becoming thicker towards the northern flank.

Neogene deposits are characterized by coarse grained sedimentation and increase in sedimentation rates (see Part D of this manuscript). The oldest matrix-supported conglomerates is described in the Late Early Miocene deposits (MD 61Bis=83) and sedimentary deposits became thicker and coarser during Middle Miocene period (MD 244), suggesting that active relief creation and erosion occurred in the Late Early Miocene times. In addition, an intra-Tertiary décollement level (F3) has been interpreted on seismic sections Hepc-09-01, Hepc-09-02, Hepc-09-04, Hepc-09-17 and Hepc-09-16, and has been mapped in Figure 11. This surface is located within deposits which are Early Middle Miocene in age (outcrop MD 67; Antoine et al., 2012, see Annex nº7). Thrusting of the Salvación syncline is consequently no older than Early middle Miocene.

In the Salvación thrust footwall, seismic section Hepc-09-04 also shows more little-scale growth strata between the Early Middle Miocene seismic horizon (T1) and the Late Miocene seismic marker (T2) (see enlarged view corresponding to the black rectangle in Figure 56). In details, these growth strata are situated above seismic marker T1 (Early Middle Miocene) and just below an unconformity surface represented by a dashed line in Figure 55 and Figure 56. This surface is interpreted to correspond to a Middle Miocene erosion. It has also been documented in other seismic sections (see the composite seismic section, Figure 21).

Figure 57 is a tentative reconstruction of the deformation history based on seismic sections localized south to the Pongo de Coñeq section. Indeed, the restoration is mainly based on the interpretation of seismic section Hepc-09-04 where growth strata are preserved, but can be considered as regional model in the Madre de Dios foothills. Note that further north, seismic line Hepc-09-01 (crossing over the Salvación syncline and the Pantiacolla anticline) doesn't show any Neogene growth strata. This can be due to the strong erosion of the southern flank syncline, and the younger Pantiacolla anticline uplift towards the northern flank of the syncline. According to our interpretation, we propose the six following stages in the deformation history of the Pongo de Coñeq SAZ (around Hepc-09-04 area) (Figure 57):

- A. Early Middle Miocene (15-6 to 14.7 Ma): no deformation registered or preserved in the present-day Pongo de Coñeq SAZ.
- B. Post Early Middle Miocene (post 15.6-14.7 Ma to ?): the Late Paleozoic to Early Middle Miocene sequence is deformed by two fault propagation folds, which are probably linked to a basal intra-Paleozoic detachment level. Growth strata developed between the two folded structures. Uplift of the two frontal folds (Figure 56) recorded by fold limbs fold limb growth strata sedimentation and onlaps on the northern limb of the hinterland fold (black circles in Figure 56-C). Because of their relative geometry and stratigraphic position, these growth strata are post-Early Middle Miocene and pre-Late Miocene in age (Orange seismic Horizon or T2). We thus propose a first deformation period during Middle Miocene times (Period 1).
- C. Middle to Late Miocene (? To 10 Ma): an unconformity developed above the growth strata which progressively flatten towards the top. This unconformity has been documented in the overall Pongo de Coñeq area and probably documents erosion during Middle Miocene times. To simplify the figures, this unconformity is depicted by a bold black dashed line in the other illustrations Figure 56-D, -E and -F). The deposits overlying the erosive surface are often related to the intra-Tertiary décollement level already presented (F3). These deposits are probably made of fine-grained sedimentary rocks.
- D. Late Miocene to Pliocene (~10-2.6 Ma): the growth stratal geometry documented between seismic markers T2 and T3 in the present-day Salvación syncline is interpreted as the result of the duplex formation and uplift below the present-day Pongo de Coñeq Canyon and the southern flank of the syncline.
- E and F. Post Pliocene to present-day (post ~2.6-0 Ma): the duplex is still growing during this period as attested by the continuous presence of the growth strata already described in the stratigraphic interval comprised between T2 (Late Miocene to Pliocene) and the uppermost strata (Quaternary). Activation of the Intra-Tertiary décollement level is probably contemporaneous of the duplex growth which enables higher slip transfer toward the foreland (Zoetemeijer, 1993).To compensate the shortening induced by the growing, ramps (F6 and F9 in Figure 57) developed from the intra-Tertiary décollement level across the overlying Late Miocene to Quaternary sequence and progressively induced piggy-back structures. These piggy-back structures are visible in the present-day geometry of the Salvación syncline. Thrust Fault F9 probably corresponds to the reactivation of ancient structures. F6 and F9 are visible at the surface and correspond to fault scarps on map view (see F6 and F9 on the DEM, Figure 11). Stages D, E and F correspond to deformation Period 2.

Note that very similar piggy-back structures have been documented in the Bolivian Subandes by Baby et al. (1995). The same structures have later been modelled by “sand boxes” and numerical approach by Leturmy et al. (2000) in order to study the retroactive effects of tectonics on piggy-back development in thin-skinned thrust belts. Conclusions are that i) erosion promotes fault reactivation and tectonic delamination (passive roof duplex) while ii) sedimentation promotes forward shifting of the frontal thrust and consequently piggy-

back development (Leturmy et al., 2000). Authors also conclude that the step-by-step history of the thrust belt predicts that each change in tectonic location is recorded with large unconformities in basins (Leturmy et al., 2000). This could explain the presence of the unconformity documented in the Pongo de Coñeq area within the Middle-Late Miocene sequence.

The structure of the Pongo de Coñeq SAZ shows striking similarity to the geometry obtained with Leturmy's model characterized by "basement tilting, sedimentation and no erosion" (second model performed by the authors referred as the "Syn-orogenic wedge-shaped basin" model) (Leturmy et al., 2000) (Figure 58).

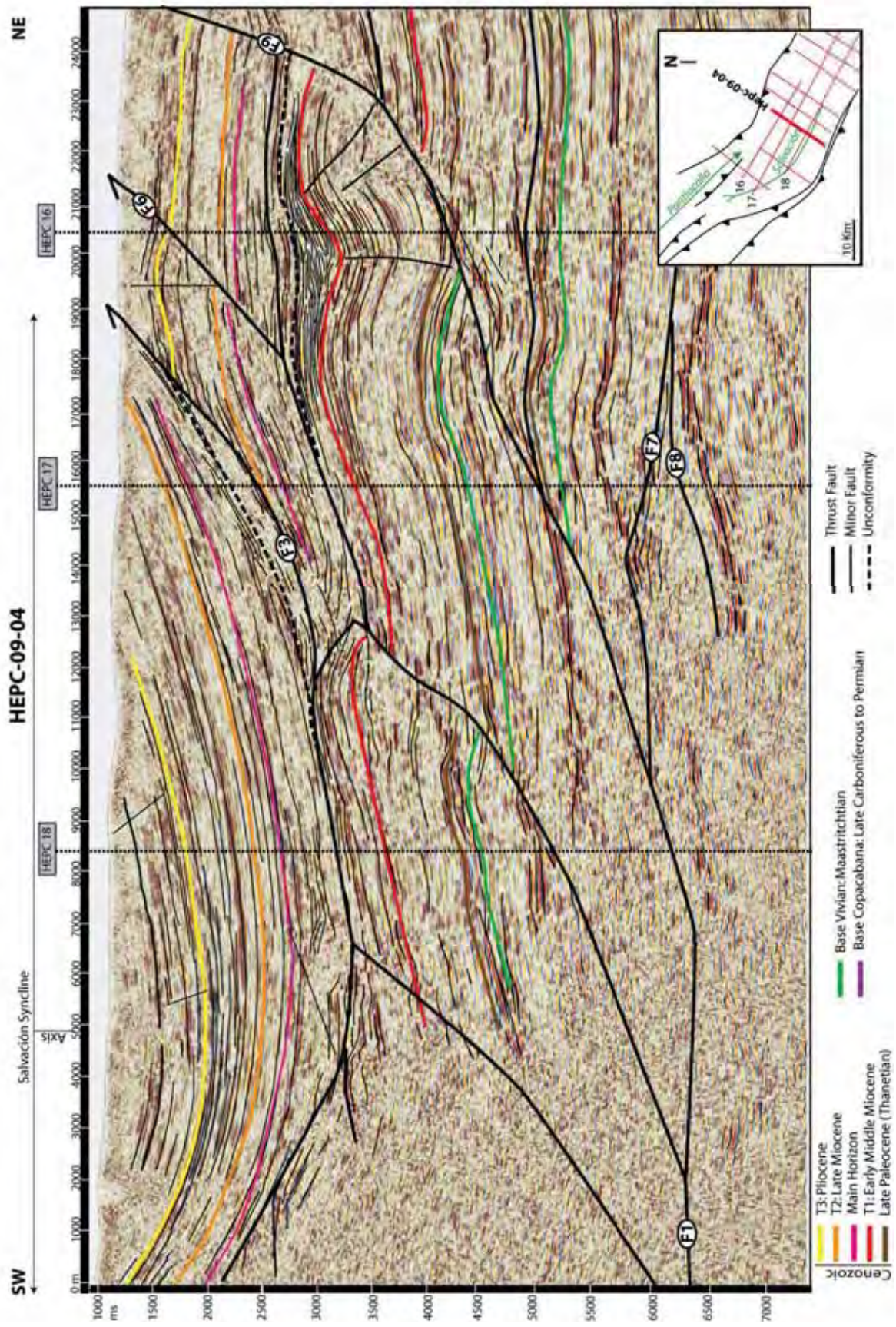

Figure 55: Interpreted 2D seismic section Hepc-09-04 (location on Figure 12). Seismic markers (coloured bold lines) are correlated with the reference line Hepc-01 thanks to the transverse seismic sections Hepc-17 and Hepc-18. These seismic markers correspond to time lines.

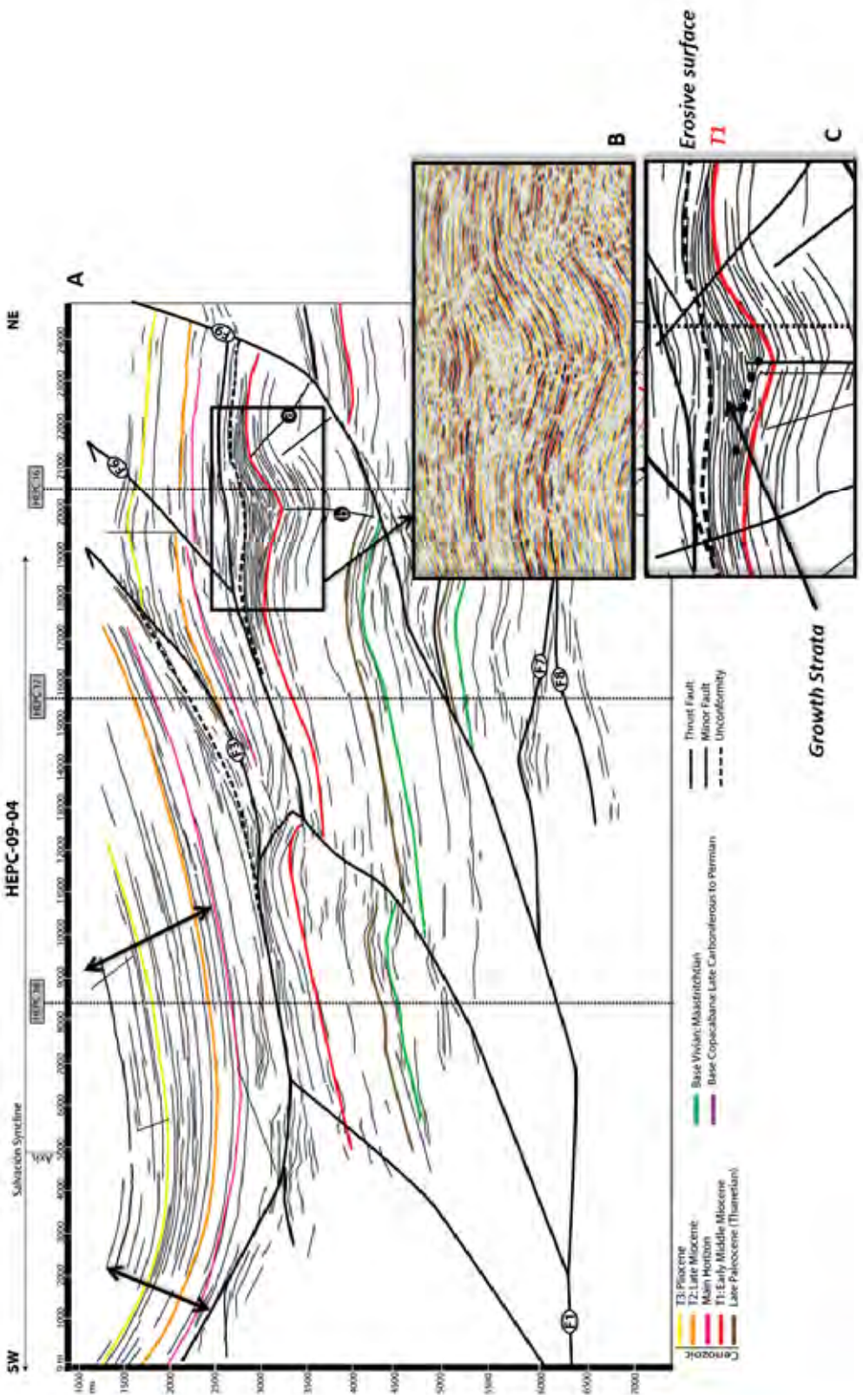

Figure 56: A) Line drawing of the interpreted seismic line Hepc-09-04. Black arrows indicate the general growth stratal geometry displayed here by the post Early Middle Miocene (near T2 horizon) to Plio-Quaternary strata (above T3 horizon). B) Enlarged view of the seismic line area corresponding to the black rectangle on A). C) Line-drawing interpretation of the enlarged view. Note the small-scale growth strata which developed between T1 red horizon (Early Middle Miocene) and the dashed black line, corresponding to an unconformity. According to their stratigraphic position, the strata that are just underlying this dashed line are also situated beneath the orange T2 seismic horizon corresponding to Late Miocene age. They consequently are post- Early Middle Miocene and pre-Late Miocene in age.

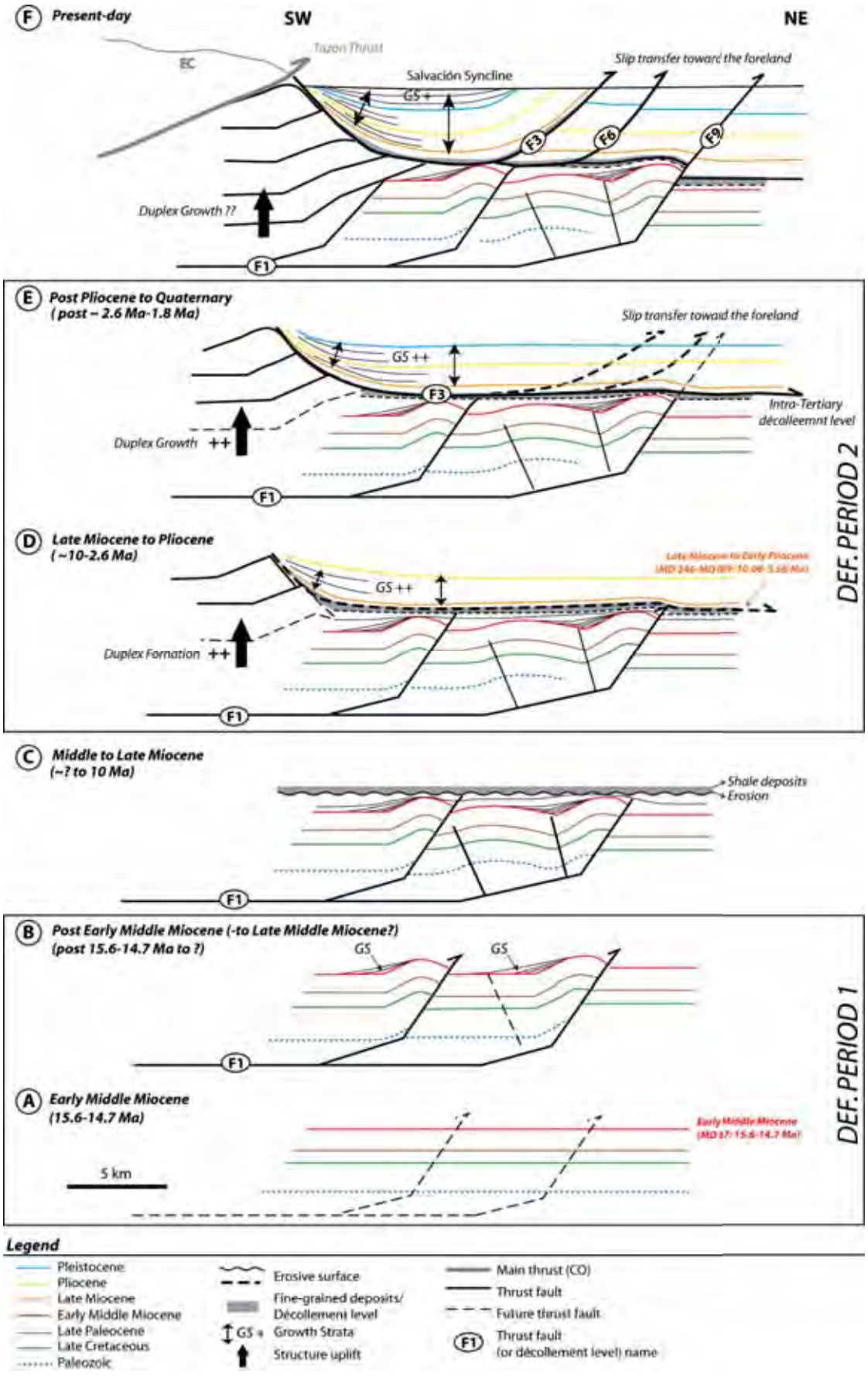

Figure 57: Synthetic restoration of seismic section Hepc-09-04 inferred from present-day geometry, syn-sedimentary features and biostratigraphic content. GS= Growth Strata. See details in the text.

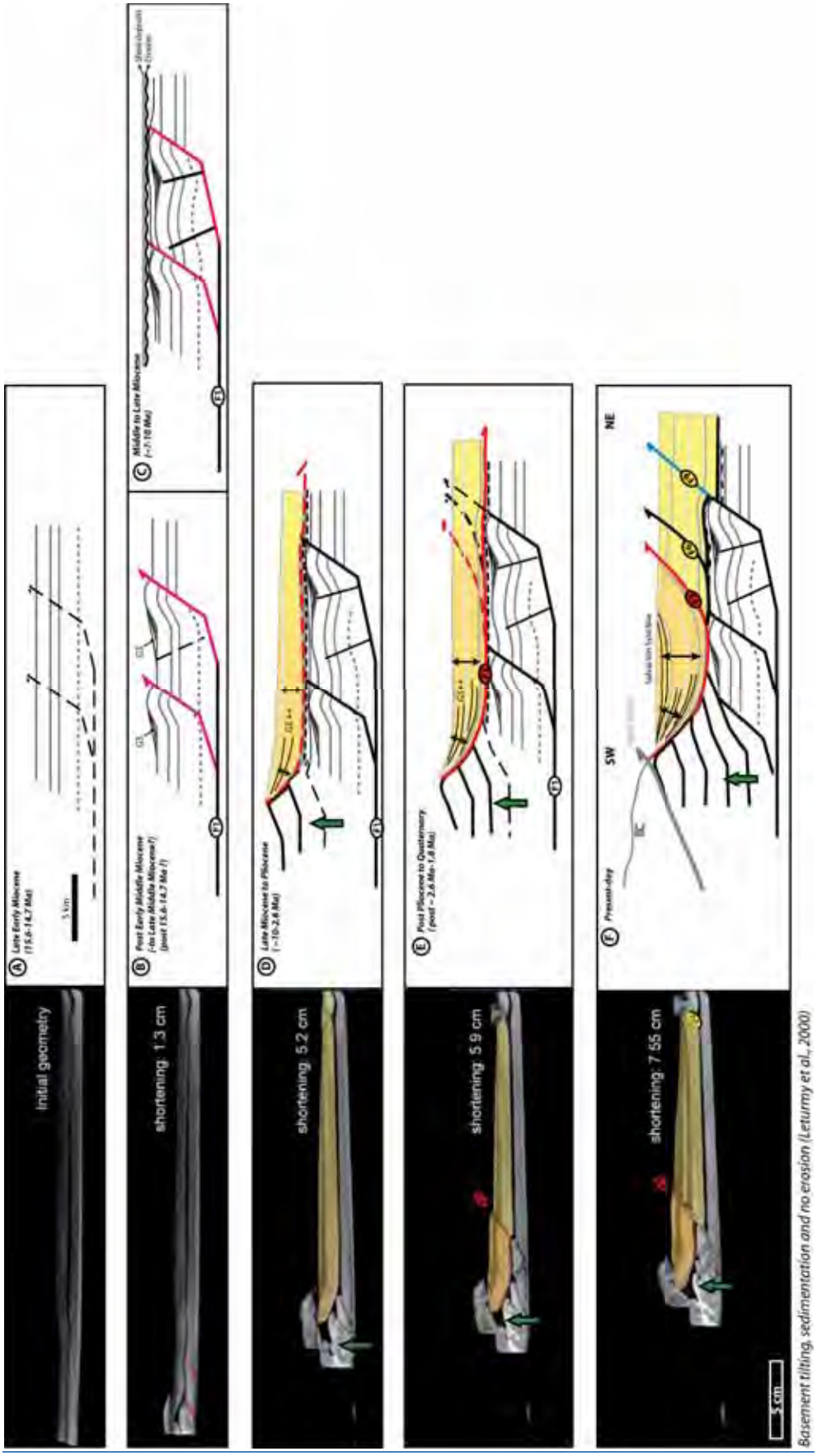

Figure 58: Comparison of seismic section Hepc-09-04 deformation history (fugures A to F on the right) and modelling realized by Leturmy et al. (2000) in the Bolivian Subandes (modified X-ray tomograph pictures, at the left of the figure).

5.2.2.2. Inambari area

In the southern Inambari area, the Cenozoic filling of the Punquiri syncline is also characterized by alternation of thick continental to shallow marine deposits (see part D of the manuscript). As observed in the Salvación syncline, the southern Punquiri syncline also shows growth stratal geometry. These growth strata are highlighted by both i) dip data projected onto seismic line Mob-109 (Figure 59), and ii) the geometry of Neogene to Pleistocene strata on the field (Figure 60).

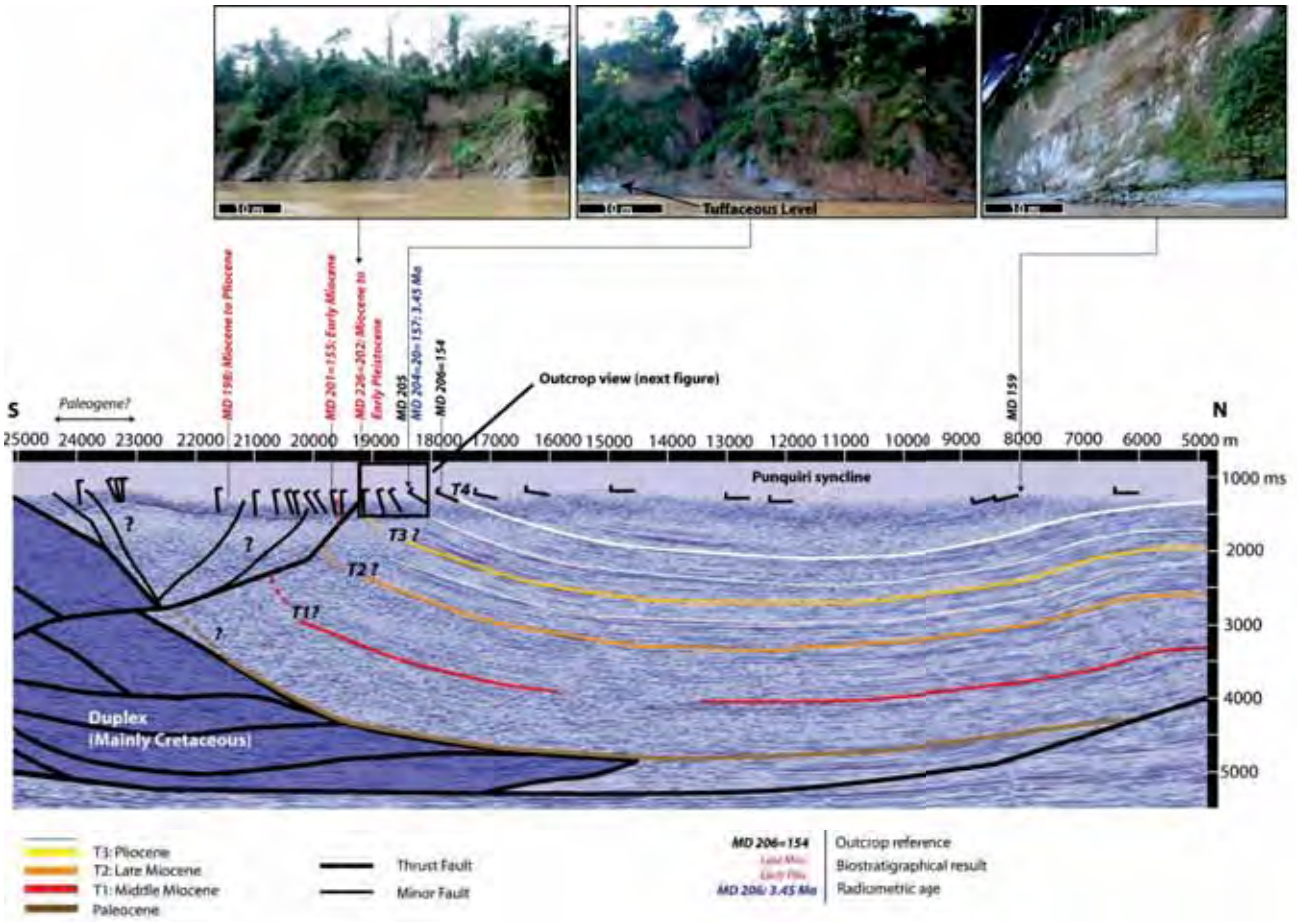

Figure 59: Seismic section Mob-109 focused on the Punquiri syncline (location on Figure 12). Structural interpretation has been simplified. The locations of the seismic markers (T, T2, T3 and T4) in time (vertical axis in TWT) are tentative as very few biostratigraphic data exist in this area. Dip and biostratigraphic data have been projected above the topography using Move software. Photographs illustrate the evolution of layers dip.

Figure 60 (previous page): Outcrop view (panoramic photo montage) of localities MD 202-204-205 (see previous figure for location on the seismic line). Stratification is highlighted by bold yellow lines to illustrate the change in the dip data forming overall growth stratal geometry, the layers flattening towards the syncline axis.

The growth strata from the Punquiri syncline are thus related to the second period of deformation registered in the Pongo de Coñeq area and interpreted to be Late Miocene and Pliocene in time (Figure 57-D and E).

Because seismic data quality is not as good as in the Pongo de Coñeq area and because of the few biostratigraphic constraints existing in the Inambari SAZ, the timing of deformation is more difficult to assess. However, based on the geometry of the present-day Inambari SAZ and on the results obtained in the northern Pongo de Coñeq SAZ, we propose a tentative 2-steps history of deformation (Figure 61).

During the first deformation period (Period 1; Figure 61-A), growth strata developed:

i) Onto the imbricate system which are interpreted as the equivalent structures to those observed in the Pongo de Coñeq area and related to the same deformation event (see little-scale growth strata "GS-1" coloured in red in Figure 61-A for the Inambari area and the growth strata of Figure 57-B for the Pongo de Coñeq SAZ), and

ii) towards the Madre de Dios foredeep, in the growing Punquiri piggy-back syncline ("GS-2", also coloured in red in Figure 61-A).

At present-time, this first period of deformation which is conserved in the Pongo de Coñeq area (Figure 56-A and B) is not visible in southern Inambari SAZ. This could be due to the poor seismic quality of seismic section Mob-109 preventing their detection, but we assume that it is mainly due to the higher deformation rate in the Inambari area relative to the Pongo de Coñeq area. We propose that Period 1 related growth strata of the Inambari SAZ have been eroded or incorporated by younger Period 2 (Late Miocene to Pliocene times) thrust related structures (Figure 61).

During Period 2, the deformation mainly accommodated by the growth of the internal duplex (Figure 61-B). Period 1 fault propagation folds structures as well as their associated growth strata may have been partly eroded and partially incorporated in this duplex and are now part of the internal duplex. We propose that the growth strata which deposited in the incipient Punquiri syncline during Period 1 (Figure 61-A) have also partly been eroded during Period 2 by the uplift of the southern flank of the Punquiri syncline which have been facilitated by the development and activity of the basal Tertiary- related décollement level situated at the base of the piggy-back Punquiri syncline. The activity of the basal-Tertiary décollement level is also directly linked to the duplex growth.

Today, the only growth strata documented in the Punquiri syncline (Figure 59 and Figure 60) are related to the second period of deformation (Late Miocene to Pliocene) and thus to the duplex growth (Figure 61-B).

Because AFT results of sandstones sampled in the Imbricates area indicate cooling ages around 4 and 5 Ma, the formation of the imbricates is most probably linked to Period 2 deformation (Late Miocene to Pliocene).

Note that the Nusiniscati syncline (Figure 61-B) is mostly formed by Cretaceous to Early Neogene deposits, and thus cannot be related to Period 2 deformation.

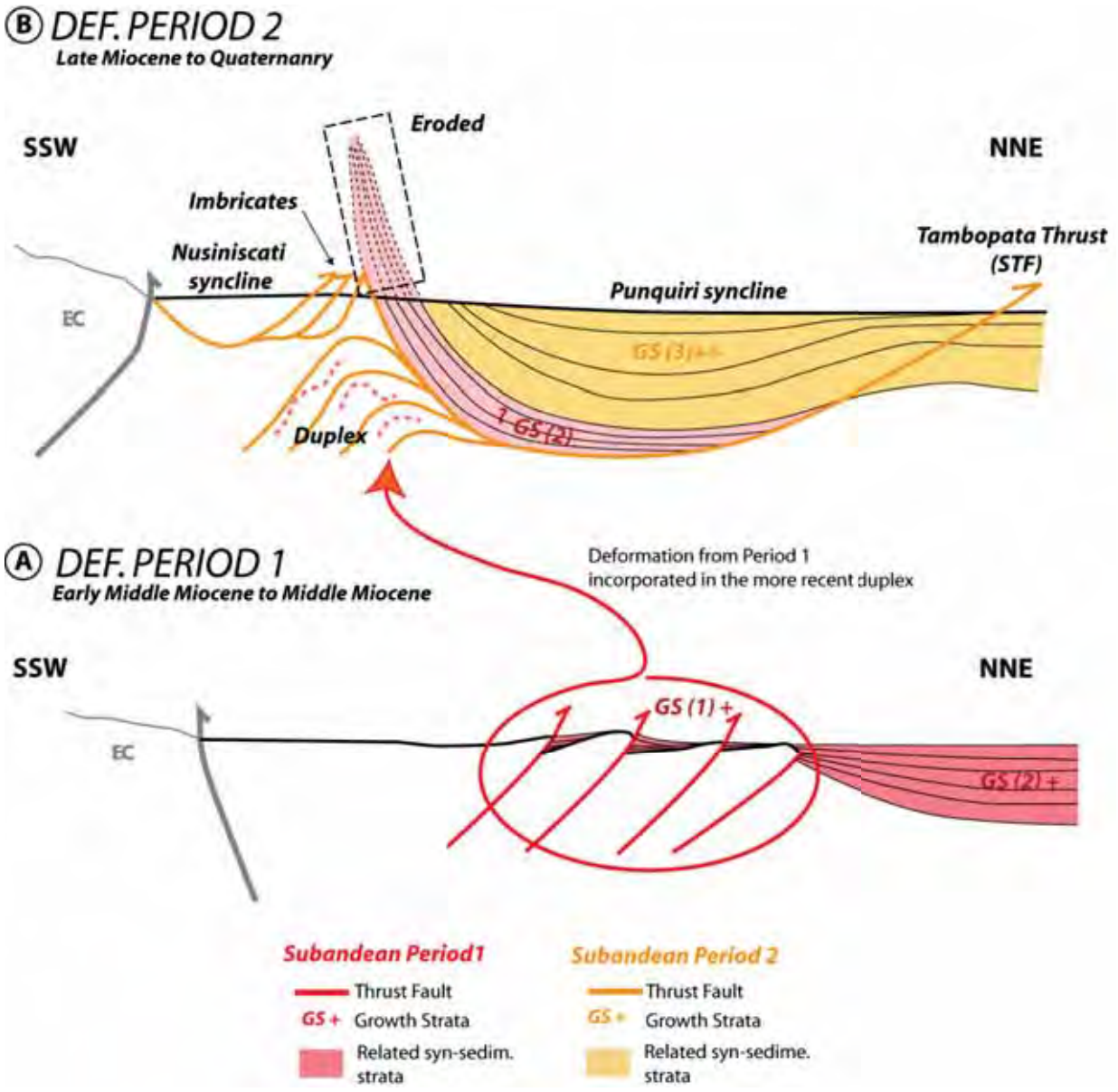

Figure 61: Synthetic sketch of the timing of deformation in the Inambari SAZ. GS= Growth Strata. STF= Subandean Thrust Front. More details in the text.

As we already highlighted in the Punquiri area, the present-day geometry of the main Inambari structural cross-section also shows striking similarity to the geometry obtained with Baby's syn-sedimentary analog sandbox experiment (Baby et al., 1995) in the Alto Beni (Bolivian Subandes). In this experiment, the piggy-back basin develops in the core of a syncline which is structuring on the roof thrust of the duplex (Figure 62-B). The development of the syncline borders synchronizes with the duplex shortening which constitutes the "motor" of the basin formation (Baby et al., 1995).

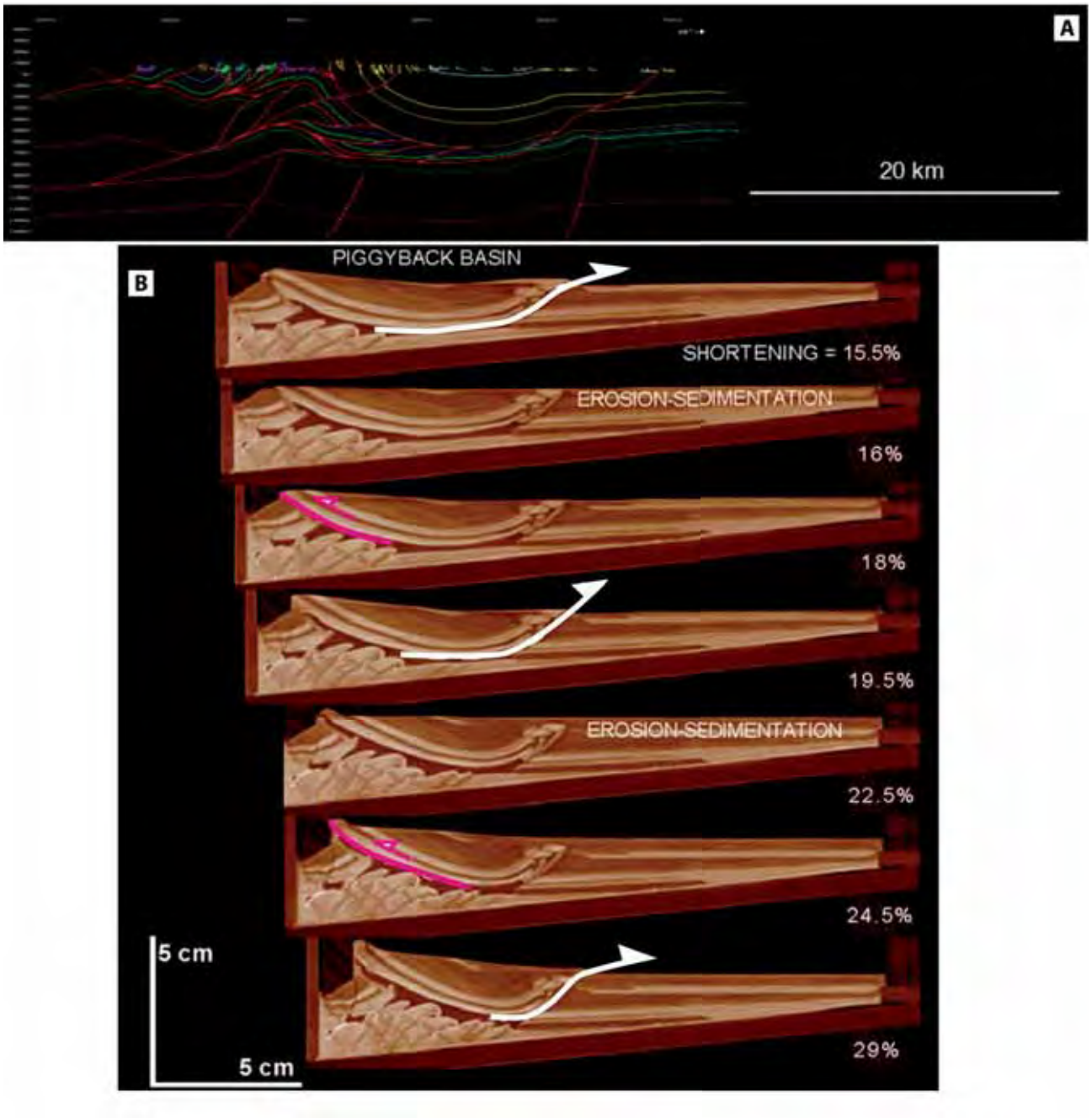

Figure 62: Commparison between the present day geometry of the Inambari SAZ (A) and Baby's et al (1995) sand-box experiment destined to modelling the Alto Beni iin the Bolivian Subandes. Red bold lines corresponds to back-thrust whereas white bold lines display forward thrusts (toward the foreland).

5.3. Synthesis

The earliest Cenozoic evidences of deformation and exhumation in the present-day EC and SAZ of the Peruvian Central Andes consist of:

i) AFT cooling ages recorded by Paleozoic rocks of the Pongo de Coñeq Canyon (SAZ) and which indicate a ~25±5 Ma cooling age (MD 56-FT),

ii) Growth strata mainly documented within the Middle Miocene (15.6-14.7 Ma) strata in the Salvación syncline (SAZ).

Both evidences have been documented in the Pongo de Coñeq SAZ. Middle Miocene structures (fault related folds) and their associated growth strata (Period 1) are well developed around seismic section Hepc-09-04, Hepc-09-05 and Hepc-09-06 as illustrated by the synthetic section B, Figure 63. The northernmost seismic sections in the Pongo de Coñeq SAZ show almost no or very few of these evidences (Hepc-09-01 and Hepc-09-02; Figure 63-A). No Period 1 related deformation nor exhumation evidences have been registered in the southern Inambari SAZ but we believe that it is highly probable that equivalent Middle Miocene structures were further integrated in the recent internal duplex, as illustrated by Figure 63-C.

We acknowledge a time gap between the age of exhumation in the western border of the SAZ (~25 Ma; Late Oligocene) and the age of deformation documented in the Pongo de Coñeq SAZ (post Early Miocene). To explain this time gap, we propose that exhumation started as early as Late Oligocene times (~25±5 Ma) and continued until Late Early Miocene (post 15.6-14.7 Ma) to possibly Early Late Miocene times. This implies that the very beginning of deformation and exhumation of the eastern Central Andean wedge has not been recorded (or preserved ?) in the present-day sedimentary filling of the SAZ. This hypothesis is confirmed by the absence of Period-1 related features in the Inambari SAZ. Thus, we consider that Period 1 deformation started at least ~25±5 Ma ago and continued at least until Middle Miocene period (post 15.6-14.7 Ma).

Period 1 structures are separated from Period 2 structures by an erosive surface. This Middle to Late (?) Miocene erosion is probably linked to a regional tectonic event. Because overlying deposits are interpreted to be fine-grained deposits (intra-Tertiary décollement level-F3), it is very probable that this Middle to Late (?) Miocene period was related to tectonic quiescence.

Present-day geometry of the SAZ majorly results from deformation Period 2. It is characterized by:

i) Large-scale growth stratal geometries in both the Salvación and the Punquiri synclines,

ii) Formation of duplexes (in both the Pongo de Coñeq and the Inambari SAZ),

iii) Intra-Tertiary décollement-level activation (only in the Pongo de Coñeq SAZ?)

iv) Forward thrusting (F6 and F9),

v) Pliocene AFTA erosional cooling ages in the whole EC and SAZ

vi) Younger Plio-Pleistocene erosional cooling AHe ages in the whole EC

vii) Co-variation of AFT and AHe ages with elevation for the Inambari EC profiles

Large-scale growth stratal geometries that constitute the Salvación and the Punquiri synclines are related to the growth of duplexes in the Pongo de Coñeq SAZ and in the Inambari SAZ (internal passive and/or active duplexes). Because growth strata are continuous in both areas, deformation has certainly been continuous from Late Miocene to present-day.

Intra-Tertiary décollement level as well as forward thrusts (F3 and F6 for example) probably became active during the formation of the duplex as it cuts through an almost complete Noegene sequences. Thrust F9 is subsequent to thrusts F3 and F6. These recent thrust are probably the result of slip transfer towards the foreland. Note that these structures are particularly developed in the southern Pongo de Coñeq area (seismic sections Hepc-09-04, Hepc-09-05 and Hepc-09-06).

Low temperature thermochronology (AFT and Ahe ages) indicate Early Pliocene and Plio-Pleistocene exhumation ages respectively. These results imply that the second period of exhumation was recorded in both the EC and the SAZ and started at least ~5 Ma ago. Thermochronological ages are thus consistent with Period 2 deformation. Period 1 deformation was not recorded by thermochronological ages of the Inambari EC and SAZ. Associated with the fact that Period 1 growth strata were eroded or incorporated into Period 2 thrust structures, we suggest that the Inambari EC and SAZ was more deformed during period 2 when compared with the Pongo de Coñeq EC and SAZ.

Difference between both areas could be explained by different deformation transfer processes toward the SAZ in relation with sedimentation rates.

5.4. Discussion

Our results have implications regarding two fundamental problems in Andean geology: i) the putative effect of Pliocene climatic control on erosion and ii) the mechanisms responsible for the growth of the Altiplano.

Regarding the first problem, many recent studies have emphasized the potential climatic control on the Neogene erosion exhumation and deformation of the Eastern Andean orogenic wedge (EC and SAZ). Contrasting climatic conditions between wet (north to latitude 15-16°S) and dry (south to 21°S) is supposed to have controlled the amount of shortening during the Miocene (ca. 19 or ca. 8 Ma) potentially limiting the width of the Andes north to latitude 15-16°S (McQuarrie et al., 2008). Based on the construction of two crustal scale balanced cross-sections, these authors suggested that a wetter climate is responsible for the greater percentage of shortening in the northern actively deforming SAZ relative to southern SAZ (41±2% on north versus 32±2% on south, Mc Quarrie et al., 2008). In addition, Pliocene erosion of the Eastern Cordillera of Bolivia and Southern Peru apparently decoupled from active deformation as recorded by low-temperature thermochronometers cooling ages was interpreted to be controlled by a shift in global climate from early Pliocene warmth to late Pliocene cooling driven by sea surface temperature changes (Lease and Ehlers, 2013). Regarding the later point, our results are in contradiction with Lease and Elhers 2013's conclusions. These authors used thermochronological ages and absence of deformation in the subandes since 15 Ma to exclude a tectonic control on erosional rate. In particular, based on the same similar vertical profile we made, they detect change in (U-Th)/He on zircon ages (ZHe, Closure temperature of ~180°C, Reiners 2005)

from young early Miocene ZHe ages in the hanging wall of the Ollachea fault toward old ZHe ages in the footwall which they interpret as being due to Ollachea back-trust activity in the Early Miocene. As all analyzed AHe ages give similar Pliocene AHe ages in the same vertical profile, they conclude that the Ollachea thrust was inactive during the Pliocene. They interpret invariant AHe ages in both sides of the Ollachea fault (or Eastern Cordillera faults) as being due to a global climate shift from early Pliocene warmth to Late Pliocene cooling (Lease and Elhers, 2013). Our AFT and AHe data show younger ages above the thrust suggesting that erosion is non uniform across the EC (Figure 52). Rather, younger FTA and AHe ages are best explained by the movement on a ramp thrust fault (the Ollachea fault) that could drive surface uplift of the upper part of the EC and Altiplano. Hence in the light of our thermochronologicl data, we do conclude that erosional cooling of the southern Peruvian EC is not controlled by a Pliocene climatic shift but rather by Plio-Pleistocene tectonic antiformal stacking of thrust faults. This is in agreement with the presence of numerous Period 2 growth strata identified in both the Inambari and the Pongo de Coñeq SAZ.

Regarding the second point, three processes are generally proposed to explain the rise of the Altiplano: removal of dense lithosphere, lower crustal flow and crustal shortening. Removal of dense lithosphere including eclogitized lower crust, with secondary contributions of crustal shortening and lower crustal flow, is supported by relatively low magnitude of shortening rates and synchronous Late Miocene surface uplift across the entire Andean Plateau (Garzione et al., 2008; Hoke and Garzione, 2008). This lower lithospheric loss would have favored eastward transfer of shortening and formation of the Subandean zone adjacent to the Andean Plateau after ~10 Ma (Garzione et al., 2006). However, the study of Ehlers and Poulsen (2009) suggests that this rapid rise of the Andean Plateau would be overestimated mainly because paleoclimate changes have not been considered and rather propose a constant slow growth of the Andean Plateau over the last 25 Ma for plateau evolution. Hence, the timing of deformation in the Subandean zone of the Andean Plateau is taken as a proxy to validate the timing of the lower lithospheric loss model or Altiplano rise by crustal thickening. Our AFT ages from the innermost preserved structure of the Madre de Dios basin, coupled with structural restoration and timing reconstruction attempts, suggest a ~25 Ma age for the Andean transfer of shortening into the Subandean zone from the northern Andean Plateau. This age is the similar to that invoked by Ehlers and Poulsen (2009) which propose a slow growth of the Andean Plateau over the last 25 Ma. Thus similar to what is found by Espurt et al. (2011), the transfer of shortening from the Andean Plateau to the Subandean zone occurred prior to the removal of dense lithosphere event given by Garzione et al. (2006). This lithospheric loss model does not seem to be responsible for the formation of the Subandean zone (also discussed by Espurt et al., 2011). Our data in light with the data of Espurt et al. 2011 indicate that the rise of the Altiplano is a slow processes resulting from a possible combination of tectonic crustal thickening and lower crustal flow.

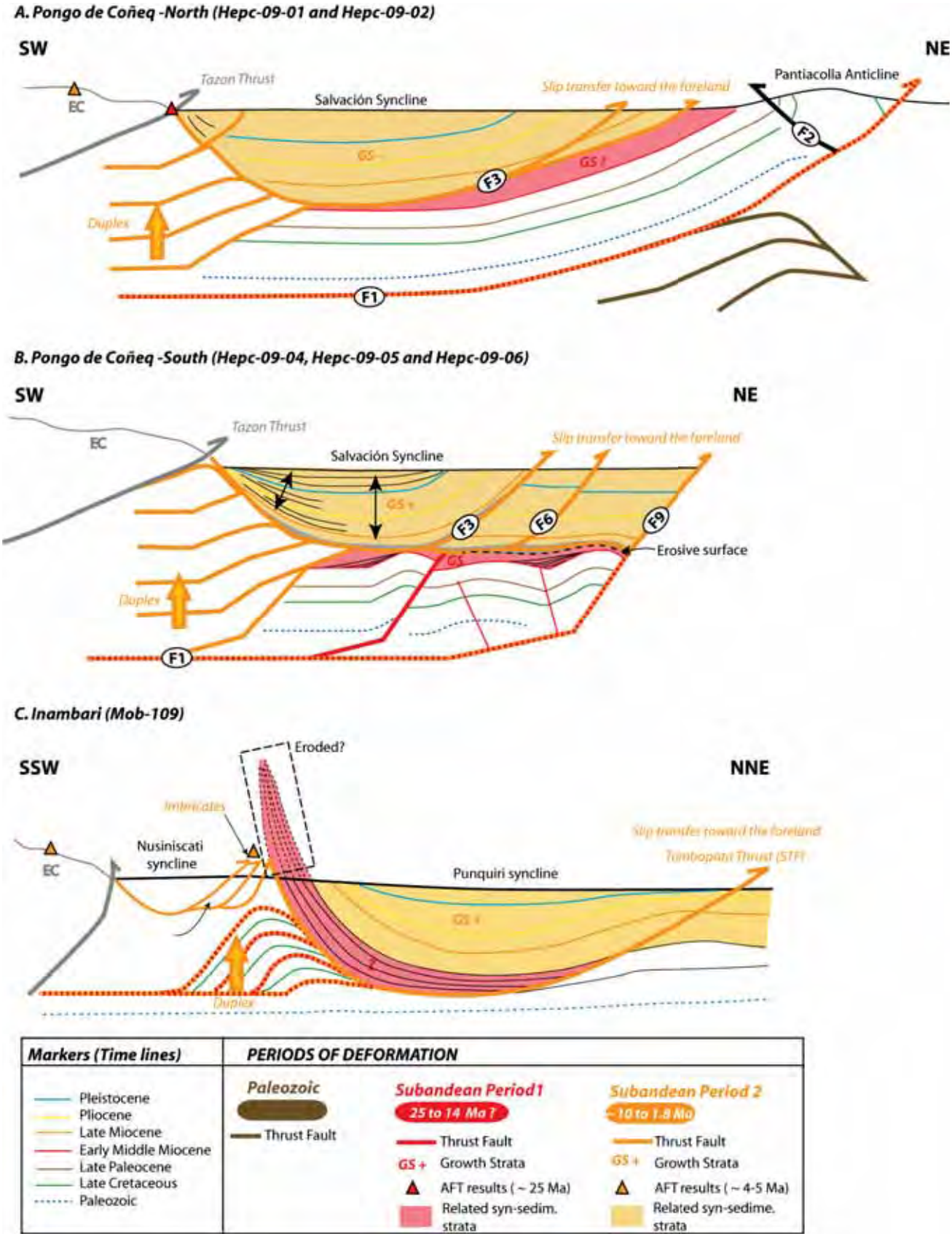

Figure 63: Synthetic sketch for the timing of deformation in the Pongo de Coñeq (A and B) and in the Inambari areas (C). Faults are also mapped on Figure 11.

6. References

Aleman, A., Valasek, D., Ardiles, C., Wood, G., Wahlman, G. and Groves, J., 2003. Petroleum Systems and Tectono-Stratigraphic Evolution of the Madre de Dios Basin and its Associated Thrustbelt in Perú and Bolivia, 8th Simposio Bolivariano-Exploracion Petrolera en las Cuencas Subandinas.

Alemán, A.M. and León, W., 2002. A Carboniferous volcanic arc along the Coastal Cordillera, Fifth International Symposium of Andean Geodynamics, Extended Abstracts, pp. 23-26.

Aliaga Lopez, E., 1985. Palinoestratigrafia del Paleozoico: section Pongo de Conec, Cuenca Madre de Dios, sureste del Peru. Quito, Ecuador: Asistencia Reciproca Petrolera Estatal Latinoamericana (ARPEL), Exploracion y desarrollo de hidrocarburas en horizontes precretacicos, LV Reunion de ARPEL, 2.

Anadón Monzón, P., 1986. Las facies lacustres del Oligoceno de Campins (Vallés Oriental, prov. de Barcelona).

Antoine, P.O., Roddaz, M., Brichau, S., Tejada-Lara, J., Salas-Gismondi, R., Altamirano, A., Louterbach, M., Lambs, L., Otto, T. and Brusset, S., 2013. Middle Miocene vertebrates from the Amazonian Madre de Dios Subandean Zone, Peru. Journal of South American Earth Sciences, 42: 91-102.

Audebaud, E., Bard, J.-P., Raymond, C., Dalmayrac, B., Marocco, R., Megard, F. and Paredes, J., 1971. Le métamorphisme précambrien de basse pression des Andes orientales du Pérou. CRAS Paris, 273: 450-453.

Baby, P., Colletta, B. and Zubieta, D., 1995. Étude géométrique et expérimentale d'un bassin transporté : exemple du synclinorium de l'Alto Beni (Andes centrales). Bulletin de la Société Géologique de France(6): 797-811.

Baby, P., Hérail, G., Lopez, J.M., Lopez, O., Oller, J., Pareja, J., Sempere, T. and Tufiño, D., 1989. Structure de la zone subandine de Bolivie: influence de la géométrie des séries sédimentaires antéorogéniques sur la propagation des chevauchements. Tectonique, 309: 1717-1722.

Baby, P., Hérail, G., Salinas, R. and Sempere, T., 1992. Geometry and kinematic evolution of passive roof duplexes deduced from cross section balancing: Example from the foreland thrust system of the southern Bolivian Subandean Zone. Tectonics, 11(3): 523-536.

Baby, P., Rochat, P., Mascle, G. and Hérail, G., 1997. Neogene shortening contribution to crustal thickening in the back arc of the Central Andes. Geology, 25(September 2009): 883-886.

Barbarand, J., Carter, A., Wood, I. and Hurford, T., 2003a. Compositional and structural control of fission-track annealing in apatite. Chemical Geology, 198(1): 107-137.

Barbarand, J., Hurford, T. and Carter, A., 2003b. Variation in apatite fission-track length measurement: implications for thermal history modelling. Chemical geology, 198(1): 77-106.

Barker, C.E. and Pawlewicz, M., 1986. The correlation of vitrinite reflectance with maximum temperature in humic organic matter, Paleogeothermics. Springer, pp. 79-93.

Beck, S.L., Zandt, G., Myers, S.C., Wallace, T.C., Silver, P.G. and Drake, L., 1996. Crustal-thickness variations in the central Andes. Geology, 24(5): 407-410.

Benavides, V., 1991. Cuencas Paleozoicas en el subandino peruano, 4th Simposio Bolivariano-Exploracion Petrolera en las Cuencas Subandinas.

Bevis, M., Kendrick, E., Smalley, R., Brooks, B., Allmendinger, R. and Isacks, B., 2001. On the strength of interplate coupling and the rate of back arc convergence in the central Andes: An analysis of the interseismic velocity field. Geochemistry, Geophysics, Geosystems, 2(11).

Boyer, S.E. and Elliott, D., 1982. Thrust systems. AAPG Bulletin, 66(9): 1196-1230.

Brandon, M.T., 1992a. Decomposition of fission-track grain-age distributions. American Journal of Science, 292: 535-564.

Brandon, M.T., 1992b. Decomposition of fission-track grain-age distributions. American Journal of Science, 292: 535-535.

Brandon, M.T., 1996a. Probability density plot for fission-track grain-age samples. Radiation Measurements, 26(5): 663-676.

Brandon, M.T., 1996b. Probability density plots for fission-track age distributions. Radiation Measurements, 26: 663-676.

Brandon, M.T., 2002. Decomposition of mixed grain-age distributions using BINOMFIT. On Track, 24: 13-18.

Brandon, M.T., Roden-Tice, M.K. and Garver, J.I., 1998. Late Cenozoic exhumation of the Cascadia accretionary wedge in the Olympic Mountains, northwest Washington State. Geological Society of America Bulletin, 110(8): 985-1009.

Burbank, D., Meigs, A. and Brozovic, N., 1996. Interactions of growing folds and coeval depositional systems. Basin Research, 8(3): 199-223.

Burtner, R.L. and Nigrini, A., 1994. Thermochronology of the Idaho-Wyoming thrust belt during the Sevier orogeny: a new, calibrated, multiprocess thermal model. AAPG bulletin, 78(10): 1586-1612.

Carrera, N. and Muñoz, J.A., 2008. Thrusting evolution in the southern Cordillera Oriental (northern Argentine Andes): Constraints from growth strata. Tectonophysics, 459(1): 107-122.

Crampton, S. and Allen, P., 1995. Recognition of forebulge unconformities associated with early stage foreland basin development: example from the North Alpine foreland basin. AAPG bulletin, 79(10).

Chew, D.M., Magna, T., Kirkland, C.L., Mišković, A., Cardona, A., Spikings, R. and Schaltegger, U., 2008. Detrital zircon fingerprint of the Proto-Andes: Evidence for a Neoproterozoic active margin? Precambrian Research, 167(1): 186-200.

Chew, D.M., Schaltegger, U., Košler, J., Whitehouse, M.J., Gutjahr, M., Spikings, R.A. and Miškovíc, A., 2007. U-Pb geochronologic evidence for the evolution of the Gondwanan margin of the north-central Andes. Geological Society of America Bulletin, 119(5-6): 697-711.

Dahlstrom, C., 1969. Balanced cross sections. Canadian Journal of Earth Sciences, 6(4): 743-757.

Dalmayrac, B., Laubacher, G. and Marocco, R., 1980. Géologie des Andes péruviennes. ORSTOM.

Dalmayrac, B. and Molnar, P., 1981. Parallel thrust and normal faulting in Peru and constraints on the state of stress. Earth and Planetary Science Letters, 55(3): 473-481.

Dávila, J. and Ponce de León, V., 1971. La sección del río Inambari en la Faja subandina del Perú y la presencia de sedimentitas de la Formación Cancañiri (Zapla) del Silúrico. Revista Técnica de YPFB, 1(1): 67-85.

DeCelles, P.G. and Giles, K.a., 1996. Foreland basin systems. Basin Research, 8(2): 105-123.

DeCelles, P.G. and Horton, B.K., 2003. Early to middle Tertiary foreland basin development and the history of Andean crustal shortening in Bolivia. Geological Society of America Bulletin, 115(1): 58-77.

Diaz Martinez, E. and Choque Mamani, N., 1995. Paleozoico superior y cretacico del area Huaranca (Sapahaqui-Rio La Paz), Cordillera Oriental de Bolivia. Revista Tecnica de Yacimientos Petroliferos Bolivianos, 16(1-2): 161-167.

Dunbar, C.O. and Newell, N.D., 1946. Marine early Permian of the central Andes and its fusuline-faunas. American Journal of Science, 244(6): 377-402.

Echavarria, L., Hernandez, R., Allmendinger, R. and Reynolds, J., 2003a. Subandean thrust and fold belt of northwestern Argentina: Geometry and timing of the Andean evolution. AAPG bulletin, 87(6): 965-985.

Echavarria, L., Hernandez, R., Allmendinger, R. and Reynolds, J., 2003b. Subandean thrust and fold belt of northwestern Argentina; geometry and timing of the Andean evolution. AAPG Bull., 87: 965-985.

Elger, K., Oncken, O. and Glodny, J., 2005. Plateau-style accumulation of deformation: Southern Altiplano. Tectonics, 24(4).

Espitalié, J., Laporte, J.L., Madec, M., Marquis, F., Leplat, P., Paulet, J. and Boutefeu, A., 1977. Méthode rapide de caractérisation des roches mètres, de leur potentiel pétrolier et de leur degré d'évolution. Oil & Gas Science and Technology, 32(1): 23-42.

Espurt, N., 2007. Influence de la subduction d'une ride asismique sur la dynamique de la plaque continentale chevauchante: exemple de la ride de Nazca et du bassin Amazonien, 1-326 pp.

Espurt, N., Baby, P., Hermoza, W., Bolan, R., Uyen, D. and Déramond, J., 2008. Paleozoic structural controls on shortening transfer in the Subandean foreland thrust system , Ene and southern Ucayali basins , Peru. Tectonics, 27: 1-21.

Espurt, N., Barbarand, J., Roddaz, M., Brusset, S., Baby, P., Saillard, M. and Hermoza, W., 2011. A scenario for late Neogene Andean shortening transfer in the Camisea Subandean zone (Peru, 12 S): Implications for growth of the northern Andean Plateau. Geological Society of America Bulletin, 123(9-10): 2050-2068.

Farley, K., Wolf, R. and Silver, L., 1996. The effects of long alpha-stopping distances on (U ▪ Th)/He ages. Geochimica et Cosmochimica Acta, 60(21): 4223-4229.

Galbraith, R., 1988a. Graphical display of estimates having differing standard errors. Technometrics, 30(3): 271-281.

Galbraith, R. and Green, P., 1990a. Estimating the component ages in a finite mixture. International Journal of Radiation Applications and Instrumentation. Part D. Nuclear Tracks and Radiation Measurements, 17(3): 197-206.

Galbraith, R.F., 1981. On statistical models for fission-track counts. Journal of Mathematical Geology, 13: 471-478.

Galbraith, R.F., 1988b. Graphical display of estimates having differing standard errors. Technometrics, 30: 271-281.

Galbraith, R.F. and Green, P.F., 1990b. Estimating the component ages in a finite mixture. Nuclear Tracks and Radiation Measurements, 17: 197-206.

Gautheron, C., Tassan-Got, L. and Farley, K., 2006. (U–Th)/He chronometry. Earth and Planetary Science Letters, 243(3): 520-535.

Gil, W., Baby, P. and Ballard, J.-f., 2001. Structure et contrôle paléogéographique de la zone subandine péruvienne. Sciences-New York, 333: 741-748.

Gil, W., Marocco, R. and Ballard, J.F., 1999. North-South structural evolution of the Peruvian subandean zone, ISAG, Goettingen, Germany, pp. 278-282.

Gil, W.F., 2001. Evolution latérale de la déformation d'un front orogénique: exemples des bassins subandins entre 0° et 16°S, University Paul Sabatier, Toulouse.

Gotberg, N., McQuarrie, N. and Caillaux, V.C., 2010. Comparison of crustal thickening budget and shortening estimates in southern Peru (12 – 14 ° S): Implications for mass balance and rotations in the " Bolivian orocline ". Plateau.

Green, P.F., 1981. A new look at statistics in fission-track dating. Nuclear Tracks and Radiation Measurements, 5: 77-86.

Gubbels, T., Isacks, B. and Farrar, E., 1993. High-level surfaces, plateau uplift, and foreland development, Bolivian central Andes. Geology, 21(8): 695-698.

Gutierrez, M., 1982. Evaluacion potencial petrolifero cuencas Huallaga, Ucayali y Madre de Dios. Zonacion bioestratigrafica del intervalo Cretacico superior-Tertiario inferior, Petroperu, Internal Report, Lima.

Hardy, S., Poblet, J., McClay, K. and Waltham, D., 1996. Mathematical modelling of growth strata associated with fault-related fold structures. Geological Society, London, Special Publications, 99(1): 265-282.

Haschke, M. and Günther, A., 2003. Balancing crustal thickening in arcs by tectonic vs. magmatic means. Geology, 31(11): 933-936.

Hendriks, B.W.H., 2005. Analytical methods for physicochemical characterization: Fission Track Analysis, pp. 161-72.

Hermoza, W., 2004. Dynamique tectono-sedimentaire et restauration sequentielle du retro-bassin d'avant-pays des Andes Centrales, Univeristé Paul Sabatier, Toulouse, 196 pp.

Hindle, D., Kley, J., Oncken, O. and Sobolev, S., 2005. Crustal balance and crustal flux from shortening estimates in the Central Andes. Earth Planet. Sci. Lett., 230: 101016/jepsl200411004-101016/jepsl200411004.

Horton, B.K., 1999. Erosional control on the geometry and kinematics of thrust belt development in the central Andes. Tectonics, 18(6): 1292-1304.

House, N.J., Carpenter, D.G., P.S., C. and Berumen, M., 1999. Influence of Paleozoic arches on structural style and stratigraphy in the Madre de Dios basin in Southern Peru and Northern Bolivia, INGEPET Exploration and Exploration of Petroleum and Gas.

Hovikoski, J., Räsänen, M., Gingras, M., Roddaz, M., Brusset, S., Hermoza, W., Pittman, L.R. and Lertola, K., 2005. Miocene semidiurnal tidal rhythmites in Madre de Dios, Peru. Geology, 33(3): 177-180.

Isaacson, P. and Diaz Martinez, E., 1995. Evidence for Middle-Late Paleozoic Foreland Basin and Significant Paleolatitudinal Shift, Central Andes. Memoirs- American Association of Petroleum Geologists 231-231.

Jaillard, E., 1993a. The Senonian to Palaeocene tectonic evolution of the Peruvian margin and its relationships with geodynamics. Bulletin de la Société Géologique de France, 164(6): 819-830.

Jaillard, E., Carlotto, V., Cardenas, J., Chavez, R. and Gil, W., 1993b. La "Nappe des Couches Rouges" de Cuzco (Sud du Pérou): mise en évidence stratigraphique, interprétations tectoniques et paléogéographiques. C. R. Acad. Sci. Paris, 36(Série II): 379-386.

Jamison, W. and Pope, A., 1996. Geometry and evolution of a fault-bend fold: Mount Bertha anticline. Geological Society of America Bulletin, 108(2): 208-224.

Kay, S.M., Mpodozis, C. and Ramos, V.A., 2005. Andes, pp. 118-131.

Kennan, L., Lamb, S. and Rundle, C., 1995. K-Ar dates from the Altiplano and Cordillera Oriental of Bolivia: implications for Cenozoic stratigraphy and tectonics. Journal of South American Earth Sciences, 8(2): 163-186.

Khazaradze, G. and Klotz, J., 2003. Short-and long-term effects of GPS measured crustal deformation rates along the south central Andes. Journal of Geophysical Research: Solid Earth (1978–2012), 108(B6).

Kley, J., 1996. Transition from basement-involved to thin-skinned thrusting in the Cordillera Oriental of southern Bolivia. Tectonics, 15(4): 763-775.

Kummel, B., 1948. Geological Reconnaissance of the Contamana Region, Peru. Bulletin of the Geological Society of America, 59: pp.1217-1266.

Lamb, S., 2000. Active deformation in the Bolivian Andes, South America. Journal of Geophysical Research: Solid Earth (1978–2012), 105(B11): 25627-25653.

Laubacher, G., 1974. Le Paleozoïque inférieur de la Cordillère Orientale du Sud-Est du Pérou. Géologie de l'ORSTOM, VI(1): 19-40.

Laubacher, G., 1977. Géologie des Andes péruviennes: géologie de l'Altiplano et de la Cordillère orientale au nord et nord-ouest du lac Titicaca (Pérou). Académie de Montpellier.

Laubacher, G., 1978. Geology of the Peruvian Andes: geology of the eastern Cordillera and of the Altiplano to the north and north west of Lake Titicaca. Travaux et Documents de l'ORSTOM.

Laubacher, G., Mégard, F., Pitcher, W., Atherton, M., Cobbing, J. and Beckinsale, R., 1985. The Hercynian basement: a review. Magmatism at a plate edge. Blackie, Glasgow: 29-35.

Laubacher, G. and Naeser, C., 1994. Fission-track dating of granitic rocks from the Eastern Cordillera of Peru: evidence for Late Jurassic and Cenozoic cooling. Journal of the Geological Society, 151(3): 473-483.

Lawton, D.C., Spratt, D.A. and Hopkins, J.C., 1994. Tectonic wedging beneath the Rocky Mountain foreland basin, Alberta, Canada. Geology, 22(6): 519-522.

Lease, R.O. and Ehlers, T.A., 2013. Incision into the Eastern Andean plateau during Pliocene cooling. Science, 341(6147): 774-776.

Leigh, R. and Rejas, A., 1966. Columna estratigráfica Pongo de Paquitzapango, Río Ene. Reporte Inédito. PETROPERU.

Leturmy, P., Mugnier, J., Vinour, P., Baby, P., Colletta, B. and Chabron, E., 2000. Piggyback basin development above a thin-skinned thrust belt with two detachment levels as a function of interactions between tectonic and superficial mass transfer: the case of the Subandean Zone (Bolivia). Tectonophysics, 320(1): 45-67.

Liu, M., Yang, Y., Stein, S., Zhu, Y. and Engeln, J., 2000. Crustal shortening in the Andes: Why do GPS rates differ from geological rates? Geophysical Research Letters, 27(18): 3005-3008.

Louterbach, M., Roddaz, M., Baby, P., Bailleul, J., Antoine, P.-O., Adnet, S., Kim, J.H., Van Soelen, E., Parra, F., Gérard, J., Calderon, Y., Gagnaison, C. and Sinninghe Damsté, J.S., Submitted. Evidences for a late Paleocene marine incursion in Southern Amazonia (Madre de Dios Sub-Andean Zone, Peru). Palaeogeography, Palaeoclimatology, Palaeoecology.

Marocco, R., 1978. Estudio geológico de la Cordillera de Vilcabamba-[Boletín D 4], INGEOMIN.

McClay, K.R. and Price, N.J., 1981. Thrust and nappe tectonics. Wiley-Blackwell.

McQuarrie, N., Barnes, J.B. and Ehlers, T.A., 2008b. Geometric, kinematic, and erosional history of the central Andean Plateau, Bolivia (15–17°S). Tectonics, 27(3): 1-24.

Medwedeff, D. and Suppe, J., 1986. Kinematics, timing and rates of folding and faulting from synthetonic sediments geometry. Eos, 67(44): 1223.

Medwedeff, D.A., 1989. Growth fault-bend folding at southeast Lost Hills, San Joaquin Valley, California. AAPG Bulletin, 73(1): 54-67.

Mégard, F., 1978. Etude géologique des Andes du Pérou central: contribution à l'étude géologique des Andes, 1. Orstom.

Mégard, F., 1996. Geología de los cuadrángulos de Tarma, La Oroya y Yauyos 23-l, 24-l, 25-l–[Boletín A 69], INGEMMET.

Mora, A., Baby, P., Roddaz, M., Parra, M., Brusset, S., Hermoza, W. and Espurt, N., 2010. Tectonic history of the Andes and sub-Andean zones : implications for the development of the Amazon drainage basin, pp. 38-60.

Moser, F., Hann, H.P., Dunkl, I. and Frisch, W., 2005. Exhumation and relief history of the Southern Carpathians (Romania) as evaluated from apatite fission track chronology in crystalline basement and intramontane sedimentary rocks. International Journal of Earth Sciences, 94(2): 218-230.

Müller, H., 1982. Evaluación Potencial Petrolífero cuencas Huallaga, Ucayali y Madre de Dios., Cooperación Técnica Peruana-Alemana.

Müller, J.P., Kley, J. and Jacobshagen, V., 2002. Structure and Cenozoic kinematics of the Eastern Cordillera, southern Bolivia (21 S). Tectonics, 21(5): 1037.

Naeser, C.W., Zimmermann, R. and Cebula, G., 1981. Fission-track dating of apatite and zircon: an interlaboratory comparison. Nuclear Tracks, 5(1): 65-72.

Newell, N.D., 1945. Investigaciones geologicas en las zonas circunvecinas al Lago Titicaca: Soc. Geol. Peru Bol, 18: 44-52.

Norabuena, E., 1998. Space Geodetic Observations of Nazca-South America Convergence Across the Central Andes. Science, 279(5349): 358-362.

Oncken, O., Hindle, D., Kley, J., Elger, K., Victor, P. and Schemmann, K., 2006. Deformation of the central Andean upper plate system—Facts, fiction, and constraints for plateau models, The Andes. Springer, pp. 3-27.

Peters, K.E. and Cassa, M.R., 1994. Applied source rock geochemistry. Memoirs of the american Association of Petroleum Geologists: 93-93.

Price, R.A., 1986. The southeastern Canadian Cordillera: thrust faulting, tectonic wedging, and delamination of the lithosphere. Journal of Structural Geology, 8(3): 239-254.

Ring, U., 1999. Exhumation processes: normal faulting, ductile flow and erosion. Geological Society of London.

Roddaz, M., Baby, P., Brusset, S., Hermoza, W. and Maria Darrozes, J., 2005b. Forebulge dynamics and environmental control in Western Amazonia: The case study of the Arch of Iquitos (Peru). Tectonophysics, 399(1–4): 87-108.

Roddaz, M., Hermoza, W., Mora, A., Baby, P., Parra, M., Christophoul, F., Brusset, S. and Espurt, N., 2010. Cenozoic sedimentary evolution of the Amazonian foreland basin system. In: Blackwell (Editor), Amazonia, Landscape and Species Evolution, pp. 61-88.

Roddaz, M., Viers, J., Brusset, S., Baby, P. and Hérail, G., 2005a. Sediment provenances and drainage evolution of the Neogene Amazonian foreland basin. Earth and Planetary Science Letters, 239(1–2): 57-78.

Ruiz, G.M.H., Victor, V., P. and Andriessen, P.A.M., 2009. Steady-state exhumation pattern in the Central Andes - SE Peru, London, pp. 307-316.

Sanchez, C., 2012. Provenance des sédiments du bassin d'avant-pays sud Amazonien (Madre de dios, Pérou): analyses géochimiques (majeurs, traces et isotopie Nd-Sr) et minéralogiques RX et minéraux lourds), University Paul Sabatier de Toulouse, France.

Shaw, J.H., Bilotti, F. and Brennan, P.A., 1999. Patterns of imbricate thrusting. Geological Society of America Bulletin, 111(8): 1140-1154.

Shepherd, R.D., House, N. and Webster, R.E., 2002. Assessment of potentially large, shallow stratigraphic traps, Manu Arch, Madre de Dios Basin, INGEPET, Lima, Peru.

Silva González, P., 2004. variations The Tertiary South-Altiplano-Basin (Bolivia): Sedimentology and Tectonic Implications.

Suppe, J., Chou, G.T. and Hook, S.C., 1992. Rates of folding and faulting determined from growth strata, Thrust tectonics. Springer, pp. 105-121.

Sweeney, J.J. and Burnham, A.K., 1990. Evaluation of a Simple Model of Vitrinite Reflectance Based on Chemical Kinetics (1). AAPG Bulletin, 74(10): 1559-1570.

Tassinari, C.C.G., Castroviejo, R., Rodrigues, J.F., Acosta, J. and Pereira, E., 2011. A Neoproterozoic age for the chromitite and gabbro of the Tapo ultramafic Massif, Eastern Cordillera, Central Peru and its tectonic implications. Journal of South American Earth Sciences, 32(4): 429-437.

Teichmüller, M., 1987. Recent advances in coalification studies and their application to geology. Geological Society, London, Special Publications, 32(1): 127-169.

Valdivia, H., 1974. Estratigrafia de la Faja Subandina de la region de Madre de Dios.

Vergés, J., Marzo, M. and Muñoz, J., 2002. Growth strata in foreland settings. Sedimentary Geology, 146(1): 1-9.

Victor, P., Oncken, O. and Glodny, J., 2004. Uplift of the western Altiplano plateau: Evidence from the Precordillera between 20 and 21 S (northern Chile). Tectonics, 23(4): TC4004.

Wagner, G., 1968. Fission track dating of apatites. Earth and Planetary Science Letters, 4(5): 411-415.

Wigger, P.J., Schmitz, M., Araneda, M., Asch, G., Baldzuhn, S., Giese, P., Heinsohn, W.-D., Martínez, E., Ricaldi, E. and Röwer, P., 1994. Variation in the crustal structure of the southern Central Andes deduced from seismic refraction investigations, Tectonics of the southern central Andes. Springer, pp. 23-48.

Willner, A.P., Castroviejo Bolibar, R., Rodrigues, J.F., Acosta, J. and Rivera Feijóo, M., 2010. High pressure metamorphic conditions in garnet amphibolite from a collisional shear zone related to the Tapo ultramafic body, Eastern Cordillera of Central Peru.

Yuan, X., Sobolev, S., Kind, R., Oncken, O., Bock, G., Asch, G., Schurr, B., Graeber, F., Rudloff, A. and Hanka, W., 2000. Subduction and collision processes in the Central Andes constrained by converted seismic phases. Nature, 408(6815): 958-961.

Yuan, X., Sobolev, S.V. and Kind, R., 2002. Moho topography in the central Andes and its geodynamic implications. Earth and Planetary Science Letters, 199: 389-402.

Zandt, G., Velasco, A.A. and Beck, S.L., 1994. Composition and thickness of the southern Altiplano crust, Bolivia. Geology, 22(11): 1003-1006.

Zoetemeijer, B.P., 1993. Tectonic modelling of foreland basins: thin skinned thrusting, syntectonic sedimentation and lithospheric flexure.

7. Figures

B. Onset of Southern Amazonian foreland basin as inferred from Late Maastrichtian forebulge uplift (Madre de Dios basin, Peru)

Introduction au chapitre:

La première partie de la thèse (Partie A) résout en grande partie les questions scientifiques relatives à la géométrie ainsi qu'à la chronologie de la déformation de la Cordillère Orientale et de la zone Subandine au sud du Pérou. Cependant, le débat relatif à la formation du bassin d'avant-pays amazonien adjacent (bassin de Madre de Dios) reste ouvert. Par exemple, quand le bassin d'avant pays se constitue-t-il ? A partir de quand la charge orogénique engendrée par les nouvelles structures Andines fut-elle suffisante pour engendrer une flexure lithosphérique et ainsi la segmentation du bassin d'avant-pays ? Certains auteurs suggèrent que le bassin d'avant pays Amazonien au sens large fut mis en place dès le Crétacé supérieur ou le Paléocène inférieur (Balkwill et al., 1995; DeCelles and Horton, 2003; Horton et al., 2001; Martin-Gombojav and Winkler, 2008; Roddaz et al., 2010; Sempere et al., 1997) alors que d'autres proposent un début de formation pendant l'Éocène (Viramonte et al., 1999) ou même plus tard (Jordan et al., 2001; Jordan et al., 2010).

D'après certains auteurs, la mise en place des bassins d'avant-pays est contemporaine de la formation et du soulèvement d'un « forebulge », qui n'est autre que la réponse flexurale à la charge orogénique induite par la construction de la chaîne andine (e.g. Beaumont, (1981) and Crampton and Allen,(1995)). La présence avérée d'un forebulge, tout comme celle des autres zones de dépôts ou « depozones » (wedge-top, foredeep ou back-bulge) sensu DeCelles and Giles (1996) permet de démontrer l'existence d'un bassin d'avant-pays à l'époque concernée. Dans l'enregistrement sédimentaire, le soulèvement d'un forebulge peut être déduit d'un changement d'environnement de dépôt et d'une diminution des taux de sédimentation (Uba et al., 2006), d'un changement de provenance sédimentaire (DeCelles and Horton, 2003; Horton and DeCelles, 2001; Hulka and Heubeck, 2010), de la présence d'une discontinuité majeure associée au développement d'un paléosol plus ou moins conséquent (DeCelles et al., 2011), du développement de surfaces d'érosions majeures à l'échelle du bassin (Crampton and Allen, 1995), de la présence d'onlaps progressifs recouvrant le craton (Crampton and Allen, 1995) ou encore de la combinaison de plusieurs de ces paramètres (Fuentes et al., 2009). Si certaines études concernent les prémices du bassin d'avant pays Bolivien (DeCelles and Horton, 2003) (Uba et al., 2006), très peu d'études (Gil, 2001; Hermoza, 2004) ont été menées sur cette thématique dans notre zone d'étude, au sud du Pérou.

Dans ce chapitre, rédigé à la manière d'un article court, nous présentons de nouvelles données biostratigraphiques, sédimentologiques et géochimiques (provenance sédimentaire) afin de documenter l'évolution spatiale et la chronologie de mise en place du bassin de Madre de Dios entre le Maastrichtien (Crétacé supérieur) et le Paléocène supérieur. Il s'agit des toutes premières données jamais présentées

suggérant la présence d'un bassin d'avant-pays de type « retro-arc » dès le Maastrichtien dans les Andes Centrales.

Résumé:

Situé au sud du Pérou, le bassin actuel de Madre de Dios (situé entre les latitudes 12ºS et 14ºS) peut être divisé en plusieurs zones de dépôt spécifiques aux bassins d'avant-pays retro-arc telles que définies par DeCelles and Giles (1996). Ainsi, la zone Subandine actuelle, adjacente à la Cordillère Orientale, correspond à la zone de wedge-top. Le reste du bassin d'avant-pays, depuis le front de déformation subandin jusqu'à la bordure Est du bassin correspond au foredeep. Suite au soulèvement récent de l'Arche de Fitzcarrald (Espurt, 2007) situé au Nord-Ouest de la zone d'étude, le bassin de Madre de Dios ne présente aucun forebulge ni backbulge actuels. Cependant, ces quatre zones de dépôts particulières ont existé depuis le début de la mise en place du bassin d'avant-pays de Madre de Dios et ont évolué en fonction de la migration et de l'intensité de la déformation Andine au cours du temps. A partir d'une coupe stratigraphique de 270 m d'épaisseur levée sur le terrain dans le synclinal de Salvación au Nord-Ouest de la zone Subandine de Madre de Dios, et en nous basant sur des résultats biostratigraphiques, sédimentologiques et géochimiques (concentrations isotopiques en Nd-Sr), nous montrons qu'un forebulge était déjà présent dans cette zone dès le Maastrichtien.

Pendant le Campanien supérieur jusqu'au Maastrichtien inférieur, les dépôts attestent d'un environnement de dépôt marin peu profond, de taux de sédimentation relativement bas et d'une provenance sédimentaire similaires aux sédiments issus du Craton Brésilien (εNd(0)= -16,4 to -13.91). Ces caractéristiques suggèrent que la coupe étudiée se situait alors en position de backbulge. Les dépôts du Maastrichtien inférieur sont séparés des dépôts du Maastrichtien supérieur par une surface d'érosion subaérienne. Les dépôts continentaux du Maastrichtien supérieur sont recoupés par des failles normales syn-sédimentaires. La surface d'érosion est de plus caractérisée par un changement brutal de provenance sédimentaire puisque les dépôts situés au-dessus (Maastrichtien supérieur) présentent une signature isotopique typique des sédiments provenant des Andes (εNd(0)= -12,6) et non plus du craton. Ces données attestent de la présence d'un forebulge dès le Maastrichtien supérieur au niveau de la coupe étudiée. Les dépôts marins du Paléocène supérieur sont transgressifs et caractérisés par une provenance sédimentaire similaire aux sédiments dérivés du volcanisme Andin (εNd(0)= -10,7 to -6,2). Ceci est probablement expliqué par l'activité de l'Arc volcanique Toquepala (Cordillère Occidentale) pendant le Paléocène (Mamani et al., 2010). Les dépôts du Paléocène supérieur présentent enfin les taux de sédimentation les plus bas de toute la coupe stratigraphique présentée dans cette étude (~3 m/My). Ces caractéristiques sont en accord avec un forebulge (cette fois-ci immergé) ou bien avec un foredeep encore très proche du forebulge pendant le Paléocène supérieur.

Les données proposées dans cette étude attestent donc de la présence d'un forebulge dès le Maastrichtien supérieur et suggèrent la migration vers l'Est d'un bassin d'avant-pays au cours du Crétacé supérieur jusqu'au Paléogène au moins. Le bassin d'avant-pays du sud du Pérou a donc été actif au moins depuis le Maastrichtien supérieur.

Onset of Southern Amazonian foreland as inferred from Late Maastrichtian forebulge uplift (Madre de Dios basin, Peru)

Mélanie Louterbach[1,2,5], Martin Roddaz[1], Caroline Sanchez[1], Pierre-Olivier Antoine[3], Laurent Marivaux[3], Julien Bailleul[2], Elton Dantas[6], Patrice Baby[1] and Ysabel Calderon [1-4]

[1]Géosciences-Environnement Toulouse, Université de Toulouse; UPS (SVT-OMP); LMTG; CNRS; IRD; 14 Avenue Édouard Belin, F-31400 Toulouse, France

[2]Bassins-Réservoirs-Ressources, Institut Polytechnique Lasalle Beauvais, Département Géosciences, 19 rue Pierre Waguet, F-60026 Beauvais Cedex, France

[3]Laboratoire de Paléontologie, Institut des Sciences de l'Évolution (ISE-M, UMR - CNRS 5554), c.c. 64, Université Montpellier 2, Place Eugène Bataillon, F-34095 Montpellier Cedex 05, France

[4] PERUPETRO S.A., Luis Aldana 320 - San Borja, Lima, Peru

[5] REPSOL Exploración S.A., Calle Mendez Alavaro 44, 28045 Madrid, Spain

[6] Laboratório de Geocronologia, Instituto de Geociências, Universidade de Brasília, Brasília, DF 70910-000, Brazil

Keywords: Nd-Sr isotopes, provenance, Late Cretaceous-Paleocene, Amazonian Foreland Basin, forebulge, Central Andes, Peru.

Summary:

1. Introduction

One of the most controversial unresolved problem of the Andean belt and associated foreland basin is when does the retroarc foreland basin form? Some authors suggest that it formed during the Late Cretaceous or early Paleocene time (Balkwill et al., 1995; DeCelles and Horton, 2003; Horton et al., 2001; Martin-Gombojav and Winkler, 2008; Roddaz et al., 2010; Sempere et al., 1997) whereas others proposed an onset of formation during Eocene time (Viramonte et al., 1999) or later (Jordan et al., 2001; Jordan et al., 2010).

Onset of foreland basins is coeval to the onset of their forebulge uplift as the forebulge is a flexural response to orogenic loading (e.g. Beaumont, (1981) and Crampton and Allen,(1995)). The forebulge uplift can be inferred from changes in depositional environments and sedimentation rates (Uba et al., 2006), shift in sedimentary provenances (DeCelles and Horton, 2003; Horton and DeCelles, 2001; Hulka and Heubeck, 2010), the presence of typical forebulge-related unconformities such as supersol (DeCelles et al., 2011), bauxite formation (Singh, 2003), erosional unconformities (Crampton and Allen, 1995), the presence of cratonward migrating onlaps (Crampton and Allen, 1995) or a combination of these (Fuentes et al., 2009).

In northern Bolivia, the presence of a Late Paleocene- early Eocene forebulge is inferred in the present-day Puna-Altiplano from a shift in provenance from cratonic to Andean type and from a condensed sedimentary section (DeCelles and Horton, 2003). In the present-day Sub-andean zone of southern Bolivia, Uba et al. (2006) suggested the presence of a Late Oligocene-Middle Miocene forebulge on the basis of low sedimentation rates and of cratonic provenance. These studies deal with Bolivian foreland basins, but little data exist for the southern Peruvian foreland basins.

In this study we bring new biostratigraphical, sedimentological and provenance constraints to document the spatial and chronologic evolution of the southern Peruvian Madre de Dios foreland basin between Maastrichtian and Late Paleocene times. This unique dataset indicates the presence of a forebulge in the present-day Sub-Andean Zone (SAZ) during the Late Maastrichtian, suggesting that the development of the Andean retroarc foreland basin could have started as early as Late Maastrichtian.

2. Geological Setting and Methodology

The southern Peruvian Madre de Dios foreland basin is part of the southern Amazonian foreland basin (Roddaz et al., 2005a) (Figure 1). The present-day Madre de Dios basin is composed of the the wedge-top and foredeep depozones sensu DeCelles and Giles (1996). Sediments that accumulate on top of the frontal part of the orogenic wedge constitute the wedge-top depozone and correspond to the present-day SAZ. The structure of the SAZ is controlled by the development of deep duplexes, whose shortening is accommodated in surface by imbricates structures and the Sub-andean Thrust Front (STF). The STF transports a large Cenozoic syncline (i.e. Salvación syncline, Figure 1-A). The onset of Peruvian Sub-andean shortening started at c. 14 Ma (e.g. Espurt et al.,(2011)).

The southern Peruvian Andes can be divided into six morphostructural units which are, from west to east, the Coastal Cordillera, the Western Cordillera, the Interandean Depression or Altiplano, the Eastern

Cordillera, the SAZ and the Brazilian Shield. These units constituted the potential sources for the Maastrichtian-Late Paleocene sedimentary rocks analyzed in this study.

Onset of erosion of the Coastal Cordillera is thought to be in Eocene times (Von Huene and Suess, 1988) and hence it can be disregarded as a potential source for the Late Cretaceous-Late Paleocene sedimentary section presented in here.

The Western Cordillera is mainly made up of Late Cretaceous-Paleogene volcanic rocks as well as associated intrusive rocks (i.e. Toquepala Arc, active between 145 and 55 Ma), and of Proterozoic and Ordovician rocks of the Arequipa Massif (Decou et al., 2011; Mamani et al., 2010). Local Jurassic intrusive rocks as well as Cretaceous volcanics and sediments also constitute the Western Cordillera (according to the 1/1,000,000 digital geological map by INGEMMET).

The Altiplano is located between the Western Cordillera and the Eastern Cordillera, and is constituted by Cretaceous to tertiary volcanic and sedimentary rocks. The Altiplano is thought to have been the foredeep of the Andean retroarc foreland basin before the exhumation of the Eastern Cordillera. In the northern Bolivian Altiplano, the 70-60 Ma el Molino Formation contains shallow marine deposits suggesting that the Altiplano was at sea level at the end of the Cretaceous (Sempere et al., 1997).

The Eastern Cordillera is mainly made up of Tardi-Hercynian plutonic rocks and Pre-Cambrian to Late Paleozoic meta-sedimentary rocks (Laubacher, 1978). The exhumation and erosion of the southern Peruvian Eastern Cordillera is thought to have occurred in the Neogene (Lease and Ehlers, 2013) (Part A of this manuscript).

Finally, the Brazilian craton is constituted by Precambrian crystalline rocks (Chew et al., 2007). A Precambrian granitoid sample was analyzed in northeastern Bolivia (Roddaz et al., 2005a) and it gave a low γNd(0) value (11.7) with high radiogenic $^{87}Sr/^{86}Sr$ composition (0.893764).

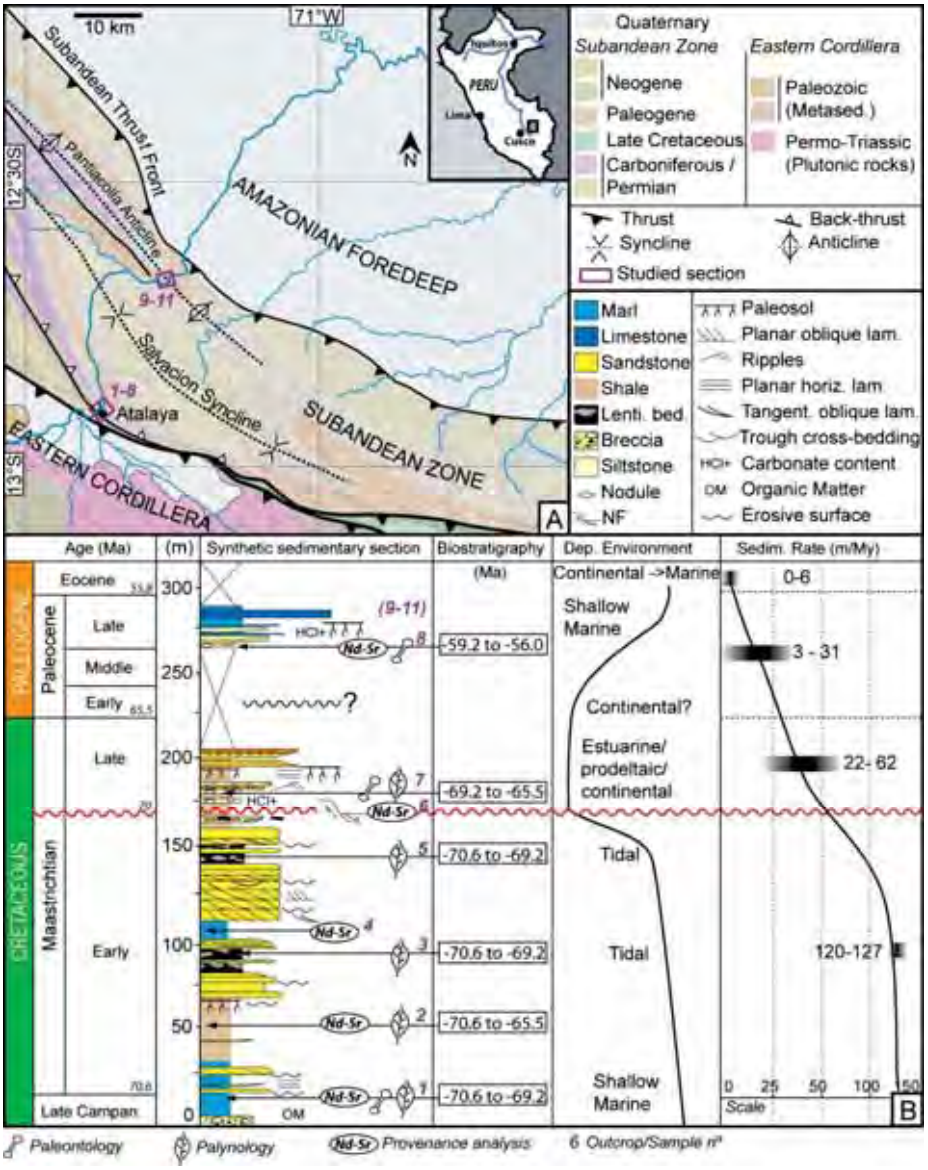

Figure 1: A/ Location of the Madre de Dios foreland basin and simplified geological map of the northwestern Salvación syncline where sedimentological observations and sampling have been performed (numbers 1 to 11). B/ Synthetic sedimentological section of the Late Campanian-Early Maastrichtian to Late Paleocene strata. Samples used for provenance analysis, paleontological and palynological studies are located along the section and numbered from 1 to 11. One sample number can be related to various analyses. Based on sedimentological observations, depositional environments have been interpreted. Sedimentary rates (m/Ma) have been calculated for each time-interval.

This paper focuses on a 270 m- thick sedimentological section of Late Cretaceous to Paleogene strata outcropping in the Pongo de Coñeq canyon. The canyon, located in the northwestern SAZ, incises the southwestern vertical flank of the transported Salvación syncline (Figure 1-A, outcrops 1 to 8). Additional outcrops are located in the northern flank of the Salvación syncline, near the Pantiacolla anticline (Figure 1-A, outcrops 9 to 11 and Supplementary Table 1). This study provides the first accurate stratigraphic, sedimentological and sedimentary provenance results related to the southern Peruvian SAZ for this interval of time (Maastrichtian-Late Paleocene). It also provides the first evidences for Late-Cretaceous deformation in the southern Peruvian Andean belt.

These data have been collected during several field trips undertaken in the northern SAZ of the Madre de Dios foreland between 2010 and 2012 (Figure 1). The Nd-Sr isotopic compositions have been measured at

both the University of Toulouse (GET, France) and the University of Brasilia (Laboratorio de Geochronología). Detailed analytical methods for the Nd-Sr isotopes measured in Toulouse can be found in Roddaz et al (2005a) and in the supplementary Dataset-A. Detailed protocol for samples analyzed in Brasilia can be found and in Dantas et al (2009). Mineralogical compositions have also been carried out at the University of Toulouse. Major, minor and trace element concentrations were measured at the Service d'Analyse des Roches et Minéraux (SARM, INSU facility, Vandoeuvre-Les-Nancy, France).

3. Biostratigraphic and sedimentological constraints

Late Cretaceous to Cenozoic strata in the Salvación syncline consist of +/- 4500 meters of mainly fluvial deposits occasionally interrupted by transgressive tidal deposits. Within the Pongo de Coñeq canyon, the late Maastrichtian to Eocene transition is recorded by a270-meters thick sedimentological section (Figure 1-B). This section yields numerous fossiliferous localities that provide very good biostratigraphical and paleo-environmental constraints for the Maastrichtian and Eocene periods. All paleontological interpretations (samples nº 1 ,2, 3, 5, 7 and 8) have been made at the University of Montpellier, and palynological results have been provided by the Smithsonian Institute of Panama and the University of Amsterdam (results are synthesized in Table 1 but detailed biostratigraphic content is available in Supplementary Table 2).

At the base of the section are 5 meters of nodular mud breccia intercalated with thin centimetric calcareous levels, where Late Campanian to Early Maastrichtian marine fauna and pollen have been found (sample nº1, collected at 20 m, see Table 1). This basal mud breccia can be interpreted as mudflow deposit. Then, the section shows 20 meters of blue to violet marls locally eroded by thin erosive lenses of fine-grained sandstone that shows planar horizontal- or trough cross-stratification (see Figure 1-B). As attested by the biostratigraphical content (supplementary Table 2), these first 25 meters of strata are characterized by confined proximal marine-related deposits and probably correspond to an estuarine or prodeltaic environment.

Above the shallow marine facies, 45 meters of reddish massive shales end with poor-developed paleosol horizons (from 25 m to 70 m, Figure 1-B). Based on sedimentary observations and biostratigraphical content (sample nº2 collected at 50 m), we suggest a more proximal continental environment such as a fluvio-tidal coastal plain. Shales from this succession also yield Early Maastrichtian palynomorph material (supplementary Table 2).

Sample nº	Palynoogy	Microfossil	Paleontology	Age	Paleobiology	Reference
1	x		x	Early Maastrichtian	Prodeltaic/estuarine plain fringe. Confined proximal marine environment of normal salinity (diverse euhaline ichtyo-fauna, but no shark). Equivalent to the Bolivian El Molino Fm.	1
	x				Marine.	
2	x			Maastrichtian	Marginal marine environment.	2
3	x			Early Maastrichtian	Marginal marine environment.	1
4	x			(Maastrichtian)	Marginal marine environment.	2
5	x			Early Maastrichtian	Marginal marine environment.	1
7	x		x	Late Maastrichtian	Prodeltaic/estuarine plain fringe. Confined proximal marine environment of normal salinity (diverse euhaline ichty-ofauna, but no shark), with terrigenous inputs (including charophyte oogonia). Ichthyo-fauna comparable to that of Toro Toro (Bolivia; Cappetta, 1975).	1
8	x		x	Thanetian (late Palaeocene)	Lagoonal/estuarine/steady bay. Confined and steady proximal marine environment of normal salinity (still more diverse euhaline ichtyo-fauna, but no shark).	1
9	x			(Paleocene)-Eocene	-	1, 2
	x			(Paleocene)-Eocene	Marginal marine environment - Supralitoral.	
			x	Thanetian (late Palaeocene)	Lagoonal/estuarine/steady bay. Confined and steady proximal marine environment of normal salinity (still more diverse euhaline ichtyo-fauna, but no shark).	
10		x		Upper Cretaceous-Ypresian	Undetermined. Probably related to terrestrial inputs + paleosoils formation.	2
11	x			Paleocene	Coastal/Estuarine plain fringe with saline/fresh water.	1, 2
	x			Paleocene	Coastal/Estuarine plain fringe with saline/fresh water.	
			x	Thanetian (late Palaeocene)	Distal fluvial/proximal estuarine-deltaic. Strong freshwater influence (fish fauna): the environment is much more proximal than other ones, i.e. distal fluvial. Shallow water.	

Table 1: Synthetic stratigraphic and paleoenvironmental constraints from paleontology, palynology and microfossil analyses. Ref=1: results from the University of Montpellier and the Smithsonian Institute. Ref=2: results from the University of Toulouse. See Supplementary Table 2 for more details.

The reddish shales are overlaid by a well-developed paleosol evolving vertically to stacked channelized fine- to medium-grained sandstone and lenticular or wavy-bedding deposits (from 70 m to 115 m in thickness). This sedimentary unit ends with more than 5 meters of massive blue shales. Sedimentological and paleontological data from sample nº3 collected in the wavy-bedded deposits (at 93 m, Figure 1-B) suggest a transition from fluvio-tidal to tidal flat towards shallow calm marine environments at the top of the blue shale (~110 m). Pollen are also in agreement with an Early Maastrichtian age.

These transgressive deposits are overlaid by vertically stacked 50 cm-thick beds mainly made up of trough and tabular- cross-stratified and fine- to medium grained sandstones (total thickness of 50 m, from 115 m to 165 m, Figure 1-B). Sandstone bars are frequently gently erosive and are interpreted as tidal-bars accretion, Early Maastrichtian in age (palynological result from sample nº5 collected at 147 m, Table 1).

From 165 to 170 m (Figure 1-B), we observe 5 meters of reworked material cut by a major erosional surface. Above this important surface boundary are 25 meters of thick reddish shale and well-developed nodular carbonaceous paleosol followed in its upper part by various 20 cm-thick silty- to sandy packages alternating with reddish shale. Ripples and climbing ripples are frequent in the sandy units. The section evolves upward into breccia levels and channelized coarse- to very coarse-grained sandstones bodies (195 m to 200 m), where Late Maastrichtian marine and continental fauna and pollen have been found (sample nº7, collected at 160 m, Table 1). This Late Maastrichtian fauna indicates proximal marine environment of normal salinity (diverse euhaline ichtyo-fauna) with terrigenous inputs (including charophyte oogonia, see results in Table 1). Syn-sedimentary normal faults and several mudlfows deposits characterize these deposits suggesting that

slope creation occurred in the Late Maastrichtian. These deposits situated above the important erosional surface are interpreted as Late Maastrichtian deposits having formed in a very proximal marine environment that suffered subsequently terrigenous inputs and important emersion. Subaerial conditions are evidenced by the well-developed calcareous nodular paleosols. The Late Maastrichtian deposits are deformed by two families of syn-sedimentary normal faults. Structural data measured on the field and rotated thereafter indicate an average azimuth direction of 171 (family 1) and 354 (family 2) and an average dip of 42°. General strike direction of all measured faults planes plots between N 81 and N87.

The uppermost part of the Pongo de Coñeq section corresponds to 15 meters of shales with several thin carbonate levels showing pedogenetic processes probably linked to successive emersions (Figure 1-B). Late Paleocene (Thanetian) fauna and palynomorphs have been found in these shales and are related to confined shallow marine environment (sample nº8, collected at 260 m, see Table 1). About 60 m of strata cannot be observed. These missing strata could correspond to either Late Maastrichtian or Early to Late Paleocene deposits.

We used the *PetroMod 1D* basin modeling software (Schlumberger S.A.) to reconstruct the burial history of the basin in the present-day Pongo de Coñeq area (Figure 1-B and Supplementary Data B). To calculate sedimentation rates, the program uses the back-stripping method. Data input consist of stratigraphic time-depth information (thicknesses, ages, lithology and depositional water depths). Different *scenarii* have been tested depending on the thickness of the Paleocene strata (60 meters maximum) and the possible erosion range. The calculated sedimentation rate for the Late Campanian to Early Maastrichtian formations range from 120 to 127 $m.Ma^{-1}$. The Late Maastrichtian sedimentation rates range from 22 to 62 $m.Ma^{-1}$ depending on the scenario. Paleocene sedimentation rates range from 3 (non-deposition or erosion) to 37.7 $m.Ma^{-1}$ (60 meters-thick). Late Paleocene deposits also present low sedimentation rates ranging from 0 to $6m.Ma^{-1}$. The Late Campanian-Early Maastrichtian to Late Paleocene section could be considered as a condensed section (270-meters thick) that spans c.a. ~20 Ma and presents decreasing sedimentation rates from ~124 to $\sim 15m.Ma^{-1}$. These decreasing sedimentation rates show similar evolution than the sedimentation rates calculated and based on the sedimentary sections recording the evolution from a backbulge to a forebulge depozones in Bolivia (Uba et al., 2006) and Argentina (DeCelles et al., 2011).

4. Mineralogical and Geochemical constraints

The Early Maastrichtian sample MD 175 consists mainly of kaolinite and dolomite and is characterized by low smectite and micas contents (see Supplementary Table 3). When compared with MD 175, the Late Maastrichtian sample MD 176 shows an increase in quartz content and a strong decrease in kaolinite content. The Late Paleocene samples are characterized by the appearance of chlorite. There are also some marked differences in geochemical concentrations between the Early to Late Maastrichtian samples and the Late Paleocene samples. MD 175 is depleted in Zr and Hf and Rare Earth Element (REE) relative to PAAS whereas MD 176 is enriched (results available in Supplementary Table 4). The Early and Late Maastrichtian samples are characterized by lower Cr/Th ratios (3.5-3.9 respectively), higher Th/Sc ratios (1.12-1.16

respectively) and more negative Eu anomalies (0.62-0.63) than those of The Upper Continental Crust or PAAS (Taylor and McLennan, 1985). Compared with Maastrichtian samples, the Late Paleocene samples show lower Eu anomalies (0.67-0.76) and lower Th/Sc ratios (0.48-0.80). The differences in mineralogy and major and trace element concentrations are accompanied by differences in Nd-Sr isotopic compositions (see Figure 2 and Supplementary Table 5). Early and Late Maastrichtian samples have low εNd(0) values (between -16,4 and -13.91 for Early Maastrichtian samples and around -12,6 for Late Maastrichtian sample), with radiogenic $^{87}Sr/^{86}Sr$ isotopic compositions (0.7247 and 0.7302 respectively). Compared with Maastrichtian samples, the Late Paleocene samples have higher εNd(0) values (from -10.7 to -6.2) with less radiogenic $^{87}Sr/^{86}Sr$ isotopic compositions (between 0.712024 to 0.7190).

Mineralogical, geochemical concentrations and isotopic compositions point to different provenance between Early Maastrichtian, Late Maastrichtian and Late Paleocene sedimentary rocks. The Early Maastrichtian sample is characterized by its high kaolinite content. High kaolinite content also characterizes present suspended sediment of Amazonian cratonic rivers (Guyot et al., 2007). Where reported in the $^{87}Sr/^{86}Sr$ versus εNd(0) diagram and compared with other relevant source fields (Figure 2), the Early Maastrichtian sample plots outside of the melange hyperbole and close to the Late Miocene to Pliocene White Sands sample, which is cratonic in provenance (Roddaz et al., 2005a), indicating hence a similar cratonic provenance. Other analyzed Early Maastrichtian samples have εNd(0) values much lower than -12.7 that confirm a cratonic provenance (Nie et al., 2012). The Late Maastrichtian sample (nº6) plots within the hyperbole and has similar Nd-Sr isotopic composition as those of the present-day suspended matter of the Madeira River (Viers et al., 2008) and as the South American Foreland Basin Neogene sediments (Roddaz et al., 2005a), indicating an overall similar Andean provenance. The Eu anomaly expressed as Eu/Eu*, Th/Sc and Cr/Th elemental ratios have proven to be useful tools for differentiating sediments derived from silicic and basic sources (see (Cullers, 2000) and references therein). However, there is no difference in Th/Sc and Cr/Th ratios and Eu anomalies between the Early and Late Maastrichtian samples indicating the change in provenance is not related to a change in the source composition. From a mineralogical point of view, the Late Paleocene samples are characterized by the appearance of chlorite. Present-day suspended sediments of Andean rivers are characterized by Mica-Chlorite assemblage which is also present in the late Paleocene samples. Lower Eu anomalies and Th/Sc ratios indicate input of more basic/volcanic detritus for late Paleocene samples when compared with Maastrichtian samples. This increasing volcanic contribution is further confirmed by Nd-Sr isotopic compositions. Amongst the analyzed sediments in this study, the late Paleocene samples plot the closest to the volcanic arc end member, indicating that the contribution of the volcanic arc material was greater in the Late Paleocene times than in the Maastrichtian times.

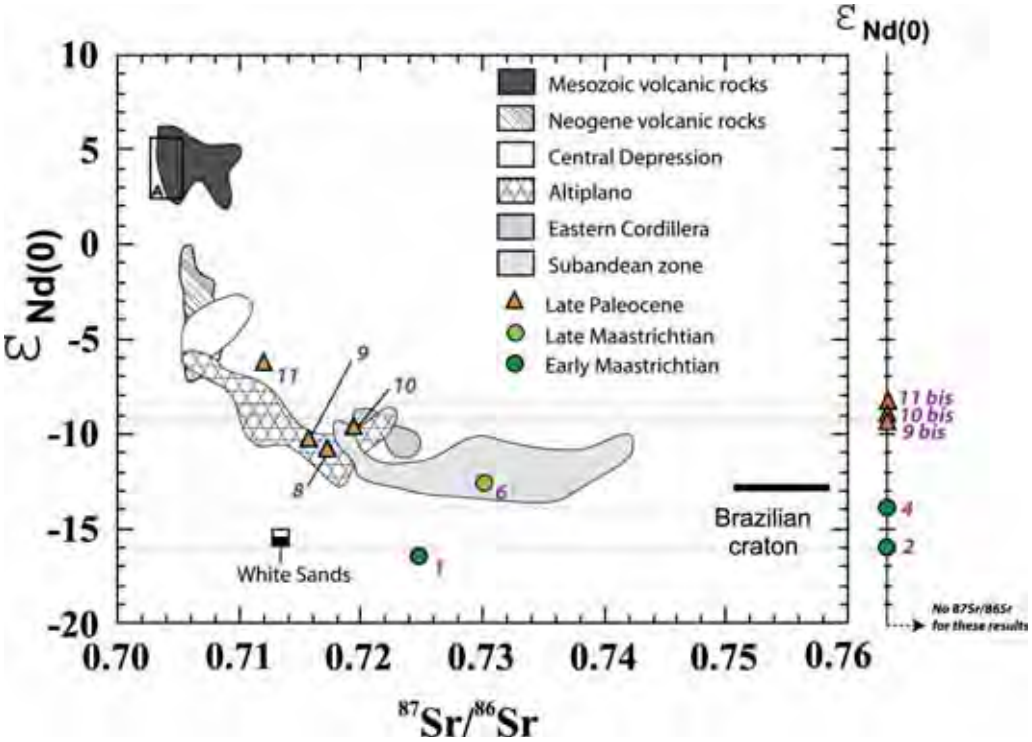

Figure 2: $^{87}Sr/^{86}Sr$ versus εNd(0) diagram for Late Campanian to Late Paleocene samples collected in the Pongo de Coñeq sedimentological section. Mesozoic and Neogene volcanic rocks are from Kay et al. and Rogers and Hawkesworth (1994; 1989); Quaternary Ecuadorian lavas from Barragan et al. (1998); Cenozoic sedimentary rocks from the Altiplano, Oriental Cordillera and SAZ of Chili and Bolivia are from Pinto (2003); modern suspended sediments from the Solimoes and Madeira rivers are from Viers et al. (2008); Neogene deposits from the Amazonian foreland basin of Bolivia, Ecuador and Peru are from Roddaz et al. (2005a), and the sand of the Peruvian White Sand (WS) formation cratonic in origin are from Roddaz et al. (2005a). On the whole, the sediments originated from the Andes define a hyperbolic relationship similar as observed by Basu et al. (1990) for the sands of the South Amazonian foreland basin and by Roddaz et al. (2005; 2012) for the Neogene sediments from the Amazonian foreland basin of Bolivia, Peru and Ecuador, with one end member being the primitive arc ("Mesozoic volcanic rocks")) and the other, the upper continental crust of the cratonic shield ("Brazilian Craton").

The transition from shallow marine Early Maastrichtian deposits to continental Late Maastrichtian strata is hence accompanied by a strong shift in Nd-Sr isotopic values, indicating a change from a cratonic source during the Early Maastrichtian times towards an Andean source during the Late Maastrichtian to Late Paleocene times.

5. Discussion and Conclusion

Based on the evolution of depositional environments, sedimentation rates and sedimentary provenance, we propose a foreland basin evolution model sensu DeCelles and Giles (1996) and DeCelles and Horton (2003) for the Southern Amazonian retroarc foreland basin between Late Campanian to Late Paleocene times.

Shallow marine depositional environment, low sedimentation rates and cratonic provenance during Late Campanian to Early Maastrichtian suggest deposition in a low accommodation setting in agreement with a backbulge setting (Figure 3-A). Coeval Sicuani conglomerates described by Jaillard et al. (Jaillard, 1993a) and outcropping in the present day Altiplano could constitute the wedge-top deposits of the Southern Amazonian retroarc foreland basin system. We suggest that the Sicuani conglomerates were sourced from the growing proto Western Cordillera.

The Late Maastrichtian deposits (Figure 3-B) are separated from the Early Maastrichtian deposits by a subaerial erosive surface associated with a change in depositional environment from shallow marine to continental. This overall regressive pattern could be ascribed to the global sea-level fall in the Late Maastrichtian times (Haq et al., 1987). However, change in provenance from cratonic to Andean and lowering in sedimentation rates associated with the presence of localized normal faults advocate for the uplift of a flexural forebulge. Similar syn-sedimentary normal faults have already been described in the forebulge depozone of the northern Peruvian foreland basin (Roddaz et al., 2005b) and are interpreted to be formed by inelastic flexural extension in area of high curvature (Bradley and Kidd, 1991; Londoño and Lorenzo, 2004). The presence and development of thick paleosol horizon is interpreted as potential forebulge indicator in other foreland systems (e.g. in the western Himalayan foreland basin in Singh (2003) and in Bolivia in DeCelles et al (2011)). In this configuration the coeval deposits of the El Molino Formation (Bolivian Altiplano) and the Vilquechico Formation (Peruvian Altiplano) could represent distal foredeep deposits as they are characterized by higher sedimentation rates and Andean provenance, attested by the presence of Andean volcanic tuff (Jaillard et al., 1993c; Sempere et al., 1997).

Finally, the late Palaeocene deposits (Figure 3-C) are characterized by transgressive shallow marine deposits associated with the input of volcanic detritus. We suggest that the shallow marine strata registered here for the Late Paleocene period may have been deposited in a distal foredeep setting, according to the low sedimentation rates calculated (3 to 3 m/My). The occurrence of volcanic detrital input may be associated with the activity of the Toquepala volcanic Arc (Western Cordillera) during Paleocene times (Louterbach et al., Submitted; Mamani et al., 2010). Louterbach et al. (submitted) suggest that the Paleocene marine incursion registered in the Madre de Dios SAZ could be related to proto western Cordillera loading (see PART B of the manuscript for more details or Louterbach et al., submitted).

In conclusion, the data presented here are best explained by an eastward migrating foreland basin system and by the presence of a Late Maastrichtian forebulge in the present-day SAZ. Hence, data suggest that a retroarc foreland basin system became active in southern Peru as early as Maastrichtian time.

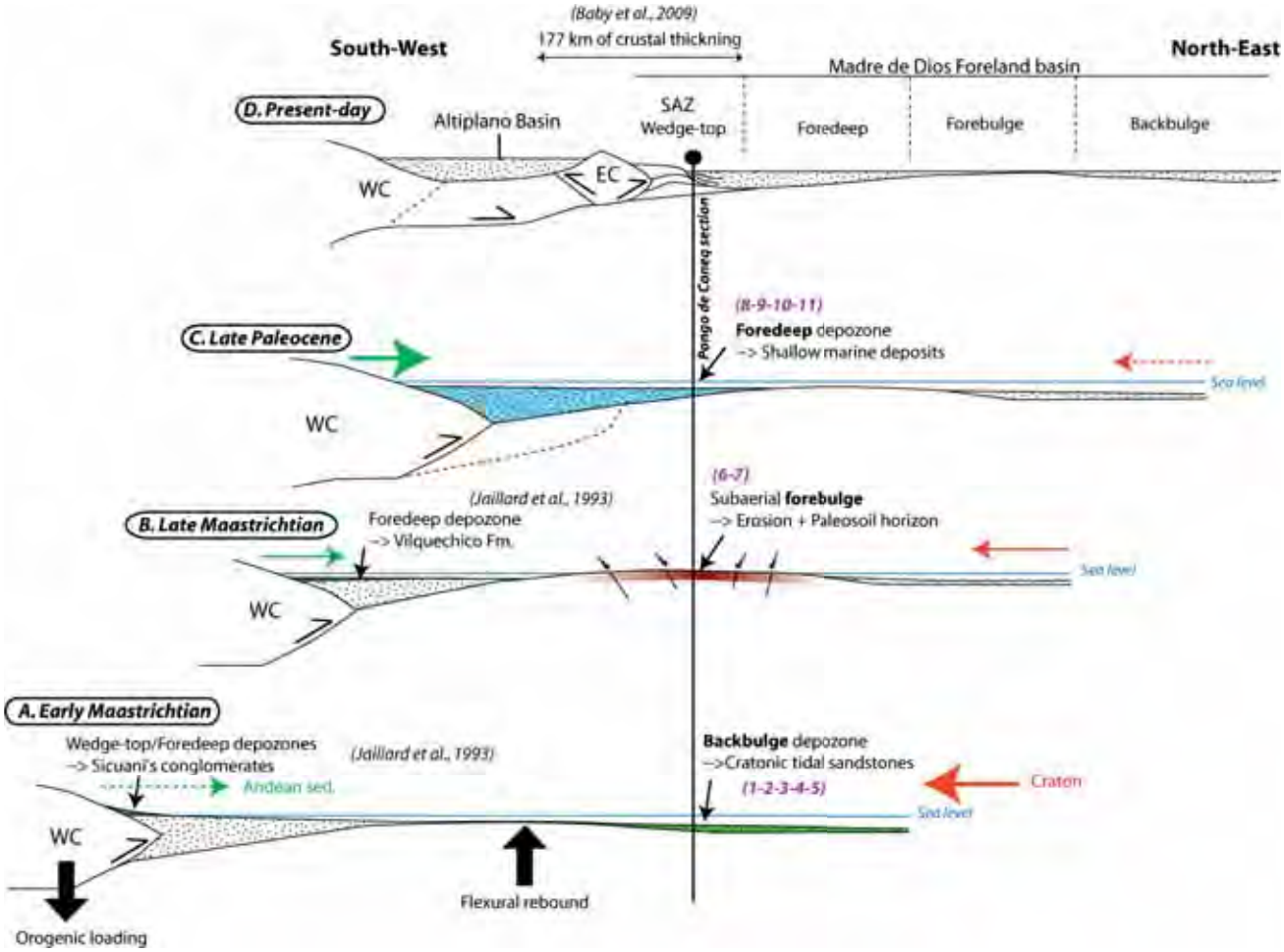

Figure 3: Synthetic cartoon showing the evolution of the Southern Amazonian foreland basin system during the Maastrichtian-Late Paleocene times (see text for details). Sedimentary sources are indicated by green (Andean) or red (cratonic) arrows. Localities are also indicated. See Figure 1 for location of the Pongo de Coñeq section and the corresponding outcrops.

6. Supplementary dataset

Outcrop ref. (Thisstudy)	Correspondingoutcrop	X	Y	Zone
1	MD 175	-71,363551	-12,89295	Pongo de Coñeq Canyon
2	MD 238	-71,36228	-12,89299	Pongo de Coñeq Canyon
3	MD 80	-71,362298	-12,893048	Pongo de Coñeq Canyon
4	MD 239	-71,36149	-12,89221	Pongo de Coñeq Canyon
5	MD 79	-71,361607	-12,891997	Pongo de Coñeq Canyon
6	MD 176	-71,3621	-12,892	Pongo de Coñeq Canyon
7	MD 82=60	-71,361424	-12,891202	Pongo de Coñeq Canyon
8	MD 177	-71,360503	-12,8903	Pongo de Coñeq Canyon
9	MD 184	-71,2659	-12,6688	Pantiacolla Anticline
10	MD 255	-71,2477	-12,6799	Pantiacolla Anticline
11	MD 85	-71,267881	-12,671605	Pantiacolla Anticline

Supplementary Table 1: Outcrop references for this study, and their corresponding reference number (Corresponding Outcrop) used in the general Madre de Dios database (PhD).

Sample nº	Palynoogy	Microfossil	Paleontology	Description	Age	Paleobiology	Reference
1	x		x	*Tricolporopollenites sp. A + Ulmoideipiteskrempii [72-65 Ma; Late Campanian-Maastrichtian] – continental environment, early Maastrichtian (MD-81-PN1)* *Chondrichthyes, Sclerorhynchiformes, Pucapristis sp. [Maastrichtian]* *Chondrichthyes, ?Ptychotrygon sp. / Sclerorhynchidae (oral tooth)* *Chondrichthyes, Schizorhizaaff. Stromeri (rostral tooth) [brachydontà late Campanian]* *Rajiformes, Pucabatis sp. [Maastrichtian]* *Osteichthyes, Pycnodontiformesindet. (small)Osteichthyes, Tetraodontiformes, Eotrigonodontidae, cf. Stephanodus sp.*	Early Maastrichtian	Prodeltaic/estuarine plain fringe. Confined proximal marine environment of normal salinity (diverse euhaline ichtyo-fauna, but no shark). Equivalent to Bolivan El Molin Fm.	1
	x						
	x					Marine	
2	x			*Rzehakinalata Cushman & Jarvis, 1928 (5)* *Rzehakina minima Cushman &Renz (1946) (8)* *RzehakinaepigonaRzehak (1895) (2)* *RzehakinafissistomataGrzybowski, 1901 (2)* *SpirosigmoilinellacompressaMatsunaga (1955) (13)* *SilicosigmoilinaangustaTurenko, 1983 (2)* *Ammobaculites sp. Cushman, 1910 (1)* *cf. Trochammina Parker & Jones, 1859 (2)* *Miliammina sp. Heron-Allen &Earland, 1930 (2)* *SigmoilinadistortaPhleger& Parker, 1951 (2)*	Maastrichtian	Marginal marine environment	2
3	x			*Reworked Cenomanian material*	Early Maastrichtian	Marginal marine environment	1
4	x			*cf. RotaliidaeEhrenberg, 1839 (1)* *SpirosigmoilinellacompressaMatsunaga, 1955 (1)* *SilicosigmoilinaangustaTurenko 1983 (1)* *Dientes (5)Karrerulina horrida (Mjatlivk, 1970) (2)* *Karrerulinaconiformis (Grzybowski, 1898) (2)* *cf. fragmentos de arenáceos indeterminados (2)* *Foraminíferos ennegrecidos retrabajados (4)* *Dientes (8)*	(Maastrichtian)	Marginal marine environment	2
5	x			*Reworked Aptian/Albian material*	Early Maastrichtian	Marginal marine environment	1
7	x		x	*Charophyta, oogonia (numerous)* *Unidentifiable gastropod casts (11), probably including cerithioideans* *Aylacostoma sp. 1 (2) [fresh water]* *Chondrichthyes, Ischyrhizahartenbergeri [Maastrichtian]* *Chondrichthyes, Rajiformes, Dasyatoidea, Dasyatisschaefferi [Maastrichtian]* *Cheloniaindet.*	Late Maastrichtian	Prodeltaic/estuarine plain fringe. Confined proximal marine environment of normal salinity (diverse euhaline ichtyo-fauna, but no shark), with terrigenous inputs (including charophyteoogonia). Ichthyo-fauna comparable to that of Toro Toro (Bolivia; Cappetta, 1975).	1
8	x		x	*Charophyta, oogonia (very few)* *Mollusca, Gastropodaindet.* *Mollusca, Bivalviaindet. (possibly corbiculid clams/marine lucinid clams)* *Arthropoda, Ostracodaindet.* *Chondrichthyes, Myliobatiformes, Ouledia sp. [Thanetian FAD; first American occurrence; large size indicative of Eocene]* *Chondrichthyes, Dasyatoidea, ?Dasyatidaeindet.* *Osteichthyes, Pycnodontiformes, cf. Coelodus sp. (many teeth) [LAD: early middle Eocene]* *Osteichthyes, Characiformesindet. (multicuspidate teeth)* *Mammalia, ?Metatheriaindet. (broken canine)*	Thanetian (late Palaeocene)	Lagoonal/estuarine/steady bay . Confined and steady proximal marine environment of normal salinity (still more diverse euhaline ichtyo-fauna, but no shark).	1
9	x			*?Polymesoda/Rangia (other possibilities include species of Unionoidea or Veneroidea. It concerns at least three species (6 + c 30/2))* *Corbiculas.l. indet.? (2/2, ribbed imprints)* *Cerithioideaindet. (6)* *Pachychilidaeindet. (2)* *?Aylacostomaindet. (1)* *Chondrichthyes, Pristiformes, Pristidaeindet. [FAD: early Eocene]* *Chondrichthyes, Myliobatiformes, Ouledia sp. (Thanetian FAD; many teeth)* *Chondrichthyes, Rajiformes, Dasyatoideaindet. [Dasyatidae / Potamotrygonidae]* *Osteichthyes, Pycnodontiformes, cf. Coelodus sp. (many teeth) [LAD: middle Eocene]* *Osteichthyes, Characiformesindet. (multicuspidate teeth)*	(Paleocene)-Eocene		1, 2
	x				(Paleocene)-Eocene	Marginal marine environment - Supralitoral.	
			x		Thanetian (late Palaeocene)	Lagoonal/estuarine/steady bay. Confined and steady proximal marine environment of normal salinity (still more diverse euhaline ichtyo-fauna, but no shark).	
10		x		*Karreriella conversa (3)* *Nothiasp. (5)* *Incertaesedis cf. cangrejo (1)*	Upper Cretaceous-Ypresian	Undetermined. Probably related to terrestrial imputs + paleosoils formation.	2
11	x			*Charophyta, oogonia (numerous)* *Mollusca, Gastropodaindet.* *Chondrichthyes, Myliobatiformes, Ouledia (Thanetian FAD; one tooth; eroded)* *Chondrichthyes, Dasyatoidea, Potobatisnov.gen. Cappetta, submitted [age?]* *Osteichthyes, Pycnodontiformes, cf. Coelodus sp. (many teeth) [LAD: middle Eocene]* *Osteichthyes, Characiformesindet. (multicuspidate teeth)* *Mammalia indet. (tooth fragment)*	Paleocene	Coastal/Estuarine plain fringe with saline/fresh water	1, 2
	x				Paleocene	Coastal/Estuarine plain fringe with saline/fresh water	
			x		Thanetian (late Palaeocene)	Distal fluvial/proximal estuarine-deltaic. Strong freshwater influence (fish fauna): the environment is much more proximal than other ones, i.e. distal fluvial. Shallow water.	

Supplementary Table 2: Detailed stratigraphic constraints from Paleontology, Palynology and microfossil study. Ref=1: results interpreted by the University of Montpellier (Pierre Olivier Antoine, Laurent Marivaux, Sylvain Adnet) and the Smithsonian Institute (Carlos Jaramillo). Ref=2: results interpreted by the University of Toulouse (Francisco Parra).

Age	Sample	Quartz	Kaolinite	Calcite	Smectite	Micas	Chlorite	Dolomite
Maastrichtian	MD 175 A	**	***	*	*	*	o	**
	MD 176 A	***	*	o	*	*	o	o
Late Paleocene	MD 85	**	*	***	*	*	*	o
	MD 85 A	**	*	*	*	*	*	o
	MD 184 A	**	*	*	*	*	o	o
	MD 177 A	**	*	*	*	*	*	o

Supplementary Table 3: Mineralogical results (shales). +: few content; ++: moderate content; +++: high content; o: not present. See Caroline Sanchez' Master Thesis (2012) for more details.

Supplementary Table 4: Major and Trace elements concentrations of analyzed sediments; LOI: Lost Of Ignition; CIA: Chemical Index of Alteration (Nesbitt and Young, 1982) .

(Next Page)

Outcrop Ref. (Thisstudy)	CorrespondingOutcrop	Correspondingsamples	Lithology	Sr (ppm)	Nd (ppm)	143Nd/144Nd	± 2σ	eNd(0)	87Sr/86Sr	± 2σ1	REF
1	MD 175	MD 175 A	Mudstone	104	49,94	0,511797	6	-16,40533866	0,724795	9	1
2	MD 238	MD 238 Nd	Mudstone	NM	21,43	0,51186	14	-15,18	NM	NM	2
4	MD 239	MD 239 B Nd	Mudstone	NM	18,092	0,511925	51	-13,91	NM	NM	2
6	MD 176	MD 176 A	Mudstone	56,18	27,87	0,511991	4	-12,62099181	0,730209	8	1
8	MD 177	MD 177 A	Mudstone	244,3	38,2	0,512087	3	-10,7	0,717287	10	1
9	MD 184	MD 184 A	Mudstone	269,7	42,39	0,512117	6	-10,16311705	0,715741	10	1
9 bis		MD 184 F Nd	Mudstone	NM	27,157	0,512155	16	-9,43	NM	NM	2
10	MD 255	MD 255 Nd	Mudstone	NM	NM	0,512126	6	-10,0	0,719026	10	1
10 bis		MD 255 NdBr	Mudstone	NM	14,73	0,512168	3	-9,17	NM	NM	2
11 bis	MD 85	MD 85 B	Mudstone	NM	0,38	0,512178	9	-8,97	NM	NM	2
11		MD 85	Mudstone	295,5	28,33	0,512318	5	-6,242221607	0,712024	8	1

Supplementary Table 5: Detailed Nd/Sr isotopic results for the Late Campanian to Late Paleocene samples from the Salvación syncline, Madre de Dios basin. 1: analyses carried out at the University of Toulouse (GET, France); 2: analyses carried out at the University of Brasilia (Laboratorio de Geochronologia, Brasil).

Samples:	MD 175	MD 176	MD 177	MD 184	MD 85 A	MD 85
SiO2	50,07	73,16	55,30	53,47	52,78	46,57
Al2O3	18,39	11,16	16,48	16,48	15,69	14,82
Fe2O3	5,63	4,73	6,68	7,89	6,87	6,87
MnO	0,08	0,05	0,05	0,08	0,10	0,14
MgO	3,03	1,07	2,82	2,67	3,73	5,30
CaO	4,13	0,74	2,91	2,59	3,20	7,04
Na2O	0,09	0,09	0,51	0,26	0,54	0,41
K2O	2,50	1,92	3,15	3,13	3,55	2,69
TiO2	0,77	0,74	0,81	0,81	0,77	0,69
P2O5	0,14	0,15	0,27	0,28	0,11	0,22
LOI	16,34	6,59	12,13	13,03	14,00	15,65
Total	101,16	100,39	101,10	100,69	101,32	100,40
Sc	16,35	10,57	16,49	17,78	17,35	17,23
Rb	115,10	91,66	126,00	125,60	121,50	93,49
Cs	5,52	4,51	7,15	6,05	6,59	7,48
Ba	185,10	233,00	609,90	2562,00	380,20	194,30
Sr	104,00	56,18	244,30	269,70	207,90	295,50
Th	18,26	12,31	13,17	10,75	9,84	8,35
U	4,14	2,58	3,19	1,80	2,47	2,33
Y	30,92	27,77	32,21	34,63	24,44	25,52
Zr	125,90	453,50	163,20	155,10	149,20	135,40
Nb	17,34	15,48	13,87	10,95	10,14	10,00
Hf	3,53	11,07	4,63	4,47	4,26	3,52
Ni	28,75	25,43	41,26	32,64	27,65	26,52
Cr	64,11	47,60	75,11	65,46	54,46	40,90
Co	13,99	9,42	15,30	14,23	14,16	20,31
V	95,12	81,04	140,10	99,42	69,77	114,70
La	56,35	31,76	38,92	40,64	29,11	27,49
Ce	122,90	66,33	84,05	84,48	61,23	58,08
Pr	14,14	6,99	9,23	9,95	6,66	6,68
Nd	49,94	27,87	38,20	42,39	27,27	28,33
Sm	9,14	5,39	7,59	8,72	5,57	5,82
Eu	1,63	1,05	1,54	1,95	1,24	1,36
Gd	6,96	4,80	6,54	7,77	4,76	5,12
Tb	1,06	0,77	1,01	1,15	0,76	0,75
Dy	6,00	4,68	5,84	6,62	4,60	4,40
Ho	1,15	0,98	1,15	1,25	0,92	0,85
Er	3,19	2,92	3,26	3,44	2,66	2,35
Tm	0,49	0,47	0,49	0,49	0,41	0,35
Yb	3,31	3,33	3,30	3,30	2,86	2,34
Lu	0,50	0,54	0,51	0,50	0,44	0,37
Eu/Eu*	0,62	0,63	0,67	0,73	0,73	0,76
Cr/Th	3,51	3,87	5,70	6,09	5,54	4,90
Th/Sc	1,12	1,16	0,80	0,60	0,57	0,48
Zr/Sc	7,70	42,90	9,90	8,72	8,60	7,86
CIA	85,94	82,46	76,35	79,50	73,61	77,65

Supplementary Data A: Analytical Methods for provenance analyses

The mineralogical composition of the six mudstones was determined at Geosciences Environment Toulouse (GET) by X-ray diffraction (XRD) using a Philips PW1050 diffractometer (INGEIS) with Cu K radiation operated at 40 mA and 30 kV.

The eleven selected samples were finely crushed in an agate mortar. They were then analyzed for major and trace element concentrations and Nd-Sr isotopic compositions. Major, minor and trace element concentrations were measured at the Service d'Analyse des Roches et Minéraux (SARM, INSU facility, Vandoeuvre-Les-Nancy, France, analytical details available on http://helium.crpg.cnrs-nancy.fr/SARM/), by ICP-AES and ICP-MS after alkali fusion. Uncertainties are lower than 5% for major elements, and lower than 10% for minor and trace elements.

The Nd-Sr isotopic compositions were measured at Geosciences Environment Toulouse (GET) in France and at Laboratorio de Geochronología de Brasilia.

Methodology at Geoscience Environnement Toulouse:

The analyzed samples for Nd-Sr isotopic composition were firstly digested in hydrogen peroxide for 24 hours at ambient temperature, and then digested in HNO3 for 24 hours at 80°C followed by HF- HNO3 for 24 hours at 80°C, and, finally HCl+HNO3 for 24 hours at 115°C. Blank tests were performed to estimate the level of contamination induced by the acid digestion, but it was found to be negligible. Aliquots containing about 1000 ng of Sr and Nd were loaded into the ion exchange columns. Sr and Nd were separated using the Sr-SPEC, TRU-SPEC and LN-SPEC resins (Eichrom). Nd and Sr isotopic ratios were measured using a Finnigan Mat 261 thermal ionization mass spectrometer in dynamic mode. During the Nd run, the $^{146}Nd/^{144}Nd$ (=0.7219) was used to correct the signal for mass fractionation. For each sample, checks were made for the absence of samarium (Sm). The accuracy of the measurements was estimated on the Rennes University standard for Nd (0.511961+/- 14). This value was calibrated relative to the La Jolla standard by the Brest, Toulouse and Rennes laboratories (Lacan, 2002). During the Sr run, $^{86}Sr/^{88}Sr$ (= 0.1194) was used to correct the signal for mass fractionation. The accuracy of the measurements was checked against the NBS 987 standard (=0.710240). The average values fall within the range given for these standards, so that no instrumental bias needs to be taken into account. The repeatability on these standards is around 15 ppm. This value is adopted for the overall uncertainty of all measurements, even if some individual samples yield results with a lower internal precision. Total blanks (acid digestion plus column chemistry) for Nd and Sr were checked by ICP-MS and found to be negligible compared to the Nd and Sr amounts loaded onto the columns. The measured $^{143}Nd/^{144}Nd$ ratios are expressed as the fractional deviation in parts per 104 (units) from $^{143}Nd/^{144}Nd$ in a Chondritic Uniform Reservoir (CHUR) as measured at the present day:

$\varepsilon Nd(0) = (((^{143}Nd/^{144}Nd)S / ICHUR(0) - 1)*104$, where $(^{143}Nd/^{144}Nd)S$ is the present-day ratio measured in the sample and ICHUR(0) is the $^{143}Nd/^{144}Nd$ in the CHUR reference reservoir at the present (ICHUR(0)=0.512638 (Jacobsen and Wasserburg, 1980).

Supplementary Data B: Sedimentation Rates from Petromod1D

71	69	65	53	34	23,5	Age (Ma)
Lower Maastrichtian	Upper Maastritchian	Paleocene	Eocene	Oligocene	Early Miocene	Geol. Age
CAS 1A						PetroMod calculated Sed. Rates (m/Ma)
121,56	61,96	4,71	0,99	0,00	230,02	
CAS 1B						
124,29	22,21	3,14	3,14	0,00	234,05	
CAS 1C						
124,34	22,22	31,35	0,00	0,00	209,89	
CAS 1D						
124,37	22,22	31,35	5,91	0,00	197,85	
CAS 1E						
120,16	61,97	3,14	0,00	0,00	234,46	
CAS 1F						
120,19	61,97	3,14	5,94	0,00	222,36	
CAS 1G						
120,26	61,98	31,29	0,00	0,00	198,25	
CAS H						
120,29	61,99	31,29	5,90	0,00	186,24	

min	min	min	min	min	min	Minimum Sed. Rate (m/Ma)
120,19	**22,21**	**3,14**	**0,00**	**0,00**	**186,24**	
max	max	max	max	max	max	Maximum Sed. Rate (m/Ma)
127,37	**61,99**	**31,35**	**5,94**	**0,00**	**234,46**	

Table B1: Syntethic table presenting the different sedimentation rates calculated by PetroMod 1D software for each case (8 cases). See Table B2 for details related to each case.

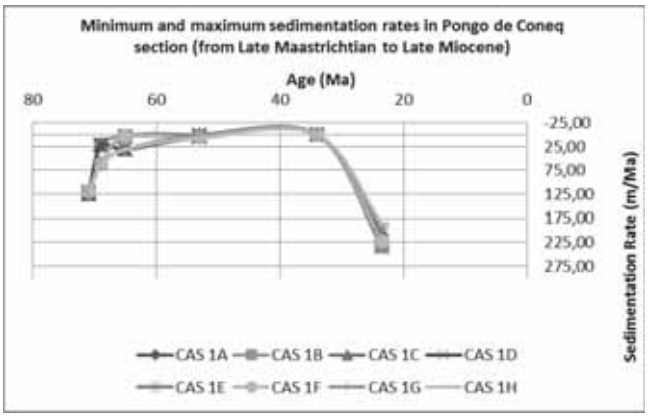

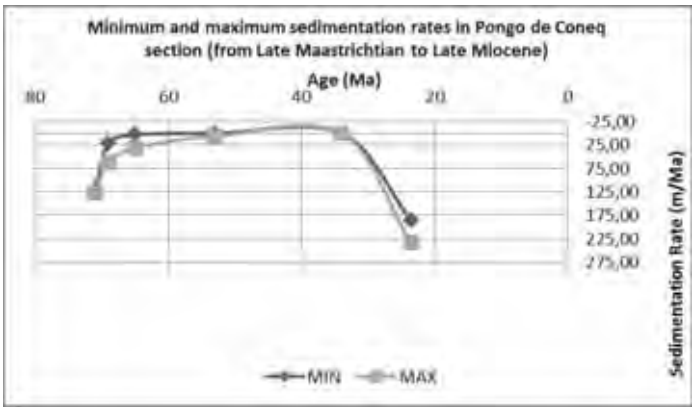

Figure B1 (left) and B2 (right): diagram of sedimentation rates evolution through time, for each of the 8 cases (left) and for the minimum and maximum sedimentation rates computed. Note that the studied time interval here is from the Late Maastrichtian to the Late Miocene.

Case 1A							Case 1E						
Layer	Top	Base	Thick	Eroded	Depo. From (Ma)	Depo. To (Ma)	Layer	Top	Base	Thick	Eroded	Depo. From (Ma)	Depo. To (Ma)
Late Miocene	0	2129	2129		11,00	0,10	Late Miocene	0	2129	2129		11	0,1
Middle Miocene	2129	3249	1120		16,00	11,00	Middle Miocene	2129	3249	1120		16	11
Early Miocene	3249	4497	1248		23,50	16,00	Early Miocene	3249	4441	1192		23,5	16
Oligocene	4497	4497	0		34,00	23,50	Oligocene	4441	4441	0		34	23,5
Eocene	4497	4497	0		53,00	34,00	Eocene	4441	4441	0		53	34
Paleocene	4497	4517	20		65,00	53,00	Paleocene	4441	4461	20		65	53
Upper Maastritchian	4517	4549	32		69,00	65,00	Upper Maastritchian	4461	4551	90		69	65
Lower Maastrichtian	4549	4719	170		71,00	69,00	Lower Maastrichtian	4551	4721	170		71	69
						71,00							71
Case 1B							Case 1F						
Layer	Top	Base	Thick	Eroded	Depo. From (Ma)	Depo. To (Ma)	Layer	Top	Base	Thick	Eroded	Depo. From (Ma)	Depo. To (Ma)
Late Miocene	0	2129	2129		11	0,1	Late Miocene	0	2129	2129		11	0,1
Middle Miocene	2129	3249	1120		16	11	Middle Miocene	2129	3249	1120		16	11
Early Miocene	3249	4439	1190		23,5	16	Early Miocene	3249	4381	1132		23,5	16
Oligocene	4439	4439	0		34	23,5	Oligocene	4381	4381	0		34	23,5
Eocene	4439	4499	60		53	34	Eocene	4381	4441	60		53	34
Paleocene	4499	4519	20		65	53	Paleocene	4441	4461	20		65	53
Upper Maastritchian	4519	4551	32		69	65	Upper Maastritchian	4461	4551	90		69	65
Lower Maastrichtian	4551	4721	170		71	69	Lower Maastrichtian	4551	4721	170		71	69
						71							71
Case 1C							Case 1G						
Layer	Top	Base	Thick	Eroded	Depo. From (Ma)	Depo. To (Ma)	Layer	Top	Base	Thick	Eroded	Depo. From (Ma)	Depo. To (Ma)
Late Miocene	0	2129	2129		11	0,1	Late Miocene	0	2129	2129		11	0,1
Middle Miocene	2129	3249	1120		16	11	Middle Miocene	2129	3249	1120		16	11
Early Miocene	3249	4319	1070		23,5	16	Early Miocene	3249	4261	1012		23,5	16
Oligocene	4319	4319	0		34	23,5	Oligocene	4261	4261	0		34	23,5
Eocene	4319	4319	0		53	34	Eocene	4261	4261	0		53	34
Paleocene	4319	4519	200		65	53	Paleocene	4261	4461	200		65	53
Upper Maastritchian	4519	4551	32		69	65	Upper Maastritchian	4461	4551	90		69	65
Lower Maastrichtian	4551	4721	170		71	69	Lower Maastrichtian	4551	4721	170		71	69
						71							71
Case 1D							Case 1H						
Layer	Top	Base	Thick	Eroded	Depo. From (Ma)	Depo. To (Ma)	Layer	Top	Base	Thick	Eroded	Depo. From (Ma)	Depo. To (Ma)
Late Miocene	0	2129	2129		11	0,1	Late Miocene	0	2129	2129		11	0,1
Middle Miocene	2129	3249	1120		16	11	Middle Miocene	2129	3249	1120		16	11
Early Miocene	3249	4259	1010		23,5	16	Early Miocene	3249	4201	952		23,5	16
Oligocene	4259	4259	0		34	23,5	Oligocene	4201	4201	0		34	23,5
Eocene	4259	4319	60		53	34	Eocene	4201	4261	60		53	34
Paleocene	4319	4519	200		65	53	Paleocene	4261	4461	200		65	53
Upper Maastritchian	4519	4551	32		69	65	Upper Maastritchian	4461	4551	90		69	65
Lower Maastrichtian	4551	4721	170		71	69	Lower Maastrichtian	4551	4721	170		71	69
						71							71

Table B2: Details for each studied case used to compute the sedimentation rates through time. Top, Base and thickness are in meters.

7. References

Balkwill, H., Rodrigue, G., Paredes, F. and Almeida, J., 1995. Northern part of Oriente basin, Ecuador: reflection seismic expression of structures. AAPG Special Volumes: 559-571.

Barragan, R., Geist, D., Hall, M., Larson, P. and Kurz, M., 1998. Subduction controls on the compositions of lavas from the Ecuadorian Andes. . Earth and Planetary Science Letters 154: p.153-166

Beaumont, C., 1981. Foreland l* n Oa. physical Journal nf Royal Astmomical Society, 65: 291-329.

Bradley, D. and Kidd, W., 1991. Flexural extension of the upper continental crust in collisional foredeeps. Geological Society of America Bulletin, 103(11): 1416-1438.

Crampton, S. and Allen, P., 1995. Recognition of forebulge unconformities associated with early stage foreland basin development: example from the North Alpine foreland basin. AAPG bulletin, 79(10).

Cullers, R.L., 2000. The geochemistry of shales, silstones and sandstones of Pennsylvanian-Permian age, Colorado, USA: implications for provenance and metamorphic studies. Lithos, 51: 181-203.

Chew, D.M., Schaltegger, U., Košler, J., Whitehouse, M.J., Gutjahr, M., Spikings, R.A. and Miškovíc, A., 2007. U-Pb geochronologic evidence for the evolution of the Gondwanan margin of the north-central Andes. Geological Society of America Bulletin, 119(5-6): 697-711.

Dantas, E.L., Alvarenga, C.J.S.d., Santos, R.V. and Pimentel, M.M., 2009. Using Nd isotopes to understand the provenance of sedimentary rocks from a continental margin to a foreland basin in the Neoproterozoic Paraguay Belt, Central Brazil. Precambrian Research, 170(1): 1-12.

DeCelles, P.G., Carrapa, B., Horton, B.K. and Gehrels, G.E., 2011. Cenozoic foreland basin system in the central Andes of northwestern Argentina: Implications for Andean geodynamics and modes of deformation. Tectonics, 30(6): TC6013.

DeCelles, P.G. and Giles, K.a., 1996. Foreland basin systems. Basin Research, 8(2): 105-123.

DeCelles, P.G. and Horton, B.K., 2003. Early to middle Tertiary foreland basin development and the history of Andean crustal shortening in Bolivia. Geological Society of America Bulletin, 115(1): 58-77.

Decou, a., von Eynatten, H., Mamani, M., Sempere, T. and Wörner, G., 2011. Cenozoic forearc basin sediments in Southern Peru (15–18°S): Stratigraphic and heavy mineral constraints for Eocene to Miocene evolution of the Central Andes. Sedimentary Geology, 237(1-2): 55-72.

Espurt, N., 2007. Influence de la subduction d'une ride asismique sur la dynamique de la plaque continentale chevauchante: exemple de la ride de Nazca et du bassin Amazonien, 1-326 pp.

Espurt, N., Barbarand, J., Roddaz, M., Brusset, S., Baby, P., Saillard, M. and Hermoza, W., 2011. A scenario for late Neogene Andean shortening transfer in the Camisea Subandean zone (Peru, 12 S): Implications for growth of the northern Andean Plateau. Geological Society of America Bulletin, 123(9-10): 2050-2068.

Fuentes, F., DeCelles, P. and Gehrels, G., 2009. Jurassic onset of foreland basin deposition in northwestern Montana, USA: Implications for along-strike synchroneity of Cordilleran orogenic activity. Geology, 37(4): 379-382.

Gil, W.F., 2001. Evolution latérale de la déformation d'un front orogénique: exemples des bassins subandins entre 0° et 16°S, University Paul Sabatier, Toulouse.

Haq, B.U., Hardenbol, J. and Vail, P.R., 1987. Chronology of fluctuating sea levels since the Triassic. Science, v. 235: p. 1156–1167.

Hermoza, W., 2004. Dynamique tectono-sedimentaire et restauration sequentielle du retro-bassin d'avant-pays des Andes Centrales, Univeristy Paul Sabatier, Toulouse, 196 pp. pp.

Horton, B. and DeCelles, P., 2001. Modern and ancient fluvial megafans in the foreland basin system of the central Andes, southern Bolivia: implications for drainage network evolution in fold-thrust belts. Basin research, 13(1): 43-63.

Horton, B.K., Hampton, B.A. and Waanders, G.L., 2001. Paleogene synorogenic sedimentation in the Altiplano plateau and implications for initial mountain building in the central Andes. Geological Society of America Bulletin, 113(11): 1387-1400.

Hulka, C. and Heubeck, C., 2010. Composition and provenance history of late Cenozoic sediments in southeastern Bolivia: implications for Chaco foreland basin evolution and Andean uplift. Journal of Sedimentary Research, 80(3): 288-299.

Jacobsen, S.B. and Wasserburg, G., 1980. Sm-Nd isotopic evolution of chondrites. Earth and Planetary Science Letters, 50(1): 139-155.

Jaillard, E., 1993a. The Senonian to Palaeocene tectonic evolution of the Peruvian margin and its relationships with geodynamics. L'evolution tectonique de la marge peruvienne au Senonien et Paleocene et ses relations avec la geodynamique, 164(6): 819-830.

Jaillard, E., Cappetta, H., Ellenberger, P., Feist, M., Grambast-Fessard, N., Lefranc, J. and Sigé, B., 1993c. Sedimentology, palaeontology, biostratigraphy and correlation of the Late Cretaceous Vilquechico Group of southern Peru. Cretaceous Research, 14(6): 623-661.

Jordan, T.E., Burns, W.M., Veiga, R., Pángaro, F., Copeland, P., Kelley, S. and Mpodozis, C., 2001. Extension and basin formation in the southern Andes caused by increased convergence rate: A mid-Cenozoic trigger for the Andes. Tectonics, 20(3): 308-324.

Jordan, T.E., Nester, P.L., Blanco, N., Hoke, G.D., Dávila, F.M. and Tomlinson, A.J., 2010. Uplift of the Altiplano-Puna plateau: A view from the west. Tectonics, 29(5).

Kay, S.M., Coira, B. and Viramonte, J., 1994. Young mafic back arc volcainc-rocks s indicators of continental lithospheric delamination beneath the Argentine Puna plateau, Central Andes Journal of Geophysical Research-Solid Earth, 99(B12): 24323-24339.

Lacan, F., 2002. Masses d'eau des Mers Nordiques et de l'Atlantique Subarctique tracées par les isotopes du néodyme, Université Paul Sabatier-Toulouse III.

Laubacher, G., 1978. Geology of the Peruvian Andes: geology of the eastern Cordillera and of the Altiplano to the north and north west of Lake Titicaca. Travaux et Documents de l'ORSTOM.

Lease, R.O. and Ehlers, T.A., 2013. Incision into the Eastern Andean plateau during Pliocene cooling. Science, 341(6147): 774-776.

Londoño, J. and Lorenzo, J.M., 2004. Geodynamics of continental plate collision during late tertiary foreland basin evolution in the Timor Sea: constraints from foreland sequences, elastic flexure and normal faulting. Tectonophysics, 392(1): 37-54.

Louterbach, M., Roddaz, M., Baby, P., Bailleul, J., Antoine, P.-O., Adnet, S., Kim, J.H., Van Soelen, E., Parra, F., Gérard, J., Calderon, Y., Gagnaison, C. and Sinninghe Damsté, J.S., Submitted. Evidences for a late Paleocene marine incursion in Southern Amazonia (Madre de Dios Sub-Andean Zone, Peru). Palaeogeography, Palaeoclimatology, Palaeoecology.

Mamani, M., Worner, G. and Sempere, T., 2010. Geochemical variations in igneous rocks of the Central Andean orocline (13 degrees S to 18 degrees S): Tracing crustal thickening and magma generation through time and space. Geological Society of America Bulletin, 122(1-2): 162-182.

Martin-Gombojav, N. and Winkler, W., 2008. Recycling of proterozoic crust in the andean amazon foreland of Ecuador: Implications for orogenic development of the Northern Andes. Terra Nova, 20(1): 22-31.

Nesbitt, H. and Young, G., 1982. Early Proterozoic climates and plate motions inferred from major element chemistry of lutites. Nature, 299(5885): 715-717.

Nie, J., Horton, B.K., Saylor, J.E., Mora, A., Mange, M., Garzione, C.N., Basu, A., Moreno, C.J., Caballero, V. and Parra, M., 2012. Integrated provenance analysis of a convergent retroarc foreland system: U–Pb ages, heavy minerals, Nd isotopes, and sandstone compositions of the Middle Magdalena Valley basin, northern Andes, Colombia. Earth-Science Reviews, 110(1-4): 111-126.

Pinto, L., 2003. Traçage de l'érosion Cénozoïque des Andes Centrales à l'aide dela minéralogie et de la géochmie des sédiments (Nord du Chili et Nord-Ouest de la Bolivie), University Paul Sabatier, Toulouse.

Roddaz, M., Baby, P., Brusset, S., Hermoza, W. and Maria Darrozes, J., 2005b. Forebulge dynamics and environmental control in Western Amazonia: The case study of the Arch of Iquitos (Peru). Tectonophysics, 399(1–4): 87-108.

Roddaz, M., Hermoza, W., Mora, A., Baby, P., Parra, M., Christophoul, F., Brusset, S. and Espurt, N., 2010. Cenozoic sedimentary evolution of the Amazonian foreland basin system, pp. 61-88.

Roddaz, M., Viers, J., Brusset, S., Baby, P. and Hérail, G., 2005a. Sediment provenances and drainage evolution of the Neogene Amazonian foreland basin. Earth and Planetary Science Letters, 239(1–2): 57-78.

Rogers, G. and Hawkesworth, C.J., 1989. A geochemical traverse across the North Chilean Andes: evidence for crust generation from the mantle wedge. Earth and Planetary Science Letters, 91(3–4): 271-285.

Sempere, T., Butler, R.F., Richards, D.R., Marshall, L.G., Sharp, W. and Swisher, C.C., 1997. Stratigraphy and chronology of upper Cretaceous lower Paleogene strata in Bolivia and northwest Argentina. Geological Society of America Bulletin, 109(6): 709-727.

Singh, B.P., 2003. Evidence of growth fault and forebulge in the Late Paleocene (~57.9–54.7 Ma), western Himalayan foreland basin, India. Earth and Planetary Science Letters, 216(4): 717-724.

Taylor, S.R. and McLennan, S.M., 1985. The continental crust: its composition and evolution.

Uba, C.E., Heubeck, C. and Hulka, C., 2006. Evolution of the late Cenozoic Chaco foreland basin, Southern Bolivia. Basin Research, 18(2): 145-170.

Viers, J., Roddaz, M., Filizola, N., Guyot, J.L., Sondag, F., Brunet, P., Zouiten, C., Boucayrand, C., Martin, F. and Boaventura, G.R., 2008. Seasonal and provenance controls on Nd-Sr isotopic compositions of Amazon rivers suspended sediments and implications for Nd and Sr fluxes exported to the Atlantic Ocean. Earth and Planetary Science Letters, 274(3-4): 511-523.

Viramonte, J.G., Kay, S.M., Becchio, R., Escayola, M. and Novitski, I., 1999. Cretaceous rift related magmatism in central-western South America. Journal of South American Earth Sciences, 12(2): 109-121.

Von Huene, R. and Suess, E., 1988. Ocean Drilling Program Leg 112, Peru continental margin: part 1, tectonic history. Geology, 16(10): 934-938.

8. Figures

C. Evidences for a late Paleocene marine incursion in Southern Amazonia (Madre de Dios Sub-Andean Zone, Peru)

Introduction au chapitre:

Le chapitre C correspond à la version finale d'un article soumis en octobre 2012 à la revue Palaeogography, Palaeoclimatology and Palaeoecology. *L'article devrait être publié après révisions mineures à majeures en accord avec la réponse de l'éditeur reçue en mai 2014 (voir commentaires des correcteurs, Annexe nº5).*

Après une première estimation de l'âge du début de la formation du bassin d'avant-pays de Madre de Dios (Partie B), nous proposons dans ce chapitre une étude multidisciplinaire (paléontologie, sédimentologie, provenance et origine de la matière organique) des dépôts Paléocène décrits dans la partie nord du bassin (synclinal de Salvación). Il s'avère en effet que ces dépôts traditionnellement interprétés comme continentaux présentent finalement des caractéristiques marines.

Les principaux objectifs de cette étude sont de i) déterminer l'âge des dépôts décrits, ii) caractériser les paléo-environnements de dépôts associés et finalement de iii) proposer une première carte paléogéographique. Le contrôle de la déformation Andine sur ces dépôts sera aussi discuté, tout comme les conséquences d'une telle incursion marine sur la biodiversité Néotropicale.

Résumé:

Cet article présente de nouveaux résultats biostratigraphiques, une analyse de facies complète, des résultats de géochimie organique ainsi que de nouvelles données de provenance sédimentaire pour cinq affleurements du bassin d'avant-pays de Madre de Dios au sud du Pérou (MD-85, MD-177, MD-184, MD-255 and MD-256). Nous documentons pour la première fois une incursion marine au Thanétien (Paléocène supérieur) dans cette partie du bassin Amazonien.

La présence de foraminifères benthiques agglutinés de type Karreriella conversa, d'ostracodes de type Protobuntonia et de charophytes de type Peckichara-varians meridionalis suggère un âge Thanétien pour les dépôts étudiés. Quinze faciès ont été reconnus et ont été regroupés en 3 associations de faciès. La première, l'association de facies A, correspond au remplissage sédimentaire d'un chenal méandriforme influencé par la marée et formé dans la zone de transition côtière « fluviale-tidale ». L'association de faciès B correspond quant à elle à des dépôts de replats tidaux plus distaux recoupés par de petits chenaux tidaux ainsi qu'a des dépôts de « saltmarshes ». L'association de faciès C correspond finalement à un environnement de baie ou de lagon, ou plus généralement à un milieu marin peu profond. La valeur de $\delta^{13}C_{TOC}$ (-23.4 ‰) obtenue pour l'affleurement MD-184 est enrichie en 13C en comparaison avec les valeurs obtenues pour les autres affleurements, ce qui suggère la présence d'une concentration notable de matière organique d'origine marine pour MD-184. En contrepartie, les valeurs de $\delta^{13}C_{TOC}$ obtenues pour les autres affleurements (de -27.3 à -29.8 ‰) indiquent que l'origine de la matière organique est mixte et caractérise donc un environnement

continental à côtier. Les sédiments analysés dans cette étude ont une composition isotopique en Nd-Sr similaire à celles obtenues pour les sédiments Cénozoïques de l'Altiplano (valeurs de ƐNd(0) entre -6.2 et -10.7 et compositions 87Sr/86Sr de 0.712024 à 0.719026), ce qui indique une source volcanique similaire à ces sédiments.

L'intégration des différentes données documente la présence d'un estuaire dominé par la marée débouchant dans une baie marine peu profonde et alimenté par la proto Cordillère Occidentale pendant le Thanétien. Cette transgression est certainement due à la subsidence créée en réponse au chargement orogénique de la Cordillère Occidentale située bien plus à l'ouest. Finalement, nous suggérons que l'incursion Paléogène décrite ici a pu jouer un rôle déterminant dans la dynamique de biodiversité Neotropicale amazonienne en favorisant l'isolation bio-géographique et en promouvant la spéciation allopatrique des organismes terrestres. Ces mêmes processus sont d'ailleurs connus et décrits pour les incursions Miocène plus tardives affectant le méga-système marécageux Pebas et associées de la même manière au soulèvement des Andes.

Evidences for a late Paleocene marine incursion in Southern Amazonia (Madre de Dios Sub-Andean Zone, Peru)

M. Louterbach[1,2,5,] *, M. Roddaz[1], J. Bailleul[2], P-O. Antoine[3], S. Adnet[3], J.H. Kim[4], E. van Soelen[4], F. Parra[1], J. Gérard[5], Y. Calderon[6], C. Gagnaison[2], J. S. Sinninghe Damsté[4] and P. Baby[1]

[1]Géosciences-Environnement Toulouse, Université de Toulouse; UPS (SVT-OMP); LMTG; CNRS; IRD; 14 Avenue Édouard Belin, F-31400 Toulouse, France

[2]Bassins-Réservoirs-Ressources, Institut Polytechnique Lasalle Beauvais, Département Géosciences, 19 rue Pierre Waguet, BP 30313, F-60026 Beauvais Cedex, France

[3]Institut des Sciences de l'Évolution (ISE-M, UMR - CNRS 5554), c.c. 64, Université Montpellier 2, Place Eugène Bataillon, F-34095 Montpellier Cedex 05, France

[4]NIOZ Royal Netherlands Institute for Sea Research, NL-1790 AB Den Burg, the Netherlands

[5]REPSOL Exploracion S.A., Calle Mendez Alavaro 44, 28045 Madrid, Spain

[6]PERUPETRO S.A., Luis Aldana 320 - San Borja, Lima, Peru

*Corresponding author

E-mail: melanie.louterbach@hotmail.fr

Summary

Abstract

This article presents new biostratigraphic dating, facies analysis, organic geochemical data and Nd-Sr isotopic provenance from five outcrops of southern Amazonian (MD-85, MD-177, MD-184, MD-255 and MD-256) to document for the first time the presence of a Thanetian shallow marine ingression in the southern Amazonian basin. The presence of agglutinated benthic foraminifer *Karreriella conversa,* ostracod *Protobuntonia* and charophyte *Peckichara* cf. *varians meridionalis* suggest a Thanetian age for the studied deposits. Fifteen facies have been recognized and have been grouped into three facies assemblages. Facies association A corresponds to the sedimentary filling of a tide-influenced meandering channel formed in the fluvial-tidal transition zone. Facies association B is related to more distal tidal-flats, little channelized tidal inlets and saltmarshes deposits. Facies association C corresponds to a stressed shallow marine environment such as a bay or a lagoon. The $\delta^{13}C_{TOC}$ value (-23.4 ‰) of MD-184 is enriched in ^{13}C compared to the other samples suggesting the presence of substantial amounts of marine organic matter in MD-184. The $\delta^{13}C_{TOC}$ values of samples from other outcrops (-27.3 to -29.8 ‰) indicate a mixed organic matter origin, from terrestrial to brackish environments. The analyzed sediments have similar Nd-Sr isotopic compositions as those of the Cenozoic sediments of the Altiplano (εNd(0) values from –6.2 to -10.7 and $^{87}Sr/^{86}Sr$ compositions from 0.712024 to 0.719026) indicating a similar volcanic source. Our multidisciplinary dataset documents the presence of a tide-dominated estuary sourced by the proto Western Cordillera debouching into a shallow marine bay during Thanetian times. This transgression is best explained by subsidence created in response to the proto-Western Cordillera loading. Finally, we suggest that similarly to Miocene marine incursions affecting the Pebas megawetland, Paleogene marine incursions in the Amazonian foreland basin associated with Andean uplift may have played a role in the Neotropical biodiversity dynamics in favouring biogeographical isolation and promoting allopatric speciation for terrestrial organisms.

Keywords: Paleogene; Marine ingression; Amazonian foreland basin; Nd-Sr isotopes; Madre de Dios basin; Peru

1. Introduction

The Amazon basin is the world's largest Cenozoic fluvial basin with an actual drainage area of 5.8×106 km^2 and a depositional area of approximately 2.5-3×106 km^2. The Amazon rainforest, with an area of about 5.6×106 km^2, is the largest rainforest ecosystem, representing nearly 50% of the total tropical rainforest area on Earth. The Amazon rainforest plays a significant role in global climate, the carbon cycle and biodiversity and is the most species-rich terrestrial ecosystem in the world. However, the timing of the origin and evolutionary causes of this diversity are still highly debated. A recent synthesis by Hoorn et al. (2010) has highlighted the complex links between Andean building, climate variability and biodiversity development throughout Cenozoic times in the Amazonian basin. In particular the occurence of inland seaway is particularly important not only in promoting biogeographical isolation and allopatric speciation but also in controlling the precipitation rates in the Amazon basin (Jeffery et al., 2012). Consequently, determining the number, timing and duration of Cenozoic marine incursions recorded in Amazonian basin is fundamental not only for reconstructing paleo-Amazonian landscapes and ecosystems through time but also for understanding the close relationships between Andean building and the Cenozoic climate and biotic evolution of South America.

Several marine incursions have already been described in the Cenozoic sedimentary record of the Amazonian foreland basins (Roddaz et al., 2010). For instance, the existence and persistence of the Early to Middle Miocene Pebas "mega wetland system" in northern Amazonia is thought to have promoted the high biodiversity of the Amazon rainforest (for a review, see (Hoorn et al., 2010) and references therein) . However, the extent of this Pebas system and the number of marine ingressions that have occurred is still under debate (Campbell et al., 2006; Hoorn et al., 2010; Hovikoski et al., 2007) mainly because of poor stratigraphic dating and the lack of regional data integration. In comparison, few studies document Paleogene marine incursions in the Amazonian basin. For instance, there is some evidence of a marine ingression during Eocene to Oligocene times in Colombia (Christophoul et al., 2002; Santos et al., 2008), Ecuador (Christophoul et al., 2002) and northern Peru (Hermoza et al., 2005b), but no data exist for earlier marine incursions.

In this study, we bring new biostratigraphical, sedimentological and geochemical data to highlight a late Paleocene marine ingression in southern Peru, Madre de Dios basin, and we propose a new paleo-depositional model for these shallow marine deposits. We further discuss the paleogeography and paleo-extension of this shallow marine ingression.

2. Geological background

2.1. Paleocene sedimentary record in the Amazonian foreland basins

In nearly all the Central Andean sedimentary basins, Late Eocene to Early Oligocene times are marked by a widespread sedimentary hiatus (Marocco et al., 1995; Mpodozis and Allmendinger, 1993) corresponding to a major tectonic phase primarily called "Incaic 1 phase" (Jaillard, 1996; Noble et al., 1990). However, there are

some localities in northern and Central Andean foreland basins where Paleocene strata have been preserved and can be described (Figure 1 and Figure 2).

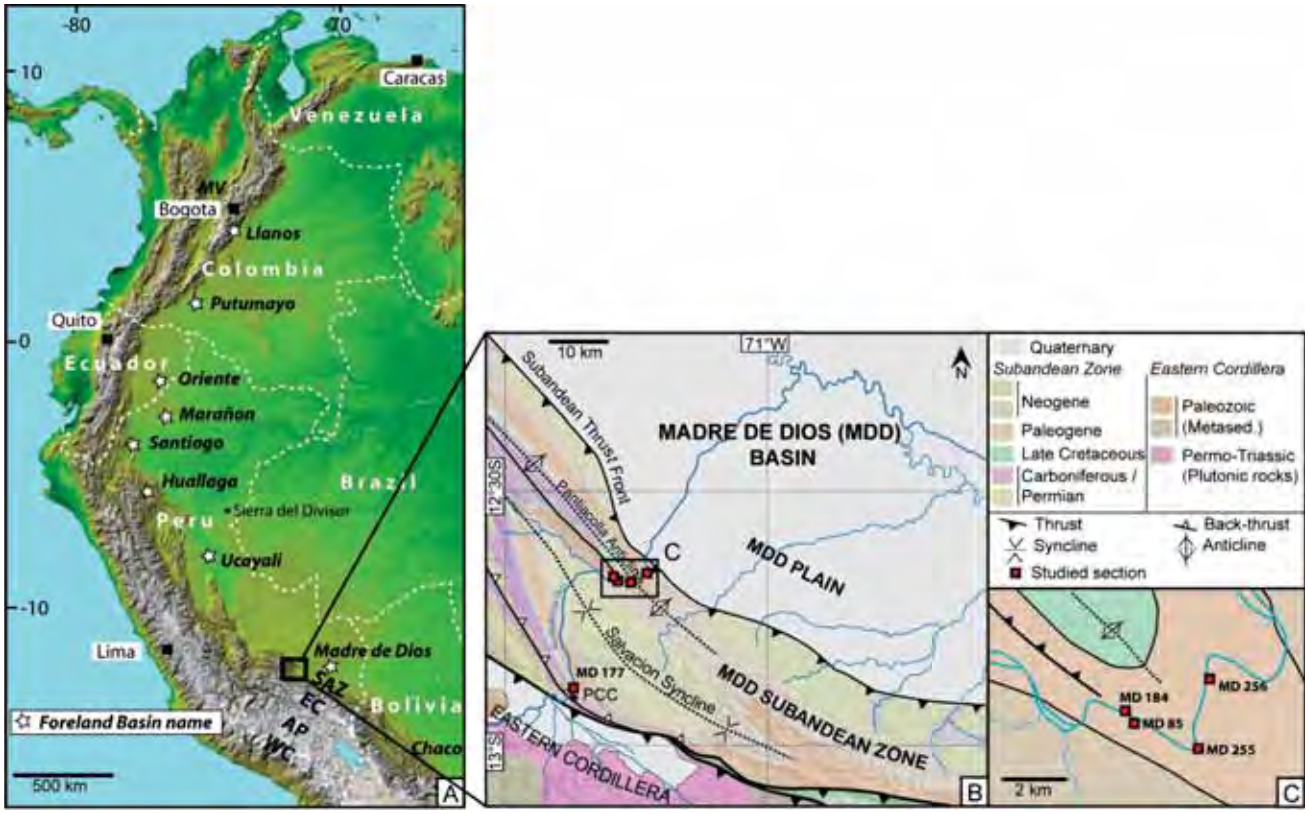

Figure 1: A/ White stars display Amazonian foreland basins location (northern Andes and part of Central Andes). B) Simplified geological and structural map of the study area. Red squares display the location of the outcrops used for this study. PCC= Pongo de Coñeq Canyon. C) Zoom of Pantiacolla Anticline area, and location of the outcrops.

In central Colombia, the Cuervos formation is Late Paleocene in age (Jaramillo and Dilcher, 2000; 2001) and its sedimentary rocks correspond to mudstones deposited in a distal alluvial to coastal plain environment, in a foredeep position (Parra et al., 2009). In the Putumayo basin (southern Colombia), the early Paleocene Rumiyaco Formation is characterized by shallow marine to continental siliciclastic sedimentary rocks. In the Ecuadorian Oriente basin, Paleocene strata dated by charophytes (Faucher and Savoyat, 1973) are represented by the deposits of the fluvial Tena formation. Various studies demonstrated that sediments from Tena formation are derived from the Eastern Cordillera of Ecuador (Martin-Gombojav and Winkler, 2008; Ruiz et al., 2004; Ruiz et al., 2007).

In Peru, Paleocene strata are very scarce and are only identified in the eastern border of the Altiplano (Vilquechico Group and Lower Muñani Formation), in the Cusco-Sicuani area (Puquin Formation) or in the present-day foreland basin (Yahuarango or Huayabamba Formations) (Sigé et al., 2004). These strata generally consist of fine-grained “red beds” continental deposits (Jaillard et al., 1993b; Naeser et al., 1991). The Lower Muñani Formation is dated between 55.9 and 53.4 Ma by mammalian biostratigraphy and by magnetostratigraphy (Cande and Kent, 1992; Sigé et al., 2004). The Yahuarango (Huallaga and Marañon basins) and Huayabamba (Madre de Dios and Beni basins) formations are poorly constrained. Only few

charophytes have been documented and provide a Paleocene age (Gutierrez, 1982) for these fluvial deposits (Figure 2).

In Bolivia, Paleocene strata are absent in the Amazonian foreland basin (Roddaz et al., 2010) (Figure 2). Paleocene deposits documented in the Eastern Cordillera of southern Bolivia correspond to the continental Santa Lucia and Cayara formations, Danian and Thanetian in age, respectively (DeCelles and Horton, 2003; Marshall et al., 1997).

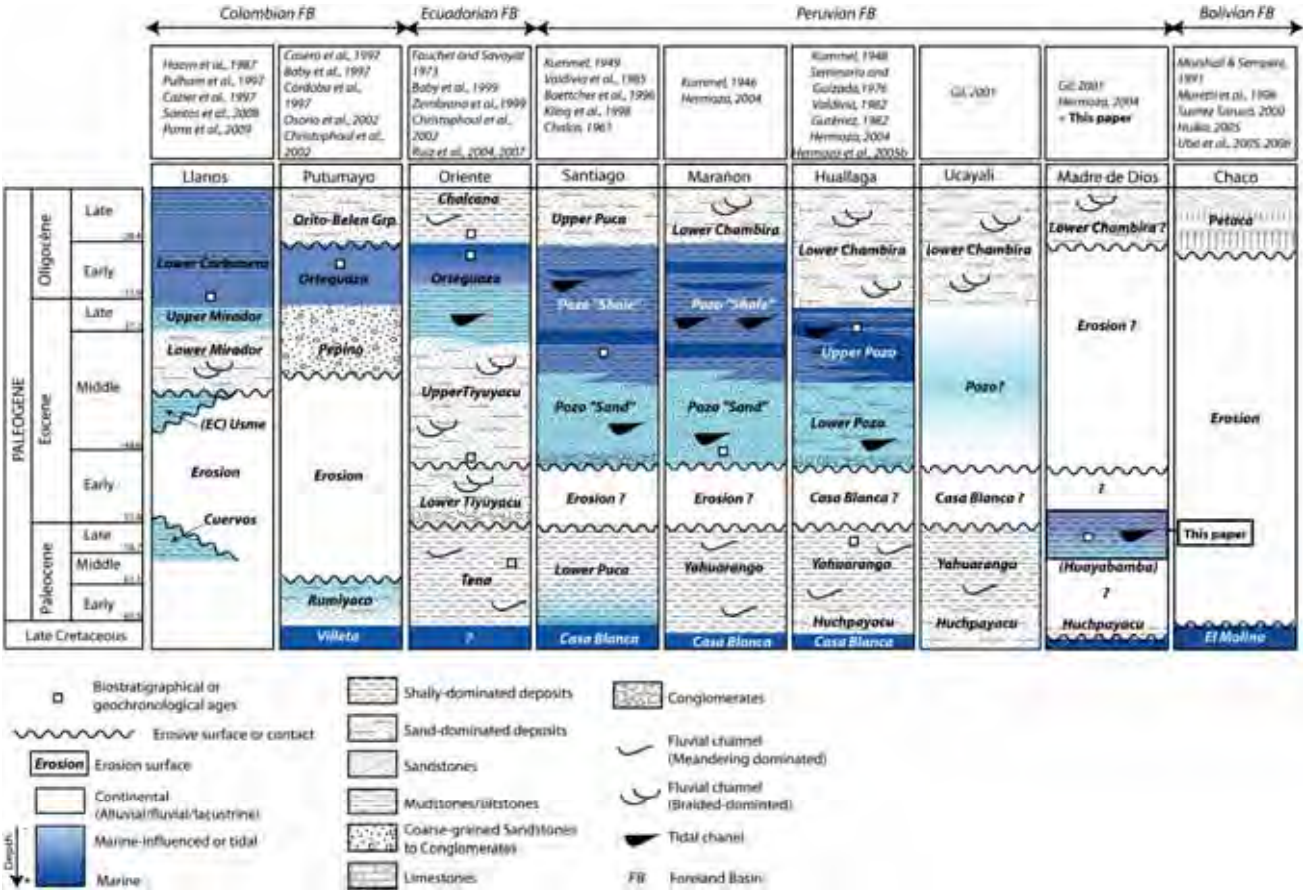

Figure 2: Stratigraphic correlation chart for Paleogene strata between Amazonian foreland basins from Colombia to northern Bolivia. Marine and marine-related deposits are coloured in blue. Important biostratigraphical or geochronological references are displayed by white squares.EC= Eastern Cordillera.

2.2. Stratigraphy and structure of the Madre de Dios basin

The Madre de Dios basin is part of the southern Amazonian foreland basins system (Roddaz et al., 2005). The Madre de Dios foreland basin is located north-eastward to the Eastern Cordillera (EC) of southern Peru and can be subdivided into the Sub-Andean Zone (SAZ) and the Madre de Dios plain tectonomorphic units (Figure 1) (Gil, 2001; Hermoza, 2004). The SAZ is characterized by both sedimentary filling and active deformation. In the SAZ, propagation of deformation towards the Madre de Dios plain is controlled by the development of deep duplexes, whose shortening is accommodated in surface by imbricates and by the Sub-Andean thrust front. The Sub-Andean thrust front corresponds to the eastern border of the SAZ and is responsible for transportation of a piggy-back basin, which outcrops as a large syncline called Salvación

syncline in the study area (Figure 1). The deformed and still active SAZ only corresponds to the internal (western) part of Madre de Dios foreland basin. The external (eastern) part of the basin is situated east to the Sub-Andean thrust front and corresponds to the non-deformed part of the system, the Madre de Dios plain. In this study, we will only focus on outcropping strata from the Salvación syncline, in the SAZ of Madre de Dios basin (Figure 1).

Late Cretaceous to Cenozoic strata in Salvación piggy-back basin consist of ca.4500 m of an alternance of marine, tide-influenced and fluvial deposits (Gil, 2001; Hermoza, 2004). Because of the very scarce outcrops, fauna and palynomorph material available in the studied area, the general chronostratigraphy of this succession is quite difficult to assess and many interrogations subsist for the Cretaceous-Paleogene interval (Gil, 2001; Hermoza, 2004; Roddaz et al., 2010), while Miocene deposits are much better constrained in terms of biochronology and chronostratigraphy (Antoine et al., 2013; Marivaux et al., 2012). Paleogene strata in the Salvación series and more broadly in the Madre de Dos basin are supposed to correspond to the fluvial Huayabamba or “Red beds” formation.

3. Methodology

In the Madre de Dios basin, Paleogene deposits crop out along the Alto Madre de Dios River between the Pongo de Coñeq Canyon and the Pantiacolla anticline, which correspond to the verticalized flanks of the Salvación Syncline (Figure 1-B). This paper focuses on five selected exposures in cutbanks along the Alto Madre de Dios River. The section includes MD-177, MD-85, MD-184, MD-256 and MD-255outcrops (Figure 1-B and 1-C). Their precise locations are given in the online supplementary dataset (Table A). The five concerned localities yield similar faunas (foraminiferans, molluscs, ostracods, chondrichthyan, and actinopterygian fishes) and floras (charophytes), which allows us to consider them as being time equivalent (Table 1). Fifteen sedimentary facies are characterized on the basis of their lithologies, their physical and biogenic sedimentary structures, their palynological and palaeontological content, and their general geometry (Table 2). For limestone layers of MD-184, standard microfacies descriptions have also been realized. Each of these fifteen facies is interpreted in terms of depositional processes and related depositional environment. On the basis of these interpretations and with regards to the geometrical relationships between the facies, three facies associations are proposed (Table 2).

In order to determine the nature of the organic matter (terrestrial versus marine), we analyzed four samples for the total organic carbon (TOC) content and stable carbon isotope ($\delta^{13}C_{TOC}$) at NIOZ, the Netherlands (Table 3). The dried sediment samples were decarbonated with 2 mol L^{-1}HCl (overnight at 50°C). All samples were analyzed with a Flash EA 1112 Elemental Analyzer interfaced with a Thermo Finnigan Delta Plus mass spectrometer. TOC is expressed as the weight percentage of dry sediment (wt. %). Isotope values were calibrated to a benzoic acid standard ($\delta^{13}C_{TOC}$ = -27.8 ‰ with respect to Vienna Pee Dee Belemnite (VPDB) calibrated on NBS-22 and corrected for blank contribution. The $\delta^{13}C_{TOC}$ values are reported in the standard delta notation relative to VPDB standard (‰ VPDB). All the analyses were determined at least in duplicates.

Four selected samples of mudstones from outcrops MD-177, MD-85, MD-184 and MD-255 were measured at the University of Toulouse for their Nd-Sr isotopic compositions, providing sedimentary provenance information (Table 4). Aliquots containing about 1000 mg of Sr and Nd were loaded onto the ion-exchange columns. Sr and Nd were separated using the Sr-SPEC, TRU-SPEC and LN-SPEC resins (Eichrom®). Nd-Sr isotopic ratios were measured using a Finnigan Mat 261 thermal ionization mass spectrom in dynamic mode following Viers et al. (2008). The measured $^{143}Nd/^{144}Nd$ ratios are presented as the fractional deviation in parts per 10^4 (units) from $^{143}Nd/^{144}Nd$ in a Chondritic Uniform Reservoir (CHUR) as measured at the present-day:

$$\varepsilon Nd(0)= [(^{143}Nd/^{144}Nd)_S/I_{CHUR}(0)\_1]*10^4$$

where $(^{143}Nd/^{144}Nd)_S$ is the present-day ratio measured in the sample, and $I_{CHUR}(0)$ is the $^{143}Nd/^{144}Nd$ in the CHUR reference reservoir at the present ($I_{CHUR}(0)$ = 0.512638 (Jacobsen and Wasserburg, 1980).

4. Results

4.1. New Biostratigraphical and paleoenvironmental constraints from fossil assemblage

4.1.1. Biostratigraphy

The dominant taxon among vertebrate remains in the concerned deposits is the batoid *Ouledia* sp. (MD-177; MD-184; MD-85; see Table 1 for biostratigraphical results details), ranging from the Thanetian up to the Priabonian (Cappetta, 2012). In MD-184, *Ouledia* is found in association with a pristid sawfish. This family is restricted to Cenozoic localities at world scale (Cappetta, 2012). This assemblage also includes an unidentified pycnodontiform bony fish (MD-177, MD-184). Pycnodontiforms are well represented in Mesozoic and early Paleogene localities before the group gets extinct during the middle Eocene (Gayet et al., 1993).

Being only recognized at genus, family level, or above, the molluscs found in MD-177, MD-184, and MD-85 are of no use in terms of biostratigraphy. The same occurs for unidentified Charophyta and Ostracoda in MD-177 and MD-184. However, microfossils of high biostratigraphical interest were recovered in MD-255 and MD-85. The agglutinated benthic foraminifer *Karreriella conversa* (Eggerellidae), found in MD-255, has an Upper Cretaceous-Ypresian range (Valchev, 2007). The best constrained locality is MD-85, with a diversified charophyte flora (17 specimens of *Peckichara* cf. *varian smeridionalis*; 10 specimens of *Platycharaperlata*?; 15 specimens of *Feistiella* cf. *gildemeisteri*), the ostracod *Protobuntonia* sp., and benthic foraminifers (*Reophax* sp., *Bathysiphon* sp., and *Rhabdammina* sp.). The charophyte *Peckichara* cf. *varians meridionalis* is restricted to the Thanetian (e.g., (Aubry et al., 2005)), while the ostracod *Protobuntonia* has a Coniacian-Paleocene range. Interestingly, the charophyte *Feistiella* cf. *gildemeisteri* was previously recorded in the Paleocene Yahuarango Formation from Huallaga area, in northern Peru (Hermoza et al., 2005b; Roddaz et al., 2010).

Once combined, all these biostratigraphical data preclude any referral to the Upper Cretaceous or Eocene interval and they further concur to indicate a late Paleocene age (i.e., Thanetian) for the deposits described in the northern part of the Madre de Dios Basin.

Outcrop	Samples	Palynology	Microfossil	Paleontology	*Description*	Age	Depositional Environment (inferred from biostratigraphical material)	Facies Code
MD 177	MD 177 Pal 1 MD 177 Pal 2 MD 177 Bio	X			*Charophyta, oogonia (very few)*	Thanetian (late Palaeocene)	Lagoonal/estuarine/steady bay (confined marine environment). Confined and steady proximal marine environment of normal salinity (still more diverse euhaline ichtyofauna, but no shark), maximal depth: 10m.	C1 and C2
				X	*Mollusca, Gastropoda indet.*			
					Mollusca, Bivalvia indet. (possibly corbiculid clams/marine lucinid clams)			
					Arthropoda, Ostracoda indet.			
					Chondrichthyes, Myliobatiformes, Ouledia sp. 1, dozens of teeth [marine; Thanetian-Priabonian; dominant selachian in MD177]			
					Chondrichthyes, Dasyatoidea, ?Dasyatidae indet. sp. 1 (small) [marine]			
					Chondrichthyes, Dasyatoidea, ?Dasyatidae indet. sp. 2 (large)			
					Osteichthyes, Pycnodontiformes indet. (many teeth) [Last Appearance Datum at family level: early middle Eocene]			
					Osteichthyes, Characiformes indet. (multicuspidate teeth) [freshwater]			
MD 85	MD 85 Pal1 MD 85 Pal 2 MD 85 Bio A MD85 Bio B	X			*Charophyta, Peckichara cf. varians meridionalis, 17 specimens [Palaeocene]*	Thanetian (late Palaeocene)	Distal fluvial/proximal estuarine-deltaic. Strong freshwater influence (fish fauna): the environment is much more proximal than other ones, i.e. distal fluvial. Shallow water (maximal depth: 10m). Potentially reworked elements.	C1 and C2
					Charophyta, Platychara perlata?, 10 specimens			
					Charophyta, Feistiella cf. gildemeisteri, 15 specimens ["Palaeocene" Huayabamba Fm. in northern Peru]			
					Arthropoda, Ostracoda, Podocopida, Protobuntonia sp., 2 specimens [Coniacian-Thanetian]			
			X		*Foraminifera, Reophax sp., 1 specimen [marine]*			
					Foraminifera, Bathysiphon sp., 5 specimens [marine]			
					Foraminifera, Rhabdammina sp., 3 specimens [marine]			
				X	*Mollusca, Gastropoda indet., shell fragments (some reworked)*			
					Chondrichthyes, Myliobatiformes, Ouledia sp. 1 [marine ; Thanetian-Priabonian; one tooth, eroded]			
					Chondrichthyes, Dasyatoidea, Potobatis sp., tooth likely to be reworked [marine ; similar to that from the Santa Lucia Fm., early Palaeocene, Bolivia]			
					Osteichthyes, Characiformes indet. (multicuspidate teeth)			
MD 184	MD 184 Pal 1 MD 184 Pal2 MD 184 Pal 3	X			*Arthropoda, Ostracoda indet.*	Thanetian (late Palaeocene)	lagoonal/estuarine/steady bay (confined marine environment). Confined and steady proximal marine environment of normal salinity (still more diverse euhaline ichtyofauna, but no shark), maximal depth: 10m.	C1, C2 and C3
				X	*Mollusca, Bivalvia, Corbicula s. l. indet.?*			
					Mollusca, Gastropoda, Cerithioidea indet.			
					Mollusca, Gastropoda, Pachychilidae indet.			
					Mollusca, Gastropoda, ?Aylacostoma indet.			
					Mollusca, Bivalvia, ?Polymesoda/Rangia			
					Chondrichthyes, Pristiformes, Pristidae indet. [marine; Cenozoic]			
					Chondrichthyes, Myliobatiformes, Ouledia sp. 1 [marine; Thanetian-Priabonian; dominant selachian in MD184]			
					Chondrichthyes, Rajiformes, Dasyatoidea indet. [marine or freshwater]			
					Osteichthyes, Pycnodontiformes indet. (many teeth) [Last Appearance Datum at family level: early middle Eocene]			
					Osteichthyes, Characiformes, Serrasalminae indet. (multicuspidate teeth)			
					Osteichthyes, Characiformes indet. (multicuspidate teeth)			
MD 255	MD 255 Bio	0	X		*Benthic foraminifera, Eggerellidae, Karreriella conversa (agglutinated) (6) E14 [marine]*	Upper Cretaceous-Ypresian	shallow marine platform, with unstable environmental conditions (continental influx)	A4
MD 256	MD 256 Bio A MD 256 Bio B		0	X	*Benthic Foraminifera (reworked)*		Marine ?	B1

Table 1: Biostratigraphical results related to Paleocene deposits of the northern Madre de Dios basin.

4.1.2.Paleoenvironments

Thus far, Upper Cretaceous and Paleocene selachian faunas from Andean and sub-Andean basins consist only of batoids (i.e. no shark is recorded), further known to be highly endemic (Cappetta and Gayet, 2013; Gayet et al., 1993). Together with the complete absence of associated sharks, the co-occurrence of *Ouledia* (MD-177; MD-184; MD-85), *Potobatis* (MD-85), two unidentified dasyatoids (MD-177), and a pristid (MD-184) point to shallow waters in a proximal marine or estuarine environment for the Thanetian deposits described in this study (Cappetta, 2012; Cappetta and Gayet, 2013). The ichthyofauna also includes a high number of pycnodontiform bony fish remains (Gyrodontidae indet.; MD-177; MD-184; MD-85, see Table 1),

some of them being found in partial anatomical connection (i.e., no transport). This extinct group is only recorded in marine deposits (shallow water seas; (Gayet et al., 1993)). However, a freshwater influence is supported by the presence of numerous isolated teeth of characiform bony fishes (MD-177; MD-184; MD-85). Today, characiforms are strictly restricted to freshwaters (Aubry et al., 2005). Serrasalmine characiform teeth with a plesiomorphic pattern (*Colossoma*-like) were in particular recognized in MD-184.

The agglutinated foraminifer assemblage, including *Karreriella conversa* (MD-255), *Reophax*, *Bathysiphon*, and *Rhabdammina* (MD-85), points to a shallow marine inner platform, under unstable environmental conditions, with frequent detrital/terrigenous influxes. Such a continental influence is further attested by the presence of numerous charophyte oogonia (likely to be transported during river flooding episodes) and riverine to brackish molluscs (e.g., *Corbicula* and *Aylacostoma*). No open sea indicator, such as dinoflagellates or planctonic foraminifers, has been recorded throughout the sections.

To sum up, the macro- and microfossil assemblages (vertebrates, molluscs, ostracods, foraminifers, and charophytes) as documented in MD-177, MD-184, MD-255, and MD-85 (Table 1) give us an initial idea of the depositional environment: a shallow marine inner platform, under unstable environmental conditions, with frequent detrital/terrigenous influxes from a river estuary or delta.

4.2. Depositional environments from sedimentary analysis

In this section, the facies associations are described and interpreted. Diagnostic criteria of the facies are summarized in Table 2.

Outcrops	FA	Code	Facies description	Thickness	Physical Sedimentary strucutres	Bioturbation	Observations	Microfacies and Biostratigraphy	Depositional Environment	
MD 255	Facies Association A	A1	Tangential cross-bedded fine- to medium-grained sandstone	20 cm to 120 cm	Massive/Large scale cross-bedding with reactivation surfaces in rhythmic bundles/Ripples/Planar lamination. Lag deposit possible at the base with millimetric to centimetric mud clasts. Millimetric mud drapes.	*Arenicoltes, Dactiloides* (?) at the top	Occasional bidirectionality + Rhythmicity		Compound dune/ Tidal dune of Channel infill	Fluvio-tidal transition
MD 255		A2	Oblique Hetrolithic strata with climbing rippled cross-stratification	1 to 1,20 m	Flaser-bedding with asymmetrical ripples+mud drapes/wavy or plana bedding . Coarsening-up patterns.	Higly Bioturbated	Current direction orthogonal to dipping + Rhythmicity		Lower part of tidal influenced point bar (IHS)	
MD 255		A3	Oblique Hetrolithic strata with tangential cross-bedding	>60 cm	Sandy beds (20-40 cm-thick) with tangential cross-bedding and planar lamination at the base+mud drapes/ muddy to silty beds (2 to 5 cm)	Bioturbated	Current direction orthogonal to dipping + Rhythmicity+ Bidir.		Upper part of tidal influenced point bar (IHS)	
MD 255		A4	Mudstone to siltstone, occasional rippled fine-grained sandstone	2m, sandy layers: 10 cm	Planar stratification, ripples and climbing ripples in the silty and sandy layers	Roots traces at the top. Bioturbated		Marine+terrestrial (Table 2)	Channel abandonment + Floodplain (crevasse splay)	
MD 256/MD 85b	Facies Association B	B1	Fine- to medium-grained sandstone	1 to 1,50 m	Massive, lag deposits possible at the base, sigmoid bedding (heights of set: 45 cm). Climbing Ripples, Trough cross-bedding at the top. FU general setting			Marine (Table 2)	Inlet tidal channel fill / Estuarine tidal bar	Tide-dominated environment
MD 256		B2	Red mudstone	20 m	Gypsum nodules at the top	Bioturbated, roots traces			Supratidal saltmarshes	
MD 256		B3	Siltstone & mudstone	0,50 to 4 m	Scattered lenticular bedding (with carbonaceous sand) or centimetric fine-grained sandstone.	Bioturbated		Marine (Table 2)	Intertidal Mud flats	
MD 256		B4	Highly burrowed sandstone/siltstone & heterolithic sandstone	1 to 5m	Mud drapes,wavy and lenticular bedding. Fluid escape structures	Higly Bioturbated	Ocasional bidirectionality		Intertidal to subtidal mixed to sandy flats	
MD 256		B5	Rippled fine-grained sandstone	20 to 30 cm	Ripples				Top of sand flats (subtidal?)	
MD 184/ MD 85/md 177	Facies association C	C1	Violet-reddish carbonaceous mudstone to siltstone with centimetric fine-grained sandy layers + thin carbonaceous layers	50 cm to >2 m	Ripples andclimbing ripples within sandy layers			Marine (Table 2)	Confined marine environment with some flood events	Bay/ Shallow marine
MD 184/ MD 85/md 177		C2	Bioturbated Facies C1	80 cm to 1 m	Common sandy/carbonaceous nodules, possible gypsium nodules,	Root traces, Bioturbation			Paleosoil developed on emerged shallow marine deposits (C1)	
MD 184		C3	Sand nodules breccia with muddy to silty matrix	15 to 50 cm	Sand nodules in a muddy matrix			(Table 2)	Episodic channel flow	
MD 184/MD 85		C4	Alternation of marl/Limestone	10 to 25 cm	Dessiccation cracks at the top. Frequent carbonate nodules	Root traces at the top, burrows		Shallow marine: Oysters, fish vertebrae, annelids, ostracods, gasteropods.	Confined intertidal to palustre environment	
MD 184		C5	Stromatholitic Limestone	25 to 80 cm	dessiccation cracks at the top			Shallow marine: Stromatholith, annelids, ostracods	Confined and stressed marine environment, Intertidal	
MD 184		C6	*Ostrea* Limestone	10 to 25 cm	dessiccation cracks at the top	Root traces at the top, burrows		Shallow marine: Blue algae, Fish coprolith, ostracods,oysters	Confined marine environment, intertidal / infralitoral sup	

Table 2: Descriptions and interpretations of sedimentary facies used in this study. FA= Facies Association.

4.2.1.Facies association A: the Fluvial-tidal transition zone

Description:

Facies association A is made up of four facies: A1, A2, A3, and A4. These four facies have only been described at the location of outcrop MD-255 (Figure 1-C). Outcrop MD-255 displays two channel-shape stacked bodies showing concave-up basal surfaces. The lateral extension of these sedimentary bodies is close to 150 m long and their thickness reach 4 to 5 m (Figure 3A and 3-B). Facies A1, A2 and A3 have been recognized within the channelized bodies, whereas facies A4 has been observed above and laterally to the channels (Figure 3-C).

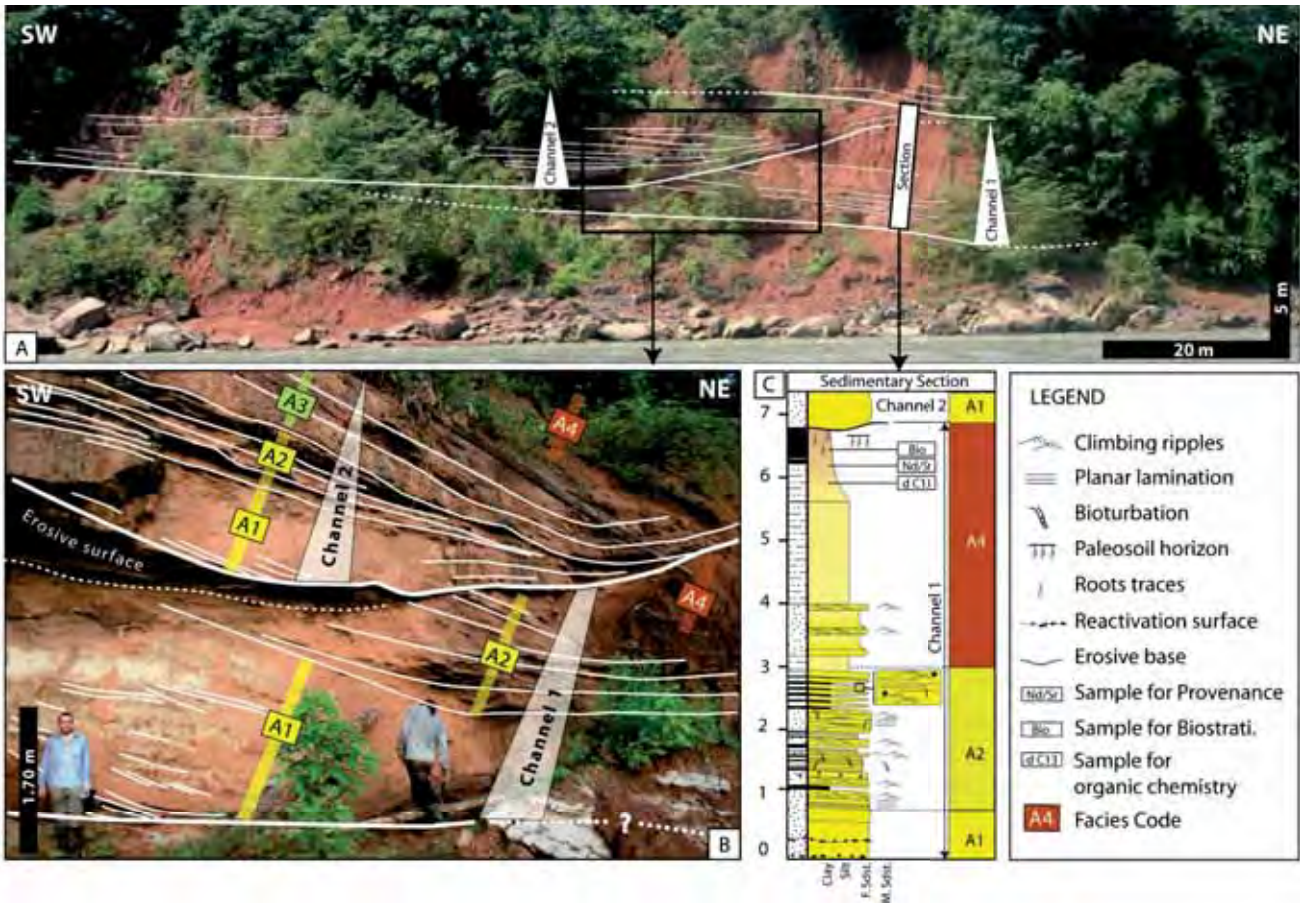

Figure 3: Outcrop MD-255. A) General outcrop view along the river cutbank. B) Zoom from A. Interpreted photograph of two stacked channels. C/Sedimentary section with Facies code (see Table 2 for details).

Facies A1 (total thickness of 20- to 120 cm) has been observed at the base of the channel-shape bodies. It generally starts with anaccumulation of millimetric to centimetric mud clasts scattered in fine- to medium-grained sandstone, forming a few cm-thick micro-conglomeratic matrix-supported mud breccias, erosive at its base. Mud clasts disappear upwards and the facies evolves into fine- to medium-grained sandstones. These sandstones are massive or are organized into tangential cross-bedding forming 30 cm- thick tangential co-sets (Figure 4-A). Some reactivation surfaces can be observed. Both tangential sets and co-sets can be highlighted by thin mud drapes and generally present the same dip direction. However, some tangential cross-bedding can dip in the opposite direction. Facies A1 ends with an undulate rippled surface with heights

of 1–2.5 cm and wavelengths of 15–20 cm, showing ichnofabrics *Arenicolites* and possible *Dactiloides* (Figure 4-B and 4-C).Facies A1 corresponds to the coarsest deposits described in the area.

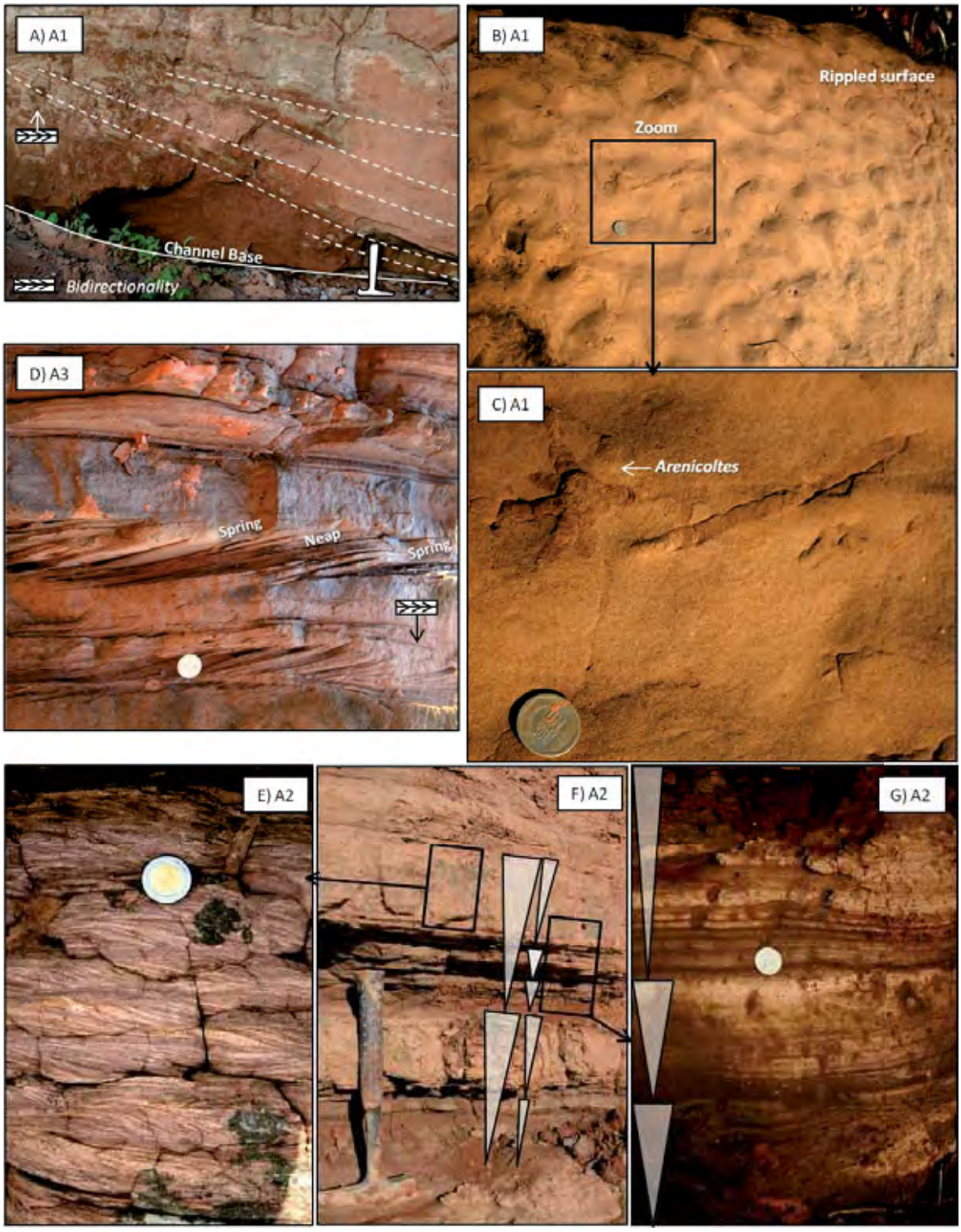

Figure 4: Facies Photographs for Facies Association A (FA-A). A) Facies A1, showing fine-grained sandstone with tangential cross-bedding and sets prograding in the same direction. Note that bidirectionality has been observed in this facies. B) Photograph of the rippled-surface of Facies A1. Square indicates the location of photograph C. C) Ichnofabrics from Facies A1 top surface: Arenicolite sand possible Dactiloides (tubular trace). D) Facies A3.Tangential cross-bedding with planar laminations at their base. Rare asymmetrical ripples in the opposite direction can also be observed at the top of the tangential laminations, suggesting bidirectionality. Regular changes in thickness suggest cyclycity, possibly Neap and Spring cycles (?). E) Photograph of climbing-rippled cross-stratification of Facies A2, from the zoom section displayed on F). F) View of the heterolithic and cyclic deposits of Facies A2. Black squares indicate the location of photographs E) and G). G) Photograph of Facies A2, with massive fine-grained sandstones or flaser bedding alternating with wavy- or planar muddy lamination.

Facies A2 (total thickness of 1 to 1.20 m) consists of slightly oblique heterolithic strata (Figure 4-F) overlying Facies A1 after a sharp transition (Figure 3-B). Massive fine-grained sandstones or flaser bedding with asymmetrical climbing ripples highlighted by frequent mud drapes (15 to30 cm-thick) (Figure 4-E) alternates with wavy bedding or planar muddy lamination in fine-grained sandstones (10 to 20 cm) (Figure 4-G). The distribution of the thin planar mud drapes observed within the fine-grained sandstones of the wavy bedding often displays a rhythmic pattern, with intervals of inframillimetric sandstone beds evolving gradually to millimetric and then centimetric thicker sandy beds suggesting coarsening-up cycles (Figure 4-G and 4-F). Mud accumulation can be 1 mm- to 1 cm-thick. Horizontal and to a lesser extent vertical undetermined burrows are occasionally present.

Facies A3 also corresponds to slightly oblique heterolitic strata (total thickness > 60 cm). In comparison with Facies A2, Facies A3 is coarser as it is made up of thicker sandy beds (20 to 40 cm-thick) intercalated with thin muddy to silty beds (2 to 5 cm thick). Fine-grained sandstones present tangential cross-bedding with planar laminations at their base representing their bottomset (Figure 4-D). Rare asymmetrical ripples in the opposite direction can also be observed at the top of the tangential laminations. These sansdstones are also heterolithic as almost all the sandy tangential and planar laminae are highlited by thin mud drapes. Regular chanching thicknesses of millimetric to centimetric sandy layers and inframillimetric to millimetric muddy layers suggests a rhythmic pattern (Figure 4-D). Facies A1 and A3 are both made up of tangential cross-bedding in fine-grained sandstones, but differences with Facies A1 result in: i) the scale of the structures (Facies A1 is made up of larger-scale cross-bedding compared to Facies A3), ii) the general geometry of the bodies (Facies A1 corresponds to the laterally filling of a channelized body whereas Facies A2 corresponds to more tabular deposits) and 3) the texture and internal organization of the sediments (more finer texture and more heterolithic and rhythmic patterns for Facies A1).
Strata from both facies A2 and A3 present an oblique pattern, prograding from the south-eastern channel margin towards the north-western margin of the channel (Figure 3-A and 3-B).

Facies A4 corresponds to siltstone layers (2 m thick) intercalated with fine-grained sandstone layers (10 cm thick). These sandstones present a sharp contact with the underlying siltstones and show climbing-ripples structures. Siltstones evolve upwards into mudstones (>2m thick), where root traces develop at the top of the section. Rare benthic foraminifera *Karreriella conversa* can be preserved in this facies.

Interpretation:

Stacked channels geometries as observed at MD-255 are common in fluvial and tidal settings. In both cases channels are erosive at their base and can be composed of fining- and thinning-up strata evolving gradually upwards into shaly strata. These shales can correspond to either fluvial floodplain or tidal flat deposits depending on the depositional environment.
The massive or cross-bedded fine- to medium-grained sandstones with basal mud clasts above erosive surfaces (Facies A1) could represent purely fluvial channel filling with bottom reworking lag deposits (Facies

Gt and Gh from Miall (1996)). However the presence of ichnofabric *Arenicolites* (and possible *Dactiloides*?) observed at the top of this facies (Figure 4-C) and the presence of benthic foraminifera *Karriella conversa* (Facies A4) suggest deposition in, respectively, tide-influenced environment (deltaic or estuarine) and deposition in shallow marine platform with continental influx (see Table 1). Facies Association A is therefore related to both tidal and fluvial environments.

Reactivation surfaces as observed within the cross-bedded sandstones of facies A1 can be caused by tidal current reversals (de Mowbray and Visser, 1984; Klein, 1970) even if these surfaces could also be produced by river-discharge variations and erosion of brink by arrival of a new bedform in fluvial settings (Dalrymple, 1984). The occurrence of rare bidirectional trough cross-bedding (Figure 4-A) suggests a depositional area receiving opposite-direction currents, dominated either by flood or ebb currents. The prograding pattern displayed by the tangential cross-bedded sandstones suggests lateral accretion processes. Mud clasts have been deposited at the base of the channels by gravity processes. They are common in channel bottom deposits in many tide-dominated or influenced environments because of the re-erosion by high-energy currents of thin muddy layers forming slack water drapes, or because of theerosion by lateral accretion of muddy tidal-flat and salt-marsh deposits (Dalrymple and Choi, 2007). In conclusion, we interpret Facies A1 as dune deposits formed during the early-stage of a tide-influenced channel settlement controlled by both fluvial and tidal processes.

Facies A2 and A3 overly the basal filling of the channelized bodies and constitute small-scale Inclined Heterolithic Stratification (IHS). These IHS developed by lateral accretion within the channels (Figure 3-A and 3-B). Although IHS may be observed in fluvial environments (Jackson, 1981; Page et al., 2003), they are most common in tide-influenced settings (Dalrymple et al., 2003; Gingras et al., 1999; Gingras et al., 2002; Martinius et al., 2001; Shanley et al., 1992; Shanmugam et al., 2000; Thomas et al., 1987). In addition, Facies A2 and A3 often display rhythmic patterns and heterolithic textures. Interlamination of mud and fine-grained sands results from suspension and weak traction current and may occur in fluvial overbank deposits (Lithofacies Fl, (Miall, 1996)). However, alternation of sand and mud laminae within millimetric wavy and flaser beddings (Facies A2 and A3) is more frequent in tidal depositional environment. Concerning Facies A2 and A3, the abundance of wavy and flaser bedding, mud drapes and rhytmicity rather suggests tidal influence on deposition (Nio and Yang, 1991). Recurrent thickness fluctuations observed within the cross-bedded sandstones in the successive sandy beds of Facies A3 (Figure 4-D) may be interpreted as the result of neap-spring influence (Eriksson and Simpson, 2004; Eriksson et al., 1998; Mazumder and Arima, 2005). Similar rhythmicity has also been found within facies A2 (Figure 4-F and 4-G). The presence of few thin mud drapes observed within these sandstones may therefore represent deposition during tidal slack-water periods. Facies A2 corresponds to lower hydrodynamic conditions than Facies A3 (coarser sandstones). However, they both constitute IHS, and are interpreted to have been deposited by lateral accretion in a channelized body. Therefore, facies A2 and A3 are both interpreted as tide-influenced point-bar deposits in a meandering channel. Because Facies A3 is situated above Facies A2 (Figure 3), Facies A3 should be related to a higher energy recovery during the channel deposition history.

Facies A4 corresponds to the uppermost- and finest strata deposited at the top of the channels succession. This silty facies could firstly be interpreted as channel abandonment, fluvial floodplain or tidal-flat deposits. The presence of *Karreriella conversa* indicates deposition in a coastal, brackish water environment (Valchev, 2007) and supports a tidal flat interpretation for facies A4. According to Dalrymple and Choi (2007), the pedogenic structures described in the mudstones at the top of facies A4 could be associated to a period of emersion of a tidal mud flat (Dalrymple and Choi, 2007).

To conclude, Facies association A corresponds to a moderate-energy channel filling history. According to the IHS geometry resulting from lateral accretion processes, this channel is interpreted to be related to a meandering system. Because of the proximity of pedogenetic features and because of the preponderance of fine-grained texture in the facies association, this meandering system could be purely fluvial. However, the evidences of tidal- or marine-related environment (benthic foraminifera, *Arenicolites*) and the evidences of tidal-processes (rhythmic patterns, HIS, mud drapes) finally suggest a mixed fluvial-tidal environment. Facies association A corresponds to the sedimentary infilling and abandonment of tide-influenced meandering channels migrating laterally in surrounding tidal-flats and floodplain.

4.2.2.Facies association B: Tide-dominated environment

Facies association B consists of 5 facies: B1, B2, B3, B4 and B5. They all have been found in MD-256 (Figure 5) and partially in MD-85 (Figure 7) and are summarized in Table 2.

Facies B1 corresponds to the infill of isolated channelized sedimentary bodies (~60- to 150-m width and ~1- to 1.50 m in thickness) and has been observed at both MD-256 and MD-85 localities. No stacking or amalgamated pattern has been noticed. The base of this facies corresponds to a channel-shaped surface. This surface is highlighted by elongated millimetric to centimetric mudclasts forming a breccia of few centimetres-thick and evolving upwards into massive medium- to fine- or very fine-grained sandstone. Internal sigmoid cross-beddings (45cm in height) are often present in the basal part of these sandstones. Fine-grained sandstones may also display high-angle climbing ripples at their base evolving upwards into low-angle climbing ripples (Figure 6-A). At the top of the deposits, climbing ripples cross-stratification changes upward into more flattened trough cross-stratification (see channel sedimentary structures within the channel of outcrop MD-85, Figure 7). Reworked charophyte oogonia, stingray teeth (MD-85), and benthic foraminifera (MD-256) are observed in this facies (Table 2).

Facies B2 (total thickness of ~20 m) consists of reddish mudstones. Root traces and gypsum or anhydrite nodules can develop at the top of the facies (Figure 6-B). This facies has been observed at the top of the sedimentary section and presents a sharp contact with the underlying Facies B3 (Figure 5). It is also laterally associated with Facies B1.

Facies B3 and B4 are closely related and often alternate in the section described (Figure 5). In this case, the contact between the two facies is sharp or progressive.

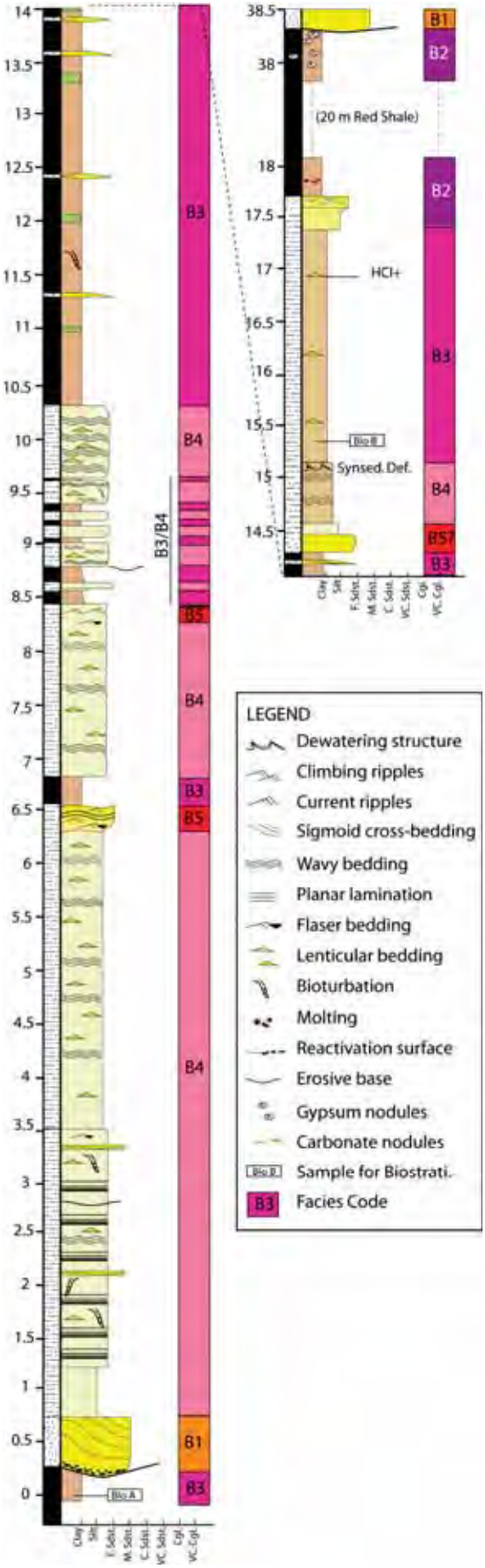

Facies B3 (total thickness of 0.50 to 4m) consists of bioturbated and burrowed reddish mudstones to rare siltstones. Occasional lenticular bedding can occur within the mudstones.

Facies B4 (total thickness of 1 to 5m) corresponds to highly burrowed heterolithic deposits showing regular alternations of very fine to fine-grained sandstones with muddy or silty layers displaying planar horizontal, wavy bedding and lenticular bedding (sets of 10 cm thick) (Figure 6-C, 6-D and 6-E). Burrows are horizontal or vertical but no specific ichnofabric can be determined (Figure 6-4D). Colour is dark grey to violet. The sedimentary structures in sandstones are highlighted by thin (2-3 mm thick) laminae of mud and silty drapes. Thin sand layers can occasionally be intercalated by mud drapes, thus forming mud couplets. Opposite current dips have been observed in this facies. At the top of sandy strata, fluid escape structures can be observed (Figure 6-E).

Facies B5 (total thickness of ~20 cm) is generally observed above facies B4, after a sharp or progressive contact (Figure 5). It is made up of clean fine-grained sandstone often ending with a wave-rippled surface (ripples are 1 to 1.5 cm in height with wavelength of 6.5 to 8.5 cm) (Figure 6-F).

Figure 5: Sedimentary section from outcrop MD-256.

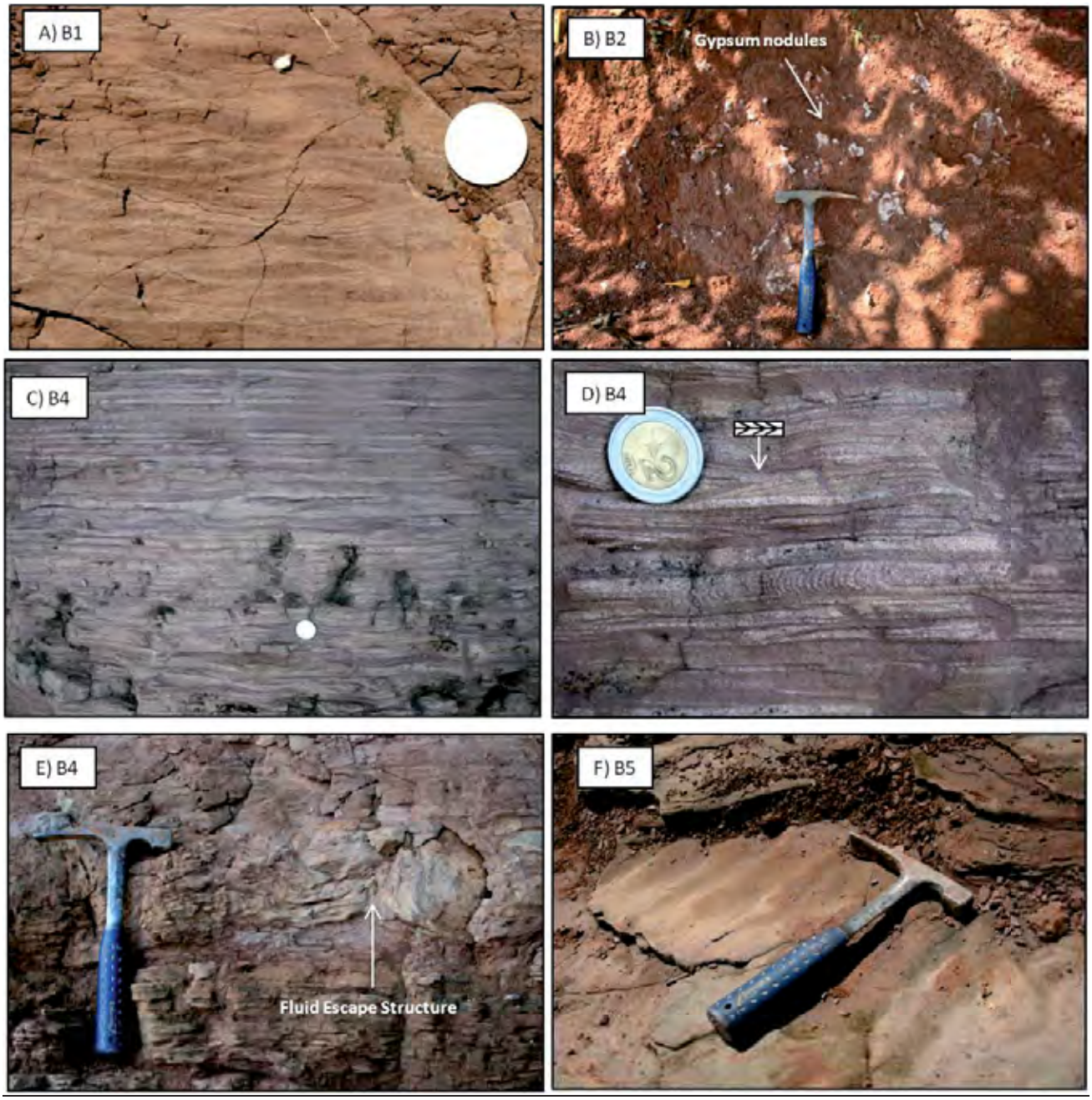

Figure 6: Facies photographs of Facies Association B (FA-B). A) Fine-grained sandstone with climbing ripples. B) Root traces and gypsum or anhydrite nodules developing at the top of the reddish mudstones of Facies B2.C) Facies B4.Highly burrowed heterolithic deposits showing regular alternations of very fine to fine-grained sandstones with muddy or silty layers displaying planar horizontal and wavy bedding. D) Horizontal and vertical burrows in Facies B4. E) Fluid-escape structure within deposits of Facies B4. F) Facies B5 with rippled-surface.

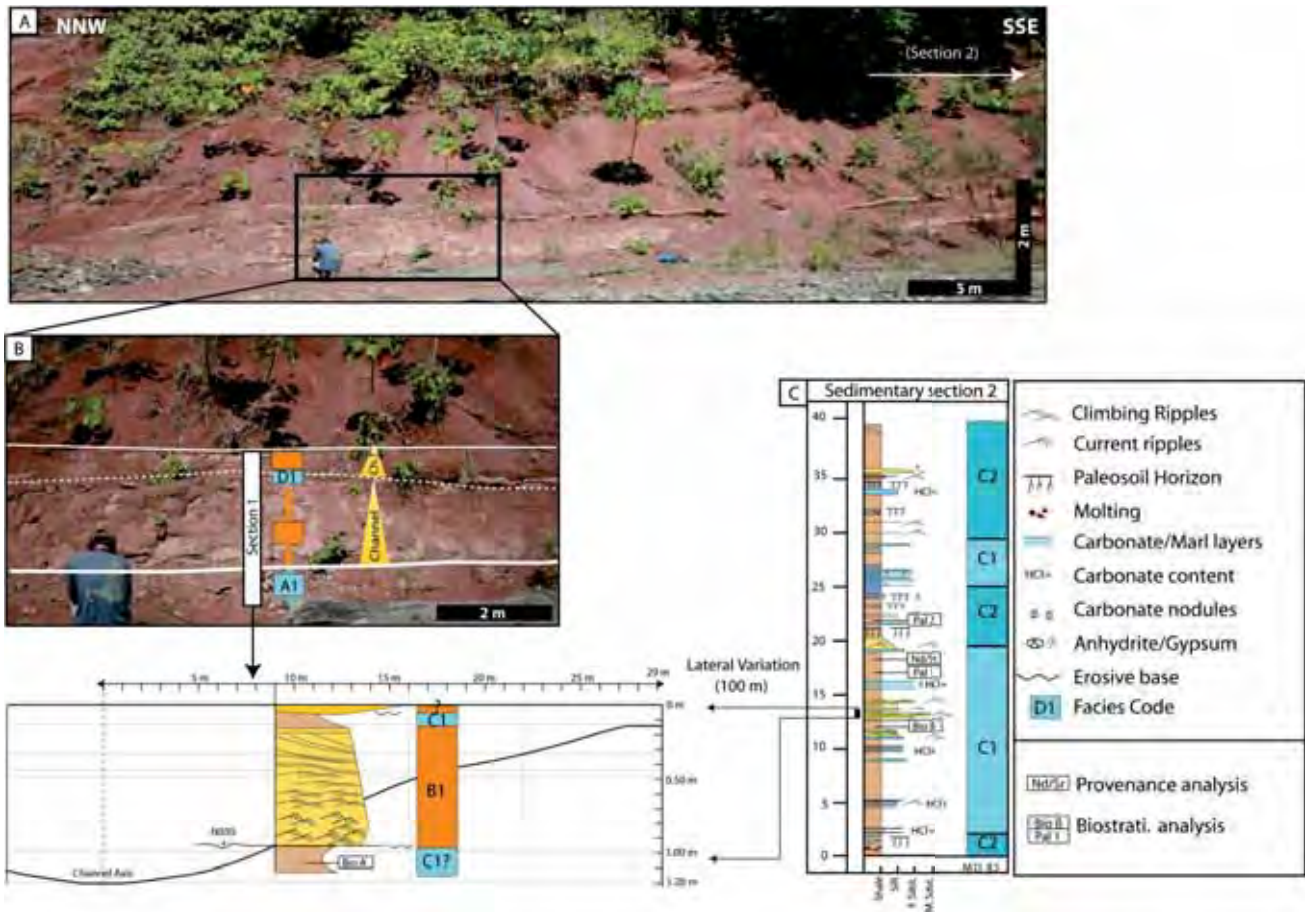

Figure 7: Outcrop MD-85 near Pantiacolla antincline. A) General view of the outcrop. Black rectangle precise the location of photograph B. B) Enlarged view from A with the location of the sedimentary section 1 described. C) Sedimentary section 2 and Facies code. Note that 100 m separates the two sedimentary sections.
Figure 8: Sedimentary sections from outcrop MD-177 (Sedimentary section 1) and MD-184 (Sedimentary section 2).

Interpretation:

Facies B1 corresponds to channel infill deposits. Climbing-ripple cross-stratification is a common feature in a wide range of depositional environments in which suspension exceeds the rate of traction transport (Allen, 1970; Ashley et al., 1982; Jopling and Walker, 1968). However, sigmoidal cross-bedding associated with the presence of brackish-water fossils (benthic foraminifera, see Table 1) suggests deposition within a tide-influenced environment. Climbing ripples from tidal environments are different from non-tidal climbing ripples by having common mud drapes and finer-grained texture (Choi, 2010). In a tidal environment, they can be characteristic of tidal inlet infillings in the fluvial-tidal transition zone of estuaries (Dalrymple et al., 1992; Hovikoski et al., 2008; Tessier, 1996). Flood dominated Climbing Ripples Facies (CRF) can also be associated with tidal channel levees found in the inner/straight channel zone of the fluvial-estuarine transition (cf. Mont St Michel estuary (Tessier, 1996)). In case of ebb-dominated context, CRF are found in chute channels and chute bars in the meandering zone of the fluvial-estuarine transition (Tessier, 1996). In comparison with Facies A1, Facies B1 is finer-grained and is related to decreasing flow processes (climbing ripples). Geometrically, Facies B1 only concerns isolated channels whereas Facies A1 is related to stacked and thick channels overlain by laterally migrating strata (IHS deposits; Facies A2 and A3, Figure 3). Channels from Association A represent higher energy channels in comparison with those from Facies Association B

(Facies B1). We interpret Facies B1 as tidal inlet deposits. Facies B2 is generally structureless but contains paleosoil horizons and gypsum nodules in a very fine shaly matrix. As it is laterally associated with facies B1, it has been interpreted as salt marshes in a supratidal environment. Facies B3, characterized by muddy deposits with scarce lenticular bedding, could correspond to mud flat deposits in an intertidal environment. Facies B4 is characterized by highly burrowed heterolithic deposits with double mud drapes, wavy and lenticular beddings that are typical sedimentary structures of tide-influenced environments (Dalrymple and Choi, 2007; Dalrymple et al., 1992; Nio and Yang, 1991). We consequently interpret facies B4 as mixed muddy/sandy flat deposits.

To conclude, Facies association B is constituted by all the surrounding "flats" influenced by tidal processes, from the subtidal area (tidal inlet -Facies B1), mixed tidal flats with double mud drapes (Facies B4 and B5) to the intertidal/surpatidal environments (mud flats and saltmarshes, respectively Facies B2 and B3).

4.2.3.Facies association C: Bay and shallow marine environments

Facies association C is composed of six facies: C1, C2, C3, C4, C5 and C6. All the facies have sheet-like geometries, and have been described at outcrops MD-85 (Figure 7), MD-177 and MD-184 (Figure 8, respectively section 1 and 2).

Facies C1 (total thickness of 50 cm to >2 m) corresponds to blue-violet-reddish marls to carbonated siltstones with centimetric thick fine-grained sandy layers and occasional centimetric thick carbonaceous layers (¡¡Figure 9-A). Ripples and climbing ripples are present within the sandy layers. Facies C1 contains benthic foraminifera (*Bathysiphon,* Figure 9-B), Mollusca (Bivalvia: Corbicula and Polymesoda; Gastropoda: Cerithioidea, Pachychilidae, and? *Aylacostoma*), Ostracoda, Chondrichthyes (Myliobatiformes: *Ouledia* sp., Pristidae, and Dasyatoidea), Osteichthyes (Pycnodontiformes: *Coelodus*; Characiformes: Serrasalminae and indet.) (see Table 1).

Facies C2 (total of thickness 80 cm to 1 m) is always closely related to facies C1 and the contact (basal and top) between the two facies is progressive. Facies C2 is similar to facies C1 but contains common sandy and gypsum nodules, root traces and bioturbation.

Facies C3 (total thickness of 15 to 50 cm) corresponds to millimetric to centimetric sandy nodules scattered into a violet muddy to silty matrix, forming a matrix-supported breccias. This facies contains numerous organic fragments such as fish vertebrae and ostracods.

Facies C4 corresponds to an alternation of marl (5 to 10 cm) and thin limestone strata (2 to 5 cm). Carbonate nodules are frequent within the marls. Limestones often present well-developed desiccation crack surfaces at the top of the strata as well as burrows and root traces. Little oyster shells (2 to 4 cm in length) are visible within the limestone strata. Microfacies analysis of thin sections allowed the recognition of oysters (little size species), fish vertebrae fragments, annelid burrows, numerous ostracods and/or phylopods, and

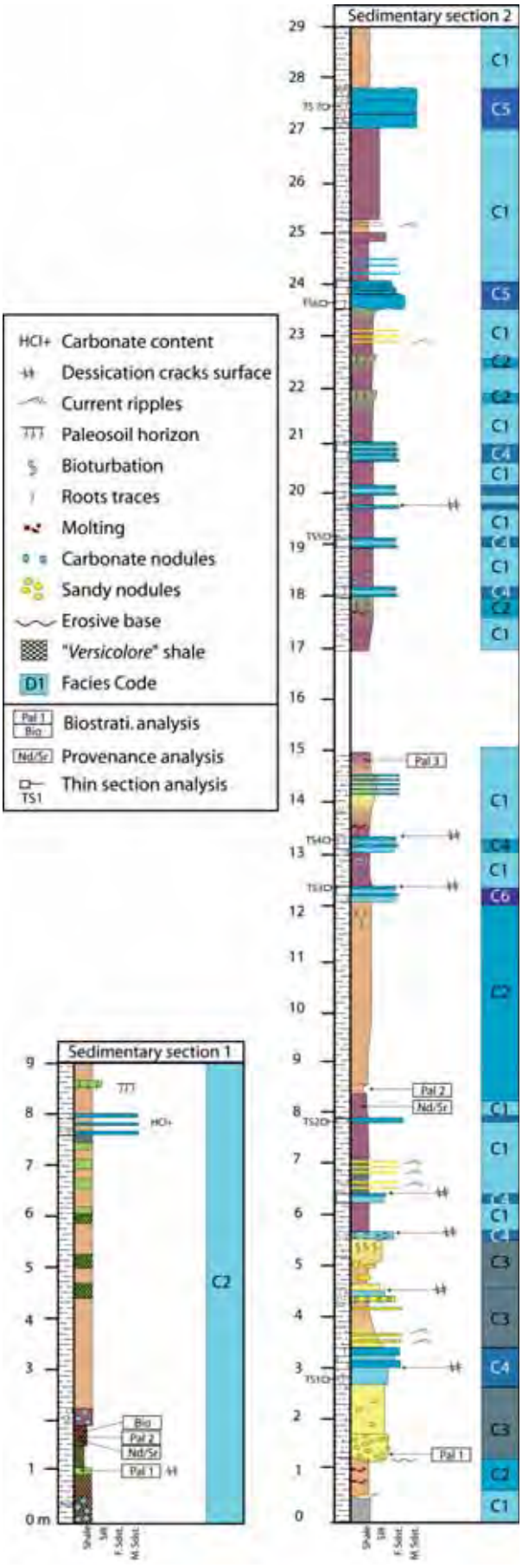

undifferentiated gastropods (Figure 10-A, 10-B, 10-C and 10-D). Only very few ostracods and phylopods present a complete carapace with paired valves but they all present a smooth surface. According to Dunham's classification (Dunham, 1962), the observed limestones can be classified as wackstone to packstone. The matrix is generally micritic or microsparitic. Peloidal micrite (Figure 10-A and 10-B) could constitute secondary cementation better than primary matrix. Secondary sparite grains are common, and can form drusic or bird-eyes cements (Figure 10-b and 10-D).

Facies C5 (strata presenting thickness of 25 to 80cm) also corresponds to limestone deposits showing desiccation cracks at the top (Figure 9-C and 9-D). These strata present undulated base and top. Thin-section shows stromatolith filaments entangled with ostracod carapaces and annelid burrows (Figure 10-E and 10-F). The matrix is micritic to microsparitic.

Facies C6 correspond to limestone strata (10 to 25cm thick) with abundant small-size oysters (2 to 4 cm in length). Thin-section reveals numerous oysters with lamellar and multilayered structures, annelids burrows, blue (?) algae filaments, fish coprolith and some ostracodes Figure 10-G, 10-H, 10-I and 10-J). Root traces are also present. The matrix is made up of micrite or small microsparite crystals. Some bivalve's shells are rounded by a micrite envelope (Figure 10-G). This facies is separated from the other because of its greatest oysters content.

Figure 8: Sedimentary sections from outcrop MD-177 (Sedimentary section 1) and MD-184 (Sedimentary section 2).

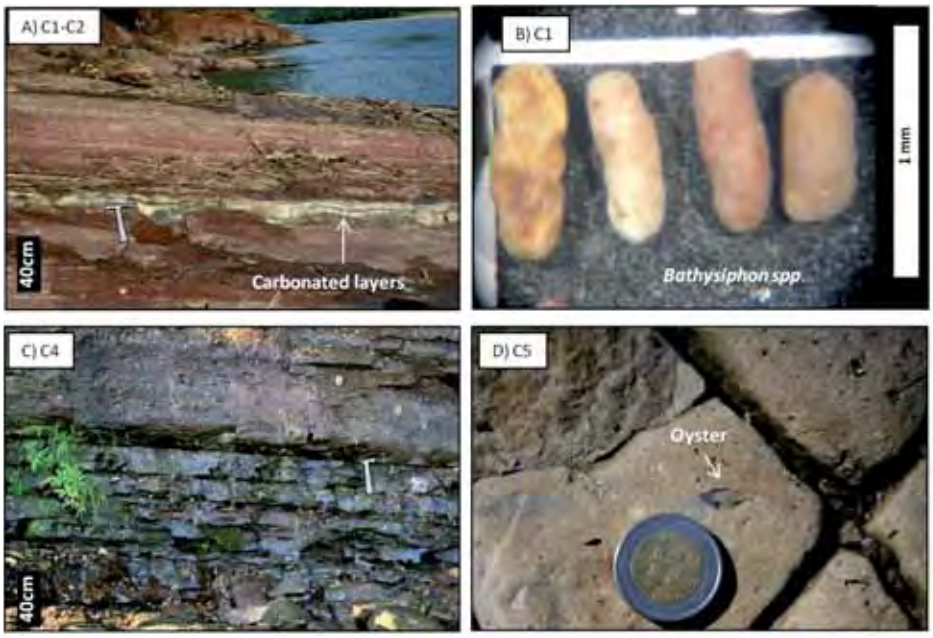

Figure 9: Photographs from outcrop MD-184. A) Outcrop view of alternating Facies C1 and C2. Note undulated marls/carbonated layers. B) Benthic foraminifera Bathysiphon sp. found in facies C1. C) Outcrop view of carbonated layers from Facies C4. D) Desiccation cracks at the top of a carbonated layer in Facies C5. Note little-sized oyster visible on that surface.

Interpretation:

Ichtyofauna from Facies C1 and C3 are characteristic of a shallow marine environment, with variations from a strong freshwater influence in a more proximal environment to a confined and steady proximal marine environment of normal salinity (as attested by the wide array of obligate marine taxa, such as chondrichthyans and pycnodontiform actinopterygians (Cappetta, 2012)).Absence of high energy sedimentary structure in facies C1 suggests deposition in a protected shallow marine environment. Pedogenic structures of Facies C2 are related to episodic emersions of these shallow-marine deposits (originally Facies C1). Facies C3 is interpreted to have been deposited by an episode of higher energy in this shallow marine environment, maybe related to bank collapsing. Facies C4, C5 and C6 correspond to limestones deposited in a subaquatic environment submitted to frequent subaerial exposures as attested by the desiccation cracks and root traces and burrows found at the top of the beds The presence of little-sized oysters (characteristic of a stressed environment), smooth-carapaces ostracodes and annelids are consistent with a shallow marine environment (Armstrong and Brasier, 2005) whereas micrite envelopes rounding bivalve's bioclasts indicate an intertidal context. Evidences of frequent subaerial exposures indicate a short-lived and frequently changing depositional environment, from intertidal to lacustrine. Stromatholitic carbonates of Facies C5 are related to a confined and stressed intertidal environment (Wattinne, 2004), whereas the Ostrea limestones of Facies C6 are in agreement with a deeper confined marine environment (Enay, 1990) intertidal to upper infralitoral. Because of the presence of some fresh water fossils and the occurrence of frequent emersion, the depositional setting should be quite close to the coast.

To conclude, we interpret facies association C to represent deposition in a bay/lagoon or stressed shallow marine-environment.

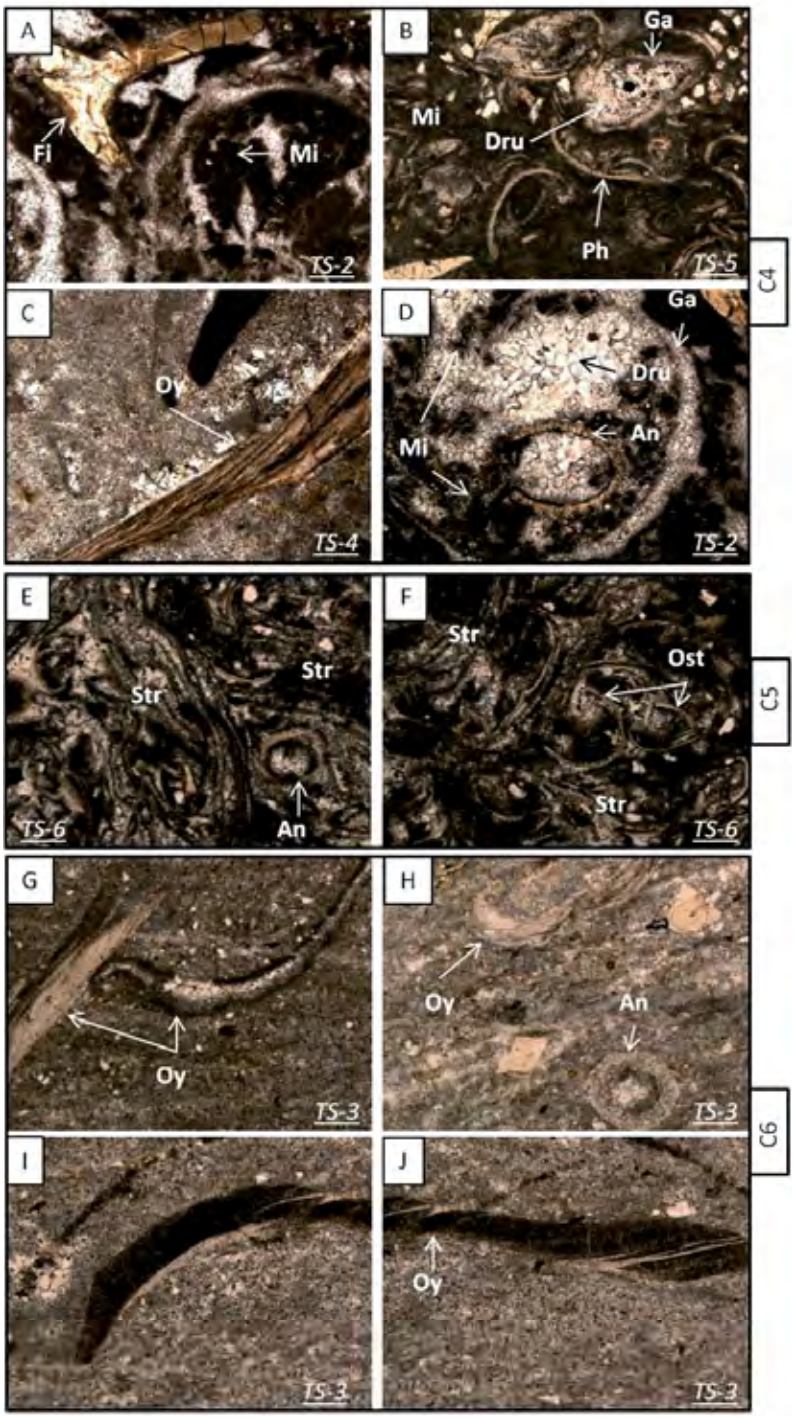

Figure 10: Thin sections photographs from Facies C4, C5 and C6, sampled at MD-184. The number of each thin-section is indicated by "TS-n°". They are located on the sedimentary section 2 of Figure 8. A), B), C) and D) correspond to thin-sections of alternated marls and limestones strata from Facies C4. E) and F) correspond to the stromatolithic Limestones of Facies C5. G), H), I) and J) correspond to the Oyster limestones of Facies C6. Fi=Fish vertebra, Mi= Micritic pellets, Dru= Drusic cement, Ga= Gasteropod, Ph= Phylopod, Oy= Oyster, An= Annelid, Str= Stromatolith filaments.

4.3. Organic Geochemistry

The TOC contents of the samples were in general very low, ranging from 0.001 to 0.06 wt. % (Table 3). Therefore, care should be taken to interpret the organic geochemical data. Nonetheless, the reproducibility of TOC contents and $\delta^{13}C_{TOC}$ was better than 0.002 wt. % and 0.3 ‰, respectively. The $\delta^{13}C_{TOC}$ values varied -23.4 to -29.8 ‰ (Table 3).

The $\delta^{13}C_{TOC}$ of higher plants that use the Calvin-Benson cycle of carbon fixation (i.e. so-called C_3 plants) ranges from -29.3 to -25.5 ‰, with an average value of about -27 ‰ (e.g. Tyson (1995)). The typical marine $\delta^{13}C_{TOC}$ values are in the range of -18 to -22 ‰ (e.g. Meyers (1997)). The $\delta^{13}C_{TOC}$ values (-27.3 to -29.8 ‰) of MD-177, MD-85, and MD-255 are hence typical of C_3 vegetation. In contrast, the $\delta^{13}C_{TOC}$ value (-23.4 ‰) of MD-184 is enriched in ^{13}C compared to the other samples, closer to typical marine $\delta^{13}C_{TOC}$ values. This suggests the presence of substantial amounts of marine organic matter in MD-184. The three other samples (from outcrops MD-85, MD-255, and MD-177) indicate a mixed organic matter origin, from terrestrial to brackish environments.

Outcrops	$D^{13}C_{TOC}$ (%VPDB)	Stdev $\delta^{13}C_{TOC}$	TOC (wt.%)	Stdev TOC (wt.%)
MD 177	-27.3	0,13	0,01	0,003
MD 85	-29.8	0,04	0,01	0,003
MD 184	-23.4	0,24	0,06	0,017
MD 255	-27.9	0,34	0,001	0,002
MD 256	no sample	no sample	no sample	no sample

Table 3: Organic geochemistry results.

4.4. Nd-Sr isotopic composition

The Nd-Sr isotopic compositions of the Thanetian sedimentary rocks are shown in Table 4. Overall, the sediments have quite variable εNd(0) values (ranging from –6.2 to -10.7) with a comparatively narrow range of $^{87}Sr/^{86}Sr$ compositions (0.712024 to 0.719026) (Table 4).

Outcrop	Sample	Lithology	Sr (ppm)	Nd (ppm)	143Nd/144Nd	± 2σ	eNd(0)	87Sr/86Sr	± 2σ1
MD 177	MD 177 A	Mudstone	244,3	38,2	**0,512087**	3	**-10,7**	0,717287	10
MD 85	MD 85 Nd	Mudstone	295,5	28,33	**0,512318**	5	**-6,2**	0,712024	8
MD 184	MD 184 A	Mudstone	269,7	42,39	**0,512117**	6	**-10,2**	0,715741	10
MD 255	MD 255 Nd	Mudstone	NM	NM	**0,512126**	6	**-10,0**	0,719026	10
MD 256	MD 256	no sample	no sample	no sample	no sample	no sample	no sample	no sample	no sample

Table 4: Nd-Sr isotopic compositions for provenance analysis.

The four samples analyzed for their Nd-Sr isotopic compositions have been reported in the $^{87}Sr/^{8S}Sr$ versus εNd(0) diagram (Figure 11). The isotopic results are compared with several other relevant source fields: Mesozoic and Neogene volcanic rocks (Kay et al., 1994; Rogers and Hawkesworth, 1989). Quaternary Ecuadorian lavas (Barragan et al., 1998); Cenozoic sedimentary rocks from the Depression, Altiplano, Oriental Cordillera and Subandean zone of Chili and Bolivia (Pinto, 2003); modern suspended sediments from the Solimoes and Madeira rivers (Viers et al., 2008); Neogene deposits from the Amazonian foreland basin of Bolivia, Ecuador and Peru (Roddaz et al., 2005a), and the sand of the Peruvian White Sand (WS) formation cratonic in origin (Roddaz et al., 2005a). Nd-Sr isotopic compositions of sediments deposited by an Andean drainage define plot within a mélange hyperbole as observed by Basu et al. (1990) and Roddaz et al. (2012; 2005a) for Neogene sediments of the Amazonian foreland basins, with one end member being the primitive volcanic arc and the other the upper continental crust of the Brazilian shield. The four analyzed Thanetian

samples plot within the field of the Cenozoic Altiplano sediments, indicating a similar Andean provenance. When compared with Neogene Subandean zone sediments, they plot closer to the volcanic arc end member, indicating a greater contribution of the volcanic arc rocks end member for the Thanetian sedimentary rocks relative to Neogene SAZ sediments.

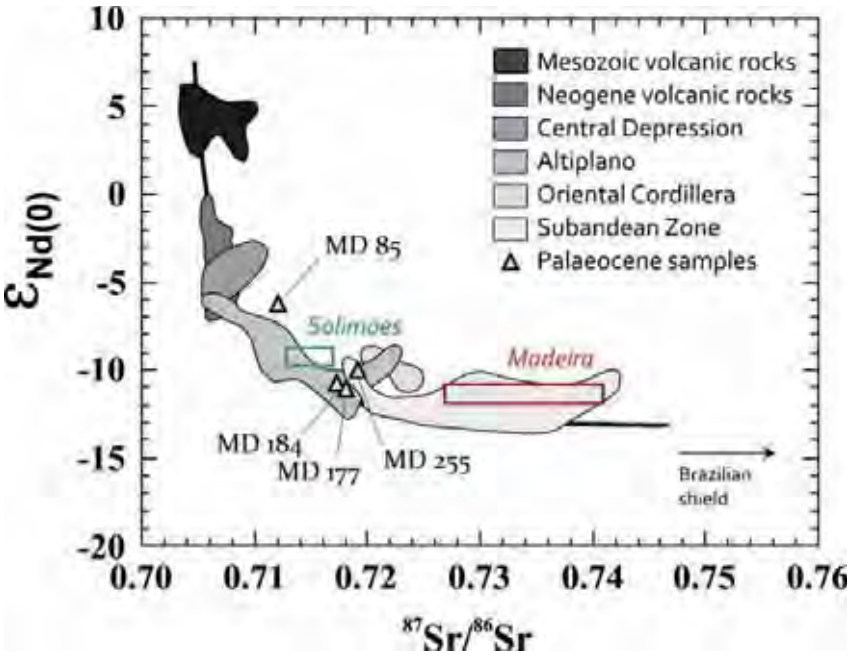

Figure 11: $^{87}Sr/^{86}Sr$ versus εNd(0) diagram. Yellow triangles correspond to the Late Paleocene samples analyzed in this study. Note that they all plot within the melange hyperbole, indicating an Andean provenance.

5. Depositional environment synthesis

Our biostratigraphical results, sedimentary facies interpretations and organic geochemistry analysis indicate the presence of a tide-influenced shallow marine paleoenvironment during the Late Paleocene period in the northern Madre de Dios Basin. Facies association A corresponds to the sedimentary filling of a tide-influenced meandering channel deposited in the fluvial-tidal transition zone. Facies association B corresponds to tidal flats deposits, tidal inlets and also characterizes a tide-influenced environment but with more distal facies than facies association A. Facies association C, interpreted as deposited in a bay/lagoon or stressed shallow marine-environment, is the most distal facies association. The facies of this association do not show any evidence of tidal nor oscillatory currents.

The transition between the land and the sea in tide-dominated coastal environments is among the most complex on Earth, because of the interaction of numerous physical, chemical and biological processes (Dalrymple and Choi, 2007). Existing depositional models are therefore preliminary because the number of case studies of many of the sub-environments is rather small. However, our dataset makes the possibility to distinguish between tide-dominated delta and tide-dominated estuary. First, from a geological point of view, estuaries are transgressive whereas deltas are regressive (Dalrymple et al., 1992). The tide-dominated Late Paleocene deposits studied in this paper overly continental deposits of the Yahuarango formation. This

stratigraphic succession therefore suggests that the tide-dominated Late Paleocene deposits are transgressive and related to an estuary. The presence of a late Paleocene tide-dominated estuary is further attested by the occurrence of a well expressed tide-influenced meandering zone. According to several works (Dalrymple and Choi, 2007; Dalrymple et al., 1992), only the fluvio-estuarine transition zone in a tide-dominated estuary could explain the occurrence of both opposite current and meandering channels in a tide-influenced environment. Facies association A could be an illustration of this precise fluvial-tidal environment, as it shows evidences of meandering channels influenced by both fluvial and tidal currents (). According to this interpretation, Facies association B could be interpreted as deposited in the outer part of this tide-dominated estuary, where tidal inlets are still present and can laterally be connected to muddy and mixed tidal-flat deposits.

Finally, as Facies association C does not show any evidences of tidal currents, we suggest deposition in a shallow confined marine environment (Figure 12).

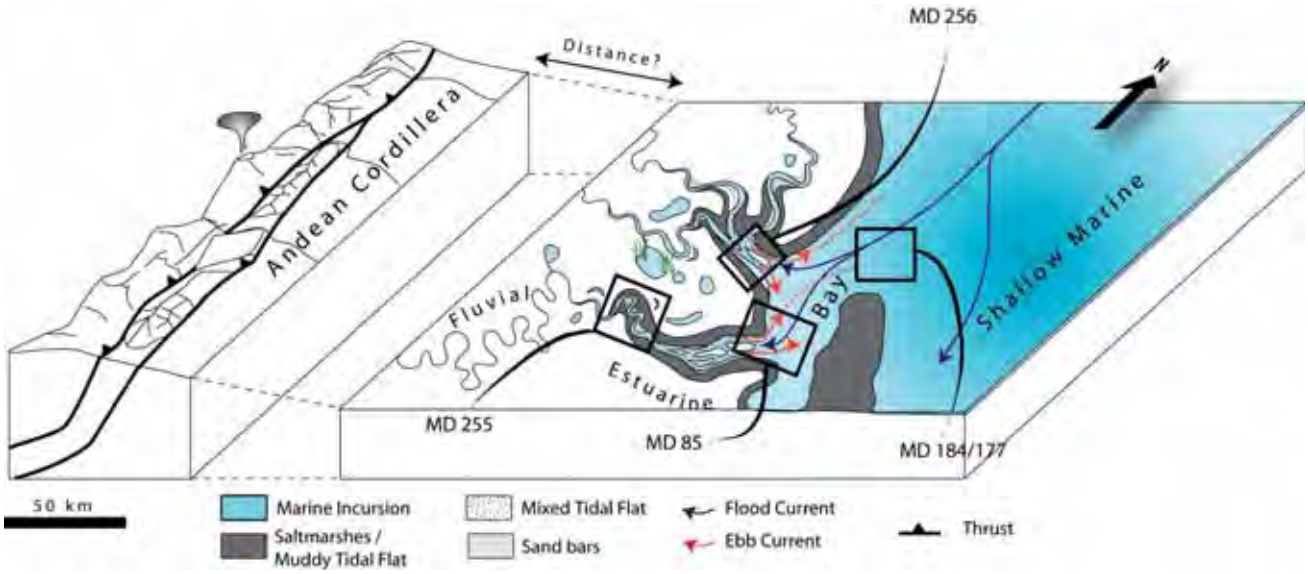

Figure 12: Interpretative diagram for Late Paleocene Times. Andean relief is active yet and produces sedimentary supply for the fluvial and then estuary system debouching in a shallow interior sea. Black rectangles correspond to the interpretative depositional contexts location of each outcrop: MD-255 corresponds to the fluvio-estuarine meandering transition zone in the proximal estuarine system; MD-256 corresponds to the inner (?) part of the estuary; MD-85 corresponds to the outer part of the estuary system and MD-184/177 corresponds to the most distal environment, also located around the outer part of the estuary system but more connected to a bay or calm confined shallow marine basin.

6. Paleogeographic and tectonic implications

Our data document for the first time the existence of a Late Paleocene tide dominated estuary debouching into a shallow marine bay in the western Amazonian foreland basin. Older Paleocene and most of the time equivalent Thanetian sedimentary rocks of other parts of the Andean/Amazonian foreland basin were deposited in a distal fluvial environment (see Figure 2). The presence of estuarine deposits overlying continental deposits indicates a marine transgression during the Thanetian. Late Paleocene times are characterized by a lowstand period (Haq et al., 1987; Hardenbol et al., 1998) and consequently the recorded transgression cannot be related to a rise in global sea-level. Flexural tectonic subsidence in response to

Andean tectonic loading is the best candidate to explain the development of a Thanetian estuary in Western Amazonia. This is in agreement with our Nd-Sr isotopic provenance data that show an Andean provenance and hence the presence of an Andean relief in Late Paleocene times. However the entrance of this Late Paleocene marine ingression (Altantic Ocean, Pacific Ocean or Caribbean Sea) and the nature/of the Andean source (Western or Eastern Cordillera) remain to be elucidated. Regarding the oceanic connection, very few Late Paleocene marine or coastal deposits are documented in the Andean/Amazonian foreland basins. The Late Paleocene Los Cuervos formation in Colombia shows evidences of marine influence (Figure 2) but contemporaneous formations of Ecuador and elsewhere in Peru show no evidences of marine or coastal deposits (Figure 2). In the Bolivian Altiplano and the Eastern Cordillera there is no evidence of any marine influence attested so far. Hence the Late Paleocene paleogeogaphical map proposed here (Figure 13-A) is tentative. In conjunction with the presence of shallow marine deposits in the Colombian Los Cuervos formation, our data suggest a northern connection with the Caribbean Sea or the Pacific Ocean. In any case, more, detailed sedimentological works are needed to decipher the locus of this Late Paleocene marine entrance.

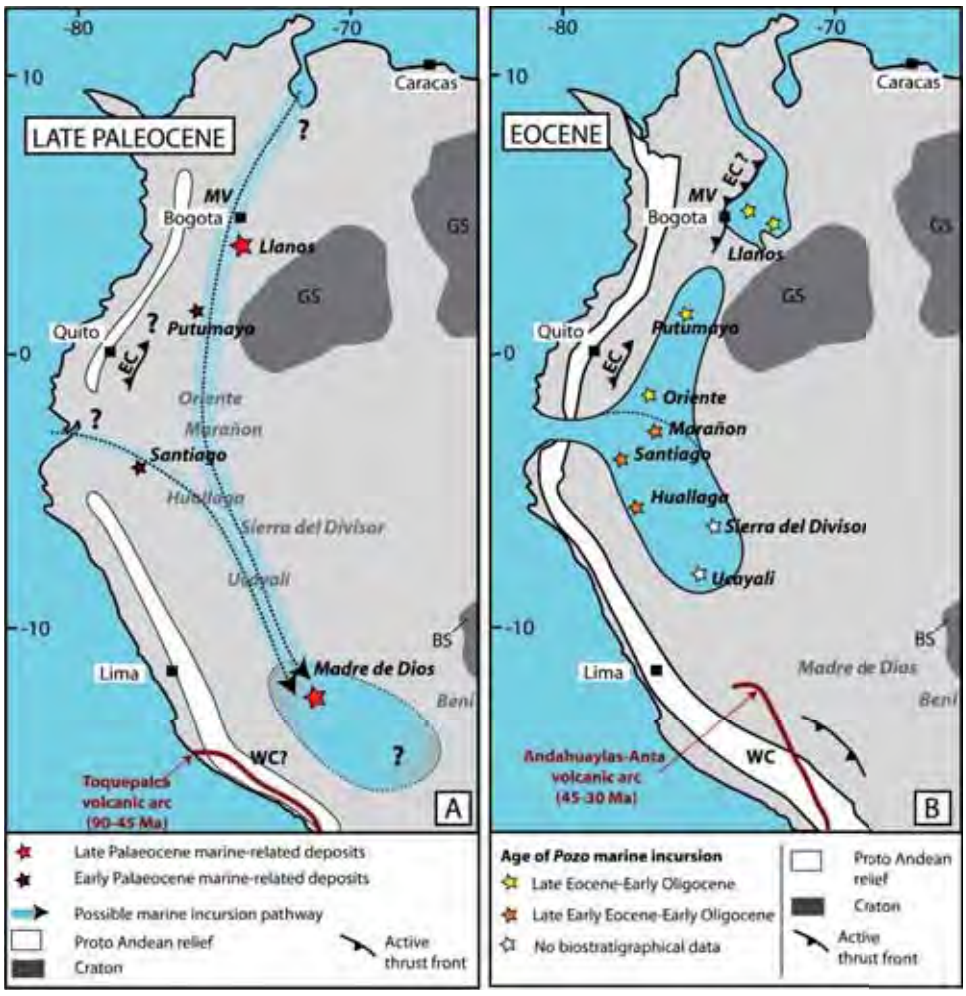

Figure 13: Paleogeographical reconstructions for Paleogene times. A) Paleogeographic reconstruction of Late Paleocene Times. The shallow marine sea described in this paper in the Amazonian foreland basin does not present clear connection with existing oceans. This shallow marine incursion could have come from the Caribbean Sea from Vennezuela or from the Pacific Ocean by the Guyaquil Gulf. Southern connection through Bolivia is much unlikely. B) Paleogeographic reconstruction for Eocene Times, related to Pozo shallow marine incursion.

The location of the Andean relief that was the source for the sediments deposited within the Late Paleocene estuary also remains unclear. Thermochronological evidences suggest that the first exhumation and/or deformation pulse in the Eastern part of the Altiplano or in the Eastern Cordillera of Central Andes occurred

in the Late Eocene (Barnes et al., 2006; Kontak et al., 1990). Jaillard et al. (1993a) interpreted the absence of strata close to the Cretaceous-Paleogene boundaty in the Cusco basins as the consequence of an uplift of a proto-eastern cordillera occurring as early as the Early to Late Paleocene. However our provenance data suggest that the Thanetian estuarine sediments are characterized by a contribution from a volcanic arc source. According to Mamani et al. (2010), the only active volcanic arc during the Paleocene was the Toquepala volcanic arc (91-45 Ma) located in the present-day Coastal/Western Cordillera. This suggests the absence of any significant proto-eastern cordillera relief capable of acting as a barrier to sediments originating from the Western Cordillera Arc. In conclusion, our data suggest that the Late Paleocene marine incursion could be related to proto western Cordillera loading. This orogenic loading can be related to a drastic change in convergence direction of the subduction from NE to ENE (Soler and Bonhomme, 1990) that might have provoked the major Late Paleocene tectonic event formerly called “Incaic 1” tectonic event (Noble et al., 1990; Sempere et al., 1997).

The documented Late Paleocene marine transgression predates a well-known Eocene transgression occurring in the Colombian, Ecuadorian and northern Peruvian Amazonian foreland basins and recorded by the Lower Carbonera, Orteguaza and Pozo formations (Christophoul et al., 2002; Hermoza et al., 2005b; Roddaz et al., 2010). According to these authors, this Eocene marine incursion would come from both the Guyaquil Gulf and the Caribbean Sea (Figure 13-B). Data from Colombia suggest that a Late Eocene transgression flooded south-western Colombia, coming from the south through the Ecuadorian coast (Osorio, 2002; Santos et al., 2008). The presence of marine deposits in the Eastern Cordillera and the Central-Eastern Llanos Foothills is more difficult to explain and authors propose a possible corridor through the proto-Lower Magdalena Valley that connected the Caribbean Sea and the Central Llanos Foothills (Santos et al., 2008). In Ecuador and northern Peru, the Eocene shallow marine transgression is recorded by the deposits of Orteguaza and Pozo formation (Figure 2) as the result of the Western Cordillera loading (Roddaz et al., 2010). The southern limit of this marine incursion is not well-constrained but no Eocene deposits have been recognized in the southern Peruvian and Bolivian Amazonian basin (Figure 2).

Our data and literature review indicate that at least two marine incursions occurred in the Amazonian foreland basin in early Palaeogene times (late Palaeocene and Eocene, respectively). Both shallow marine incursions are induced by Andean tectonic loading but they did not affect similar area in the Amazonian foreland basins. Many studies (see (Hoorn et al., 2010) have emphasized the role played by the Miocene long-lived Pebas megawetland system in preventing in situ speciation and floristic and plants dispersal between the Andes and Amazonia for at least 6 Ma (Antonelli et al., 2009) and favouring evolutionary transition from marine to freshwater habitats of Neotropical fishes (Lovejoy et al., 2006; 2009; Lundberg et al., 1998).Recurrent Paleogene marine incursions in the Amazonian foreland basin associated with Andean uplift could have provoked biogeographical isolation and promoted allopatric speciation for terrestrial organisms. Unfortunately, such a hypothesis is virtually untestable at the time being, as a very few Thanetian-Ypresian vertebrate-yielding localities are documented at South American scale so far (Gelfo et al., 2009).

7. Conclusion

Based on a multidisciplinary approach, this paper documents for the first time the presence of a tide-influenced shallow marine paleoenvironment during the Late Paleocene interval (Thanetian) in the Amazonian basin. In details, based on sedimentary facies analysis, organic geochemistry and fossil assemblages, we define three facies associations related to a tide-dominated estuary debouching into a shallow-marine bay or lagoon. Facies association A corresponds to the sedimentary filling of a tide-influenced meandering channel formed in the fluvial-tidal transition zone. Facies association B is related to more distal tidal-flats, little channelized tidal inlets and saltmarshes deposits. Facies association C corresponds to a stressed shallow marine environment such as a bay or a lagoon.

The presence of these transgressive estuarine deposits overlying older continental facies is best explained by flexural tectonic subsidence in response to Andean tectonic loading. This is in agreement with our Nd-Sr isotopic provenance data that show an Andean provenance and hence the presence of an Andean relief during Thanetian times. The volcanic contribution recorded in the Nd-Sr isotopic compositions can be related to the Toquepala volcanic arc (91-45 Ma) located in the present-day Coastal/Western Cordillera. This suggests the absence of any significant proto-Eastern Cordillera relief that would have stopped the drainage and the sedimentary influxes from this Western Andean volcanic relief towards the Amazonian basin during Thanetian times. Consequently our data suggest that the Thanetian marine incursion can be related to the subsidence created in response to the proto-Western Cordillera loading.

Finally, we suggest that similarly to Miocene marine incursions affecting the Pebas megawetland, Paleogene marine incursions in the Amazonian foreland basin associated with Andean uplift may have played a role in the Amazon biodiversity in favouring biogeographical isolation and promoting allopatric speciation for terrestrial organisms.

Acknowledgements

We thank Denise Dorhout for analytical support at NIOZ. We are much indebted to Frank P. Wesselingh for mollusk taxonomic identification. The research leading to these results has received funding from the European Research Council under the European Union's Seventh Framework Program (FP7/2007-2013) / ERC grant agreement n° [226600].

Supplementary Table A:

Outcrop	Area	X	Y
MD 177	Pongo de Coñeq	-71,360503	-12,890300
MD 85	Pantiacolla	-71,271500	-12,668700
MD 184	Pantiacolla	-71,265917	-12,668783
MD 255	Pantiacolla	-71,247700	-12,679900
MD 255	Pantiacolla	-71,244260	-12,662260

References

Allen, J.R.L., 1970. A quantitative model of climbing ripples and their cross-laminated deposits. Sedimentology, 14(1-2): 5-26.

Antoine, P.O., Roddaz, M., Brichau, S., Tejada-Lara, J., Salas-Gismondi, R., Altamirano, A., Louterbach, M., Lambs, L., Otto, T. and Brusset, S., 2013. Middle Miocene vertebrates from the Amazonian Madre de Dios Subandean Zone, Peru. Journal of South American Earth Sciences, 42: 91-102.

Antonelli, A., Nylander, J.A.A., Persson, C. and Sanmartin, I., 2009. Tracing the impact of the Andean uplift on Neotropical plant evolution. PNAS.

Armstrong, H.A. and Brasier, M.D., 2005. Microfossil In: M. Hart (Editor), Geological Magazine. Blackwell Publishing, Malden, Oxford, Carlton, pp. 296 pp. .

Ashley, G.M., Southard, J.B. and Boothroyd, J.C., 1982. Deposition of climbing-ripple beds: a flume simulation. Sedimentology, 29(1): 67-79.

Aubry, M.-P., Thiry, M., Dupuis, C. and Berggren, W., 2005. The Sparnacian deposits of the Paris Basin: A lithostratigraphic classification. . Stratigraphy, 2: 65-100.

Barnes, J.B., Ehlers, T.A., McQuarrie, N., O'Sullivan, P.B. and Pelletier, J.D., 2006. Eocene to Recent variations in erosion across the Central Andean fold-thrust belt, northern Bolivia; Implications for plateau evolution: Earth and. Planetary Science Letters, v: 101016/jepsl200605018-101016/jepsl200605018.

Barragan, R., Geist, D., Hall, M., Larson, P. and Kurz, M., 1998. Subduction controls on the compositions of lavas from the Ecuadorian Andes. . Earth and Planetary Science Letters 154: p.153-166

Basu, A.R., Sharma, M. and Decelles, P.G., 1990. Nd, Sr-Isotopic provenance and trace-element geochemistry of Amazonian foreland basin fluvial sands, Bolivia and Peru. Implications for ensialic Andean orogeny. . Earth and Planetary Science Letters, 100(1-3): 1-17.

Campbell, K.E., David, C. and Romero-pittman, L., 2006. The Pan-Amazonian Ucayali Peneplain , late Neogene sedimentation in Amazonia , and the birth of the modern Amazon River system. October.

Cande, S.C. and Kent, D.V., 1992. A new geomagnetic polarity time scale for the Late Cretaceous and Cenozoic. Journal of Geophysical Research: Solid Earth, 97(B10): 13917-13951.

Cappetta, H., 2012. Chondrichthyes (Mesozoic and Cenozoic Elasmobranchii: teeth). In: H.-P. Schultze (Editor), Handbook of Paleoichthyology, Munich (Pfeil).

Cappetta, H. and Gayet, M., 2013. A new elasmobranch genus (Myliobatiformes, Dasyatoidea) from the Danian of Potosí (Bolivia). Neues Jahrbuch f??r Geologie und Pal??ontologie - Abhandlungen, 269(3): 285-290.

Choi, K., 2010. Rhythmic Climbing-Ripple Cross-Lamination in Inclined Heterolithic Stratification (IHS) of a Macrotidal Estuarine Channel, Gomso Bay, West Coast of Korea. Journal of Sedimentary Research, 80(6): 550-561.

Christophoul, F., Baby, P. and Dávila, C., 2002. Stratigraphic responses to a major tectonic event in a foreland basin: the Ecuadorian Oriente Basin from Eocene to Oligocene times. Tectonophysics, 345(1–4): 281-298.

Dalrymple, R.W., 1984. Runoff microdeltas; a potential emergence indicator in cross-bedded sandstones. Journal of Sedimentary Research, 54(3): 825-830.

Dalrymple, R.W., Baker, E.K., Harris, P.T. and Hughes, M.G., 2003. Sedimentology and stratigraphy of a tide-dominated, foreland-basin delta (Fly River, Papua New Guinea. In: F.H. Sidi, Nummedal, D., Imbert, P., Darman, H., and Posamentier, H.W., eds. (Editor), Tropical Deltas of Southeast Asia—Sedimentology, Stratigraphy, and Petroleum Geology. SEPM, Special Publication, pp. p. 147-173.

Dalrymple, R.W. and Choi, K., 2007. Morphologic and facies trends through the fluvial–marine transition in tide-dominated depositional systems: A schematic framework for environmental and sequence-stratigraphic interpretation. Earth-Science Reviews, 81(3-4): 135-174.

Dalrymple, R.W., Zaitlin, B.A. and Boyd, R., 1992. Estuarine facies models; conceptual basis and stratigraphic implications. Journal of Sedimentary Research, 62(6): 1130-1146.

de Mowbray, T. and Visser, M.J., 1984. Reactivation surfaces in subtidal channel deposits, Oosterschelde, Southwest Netherlands. Journal of Sedimentary Research, 54(3): 811-824.

DeCelles, P.G. and Horton, B.K., 2003. Early to middle Tertiary foreland basin development and the history of Andean crustal shortening in Bolivia. Geological Society of America Bulletin, 115(1): 58-77.

Dunham, R.J., 1962. Classification of carbonate rocks according to depositional texture. In: e. W. E. Ham (Editor), Classifications of carbonate rocks - a symposium, pp. p. 108–121.

Enay, R., 1990. Paléontologie des invertébrés Collection Géosciences, Paris, 233 p. pp.

Eriksson, K.A. and Simpson, E.L., 2004. Precambrian tidalites: recognition and significance. In: P.G. Eriksson, Altermann, and N. W., D., Mueller, W., Cateneau, O., Strand, K. (Eds.) (Editors), Tempos and Events in Precambrian Time. Developments in Precambrian Geology. Elsevier, Amsterdam, pp. pp. 631–642.

Eriksson, P.G., Condie, K.C., Tirsgaard, H., Mueller, W.U., Altermann, W., Miall, A.D., Aspler, L.B., Catuneanu, O. and Chiarenzelli, J.R., 1998. Precambrian clastic sedimentation systems. Sedimentary Geology, 120(1–4): 5-53.

Faucher, B. and Savoyat, E., 1973. Esquisse géologique des Andes de l'Equateur. Revue de géographie physique et de géologie dynamique, 15(1-2): 115-142.

Gayet, M., Sempre, T., Cappetta, H., Jaillard, E. and Lévy, A., 1993. La présence de fossiles marins dans le Crétacé terminal des Andes centrales et ses conséquences paléogéographiques. Palaeogeography, Palaeoclimatology, Palaeoecology, 102(3–4): 283-319.

Gelfo, J.N., Goin, F.J., Woodburne, M.O. and Muizon, C.D., 2009. Biochronological relationships of the earliest South American Paleogene mammalian faunas. Palaeontology, 52(1): 251-269.

Gérard, J., 2008. ICHNOFABRICS IN CLASTIC SEDIMENTS: Applications to sedimentological core studies. a practical guide by Jean R.F. GERARD & Richard G. BROMLEY. Jean Gérard, Madrid, 100 pp.

Gil, W.F., 2001. Evolution latérale de la déformation d'un front orogénique: exemples des bassins subandins entre 0° et 16°S, University Paul Sabatier, Toulouse.

Gingras, M.K., Pemberton, S.G., Saunders, T. and Clifton, H.E., 1999. The ichnology of modern and Pleistocene brackish-water deposits at Willapa Bay, Washington; variability in estuarine settings. PALAIOS, 14(4): 352-374.

Gingras, M.K., Räsänen, M. and Ranzi, A., 2002. The Significance of Bioturbated Inclined Heterolithic Stratification in the Southern Part of the Miocene Solimoes Formation, Rio Acre, Amazonia Brazil. PALAIOS, 17(6): 591-601.

Gutierrez, M., 1982. Evaluacion potencial petrolifero cuencas Huallaga, Ucayali y Madre de Dios. Zonacion bioestratigrafica del intervalo Cretacico superior-Tertiario inferior, Petroperu, Internal Report, Lima.

Haq, B.U., Hardenbol, J. and Vail, P.R., 1987. Chronology of fluctuating sea levels since the Triassic. Science, v. 235: p. 1156–1167.

Hardenbol, J., Thierry, J., Farley, M.B., Jacquin, T., De Graciansky, P.C. and VailP.R., 1998. Mesozoic–Cenozoic sequence chronostratigraphy of european basins. 60SEPM Special Publication, Tulsa: pp. 1–786.

Hermoza, W., 2004. Dynamique tectono-sedimentaire et restauration sequentielle du retro-bassin d'avant-pays des Andes Centrales, Univeristy Paul Sabatier, Toulouse, 196 pp. pp.

Hermoza, W., Brusset, S., Baby, P., Gil, W., Roddaz, M., Guerrero, N. and Bolaños, R., 2005b. The Huallaga foreland basin evolution: Thrust propagation in a deltaic environment, northern Peruvian Andes. Journal of South American Earth Sciences, 19(1): 21-34.

Hoorn, C., Wesselingh, F.P., ter Steege, H., Bermudez, M.a., Mora, a., Sevink, J., Sanmartín, I., Sanchez-Meseguer, a., Anderson, C.L., Figueiredo, J.P., Jaramillo, C., Riff, D., Negri, F.R., Hooghiemstra, H., Lundberg, J., Stadler, T., Särkinen, T. and Antonelli, a., 2010. Amazonia through time: Andean uplift, climate change, landscape evolution, and biodiversity. Science (New York, N.Y.), 330(6006): 927-31.

Hovikoski, J., Gingras, M., Räsänen, M., Rebata, L., Guerrero, J. and Ranzi, A., 2007. The nature of Miocene Amazonian epicontinental embayment: High-frequency shifts of the low-gradient coastline. GSA Bulletin, 119: 1506-1520.

Hovikoski, J., Räsänen, M., Gingras, M., Ranzi, A. and Melo, J., 2008. Tidal and seasonal controls in the formation of Late Miocene inclined heterolithic stratification deposits, western Amazonian foreland basin. Sedimentology, 55(3): 499-530.

Jackson, R.G., 1981. Sedimentology of muddy fine-grained channel deposits in meandering streams of the American Middle West. Journal of Sedimentary Research, 51(4): 1169-1192.

Jacobsen, S.B. and Wasserburg, G.J., 1980. Sm-Nd isotopic evolution of chondrites. Earth and Planetary Science Letters, 50(1): 139-155.

Jaillard, E., 1993a. The Senonian to Palaeocene tectonic evolution of the Peruvian margin and its relationships with geodynamics. L'evolution tectonique de la marge peruvienne au Senonien et Paleocene et ses relations avec la geodynamique, 164(6): 819-830.

Jaillard, E., 1996. Cretaceous to early Paleogene tectonic evolution of the northern Central Andes (0–18°S) and its relations to geodynamics. Tectonophysics, 259(1-3): 41-53.

Jaillard, E., Carlotto, V., Cardenas, J., Chavez, R. and Gil, W., 1993b. La "Nappe des Couches Rouges" de Cuzco (Sud du Pérou) : mise en évidence stratigraphique, interprétations tectoniques et paléogéographiques C. R. Acad. Sci. Paris, 36(Série II): 379-386.

Jaramillo, C.A. and Dilcher, D.L., 2000. Microfloral diversity patterns of the late Paleocene–Eocene interval in Colombia, northern South America. Geology, 28(9): 815-818.

Jaramillo, C.A. and Dilcher, D.L., 2001. Middle Paleogene palynology of Central Colombia, South America: A study of pollen and spores from tropical latitudes. Palaeontographica Abteilung B, 258(4-6): 87-213.

Jeffery, M.L., Poulsen, C.J. and Ehlers, T.A., 2012. Impacts of Cenozoic global cooling, surface uplift, and an inland seaway on South American paleoclimate and precipitation δ18O. Geological Society of America Bulletin, 124(3-4): 335-351.

Jopling, A.V. and Walker, R.G., 1968. Morphology and origin of ripple-drift cross-lamination, with examples from the Pleistocene of Massachusetts. Journal of Sedimentary Research, 38(4): 971-984.

Kay, S.M., Coira, B. and Viramonte, J., 1994. Young mafic back arc volcainc-rocks s indicators of continental lithospheric delamination beneath the Argentine Puna plateau, Central Andes Journal of Geophysical Research-Solid Earth, 99(B12): 24323-24339.

Klein, G.d., 1970. Depositional and dispersal dynamics of intertidal sand bars. Journal of Sedimentary Research, 40(4): 1095-1127.

Kontak, D.J., Farrar, E., Clark, A.H. and Archibald, D.A., 1990. Eocene tectono-thermal rejuvenation of an upper Paleozoic-lower Mesozoic terrane in the Cordillera de Carabaya, Puno, southeastern Peru, revealed by K-Ar and 40Ar/39Ar dating. Journal of South American Earth Sciences, 3(4): 231-246.

Lovejoy, N.R., Albert, J.S. and Crampton, W.G.R., 2006. Miocene marine incursions and marine/freshwater transitions: Evidence from Neotropical fishes. Journal of South American Earth Sciences, 21(1-2): 5-13.

Lovejoy, N.R., Willis, S.C. and Albert, J.S., 2009. Molecular signatures of Neogene biogeographical events in the Amazon fish fauna.

Lundberg, J.G., Marshall, L.G. and Guerrero, J., 1998. The Stage of Neotropical Fish Diversification: A History of Tropical South American Rivers. In: L.R. Malabarba, R.E. Reis, R.P. Vari, Z.M. Lucena and C.A.S Lucena (eds) (Editor), Phylogeny and Classification of Neotropical Fishes. Edipucrs, Porto Alegre, pp. 603 pp.

Mamani, M., Worner, G. and Sempere, T., 2010. Geochemical variations in igneous rocks of the Central Andean orocline (13 degrees S to 18 degrees S): Tracing crustal thickening and magma generation through time and space. Geological Society of America Bulletin, 122(1-2): 162-182.

Marivaux, L., Salas-Gismondi, R., Tejada, J., Billet, G., Louterbach, M., Vink, J., Bailleul, J., Roddaz, M. and Antoine, P.O., 2012. A platyrrhine talus from the early Miocene of Peru (Amazonian Madre de Dios Sub-Andean Zone). Journal of Human Evolution, 63(5): 696-703.

Marocco, R., Baudino, R. and A., L., 1995. The intermontane Neogene continental basins of the Central Andes of Ecuador and Peru: Sedimentologic, tectonic and geodynamic implications. In: R.S. A.J. Tankard, H.J. Welsink (Eds.) (Editor), Petroleum Basins of South America. Am. Assoc. Pet. Geol. Mem., pp. pp. 597–613.

Marshall, L.G., Sempere, T. and Butler, R.F., 1997. Chronostratigraphy of the mammal-bearing Paleocene of South America. Journal of South American Earth Sciences, 10(1): 49-70.

Martin-Gombojav, N. and Winkler, W., 2008. Recycling of proterozoic crust in the andean amazon foreland of Ecuador: Implications for orogenic development of the Northern Andes. Terra Nova, 20(1): 22-31.

Martinius, A.W., Kaas, I., N¹ss, A., Helgesen, G., Kj¹refjord, J.M. and Leith, D.A., 2001. Sedimentology of the heterolithic and tide-dominated tilje formation (Early Jurassic, Halten Terrace, Offshore Mid-Norway). In: J.M. Ole and D. Tom (Editors), Norwegian Petroleum Society Special Publications. Elsevier, pp. 103-144.

Mazumder, R. and Arima, M., 2005. Tidal rhythmites and their implications. Earth-Science Reviews, 69(1–2): 79-95.

Meyers, P.A., 1997. Organic geochemical proxies of paleoceanographic, paleolimnologic, and paleoclimatic processes. Organic Geochemistry, 27(5-6): 213-250.

Miall, A.D., 1996. The geology of fluvial deposits: sedimentary facies, basin analysis and petroleum geology. Springer-Verlag Inc Berlin, 582 pp. pp.

Mpodozis, C. and Allmendinger, R.W., 1993. Extensional tectonics, Cretaceous Andes, northern Chile (27°S). Geological Society of America Bulletin, 105(11): 1462-1477.

Naeser, C.W., Crochet, J., Jaillard, E., Laubacher, G., Mourier, T. and Sige, B., 1991. Tertiary fission-track ages from the Bagua syncline (northern Peru): Stratigraphic and tectonic implications. Journal of South American Earth Sciences, 4(1-2): 61-71.

Nio, S.D. and Yang, C.S., 1991. Diagnostic attributes of clastic tidal deposits: a review. In: D.G. Smith, Reinson, G.E., Zeitlin, B.A. and R.A. Rahmani (Editor), Clastic Tidal Sedimentology. Canadian Society of Petroleum Geologists, pp. p. 3-28.

Noble, D.C., McKee, E.H., Mourier, T. and Mégard, F., 1990. Cenozoic stratigraphy, magmatic activity, compressive deformation, and uplift in Northern Peru. Geological Society of America Bulletin, 102: p. 1105-1113.

Osorio, 2002. Stratigraphy of the Tertiary sequences — Upper Magdalena and the Putumayo basins, a different point of view for hydrocarbon exploration. Memorias de la Segunda Convención técnica de la Asociación Colombiana de Geólogos y Geofísicos del Petróleo, Bogotá, Colombia 10 pp.

Page, K.J., Nanson, G.C. and Frazier, P.S., 2003. Floodplain Formation and Sediment Stratigraphy Resulting from Oblique Accretion on the Murrumbidgee River, Australia. Journal of Sedimentary Research, 73(1): 5-14.

Parra, M., Mora, A., Jaramillo, C., Strecker, M.R., Sobel, E.R., Quiroz, L., Rueda, M. and Torres, V., 2009. Orogenic wedge advance in the northern Andes : Evidence from the Oligocene-Miocene sedimentary record of the Medina Basin , Eastern Cordillera , Colombia. Geological Society Of America Bulletin(May).

Pinto, L., 2003. Traçage de l'érosion Cénozoïque des Andes Centrales à l'aide dela minéralogie et de la géochmie des sédiments (Nord du Chili et Nord-Ouest de la Bolivie), University Paul Sabatier, Toulouse.

Roddaz, M., Christophoul, F., Zambrano, J.D.B., Soula, J.C. and Baby, P., 2012. Provenance of late Oligocene to quaternary sediments of the Ecuadorian Amazonian foreland basin as inferred from major and trace element geochemistry and Nd-Sr isotopic composition. Journal of South American Earth Sciences, 37: 136-153.

Roddaz, M., Hermoza, W., Mora, A., Baby, P., Parra, M., Christophoul, F., Brusset, S. and Espurt, N., 2010. Cenozoic sedimentary evolution of the Amazonian foreland basin system, pp. 61-88.

Roddaz, M., Viers, J., Brusset, S., Baby, P. and Hérail, G., 2005a. Sediment provenances and drainage evolution of the Neogene Amazonian foreland basin. Earth and Planetary Science Letters, 239(1–2): 57-78.

Rogers, G. and Hawkesworth, C.J., 1989. A geochemical traverse across the North Chilean Andes: evidence for crust generation from the mantle wedge. Earth and Planetary Science Letters, 91(3–4): 271-285.

Ruiz, G.M.H., Seward, D. and Winkler, W., 2004. Detrital thermochronology - A new perspective on hinterland tectonics, an example from the Andean Amazon Basin, Ecuador. Basin Research, 16(3): 413-430.

Ruiz, G.M.H., Seward, D. and Winkler, W., 2007. Evolution of the Amazon Basin in Ecuador with Special Reference to Hinterland Tectonics: Data from Zircon Fission-Track and Heavy Mineral Analysis pp. 907-934.

Santos, C., Jaramillo, C., Bayona, G., Rueda, M. and Torres, V., 2008. Late Eocene marine incursion in north-western South America. Palaeogeography, Palaeoclimatology, Palaeoecology, 264(1–2): 140-146.

Sempere, T., Butler, R.F., Richards, D.R., Marshall, L.G., Sharp, W. and Swisher, C.C., 1997. Stratigraphy and chronology of upper Cretaceous lower Paleogene strata in Bolivia and northwest Argentina. Geological Society of America Bulletin, 109(6): 709-727.

Shanley, K.W., McCabe, P.J. and Hettinger, R.D., 1992. Tidal influence in Cretaceous fluvial strata from Utah, USA: a key to sequence stratigraphic interpretation. Sedimentology, 39(5): 905-930.

Shanmugam, G., Poffenberger, M. and Toro Álava, J., 2000. Tide-Dominated Estuarine Facies in the Hollin and Napo ("T" and "U") Formations (Cretaceous), Sacha Field, Oriente Basin, Ecuador. AAPG Bulletin, 84(5): 652-682.

Sigé, B., Sempere, T., Butler, Robert F., Marshall, Larry G. and Crochet, J.-Y., 2004. Age and stratigraphic reassessment of the fossil-bearing Laguna Umayo red mudstone unit, SE Peru, from regional stratigraphy, fossil record, and paleomagnetism. Geobios, 37(6): 771-794.

Soler, P. and Bonhomme, M.G., 1990. Relation of magmatic activìty to plate dynamics In central Peru from Late Cretaceous to present. In: S.M. Kay, and Rapela, C. W., eds (Editor), Plutonism from Antarctica to Alaska: Boulder, Colorado. Geological Society of America Special Paper.

Tessier, B., 1996. River-Ocean Interaction Zone: a Facies Model with climbing Ripple Bedding. In: N.I.o.M.G.a.G.-e.o. Romania (Editor), GEO-ECO-MARINA 2.Workshop on "Fluvial-Marine Interactions", Malnas, Romania.

Thomas, D.S.G., Martin, H.E. and Lancaster, N., 1987. Grain-size characteristics of linear dunes in the southwestern Kalahari; discussion and reply. Journal of Sedimentary Research, 57(3): 572-574.

Tyson, R.V., 1995. Sedimentary organic matter: organic facies and palynofacies. Springer.

Valchev, B., 2007. Representatives of Family Eggerellidae Cushman, 1937 from the Palaeocene of the Coastal Part of East Stara Planina. Review of the Bulgarian Geological Society, 68: 36-40.

Viers, J., Roddaz, M., Filizola, N., Guyot, J.L., Sondag, F., Brunet, P., Zouiten, C., Boucayrand, C., Martin, F. and Boaventura, G.R., 2008. Seasonal and provenance controls on Nd-Sr isotopic compositions of Amazon rivers suspended sediments and implications for Nd and Sr fluxes exported to the Atlantic Ocean. Earth and Planetary Science Letters, 274(3-4): 511-523.

Wattinne, A., 2004. Évolution d'un environnement carbonate lacustre à bioconstructions, en limagne bourbonnaise (Oligo-Miocène, Massif Central, France), Paris, 195 p. pp.

Figures

D. Facies analysis and sedimentary evolution of the Neogene southern Amazonian foreland basin

Introduction au chapitre:

La plus grande partie du remplissage sédimentaire du bassin de Madre de Dios est Néogène. Cependant, ces dépôts sont peu décrits dans la littérature (Gil, 2001; Hermoza, 2004). L'accès difficile aux affleurements dans cette région de l'Amazonie est tout aussi problématique et contraint nettement la qualité des observations. Mais la principale difficulté rencontrée par ces auteurs est liée au manque de contenu paléontologique et palynologique nécessaire pour dater ces dépôts cénozoïques majoritairement décrits comme continentaux.

Cependant, plusieurs incursions marines ont déjà été décrites dans l'enregistrement sédimentaire néogène du bassin d'avant-pays Amazonien (Hovikoski et al., 2010; Roddaz et al., 2010). Il a de plus déjà été démontré que les incursions marines, surtout en Amazonie, influent de manière importante la biodiversité et la paléo-écologie. Par exemple, l'existence et la persistance d'un système marécageux très étendu pendant le Miocène inférieur à moyen dans le nord de l'Amazonie (le système « Pebas ») est certainement en grande partie responsable de la très grande biodiversité de la forêt amazonienne (Hoorn et al., 2010). Cependant, l'extension du système Pebas ainsi que le nombre exact d'incursions marine qui ont eu lieu en Amazonie au Tertiaire restent toujours débattus et peu compris (Campbell et al., 2006; Hoorn et al., 2010; Hovikoski et al., 2007b). Une synthèse récente (Hoorn et al., 2010) souligne les liens complexes existant entre la formation des Andes, les changements climatiques et le développement de la biodiversité au cours du Cénozoïque dans le bassin Amazonien. Ces auteurs insistent notamment sur les conséquences et le rôle des incursions marines sur les taux de précipitations enregistrés dans les zones concernées (Jeffery et al., 2012). Il apparaît donc primordial de déterminer le nombre, l'âge et la durée des incursions marines ayant atteint le bassin Amazonien au cours du Cénozoïque pour i) reconstruire la paléogéographie de l'époque, et ii) préciser les relations entre la formation des Andes, les changements climatiques et l'évolution de la biodiversité en Amazonie du Sud.

Dans ce chapitre, nous présentons de nouvelles données biostratigraphiques et radiométriques (palynologie, paléontologie, datations Ar/Ar), des descriptions sédimentologiques ainsi que des résultats géochimiques (composition isotopique du Nd-Sr) pour les sédiments néogènes du bassin de Madre de Dios. Plus précisément, le caractère continental versus marin des dépôts néogènes est particulièrement discuté, tout comme la relation entre la déformation Andine, la dynamique du bassin d'avant-pays et le type de dépôts associés. L'objectif principal de ce chapitre est de documenter le remplissage sédimentaire néogène du bassin d'avant-pays sud Amazonien.

Les résultats biostratigraphiques, la localisation des échantillons ainsi que les coupes stratigraphiques en format A3 sont disponibles séparemment, en Annexes.

Résumé :

Les dépôts néogènes à pléistocènes du bassin de Madre de Dios (zone Subandine actuelle) correspondent à une méga-séquence de dépôt grano et strato-croissante. Cette méga-séquence strato- et grano-croissante dominée par des dépôts continentaux/fluviatiles évolue de dépôts distaux de faible énergie pendant le début du Néogène vers des dépôts proximaux de haute énergie pendant le Néogène terminal et le Pléistocène. Une telle séquence suggère le rapprochement progressif de la source sédimentaire et donc la migration du front orogénique Andin vers l'Est. Cette migration est illustrée par des dépôts distaux de faible énergie pendant le début du Néogène évoluant ensuite vers des dépôts proximaux de haute énergie pendant le Néogène terminal et le Pléistocène. Si la migration vers l'Est de la déformation andine peut facilement expliquer l'évolution générale des dépôts, elle n'explique cependant pas les variations à plus petites échelles enregistrées par les sédiments.

Dans cette étude, 3 séquences de dépôt séparées les unes des autres par des surfaces d'érosion ou des gaps stratigraphiques ont été identifiées dans chacun des transects Néogène étudiés (celui de Pongo de Coñeq au Nord-Ouest et celui d'Inambari au sud) :

1. *Une première séquence pendant le Miocène inférieur à Moyen (et divisée en deux sous-séquences),*
2. *Une deuxième séquence du Miocène supérieur jusqu'au Pliocène,*
3. *Une troisième et dernière séquence de la fin du Pliocène jusqu'au Pléistocène.*

Ces séquences de dépôts sont généralement caractérisées par : i) l'évolution d'un environnement de dépôt continental à deltaïque, ii) des chenaux (fluviaux ou deltaïques) de moins en moins fréquents et plus espacés depuis la base de la séquence jusqu'à son sommet, et iii) une granulométrie de plus en plus grossière vers le haut de la séquence. L'évolution d'un environnement de dépôt fluvial vers un environnement de dépôt côtier (deltaïque) suggère une transition depuis un bassin suralimenté (« overfilled ») à alimenté (« filled »). En tout, trois incursions marines peu profondes ont été documentées dans ce chapitre (au Miocène inférieur, au Miocène moyen vers ~17-15 Ma et au Pliocène à 3,45 Ma). Elles correspondent chacune à la fin d'une séquence ou sous-séquence de dépôt.

Parce ces séquences sont associées à la présence de discordances progressives et à une augmentation du taux de sédimentation, nous suggérons que ces séquences de dépôts correspondent à des cycles du système orogénique andin, depuis des périodes de quiescence tectonique (« unloading ») à des périodes de chargement tectonique (« loading »). Nous interprétons ces rétrogradations successives (continental à deltaïque) comme l'enregistrement stratigraphique de la déformation andine au cours du Cénozoïque . Dans le détail, chacune des séquences de dépôt enregistre une augmentation ou un pulse de l'activité tectonique dans la cordillère Orientale et la zone Subandine actuelle. Ces pulses tectoniques entraînent par flexure lithosphérique une augmentation de l'espace d'accommodation dans le bassin d'avant-pays (chenaux de moins en moins empilés verticalement) et se traduisent finalement par une incursion marine (transition des faciès fluviaux à deltaïques).

Les taux de sédimentation calculés pour le remplissage cénozoïque du bassin de Madre de Dios montrent une forte augmentation à partir du début du Néogène. Cette augmentation est certainement liée au passage et

donc au dépôt de sédiments dans le foredeep. D'autre part, un pulse particulièrement important pour la période du Miocène supérieur à Pliocène a été documenté, interprété cette fois comme la conséquence directe d'un pulse d'activité tectonique. Cette période correspond notamment à un changement climatique important et à l'intensification de la mousson (Mulch et al., 2010; Poulsen et al., 2010; Uba et al., 2007).

Tout comme Uba et al. (2007) l'ont décrit pour le remplissage néogène de l'avant-pays Bolivien, nous proposons finalement d'interpréter Le remplissage néogène de Madre de Dios comme un système fluvial de type « Mégafan » (Rossetti et al., 2012; Wilkinson et al., 2009) ou « Distributive Fluvial System » (Davidson et al., 2013) migrant progressivement vers l'Est et périodiquement envahit par des incursions marines peu profondes. Dans ce cas précis, le système distal du mégafan débouche probablement sur une baie et provoque la formation d'un système deltaïque.

La première incursion marine (25-20 Ma) pourrait correspondre à la phase précoce de développement du méga-système marécageux enregistré en Colombie, au Pérou et dans le bassin intracratonique de Solimoes au Brésil par Hoorn et al. (2010). La seconde incursion (17-15 Ma) correspond probablement à l'incursion Pebas enregistrée plus au Nord. Cependant, les faciès décrits à Madre de Dios ne correspondent pas à ceux déjà décrits pour le Miocene moyen à supérieur (Hoorn et al., 2010). Finallement, la troisième incursion correspond à l'incursion marine la plus récente jamais enregistrée dans le bassin Amazonien et reste mystérieuse quand à son extension et ses connections maritimes extérieures.

Summary:

1. Introduction

The modern foreland basin system adjacent to the central Andes is an exemplary case of a retroarc foreland basin (Horton and DeCelles, 1997; Jordan, 1995; Jordan et al., 1983). In southern Bolivia, this system defines a four component foreland basin system (wedge-top, foredeep, forebulge and backbulge depozones, after (DeCelles and Giles, 1996) mainly characterized by fluvial sedimentation throughout the Tertiary (DeCelles and Horton, 2003; Uba et al., 2005; Uba et al., 2006) interrupted by a Late Miocene marine incursion due to Andean tectonic loading (Uba et al., 2005). In southern Peru, the present-day Madre de Dios foreland basin (Figure 1) does not show this four-components partitioning due to Plio-Pleistocene uplift of the Nazca ridge (Espurt, 2007), even if forebulge and backbulge depozones have been recognized during the Late Maastrichtian to Paleocene times in the Madre de Dios SAZ (Louterbach et al., in preparation, and Part B of the manuscript). Due to very scarce fauna material and the difficulty to access the outcrops in the Amazonian plain, only few studies exist concerning the Cenozoic stratigraphic infilling of Amazonian foreland basin (Gil, 2001; Hermoza, 2004; Roddaz et al., 2010).

The general trend for Neogene deposits is a coarsening upward megasequence evolving from fluvial to alluvial depositional environments (Hermoza, 2004). However, several marine incursions have already been described in the Neogene sedimentary record of the Amazonian foreland basins (Hovikoski et al., 2010; Roddaz et al., 2010). For instance, the existence and persistence of the Early to Middle Miocene Pebas “mega wetland system” in northern Amazonia is thought to have promoted the high biodiversity of the Amazon rainforest (for a review, see (Hoorn et al., 2010) and references therein). A recent synthesis by Hoorn et al. (2010) has highlighted the complex links between Andean building, climate variability and biodiversity development throughout Cenozoic times in the Amazonian basin. These authors emphasized that the potential occurrence of Neogene inland seaway is particularly important not only in promoting biogeographical isolation and allopatric speciation but also in controlling the precipitation rates in the Amazon basin (Jeffery et al., 2012). Consequently, determining the number, timing and duration of Neogene marine incursions recorded in Amazonian basin is fundamental not only for reconstructing paleo-Amazonian landscapes and ecosystems through time but also for understanding the close relationships between Andean building and the Cenozoic climate and biotic evolution of South America. However, the extent of this Pebas system and the number of marine ingressions that have occurred is still under debate mainly because of poor stratigraphic dating and the lack of regional data integration (Campbell et al., 2006; Hoorn et al., 2010; Hovikoski et al., 2007a).

In this study we bring new radiometric, biostratigraphic, subsurface, sedimentological and isotopic data data to reconstruct the Neogene stratigraphic infilling of the South Amazonian foreland basin (Madre de Dios basin, Figure 1).

In particular we document three marine incursions that have occurred in the Early Miocene, Middle Miocene and Pliocene-Pleistocene times and document how the different stages of the sedimentary filling are controlled by the complex interplay of tectonic loading subsidence and increasing sedimentary supply caused by surface uplift and relief acquisition in the Andes.

2. Geological setting

The Madre de Dios basin is part of the southern Amazonian foreland basins system (Roddaz et al., 2005b). It is located to the northeast of the Eastern Cordillera (EC) of southern Peru and can be subdivided into the Sub-Andean Zone (SAZ) and the Madre de Dios plain foredeep (Gil, 2001; Hermoza, 2004) (Figure 1). The SAZ is characterized by both sedimentary filling and active deformation. In the SAZ, propagation of deformation towards the Madre de Dios foredeep is controlled by the development of deep duplexes, whose shortening is accommodated in surface by imbricates and by the Sub-Andean thrust front. The Sub-Andean thrust front corresponds to the northeastern border of the SAZ and is responsible for the transportation of two piggy-back basins, which outcrops as two large synclines called the Salvación and the Punquiri synclines. The Salvación syncline is located in the north-western Madre de Dios SAZ termed hereafter "Pongo de Coñeq SAZ" whereas the Punquiri syncline is situated in the south-western Madre de Dios SAZ and is referred in the following as "Inambari SAZ" (Figure 1).

Cenozoic strata in the Salvación piggy-back basin consist of ca. 4000 m of deposits traditionally interpreted as mostly fluvial (Roddaz et al., 2010) . The basal Late Paleocene strata have recently been interpreted as estuarine or bay deposits that are unconformably overlaid by Neogene strata. Eocene or Oligocene deposits are absent (Louterbach et al., Submitted) (See also Part C of this PhD).

The Cenozoic filling of the Punquiri syncline consists of more than 5000 m of sediments originally interpreted as mainly deposited in fluvial to alluvial environments (Roddaz et al., 2010). Contrary to former studies (Gil, 2001; Hermoza, 2004), we documented no Paleocene deposit at the base of the syncline.

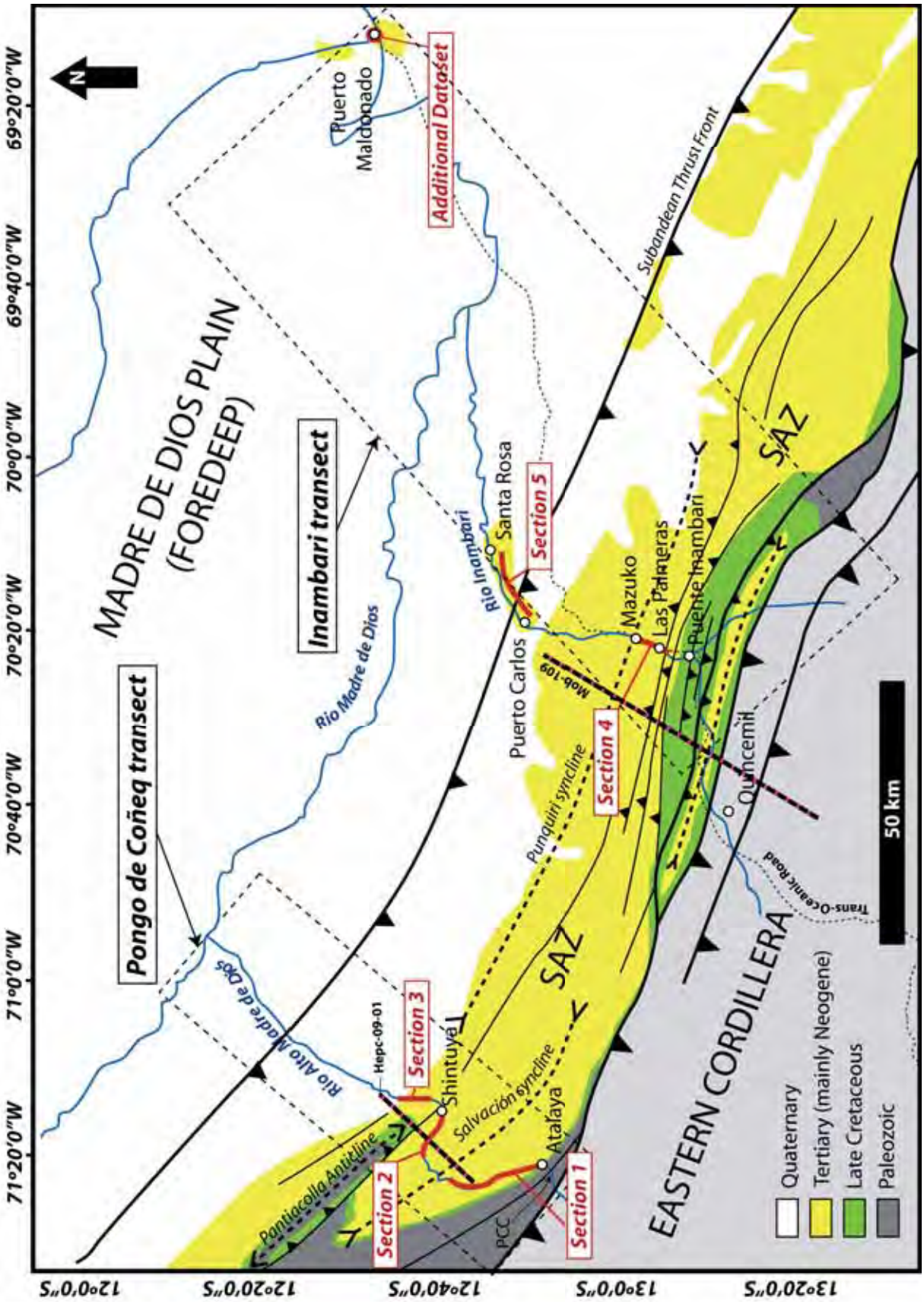

Figure 1: Simplified geological and structural map of the Madre de Dios foreland basin. Sedimentary sections described in this study are localized along the Alto Madre de Dios River (section 1, 2 and 3), in the Pongo de Coñeq SAZ and along both the Inambari River and the Interoceanic road in the Inambari SAZ (sections 4 and 5). Additional set of data is localized near Puerto Maldonado city. SAZ= Sub-Andean Zone. PCC=Pongo de Coñeq Canyon.

3. Former stratigraphic studies

The chronostratigraphy of the southern Amazonian foreland basin is supported by palynological data (Carpenter and Berumen, 1999; Cooperación Técnica Peruana-Alemana, 1982; Gutierrez, 1982; Valdivia, 1974), thermochronological analysis (Apatite to Zircon Inc., 2004; Hermoza, 2004) and radiometry ($^{40}Ar/^{39}Ar$ on feldspar and biotites (Campbell et al., 2001; Gil, 2001; Mobil Oil Corporation, 1998)). These data are scarce, and were not sufficient to construct a precise chronostratigraphic chart until now. Two principal reasons can explain the lack of stratigraphic constraints in the Madre de Dios basin: (1) outcrops are scarce and difficult to access in the Amazonia, and (2) the Neogene sedimentary record offers very poor paleontological and palynological material to date in this area.

Despite these difficulties, W. Gil (2001), W. Hermoza (2004) and more recently M. Roddaz (2010) realized synthetic studies about the stratigraphy of the Madre de Dios basin using published results and additional well data from the industry (Karene and Candamo wells). According to these authors, three Cenozoic stratigraphic units are traditionally observed in the SAZ of the Madre de Dios foreland basin: the Paleocene Huayabamba formation, the Miocene Ipururo Group and the Plio-Pleistocene (?) Mazuko formation (Gil, 2001; Hermoza, 2004). In the foredeep, three stratigraphic units have been documented: the Paleocene Huayabamba Fm., the Miocene Ipururu Group and the Late Miocene to Pliocene Madre de Dios Fm. (Campbell et al., 1996; Campbell et al., 2001; Gil, 2001; Hermoza, 2004).

In the SAZ, the Ipururo Group (Valdivia, 1974) comprises Late Oligocene to Miocene deposits of southern Peru and Bolivia. In Bolivia, the Ipururo group is divided into three formations (Roddaz et al., 2010): the Bala Formation, the Quendeque Formation and the overlying Charqui Formation. These formations were traditionally interpreted as fluvial to alluvial formations (Gil, 2001; Hermoza, 2004; Roddaz et al., 2010). However, alluvial, deltaic an estuarine coastal plain facies have been described in the Miocene Bolivian Quendeque formation (Hovikoski et al., 2007b; Hovikoski et al., 2007c). In the Bolivian Beni-Mamore basin which is adjacent to the Madre de Dios basin, Roddaz et al. (2006) also described Miocene tidal-influenced deposits.

In the Peruvian foredeep, the Ipururo Group comprises the Ipururo Formation and Unit A and B of the Madre de Dios Formation *sensu* Campbell et al. (2001). Based on stratigraphic correlations, the Ipururo Formation is estimated to be Miocene in age (Hermoza, 2004). The Ipururo Formation is continuously present in wells and seismic sections all along the Madre de Dios foredeep and the Madre de Dios Formation also outcrops continuously across the Madre de Dios foredeep. Subsurface data indicate that the thickness of the Ipururo Formation ranges from 1100 to 1300 m. The upper part of the Ipururo Formation consists of subtidal channel sediments deposited in a tide-dominated delta (Roddaz, 2004). The Madre de Dios Formation is Late Miocene ($^{40}Ar/^{39}Ar$ dating on feldspars at 9.01 ± 0.28 Ma, Campbell et al. 2001). The Madre de Dios Formation can thus be considered as a lateral equivalent of the Bolivian Charqui Formation (Roddaz et al., 2010).

According to subsurface data (seismic and wells), the thickness of the Madre de Dios Formation is fairly constant (~400 m according to Hermoza, 2004). The Unit A and B of the Madre de Dios Formation were interpreted to have been deposited in tide-dominated estuaries (Hovikoski et al., 2005; Roddaz et al., 2006).

4. Material and methods

4.1. Sedimentary facies, stratigraphic sections and correlations

In the north-western part of the Madre de Dios basin, Neogene deposits crop out along the Alto Madre de Dios River between the Pongo de Coñeq Canyon and the Pantiacolla anticline, which both correspond to the southern and the northern flanks of the Salvación Syncline, respectively (Figure 1). In this area, we studied 3 stratigraphic sections along the banks of the Alto Madre de Dios River: i) across the south-western flank of the Salvación syncline, between the locality of Salvación and the axis of the syncline (Section 1), ii) across the northeastern flank of the Salvación syncline, near the village of Shintuya (Section 2) and iii) across the northern flank of the Pantiacolla anticline (Section 3).

In the south-eastern part of the Madre de Dios basin, Neogene deposits crop out along the Inambari River, from the south-western flank of the Punquiri syncline towards the Madre de Dios foredeep (Figure 1). In this south-eastern area, two stratigraphic sections have been studied: i) one along the Inambari River across the southern flank of the Punquiri syncline, near the locality of Las Palmeras (section 4) and ii) along both the Transoceanic road and the Inambari River, from the locality of Puerto Carlos (River cut banks) to the locality of Santa Rosa (road cuts) (Section 5). Isolated outcrops have been studied in the Madre de Dios foredeep near Puerto Maldonado city (La Pastora harbour, situated along the Rio Madre De Dios cut banks). They constitute the most distal outcrops we described in this study.

For each section, sedimentological descriptions, biostratigraphical and paleontological analysis have been carried out. We present in this chapter 28 new biostratigraphic results, 1 new AFTA result interpreted as detrital age and 1 new $^{40}Ar/^{39}Ar$ radiometric age (see Table 1 and Table 2). Paleontological material collected on field in 2012 is also presented, and some fossil of interest (outcrops/samples MD 61 and MD 67) have already been published (Antoine et al., 2013b; Marivaux et al., 2012). These data helped us to establish a new chronostratigraphic framework for the Madre de Dios Neogene sedimentary infilling. For precise geographic situation of the samples, please refer to Annex-Maps 4 to 8. Detailed biostratigraphic results can also be consulted in Annexes nº2, 3, 6 and 7. Precise stratigraphic dating results from both areas have been projected onto 2D seismic sections: stratigraphic sections 2 and 3 were projected onto seismic section Hepc-09-01 for the Pongo de Coñeq transect whereas stratigraphic sections 4 and 5 have been projected onto seismic section Mob-109 for the Inambari transect (Figure 1). Then, along strike stratigraphic correlations have been made between the Pongo de Coñeq and the Inambari SAZ, using other available 2D seismic lines: Hepc-09-02, Hepc-09-04, Hepc-09-05, Hepc-09-06, Hepc-09-016, Hepc-09-17 and Hepc-09-18 (see locations of seismic sections in Annex-Map 2 and correlations in Part A of this PhD). Finally, correlations between the Inambari sections (from the southwest to the northeast) were made based on additional sedimentary

observations and biostratigraphical data collected in Santa Rosa (section 5) and Puerto Maldonado (see additional dataset in Figure 1).

Twenty-one sedimentary facies were defined on the basis of their lithologies, their physical and biogenic sedimentary structures, their palynological and palaeontological content, and their geometries (Table 1, Table 2 and Table 3). Natural affinities with modern taxa and their present habitat (see interpretations in Table 1 and Table 2) were taken from Lorente et al. (1986), Latrubesse et al. (2007), and Hoorn (1993). Special care was taken in the recognition of marine or marine-related faunas and facies associations.

On the basis of these interpretations and with regards to the geometrical relationships between the facies, six facies associations are proposed (Table 4).

4.2. Sedimentation rates and burial history

Burial history and sedimentation rates were computed with PetroMod-1D software (Schlumberger) for both the Pongo de Coñeq and the Inambari sections. In order to observe the overall trend of sedimentation rates evolution during Cenozoic period, we started the model from Late Cretaceous times and stoped it to present-day. The method is based on the decompaction of the sedimentary record and on the removing of sediment loading (backstripping procedure). For such analysis, data on strata thickness, lithology, age constraints, paleobathymetry, surface-water interface temperature and heat flux were required. All data but surface-water temperature and heat flux were provided by the dataset and the interpretations we present in this study. Surface-water interface temperature (SWIT) was automatically computed using the automatic "auto-SWIT" parameter (Wygrala, 1989) available in the PetroMod software for a mean latitude of 16ºS in the South American continent. Heat Flux was determined in function of the geodynamic context from the Late Cretaceous to present-day (from 85 mW/m^2 to 60 mW/m^2). Detailed input data and boundary conditions are available for each model on Supplementary Data 1.

4.3. Nd-Sr isotopic analysis

Eleven mudstones from sections 1, 2 and 3 in the Pongo de Coñeq area and from section 4 in the Inambari area were measured at the University of Toulouse for their Nd-Sr isotopic compositions. Aliquots containing about 1000 mg of Sr and Nd were loaded onto the ion-exchange columns. Sr and Nd were separated using the Sr-SPEC, TRU-SPEC and LN-SPEC resins (Eichrom®). Nd-Sr isotopic ratios were measured using a Finnigan Mat 261 thermal ionization mass spectrom in dynamic mode following Viers et al. (2008). The measured $^{143}Nd/^{144}Nd$ ratios are presented as the fractional deviation in parts per 10^4 (units) from $^{143}Nd/^{144}Nd$ in a Chondritic Uniform Reservoir (CHUR) as measured at the present-day:

$$\varepsilon Nd(0)= [(^{143}Nd/^{144}Nd)_S/I_{CHUR}(0)\_1]*10^{4,}$$

where $(^{143}Nd/^{144}Nd)_S$ is the present-day ratio measured in the sample, and $I_{CHUR}(0)$ is the $^{143}Nd/^{144}Nd$ in the CHUR reference reservoir at the present ($I_{CHUR}(0)$ = 0.512638 (Jacobsen and Wasserburg, 1980).

5. Results

5.1. Stratigraphic dating and correlations

5.1.1.Pongo de Coñeq transect

5.1.1.1. Biostratigraphy

In the northeastern Salvación syncline, three localities (MD 61, MD 84bis=62 and MD 67; see Annex-Map 4, Annex-Map 5 and Annex-Map 6 for location) have yielded paleontological material and led to stratigraphic and paleobiological results (see Table 1 for exhaustive list).

Outcrop MD 61 corresponds to the most basal and oldest deposits analyzed for this study in the Salvación syncline. It yielded the typical Pinturan dinomyid rodent *Scleromys quadrangulatus*, which has been found associated to a well-preserved right talus of a small-bodied anthropoid primate (MUSM-2024, see Marivaux et al., 2012). According to the authors, MD 61 is thus related to Early Miocene times ("Pinturan biochronological unit ~18.75-16.5 Ma, see Marivaux et al. (2012) in Annex 6).

Just above MD 61, MD 67 outcrop yielded the first early middle Miocene vertebrate fauna ever described in the Peruvian Amazonia (Antoine et al., 2013a): the marsupials Sipalocyon sp. (Hathlyacynidae) and Marmosa (Micoureus) cf. laventica (Didelphidae), as well as an unidentified glyptodontine xenarthran and the rodents Guiomys sp. (Caviidae), "Scleromys" sp., cf. quadrangulatus-schurmanni-colombianus (Dinomyidae), Acaremys sp. (Acaremyidae), and cf. Microsteiromys sp. (Erethizontidae). According to the authors, detrital AFT ages (17.1+/-2.4 M)a and additional biochronological results (Colloncuran South American Land Mammal) are concordant for the locality.

Finally, MD 84bis=62 outcrop yielded diverse paleontological material (see Table 1) related to Middle Miocene times (15-13 Ma, Antoine et al., in preparation).

Miliammina foraminifer facies zone (*Miliammina–Trochammina* or *Miliammina-Nothia latissama* associations) corresponds to a Neogene time period (Grzybowski, 1898; Heron-Allen and Earland, 1930). This zonation has been recognized in several samples collected in the Salvación syncline (see Table 1). In some cases (e.g. MD 61), *Miliammina* facies zone is associated with *Bathysiphon* foraminifera, indicating a Late Oligocene to mainly Miocene stratigraphic interval (Carpenter and Berumen, 1999). Palynomorphs *Echitricolporites spinosus* and *Multimargenites vanderhammeni* are found in MD 189 and MD 246, which represent the uppermost strata described in the Salvación syncline, and are characteristic of the Late Miocene (Mobil Oil Corporation, 1998). However we found other palynomorphs better suggesting a Late Miocene to Pliocene period (Table 1).

5.1.1.2. AFT analysis

MD 67 AFT age has been interpreted as an Early Miocene detrital age (Antoine et al., 2013). MD 68 AFT age indicates an Oligocene age (30.3 +/- 3 Ma), which is older than the age inferred from its stratigraphic position. This age is also interpreted as a detrital age. For details related to AFT method and results, refer to Part A of the manuscript (Part A-Table 3).

5.1.1.3. Stratigraphic correlations and seismic interpretation

Results from biostratigraphy as well as sedimentological observations from the Salvación syncline have been projected along seismic section Hepc-09-01 (see Figure 1 for location and Figure 3 for the interpretation of the seismic line).

From northeast to southwest, seismic line Hepc-09-01 shows the Pantiacolla anticline and the northeastern flank of the Salvación syncline. Outcrops with stratigraphic constraints from sections 2 and 3 have been projected onto the seismic profile Hepc-09-01 and four significant seismic markers have been interpreted for the Cenozoic interval based on their proximity to biostratigraphic constraints on surface (Figure 3):

- T1 marker corresponds to MD 67 outcrop in surface and is thus related to an Early Middle Miocene horizon
- T2 marker is stratigraphically located just below outcrop MD 189/66 and is thus related to a Late Miocene to Early Pliocene age
- Due to its stratigraphic position, T3 marker is probably Pliocene in age.
- T4 marker is the uppermost seismic marker interpreted here and it corresponds to the youngest main erosive surface documented in the overall Cenozoic filling. It is thought to be Pliocene to Quaternary in age.

The pink seismic marker situated between T1 and T2 probably corresponds to an erosive surface and is only visible in the northern Pongo de Coñeq SAZ. These kind of progressive erosive surfaces are frequent within the Neogene sedimentary filling of both the Salvación and the Punquiri synclines. They are interpreted as progressive unconformities linked to Neogene thrust deformation (see Part A).

On the bases of biostratigraphical results related to stratigraphic section 1, 2 and 3 and of seismic markers continuity visible on seismic line Hepc-09-01 (Figure 3), stratigraphic correlations from the well-constrained northern flank of the Salvación syncline toward the southern flank are then proposed (Figure 2).

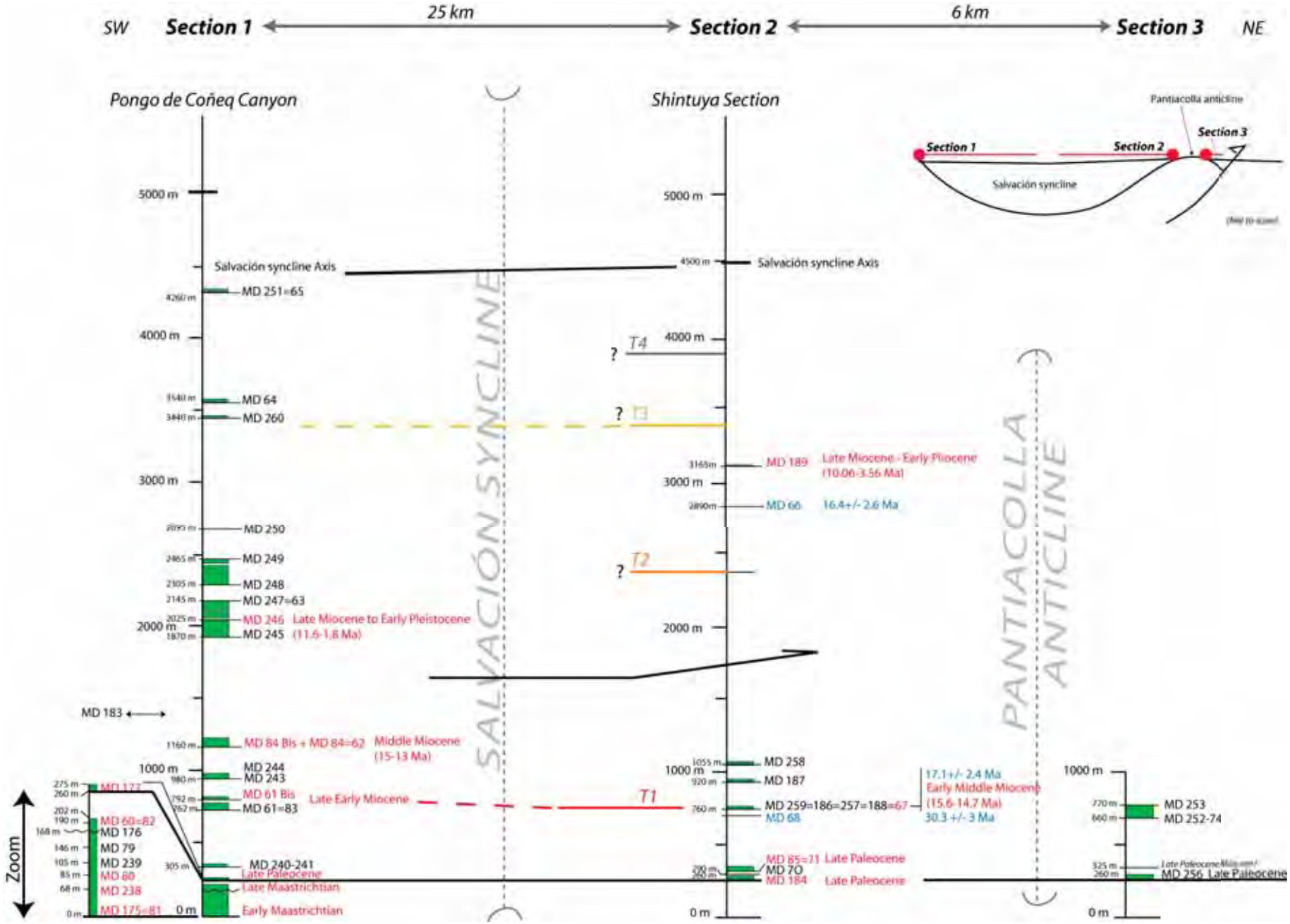
SW
Section 1
25 km
Section 2
6 km
Section 3
NE
Pongo de Coñeq Canyon
Shintuya Section
Pantiacolla anticline
Section 1
Section 2
Section 3
Salvación syncline
5000 m
Salvación syncline Axis
MD 251=65
4000 m
T4
MD 64
MD 260
MD 189
Late Miocene - Early Pliocene
(10.06-3.56 Ma)
3000 m
MD 66
16.4+/- 2.6 Ma
MD 250
MD 249
MD 248
MD 247=63
MD 246
Late Miocene to Early Pleistocene
MD 245
(11.6-1.8 Ma)
2000 m
T2
MD 183
MD 84 Bis + MD 84=62
Middle Miocene
(15-13 Ma)
1000 m
MD 244
MD 243
MD 61 Bis
Late Early Miocene
MD 61=83
T1
MD 258
MD 187
MD 259=186=257=188=67
MD 68
17.1+/- 2.4 Ma
Early Middle Miocene
(15.6-14.7 Ma)
30.3 +/- 3 Ma
MD 253
MD 252-74
MD 177
MD 60=82
MD 176
MD 79
MD 239
MD 80
MD 238
MD 175=81
MD 240-241
Late Paleocene
Late Maastrichtian
Early Maastrichtian
MD 65=71
Late Paleocene
MD 70
MD 184
Late Paleocene
MD 256
Late Paleocene
0 m
Zoom
SALVACIÓN SYNCLINE
PANTIACOLLA ANTICLINE

Figure 2 (previous page): Daring results and stratigraphic correlations between the different sedimentary sections measured in the Salvación syncline and the Pantiacolla anticline, along the Pongo de Coñeq transect. Green rectangles correspond to the observations made on field. T1, T2, T3 and T4 correspond to significant seismic markers interpreted from 2D seismic line Hepc-09-01 (Figure 3). MD=Samples/Outcrops. See Figure 1 for location of stratigraphic sections 1, 2 and 3.

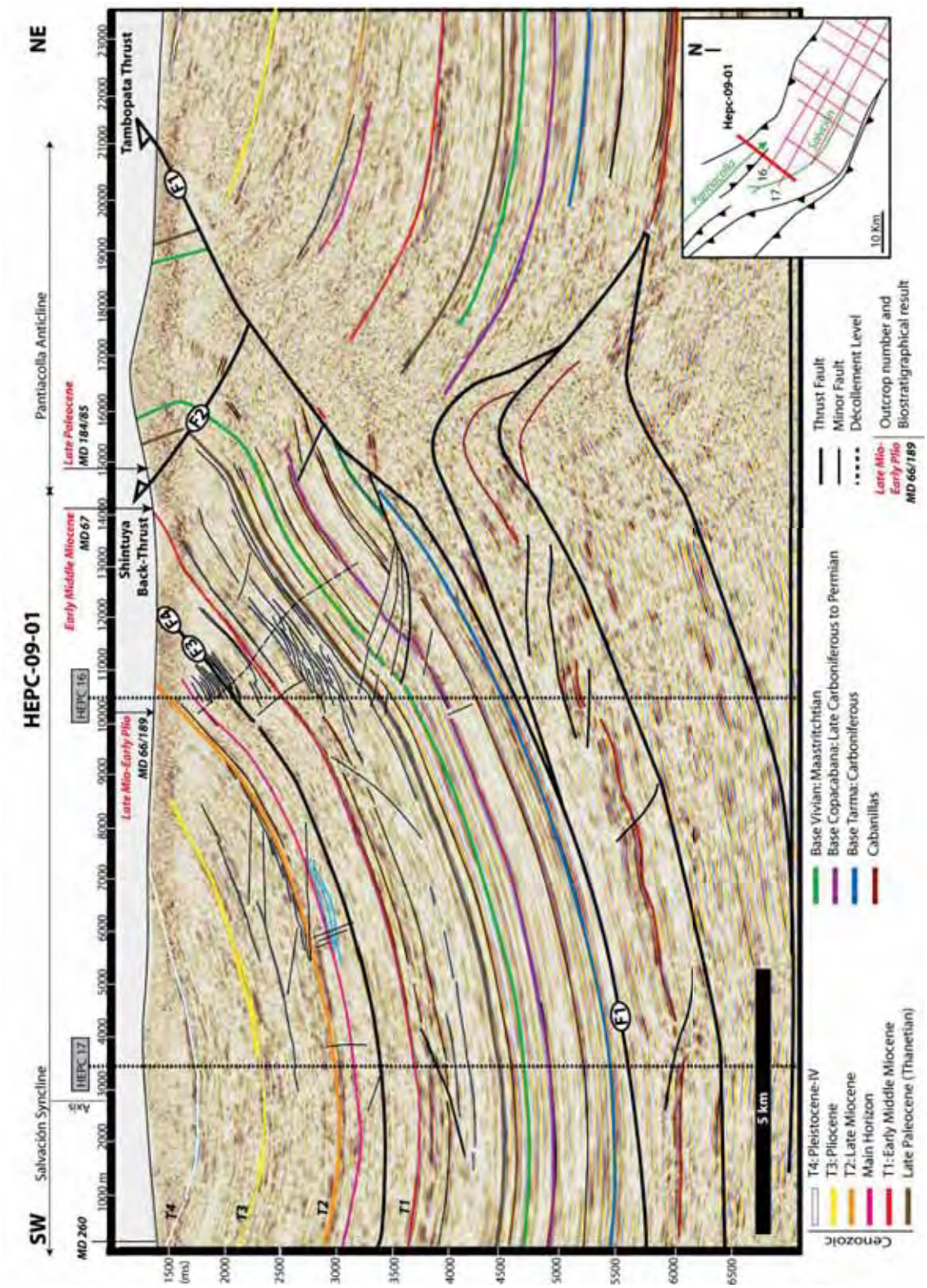

Figure 3: 2D seismic line Hepc-09-01, showing the Salvación syncline and the Pantiacolla anticline in the Pongo de Coñeq SAZ transect. Samples with biostratigraphic constraints have been localized on the section and used to date significant seismic horizons (T1, T2, T3 and T4). See Figure 1 for location of the seismic line. See chronostratigraphic chart from Part A/Figure 8 for pre-Neogene Formations names.

5.1.2. Inambari transect

5.1.2.1. Biostratigraphy

The Inambari sedimentary section has fewer biostratigraphical constraints than the Pongo de Coñeq section (Annex-Map 7 for samples collected along section 4). The base of the section is constrained by MD 198 outcrop which palynological content indicates a Miocene to Pliocene age (see Table 2). Stratigraphically above MD 198, the MD 201=155 outcrop yield Early Miocene palynomorphs (*Echinatosporis brevispinosus*and *Echitricolporites spinsosus*species, Jaramillo et al. (2010)). The presence of *Echitricolporites spinsosus* and *Psilabrevitricolporites devriesii* supports a Miocene to Early Pleistocene age for the overlying MD 202 deposits. In the uppermost strata (section 4), the MD 204 outcrop yield Early to Middle Miocene palynomorphs such as *Echitricolporites spinsosus*and *Polypodiaceosporites fossulatus*. In the Santa Rosa section (section 5) palynomorphs and microfossils from MD 208 outcrop suggests a Late Miocene to Pleistocene age (Table 2). In the Madre de Dios foredeep (Puerto Maldonado area), palynomorphs from outcrops MD51 and MD325 support a Pliocene to Pleistocene age (Table 2). This is in agreement with published $^{40}Ar/^{39}Ar$ radiometric dating of a tuffaceous level suggesting a 3.12 +/- 0.02 stratigraphic age for the Neogene strata described in the same area (Campbell et al., 2001).

5.1.2.2. Radiometry and AFT ages

Ar/Ar dating on biotite has been measured on a tuffaceous sample recently collected in the Punquiri syncline (MD 204, section 4). This sample gave a Pliocene age (~3.45 ± 0.15 Ma). Consequently, MD 204 locality provided two non-consistent biostratigraphic and radiometric results, as palynology indicates an Early-Middle Miocene age (17.41-13.17 Ma). Sedimentary reworking certainly causes the age inconsistency for this sample. On the basis of the stratigraphic position of the considered strata, of the seismic interpretation of the Punquiri syncline and because of the precision of the radiometric $^{40}Ar/^{39}Ar$ dating in comparison with the biostratigraphical method accuracy, we decided to interpret MD 204 as Pliocene.

AFT age obtained from MD 22 (section 4) corresponds to an Early-Middle Miocene detrital age (14.4 +/- 3.5 Ma) and is consistent with palynological results (Miocene to Early Pleistocene).

AFT age obtained from the overlying MD 204=20 outcrops suggests a Late Miocene age (7.20 +/- 2.7 Ma). This age is considered as a detrital age as radiometric data indicates a 3 Ma.

5.1.2.3. Stratigraphic correlations and seismic interpretation

Field observations and biostratigraphic results from the Inambri area have been projected onto 2D seismic line Mob-109 (Figure 1 for location of the seismic line). However, fewer data exist for the Inambari area. The Neogene sedimentary infilling of the Punquiri syncline is mainly interpreted based on section 4. Santa Rosa section (section 5) and Puerto Maldonado dataset correspond to isolated outcrops so that precise correlations between the two flanks of the Punquiri syncline are somewhat tentative.

2D Seismic line Mob-109 crosses over the Punquiri syncline and stops nearby the village of Santa Rosa towards the northeast.

On its south-western flank, the Punquiri syncline is transported onto a duplex (internal duplex) accommodated in surface by several southwest-verging back-thrusts and northeast-verging thrusts (Figure 5). These thrusts developed into Paloegene (?) - to Neogene strata corresponding to the basal sedimentary infilling of the syncline. Two main thrusts are of relative importance for this study: Thrust Fault-A located nearby outcrop MD 198 and the Thrust Fault-B located nearby outcrop MD 202 (Figure 5). The latter thrust could explain the absence of part of the Middle to Late Miocene strata as outlined by the biostratigraphical results (stratigraphic gap between MD 201 and MD 202, Figure 4). Seismic marker T3, interpreted to be Pliocene in age, is situated just below MD 202 outcrop, estimated to be Miocene to Early Pleistocene in age. Finally, seismic marker T4 is stratigraphically above outcrop MD 204 (dated ca 3.45 Ma) and very close to outcrop MD 206 so it is interpreted to be Pleistocene (Figure 4 and Figure 5). The Santa Rosa section corresponds to the northern edge of seismic line Mob-109. MD 159 and MD 160 outcrops of the upper part of Santa Rosa section are situated above seismic marker T4 whereas the rest of the Santa Rosa section is probably below it (Figure 4 and Figure 5). Because the lower part of the Santa Rosa section suggests a Late Miocene to Pleistocene age interval (see biostratigraphic results related to outcrops MD 208=207=310=13, Table 2), the Santa Rosa section is stratigraphically above seismic marker T3 (Figure 4 and Figure 5).

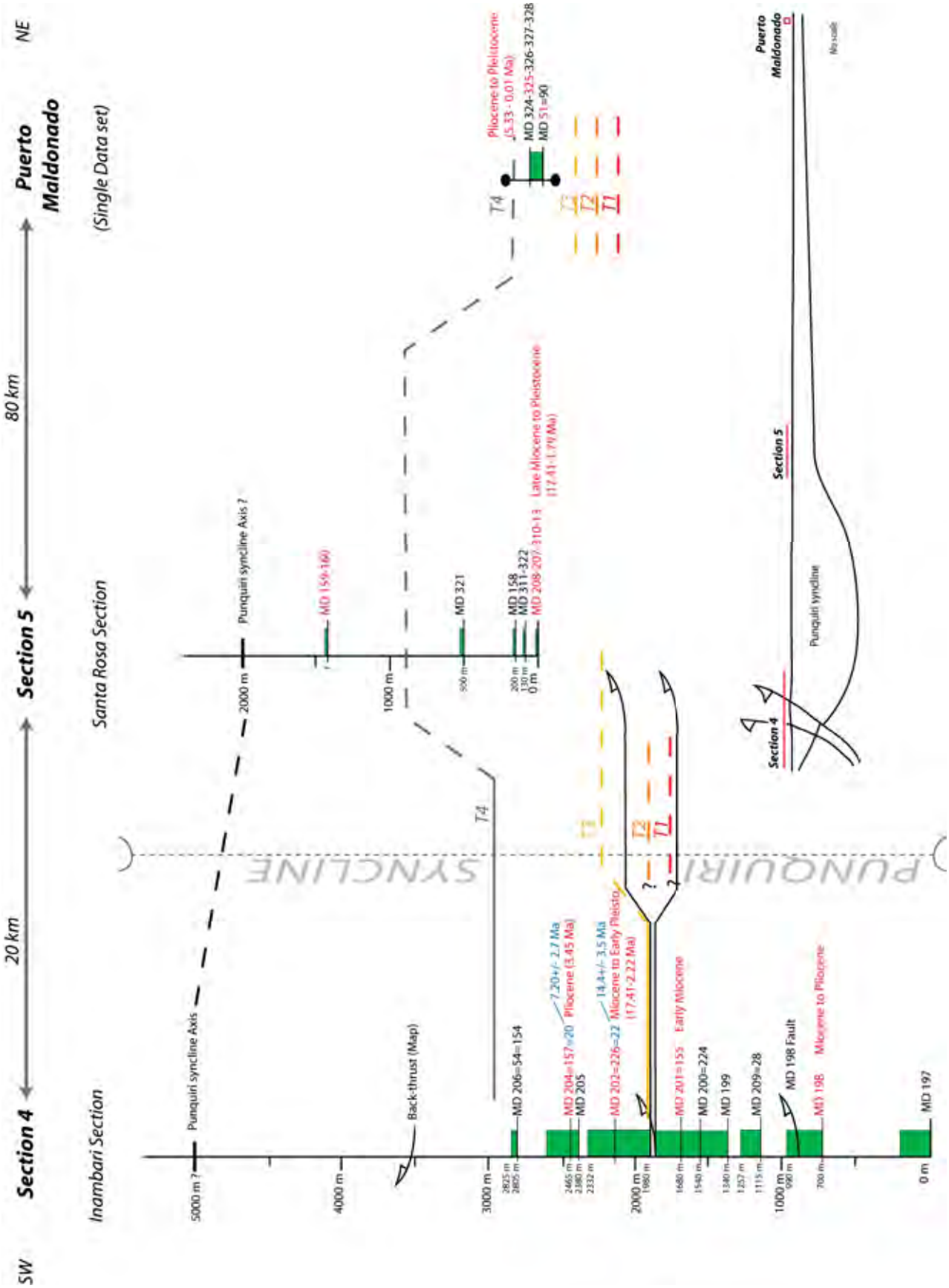

Figure 4: Dating results and stratigraphic correlations between the different sedimentary sections measured in the Punquiri syncline (section 4), near Santa Rosa (section 5) and near the city of Puerto Maldonado, along the Inambari transect. Green rectangles correspond to the observations made on field. T1, T2, T3 and T4 correspond to seismic markers interpreted from 2D seismic line Mob-109 (see Figure 5). MD=Samples/Outcrops. See Figure 1 for location of stratigraphic sections.

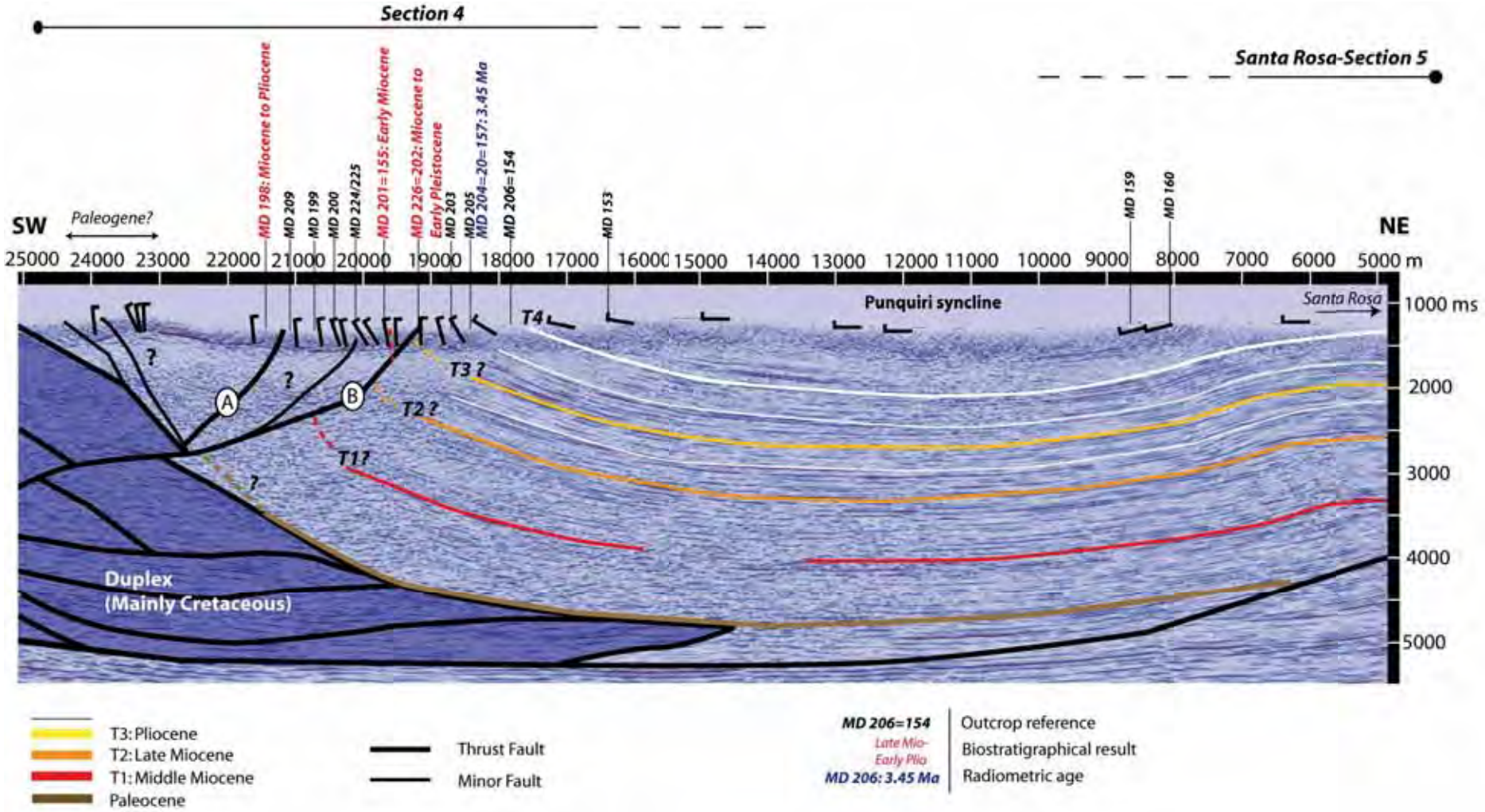

Figure 5: 2D Seismic line Mob-109 in the Inambari transect, focusing on the Tertiary sedimentary filling of the Punquiri syncline (Section 4). Projection of Section 5 (Santa Rosa) is partially visible to the NE of the seismic line. Puerto Maldonado data set is located more than 80 km from the Santa Rosa section toward the north. Samples with biostratigraphic constraints have been located on the section and used to recognize and place seismic horizons T1, T2, T3 and T4 already interpreted in the Pongo de Coñeq transect (see seismic line Hepc-09-01). See Figure 1 for location of the seismic line.

5.2. Paleoenvironmental constraint from palynological and paleontological record

Miliammina foraminifera (*Miliammina fusca, Miliammina velatina*) and *Miliamina-Trochammina* facies association are characteristic of coastal swamp. Association with the benthic foraminifera *Bathysiphon* confirms the influence of such a saline incursion.

The most recurrent marine-related palynomorphs found in the Neogene Madre de Dios deposits are *Echiperiporites stellae* and *Deltaidospora adriennis* species. The other palynomorph and fossils indicators of hyaline aquatic conditions found in the Tertiary deposits described in this study are listed in Table 1 and Table 2 (marine-related localities are colored in blue in both Tables).

In the Pongo de Coñeq area, such coastal-related associations have been found in MD 61, 244 (Bathysiphon sp.) and 246 outcrops. In the Inambari area, MD 198, MD 204, MD 208, MD 13 and MD 51 outcrops have also yielded coastal-related palynomorphs and microfossils (Table 1 and Table 2).

Except occasional coastal-related palynomorphs and microfossils, a high proportion of continental palynomorphs and microfossils have been found all across the sections in both the Pongo de Coñeq and the Inambari transects (see colorless localities in Table 1 and Table 2).

Paleontological material also brings important information about the paleo-environmental conditions. Put together, both the mammalian assemblage and lithology of the fossil-bearing level in MD 67 outcrop point to a mixture of tropical rain forest environment and more open habitats under a monsoonal-like tropical climate (Antoine et al., 2013b). Formerly interpreted as having formed in a meandering-fluvial and thus continental environment (Marivaux et al., 2012), sedimentary rocks of MD 61 outcrop are finally interpreted in this study as deposited in a coastal environment on the basis of the presence of benthic foraminifera such as Bathysiphon and Miliammina spp. (Table 1).

Sample	AF	1	2	3	4	Age (Ma)		Depositional Environment	*Material*
MD 189	FCs (Fbl)	x				10.06-3.56	Late Miocene-Early Pliocene	Undetermined (continental)	*Deltoidospora adriennis, Dicolpopollis sp., Echitricolporites spinosus, Fenestrites longispinosus, Monoporopollenites annulatus, Multimargenites vanderhammeni, Polypodiaceoisporites pseudopsilatus, Polypdodiisporites sp., Proteacidites triangulatus Psilatricolpites minutus, Psilatriletes lobatus, Retipollenites crotonicolumellatus, Unknown trilete spores, monolete spores and pollen grains*
MD 246 A	Csw (Ft)	x				23.03-5.332	Miocene (?)	Paralic environment ?	*Crab material*
MD 246 B		x	x			23.03-5.332	Miocene (?)	Coastal swamp? Unstable floor, rapid sedimentation	***Benthic foram.?, Miliammina fusca.***
MD 246 Bio	Csw (Fb)	x	x			11.608-0.0115	Late Miocene to Pleistocene	FORAM: Coastal swamp PALY: Continental	***Miliammina fusca, Deltaidospora sp.**, Monoporites annulatus, Laevigatosporites spp, Clavatriletes sp., Laevigatosporites tibuensis, Polipodiisporites spp., Lycopodium foveolate, Selaginella type, Echitricolporites spinosus, Monoporites annulatus, Psilatricolporites spp., Malvaceous pollen, Tetraploa spp.*
MD 84 bis 1= 62	FCs (Gt)			x		15-13	Middle Miocene	Continental (fluvial)	*Osteichthyes, Characiformes, Serrasalmidae indet. (pacu-like), Eusuchia, Gavialoidea indet., Mammalia, Notoungulata, Toxodontidae indet., ? Dinotoxodontidae, left P3, Mammalia, Rodentia, Caviomorpha indet.*
MD 244 Bio	Csw (Fb)	x	x			23.03-5.332	Miocene	Coastal swamp? Unstable floor, rapid sedimentation	*Benthic foram. ?:* ***Bathysiphon sp.***
MD 67	FCs (Fb)			x		15.6-14.7	Early Middle Miocene	Continental (fluvial, tropical monsoon-like climate). Mixture of tropical rain forest environment and more open habitats under a monsoonal-like tropical climate. Fully fluvial origin of the concerned sedimentary sequence.	*Mammalia, Marsupialia, Sparassodonta, Hathlyacynidae, Sipalocyon sp., Mammalia, Marsupialia, Didelphimorpha, Didelphidae, Marmosa (Micoureus) cf. laventica, Mammalia, Xenarthra, Cingulata, Glyptodontidae, Glyptodontinae indet., Mammalia, Rodentia, Caviomorpha, Dinomyidae, "Scleromys" sp., cf. quadrangulatus-schurmanni-colombianus, Mammalia, Rodentia, Caviomorpha, Acaremyidae, Acaremys sp., Mammalia, Rodentia, Caviomorpha, Caviidae, Guiomys sp., Mammalia, Rodentia, Caviomorpha, Erethizontidae, cf. Microsteiromys sp., Mammalia, Notoungulata indet., Tooth fragment*
MD 67					x	17.1-2.4	Early Miocene	Undetermined	*No material*
MD 68	(FCs)				x	30.3 +/- 3	Oligocene	Undetermined	*No material*
MD 61 Bio A	Csw (Fl)	x	x			17.5-16.5	Miocene	Marine influence?	*Benthic foram.?:* ***Miliammina sp.**, Nothia latissima*
MD 61 Bio B		x	x			17.5-16.5	Miocene	Marine influence?	*Benthic foram.?:* ***Bathysiphon sp.***
MD 61 Bio C		x				17.5-16.5	Miocene (?)	Undetermined	*Reworked vertebrate material*
MD 61 Bio F		x	x			17.5-16.5	Miocene	Swamp, unstable floor. Marine influence?	*Benthic foram.?:* ***Miliammina sp.***
MD 61.1 and 61.2 ?	CCs (Stmc)			x		17,5-16.5	Late early Miocene	Continental (fluvial). = Pinturan, Santacrucian SALMA, 17.5-16.5 Ma	*Mammalia, Xenarthra, Cingulata, Dasypodidae, Euphractinae indet. (mobil band osteoderm, distal fragment, MUSM 1978) Mammalia, Xenarthra, Pilosa, Megatherioidea (distal phalanx, right hand, MUSM 1976)Mammalia, Xenarthra, Pilosa indet. (first phalanx Mt4), Mammalia, Rodentia, Caviomorpha, Dinomyidae, Scleromys quadrangulatus ["Pinturan"], Mammalia, Rodentia, Caviomorpha indet., sp. 2, Platyrrhini, Cebidae, Cebinae indet., right astragalus (MUSM 2014), Mammalia, Notoungulata indet., Aves, Gruiformes, Gruidae indet., tibiotarsus (distal)*

Table 1: Samples list, type of analyses done (1 to 4), depositional environments interpretations and biostratigraphic constraints for the Neogene strata of the Salvación syncline (Pongo de Coñeq transect). AF= interpreted Facies Associations and Facies related to the samples. Facies are shown between brackets. 1: Palynology. 2: Microfossil analysis. 3: Paleontology. 4: AFTA analysis. Grey-colored file related to MD 67 locality has already been published (Antoine et al., 2013b). Blue lines correspond to marine-related localities. See Figure 2, Figure 13 and Figure 14 for location of samples on stratigraphic sections.

Samle	AF	1	2	3	4		Age (Ma)	Depositional Environment	*Material*
MD 325 Bio	C	x					Pliocene to Pleistocene	Continental swamp (Ferns).	*Hemitelia horrida, Psilatriletes spp., Polipodiaceoisporites pseudopsilatus, Cystopteris type, Verrutriletes spp., Laevigastoporites spp., Polypodiisporites spp., Elaphoglosus type, Polypodium type, Cingulatisporites sp., Echitriletes cf. mulleri. Polen: Monoporites annulatus*
MD 51 PN1	C	x	x				Pliocene to Pleistocene	Continental to coastal swamp, near base level (brackish water, slight marine incursion).	*Benthic foram.: Facies zone "Miliammina", **Miliammina velatina,** Cingulatisporites spp., Verrucatosporites cf. Usmensis, Cyathea type, Polypodiaceae type, Psilatriletes spp., Laevigatosporites spp.*
MD 51 PN2	C	x	x				Pliocene to Pleistocene	Continental. Swamp. Freshwater.	*Foram: reworked elements Paly: Cingulatisporites spp., Cyathea type, Polypodiaceoisporites pseudopsilatus, Psilatriletes spp., Laevigatosporites spp., Hemitelia horrida, Verrutriletes spp., Polypodiisporites spp., Monoporites anulatus, Ilex type, Psilatricolpites spp., Psilatricolporites spp., Proteacidites sp., Retitricolporites spp., Bombacacidites sp. cf. Cordia sp., Clavatricolpites sp., Alagae*
MD 51 PN3	C	x	x				Pliocene to Pleistocene	Continental to coastal swamp, near base level (brackish water, slight marine incursion).	*Benthic foram.: **Bathysiphon** (reworked). Paly.: Cyathea type; Polypodiaceoisporites pseudopsilatus; Psilatriletes spp.; Laevigatosporites spp., Verrutriletes spp., Polypodiisporites spp., Lycopodium reticulatum, Monoporites anulatus, Retitricolporites spp., Echitricolporites spinosus, Psilaperiporites minimus, Malphigiaceae type, Rubiaceae type, Algae*
MD 13 PN1	C	x	x			-	-	Continental, freshwater swamp?	*Hemitelia horrida, Malvaceae ?, Ilex type, Pediastrum sp-*
MD 13 PN2	C	x	x			-	-	Continental to coastal swamp with sporadic saline incursions	*Benthic foram.: **Trochammina sp., Miliammina sp., Haplophragmoides sp**. Paly.: Ceratopteris cf. Deltoides, Malvaceae spp., Ilex sp., Pediastrum sp.,*
MD 13 PN3	C	x	x			<5.33?	Post Miocene (?)	Continental to coastal swamp with sporadic saline incursions	*Benthic foram.: **Trochammina pacifica, Trochammina, Miliammina fusca, Haplophragmoides sp.** Paly.: Polypodiaceoisporites pseudosilatus, Echiperiporites minimus.*
MD 13 PN4	C		x			-	-	Fluvial floodplain, close to base level?	*Bacumorphomonocolpites? sp., Cyatheacidites cf. Annulatus, Pediastrum sp.*
MD 208	Csw (Ft)	x	x			23.03-2.59?	Late Miocene to Pleistocene	Supralitoral. Salinity evidences, nearshore swamp close to mangrove, poor in Ox.	***Crab, Diatomea material**, Benthic foram.: **Miliammina?, Deltaidospora spp.** Paly: **Echiperiporites stellae,** Algae, Psilatriletes spp., Deltaidospora spp., Verrucatotriletes bullatus, Laevigatosporites spp., Polypodiisporites spp., Polypodium costarricense, Echiperiporites stellae, Monoporites anulatus, Echitricolporites spinosus, Corylus type*
MD 208 Bio		x				<66.0	Post Maastr.	Continental? Coastal swamp?	*Benthic foram, Buliminido retrabajado cf. Bolivinoides decoratus, cf. Ostracoda*
MD 208_2		x				17.41-1.79	Miocene-Pleistocene	Undetermined	*Monoporopollenites annulatus, Rhoipites guianensis, Syncolporites anibalii, Retibrevitricolporites grandis, Echitricolporites spinosus, Unknown trilete spores, Unknown monolete spores, Unknown pollen grains.*
MD 20	Csw (T)			x		7.20 +/- 2.7	Late Mio.	No material	*No material*
MD 204 C		x					Miocene to Pliocene?	Coastal swamp, saline influence. Mangrove	*Verrucatosporites usmensis, Psilatriletes spp., **Deltaidospora spp**., Polipodiisporites spp., Verrucatotriletes bullatus, Polypodiaceoisporites sp., Echitriletes cf. muelleri, Laevigatosporites spp., **Echiperiporites stellae**, Malvaceous pollen, Monoporites anulatus, Algae*
MD 204 C_2		x				17.41-13.17	Early-Middle Miocene	Undetermined	*Clavainaperturites microclavatus, Psilatriletes sp., Polypodiisporites sp., Polypodiaeceoisporites pseudospilatus, Echitricolporites spinsosus, Monoporopollenites annulatus, Verrucatotriletes bullatus, Proteacidites triangulatus, Clavainaperturites clavatus, Spinizonocolpites baculatus, Momipites sp., Cingulatosporites laevigatus, Retitriletes sommeri, Polypodiaceosporites fossulatus, Echimonoletes sphericus, Echimonoletes panamensis, Echidiporites barbeitoensis, Nijssenosporites fossulatus, Foveotriletes ornatus, Unknown trilete spores, Unknown monolete spores, Unknown pollen grains*
MD 204					x	3.45 +/- 0.15	Pliocene	No material	*No material*
MD 22	Csw (T)	x				-	-	Swamp with marine influence?	***Dinoflagellates,** Algae*
MD 22 AFTA				x		14.4 +/- 3.5	Middle Miocene?	Undetermined	*No material*
MD 202 C	Csw (Fb)	x				23.03-2.588?	Miocene to Pliocene?	Continental	*Verrucatosporites usmensis, Psilatriletes spp., **Deltaidospora spp**., Polipodiisporites spp., Verrucatotriletes bullatus, Polypodiaceoisporites sp., Echitriletes cf. muelleri, Laevigatosporites spp., Camarazonosporites sp., Foveotriletes spp., Echitricolporites spinosus, Mauritiidites sp., Psiltricolporites sp., Monoporites annul atus, Syncolporites spp., Corylustype, Avicenniatype, Retitricolporites spp., Proteacidites sp., Retitricolporites sp., Retitricolpites sp., Symplocustype, Ilexpollenites sp., Podocarpites spp., Ayeniatype, Annutriporites sp., Algae.*
MD 202 C_2		x				17.41-2.22	Miocene-Early Pleistocene	Undetermined	*Monoporopollenites annulatus, Polypodiisporites sp., Psilatriletes sp., Foveotriletes ornatus (30.89-0.08), Momipites africanus, Podocarpidites sp., Echitricolporites spinsosus, Psilabrevitricolporites devriesii, Psilatricolpites papilioniformis, Unknown trilete spores, monolete spores and pollen grains*
MD 201 B	Osw (Fbl	x				17.41-16.38	Early Miocene	Undetermined	*Polypodiisporites sp., Monoporopollenites annulatus, Echinatosporis brevispinosus, Foveotriletes ornatus, Tuberositriletes verrucatus, Polypodiaeceoisporites pseudospilatus, Verrucatotriletes sp., Echitricolporites spinsosus, Proteacidites triangulatus, Psilaperiporites sp., Psilatriletes sp., Nijssenosporites fossulatus, Echinatosporis muelleri, Cingulatisporites laevigatus, Unknown trilete spores, monolete spores and pollen grains*
MD 199 B2	Osw (Fbl)	x				23.03-2.59?	Miocene to Pliocene?	Continental	*Psilatriletes spp., **Deltaidospora spp.**, Polipodiisporites spp., Echitriletes sp., Verrucatotriletes bullatus, Polypodiaceoisporites sp., Echitriletescf.muelleri, Laevigatosporites spp., Mauritiidites spp., Psiltricolporites sp., Monoporitesannulatus, cf. Polygonum, Botryococcus spp.*
MD 198 PN1	Csw (Fb)	x				23.03-2.59?	Miocene to Pliocene?	Continental with saline influence, anoxic floor. Mangrove swamp. Coastal.	***Deltaidospora spp.**, Monoporites anulatus, **Echiperiporties estelae,** Laevigatosporites spp. , Polipodiisporites spp., Laevigatosporites tibuensis, Psilatriletes spp., Psilatricolporites crassus, Monoporites anulatus, Psilatricolporites small, cf. Polygonum, Echiperiporties estelae, Tetraploa spp.*

Table 2 (previous page): Samples list, type of analyses done (1 to 4), depositional environments interpretations and biostratigraphic constraints for the Neogene strata of the Salvación syncline (Pongo de Coñeq transect). AF= interpreted Facies Associations and Facies related to the samples. Facies are shown between brackets. 1: Palynology. 2: Microfossil analysis. 3: AFTA analysis. 4: Radiometry. See Figure 4 for location of samples on stratigraphic sections. See Figure 4 and Figure 15 to Figure 18 for location of samples on the stratigraphic sections.

5.2.1.Facies analysis and depositional environments

Twenty-one sedimentary facies were identified in the Neogene of the Madre de Dios basin (Table 3) and have been combined into six facies associations (Table 4).

Facies code	Lithofacies	Sedimentary structures/other characteristics	Interpretation
Gt	Clast-supported conglomerates. Granule to Cobble.	Trough cross-stratification, normal grading with imbrications	Transverse bar, minor channel fill
Gp	Clast-supported conglomerates. Granule to Boulder, subrounded to well-rounded	Planar cross-stratification	Linguoid bar, transverse bar
Gh	Clast-supported conglomerates. Granule to Boulder, subrounded to well-rounded	Horizontally bedded, normal to inverse grading with possible imbrications	Linguoid bar, transverse bar
Gm-Gmf	"Mud breccias". Matrix-supported to clast-supported conglomerates (Gravel to pebble)	Massive or crudely bedded gravels (occasionally pebbly). Clast may be ferruginous (Gmf)	Lag deposit?
Sr	Sandstones. Very fine to medium-grained, occasionally pebbly. Moderate sorting	Rippled cross-stratification (Climbing-ripples)	2D or 3D ripples, upper flow regime
Sp	Sandstones. Very fine to medium-grained, occasionally pebbly. Moderate sorting	Planar cross-bedded, possible mud clasts at the base	Linguoid, transverse bars
Sh	Siltstones or very fine- to coarse-grained sandstones	Horizontal lamination	Planar bed flow (Lower or upper flow regime)
St	Very fine- to coarse-grained sandstones	Trough cross-stratification	3D dune migration
Stmc	Very fine- to very coarse-grained sandstones, with scattered to aligned pebbles	Trough cross-stratification, highlighted by mud clasts or occasional lithoclasts (mm to pluri-cm). Occasional wood fragments	Seasonal regime. 3D dune migration
Sm	Massive sandstones (fine to coarse-grained, with possible scattered to aligned pebbles) with moderate to well sorting	No structure. Occasional wood fragments	Rapid deposition, gravity flow
Sfu	Massive sandstones (fine to very coarse-grained), fining upward	Frequent aligned mudclasts and lithoclasts at the base. Occasional wood fragments	Fluvial bedforms and bars, waning flood
Scu	Massive sandstones (fine to very coarse-grained), coarsening upward	Frequent aligned mudclasts and lithoclasts at the base. Occasional wood fragments	Crevasse splay
Sb	Very fine- to medium-grained sandstones (reddish-yellow)	Bioturbation (continental)	
Sd	Very fine- to fine-grained shaly sandstones	Badly-sorted sandstones, dirty, frequent sandy nodules	
Fl	Siltstones, mudstones	Lamination, very small ripples. Occasional flame-structure- Occasionally Calcareous	Overbank or waning flood deposits
Fm	Siltstones, mudstones	Structureless. Occasionally calcareous	Overbank or waning flood deposits
Ft	Siltstones, mudstones (blue-grey)	Flaser or wavy laminations, frequent bioturbation	Coastal plain, coastal swamp
Fb	Mudstones to siltstones (red to purple)	Bioturbated (continental to marine). Red to green (varicolored)	Overbank or abandoned channel, incipient soil
Fbl	Mudstones to siltstones (Blue to grey/dark grey)	Structureless or some ripples	Backswamp, Oxbow-lake, anoxic environment
P	Mudstones to siltstones (red to purple). Carbonaceous nodular, gypsum levels	Frequent bioturbation and rootlets, carbonaceous nodule and stratified gypsum. Possible ferruginous pisoliths	Paleosoil
T	Tuffaceous deposit. May be more or less micaceous	Structureless, rippled or with planar lamination. Some wood debrites	Volcanoclastic lacustrine deposits

Table 3: Summary of the sedimentary facies encountered in the Neogene deposits of the Madre de Dios foreland basin.

	Intepretation	Facies
FCcg	Braided (?) Mainly gravelly to conglomeratic fluvial channel filling	Gh, Gp, Gt, Stmc, St, Sm, Sh, Sfu
FCs	Meandering (?) Sandy to gravelly fluvial channel filling. Possibly conglomeratic at the base of the channels	Sfu, Sm, Sr, Sh, Sp, St, Stmc, Fl, Gt, Gh, Gp, Gm-Gmf, (Fb)
O	Overbank: abandoned channel, paleosoil and Waning flow deposit, continental swamp or oxbow lake (Osw). Possible CU sandy crevasse splays (Ocp)	Fm, Fl, Fb, P, T, Sfu, Sm, Scu, Sr
CCcg	Coastal (Deltaic?) sandy to mainly conglomeratic channel filling/ sandy bars. CU general pattern.	Gh, Gp, Gt, Stmc, St, Sm, Sh
CCs	Coastal (Estuarine/Deltaic?) mainly sandy to possibly conglomeratic at the base of channel fill/ sandy bars	Sfu, Sm, Sr, Sh, Sp, St, Stmc, Fl, Gt, Gh, Gp, Gm-Gmf, (Fb)
C	Marine-influenced fine-grained deposits corresponding to coastal swamp (Csw) or coastal plain (C). Possible fine-grained tidal deposits (Puerto Maldonado)	Ft, Fl, Fm, P, Sr, Sfu, T

Table 4: Facies associations for the Neogene deposits of the Madre de Dios foreland basin.

5.2.2.Facies Association FCcg: conglomeratic fluvial channels

Description:

Facies association FCcg has been observed in both the Pongo de Coñeq area (sections 1, 2 and 3, Figure 13 to Figure 14) and in the Inambari area (sections 4 and 5, Figure 15 to Figure 18). This facies association is typical of the most recent deposits situated at the top of the sedimentary sections described in this paper (Pliocene to Pleistocene in age), but it has also been described within the Miocene deposits of the Salvación and the Punquiri synclines (Section 1 and Section 4, respectively).

Facies association FCcg is often alternating with facies associations O (Overbank) and FCs (Fluvial sandy Channels). Its thickness is comprised between 2 and 15 m. Facies association FCcg mainly corresponds to massive or fining-upward pebble to boulder conglomeratic deposits associated with coarse- to medium-grained sandstones, which can show a rich arkose-content. Sandy facies are generally 50 cm to >1 m-thick and form sand bedforms units.

Facies association FCcg always starts with an important erosive surface overlaid by the conglomerate deposits with trough cross-bedding (Gt, see Table 3 for detailed facies descriptions) and planar or horizontal bedding (Gp and Gh respectively, see Figure 6-B and C). The matrix of the clast-supported conglomerate facies consists of a medium to very coarse-grained sandstone. Conglomerate bodies are generally 1m to 3 m –thick. They can evolve upwards into finer-grained deposits, displaying an overall fining-up trend, or be eroded by another conglomerate body forming then an important stacking pattern (see section 4 part 3, from 2309 to 2407m, Figure 17). Clasts can beup to > 40 cm in diameter, are mainly sub rounded to well-rounded and are moderately sorted. The clast-size distribution is polymodal and shows inverse to normal grading. Imbricated clasts are present. Finer-grained deposits of facies association FCcg can be massive or fine upward from very coarse to fine-grained sandstones (Sm, Figure 6-D and Sfu, respectively), sandstones with trough cross-bedding (St, Figure 6-E) possibly highlighted by mud clasts (Stmc, Figure 6-F), and sandstones with planar bedding (Sp). Outcrop MD 206 shows this fining-up trend from conglomerates to sandstones facies (Section 4 part 3, from 2805 to 2825 m, Figure 17).

No biostratigraphic data could be collected in the deposits of facies association FCcg.

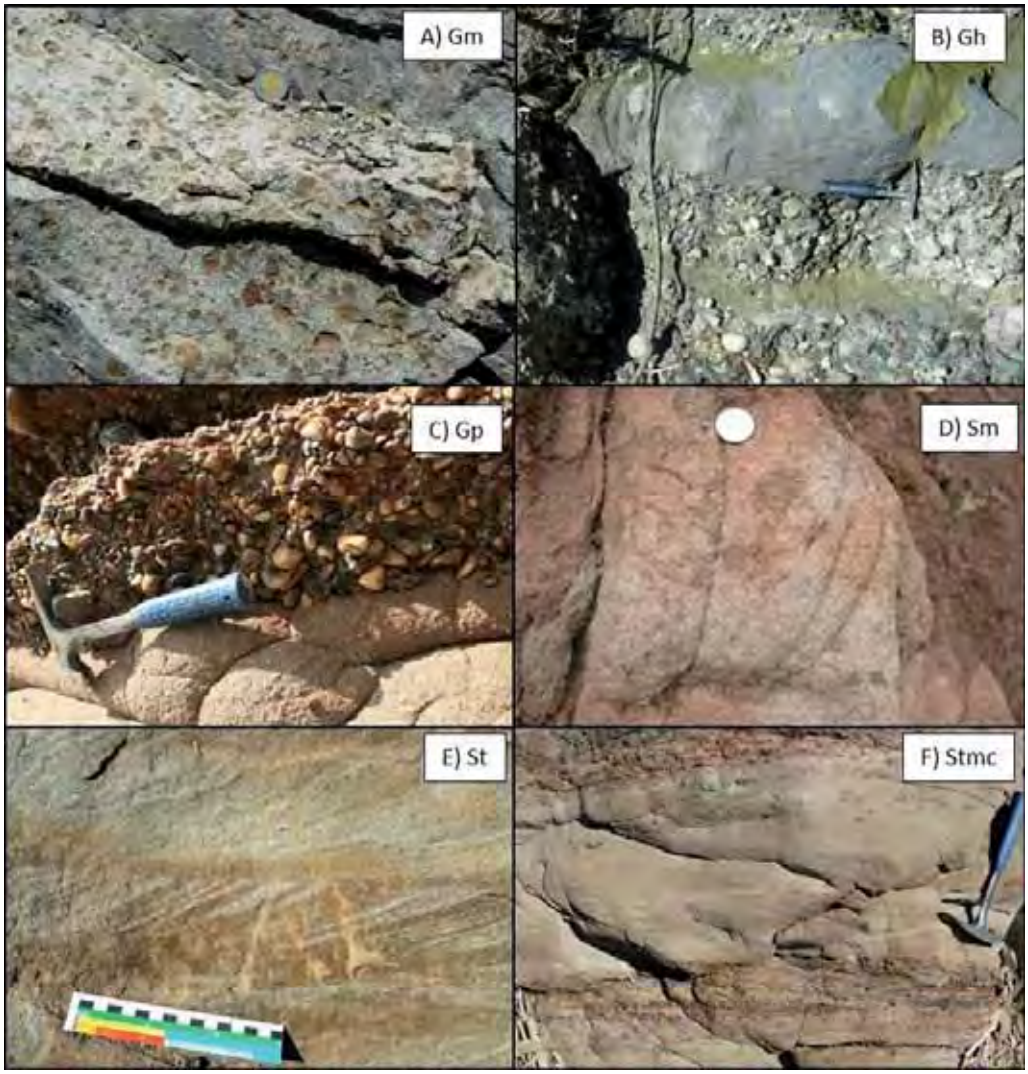

Figure 6: A) Facies Gm showing a matrix-supported conglomerate. B) Facies Gh showing a clast-supported conglomerate (pebble-grained) horizontally bedded. C) Facies Gp showing a clast-supported conglomerate above coarse-grained trough-cross bedded sandstones (St). D) Facies Sm showing structureless medium-grained massive sandstones. E) Facies St showing trough cross-bedded fine- to medium-grained sandstones. F) Facies Stmc showing trough cross-bedded fine- to medium-grained sandstones highlighted by mud clasts and occasional millimetric lithoclasts.

Interpretation:

Occasional cross-stratification and rare clast imbrications of the clast-supported pebble-to-boulder conglomerates facies associated with basal erosive surface suggest deposition from high energy floods equivalent to those produced by gravel-laden streams in poorly to well confined channels (e.g. in Ridgway and DeCelles,(1993) and Uba et al.,(2005)). The organized clast-supported conglomerate facies (Gt, Gh and Gp) with weak imbrications may be the result of incised-channel gravel bedload sedimentation under low- to waning-energy flows (Jo et al., 1997; Uba et al., 2005). The frequent erosive surface associated with overall stacking patters support this interpretation. Consequently, Gt, Gh and Gp facies may correspond to transverse or lingoid bars (Miall, 1996). Trough cross-bedded sandbodies (St) and conglomerate bodies (Gt) mainly represent deposits in channels (Miall, 1996). Sandy facies such as Sfu, Sm, Sp or Sh deposits are less frequent and mainly situated at the top of the fining-up sequences. They are interpreted to be related to loss

of energy of the streamfloods. Because facies association FCcg is closely associated with the Overbank facies association (O) where we only found continental biostratigraphic material, it is interpreted to be deposited by high-energy braided fluvial rivers deposits evolving in a fine-grained fluvial floodplain environment.

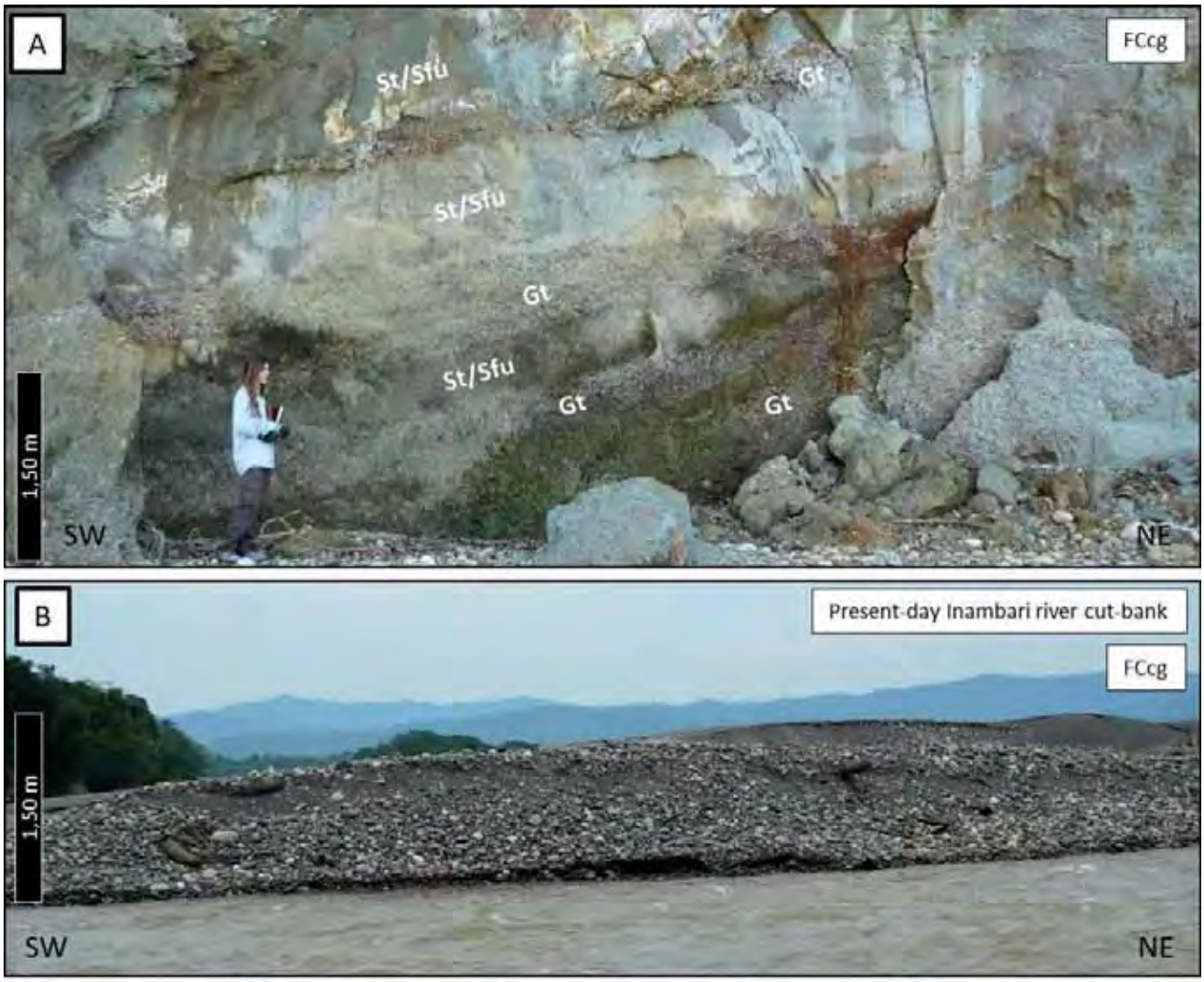

Figure 7: Inambari transect (Section 4). A) Outcrop view of MD 160 showing Late Neogene (Pliocene?) conglomeratic to sandy fluvial deposits with alternating facies St, Sfu and Gt. The corresponding facies association is FCcg. See Figure 4 for a stratigraphic position of outcrop MD 160. B) Present-day transverse bar along the Inambari River, formed by a high energy meandering fluvial system (photograph was taken nearby the axis of the Punquiri syncline). See Table 3 for facies description and Table 4 for the facies association interpretation.

5.2.3. Facies Association FCs: sandy fluvial channels

Description:

Facies association FCs can be observed in both the Salvación syncline (sections 1, 2 and 3, see Figure 13 to Figure 14) and the Punquiri syncline (sections 4 and 5, see Figure 15 to Figure 18). It is mainly made up of fine- to coarse-grained sandstones fining upwards into fine-grained to silty deposits. Occasional sandy to gravelly conglomeratic facies are present at the base of the fining-upward units. Sandstones can have arkose content. Fining-upward channelized bodies are dominant in this facies association.

The base of facies association FCs is characterized by a slightly erosive to deeply channelized surface. A 10 to 30 cm-thick mud breccia (Gm) can also be present at the base of the facies association. Clasts (<2 cm) are angular to subrounded and consist of reworked overbank mud clasts and extraformational rock fragments (ferruginous clasts (Gmf, e.g. in Section 4, at 1175 m, Inambari transect, Figure 15). These deposits can be clast- or matrix-supported.

The channels infillings can also show thin erosive gravelly- to conglomeratic levels, constituted by Gt, Gh or Gp facies (Table 3). Gt facies corresponds to conglomeratic deposits, 30 cm- to more than 3 m-thick, with trough cross-bedding. Gh and Gp facies correspond to horizontally and planar bedded conglomerates respectively, with normal to inverse grading and occasional pebble imbrications. The channel fillings typically evolve upwards into sandy facies (fine- to medium-grained sandstones). These sandstones units are 10 cm-thick to pluri-metric and can be massive (Sm), with trough cross-stratification (St), with planar (Sp) or horizontal bedding (Sh). Frequent mud clasts highlight the sedimentary structures, particularly the trough-cross bedding structures situated at the base of the sandy channel-shaped bodies (Stmc). The top of Facies association FCs is characterized by 10 cm-100 cm thick finer deposits such as fine-grained rippled sandstones (Sr) or laminated siltstones to mudstone (Fl). Facies Sfu corresponds to 50-300 cm-thick fining-upward sandstones.

Facies association FCs generally corresponds to single thick channelized sedimentary unit ranging between 50 cm and 5 m in thickness, or corresponds to several sandy stacked channel filling units (vertically stacked CH elements), 1m to 30m in thickness. No lateral accretion features is found in this facies association.

In the Pongo de Coñeq transect, outcrops MD 67, MD 84 bis=62 and MD 189, which are all interpreted as being part of facies association FCs, yielded continental palynmorphs and fauna (see Table 1 for an exhaustive list). MD 67 has been interpreted as deposited in a fluvial environment characterized by monsoon-like tropical climate (Antoine et al., 2013b). Finally, facies association FCs is generally overlaid by fine-grained overbank deposits containing continental palynological material.

Interpretation:

The channel-shape geometries and the fining-upward sequences indicate that facies association FCs is mainly produced by sandy stream floods in the waning stages of major flow events in the channels. The repeated vertical stacking patterns of the fining-upward units indicate repeated fluctuations in flow velocity. The identified facies Sp, St, Sh and the absence of lateral accretion elements suggest that sand bodies are the product of confined, high-energy stream floods and record deposition associated with subaequeous dunes and upper-stage plane beds (Miall, 1996). Facies Sm corresponds to massive sandstones deposited during sediment gravity flow or rapid deposition. Facies Sfu, Sr and Fl, situated at the top of the channel-filling sequences, are associated to a loss of stream flood energy during the channel abandonment phase. The poorly developed, disorganized and matrix-supported conglomeratic bedforms (Gm-Gmf) described at the base of the sequences suggest high sedimentation fallout rates and/or shallow flow depth (e.g. in Jo et

al. (1997) and Uba et al (2005)). We interpret facies Gt, Gh and Gp as being deposited by occasional high energy streamfloods equivalent to those produced by gravel-laden streams in poorly to well confined channels (e.g. in Ridgway and DeCelles (1993) and Uba et al. (2005)).

According to biostratigraphical contents and because facies association FCs is associated to continental fine-grained Overbank deposits (O) the sandy facies of FCs have been interpreted as fluvial channel-filling deposits. Depending on the geometry of the sandy units and their vertical stacking pattern, deposits can be associated to single-storey fluvial channel (single fining-up sandy unit) or multi-storeys channels complex (sandy units displaying an important vertical stacking).

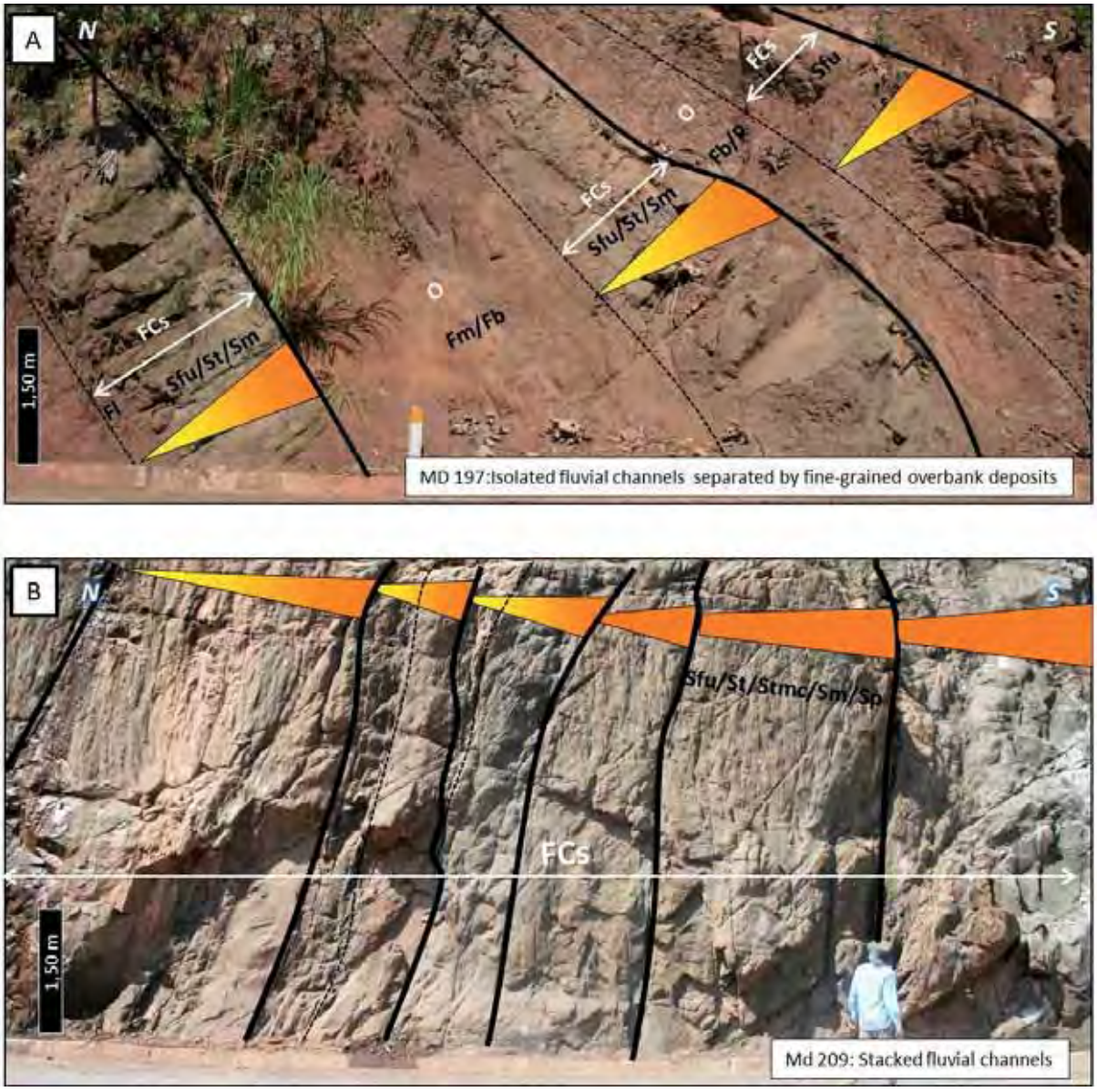

Figure 8 (previous page): Example of two different vertical organizations (stacking) of alternating Facies associations FCs and O. In both pictures, the axis of the Punquiri syncline is situated at the left (toward the North). A): Outcrop view of MD 197 (inverted strata). Isolated meter-thick and fining-upward fluvial channels (FCs) separated by thick fine-grained overbank deposits (O). B): Outcrop view of MD 209 showing vertically stacked fluvial sandstones presenting fining-upward pattern. Sandstones are mainly made up of facies Sfu, St, Stmc, Sm and Sp. Because of the important thickness of facies association FCs, lower and upper contacts with facies association O are not visible here. See Table 3 for facies description and Table 4 for facies associations' interpretations.

5.2.4.Facies Association O: Overbank deposits

Facies association O is very common in the Neogene deposit of the Madre de Dios foreland basin, in both the Pongo de Coñeq and the Inambari transects. It has been observed in all the Neogene sedimentary sections presented in this paper, and can constitute the major part of the deposits in some intervals.

Overbank deposits frequently overly the FCcg or FCs facies associations. Facies association O mainly consists of fine-grained mud bodies occasionally intersected by silty or sandy bodies and are 1- to more than 30 m-thick in total. .

Fine-grained overbank facies can correspond to massive mudstone or siltstone (Fm, Figure 9-E), laminated mud or silt deposits (Fl), bioturbated reddish or varicolored mudstone to siltstone (Fb, Figure 9-F) or blue to dark structureless or rippled mudstone to siltstone (Fbl). Facies Fb can also present occasional desiccation traces. Root trace, carbonates nodules and bioturbations can be occasionally found in muddy to silty deposits (P, Figure 9-F). All these fine-grained overbank deposits range from 20 cm- to 20 m in thickness (see important thickness in interval 1870 to 2000m in section 1, Pongo de Coñeq transect, Figure 13). Figure 10 shows an example of facies association O characterized by facies Fm, Fbl and P in the Punquiri syncline (section 4).

Coarser-grained sandy deposits, 20 - to 200 cm in thickness of massive or fining-upwards fine-grained to medium-grained sandstones (Sm or Sfu respectively), rippled sandstones (Sr) or coarsening-upwards sandstone (Scu) can be intercalated within the fine-grained overbank deposits. Example of facies Scu is shown by interval 700 to 740 m in section 4 (Figure 15). Two tuffaceous levels have been found within the overbank fine-grained sequences of the Inambari transect (at 1615 m in Figure 16 and 2465 m in Figure 17). These tuffaceous units are 30 cm to 100 cm in thickness and can show ripples or planar horizontal sedimentary structures (T, Figure 9-B). Wood fragments and leaves traces are frequent in this facies.

Only few continental palynomorphs have been found in this facies association (see samples MD 199-B and MD201-B, Table 2).

Figure 9: Example of Facies found in the Neogene of the Madre de Dios foreland basin: A) Facies Sd showing shaly fine-grained sandstone; B) Facies T showing a tuffaceous rock with plant fragments and some ripples; C) Facies Fbl showing grey mudstones to siltstones; D) Facies Ft showing wavy lamination disturbed by bioturbation; E) Facies Fm showing typical structureless reddish mudstone, and F) showing well-developed carbonaceous paleosoil (Facies P) lying above reddish mudstones with frequent root traces and continental bioturbations (Facies Fb). See Table 3 for facies description and Table 4 for facies associations' interpretations.

Interpretation:

Palynomorphs found in MD 199-B and MD 2012-B specify a continental paleoenvironement for this facies association (Table 3). Moreover, Overbank facies are always closely related to facies association FCs and FCcg, both interpreted as continental. We therefore interpret facies association O as continental.

In agreement with continental palynomorphs and with sedimentary descriptions, facies association O represents deposition in a floodplain environment (Fm, Fb, Fbl, P) occasionally disturbed by waning flow deposits (Sr, Sm, Fl) and crevasse plays sand bodies (Scu) due to its proximity to a fluvial channel. Facies Fm therefore represents deposition from low-energy flows or from standing pools of water after channel abandonment (Miall, 1996). The limited presence of desiccation cracks, the occurrence of occasional root traces and overall reddish- to purple color of Facies Fb suggest deposition under oxidizing conditions (e.g. in

Turner (1980), Miall (1996) and Retallack (1997)) with common subaerial exposure (e.g. in Esteban and Klappa (1983) and Klappa (1983)). The dark color of the fine-grained deposits of facies Fbl and its proximity to a fluvial system are consistent with deposition in an anoxic environment such as oxbow lake or continental back swamp (Miall, 1996). The thin carbonate layers, the occasional carbonate nodules and the frequent root-traces and continental bioturbation of facies P indicate pedogenic modification after deposition (e.g. in Wright and Tucker (1991) and Retallack (1997)) and are associated to a well-developed paleosoil horizon. The thin beds of fine-grained silty to sandy deposits structured by thin lamination and occasional ripples (Fl and Sr) can be indicative of low-energy streams (waning floods) associated to deposition in distal floodplains (e.g. in Uba et al. (2006)). The occasional coarsening-upward and massive sandstones of facies Sm and Scu can be related to crevasse splay deposits and crevasse-channel fillings forming in a proximal floodplain environment. Note that these sandy units can be frequent is some sedimentary successions interpreted as overbank deposits and may constitute evidences of active channel avulsion processes at that time (e.g. in DeCelles and Horton (2003)).

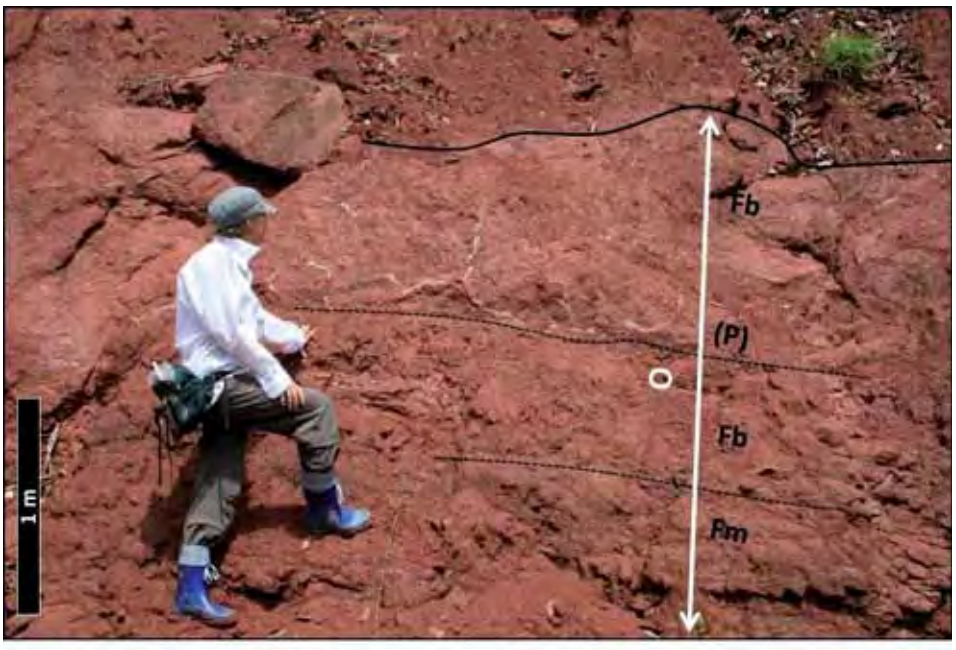

Figure 10: Example of facies association O (Overbank) observed in the Inambari transect (Section 4, outcrop MD 313). A moderately-developed paleosoil horizon (Facies P) developed above fine-grained massive and bioturbated mudstones and siltstones (Facies Fm and Fb, respectively). See Table 3 for facies description and Table 4 for facies associations' interpretations.

5.2.5. Facies Association CCcg: coastal conglomeratic channels

Description:

Facies association CCcg has been described in the uppermost Pliocene strata in the Punquiri syncline (Inambari transect, section 4, Figure 15 and Figure 16) and in the Middle Miocene and the Late-Early Miocene deposits of the Salvación syncline (Pongo de Coñeq transect, section 1, Figure 12).

Facies association CCcg consists of 2- to more than 10 m- thick deposits and often corresponds to vertically stacked units of conglomerates separated by frequent erosive surfaces. Channelized bodies are the most frequent elements.

Facies association CCcg is mainly made up of trough cross-bedded, planar and horizontally-bedded conglomeratic facies (Gt, Gp and Gh respectively) and of medium- to very coarse-grained trough cross-bedded or massive sandstones (St, Sm). The overall sequence can display a general coarsening-upward pattern, and is generally overlaid and/or underlain by the coastal fine-grained deposits of facies association C. An example of these facies succession is shown by deposits of MD 243 to MD 244 (Section 1 in the Pongo de Coñeq transect, from 950 to 1010 m, Figure 13). Note the coarsening-upward pattern displayed by deposits from 960 to 997 m. In the Inambari transect. The same kind of coarsening-up pattern can be observed from 2160 to 2174 in section 4 (Figure 16).

No biostratigraphic nor paleontological samples were collected in this facies association.

Interpretation:

Identically to facies association FCcg, the clast-supported pebble-to-boulder conglomerates (Gt, Gh, Gp) composing the facies association CCcg are interpreted as resulting from high energy in poorly to well confined channels (e.g. in Ridgway and Decelles (1993), Uba et al., (2005)). In addition, the vertical stacking pattern, the coarsening-upward trend and the geometrical and close genetic relation with facies association C (coastal fine-grained deposits) are consistent with deltaic settings. The clast-supported conglomerate facies (Gt, Gh and Gp) with rare imbrications may be therefore the result of incised-channel gravel bedload sedimentation under low- to waning-energy flows in a delta plain (Jo et al. (1997) and e.g. in Uba et al., (2005)).

5.2.6.Facies Association CCs: sandy coastal channels

Description:

Facies association CCs is found in the Late Early Miocene and in the Late Miocene-Early Pliocene strata of the Salvación syncline (Pongo de Coñeq transect, section 1, from 760 to 805 m and from 2050 to 20709 m respectively, Figure 13) and in the Early Miocene and the Late Miocene to Pliocene strata of the Punquiri syncline (Inambari transect, sections 4 from 875 to 915 m and section 5 from 0 to 7 m, respectively, both in Figure 18). Just as facies association CCcg, facies association CCs is also closely associated to fine-grained coastal deposits (Facies association C) and mainly corresponds to channelized isolated bodies and sand beds elements. The thickness of the overall sequence ranges between 1- to 4 m.

Contrary to facies association CCcg which show coarsening-upward patterns and conglomeratic deposits, facies association CCs is mainly characterized by fining-upward sequences made up of gravelly- to sandy channelized units. These units are typically 20 cm- to 2oo cm-thick massive sandstones (Sm) or fining-upward sandstones (Sfu) with occasional trough cross-bedding often highlighted by mud clasts (St and Stmc).

10 cm- to 30 cm- thick erosive beds made up of horizontally, planar or trough cross-bedded conglomerates (Gh, Gp or Gt) can also be present at the base of the sequence.

Facies association CCs brought several continental vertebrate and fauna material (see sample MD 61, Table 1, and paleo-depositional environment interpreted by Marivaux et al. (2012)). However, other undoubtedly marine-related microfossils (the benthic foraminifera *Bathysyphon* and *Miliammina* species) were found further in the same locality in the intercalated facies association C (Coastal swamp, see results for samples MD 61-A and MD 61-B).

Interpretation:

The gravelly-to-sandy fining-up channels-filled deposits and their geometric relation with coastal fine-grained deposits (facies association C) as well as the benthic foraminifera found in this closely related facies association (samples MD 61-A and B) are consistent with a coastal plain environment alimented by occasional confined to unconfined stream floods. Channelized and fining-upward deposits could hardly be interpreted as isolated deltaic channels due to the poorly developed vertical stacking pattern and the absence of general coarsening-up trend. We interpret these deposits as estuarine tidal bars or fluvio-estuarine channel fillings (Dalrymple and Choi, 2007; Dalrymple et al., 1992). Indeed, the sandy sheets or sandy channel fillings of this facies association represent distal and lower-energy stream floods in comparison with facies association CCcg which is consistent with much more higher-energy stream-floods able to transport gravel to coble clasts. In comparison with facies association FCs, channel bodies described within facies association CCs are more isolated and much thinner. Each Channel-Complex Filling unit of facies association CCs represents one channel history filling, from its establishment (erosive basal part) to its abandonment (fining-upwards deposits and coastal fine-grained deposits at the top of the sequence).

5.2.7.Facies Association C: Coastal plain deposits

Description:

Facies association C corresponds to fine-grained deposits forming 20 cm- 2 m-thick muddy units. It can occur in Section 1 in the Salvación syncline (Figure 13) and in Sections 4 and 5 in the Punquiri syncline (Figure 15 to Figure 18).

Facies association C corresponds to a 50 cm- 15-m thick sequence made up of reddish bioturbated shales (Fbl), massive shales (Fm), green to dark shales (Fbl), laminated or rippled mudstone to siltstone (Fl),thin levels of rippled fine-grained or fining-upward sandstones (Sr or Sfu respectively) and occasional tuffaceous levels (T). In some cases, 10 to 20-cm thick paleosoil horizons may have developed over the muddy facies (e.g. in section 1, at 1000 m and 1008 m).

These fine-grained facies have been separated from the fine-grained overbank deposits (facies association O) on the bases of their biostratigraphical content. Facies association C (or Csw) contains benthic foraminifera and marine-related palynomorpsh such as *Bathysiphon*, *Deltaidospora sp.* and *Miliammina fusca* in the Late Early Miocene (samples MD 61-A and MD-61-B), the Middle Miocene (MD 1441 Bio) and

the Late Miocene to Pliocene strata (MD 246 Bio, A and B) of the Pongo de Coñeq transect (see Table 1 for exhaustive list). In addition, a significant proportion of coastal to marine palynomorphs and microfossil were also found in the Early Miocene to Pliocene interval in the Inambari section (see results for samples from localities MD 198, MD 202, MD 22, MD 204, MD 208, MD 13 and MD51 in Table 2). Note the presence of rare Dinoflagellates suggesting a shallow marine environment in outcrop MD 22 (Table 2).

Where not directly available, we used the biostratigraphical material found in the associated and nearest coarser-grained Coastal Channels sandy deposits (facies association CCs). In both cases, shallow marine-related or coastal mangrove-related palynological or microfossils contents have been found.

Interpretation:

The presence of fine-grained deposits, the shallow marine to coastal microfossils and palynological material indicate a coastal plain environment. Green to dark shales are characteristic of an anoxic environment such as coastal swamp (referred as Csw) whereas the massive shales intercalated by occasional sandstones could be related to an estuarine tidal flat environment (Dalrymple and Choi, 2007; Dalrymple et al., 1992) or a delta plain environment (Dalrymple et al., 2003). The absence of deep marine facies and the presence of few paleosoil horizons developed on the fine-grained marine-related facies indicate occasional subaerial exposure of a costal to shallow-marine system, and may be related to either estuarine saltmarshes or deltaic low-energy midstream bars suffering frequent subaerial exposure. Tuffaceous deposits may have deposited in an adjacent lake or in a coastal bay or lagoon.

5.3. Nd-Sr isotopic composition

The Nd-Sr isotopic compositions of the Neogene sedimentary rocks are shown in Table 5. Overall, the sediments have quite variable εNd(0) values (ranging from –5.2 to -12.6) with a comparatively narrow range of $^{87}Sr/^{86}Sr$ compositions (0,710572 to 0,733581) (Table 5). In details, the sediments from the Inambari area differ from the sediments of the Pongo de Coñeq area having more radiogenic isotopic Sr composition with lesser Nd isotopic composition.

The eleven samples analyzed for their Nd-Sr isotopic compositions have been reported in the 87Sr/86Sr versus εNd(0) diagram (Figure 11). The isotopic results are compared with several other relevant source fields: Mesozoic and Neogene volcanic rocks (Kay et al., 1994; Rogers and Hawkesworth, 1989). Quaternary Ecuadorian lavas (Barragan et al., 1998), Cenozoic sedimentary rocks from the Central Depression, Altiplano, Oriental Cordillera and Subandean zone of Chili and Bolivia (Pinto, 2003), modern suspended sediments from the Solimoes and Madeira rivers (Viers et al., 2008), Neogene deposits from the Amazonian foreland basin of Bolivia, Ecuador and Peru (Roddaz et al., 2005a), and the sand of the Peruvian White Sand (WS) formation cratonic in origin (Roddaz et al., 2005a). Nd-Sr isotopic compositions of sediments deposited by an Andean drainage define plot within a mélange hyperbole as observed by Basu et al. (1990) and Roddaz et al. (2012; 2005a) for Neogene sediments of the Amazonian foreland basins, with one end member being the primitive volcanic arc and the other the upper continental crust of the Brazilian shield.

Sample	Grain size	Sr (ppm)	Nd (ppm)	143Nd/ 144Nd	± 2σ	eNd(0)	87Sr/86Sr	± 2σ	Transect	Geological_Age
MD 204 B	Mud	106	40,16	0,512023	7	-11,99676965	0,729826	12	Inambari	**Pliocene**
MD 202 D	Mud	86,33	38,49	0,512011	6	-12,23085296	0,728579	8	Inambari	**Miocene-Early Pleistocene**
MD 200 B	Mud	117,9	41,65	0,511997	5	-12,50395016	0,72802	11	Inambari	Early Miocene?
MD 198 E	Mud	102,4	44,17	0,511991	5	-12,62099181	0,733581	7	Inambari	**Probable Mioceno a Plioceno**
MD 197 Nd 1	Mud	113,2	51,37	0,512038	6	-11,70416551	0,724753	9	Inambari	Paleogene-Early Neogene?
MD 62 A	Mud	199,1	35,57	0,512369	7	-5,247367538	0,710572	7	Pongo de Coñeq	**Middle Miocene**
MD 62 B	Mud	249,7	48,66	0,512269	6	-7,19806179	0,715037	7	Pongo de Coñeq	**Middle Miocene**
MD 67 Nd	Mud	182,5	42,92	0,51221	5	-8,348971399	0,71662	8	Pongo de Coñeq	**Early Middle Miocene**
MD 83 Nd	Mud	208,3	42,07	0,512198	5	-9,831499031	0,714819	8	Pongo de Coñeq	Late early Miocene
MD 61 bis B	Mud	186,6	35,78	0,512263	6	-7,315103445	0,713814	8	Pongo de Coñeq	**Late early Miocene**
MD 187 A	Mud	174,2	46,59	0,512145	6	-9,616922663	0,718402	9	Pongo de Coñeq	(Early) Miocene?

Table 5: Nd–Sr isotopic systematics of the analyzed Neogene sediments from the Madre de Dios foreland basin. See samples locations on stratigraphic sections Figure 13 to Figure 18 and on Annex-Map 7.

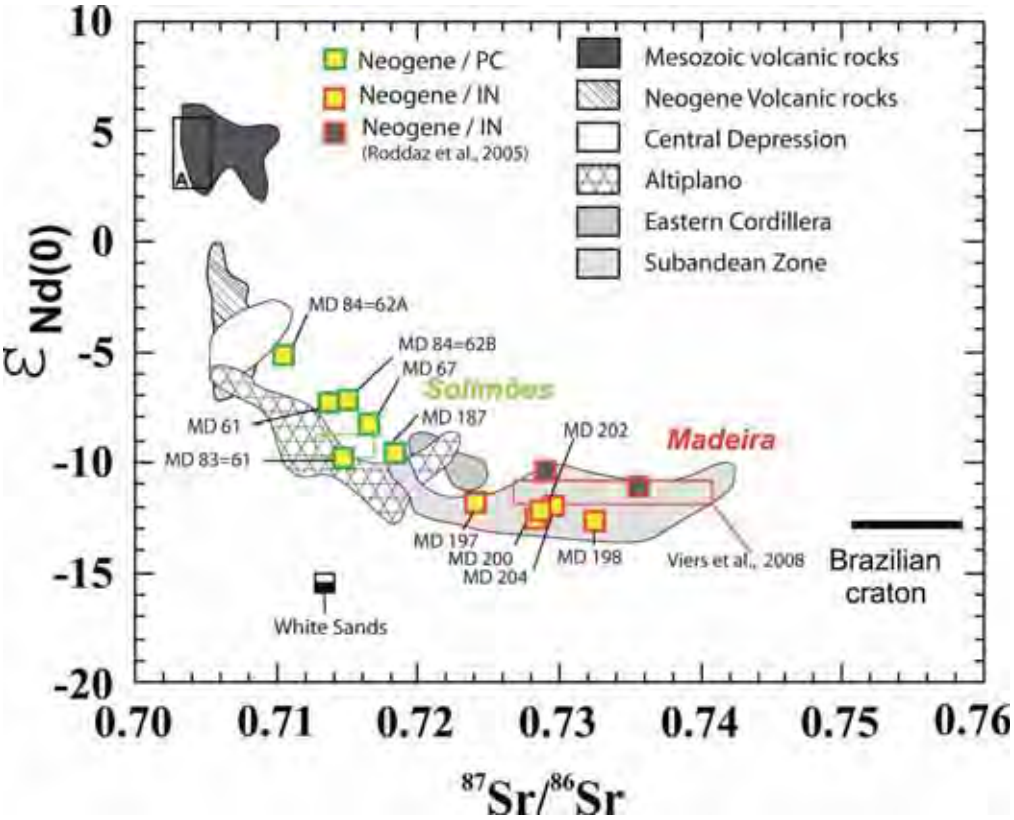

Figure 11: $^{87}Sr/^{86}Sr$-ƐNd(0) diagram for Neogene Madre de Dios foreland basin sediments. Data source: Ecuadorian volcanic lavas (A) are from Barragan, 1998; the Mesozoic and Neogene volcanic rocks are from Kay (1994) and Rogers ; data for the Central depression, the Altiplano, the Eastern Cordillera and the Subandean zone are taken from Pinto (2003) and Roddaz (2005a); Solimoes and Madeira suspended matter data are from Viers et al. (2008).

The eleven analyzed Neogene samples plot within the mélange hyperbole, indicating an overall Andean provenance. However, samples from the Pongo de Coñeq section plot in a different area in comparison with samples from the Inambari section (Sanchez et al., in preparation). Neogene samples from the Pongo de

Coñeq area plot in the field of the Cenozoic Altiplano sediments and show ƐNd(0) from -9.62 to -5.25 and $^{87}Sr/^{86}Sr$ from 0,710572 to 0,718402. Neogene samples from the Inambari area plot in the field of the Subandean zone sediments and show ƐNd(0) from 11.70 to 12.62 and $^{87}Sr/^{86}Sr$ from 0,724753 to 0,733581. Pongo de Coñeq samples plot closer to the volcanic pole than those from the Inambari area suggesting a higher volcanic contribution. They also plot in the same field than the present-day suspended sediments from the Solimoes River, whereas Inambari samples are more radiogenic and plot in the same field than the present-day Madeira suspended sediments(Viers et al., 2008). This suggests that the sediments of the Pongo de Coñeq and Inambari areas have different provenance.

6. Neogene sedimentary evolution of the Southern Amazonian foreland basin (Madre de Dios)

Note that all the stratigraphic sections described in this chapter (sections 1 to 5) are available in Annexes (enlarged views, Annexes-Figures A to G).

6.1. Pongo de Coñeq stratigraphic sections (sections 1, 2 and 3)

The sedimentary succession in the Pongo de Coñeq area can be divided into three depositional sequences separated by erosive unconformities or by absence of deposition (stratigraphic gap). Refere to Figures A to E in the Appendixes for enlarged views of the stratigraphic sections.

6.1.1.Depositional Sequence 1 (Late Early to Middle Miocene)

The first depositional sequence consists in stratigraphic order of MD61, MD61bis, MD183, MD243, MD244, MD84bis, MD84 (760m-1200m in section 1, Figure 13) and of outcrops MD 259=67, MD 187 and MD 258 in Section 2 (Figure 14) and outcrops MD 252, MD 253 and MD 254 (660-830 m, Figure 14).

In section 1 (Figure 13), the base of the Neogene sedimentary infiling of the Pongo de Coñeq area starts with MD 61 outcrop which is Late Early Miocene in age (Marivaux et al., 2012).

According to the paleontological material (Table 1), the presence of well-developed paleosoil horizons and the presence of laterally migrating sandy bars (at 780 m), the deposits of MD 61 outcrop were formerly interpreted as meandering fluvial system (Marivaux et al., 2012). However, the occurence of benthic foraminifera found in the fine-grained deposits of MD 61 and MD 244 more likely indicates a coastal environment such as a delta plain or an estuary (see Table 1). If the laterally migrating sandy bars could fit with the fluvio-estuarine meandering part of an estuary (Dalrymple et al., 1992), the vertically stacked conglomerates and the general coarsening-up pattern better suggest a deltaic environment (facies association C, Csw and CCs). Paleosoil horizons suggest subaerial conditions that may correspond to the interfluve between the distributary channels of the delta (Dalrymple et al., 2003). Alternatively, the sedimentary interval between MD 61 and MD 244 would correspond to a transgressive-regressive coastline cycle, evolving from an estuary (MD 61) to a deltaic system (MD 244).

Between MD 84 bis and MD 84=62 localities (1160-1220 m, Figure 13) Section 1 shows isolated and metric medium-grained to coarse-grained sandy packages. They correspond to single fluvial channel story deposits (FCs) separated by overbank fine-grained deposits (O). Well-developed paleosoil horizons are also frequent. Because channels are isolated and separated by overbank facies, the system is more likely to be interpreted as a meandering fluvial system. However, it is important to note that no lateral accretion has been observed in this sedimentary section.

Sedimentary rocks from outcrops MD 259=67, MD 187 and MD 258 in Section 2 (Figure 14) are also interpreted to be Middle Miocene in age. Very few meters of section are available but the alternating FCs

and O facies associations are consistent with a fluvial system. This interpretation is confirmed by paleontological and palynological data (Table 1) that suggest a fluvial system in a tropical monsoon-like climate (Antoine et al., 2013).

The stratigraphy of the sedimentary section 3 corresponding to outcrops MD 252, MD 253 and MD 254 (660-830 m, Figure 14) is not well-constrained in age. We assume an Early to Middle Miocene age (Table 1) and a continental (fluvial) environment with alternating facies associations O and FCs. However, it is important to note that the sandstones of outcrops MD 253 starts to display a vertical stacking pattern (765-800 m, Figure 14).

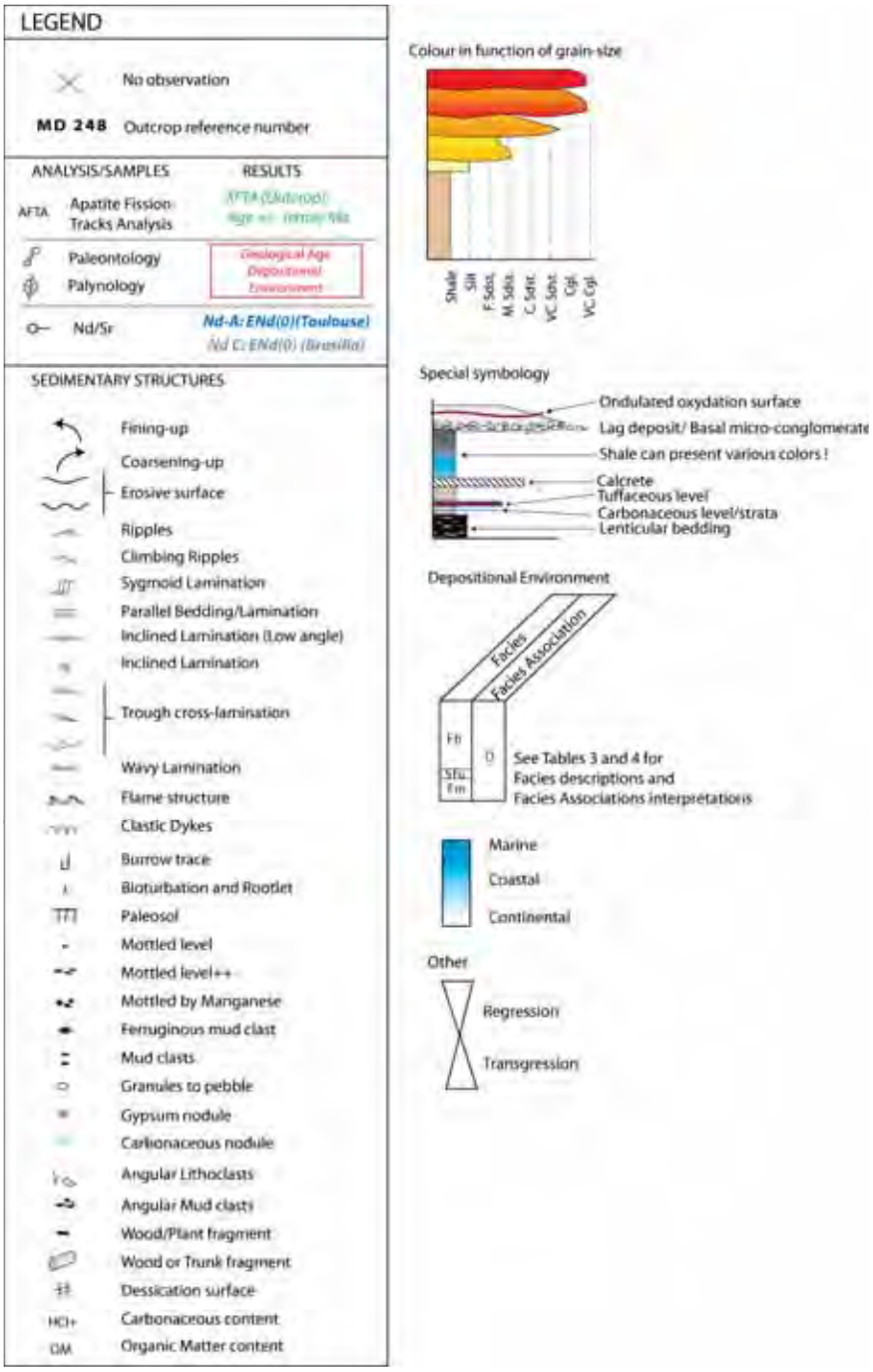

Figure 12: Legend for the stratigraphic sections presented further (Figure 13 to Figure 18). Also see Annex-Figure G.

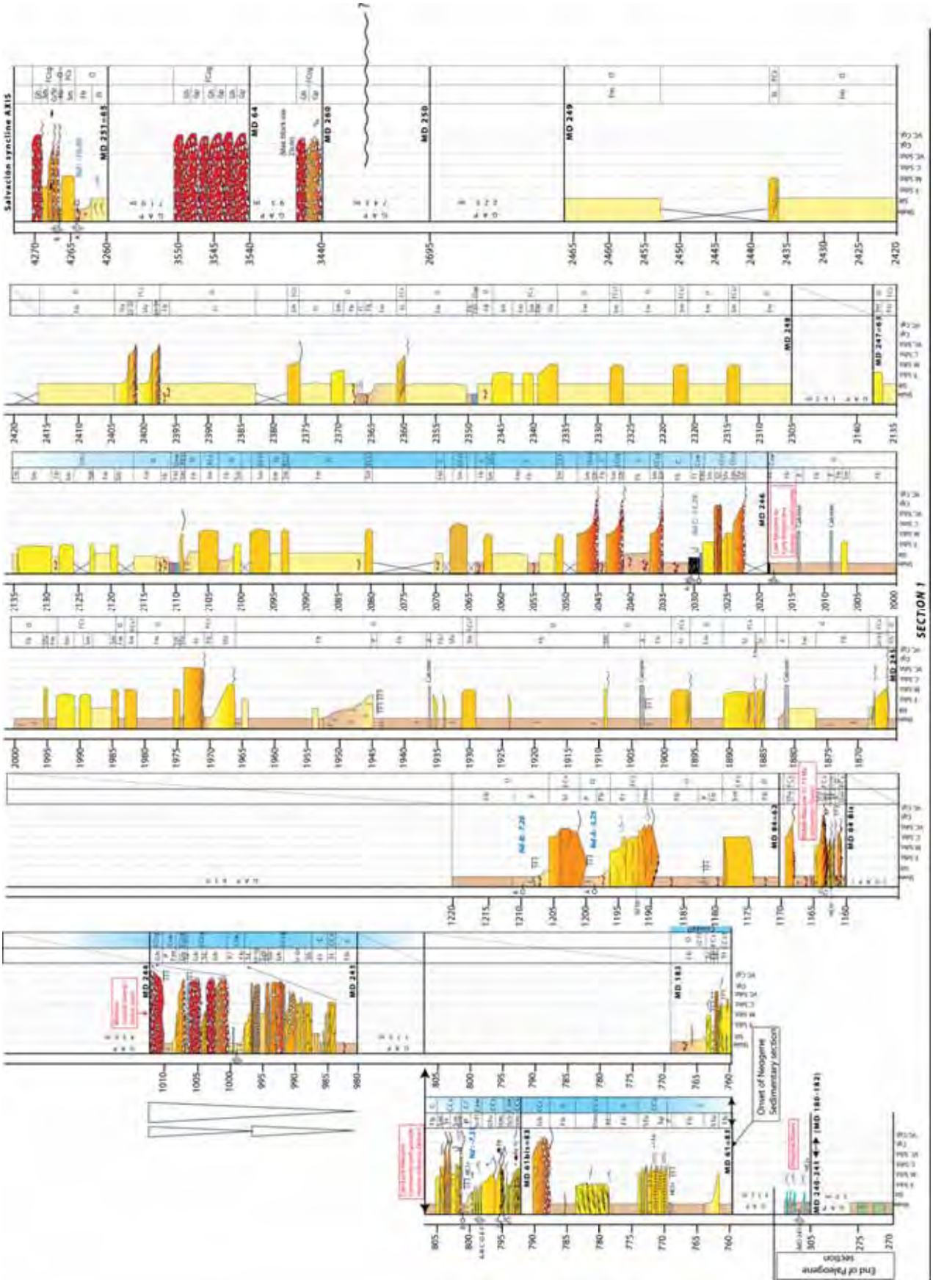

Figure 13: **Stratigraphic section 1 measured in the Salvación syncline, Pongo de Coñeq transect. See Figure 1 for location, Table 3 for facies interpretations and Table 4 for the interpretation of facies associations. Also see Annex-Figure A.**

6.1.2.Depositional Sequence 2 (Late Miocene-Early Pliocene)

The second Depositional Sequence consists of MD 245, MD246, MD 247, MD 248 and MD249 in section 1 (Figure 13) and outcrop MD189 in section 2 (Figure 14).

The base of the Depositional Sequence is characterized by an overall diminution in grain size when compared with the underlying Depositional Sequence. Between outcrops MD 245 and MD 246 (1865-2018 m, Figure 13), section 1 shows sandy packages (FCs) are more isolated and muddy to silty deposits (O) are thicker than in MD 84. Well-developed carbonate paleosoils are frequent. These indicate a fluvial system characterized by higher contribution of overbank processes than in MD 84. At the top of MD 245, near MD 246, we found benthic foraminifera and mangrove-related palynomorphs (Table 1). Hence, MD 246 may represents a transition between a fluvial system towards a coastal environment characterized by mangrove development. Between outcrops MD 246 and MD 247 (2022-2138 m, Figure 13), this coastal-system might be still present, but no other marine-related indicator has been found in this interval. The presence of isolated and channelized sandy- to conglomeratic packages (CCs and CCcg), blue to violet mudstones characteristic of anoxic environment such as swamp or coastal-swamp (Csw), the high proportion of silty deposits and the marine-related material all rather suggest an estuarine environment or a coastal plain than a delta.

Between MD 248 (at 2305 m) and MD 249 (at 2465 m) similar sedimentary succession of facies association is found as above with continental isolated sandy packages (Fcs) alternating with thick muddy- to silty overbank and floodplain deposits (0) (Figure 13). No biostratigraphical data is available but we assume this interval to be mainly continental. Overbank processes are still highly represented (O or occasional Osw). The slightly-channelized fine- to medium-grained sandy packages may be interpreted as unconfined flow deposits. Isolated and channelized coarse- to very coarse-grained deposits would thus be interpreted as episodic confined single-story channel deposits. The relatively high proportion of overbank and floodplain deposits compared to in-channel deposits indicates either a broad floodplain across in which the channel meandered or a rapid floodplain aggradation rate relative to the frequency of channel avulsion (Heller and Paola, 1996) or simply related to an increasing accommodation space.

Deposits related to outcrop MD 189 in Section 2 (3165-3175 m, Figure 14) are dated Late Miocene to Early Pliocene period (Table 1). The corresponding sedimentary section (Figure 14) shows two channelized 5-m thick fining-up sandy fluvial channel deposits (FCs) overlying a blue-colored mudstone interpreted as swamp deposits (Osw).

6.1.3. Depositional Sequence 3 (Late Pliocene to Pleistocene)

The third Depositional Sequence has only been identified in section 1 (Figure 13) and consists of MD 260 (at 3440 m), MD 64 (at 3540 m) and MD 251 (at 4260 m).

MD 64 and MD 260 both show very thick vertically stacked conglomerates corresponding to facies association FCcg. These deposits correspond to a high-energy fluvial system probably characterized by braided streams developing in proximal fluvial (to alluvial?) environment.

MD 251 corresponds to the uppermost locality described in section 1 (4260-4270 m, Figure 13). Rippled siltstone and bioturbated fine-grained deposits correspond to overbank facies (facies association O) whereas the channelized sandy- to conglomeratic bodies have been interpreted as corresponding to fluvial channels bodies (FCs and FCcg). In comparison with MD 260 and MD 64 localities, these uppermost deposits present more isolated channels, and a finer overall grain-size. Deposits probably correspond to a high-energy meandering fluvial system very similar to the present-day system (Figure 7).

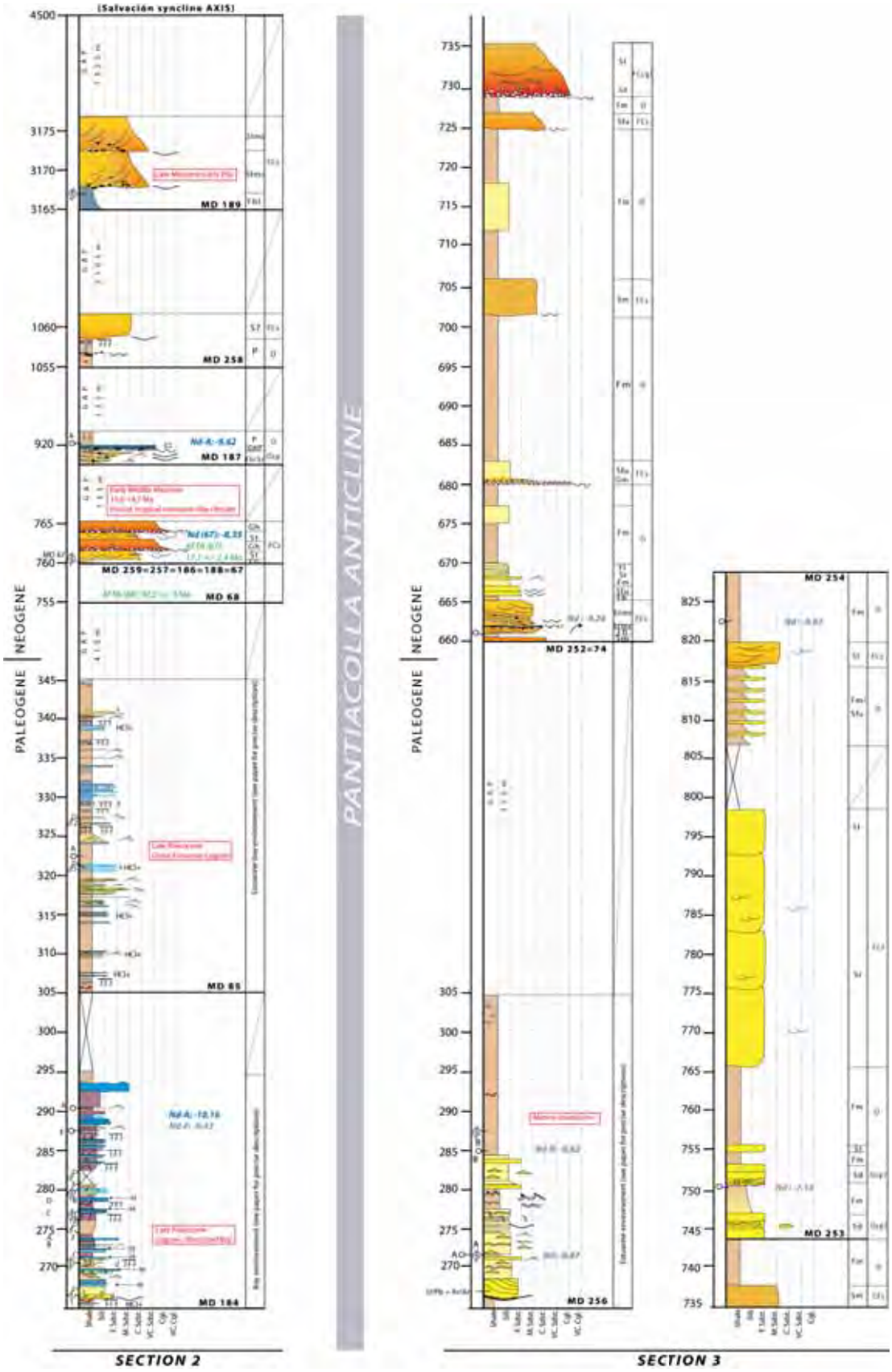

Figure 14: Stratigraphic sections 2 and 3 measured near Shintuya (northeastern flank of the Salvación syncline) and across the northeastern flank of the Pantiacolla anticline, respectively (Pongo de Coñeq transect). See Figure 1 for location, Table 3 for facies interpretations and Table 4 for the interpretation of facies associations. Also see Annex-Figure B.

6.2. Inambari stratigraphic sections (sections 4 and 5)

The sedimentary succession in the Inambari area can also be divided into three depositional sequences, separated by erosive unconformity or absence of deposition (stratigraphic gap).

6.2.1.Depositional Sequence 1 (Early-Middle Miocene)

The first Depositional Sequence is only found in Inambari section 4 and consists in stratigraphic order of MD 197, MD 198, MD 209, MD 199, MD 200, MD 201 and MD 202 (Figure 15, Figure 16 and Figure 17).

The Inambari section 4 (Figure 15, Figure 16 and Figure 17) shows a 2000 m-thick sedimentary succession related to Early Miocene deposits. However, this section is duplicated by thrust faults situated at the very beginning of the southern flank of the Punquisi syncline (see Thrust faults A and B in seismic section Mob-109, Figure 5). We thus estimate that the Early Miocene as 1000- to 1200 m in thickness.

At the base of the section (0-175 m, Figure 15), MD 197 shows isolated channelized sandstones (FCs) intercalated with fine-grained overbank deposits (O). Some muddy swamp deposits (Osw) have also been found (e.g. at 50 m). Overbank processes are important, as observed in Pongo de Coñeq area during Middle Miocene times (MD 84). This part of section 1 probably corresponds to a meandering fluvial system. However no lateral accretion process has been registered here.

MD 198 deposits evolve upwards into 20 m-thick units of stacked medium-grained sandstones (740-785 m, Figure 15) intercalated by thick fine-grained deposits (alternating facies associations FCs and O). Overbank processes are still highly represented and correspond to: blue to grey mudstones deposited in an anoxic swampy environment such as oxbow lake (Osw), fine-grained sandstone sheets probably corresponding to splays or unconfined flows and massive to bioturbated reddish mudstones typical of floodplain environment. From 875 m to 990 m, deposits also show intervals of stacked sandstones intercalated by fine-grained deposits. Little scale coarsening upward silty to sandy interval in the overbank succession (at 870 m) is interpreted as crevasse splay deposits. However, at 900 m, palynology indicates a mangrove deltaic plain environment. Strata situated between 870 m and 990 m are consequently interpreted as fluvio-deltaic deposits (coastal facies associations CCs and C for the deltaic deposits). Blue to grey-colored mudstone deposits described in this interval are the result of deposition in an anoxic coastal swamp system (Csw). The coarsening-up package made up of three different fining-up sandy units vertically stacked (870-890 m) probably corresponds to delta fan deposition. The transition between fluvial system to deltaic system may be taken with care as only one marine-related palynomorphs association has been described for this interval.

Deposits from outcrop MD 209 (1114-1257 m, Figure 15) are made up of sandy to conglomeratic units related to deposition in a fluvial channel (FCs). Fluvial overbank facies (O) proportion is very small. The high proportion of mud clasts can be explained by the erosion of well-developed adjacent muddy levees. The

highly amalgamated vertical stacking pattern as well as the preponderance of sandy units in comparison with overbank deposits is consistent with a higher-energy fluvial system (braided fluvial system?).

Deposits situated between outcrops MD 199 and MD 202 (1340-2130 m, Figure 16) are all characterized by 5 m to 20 m-thick stacked medium-grained fluvial sandstones deposits (FCs) intercalated by overbank facies (O). Some sandy intervals show important vertical amalgamated pattern (1385-1415 m and 1495-1518 m intervals) but overbank facies still concern half of the sedimentary section. Based on the high contribution of overbank processes, the fluvial system corresponding to this interval is not consistent with a pure braided system. Fluvial settings probably correspond to meandering system with occasional alternating periods of aggradation and vertical stacking according to the base level readjustment. Part of section 4 comprised between 1790 m and 2130 m has not been described in details due to difficult access conditions even if the main lithological successions have been reported.

The overlying Middle Miocene coarsening-up sequence (2160-2175 m, Figure 16) is made up of sandstones, sandy conglomerates and conglomerates interpreted as prograding deltaic fan deposits (CCcg). The marine influence is attested by the presence of Dinoflagellates and marine-related palynomorphs found in the underlying deposits (C) of MD 202 outcrop (Table 2). If we consider that the rest of the sedimentary section related to MD 202 (2215-2232 m) is continental, the corresponding facies shall be interpreted as fluvial channels and floodplain deposits (FCcg, FCs and O). Nevertheless, it is important to note that the sandy and conglomeratic units of this interval present very coarse granulometry, indicating in any cases higher energy fluvial or fluvio-deltaic system.

An important thrust, visible on seismic line 109 (Thrust fault B, Figure 5), is situated nearby MD 202. We consider for this study that the fault is located just above MD 202 deposits and that it separates the Middle Miocene deposits (MD 202) from the unconformably overlying Depositional Sequence 2 Late Miocene to Early Pliocene strata.

6.2.2. Depositional Sequence 2 (Late Miocene-Early Pliocene)

The second Depositional Sequence consists of outcrops MD 205 (at 2380 m), MD 204 (at 2465 m) and MD 206 (at 2805 m) in section 4 (Figure 17), MD 208 and MD 311 in section 5 and of MD 325 and MD 51 outcrops in Puerto Maldonado (section 5).

From MD 205 to the top of MD 204 (dated at c.a. 3.45 Ma by Ar/Ar dating) the section is characterized by thick conglomerates 10- to more than 15 m- thick intercalated with mudstones and rare sandy units. Because fine-grained deposits of outcrop MD 204 yielded marine-related palynomorphs suggesting a mangrove coastal plain, we interpret part of this succession as coastal deposits (C). Underlying and overlying conglomeratic stacked units of this interval could either correspond to deltaic deposits related to this coastal environment (CCcg and C) or deposits corresponding to high-energy braided fluvial system (FCcg and O).

Conglomeratic units are thick, but the high proportion of fine-grained overbank and floodplain facies is not consistent with an alluvial system. This may indicates a high floodplain aggradation rate relative to the frequency of channel avulsion (Heller and Paola, 1996).

Section 4 ends with the deposits of MD 206 which represent the uppermost and youngest deposits described for this section (2805-2825 m, Figure 17). These are characterized by vertically stacked units of conglomeratic deposits suggesting high energy fluvial channels (FCcg) separated by fine-grained overbank deposits (O). Conglomerates are thinner than those described at MD 205 and MD 204.

At the base of section 5, Late Miocene to Pleistocene deposits from outcrops MD 208 and MD 311 (0-140 m, Figure 18) are also related to mangrove swamp in a coastal plain environment (Csw) based on palynomorphs and microfossil associations (Table 2). The corresponding sediments show blue-colored coastal swamp deposits (Facies association C) alternating with thin coarse-grained sandy units (Ccs).

In the modern foredeep of the Madre de Dios foreland basin near the city of Puerto Maldonado, biostratigraphical data from localities MD 51 and MD 325 indicate a Pliocene to Pleistocene age and both continental and marine-related environments (see biostratigraphic results in Table 2).

6.2.3. Depositional Sequence 3 (Late Pliocene to Pleistocene)

The third Depositional Sequence has only been described in section 5 (at 1400 m, Figure 18). It is characterized by sandy-conglomeratic fluvial deposits of MD 159 and MD 160 (FCcg). Through cross-bedded conglomeratic sandstones are vertically amalgamated and could be related to either a high energy meandering or braided fluvial system. However, the coarse granulometry suggest in any cases a high-energy proximal fluvial system.

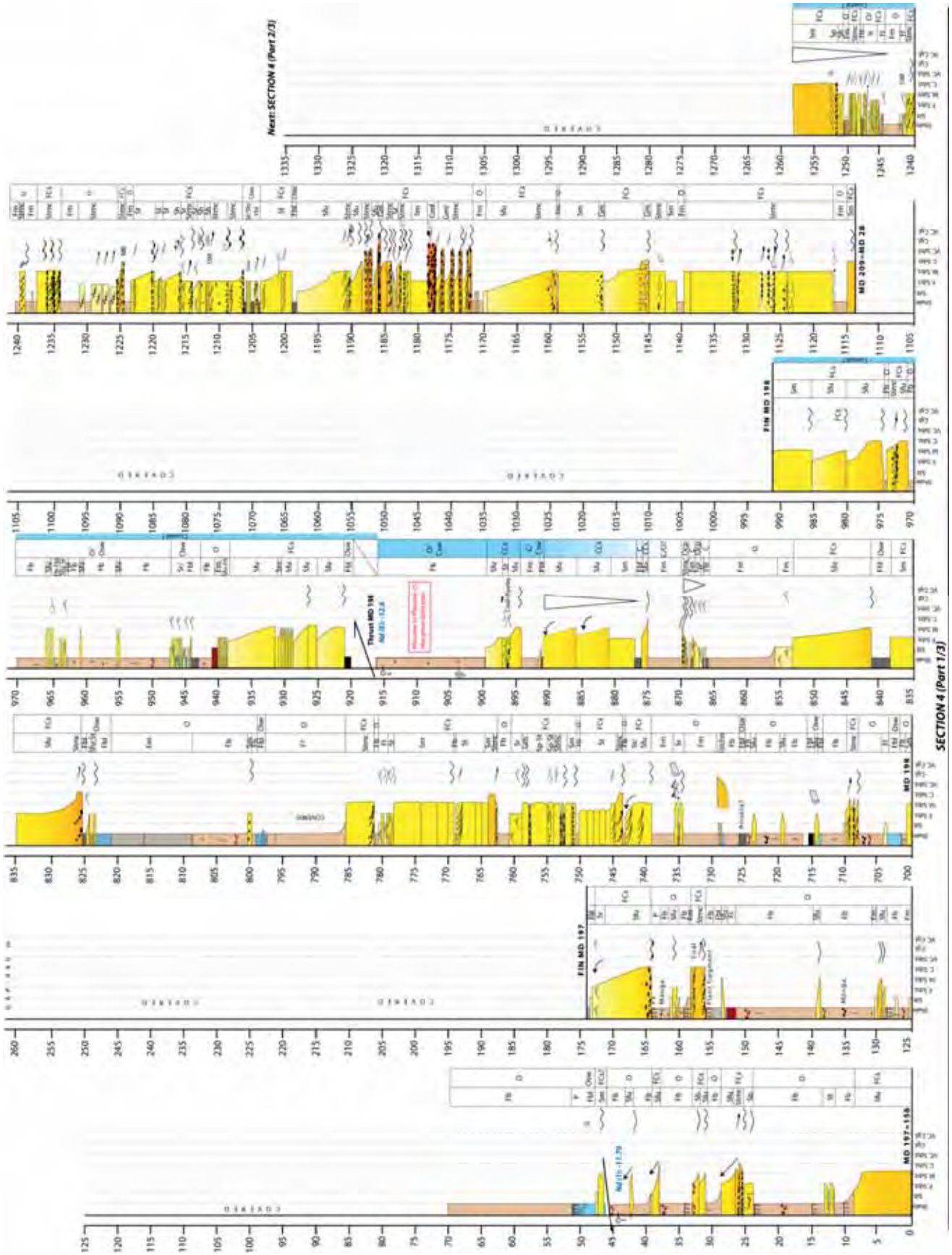

Figure 15: Stratigraphic section 4 (part 1/3) measured in the Punquiri syncline, Inambari transect. See Figure 1 for location, Table 3 for facies descriptions and Table 4 for the interpretation of facies associations. Also see Annex-Figure C.

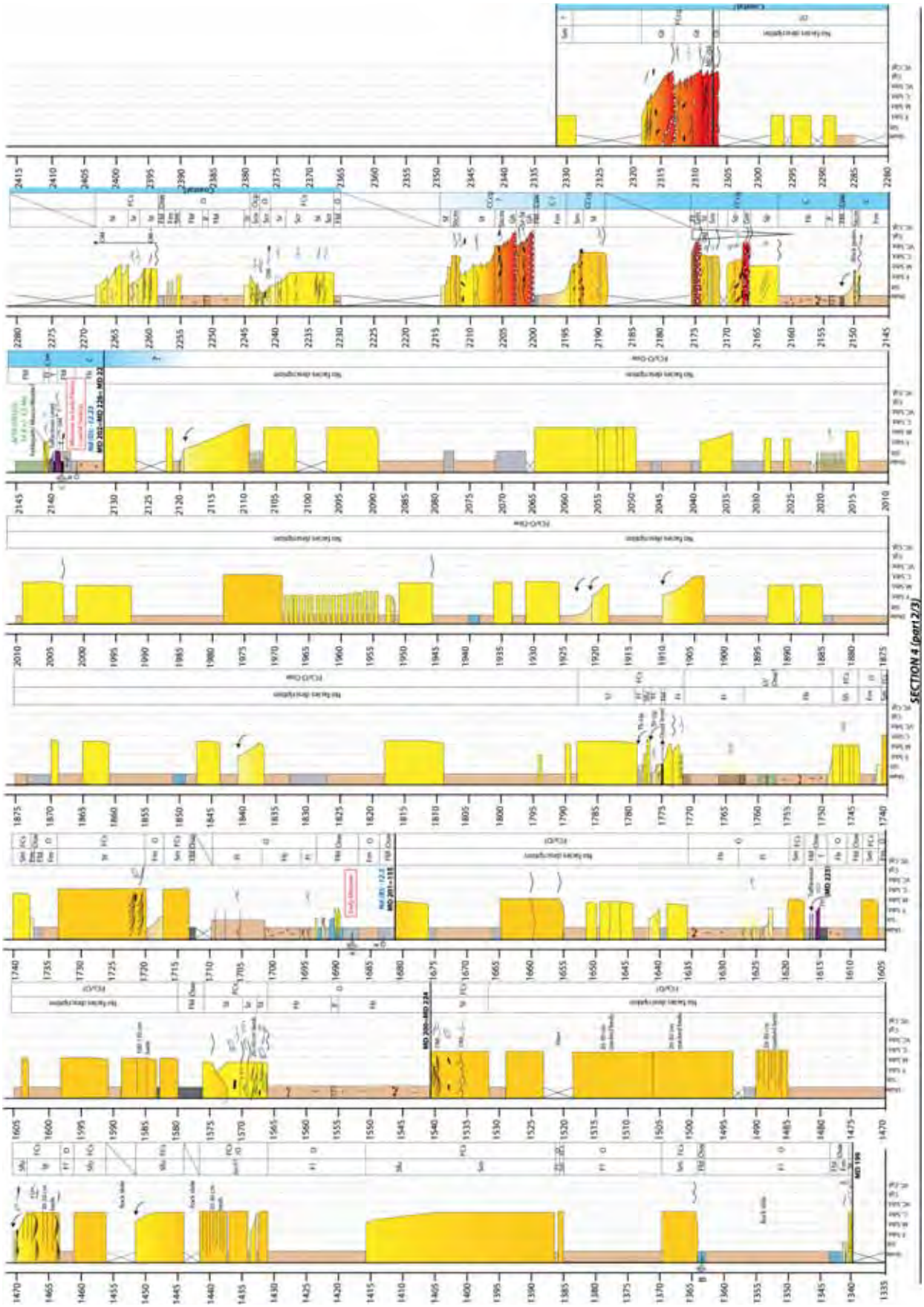

Figure 16: Stratigraphic section 4 (part 2/3) measured in the Punquiri syncline, Inambari transect. See Figure 1 for location, Table 3 for facies descriptions and Table 4 for the interpretation of facies associations. Also see Annex-Figure D.

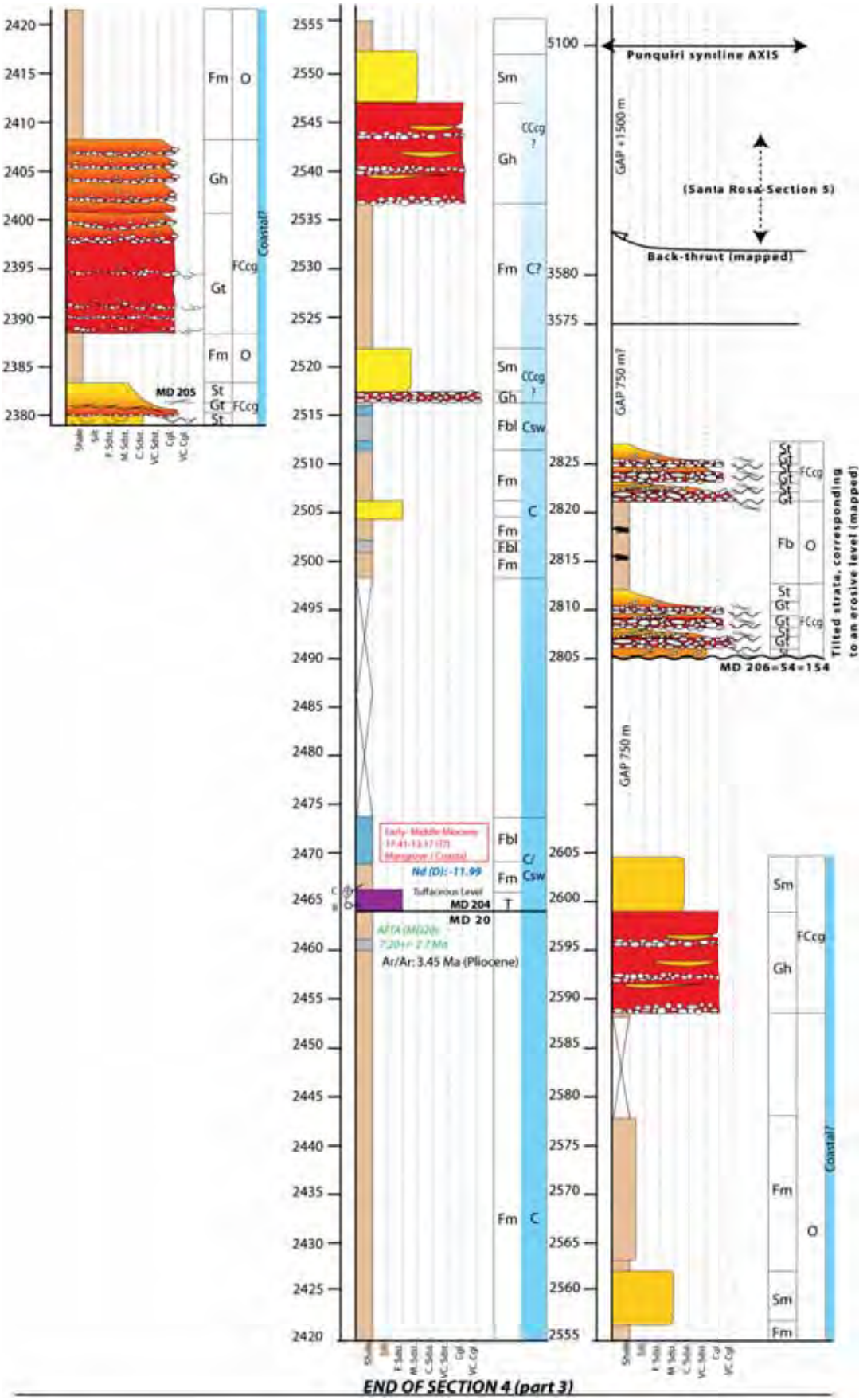

Figure 17: Stratigraphic section 4 (part3/3) measured in the Punquiri syncline, Inambari transect. See Figure 1 for location, Table 3 for facies descriptions and Table 4 for the interpretation of facies associations. Also see Annex-Figure E.

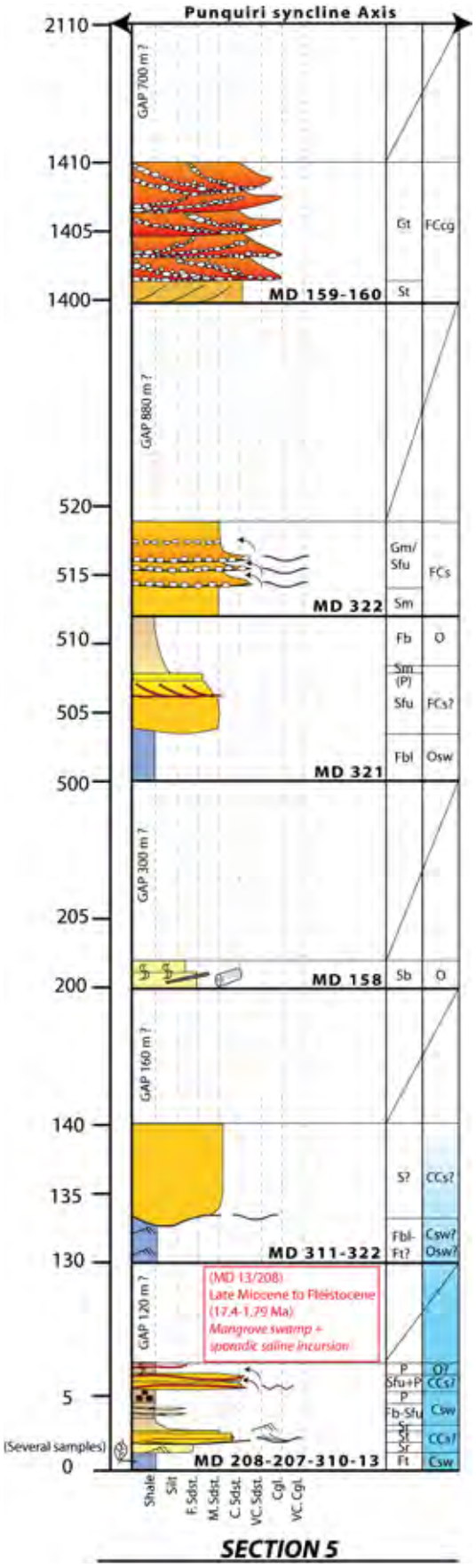

Figure 18: Stratigraphic section 5 measured near the locality of Santa Rosa, Inambari transect. See Figure 1 for location, Table 3 for facies descriptions and Table 4 for the interpretation of facies associations. Also see Annex-Figure H.

6.3. Correlation between the Pongo de Coñeq and the Inambari transects (Along-strike NW-SE stratigraphic correlation)

According to the new biostratigraphic constraints, to our sedimentological observations and to the paleo-depositional environments interpretations realized for the Pongo de Coñeq transect (sections 1, 2 and 3) and the Inambari transect (merging sections 4 and 5), we propose an along-strike stratigraphic correlation of the Neogene deposits of the Madre de Dios foreland basin (Figure 19).

In the chronostratigraphic diagram (Figure 20), both Neogene sections show an overall coarsening-upward trend from base to top (Figure 20).

In details the deposits of Depositional Sequence 1 of the Inambari section can be divided into two sub-sequences which are separated by deltaic or marine-related deposits (Figure 21). The first sub-sequence (from MD 197 to MD 198) is not complete and mainly shows evolution from fluvial to possible deltaic deposits. There is little or no variation in the channels amalgamation rates upwards and little change in the grain-size (fine-grained sandstones coarsening-upward into medium –grained sandstones). The second sub-sequence (from MD 209 to MD 202) corresponds to the most complete sequence we could document in this study. It is mainly characterized by a change in the grain-size (from sandstones to conglomerates at the top) and some changes in the vertical stacking patterns: from high amalgamated fluvial channels to isolated fluvial channels and finally isolated deltaic deposits at the top of the sequence.

Unfortunately, the early Miocene deposits corresponding to Depositional Sequence 1 are not preserved at the base of the Pongo de Coñeq section. So that it is not possible to document the presence of sub-sequence 1 in the Pongo de Coñeq area. However, the sub-sequence 2 deposits of the Inambari section are also registered in the Pongo de Coñeq section (see outcrop MD 61). This outcrop is also characterized by deltaic deposits which allow them to be correlated to those described in MD 202 (top of sub-sequence 2).

The base of Depositional Sequence 2 (Late Miocene) is poorly documented in both the Pongo de Coñeq and the Inambari transects (Figure 20). Observations made for outcrop MD 245 (Pongo de Coñeq transect) suggest a meandering fluvial system with isolated channels developing in a broad floodplain. In both transects, the very Late Miocene to Pliocene times are characterized by coarse- grained sandstones to conglomerates that developed in a shallow marine-related environment. Well-constrained by radiometric data realized in MD 204 tuffaceous deposits, this shallow marine incursion is ~ 3.45 Ma in age. The corresponding deposits suggest coastal plain (MD 246 in the Pongo de Coñeq transect and MD 208 in the Santa Rosa transect) and deltaic (MD 204 in the Inambari transect) depositional environments (Figure 20). Again, as already described for the Late Early Miocene to Early Middle Miocene (sub-sequence 2), shallow marine deposits are related to coarse-grained deltaic deposits.

Finally, the Depositional Sequence 3 (Pleistocene) is characterized in both transects by very coarse conglomerate facies with important vertical stacking patterns. These deposits are very similar to the present-day deposits of the Madre de Dios River, considered to be a high-energy meandering to occasionally braided fluvial system.

Figure 19 (next page): Stratigraphic correlations of the Neogene deposits in the Madre de Dios Sub-Andean zone. Note that the Pongo de Coñeq section is a synthetic section created from sections 1, 2 and 3 (see Figure 13, and Figure 14).

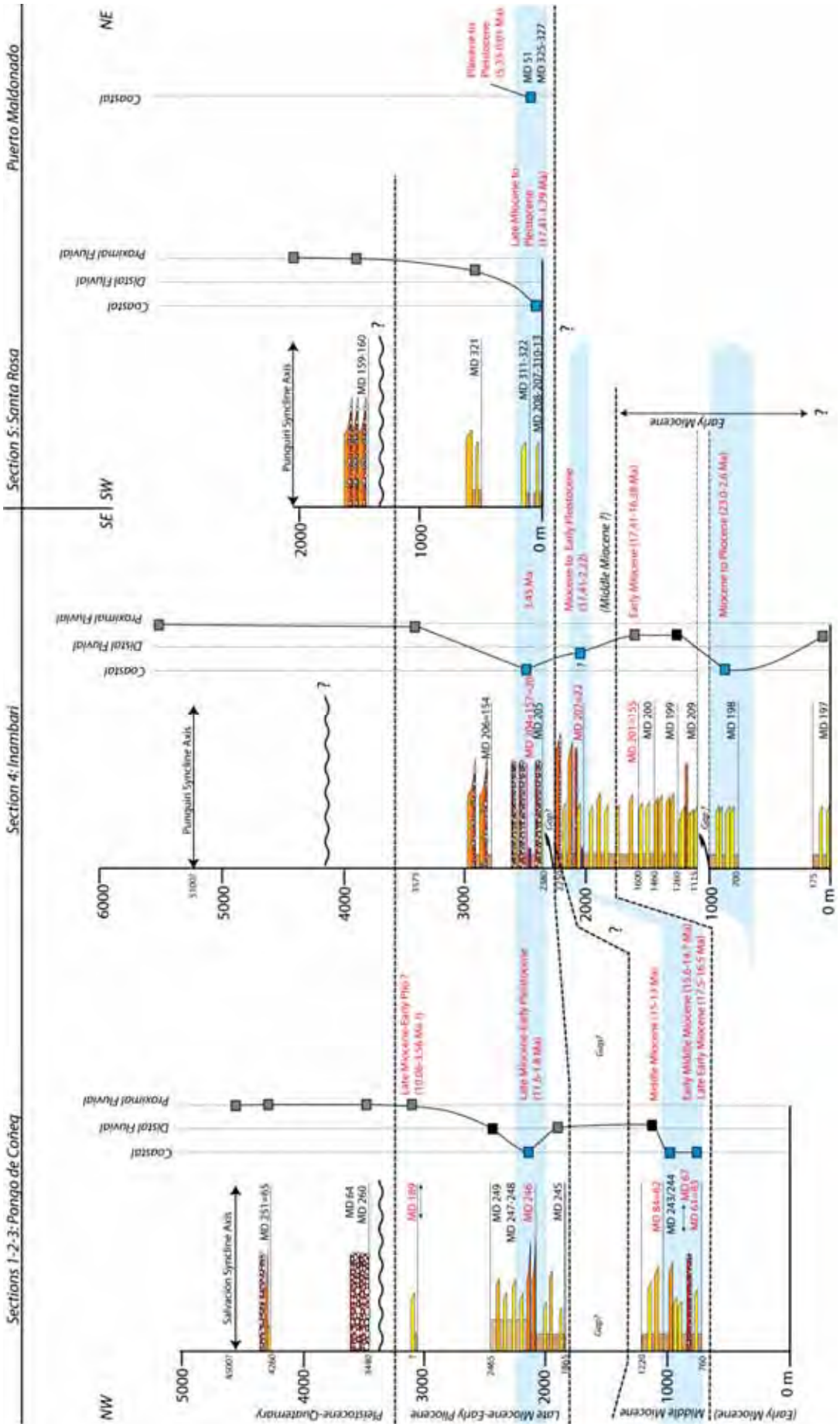
Sections 1-2-3: Pongo de Coñeq
Section 4: Inambari
Section 5: Santa Rosa
Puerto Maldonado
NW
SE
SW
NE
Coastal
Distal Fluvial
Proximal Fluvial
Salvacion Syncline Axis
Punquiri Syncline Axis
Pleistocene-Quaternary
Late Miocene-Early Pliocene
Middle Miocene
(Early Miocene)
Early Miocene
Miocene to Pliocene (23.0-2.6 Ma)
Miocene to Early Pleistocene (11.61-2.12)
(Middle Miocene ?)
3.45 Ma
Late Miocene to Pleistocene (11.61-1.79 Ma)
Pliocene to Pleistocene (5.33-0.01 Ma)
Late Miocene-Early Plio ? (10.08-3.56 Ma ?)
Late Miocene-Early Pleistocene (11.5-1.8 Ma)
Middle Miocene (11.5-11 Ma)
Early Middle Miocene (13.6-14.7 Ma)
Late Early Miocene (17.5-16.5 Ma)
Early Miocene (17.41-16.38 Ma)
MD 251+65
MD 64
MD 260
MD 189
MD 249
MD 247-248
MD 246
MD 245
MD 84+82
MD 243/244
MD 67
MD 61+63
MD 206+154
MD 205
MD 204+157+80
MD 203+82
MD 201+155
MD 200
MD 199
MD 209
MD 198
MD 197
MD 159-160
MD 321
MD 311-322
MD 208-207-310-313
MD 51
MD 325-327
Gap?
?

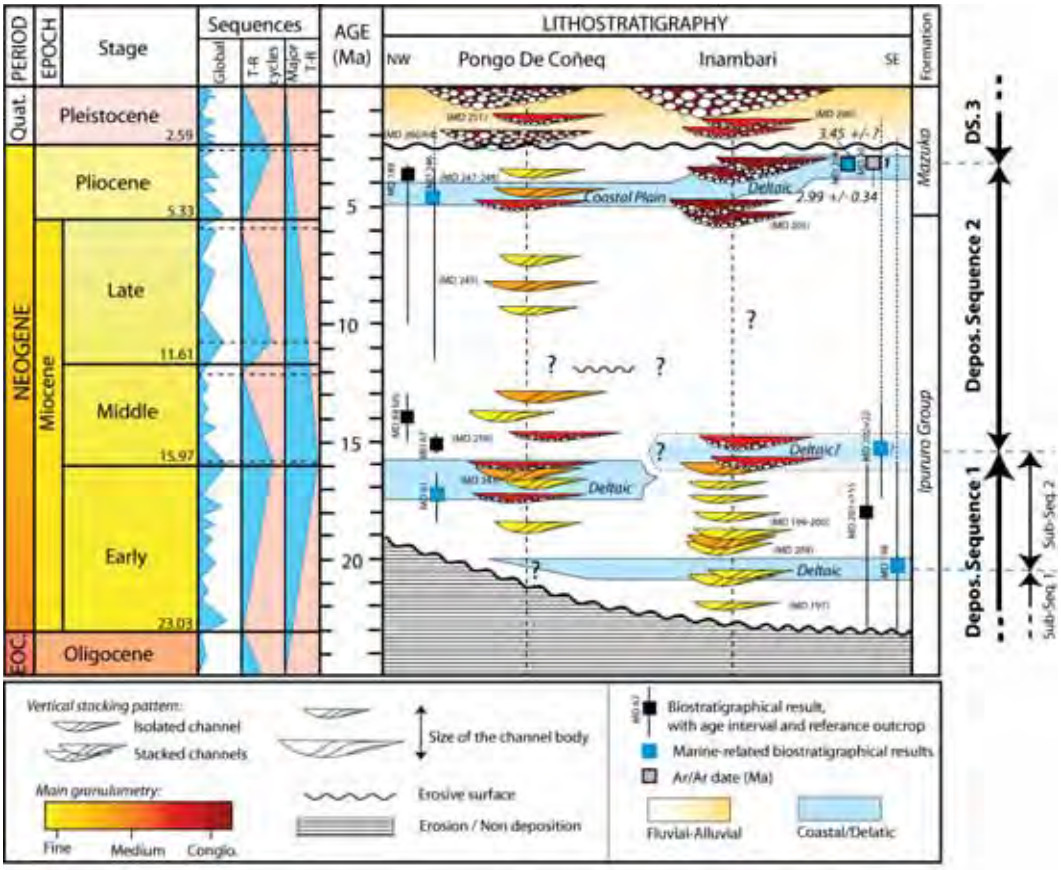

Figure 20: Wheeler diagram for the Neogene of the Pongo de Coñeq to Inambari along-strike section.

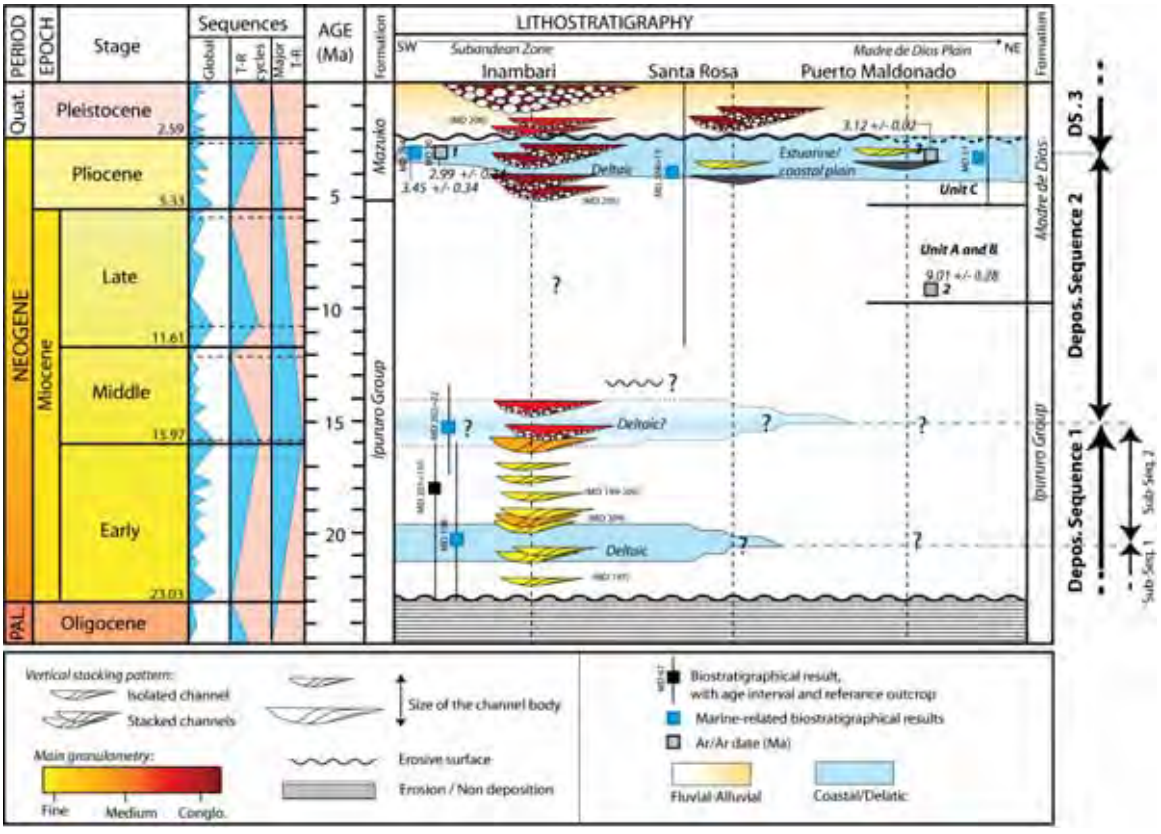

Figure 21: Wheeler diagram for the Neogene of the Inambari to Puerto Maldonado section.

6.4. Inambari to Puerto Maldonado (Proximal-distal SW-NE stratigraphic correlation)

We propose a stratigraphic correlation from the south-western most Inambari section (section 4) to the Santa Rosa section (section 5) and the Madre de Dios foredeep (Puerto Maldonado dataset) (Figure 19 and Figure 21).

Basal part of the Late Miocene to Pliocene Santa Rosa section shows tidally-influenced estuarine deposits (Hovikoski et al., 2005) and yielded shallow marine-related palynomorphs and foraminifera (Table 2). Near the city of Puerto Maldonado, samples collected in outcrops MD 51 and MD 325 also indicate a coastal swamp environment closely related to marine incursion for Late Miocene to Pliocene times (Table 2). Radiometric results from the Madre de Dios formation collected near Puerto Maldonado locality (2 and 3 in Figure 21) come from Cambell et al. (2001) and confirm our biostratigraphical results (MD 51= Pliocene to Pleistocene, see Table 2). Our new radiometric age documented for outcrop MD 204 (3.45±0.15 Ma) is also consistent with radiometric age obtained by Gil et al. (2001) in the same area (3.23±0.3 Ma). We suggest that these deposits can be correlated with the deltaic deposit documented in the Inambari section. Altogether, sedimentary observations, radiometric and biostratigraphical results from the depositional sequence 2 deposits indicate a shallow marine incursion around 3 Ma.

This marine incursion is therefore very well constrained and corresponds to the youngest marine ingression ever described in the overall Amazonia.

6.5. Burial histories and sedimentation rates

Burial histories and sedimentary deposition rates (SR) calculated for the Pongo de Coñeq transect (Figure 22) and the Inambari transect (Figure 23) are quite similar during the Cenozoic:

1) Little deposition and thus little burial from Late Cretaceous to Late Paleogene times (65-23.5 Ma),
2) A great increase in the sedimentary rate and thus in the resulting burial depth from the Early Miocene to the present (23.5-0 Ma),
3) An erosive event during the Late Middle Miocene period (see Part A of the manuscript) that separates Depositional Sequence 1 from Depositional Sequence 2, and
4) Significant very high sedimentation rates starting with the deposition of Depositional Sequence 2 during Late Miocene to Pliocene times (11-3,4 Ma).

Histogram of Figure 24 shows the mean sedimentation rates for the Pongo de Coñeq section (red bars) and the Inambari section (blue bars) over the Late Cretaceous to Cenozoic period.

The depositional Sequence 1 deposits (Early-Middle Miocene) show a great increase in sedimentation rates when compared with underlying Paleogene deposits. The sedimentation rates range from ~11 m/Ma during the Paleogene and range around ~120 m/Ma and 213m/Ma in the Pongo de Coñeq and the Inambari SAZ, respectively, during the Early Miocene (Figure 24). The difference between the sedimentation rates

calculated for the Early Miocene of the Pongo de Coñeq and the Inambari sections may be due to i) real difference in the thickness of Early Miocene strata between the two areas, ii) the very few biostratigraphic constraints available in the Inambari transect, and/or iii) the complex structural settings that characterizes the southern Punquiri syncline where the main Inambari section was measured. Faults in this area could have duplicated and thus thickened the Early Miocene strata measured on surface (see seismic section Figure 5).

Middle Miocene period shows relatively similar sedimentation rates than Early Miocene period: from 203 m/Ma to 237 m/Ma in the Inambari and Pongo de Coñeq SAZ, respectively (Figure 24). However, these sedimentation rates are poorly constrained as they are directly correlated to the thickness of eroded sediments during the erosive event of the Late Middle Miocene. We use the same default-value (150 m) for the amount of eroded sediments for both the Pongo de Coñeq and the Inambari models.

The Depositional Sequence 2 (Late Miocene to Pliocene) shows significant increase in the sedimentation rates in both sections: sedimentation rate in the Pongo de Coñeq transect is ~360 m/Ma and is ~ 385 m/Ma in the Inambari transect (Figure 24).

The Depositional Sequence 3 also shows very important sedimentation rates: ~345 m/Ma in the Pongo de Coñeq transect and ~413 m/Ma in the Inambari transect (Figure 24) and are quite similar to Depositional Sequence 2 sedimentation rates.

Finally, it is important to note that sedimentary rates reach higher values in the Inambari transect than in the Punquiri one for the Late Miocene to Quaternary period. These results are logical and predictable as the input thicknesses for the Late Miocene to present-day periods are higher for the Inambari than for the Pongo de Coñeq areas (see input data in the Supplementary dataset 1). The total thickness of the overall Late Cretaceous to Quaternary sedimentary sections is also greater in the Inambari transect (5100 m) than in the Pongo de Coñeq transect (4500 m), as the Punquiri syncline shows thicker Cenozoic sedimentary section than in the Salvación syncline.

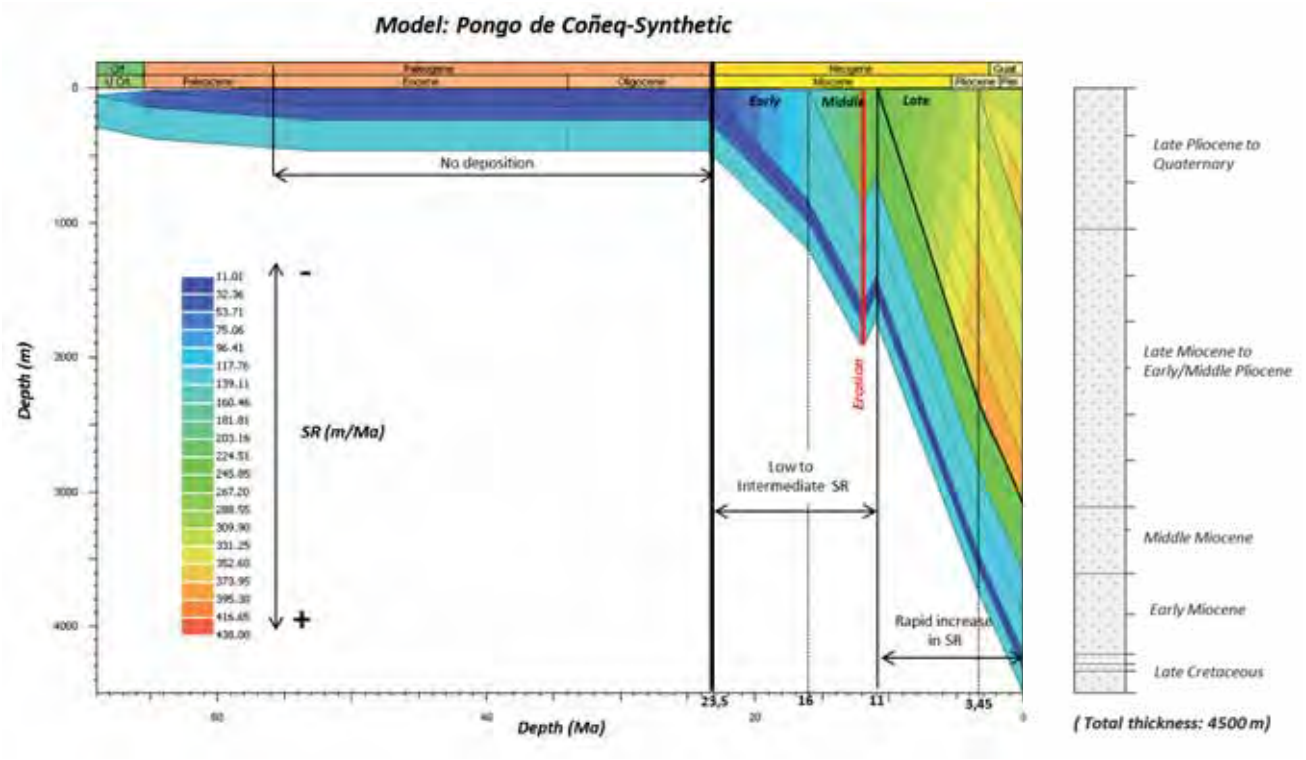

Figure 22: 1D Burial history of the Pongo de Coñeq section (4500 m of section in total) for the Late Cretaceous to present. Colors correspond to sedimentation rates values (low for blue and high for red). Software: Petromod-1D, Schlumberger. See Supplementary Dataset 1 for details about input data and boundary conditions.

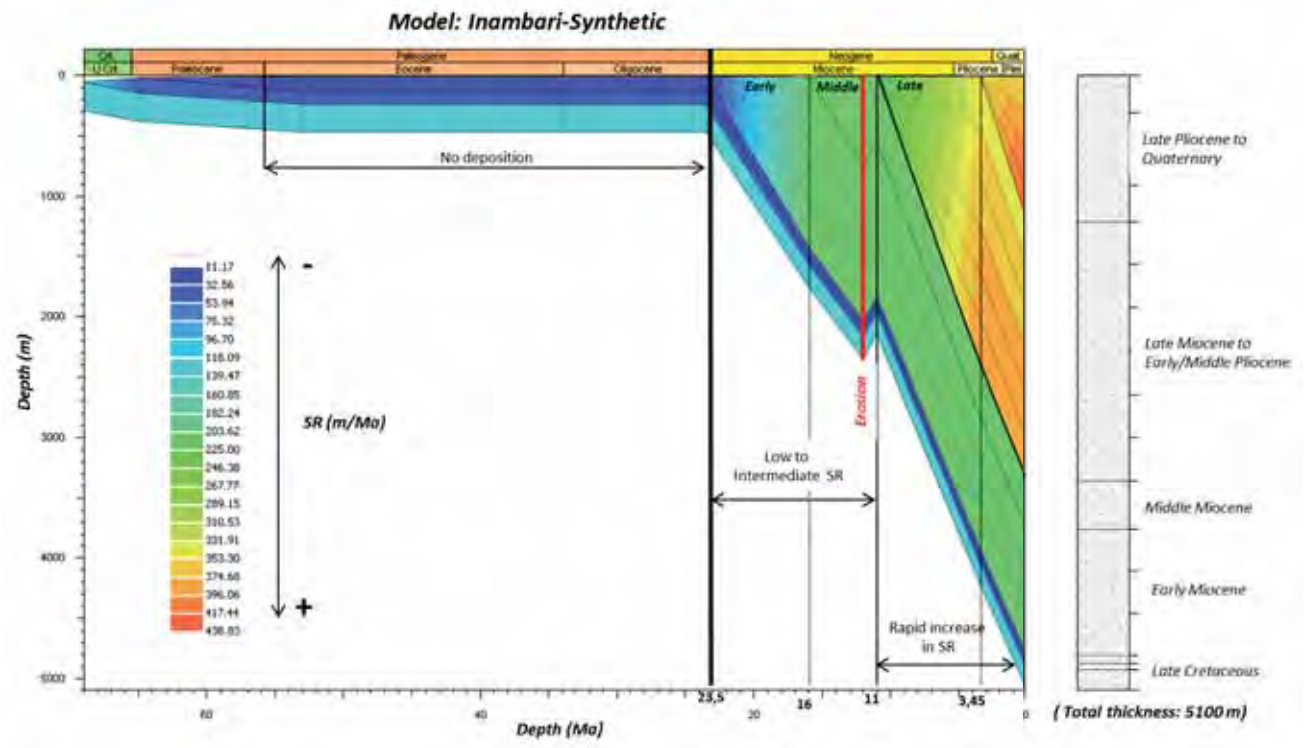

Figure 23: 1D Burial history of the Inambari section (5100 m in total) for the Late Cretaceous to present. Colors correspond to the sedimentation rates values (low for blue and high for red). Petromod-1D, Schlumberger. See Supplementary Dataset 1 for details about input data and boundary conditions.

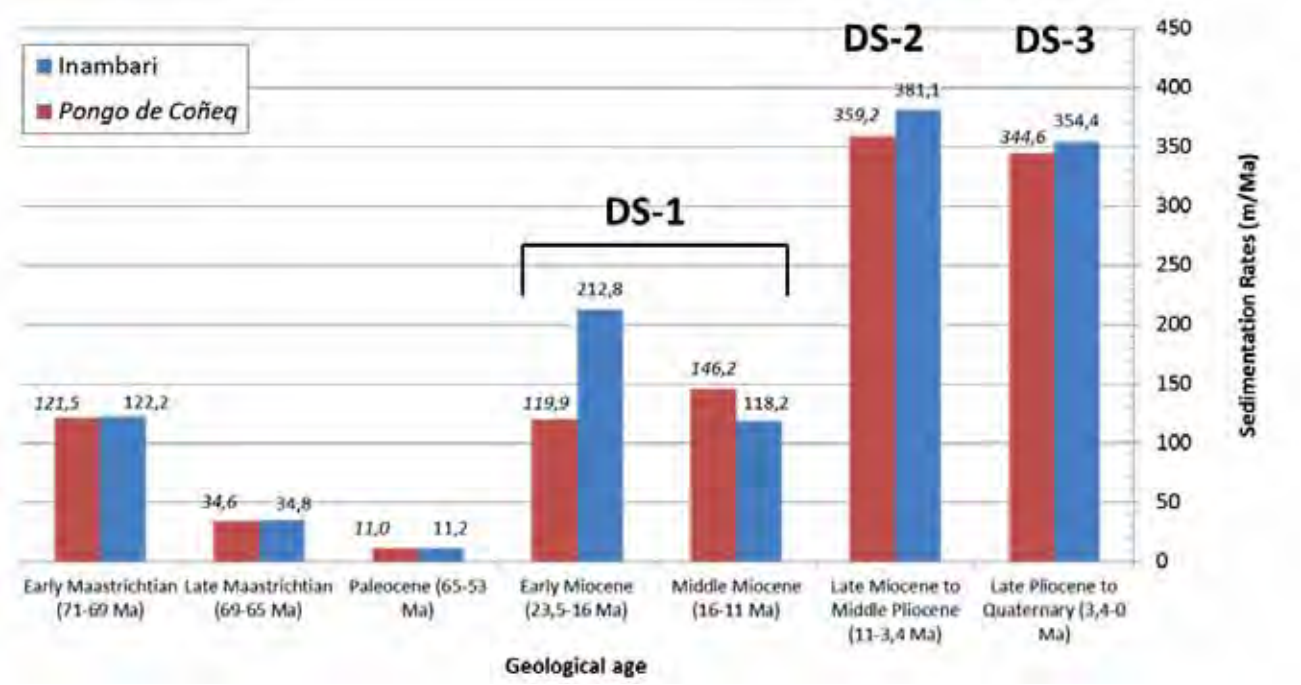

Figure 24: Histogram of the mean sedimentation rates calculated for various geological periods and for 2 stratigraphic sections: the Pongo de Coñeq section (in red) and the Inambari section (in blue). DS= Depositional Sequence. See Supplementary Dataset 1 for more details.

7. Discussion

7.1. Foreland basin stratigraphy

The overall coarsening-up trend of the Neogene sedimentary filling of the Madre de Dios SAZ suggests a depositional megasequence characterized by a strong increase in sedimentation rates. This is illustrated by the presence of distal low energy fluvial system during the Early Neogene evolving towards high energy proximal fluvial system in the Late Neogene to Pleistocene times (Figure 20 and Figure 21). In addition, the difference in Nd-Sr isotopic compositions between the Inambari and Pongo de Coñeq Neogene sedimentary rocks suggest that different source rocks fed the two systems and that two different drainage systems existed in the South Amazonian foreland basin at least since the Early Miocene. In detail, we show that the sedimentary infilling was characterized by three depositional sequences separated from each other by an erosive surface or a stratigraphic gap.

The first depositional sequence (Early-Middle Miocene) may be divided into two sub-sequences.

- The first sub-sequence (Early Miocene) has been only identified in the Inambari area (Figure 1) and consist of meandering fluvial system (MD 198) passing upward to higher energy fluvial system and fluvio-deltaic system that debouched into a shallow marine embayment (MD198, Figure 25-1).
- The second sub-sequence has been identified in both the Pongo de Coñeq and Inambari areas and show similar pattern as the first sub-sequence. It starts with high energy stacked fluvial deposits passing upward into aggrading fluvial deposits and ending with estuarine to deltaic deposits (Figure 25-2).

The second depositional sequence (Late Miocene-Pliocene) is recorded in both the Pongo de Coñeq and the Inambari areas but also in the distal part of the basin (Puerto Maldonado). It shows overall similar pattern as underlying sequences and starts with fluvial deposits (Figure 25-3) that pass upward into estuarine to deltaic deposits (Figure 25-4). The coastal upper part of the sequence could be correlated with transgressive estuarine deposits found in Puerto Maldonado (this study) and elsewhere in the Madre de Dios basin (Hovikoski et al., 2005, 2007). Compared with the first depositional sequence, the second depositional sequence is marked by a strong increase in sedimentation rates.

The last and third depositional sequence (Plio-Pleistocene) is marked by the establishment of a fluvial drainage system similar to that of present-day (Figure 25-5).

The two first sequences show similar pattern with transition from overfilled continental deposits to filled coastal deposits.

7.2. Controls on accommodation in retroarc foreland basins

Transition from overfilled to filled is caused by a increase in accommodation space which in turn depends on the interplay between sediment supply and base level chang es (Catuneanu, 2004) and references therein). In a retro-foreland basin setting, numerous mechanisms can be envisaged to account for an increase in

accommodation space including eustasy, dynamic subsidence, foreland related tectonics (i.e. loading/unloading cycles of (Catuneanu et al., 1997) and decrease in sediment supply.

First, a decrease in sediment supply is unlikely as our calculated sedimentation rates increase during the Neogene in agreement with the overall prograding and coarsening up pattern of the Neogene megasequence. Dynamic subsidence may be induced by subduction beneath the retro-foreland basin. Subduction generate long wavelength subsidence (Catuneanu, 2004; Catuneanu et al., 1997; Mitrovica et al., 1989; Pysklywec and Mitrovica, 2000) capable of maintaining foreland basin system below the base level, at filled stage (Catuneanu et al., 1997; Catuneanu, 2004) and thus of producing accommodation at the basin scale. Dynamic subsidence up to 40m/Myr has been invoked by Shephard et al. (Shephard et al., 2010)to account for the accommodation needed to explain the presence of the Middle Miocene Pebas Megawetland in the Northern part of the Amazonian basin. When compared with our calculated sedimentation rates, the subsidence induced by dynamic topography is negligible so that we believe that dynamic topography, if any, is not the main processes that have controlled the overfilled to filled sequence. Sea level variations cause global base level variations. Eustatic rise could be a good candidate to explain the overfilled to filled depositional sequence. However, strong increase in sedimentation rates and overall lowering of global-sea-level during the neogene times are not in favor of eustatic variations as a dominant process responsible for the overfilled to filled depositional sequence. In addition, the depositional sequence 2 ends with coastal deposits at ca 3 Ma, a time period during which global sea-level was lower than present-day (Haq et al., 1987) whereas depositional sequence 1 developed during time periods of relatively high sea-level. Rather, we propose that the overall coarsening-up trend of the Neogene megasequence and the transition from overfilled to filled in depositional sequences is controlled by loading/unloading cycles. The eastward migrating Andean deformation front towards the foredeep may explain the overall sedimentary facies progradation recorded by the Pongo de Coñeq and the Inambari Neogene sections, as it has been documented in the Bolivian Subandes by DeCelles and Horton (2003) and modelled by Flemings and Jordan (1990). In this case, the Neogene sedimentary infill of the Madre de Dios basin may have recorded the passage from a proximal foredeep to a wedge-top sedimentation.

Foredeep depozones are particularly characterized by high and increasing subsidence rates through time (DeCelles and Giles, 1996; DeCelles and Horton, 2003). The overall high proportion of overbank facies described in the first depositional sequence (sub-sequence 2) of both the Pongo de Coñeq and the Inambari sections combined with increase in sedimentation rates in the Early-Middle Miocene suggest high sedimentation influx associated with high subsidence rates in agreement with a deposition within the foredeep depozone. This proximal foredeep setting is also attested by the absence of growth strata in Punquiri and Salvación synclines during Period deformation 1 (see Chapter A). Coarser post Late Miocene depositional sequences 2 and 3 with similar sources as depositional sequence 1 may have recorded sedimentation within the wedge-top depozone. This is also in agreement with the growth strata documented for Period deformation 2 in both sections (see Chapter A).

At the scale of a depositional sequence, the evolution of the vertical amalgamation pattern of channel bodies as well as the evolution of the overall increase in grain-size and change in the depositional environment from continental to shallow-marine is characteristic of the Neogene infilling of the Madre de Dios basin. Similar sequences or "cyclothems" (2.4 to 15 Ma periods) have been described in foreland basins and attributed to pulses of active tectonic episodes separated by relatively quiescent periods (Blair and Bilodeau, 1988).

In the Depositional Sequence 1, between MD 209 and MD 202 (sub-sequence 2), we observe a transition from stacked fluvial channels to isolated channels and then a coarsening-upward trend ending with isolated conglomeratic deltaic channels. This sequence suggests an increasing accommodation space leading to a change in the depositional environment: from continental (overfilled-MD 209 and MD 199) to deltaic (filled-MD 202).

We suggest that the transition from filled to overfilled may be due to a tectonic quiescence stage (erosive surfaces) whereas the transition from overfilled to filled is caused by a tectonic loading period, which produced surface uplift in the adjacent Andean wedge and then higher flexural subsidence in the foredeep, leading to increasing accommodation space (isolated channels, MD 199) and finally to shallow-marine incursion (MD 202). Surface uplift and the subsequent increase in the erosion rates and sedimentary flux are attested by the increasing grain-size documented by the coarse-grained sandstones of the high-energy deltaic system (MD 202). We interpret this overall sedimentary facies retrogradation as an evidence of thrust activity. This is in agreement with the presence of coeval period 1 growth strata (see part A)

The depositional sequence 2 ends with coarse and thick deltaic deposits in both areas (Figure 19 and Figure 21). This depositional sequence 2 recorded well developed growth strata patterns (see part A) and an increase in sedimentation rates. We thus suggest a second period of tectonic loading of the growing Eastern Andean Orogenic wedge (EC-SAZ) during this period drove the more recent marine incursion registered in the Amazonian foreland (~3 Ma). This recent shallow-marine incursion represents the last filled-phase period of the Neogene stratigraphic section of both the Pongo de Coñeq and the Inambari section. The high sea-level stage documented by Haq et al. (1987) during the Pliocene possibly facilitated the incursion. The depositional sequence 2 is also accompanied by a ~ two-fold increase in sedimentation rates (up to 381m/Ma). In the Bolivian Subandes, Uba et al. (2007) correlated the Late Miocene increase in the sediment accumulation rates and the monsoon intensification to the development of a coeval fluvial megafan in the Bolivian Subandes. Modern fluvial megafans have been recognized in nonmarine foreland basins at the outlets of major rivers that drain fold-thrust belts, particularly in the Andean foreland basin systems (DeCelles and Horton, 2003; Latrubesse et al., 2012; Räsänen et al., 1992; Wilkinson et al., 2009).

On the basis of the overall coarsening-up pattern, the increase in the sedimentary rates towards the top of the section and the existence of analogues in the close Bolivian Subandes (Horton and DeCelles, 2001), we propose to interpret the Neogene fluvio-deltaic sedimentary infilling of the Madre de Dios SAZ as deposited

by an eastward migrating Distributary Fluvial System (DFS) sensu Davidson et al. (2013)or Megafan (sensu DeCelles and Cavazza (1999); Gohain and Parkash (1990); (Rossetti et al., 2012); Wilkinson et al. (2009).

7.3. Paleo-geographical implications of the marine incursions

We document the presence of three shallow marine ingressions driven by Andean tectonic loading in the Madre de Dios Basin.

Shallow marine ingression in Amazonia is still a matter of debate (Hoorn, 2006; Hoorn, 1996; Hovikoski et al., 2005; Räsänen et al., 1995) It is now well-accepted that from the Middle Miocene to the Late Miocene, western Amazonia was completely flooded by a lacustrine (Hoorn, 1993; Hoorn, 1994; Hoorn et al., 1995), and/or marine (Gingras et al., 2002a; Gingras et al., 2002b; Hovikoski et al., 2005; Räsänen et al., 1995) system or a combination thereof (Vonhof et al., 2003; Wesselingh, 2002). The southern extension of the Pebas Sea/Lake to the south and its possible connection with the Paranan and Pebas seas (Gingras et al., 2002b; Hernandez et al., 2005; Hovikoski et al., 2005; Uba et al., 2005) lack about 1100 km to sustain this connection (Roddaz et al., 2006). The tide-influenced deposits of the Beni Basin described by Roddaz et al. (2006) in Bolivia could be the northernmost deposits of the Miocene marine incursions within the Pebas system, the southernmost deposits of the Late Miocene Paranan ingression, or the Central deposits of the Miocene Amazonian interior seaway.

Because the study area is situated just at the junction of both possible Miocene marine pathway terminations, the three shallow marine incursions presented here for the Neogene period (at 25-20 Ma, 17-15 Ma and 3 Ma) could either come from the Caribbean Sea as well as from the southern Pacific Ocean. More work should be carried out to establish a more precise paleogeographical framework for these shallow-marine deposits.

The first marine incursion (25-20 Ma) could correspond to the earliest phase of the Pebas wetland development as recorded in Peru and Colombia and in the intracratonic Solimoes Basin of western Brazil by . The second marine incursion (17-15 Ma) could correspond to the Pebas incursion registered northerward, however sedimentary facies do not correspond to those described for the Middle Miocene to early Late Miocene (Pebas Phase, Hoorn et al., 2010). Finally, the third incursion corresponds to the most recent incursion ever described in the Amazonian basin.

The Neogene evolution of the Madre de Dios SAZ may be divided into several steps:

i. During the Early Miocene (25-20 Ma?, Figure 25-1), a first marine incursion is recorded in the southern present-day Inambari SAZ. This incursion probably corresponds to the final stages of a tectonic pulse in the Andean wedge which favored high subsidence and the entrance of an interior sea. We propose that the shallow marine sedimentary rocks described for that interval were deposited in the distal part of A DFS (Davidson et al., 2013), probably in a distal splay that connected with an interior sea as already illustrated by Hartley et al. (2010).

ii. From the Early Miocene (25-20 Ma?) to the very Late Early Miocene to Early Middle Miocene, fluvial deposits are characterized by an in increase in the aggradation rates. We suggest a second period of tectonic loading which ends up with another marine incursion (next step).

iii. The Late Early-Middle Miocene (~17-15 Ma, Figure 25-2) is characterized by a second marine incursion registered in the northern and southern SAZ and characterized by deltaic and coastal plain deposits. Again, we propose a distal DFS with marine termination.

iv. The Middle Miocene to Late Miocene (~15-10 Ma, Figure 25-3) period is not very well constrained as few sedimentary observations could be realized for this stratigraphic interval. We assume an overall continental depositional environment with transverse DFS terminating into a longitudinal fluvial river. Similar patterns has been interpreted in the northern Amazonian foreland basin for Late Miocene times by Roddaz et al. (Roddaz et al., 2005a).

v. The Late Miocene to Early Pliocene (~10-3 Ma) period shows very high sedimentation rates and thick fluvial deposits which may be very similar to those described for the previous period. The major part of these deposits corresponds to the sedimentary rocks deposited in the Salvación and Punquiri synclines (see seismic sections Figure 3 and Figure 5, respectively). We suggest a period of intense tectonic loading which ends up a third marine incursion.

vi. The Late Pliocene (~3 Ma, Figure 25-4) corresponds to the most recent marine incursion ever described in the Amazonian foreland. Deltaic to coastal deposits have been described in both the northern and southern Madre de Dios SAZ. We suggest that these shallow marine deposits are related to the final stage of the Late Miocene to Early Pliocene tectonic deformation phase.

vii. The post Early Pliocene to present-day (post ~3 Ma, Figure 25-5) period is characterized by the Fitzcarrald Arch uplift (Espurt, 2007; Espurt et al., 2009) and the progressive modern fluvial pattern setting up. The Pliocene DFS is replaced by a modern meandering Madre de Dios fluvial system presenting a longitudinal (NNE-SSW) fluvial drainage pattern (Rigsby et al., 2009).

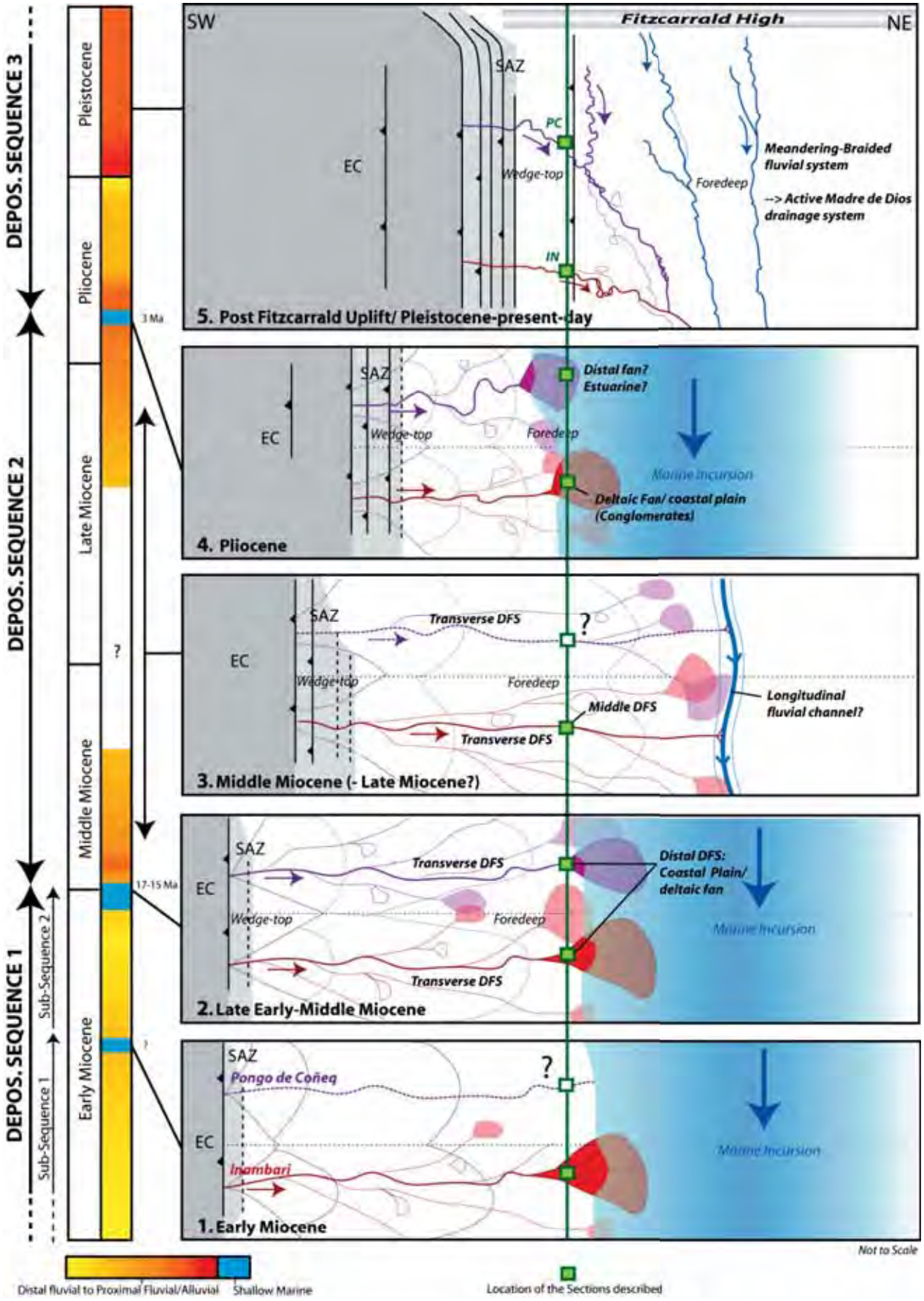

Figure 25: Synthetic figure resuming the paleogeographic evolution of the Madre de Dios foreland basin during the Neogene. IN= Inambari; PC= Pongo de Coñeq; DFS= Distributive Fluvial System; EC= Eastern Cordillera; SAZ= Subandean Zone.

Refrences

Antoine, P.-O., Roddaz, M., Brichau, S., Tejada-Lara, J., Salas-Gismondi, R., Altamirano, A., Louterbach, M., Lambs, L., Otto, T. and Brusset, S., 2013a. Middle Miocene vertebrates from the Amazonian Madre de Dios Subandean Zone, Perú. Journal of South American Earth Sciences, 42(0): 91-102.

Antoine, P.O., Roddaz, M., Brichau, S., Tejada-Lara, J., Salas-Gismondi, R., Altamirano, A., Louterbach, M., Lambs, L., Otto, T. and Brusset, S., 2013b. Middle Miocene vertebrates from the Amazonian Madre de Dios Subandean Zone, Peru. Journal of South American Earth Sciences, 42: 91-102.

Apatite to Zircon Inc., 2004. Peru samples: Apatoe and Zircon Fission-Tracks data.

Barragan, R., Geist, D., Hall, M., Larson, P. and Kurz, M., 1998. Subduction controls on the compositions of lavas from the Ecuadorian Andes. . Earth and Planetary Science Letters 154: p.153-166

Basu, A.R., Sharma, M. and Decelles, P.G., 1990. Nd, Sr-Isotopic provenance and trace-element geochemistry of Amazonian foreland basin fluvial sands, Bolivia and Peru. Implications for ensialic Andean orogeny. . Earth and Planetary Science Letters, 100(1-3): 1-17.

Blair, T.C. and Bilodeau, W.L., 1988. Development of tectonic cyclothems in rift, pull-apart, and foreland basins: sedimentary response to episodic tectonism. Geology, 16(6): 517-520.

Campbell, K.E., David, C. and Romero-pittman, L., 2006. The Pan-Amazonian Ucayali Peneplain , late Neogene sedimentation in Amazonia , and the birth of the modern Amazon River system. October.

Campbell, K.E., Frailey, C.D. and Romero-pittman, L., 1996. The Late Miocene gomphothere Amahuacatherium peruvium (Proboscidea: Gomphotheriidae) from Amazonian Peru: implications ofr the Great American Faunal Interchange. Boletin de la Sociedad Geologica del Peru, Serie D, 23: 1-152.

Campbell, K.E., Heizler, M., Frailey, C.D., Romero-Pittman, L. and Prothero, D.R., 2001. Upper Cenozoic chronostratigraphy of the southwestern Amazon Basin. Geology, 29(7): 595-598.

Carpenter, D. and Berumen, M., 1999. Geological and Geochemical Modeling of the Fold and Thrust Belt of the Southeastern, INGEPET Exploration and Exploration of Petroleum and Gas.

Catuneanu, O., 2004. Retroarc foreland systems—evolution through time. Journal of African Earth Sciences, 38(3): 225-242.

Catuneanu, O., Beaumont, C. and Waschbusch, P., 1997. Interplay of static loads and subduction dynamics in foreland basins: Reciprocal stratigraphies and the “missing” peripheral bulge. Geology, 25(12): 1087-1090.

Cooperación Técnica Peruana-Alemana, 1982. Evaluación de las cuencas Ucayali y Madre de Dios.

Dalrymple, R.W., Baker, E.K., Harris, P.T. and Hughes, M.G., 2003. Sedimentology and stratigraphy of a tide-dominated, foreland-basin delta (Fly River, Papua New Guinea. In: F.H. Sidi, Nummedal, D., Imbert, P., Darman, H., and Posamentier, H.W., eds. (Editor), Tropical Deltas of Southeast Asia—Sedimentology, Stratigraphy, and Petroleum Geology. SEPM, Special Publication, pp. p. 147-173.

Dalrymple, R.W. and Choi, K., 2007. Morphologic and facies trends through the fluvial–marine transition in tide-dominated depositional systems: A schematic framework for environmental and sequence-stratigraphic interpretation. Earth-Science Reviews, 81(3-4): 135-174.

Dalrymple, R.W., Zaitlin, B.A. and Boyd, R., 1992. Estuarine facies models; conceptual basis and stratigraphic implications. Journal of Sedimentary Research, 62(6): 1130-1146.

Davidson, S.K., Hartley, A.J., Weissmann, G.S., Nichols, G.J. and Scuderi, L.A., 2013. Geomorphic elements on modern distributive fluvial systems. Geomorphology, 180–181(0): 82-95.

DeCelles, P. and Cavazza, W., 1999. A comparison of fluvial megafans in the Cordilleran (Upper Cretaceous) and modern Himalayan foreland basin systems. Geological Society of America Bulletin, 111(9): 1315-1334.

DeCelles, P.G. and Giles, K.a., 1996. Foreland basin systems. Basin Research, 8(2): 105-123.

DeCelles, P.G. and Horton, B.K., 2003. Early to middle Tertiary foreland basin development and the history of Andean crustal shortening in Bolivia. Geological Society of America Bulletin, 115(1): 58-77.

Espurt, N., 2007. Influence de la subduction d'une ride asismique sur la dynamique de la plaque continentale chevauchante: exemple de la ride de Nazca et du bassin Amazonien, 1-326 pp.

Espurt, N., Baby, P., Brusset, S., Roddaz, M., Hermoza, W. and Barbarand, J., 2009. The Nazca Ridge and uplift of the Fitzcarrald Arch : implications for regional geology in northern South America Introduction.

Esteban, M. and Klappa, C., 1983. Carbonate depositional environ ments. AAPG Memoir, 33: 1-54.

Flemings, P.B. and Jordan, T.E., 1990. Stratigraphic modeling of foreland basins: Interpreting thrust deformation and lithosphere rheology. Geology, 18(5): 430-434.

Gil, W.F., 2001. Evolution latérale de la déformation d'un front orogénique: exemples des bassins subandins entre 0° et 16°S, University Paul Sabatier, Toulouse.

Gingras, M.K., Räsänen, M. and Ranzi, A., 2002a. The Significance of Bioturbated Inclined Heterolithic Stratification in the Southern Part of the Miocene Solimoes Formation, Rio Acre, Amazonia Brazil. PALAIOS, 17(6): 591-601.

Gingras, M.K., Rasanen, M.E., Pemberton, S.G. and Romero, L.P., 2002b. Ichnology and sedimentology reveal depositional characteristics of bay-margin parasequences in the Miocene Amazonian foreland basin. Journal of Sedimentary Research, 72(6): 871-883.

Gohain, K. and Parkash, B., 1990. Morphology of the Kosi megafan, Rachocki AH, Church M., Alluvial Fans: a Field Approach. Wiley, Chichester, pp. 151-178.

Grzybowski, J., 1898. Die Mikrofauna der Karpathenbildungen. II. Foraminiferen der naphtafährenden Schichten der Umgebung von Krosno. Bull. int. Acad., pol. Sci. Lett., Cl. Sci. math.-nat.: 180-186.

Gutierrez, M., 1982. Evaluacion potencial petrolifero cuencas Huallaga, Ucayali y Madre de Dios. Zonacion bioestratigrafica del intervalo Cretacico superior-Tertiario inferior, Petroperu, Internal Report, Lima.

Haq, B.U., Hardenbol, J. and Vail, P.R., 1987. Chronology of fluctuating sea levels since the Triassic. Science, v. 235: p. 1156–1167.

Hartley, A., Weissmann, G., Nichols, G. and Scuderi, L., 2010. Fluvial form in modern continental sedimentary basins: Distributive fluvial systems: REPLY. Geology, 38(12): e231-e231.

Hermoza, W., 2004. Dynamique tectono-sedimentaire et restauration sequentielle du retro-bassin d'avant-pays des Andes Centrales, Univeristy Paul Sabatier, Toulouse, 196 pp. pp.

Hernandez, R.M., Jordan, T.E., Farjat, A.D., Echavarria, L., Idleman, B.D. and Reynolds, J.H., 2005. Age, distribution, tectonics, and eustatic controls of the Paranense and Caribbean marine transgressions in southern Bolivia and Argentina. Journal of South American Earth Sciences, 19: 495-512.

Heron-Allen, E. and Earland, A., 1930. The Foraminifera of the Plymouth district. I. Journal of the Royal Microscopical Society, 50(1): 46-84.

Hoorn, C., 1993. Marine incursions and the influence of Andean tectonics on the Miocene depositional history of northwestern Amazonia: results of a palynostratigraphic study. Palaeogeography, Palaeoclimatology, Palaeoecology, 105(3): 267-309.

Hoorn, C., 1994. An environmental reconstruction of the palaeo-Amazon river system (Middle–Late Miocene, NW Amazonia). Palaeogeography, Palaeoclimatology, Palaeoecology, 112(3): 187-238.

Hoorn, C., 2006. Mangrove forests and marine incursions in Neogene Amazonia (lower Apaporis River, Colombia). Palaios, 21(2): 197-209.

Hoorn, C., Guerrero, J., Sarmiento, G.A. and Lorente, M.A., 1995. Andean tectonics as a cause for changing drainage patterns in Miocene northern South America. Geology, 23(3): 237-240.

Hoorn, C., Wesselingh, F.P., ter Steege, H., Bermudez, M.a., Mora, a., Sevink, J., Sanmartín, I., Sanchez-Meseguer, a., Anderson, C.L., Figueiredo, J.P., Jaramillo, C., Riff, D., Negri, F.R., Hooghiemstra, H., Lundberg, J., Stadler, T., Särkinen, T. and Antonelli, a., 2010. Amazonia through time: Andean uplift, climate change, landscape evolution, and biodiversity. Science (New York, N.Y.), 330(6006): 927-31.

Hoorn, M., 1996. Miocene deposits in the Amazonian foreland basin. Science, 273: 122-122.

Horton, B.K. and DeCelles, P.G., 1997. The modern foreland basin system adjacent to the Central Andes. Geology, 25(10): 895-895.

Hovikoski, J., Gingras, M., Räsänen, M., Rebata, L., Guerrero, J. and Ranzi, A., 2007a. The nature of Miocene Amazonian epicontinental embayment: High-frequency shifts of the low-gradient coastline. GSA Bulletin, 119: 1506-1520.

Hovikoski, J., Gingras, M., Räsänen, M., Rebata, L.A., Guerrero, J., Ranzi, A., Melo, J., Romero, L., del Prado, H.N. and Jaimes, F., 2007b. The nature of Miocene Amazonian epicontinental embayment: High-frequency shifts of the low-gradient coastline. Geological Society of America Bulletin, 119(11-12): 1506-1520.

Hovikoski, J., Räsänen, M., Gingras, M., Lopéz, S., Romero, L., Ranzi, A. and Melo, J., 2007c. Palaeogeographical implications of the Miocene Quendeque Formation (Bolivia) and tidally-influenced strata in southwestern Amazonia. Science Direct, 243: 23-41.

Hovikoski, J., Räsänen, M., Gingras, M., Roddaz, M., Brusset, S., Hermoza, W., Pittman, L.R. and Lertola, K., 2005. Miocene semidiurnal tidal rhythmites in Madre de Dios, Peru. Geology, 33(3): 177-180.

Hovikoski, J., Wesselingh, F.P., Räsänen, M., Gingras, M. and Vonhof, H.B., 2010. Marine influence in Amazonia: evidence from the geological record.

Jacobsen, S.B. and Wasserburg, G.J., 1980. Sm-Nd isotopic evolution of chondrites. Earth and Planetary Science Letters, 50(1): 139-155.

Jaramillo, C., Hoorn, C., Silva, S., Leite, F., Herrera, F., Quiroz, L., Dino, R. and Antonioli, L., 2010. The origin of the modern Amazon rainforest: implications of the palynological and palaeobotanical record, Amazonia, Landscape and Species Evolution, pp. 317-334.

Jeffery, M.L., Poulsen, C.J. and Ehlers, T.A., 2012. Impacts of Cenozoic global cooling, surface uplift, and an inland seaway on South American paleoclimate and precipitation δ18O. Geological Society of America Bulletin, 124(3-4): 335-351.

Jo, H., Rhee, C. and Chough, S., 1997. Distinctive characteristics of a streamflow-dominated alluvial fan deposit: Sanghori area, Kyongsang Basin (Early Cretaceous), southeastern Korea. Sedimentary Geology, 110(1): 51-79.

Jordan, T.E., 1995. Retroarc foreland and related basins. In: C.J. Busby and R.V. Ingersoll (Editors), Tectonics of Sedimentary Basins. Blackwell Science, Oxford, pp. 331-362.

Jordan, T.E., Isacks, B.L., Allmendinger, R.W., Brewer, J.A., Ramos, V.A. and Ando, C.J., 1983. Andean tectonics related to geometry of subducted Nazca plate. Geol. Soc. Am. Bull., 94: 341-361.

Kay, S.M., Coira, B. and Viramonte, J., 1994. Young mafic back arc volcainc-rocks s indicators of continental lithospheric delamination beneath the Argentine Puna plateau, Central Andes Journal of Geophysical Research-Solid Earth, 99(B12): 24323-24339.

Klappa, C.F., 1983. A process-response model for the formation of pedogenic calcretes. Geological Society, London, Special Publications, 11(1): 211-220.

Latrubesse, E.M., da Silva, S.A., Cozzuol, M. and Absy, M.L., 2007. Late Miocene continental sedimentation in southwestern Amazonia and its regional significance: Biotic and geological evidence. Journal of South American Earth Sciences, 23(1): 61-80.

Latrubesse, E.M., Stevaux, J.C., Cremon, E.H., May, J.-H., Tatumi, S.H., Hurtado, M.A., Bezada, M. and Argollo, J.B., 2012. Late Quaternary megafans, fans and fluvio-aeolian interactions in the Bolivian Chaco, Tropical South America. Palaeogeography, Palaeoclimatology, Palaeoecology, 356: 75-88.

Lorente, M.A., 1986. Palynology and palynofacies of the Upper Tertiary in Venezuela. J. Cramer Berlín.

Louterbach, M., Roddaz, M., Baby, P., Bailleul, J., Antoine, P.-O., Adnet, S., Kim, J.H., Van Soelen, E., Parra, F., Gérard, J., Calderon, Y., Gagnaison, C. and Sinninghe Damsté, J.S., Submitted. Evidences for a late Paleocene marine incursion in Southern Amazonia (Madre de Dios Sub-Andean Zone, Peru). Palaeogeography, Palaeoclimatology, Palaeoecology.

Marivaux, L., Salas-Gismondi, R., Tejada, J., Billet, G., Louterbach, M., Vink, J., Bailleul, J., Roddaz, M. and Antoine, P.O., 2012. A platyrrhine talus from the early Miocene of Peru (Amazonian Madre de Dios Sub-Andean Zone). Journal of Human Evolution, 63(5): 696-703.

Miall, A.D., 1996. The geology of fluvial deposits: sedimentary facies, basin analysis and petroleum geology. Springer-Verlag Inc Berlin, 582 pp. pp.

Mitrovica, J., Beaumont, C. and Jarvis, G., 1989. Tilting of continental interiors by the dynamical effects of subduction. Tectonics, 8(5): 1079-1094.

Mobil Oil Corporation, 1998. Phase I Technical Synthesis Tambopata Lot 78, Peru.

Mulch, A., Uba, C.E., Strecker, M.R., Schoenberg, R. and Chamberlain, C.P., 2010. Late Miocene climate variability and surface elevation in the central Andes. Earth and Planetary Science Letters, 290(1-2): 173-182.

Pinto, L., 2003. Traçage de l'érosion Cénozoïque des Andes Centrales à l'aide dela minéralogie et de la géochmie des sédiments (Nord du Chili et Nord-Ouest de la Bolivie), University Paul Sabatier, Toulouse.

Poulsen, C.J., Ehlers, T.A. and Insel, N., 2010. Onset of convective rainfall during gradual late Miocene rise of the central Andes. Science, 328(5977): 490-493.

Pysklywec, R. and Mitrovica, J., 2000. Mantle flow mechanisms of epeirogeny and their possible role in the evolution of the Western Canada Sedimentary Basin. Canadian Journal of Earth Sciences, 37(11): 1535-1548.

Räsänen, M., Neller, R., Salo, J. and Jungner, H., 1992. Recent and ancient fluvial deposition systems in the Amazonian foreland basin, Peru. Geological Magazine, 129(03): 293-306.

Räsänen, M.E., Linna, A.M., Santos, J.C. and Negri, F.R., 1995. Late Miocene tidal deposits in the Amazonian foreland basin. Science, 269(5222): 386-390.

Retallack, G., 1997. Palaeosols in the upper Narrabeen group of New South Wales as evidence of Early Triassic palaeoenvironments without exact modern analogues*. Australian Journal of Earth Sciences, 44(2): 185-201.

Ridgway, K.D. and Decelles, P.G., 1993. Stream-dominated alluvial fan and lacustrine depositional systems in Cenozoic strike-slip basins, Denali fault system, Yukon Territory, Canada. Sedimentology, 40(4): 645-666.

Rigsby, C.a., Hemric, E.M. and Baker, P.a., 2009. Late Quaternary Paleohydrology of the Madre de Dios River, southwestern Amazon Basin, Peru. Geomorphology, 113(3-4): 158-172.

Roddaz, M., 2004. Transition des stades alimentés à suralimentés dans les systèmes de rétro-bassin d'avant-pays.

Roddaz, M., Baby, P., Brusset, S., Hermoza, W. and Maria Darrozes, J., 2005b. Forebulge dynamics and environmental control in Western Amazonia: The case study of the Arch of Iquitos (Peru). Tectonophysics, 399(1–4): 87-108.

Roddaz, M., Brusset, S., Baby, P. and Hérail, G., 2006. Miocene tidal-influenced sedimentation to continental Pliocene sedimentation in the forebulge–backbulge depozones of the Beni–Mamore foreland Basin (northern Bolivia). Journal of South American Earth Sciences, 20(4): 351-368.

Roddaz, M., Christophoul, F., Zambrano, J.D.B., Soula, J.C. and Baby, P., 2012. Provenance of late Oligocene to quaternary sediments of the Ecuadorian Amazonian foreland basin as inferred from major and trace element geochemistry and Nd-Sr isotopic composition. Journal of South American Earth Sciences, 37: 136-153.

Roddaz, M., Hermoza, W., Mora, A., Baby, P., Parra, M., Christophoul, F., Brusset, S. and Espurt, N., 2010. Cenozoic sedimentary evolution of the Amazonian foreland basin system, pp. 61-88.

Roddaz, M., Viers, J., Brusset, S., Baby, P. and Hérail, G., 2005a. Sediment provenances and drainage evolution of the Neogene Amazonian foreland basin. Earth and Planetary Science Letters, 239(1–2): 57-78.

Rogers, G. and Hawkesworth, C.J., 1989. A geochemical traverse across the North Chilean Andes: evidence for crust generation from the mantle wedge. Earth and Planetary Science Letters, 91(3–4): 271-285.

Rossetti, D.F., Zani, H., Cohen, M.C.L. and Cremon, É.H., 2012. A Late Pleistocene–Holocene wetland megafan in the Brazilian Amazonia. Sedimentary Geology, 282(0): 276-293.

Shephard, G., Müller, R., Liu, L. and Gurnis, M., 2010. Miocene drainage reversal of the Amazon River driven by plate-mantle interaction. Nature Geoscience, 3(12): 870-875.

Turner, P., 1980. Continental red beds. Elsevier.

Uba, C.E., Heubeck, C. and Hulka, C., 2005. Facies analysis and basin architecture of the Neogene Subandean synorogenic wedge, southern Bolivia. Sedimentary Geology, 180: 91-123.

Uba, C.E., Heubeck, C. and Hulka, C., 2006. Evolution of the late Cenozoic Chaco foreland basin, Southern Bolivia. Basin Research, 18(2): 145-170.

Uba, C.E., Strecker, M.R. and Schmitt, A.K., 2007. Increased sediment accumulation rates and climatic forcing in the central Andes during the late Miocene. Geology(March 2009).

Valdivia, H., 1974. Estratigrafia de la Faja Subandina de la region de Madre de Dios.

Viers, J., Roddaz, M., Filizola, N., Guyot, J.L., Sondag, F., Brunet, P., Zouiten, C., Boucayrand, C., Martin, F. and Boaventura, G.R., 2008. Seasonal and provenance controls on Nd-Sr isotopic compositions of Amazon rivers suspended sediments and implications for Nd and Sr fluxes exported to the Atlantic Ocean. Earth and Planetary Science Letters, 274(3-4): 511-523.

Vonhof, H.B., Wesselingh, F.P., Kaandorp, R.J.G., Davies, G.R., van Hinte, J.E., Guerrero, J., Räsänen, M., Romero-Pittman, L. and Ranzi, A., 2003. Paleogeography of Miocene Western Amazonia: Isotopic composition of molluscan shells constrains the influence of marine incursions. Geological Society of America Bulletin, 115(8): 983-993.

Wesselingh, F.P., 2002. NEOGASTROPOD MOLLUSCS FROM THE MIOCENE OF WESTERN AMAZONIA , WITH COMMENTS ON MARINE TO FRESHWATER. Society, 76(2): 265-270.

Wilkinson, M.J., Marshall, L.G., Lundberg, J.G. and Kreslavsky, M.H., 2009. Megafan environments in northern South America and their impact on Amazon Neogene aquatic ecosystems.

Wright, V. and Tucker, M., 1991. Calcretes. Reprint Series Volume 2 of the International Association of Sedimentologists. Blackwell Scientific Publications.

Wygrala, B.P., 1989. Integrated study of an oil field in the southern Po basin, northern Italy. Kernforschungszentrum Karlsruhe Gmbh.

8. Figures

Conclusions et perspectives

Par une approche multidisciplinaire, cette thèse a permis d'apporter de nouvelles contraintes et des réponses aux grandes problématiques touchant la géologie andine et plus généralement le mode de construction des chaînes de montagnes en contexte non collisionnel et la façon dont se remplissent les bassins d'avant-pays retro-arc associés.

En particulier au sud du Pérou, notre étude montre au moins deux périodes de déformation dans la cordillère Orientale et la zone Subandine : i) depuis la fin de l'Oligocène jusqu'au Miocène Moyen (~25-14 Ma, Période 1), et ii) pendant le Miocène supérieur jusqu'au Pléistocène (~10-2.8 Ma, Période 2). Nos résultats ont des implications directes pour deux des plus importants problèmes fondamentaux en géologie andine, à savoir : i) l'importance du contrôle climatique Pliocène sur l'érosion et ii) les mécanismes responsables de la croissance et du soulèvement de l'Altiplano. Concernant le premier point, nos résultats thermochronologiques suggèrent que le refroidissement induit par l'érosion de la Cordillère Orientale au sud du Pérou n'est pas contrôlé par un changement climatique mais plutôt par le développement d'un empilement d'écailles ou duplex au front de la cordillère. Cette interprétation est en accord avec la présence de nombreuses strates de croissances identifiées dans les synclinaux transportés des deux transects étudiés et attribuées à la deuxième période de déformation (Miocène supérieur-Pléistocène). Concernant les mécanismes responsables de la formation de l'Altiplano, nos résultats thermochronologiques relatifs à la partie la plus interne des structures préservées du bassin de Madre de Dios ainsi que les restaurations structurales et les premiers essais de restauration séquentielles indiquent que le transfert du raccourcissement Andin depuis l'Altiplano vers la zone Subandine date de ~25 Ma. Nos résultats indiquent finalement que le soulèvement de l'Altiplano est un processus lent, résultant de la combinaison possible des processus d'épaississement crustal et de fluage de croûte inférieure.

Le bassin actuel de Madre de Dios (situé entre les latitudes 12ºS et 14ºS) peut être divisé en plusieurs zones de dépôts spécifiques aux bassins d'avant-pays retro-arc telles que définies par DeCelles and Giles (1996). Ainsi, la zone Subandine actuelle, adjacente à la Cordillère Orientale, correspond à la zone de wedge-top. Le reste du bassin d'avant-pays, depuis le front de déformation subandin jusqu'à la bordure Est du bassin correspond au foredeep. Suite au soulèvement récent de l'Arche de Fitzcarrald (Espurt, 2007) situé au Nord-Ouest de la zone d'étude, le bassin de Madre de Dios ne présente aucun forebulge ni backbulge actuels. Cependant, ces quatre zones de dépôts ont existé depuis le début de la mise en place du bassin d'avant-pays de Madre de Dios et ont évolué en fonction de la migration et de l'intensité de la déformation andine au cours du temps. A partir d'une coupe stratigraphique de 270 m d'épaisseur levée sur le terrain dans le synclinal de Salvación, au Nord-Ouest de la zone Subandine de Madre de Dios, et en nous basant sur des résultats biostratigraphiques, sédimentologiques et de provenance sédimentaire (DRX, concentrations en élément majeurs et traces et isotopie Nd-Sr), nous montrons qu'un forebulge était déjà présent dans cette zone au Maastrichtien. Les données présentées dans cette étude sont en accord avec la migration vers l'Est d'un bassin d'avant-pays ainsi qu'avec la présence d'un forebulge dès le Maastrichtien supérieur. Le bassin d'avant-pays du sud du Pérou a donc été actif au moins depuis le Maastrichtien supérieur. Nous suggérons que la flexure lithosphérique responsable de la création du forebulge a été provoquée par la charge orogénique de la Cordillère Occidentale exercée sur la lithosphère.

Par la suite, au cours du Paléocène, une incursion marine peu profonde envahit la zone Subandine actuelle. Cette incursion, enregistrée dans les dépôts Thanétien (Paléocène supérieur) de la zone Nord du bassin de Madre de Dios, n'avait jamais été décrite auparavant. Notre jeu de données, interdisciplinaires, documente la présence d'un estuaire

dominé par la marée débouchant dans une baie marine peu profonde et alimenté par la proto Cordillère Occidentale pendant le Thanétien. Finalement, nous suggérons que l'incursion Paléogène décrite ici a dû jouer un rôle déterminant dans la dynamique de la biodiversité neotropicale amazonienne en favorisant l'isolation bio-géographique et en promouvant la spéciation allopatrique des organismes terrestres. Ces mêmes processus sont d'ailleurs connus et décrits pour les incursions miocènes plus tardives affectant le méga-système marécageux Pebas et associées de la même manière au soulèvement des Andes.

Suite au début de la formation du bassin d'avant-pays de Madre de Dios au cours du Maastrichtien puis de l'incursion marine thanétienne, aucun dépôt daté de l'Eocène ou de l'Oligocène n'a été décrit. Nous suggérons une activité tectonique restreinte et des taux de sédimentation relativement bas. Il est également possible qu'un épisode érosif ait eu lieux à cette période.

Le Néogène est caractérisé dans la zone Subandine actuelle par une augmentation brutale des taux de sédimentation et par des dépôts très épais et bien conservés dans les synclinaux de Salvación et de Punquiri. Les dépôts néogènes à pléistocènes sont caractéristiques d'une méga-séquence de dépôt (dépôts de plus en plus grossiers et épais vers le sommet de la séquence), d'environ 4500 m d'épaisseur. Une telle séquence suggère le rapprochement progressif de la source sédimentaire et donc la migration du front orogénique andin vers l'Est. Ceci est illustré par des dépôts distaux de faible énergie pendant le début du Néogène évoluant ensuite vers des dépôts proximaux de haute énergie pendant le Néogène terminal et le Pléistocène. Cependant, des variations à plus petite échelle de ces séquences ont été observées. Dans cette étude, 3 principales séquences de dépôt ont été interprétées dans chacun des transects néogènes étudiés (celui de Pongo de Coñeq au Nord-Ouest et celui d'Inambari au Sud-Est du bassin) :

1. *Une première séquence pendant le Miocène inférieur à Moyen (divisée en deux sous-séquences),*
2. *Une deuxième séquence pendant le Miocène supérieur et jusqu'au Pliocène,*
3. *Une troisième et dernière séquence pendant la fin du Pliocène jusqu'au Pléistocène.*

Ces séquences de dépôts sont généralement caractérisées par : i) l'évolution d'un environnement de dépôt continental à deltaïque, ii) des chenaux (fluviaux ou deltaïques) de moins en moins fréquents et de plus en plus espacés depuis la base de la séquence jusqu'à son sommet, et iii) par une évolution grano-croissante de la granulométrie vers le haut de la séquence. L'évolution d'un environnement de dépôt fluvial vers un environnement de dépôt côtier (deltaïque) suggère une transition depuis un bassin « overfilled » à « filled » contrôlé par le chargement tectonique de la Cordillère Orientale. Nous proposons donc dans cet étude un « motif type » de remplissage sédimentaire de bassin d'avant-pays en réponse à un pulse de déformation tectonique. Ces séquences types se terminent par une augmentation considérable de l'espace d'accommodation, ce qui a provoqué aux moins deux à trois incursions marines dans le bassin Amazonien au cours du Cénozoïque.

En termes d'exploration pétrolière, les nouvelles données apportées par la thèse permettent finalement de réévaluer le potentiel pétrolier de la zone Subandine de Madre de Dios (Figure 1). La stratigraphie et la géométrie de la zone Subandine ayant été précisées, de nouveaux prospects voient le jour, par exemple au top des anticlinaux tertiaires situés sous le synclinal de Salvación au nord de la zone d'étude (Figure 1-B). Ces anticlinaux de rampe sont en effet des structures précoces probablement antérieures à la période de génération et d'expulsion des hydrocarbures. Les « oil seeps » tout comme les grès tidaux thanétiens imprégnés d'hydrocarbure et documentés vers l'anticlinal de Pantiacolla témoignent de la présence d'un système pétrolier actif (Figure 1-A). Le potentiel des réservoirs et structures pré-

crétacés (paléozoïques) a été mal documenté et minimisé jusqu'á présent (Figure 1-c) ; ces structures méritent elles aussi une réévaluation sérieuse. Enfin, les duplex situés sous le flanc sud du synclinal de Punquiri (Inambari) devraient être prioritaires en termes d'exploration (Figure 1-C) car ils renferment roches mères paléozoïques et réservoirs crétacés et sont situés en fenêtre de génération d'hydrocarbures. Des structures équivalentes ont déjà été perforées au sud de Madre de Dios (le puits Candamo) et ont montré la présence de gaz.

Finalement, afin de compléter ce travail de recherche, nous proposons de poursuivre les thématiques scientifiques suivantes:

- ***La paléogéographie précise du Crétacé supérieur au Sud du Pérou, depuis l'Altiplano jusqu'en Amazonie.*** *Cette étude devrait être réalisée sur la base de descriptions sédimentologiques précises, agrémentées d'analyses de provenance sédimentaire et d'observations structurales de terrain focalisées sur la déformation syn-sédimentaire déjà observée au Crétacé supérieur dans la zone Subandine (différents types, signification et étendue de cette déformation syn-sédimentaire ?).*
- ***La paléogéographie précise des incursions marines Cénozoïques****. Cette étude devrait se focaliser sur les connexions des incursions marines déjà décrites dans cette thèse. Des analyses de compositions isotopiques du Nd-Sr pourraient apporter des résultats originaux sur les différentes signatures géochimiques possibles selon les diverses incursions marines étudiées (signature spécifique à l'Atlantique ? au Pacifique ? aux Caraïbes?).*
- ***La restauration séquentielle du système d'avant-pays*** *amazonien sur les deux transects étudiés, depuis le Crétacé supérieur.*
- ***La modélisation stratigraphique des dépôts sédimentaires enregistrés avant, pendant et après le passage d'un forebulge****, migrant vers l'Est en contexte de bassin d'avant-pays Subandin (logiciel Dyonisos). Les différents paramètres influant sur le remplissage du bassin (pulses tectoniques, taux de précipitation, rapprochement des sources…) pourraient ainsi être testés. Cas d'étude : coupe de Pongo de Coñeq présentée en Partie B.*

References

DeCelles, P.G. and Giles, K.a., 1996. Foreland basin systems. Basin Research, 8(2): 105-123.

Espurt, N., 2007. Influence de la subduction d'une ride asismique sur la dynamique de la plaque continentale chevauchante: exemple de la ride de Nazca et du bassin Amazonien, 1-326 pp.

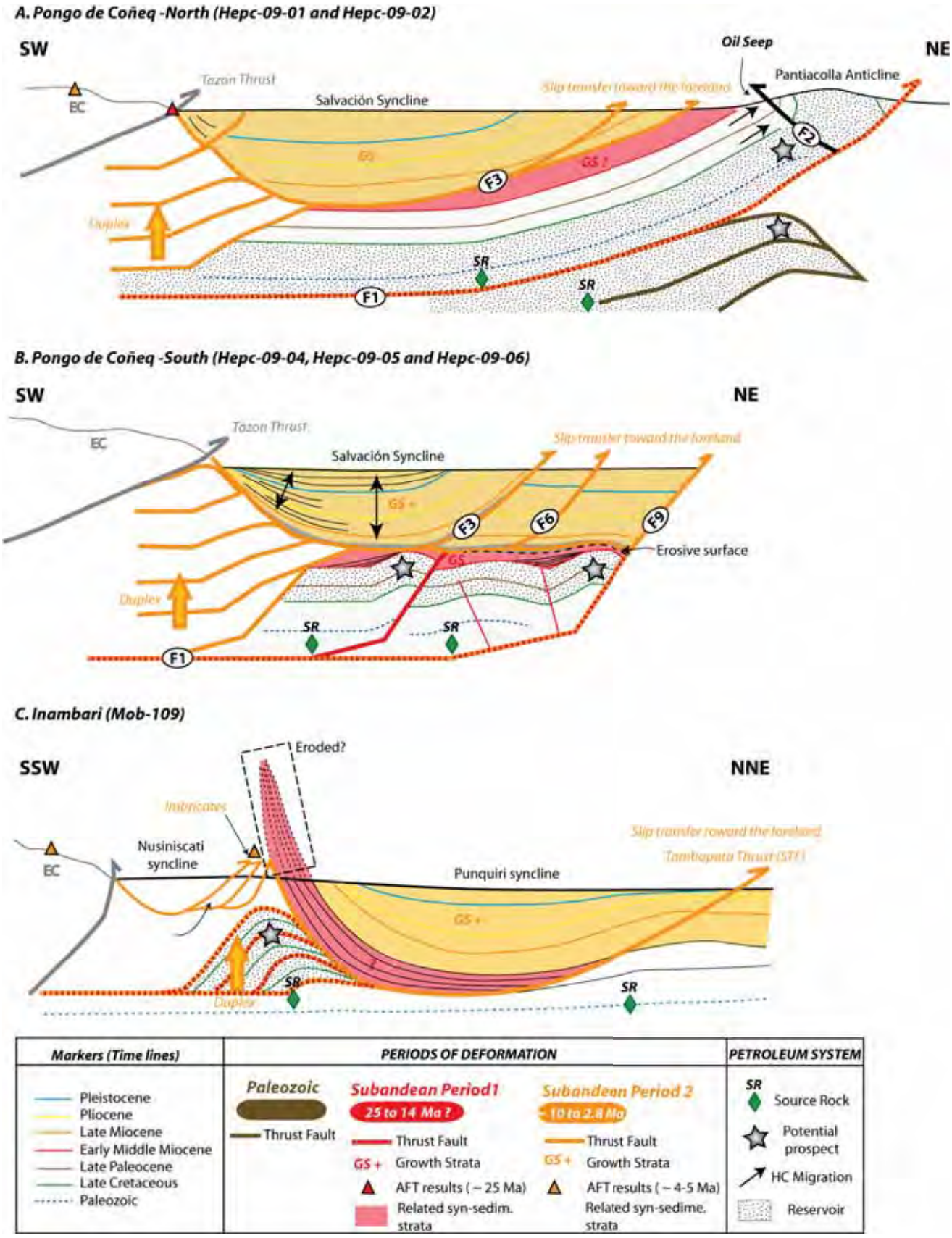

Figure 1: coupes structurales synthétiques montrant la géométrie générale, la chronologie de **déformation** et les principaux syst**èmes pétroliers des zones Subandines du Pongo de Coñeq au nord du bassin de Madre de Dios (coupes A et B) et d'Inambari au sud du bassin (C).**

Ce travail s'inscrit dans le cadre de l'étude des chaînes de montagnes et des bassins sédimentaires d'avant-pays rétro-arc associés à une subduction océanique. Il s'intéresse plus particulièrement aux facteurs qui contrôlent la croissance du prisme orogénique oriental andin et à la dynamique de remplissage du bassin d'avant-pays amazonien. La zone d'étude de cette thèse concerne le bassin de Madre de Dios (12º-14ºS) situé au sud du Pérou dans la zone Subandine (ZSA) actuelle, entre la Cordillère Orientale (CO) à l'Ouest et le bassin Amazonien à l'Est. L'approche de la thèse est multidisciplinaire (géologie structurale, thermochronologie basse température, sédimentologie, provenance). Les principaux objectifs sont de : i) déterminer la géométrie et la chronologie de déformation de la CO et de la ZSA et ii) de déterminer l'évolution du bassin d'avant-pays rétro-arc de Madre de Dios au cours du Méso-Cénozoïque. Les résultats de thermochronologie basse température (traces de fission et (U-Th)/He sur apatites) obtenus pour la CO et la ZSA ainsi que les nombreuses strates de croissances documentées en sismique et sur le terrain dans la ZSA actuelle permettent de mettre en évidence deux principales phases de déformation au sud du Pérou: i) depuis la fin de l'Oligocène jusqu'au Miocène Moyen (~25-14 Ma, Période 1) et ii) pendant le Miocène supérieur jusqu'au Pléistocène (~10-2.8 Ma, Période 2). Nos résultats suggèrent que le refroidissement induit par l'érosion de la CO au sud du Pérou n'est pas contrôlé par un changement climatique mais plutôt par le développement d'un empilement d'écailles ou duplex au front de la cordillère. L'étude du remplissage sédimentaire du bassin de Madre de Dios indique que la ZSA actuelle présentait déjà un séquençage classique de bassin d'avant-pays dès le Maastrichtien avec la mise en évidence de la surrection d'un forebulge au Maastrichtien supérieur. Au cours du Paléocène supérieur (Thanétien), nous mettons en évidence une incursion marine peu profonde jamais documentée auparavant. La paléogéographie du Thanétien se caractérise alors par la présence d'un estuaire dominé par les marées, alimenté en sédiments par la chaîne volcanique andine voisine et débouchant dans une baie peu profonde. Les dépôts Néogène du bassin de Madre de Dios sont caractéristiques d'une mégaséquence de dépôt d'environ 4500 m d'épaisseur, avec des dépôts distaux de faible énergie pendant le début du Néogène évoluant ensuite vers des dépôts proximaux de haute énergie pendant le Néogène terminal et le Pléistocène. La mégaséquence est globalement progradante et strato-croissante et interprétée comme résultant de la migration vers l'Est d'un Megafan. La mégaséquence de dépôt peut être divisée en trois sous-séquences, au cours : i) du Miocène inférieur au Miocène moyen, ii) du Miocène supérieur au Pliocène et iii) de la fin du Pliocène au Pléistocène. Ces séquences correspondent à des cycles du système orogénique Andin, enregistrant des périodes de quiescence tectonique et des périodes de chargement tectonique. Ces pulses tectoniques, enregistrés par le passage d'un stade « suralimenté » à « alimenté », entrainent par flexure lithosphérique une augmentation de l'espace d'accommodation dans le bassin d'avant-pays et se traduisent à termes par une incursion marine peu profonde. Trois incursions marines peu profondes ont ainsi été documentées au cours du Miocène inférieur, du Miocène moyen et au Pliocène (3,45 Ma). Cette dernière correspond à l'incursion marine la plus récente jamais reconnue dans le bassin Amazonien.

The Madre de Dios basin (12º-14ºS) is situated at the south of Peru in the present-day Subandean zone (SAZ), between the Eastern Cordillera (EC) at the West and the Amazonian basin at the Est. Low temperature thermochronological results (apatite fission tracks and (U-Th)/He) obtained for the EC and the SAZ, as well as the growth strata documented in seismic data and on the field allow to determine two main deformation periods in southern Peru: i) from the Oligocene to Middle Miocene (~25-14 Ma, Period 1), and ii) from the Late Miocene to Pleistocene (~10-2.8 Ma, Period 2). The cooling induced by the erosion of the EC in southern Peru is not controlled by climatic change, but better by the development of duplex in the Andean front. The study of the sedimentary infilling of the Madre de Dios basin indicates that the present day SAZ was already part of a classical foreland basin during the Late Maastrichtian, as attested by the presence of a forebulge at that period. During the Late Paleocene (Thanetian), the basin was covered by a shallow marine incursion documented at the north of the study-area. The Neogene to Pleistocene deposits of the Madre de Dios basin are characterized by a 4500 meter-thick megasequence. Sedimentary infilling is mainly continental and is interpreted as resulting from an eastward migrating Megafan fluvial system. During main tectonic pulses in the EC, the accommodation space increases in the basin. At the final stage of such orogenic loading periods, this flexure could promote shallow marine incursions such as those described in the Madre de Dios basin for the Early Miocene, Middle Miocene and Pliocene (3,45 Ma) times. These new data and interpretations allow a review of the Petroleum system of the Madre de Dios basin.